A NEW DESIGN METHODOLOGY OF REINFORCED CONCRETE SQUAT SHEAR WALLS FOR DUCTILE SEISMIC BEHAVIOR AND PREDICTABLE SHEAR STRENGTH

by

GHASSAN ALMASABHA

DISSERTATION

Submitted in partial fulfillment of the requirements
for the degree of Doctor of Philosophy at
The University of Texas at Arlington
August, 2019

Arlington, Texas

Supervising Committee:

Shih-Ho Chao, Supervising Professor
Nur Yazdani
Suyun Ham
Madan Mehta

Acknowledgements

I would like to acknowledge Professor Shih-Ho Chao for his valuable guidance and support throughout this research. His unique research mentorship reshaped the way I tackle the challenges independently, his valuable time devoted to this study is appreciated. Special thanks to the Committee members, Dr. Nur Yazdani, Dr. Suyun Ham and Dr. Madan Mehta.

I would also like to thank our research group, Ra'ed Al-Mazaidh, Ahmed Abdullah Alateeq, Seyed Missagh Shamshiri Guilvayi, Dr. Kyoung-Sub Park, Bhupendra Raj Acharya, Ashish Karmacharya and Chatchai Jiansinlapadamrong, for the support in constructing and testing throughout this study.

The favor of parents and family is invaluable, they are the source of emotions and the spirit of this life, this is the vital factor to success.

July 29, 2019

Abstract

A New Design Methodology of Reinforced Concrete Squat Shear Walls for Ductile Seismic Behavior and Predictable Shear Strength

Ghassan Almasabha, PhD

The University of Texas at Arlington, 2019

Supervising Professor: Dr.Shih-Ho Chao

Reinforced concrete (RC) squat walls (with a height-to-length ratio of 2.0 or less) have high strength and stiffness which makes them a popular seismic force-resistant system for buildings and nuclear power plants. However, extensive studies on squat shear walls showed that squat walls have limited drift ductility because a flexural yielding mechanism is difficult to achieve, thereby undermining the role of squat walls as structural fuse members in earthquake-resisting structures. This research proposes a new design methodology of squat walls for ductile seismic behavior. While ACI 318-19 requires a mesh of steel bars to reinforce squat walls, the proposed design methodology fortifies the squat walls by several steel cages which contain vertical bars enclosed by transverse hoops. These steel cages can be easily prefabricated to significantly reduce the onsite assembling work. Seven ACI compliant and proposed walls with an aspect ratio of 0.5 or 1.0 were tested under symmetric cyclic loading protocols. Similar to prior research results, ACI compliant walls exhibited a fast deterioration in shear strength at low drift ratios and failed in a sliding shear failure mode after severe damage at the wall base due to intersected compression struts under cyclic loading. On the other hand, the proposed squat walls showed excellent behavior by confining the concrete at the most critical zone of the wall base, thereby enhancing the ductility of the compression struts and eliminating the sliding shear failure. As a result, the proposed walls reached a drift

ratio as twice as that attained by the ACI compliant walls, indicating a high ductile behavior of the proposed squat walls. The proposed design methodology allows squat walls to develop a ductile seismic behavior which is essential to promote levels of safety during seismic events. An accurate strut and tie model-based proposed equation was discussed and used to evaluate shear strength of 54 previously tested walls.

CONTENTS

List of Illustrations

List of Tables

Chapter 1

Introduction

1.1. Background and research motivation

Walls and moment frames are the two major seismic-resistant systems used for reinforced concrete buildings, the high lateral stiffness and strength of walls makes them more popular than moment frames. In a survey by Eberhard and Meigs (1995), 85% of low-rise buildings in US used shear walls in high seismic zones. The walls having height to length ratio less than 2.0 are designated as squat walls that commonly used in low-rise buildings and nuclear plants. However, the insufficient drift ductility for squat walls magnifies a problem in buildings design. They have limited level of dissipating energy, and the equations and criteria used to estimate the strength of squat shear walls fail to accurately predict the shear strength. Numerous studies explore the potential of enhancing drift ductility using Fiber-reinforced Concrete (FRC), diagonal reinforcement, high-strength steel, or high-strength concrete. However, the drift ductility improvement, which is the motivation of this study, was minor.

❖ The following three research gaps in literature remain unsolved:

(1) The strength of squat shear walls cannot be accurately predicted using current procedures. Several models and equations, including the American Concrete Institute (ACI) and European codes, were proposed. However, the predicted shear strength is scattered and does not match the experimental results (Yu and Hwang 2005, Hwang et al 2001, Chandra et al 2018, Kassem 2014, and Gulec and Whittaker 2011). The reason of this discrepancy of the predicted strength is that most of those equations (ACI 318-19, Wood 1990, Barda 1977, Ramos et al 2012, and Gulec and Whittaker 2011, and Luna and Whittaker 2019) are empirical and are derived to match results of previous tested

walls based on statistical analysis. However, they cannot predict strength of future-designed walls, because these equations lack the principals and theory of shear transfer mechanism on squat walls. Recently, Hwang et al (2001), Hwang and Lee (2002), Yu and Hwang (2005), Kassem and Elsheikh (2010), Wael Kassem (2014), Weng et al. (2017), Chandra et al. (2018) proposed predicting shear strength equations based on the Strut and Tie model (STM). Although they fairly predict the shear strength, the procedure to calculate the wall strength is complicated and consumes plenty of time.

(2) Another drawback of squat shear walls is they cannot attain a satisfactory drift ductility which is essential to resist severe earthquake events (Paulay et al 1982, Hedaglo et al 2002). Most conventional walls deteriorate rapidly, and the strength drops suddenly once the peak strength is achieved at a drift of 1%. Paulay et al (1982) proposed inserting diagonal reinforcement to delay the sliding failure and increase dissipating energy of squat walls. However, results showed that improvement in maximum attained drift is minor, also this type of walls is not commonly used in practice because of the difficulties to construct the walls.

(3) Lack of experimental data about high shear strength rectangular squat walls, where essential for low-rise buildings and nuclear plants located in high seismicity zones. In a study collected experimental results of more than 400 squat walls, Gulec and Whittaker (2008) did not report any rectangular squat walls with shear strength more than $15\sqrt{f_{cm}}$ (psi); f_{cm} is the concrete compressive strength (psi). While they reported several barbell and flanged squat walls attained shear strength between 20 to $25\sqrt{f_{cm}}$ (psi).

1.2. Importance of ductile squat wall behavior

Squat walls shall have enough strength and stiffness to resist shear forces, however it is uneconomically to design a wall to remain elastic. Rather, walls shall have the ability to reach the yielding shear strength and behave nonlinearly for considerable drift ratio after the yielding, without losing significant shear strength, this quality is termed as “ductility”, which is the most preferable quality for squat walls (Figure 1-1). Ductile squat walls are essential on earthquake-resistant reinforced concrete buildings, where squat walls act as fuse members having excellent drift ductility but slightly lower shear strength compared to the adjacent concrete members, the purpose of the fuse members is to absorb energy by post-yielding deformation and redistribute internal forces from yielded members to the non-yielded members based on their stiffness ratio. The non-yielded members usually are stronger than the yielded members (ductile members) by 25% or more, but they are unnecessary to be ductile.

Although the design of elastic squat walls with insufficient ductility is expensive, they significantly lose their strength suddenly at low drift ratios without adequate warnings. Therefore, ductile squat walls are essential to promote levels of safety during seismic events and unpredicted risks.

Kircher et al. (2010) evaluated FEMA P-65 acceptance parameters (system overstrength and ductility factors) of reinforced concrete building models having different wall aspect ratio, they used OpenSees software as the investigating tool. The assessments indicate that squat walls located in short-period domain at high seismicity zones attained low story drift ratios at ultimate shear strength and failed to meet FEMA P-65 acceptance criteria. This study emphasizes the importance of having ductile squat shear walls to meet FEMA buildings safety standards.

Figure 1-1 Ductile and non-ductile wall behavior

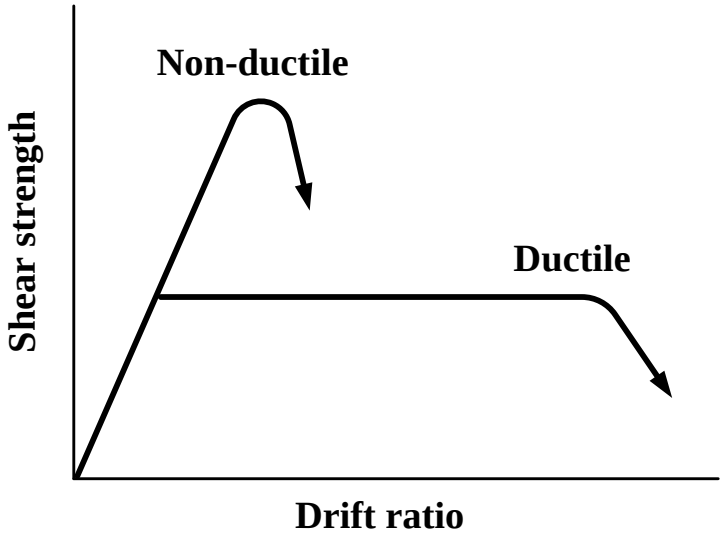

1.3. Squat walls design philosophy of ACI 318-19 versus Proposed Methodology

In this study, a new reinforcement configuration is proposed to improve squat shear walls behavior. Reinforcement layout comparison between ACI 318-19 compliant walls and proposed walls are illustrated in Figure 1-2. A typical ACI squat wall consists of vertical and horizontal steel bars, and boundary elements, while the proposed squat walls contain several steel cages of longitudinal steel bars confined by hoops. The advantages of proposed walls are: 1) Steel cages can be easily prefabricated to significantly reduce the onsite assembling work; 2) Wall web and boundaries are well-confined, thereby resulting in ductile behavior. Figure 1-3 shows the test results of an ACI compliant wall and a proposed wall that have the reinforcement layouts of Figure 1-2, both walls have same amount of vertical steel bars but different configuration of horizontal reinforcement. Once the sliding shear failure occurs on ACI walls at low drift ratio (around 1%), concrete is no longer contributes to resist shear forces, only longitudinal steel bars do by dowel action. On the other hand, concrete is still well-confined and contribute to resist shear forces until a high drift ratio (around 2% – 2.5%), which improves wall drift ductility.

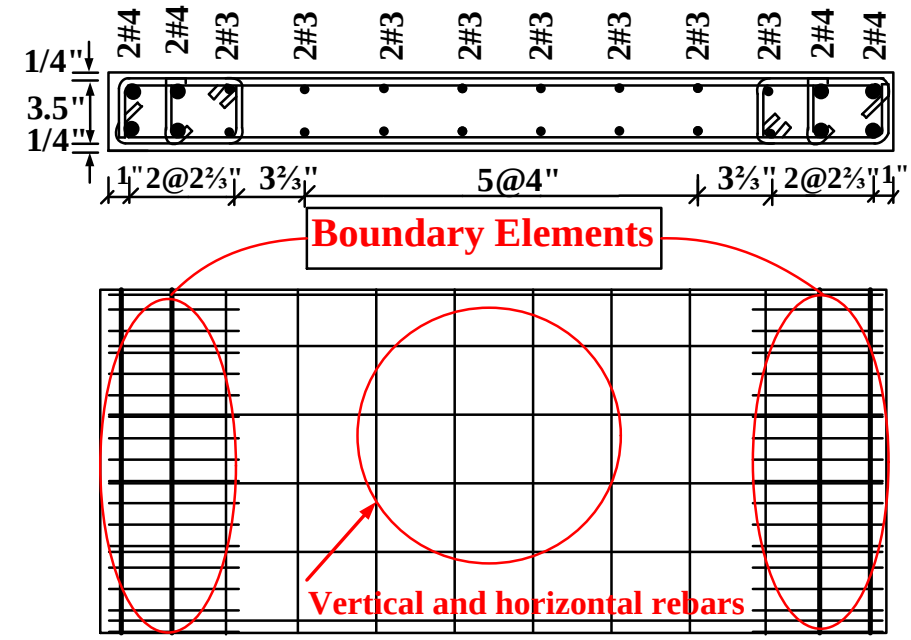

ACI wall design provisions

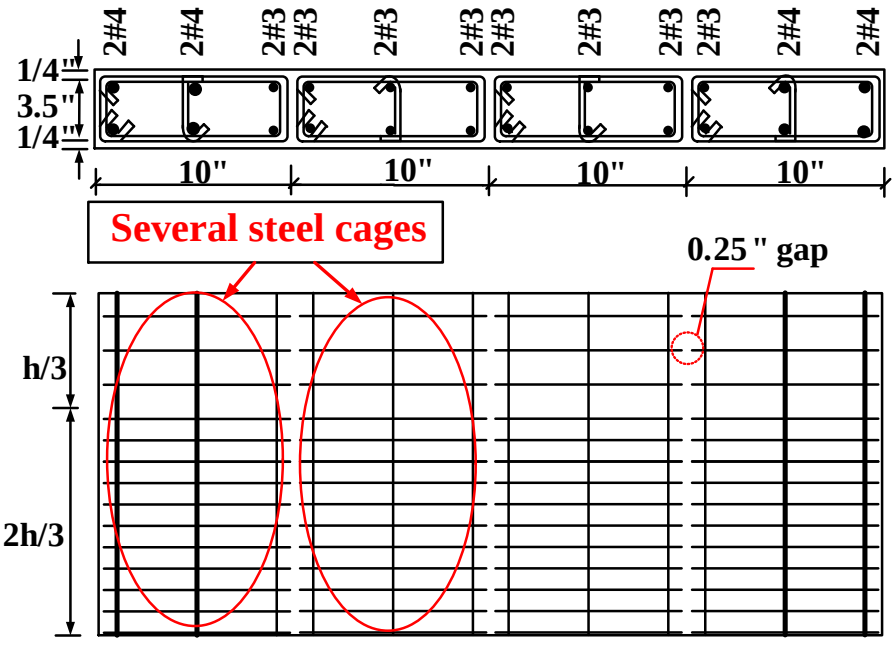

Proposed wall layout

Figure 1-2 Typical design of ACI 318-19 compliant squat wall and Proposed wall

ACI provisions-based design wall

- **No concrete resisting shear forces.**
- **Shear forces resisted by dowel action.**

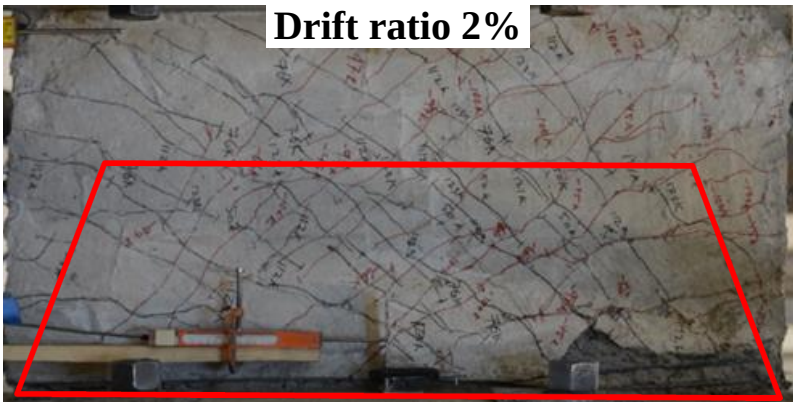

Proposed wall

- **Wall web and boundaries are confined.**
- **Enhanced concrete strength and wall ductility**

Figure 1-3 Typical shear behavior of ACI 318-19 compliant squat wall and Proposed wall

1.4. Research objectives and scope

This study aims to: (1) enhance wall drift ductility for both normal and high strength demand by changing the reinforcement layout. The conventional wall design requires vertical and horizontal steel bars. However, in this study, the proposed walls are fortified by several steel cages which consist of vertical bars and multiple horizontal

hoops, and (2) propose a new equation and criteria to predict the strength of conventional shear walls based on experimental tests considering results of previous tested walls. The new equation would eliminate the inconsistency between expected and experimental shear wall strength. In the light of squat walls results in literature, it is hypothesized that squat shear walls behave as softened strut and tie model, which eases to predict strength of squat walls. The proposed procedure stiffens the walls by hoops to confine the concrete, which enhances the wall drift ductility and eliminates the sudden deterioration on wall strength.

Seven shear walls were recently tested in the Civil Engineering Laboratory Building (CELB) at UT Arlington. The lab has abundant testing facilities which are necessary to simulate earthquake loading protocols, e.g., a 300-kips MTS Actuator and a strong floor. A set of three walls with 0.5 aspect ratio, were designed to resist high demand shear stresses and two walls to resist moderate shear stresses. While the other set of two walls with 1.0 aspect ratio were reinforced to withstand low shear stresses.

The proposed design methodology produces walls with high drift ductility which cannot be achieved using the conventional walls. Also, this study will precisely quantify the strength of the conventional walls. Therefor the new criteria is proposed to design squat shear walls which have improved level of dissipating energy. The proposed walls would fill the gap on restricted ductility walls that current design procedures cannot solve.

The following key terms are used in this proposal:

Squat shear walls are walls having aspect ratio (length/height) less than 2.0, which are commonly used on low-rise buildings, nuclear plants, industrial structures. The walls resist shear forces developed from seismic events.

Drift ratio: is the displacement of wall tip divided by the height of wall, usually the unit is percentage (%).

Drift ductility: there is many definitions of this term, however in this study it refers to the maximum wall drift achieved after the wall reaches the peak shear force and drops 15% of the peak force.

Conventional squat walls: squat walls that are designed based on current codes, e.g. ACI and European codes. The walls are usually reinforced by a steel mesh which consists of vertical and horizontal steel bars. A boundary element which contains vertical steel bars and horizontal stirrups are recommended to be provide at both wall boundaries.

Proposed squat walls: are squat walls contain multiple steel cages, each cage consists of vertical steel bars and horizontal hoops to increase the wall confinement and ductility.

1.5. Research Significance

This research investigated the seismic performance of proposed squat shear walls that have superior advantages compared to conventional walls designed by ACI 318-19 provisions which suffers sliding shear failure. The proposed wall merits are high shear ductility and easy to fabricate steel reinforcement. In previous studies, strut and tie model has been widely explored to quantify shear force transfer, however, this study accurately investigated strut and tie model components using advanced experimental measuring techniques. Numerous studies have been conducted to explain sliding shear mechanism in squat walls, however, this study clearly described the sliding shear mechanism in a simple and unique methodology.

Chapter 2

Literature Review

2.1. Introduction

Numerous studies have been devoted to investigate the behavior of squat shear walls due to their crucial role in earthquake-resistant reinforced concrete structures. Squat walls are generally governed by shear mode failure which prevents the walls to reach their full shear strength (flexural capacity). Therefore, special attention has to be considered to estimate their shear strength. Although several models and equations has been derived to predict shear wall strength, most of the estimated strength are scattered and fail to accurately predict the shear strength, which rises structural safety concerns and sometimes overestimate wall strength.

2.2. Experimentally tested walls

The downside of conventional shear walls, they cannot attain a satisfactory drift ductility which is essential to resist severe earthquake (Paulay et al 1982, Hedaglo et al 2002). Most conventional walls deteriorate rapidly, and the strength drops suddenly once the peak strength is achieved at drift of 1%. Dissipated energy has an essential role on behavior of squat shear walls constructed on severe seismic zones. In practice, walls having the ability to dissipate energy are needed since all other structural components are affected by the wall ductility. However, conventionally designed shear walls have insufficient level of dissipation energy since they are designed using a steel mesh - horizontal and vertical steel bars- which are not capable to withstand diagonal shear forces.

According to Paulay et al. (1982), sliding shear failure propagates in several stages. First, majority of shear forces are transmitted throughout the flexural compression

zone (Figure 2-1a), in this stage, the flexural steel rebars significantly yielded. Second, long cracks propagate on the wall base due to reversal loading which causes formation of flexural cracks on the pre-compressed zone (Figure 2-1b). Finally, shear forces transferred by dowel action of longitudinal steel bars (Figure 2-1c).

Paulay et al. (1982) proposed diagonally reinforced shear walls to improve the amount of dissipated energy by relieving sliding shear failure. For this study, to eliminate the sliding shear failure, diagonally reinforced walls were introduced. Four squat shear walls constructed based on either conventional design or conventional walls with diagonal reinforcement (Figure 2-2). The walls were experimentally tested to investigate the displacement ductility due to providing diagonal reinforcement on conventional squat shear walls. Results (Figure 2-3) showed that shear forces on the conventionally designed shear walls are transferred through (1) dowel action developed on not-yielded steel bars on the middle wall region, and (2) kinking of vertical bars due to significant wall slip. Inserting diagonal steel bars resists more than half of the applied shear forces on the wall, which reduces sliding shear forces, enhances the displacement ductility, and increases flexural strength.

Results also demonstrated that sliding shear forces are resisted by vertical steel bars and shear friction developed on the compressed concrete depth. Conventional squat shear walls with flanged sections have a weak shear friction resistance since the compressed concrete depth is small. Consequently, they are vulnerable to severe shear sliding. However, flanged shear walls with diagonal reinforcement showed considerable improvement on level of dissipated energy.

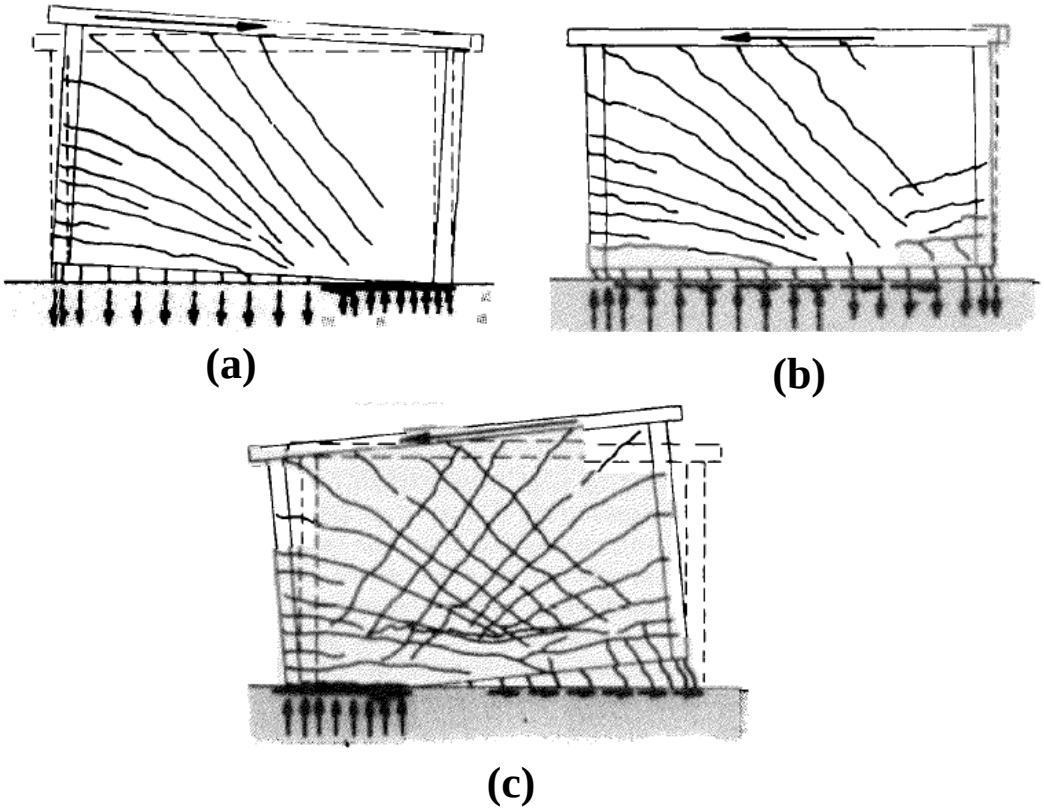

Figure 2-1 Mechanism of sliding shear failure (Paulay et al., 1982)

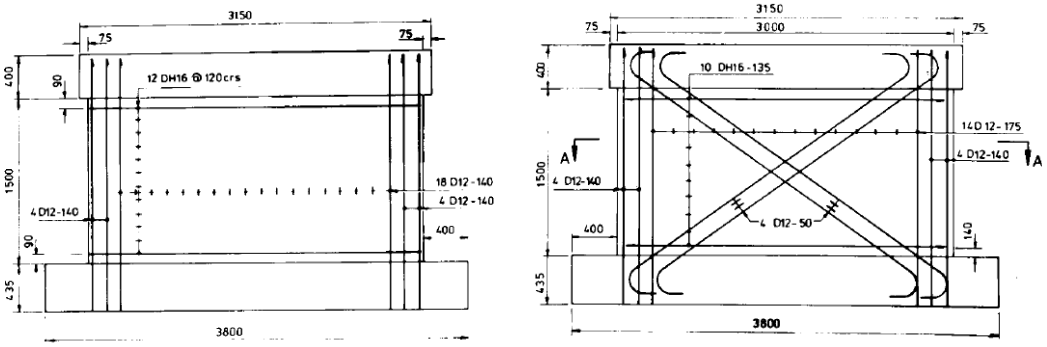

(a) Conventional wall **(b) proposed wall**

Figure 2-2 Reinforcement detailing of tested walls; dimensions mm (Paulay et al., 1982)

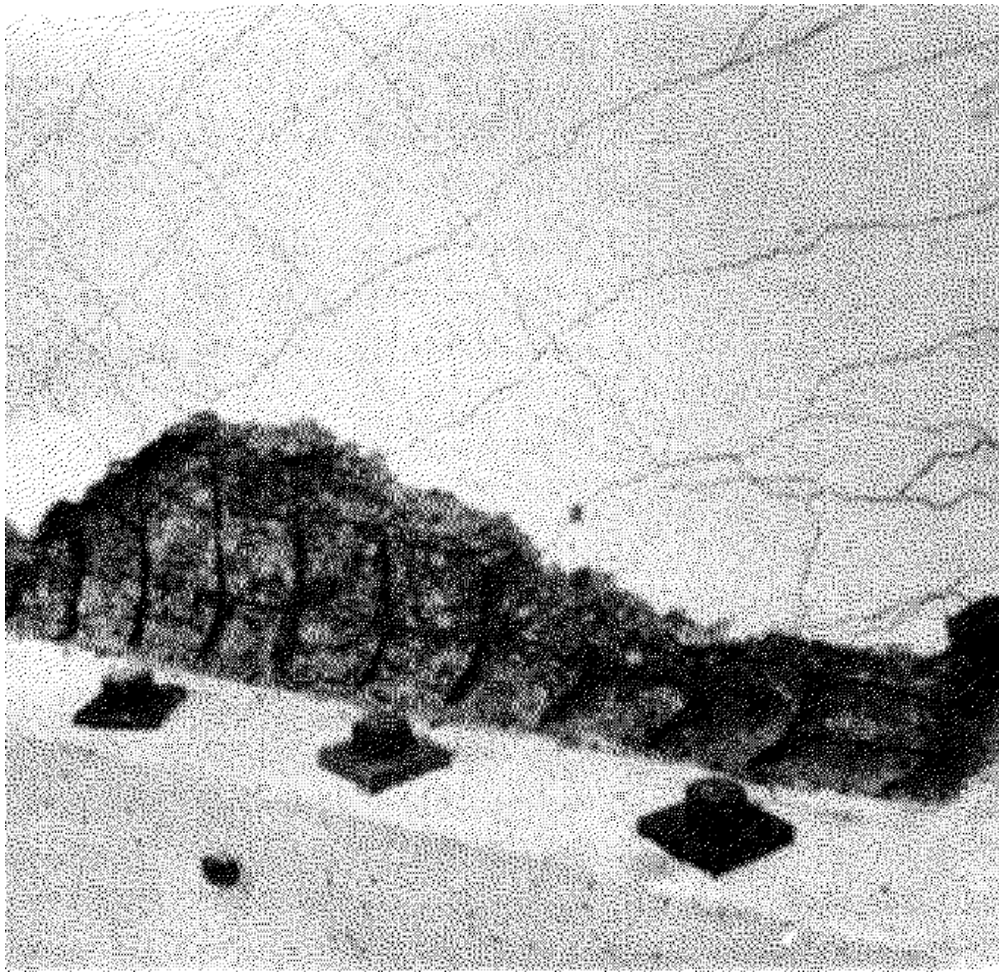

Figure 2-3 Sliding shear failure (Paulay et al., 1982)

Cardenas et. al. (1980) tested seven 1.0-aspect-ratio walls having different vertical and horizontal reinforcement ratios. Walls dimension were 75 in. X 75 in. X 3 in., longitudinal steel bars were either placed uniformly or lumped at boundaries as shown in Figure 2-4. The results showed that both vertical and horizontal steel bars are essential and contribute to resist shear forces in walls having 1.0 aspect ratio, also enough web reinforcement is a major factor to control mode failure (shear, flexural-shear, or shear-anchorage). In addition, the shear strength difference between cyclic or monotonic loading was insignificant. Figure 2-5 show the sliding shear failure of specimen SW-9.

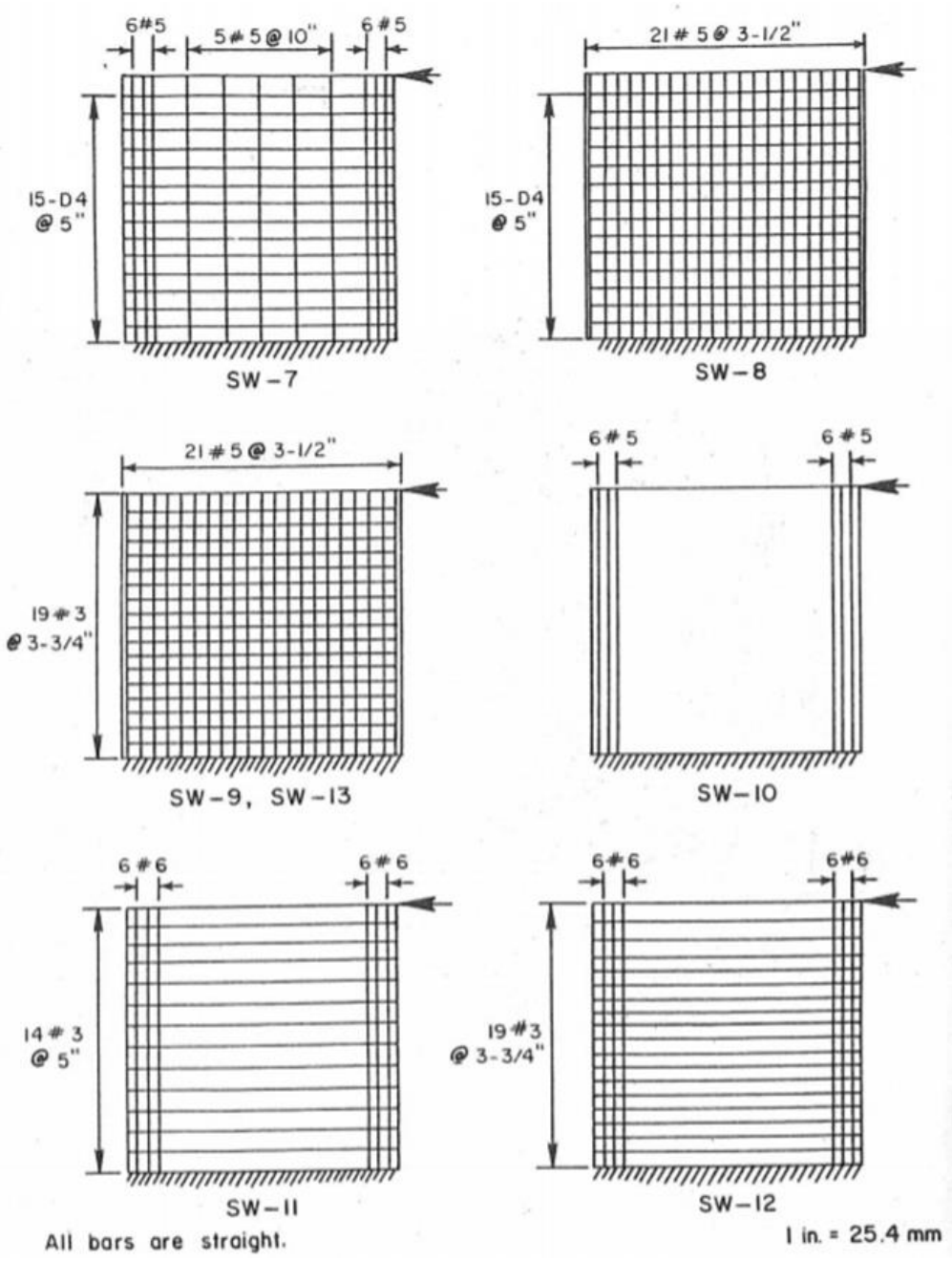

Figure 2-4 Reinforcement layout of tested walls (Cardenas et al., 1982)

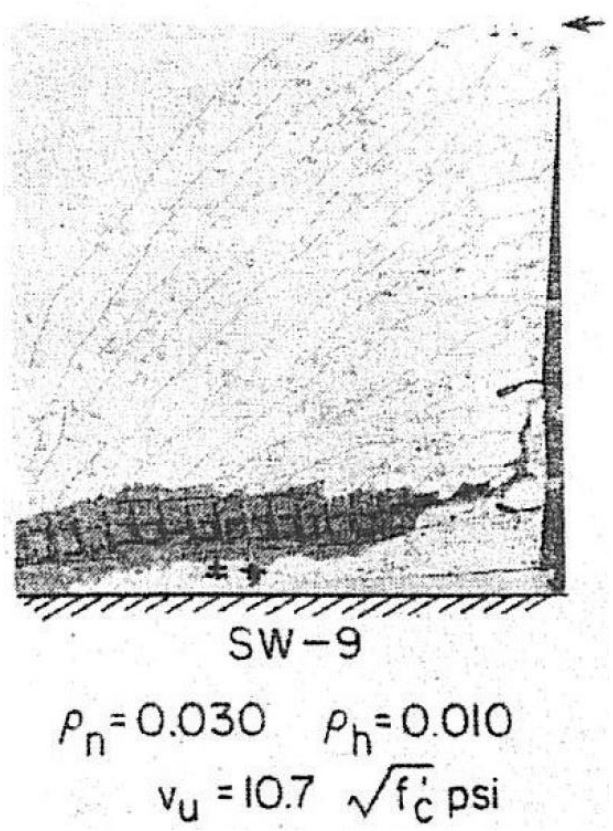

Figure 2-5 Specimen after testing (Cardenas et al., 1982)

Barda et al. (1977) tested eight flanged squat walls with aspect ratio ranges from 0.25 to 1.0, the purpose of this study was to investigate effect of vertical, horizontal, boundary reinforcement ratios on wall shear strength. Specimen B6-4 and B8-5 have 0.5- and 1.0-aspect ratios, respectively. Both walls have similar horizontal reinforcement ratio of 0.5%, B6-4 have 0.25% vertical reinforcement ratio but B8-5 reinforced by 0.5%. Both walls reached the ultimate shear stress about 12√fcm (psi) at drift ratio 0.6%, the specimens failure mode at end of test is shown in Figure 2-6 and Figure 2-7, the photos reveals the concrete crushing at the wall web.

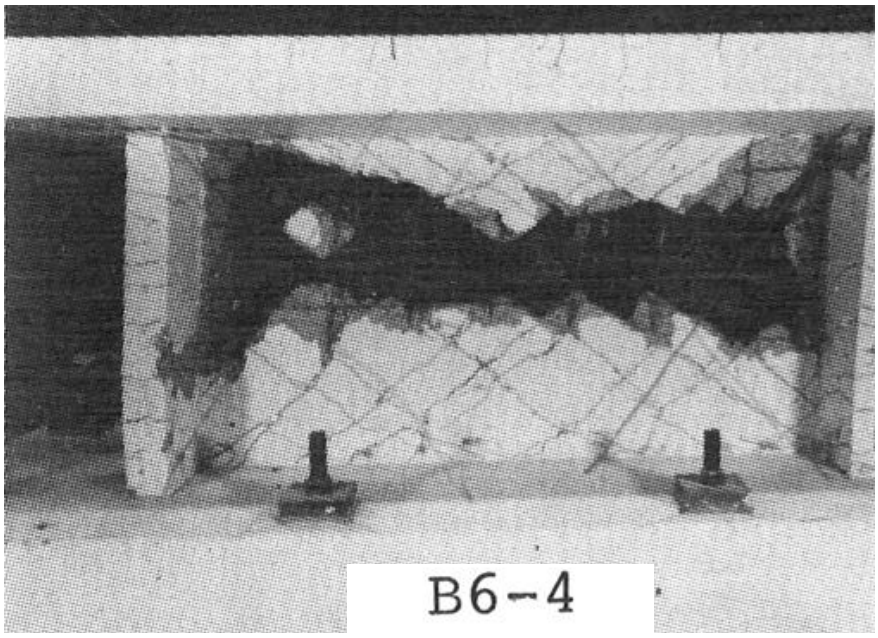

Figure 2-6 Specimen B6-4 at end of test (Bara et al. 1977)

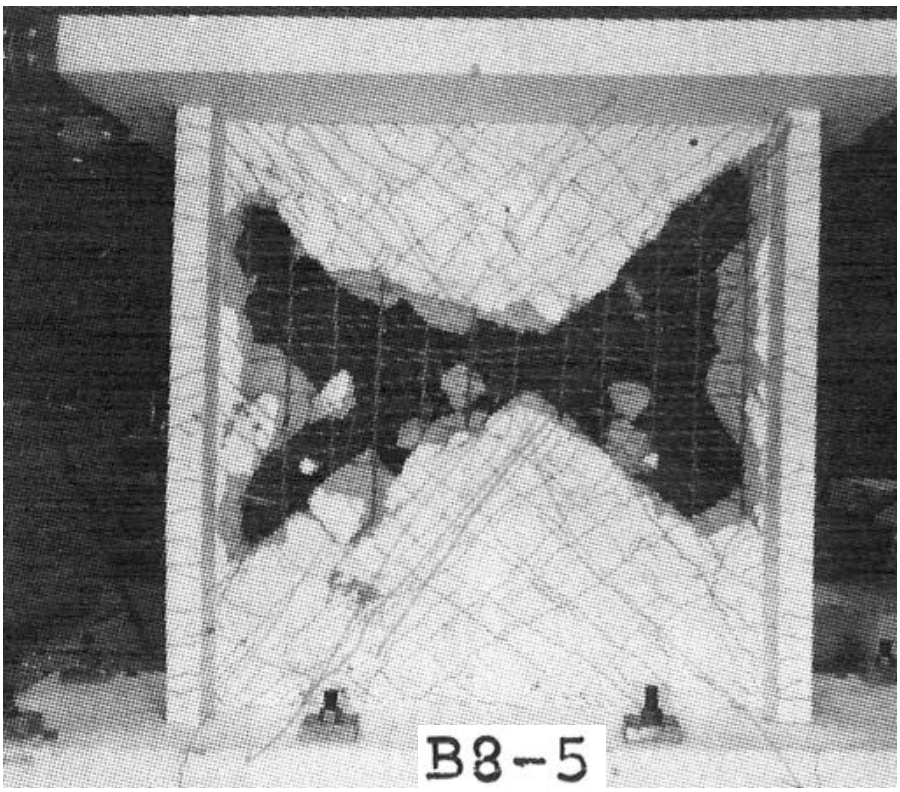

Figure 2-7 Specimen B8-5 at end of test (Bara et al. 1977)

In additional studies of squat shear walls, researchers focused on dissipated energy of walls reinforced with normal strength steel bars (Hidaglo et al., 2002) and walls reinforced with high-strength steel (HSS) bars (Cheng et al. 2016) and (Baek et al., 2017). Hidaglo et al. (2002) tested 26 full-scale specimens reinforced by normal steel strength, the major parameters of the study were wall aspect ratio (1.0, 0.69, 0.5, and 0.35), concrete compressive strength, vertical and horizontal reinforcement ratios. The results showed the failure drift and the rate of strength degradation after the peak value were adversely related to the aspect ratio (Figure 2-8). Vertical reinforcement has almost no contribution on wall strength. Also, dissipated energy seems not effected by neither aspect ratio nor amount of reinforcements. Hidaglo et al.'s work is different from Cheng et al.'s work in a number of aspects. While Cheng et al. tested five shear walls, they did so with reinforced normal steel or HSS. In particular, two walls had moderate shear strength, while the other three had high shear strength. In further detail, one of the three specimens had 50% confining reinforcement at boundaries less than the other four walls. All specimens were designed so that shear failures are avoided. Results showed that HSS specimens exhibited a 20% increase on wall drift at peak shear strength compared to normal walls. Confining reinforcements at wall boundaries were found have no contribution on overall wall performance, (Figure 2-11 and Figure 2-12). Regardless of steel grade on walls, behavior of walls has no difference, and the ultimate wall drift conversely related to shear wall demand (i.e. moderate vs high wall strength).

Similarly, Baek et al. (2017) investigated the potential use of high strength steel bars on squat shear walls, by conducting an experimental study having three main parameters: failure mode (shear or flexural), strength of steel bars (60 ksi or 80 ksi) and existence of boundary hoops. In this study, five squat walls with aspect ratio of 0.5 and seven squat wall with aspect ratio of 1.0, have been considered. To attain shear mode

failure, provided flexural reinforcement are higher than those on squat walls designed to fail in flexural mode. Results showed that the margin of errors of walls with 80 ksi reinforcement is slightly less compared to walls with 60 ksi. Inserting boundary hoops does not have any effect on behavior of walls. Overall, results show that squat walls either reinforced by steel bars with strength of 60 ksi or 80 ksi have similar performance. Figure 2-9 and Figure 2-10 show the concrete crushing at wall web at end of test Specimen NF0.5M and NF1M, the walls have 0.5- and 1.0-apect ratio, respectively. According to current studies by Cheng et al., 2016 and Baek et al., 2017, walls that constructed by high steel strength are comparable to behavior of walls reinforced with low steel strength. Therefore, current codes and procedures should adopt high steel strength on squat walls. The use of HSS on walls, reduce the required reinforcement area, as a result, walls construction become easier.

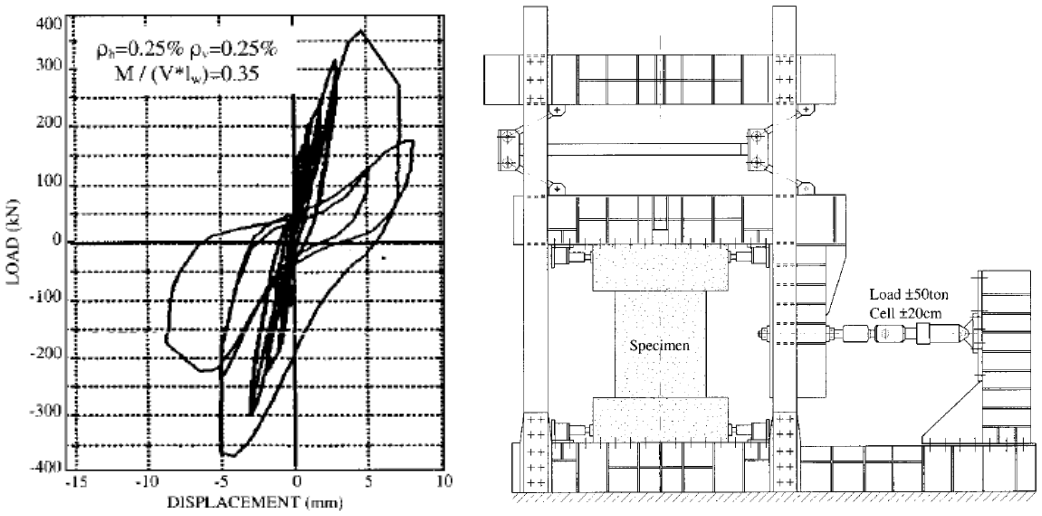

(a) Sudden strength drop of 0.35-aspect ratio specimen

(b) Test setup

Figure 2-8 Test setup and typical sliding shear behavior (Hidalgo et al., 2002)

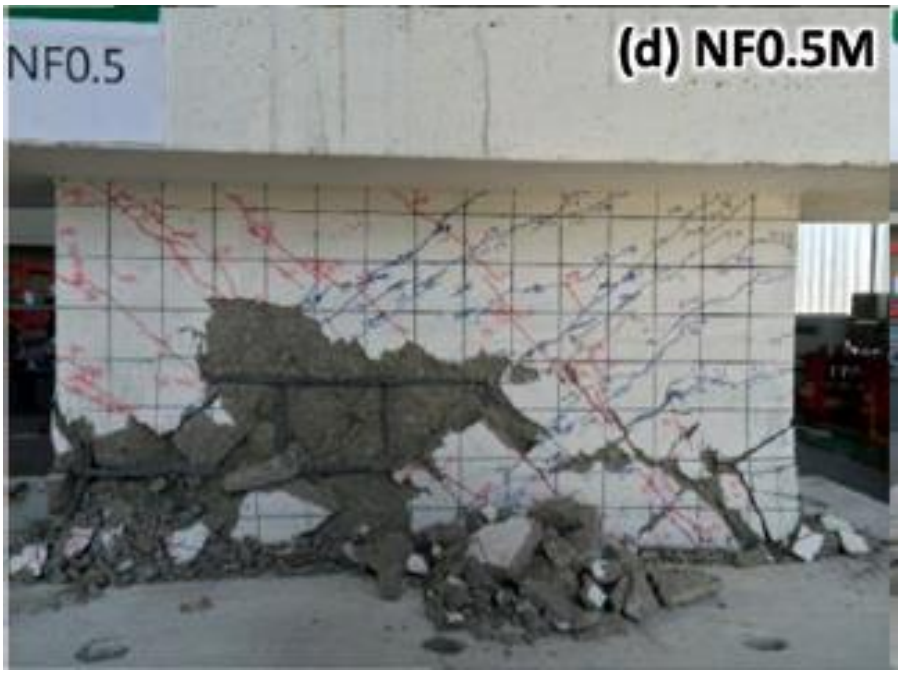

Figure 2-9 Specimen NF0.5M at end of test (Baek et al. 2017)

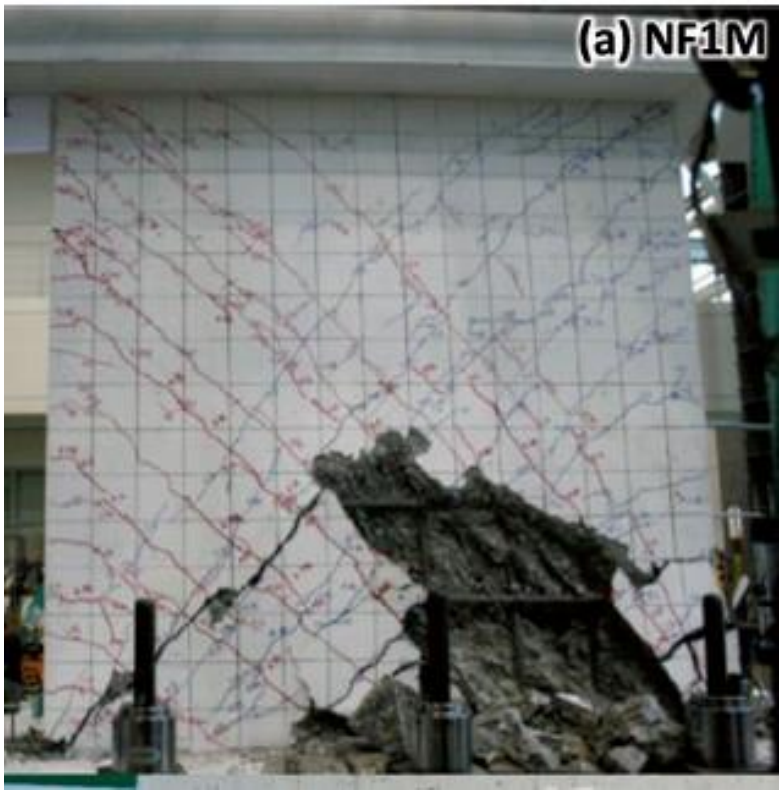

Figure 2-10 Specimen NF1M at end of test (Baek et al. 2017)

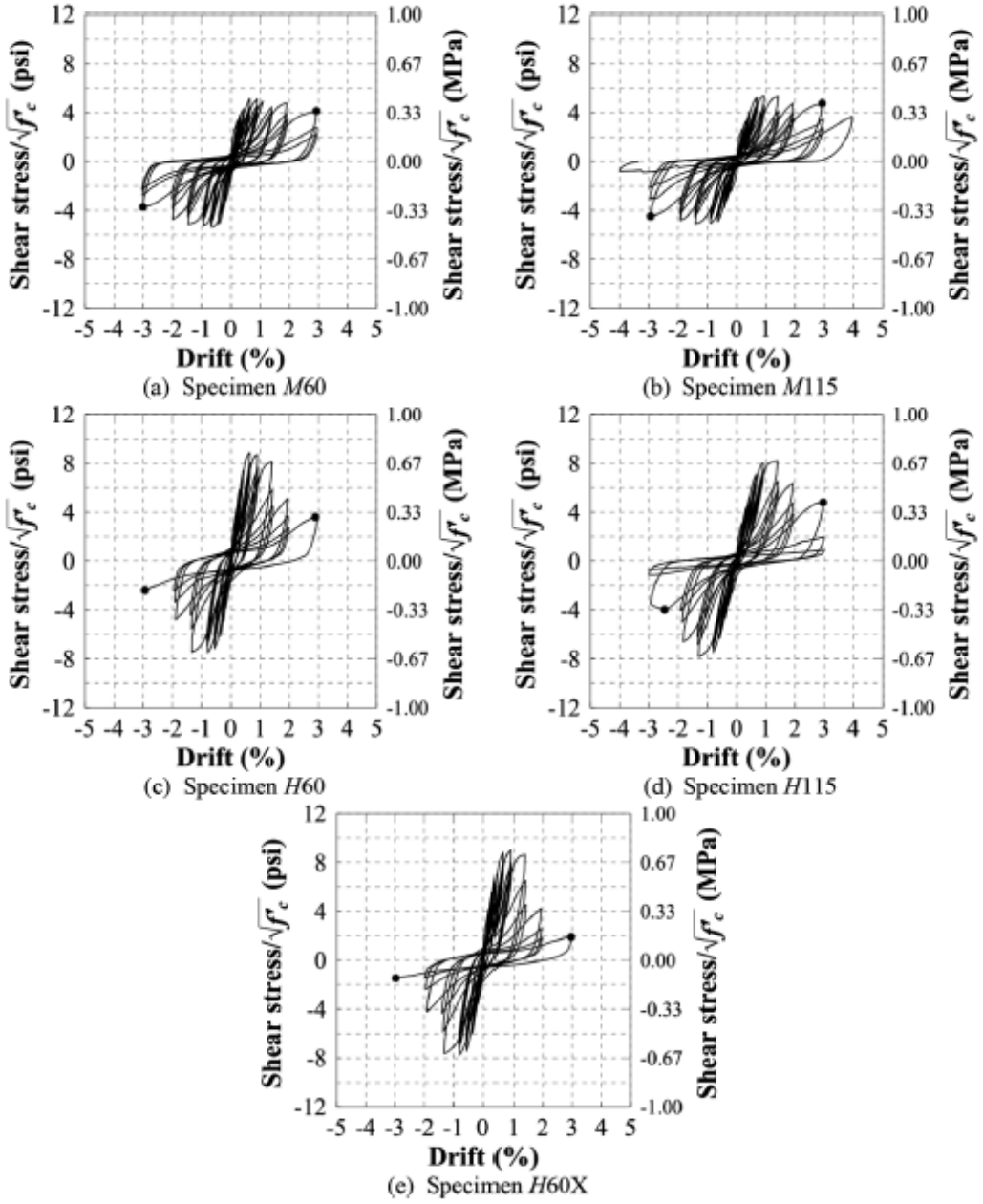

Figure 2-11 Shear strength results of tested walls; Specimens identified with letters “M” and “H” were designed for shear stresses level of 5 and 9√fc′ psi (0.42 and 0.75√fc′ MPa), respectively. Specimens H60, H115, and H60X were designed for high (“H”) shear stresses, “X” refers to 50% less hoops reinforcement at boundaries (Cheng et al., 2016)

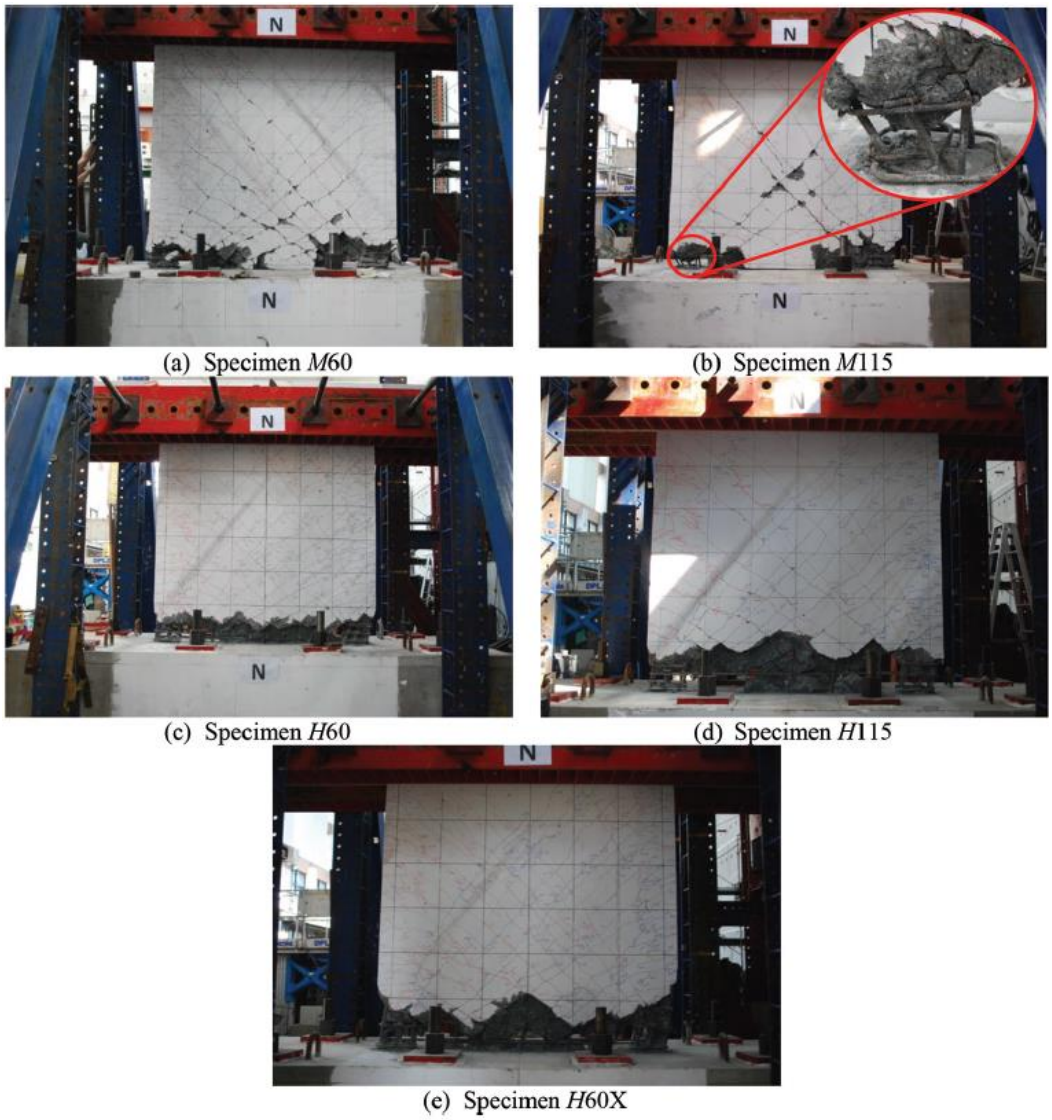

Figure 2-12 Sliding shear failure of tested walls; Specimens identified with letters “M” and “H” were designed for shear stresses level of 5 and 9√fc′ psi (0.42 and 0.75√fc′ MPa), respectively. Specimens H60, H115, and H60X were designed for high (“H”) shear stresses, “X” refers to 50% less hoops reinforcement at (Cheng et al., 2016)

Nuclear and industrial structures usually are constructed using squat shear walls with high stiffness. These walls have difficulties to be tested with hybrid simulation by usual displacement tools (like LVDTs) due to poor accuracy on displacement results. Whyte & Stojadinovic, 2014 have tried to solve this problem by using a high precision encoder technique on the hybrid simulation. At UC Berkeley, two identical walls were designed and scaled to a real wall on nuclear structure, the walls dimensions were 3 m long, 1.6 m height, and 20.3 cm thickness. The volumetric horizontal and vertical reinforcement ratios were 0.67%. A third identical wall also was tested at the State University of New York at Buffalo, but it was tested under quasi static cyclic loading. Although the walls were tested under different ground motions, performance of walls are same, they failed due to sliding shear at walls bases (Figure 2-13). Therefore, squat shear walls behavior seems not be sensitive to different types of loading protocol. The study also advanced the technique used to perform hybrid simulation, this technique accurately quantifies strength and stiffness of walls, which are hard to be estimated using conventional methods.

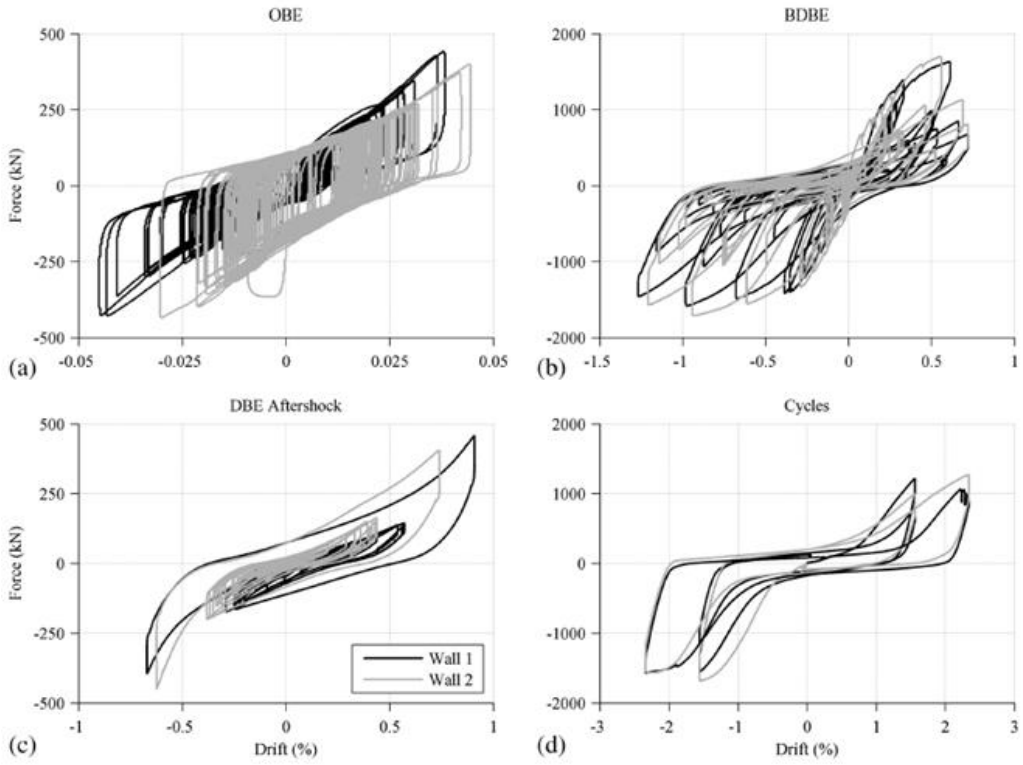

Figure 2-13 Shear strength response of Wall 1 and Wall 2 (Whyte and Stojadinovic, 2014)

2.3. Shear strength estimation based on Strut and Tie Model

Hwang et al (2001) proposed a softened strut-and-tie model to estimate wall shear strength, the softened strut considers the strength deterioration of cracked concrete which has a strength less than uniaxial compressive strength, this phenomenon represents the Modified Compression Field Theory discovered by Vecchio and Collins (1986) as shown in (Figure 2-14). The proposed softened strut-and-tie model (Figure 2-15) is similar to the model adopted to earthquake resisting beam-column joints by Hwang and Lee (1999 and 2000). The shear strength resisted proportionally by Diagonal,

Horizontal and Vertical mechanisms, the contribution percentage of each mechanism are calculated by solving a set of equations satisfying Equilibrium, Constitutive and Compatibility (Figure 1-2). Although the model predicts shear strength more accurately than equations of ACI 318-95, the solution is time-consuming and requires significant mathematical iterative efforts.

Therefore, Hwang and Lee (2002) used the same strut and tie model but simplified the methodology to calculate shear strength (Figure 2-17), the model considers the contribution of the softened concrete strut, in addition to the horizontal and vertical steel reinforcement. The shear strength $C_{d,n}$ is estimated by:

$$C_{d,n} = K\zeta f_c' A_{str}$$

Where:

$$K = \frac{-D + \frac{F_h}{\cos\theta} + \frac{F_v}{\sin\theta}}{-D + \frac{F_h}{\cos\theta}\left(1 - \frac{\sin^2\theta}{2}\right) + \frac{F_v}{\sin\theta}\left(1 - \frac{\cos^2\theta}{2}\right)} \geq 1.0$$

$$\zeta = \frac{5.8}{\sqrt{f_c'}} \frac{1}{\sqrt{1 - 400\varepsilon_r}} \leq \frac{0.9}{\sqrt{1 - 400\varepsilon_r}}$$

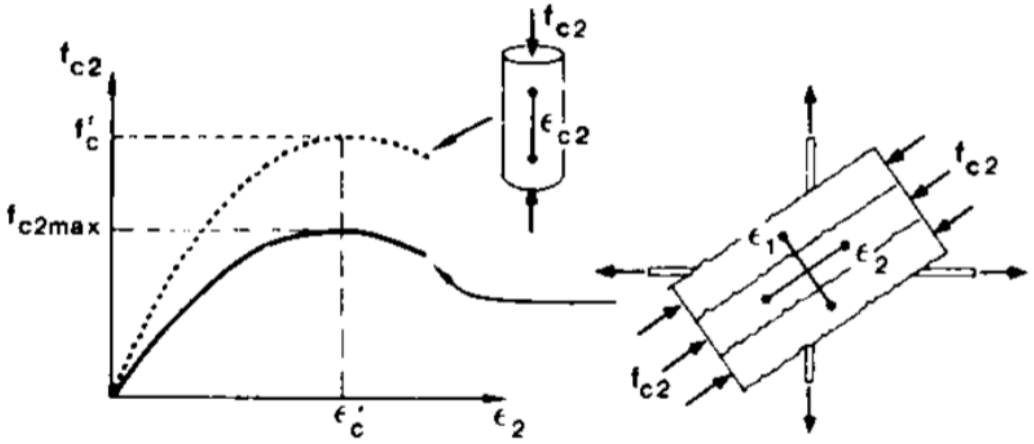

Figure 2-14 Stress-strain relationship for cracked and uncracked concrete (Vecchio and Collins 1986)

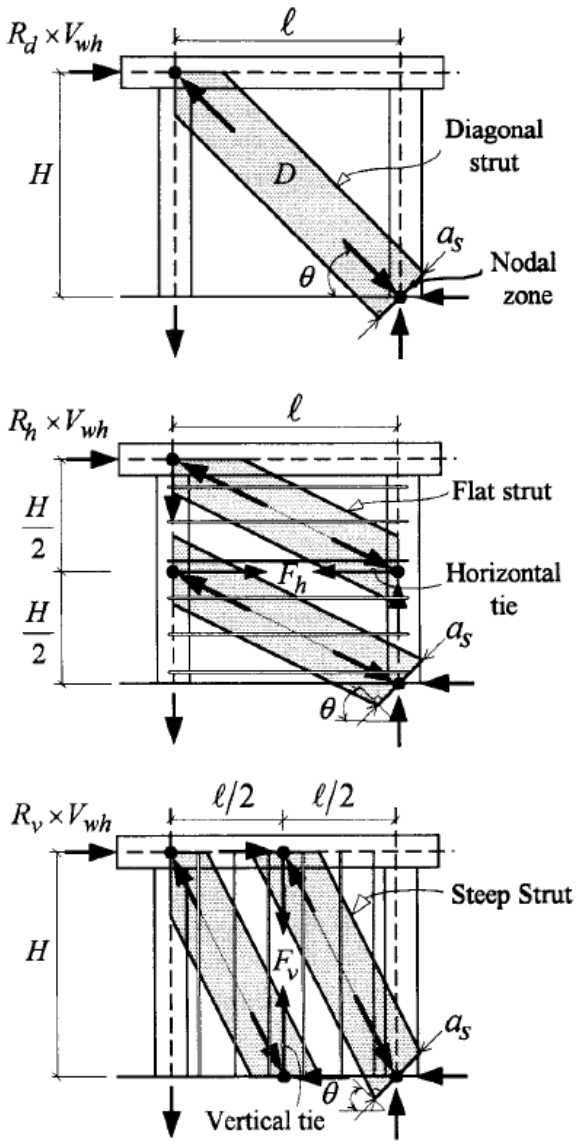

Figure 2-15 Mechanisms of shear force transfer (a) Diagonal (b) Horizontal (c) Vertical

(Hwang et al, 2001)

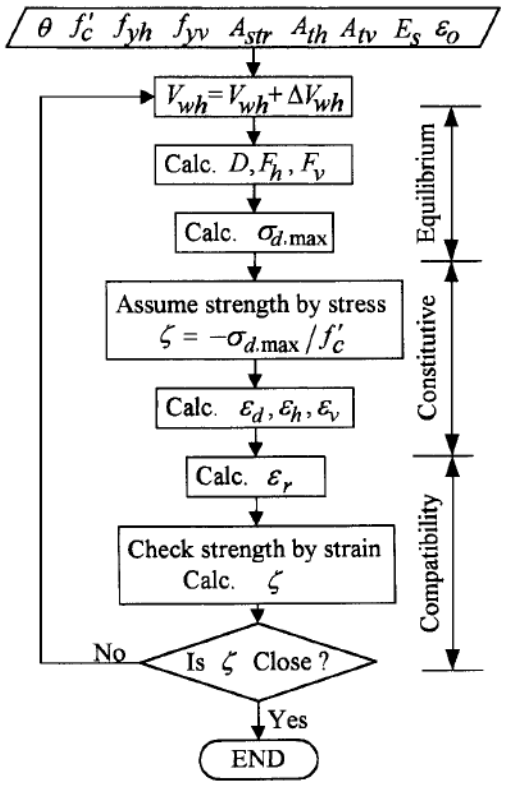

Figure 2-16 Flowchart of proposed shear strength estimation (Hwang et al, 2001)

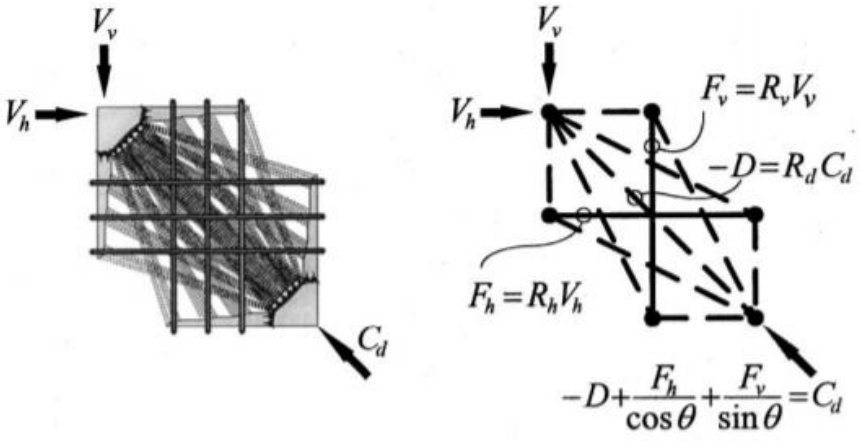

(a) Disturbed stress field (b) Strut-and-tie idealization

Figure 2-17 Strut and tie model (Hwang and Lee 2002)

Wael Kassem (2014) built on the strut-and-tie model that proposed by Hwang et al (2001), his model is shown in (Figure 2-18). The shear strength was estimated by the following single closed-form equation which is easy to calculate and more accurate to predict the shear strength.

$$v_{Rk} = 0.27 f_c' \left[\psi k_s \sin(2\alpha) + 0.11 \omega_h \frac{H_w}{d_w} + 0.3 \omega_v \cot(\alpha) \right] \le 0.83 \sqrt{f_c'} \quad \text{[MPa]}$$

$$v_{Rk} = 39.75 f_c' \left[\psi k_s \sin(2\alpha) + 0.11 \omega_h \frac{H_w}{d_w} + 0.3 \omega_v \cot(\alpha) \right] \le 10 \sqrt{f_c'} \quad \text{[psi]}$$

Where:

$$\psi = 0.95 - \frac{f_c'}{250} \quad (f_c' \text{ in MPa})$$

$$k_s = \frac{a_s}{d_w};\ a_s = \left(0.25 + 0.85 \frac{P_n}{A_w f_c'} \right) L_w$$

$$\alpha = \tan^{-1} \left(\frac{H_w}{d_w} \right)$$

$$\omega_h = \frac{\rho_h f_{yh}}{f_c'};\ \omega_v = \frac{\rho_v f_{yv}}{f_c'}$$

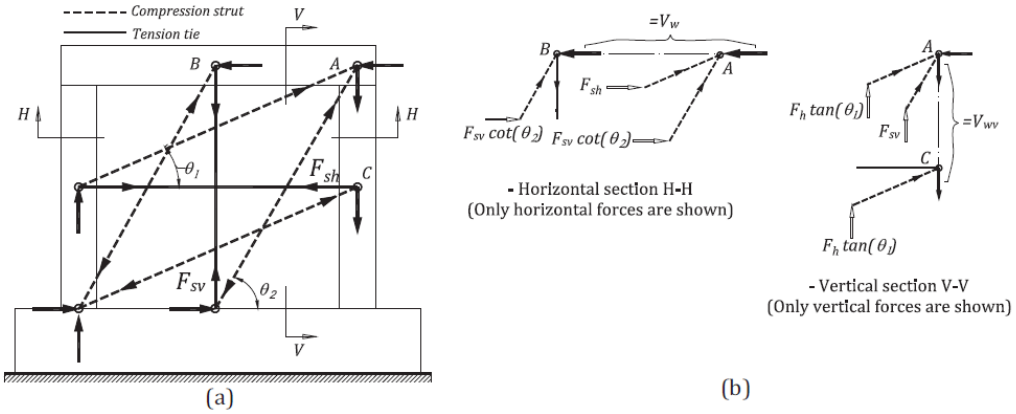

Figure 2-18 (a) Horizontal and Vertical mechanisms (b) free body diagrams (Wael Kassem 2014)

Chandra et al (2018) tested seven high strength concrete shear walls. Based on the study outcomes and results of 77 other tested walls in literature, they proposed truss model to estimate shear strength of reinforced concrete walls (Figure 2-19), the model assumes stresses are uniformly distributed, the shear strength is calculated by:

$$V_n = (\sigma_r - \sigma_d)\sin\theta\cos\theta t_w d_w + 1.64 b_{ef} d_{be} \sqrt[3]{f'_c}$$

$$\sigma_r = 0.02 f'_c$$

Where; b_{ef} is effective width of boundary element (mm), V_n is nominal shear strength of wall (Newtons), t_w is wall web thickness (mm), d_w is wall effective depth (mm).

If horizontal and vertical web reinforcement yielded before concrete strut crushing, then calculate strut strength by:

$$\sigma_d = -\zeta f'_c$$

On the other hand, if the concrete strut crushed before yielding of web reinforcement, the stresses of vertical steel bars shall be the minimum of (80% of their yielding stress or 500 MPa), then stresses on horizontal steel bars shall be calculated by satisfying equilibrium. This is in case if wall aspect ratio is 1.0 or less, otherwise, the horizontal steel bars shall be estimated to be the minimum of (80% of their yielding stress or 500 MPa), then apply equilibrium equations to calculate stresses on vertical steel bars. This is to emphasis the high contribution of horizontal reinforcement compared to vertical reinforcement for walls of aspect ratio more than 1.0.

The model more accurately predicted the shear strength of the tested walls, the average value of actual wall strength to the predicted strength was 1.36 with COV of 0.2, the study showed that horizontal reinforcement become more effective than vertical reinforcement for walls of aspect ratio higher than 1.0, also walls with boundary elements exhibits higher shear strength than their counterparts due to the dowel action of longitudinal steel bars at boundaries.

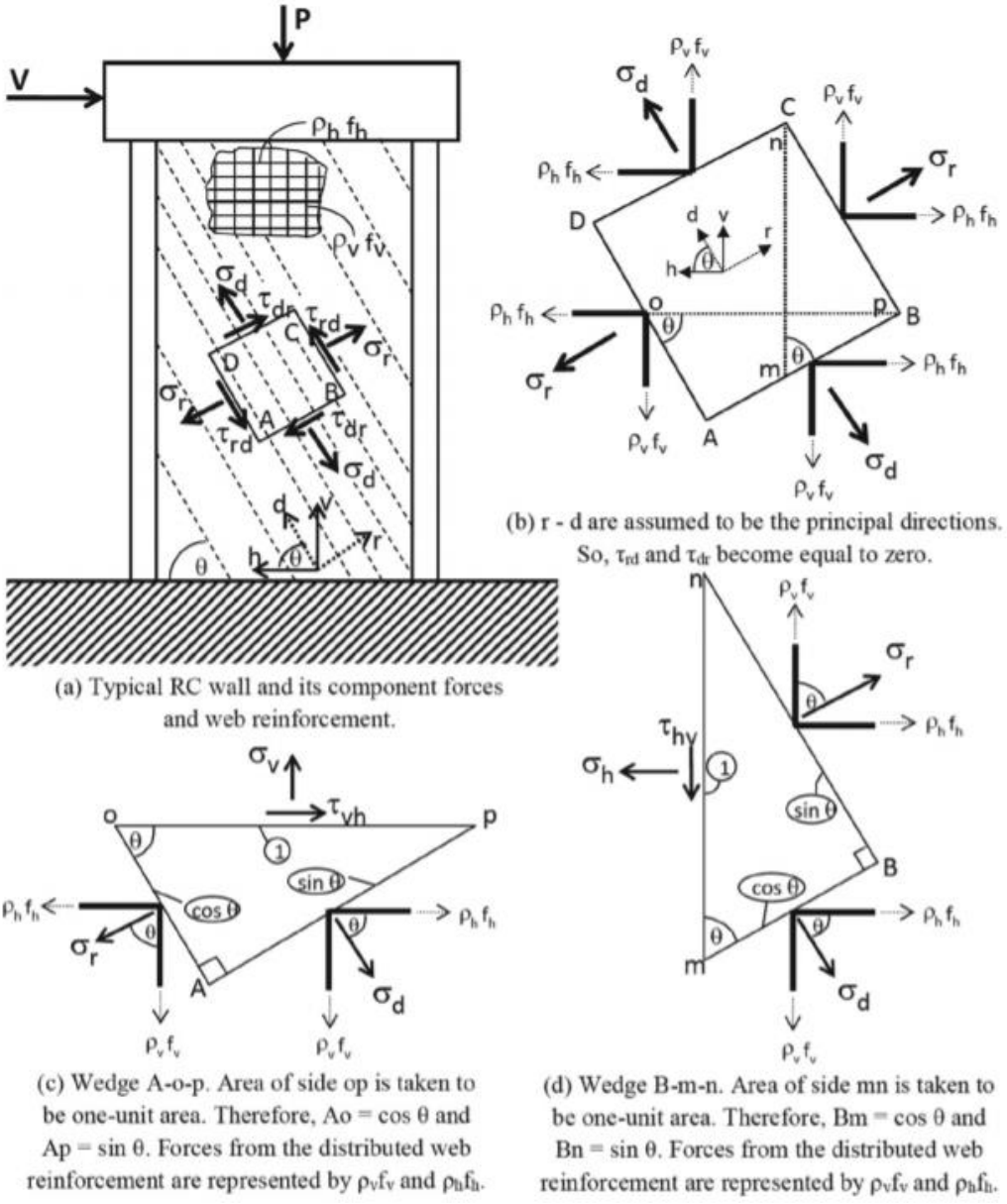

(a) Typical RC wall and its component forces and web reinforcement.

(b) r - d are assumed to be the principal directions. So, τ_{rd} and τ_{dr} become equal to zero.

(c) Wedge A-o-p. Area of side op is taken to be one-unit area. Therefore, Ao = cos θ and Ap = sin θ. Forces from the distributed web reinforcement are represented by $\rho_v f_v$ and $\rho_h f_h$.

(d) Wedge B-m-n. Area of side mn is taken to be one-unit area. Therefore, Bm = cos θ and Bn = sin θ. Forces from the distributed web reinforcement are represented by $\rho_v f_v$ and $\rho_h f_h$.

Figure 2-19 Stresses components of a reinforced concrete wall (Chandra et al 2018)

Wael Kassem and Ahmed Elsheikh (2010) used an algorithm consisting of 14-equations to estimate shear strength of reinforced concrete walls, the equations satisfy the Equilibrium, Compatibility and constitutive laws of materials, the solution based on the softened truss model (

Figure 2-20) which assumes stresses are equally distributed in the wall. Unlike Gupta (1996) who used a fixed strut angle based on wall aspect ratio, Kasseem and Elsheikh's model suggested the strut angle controlled by concrete strength, longitudinal and horizontal reinforcement volumes, yielding steel stress, wall aspect ratio and axial force. The model which is based on variable cracking angle more accurately predict shear strength compared to the model adopted by Gupta and Rangan (1998) where the cracking angle is fixed and only related to the wall aspect ratio.

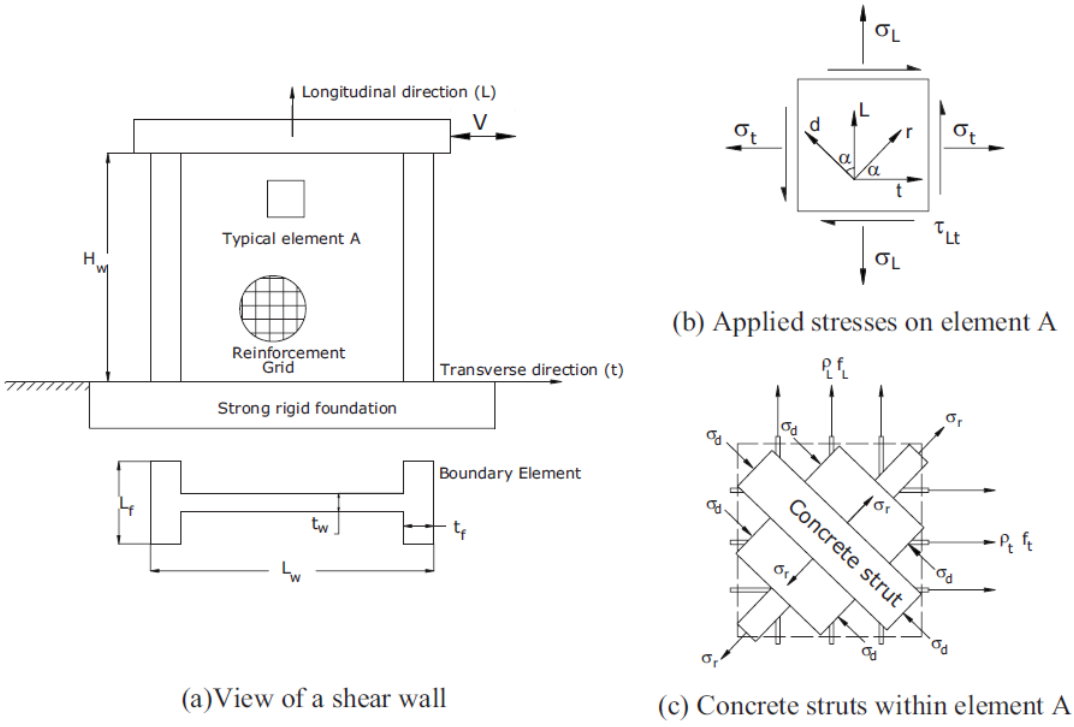

Figure 2-20 Softened truss model (Wael Kassem and Ahmed Elsheikh 2010)

Weng et al (2017) established a trilinear shear strength-lateral wall displacement curve based on the strut-and-tie model proposed by Hwang and Lee (2002), the curve is similar in concept to the curve adopted by Li and Hwang (2017) for short columns controlled by shear failure. The cracking point is estimated using initial cracking strength formula adopted by ACI 314-14 (2014), while the strength point is calculated by the procedure developed for shear strength in Hwang and Lee's model (2002). The cracking displacement (Δ_{cr}) is evaluated by summation of flexural, shear and slip deformation at onset of cracking point. The flexural and slip deformation quantified by Sezen and Moehle (2006) while the shear deformation calculated by the formula of Benjamin and Williams (1957). The model predicts shear strength, pre- and post- cracking stiffness, and the collapse displacement. The model fairly estimates strength and displacement relationship compared to ASCE/SEI 41-13. The predicted strength by ASCE/SEI 41-13 is underestimated especially for walls with aspect ratio less than 1.5, the collapse displacement decreases for walls with low aspect ratio or walls lack horizontal reinforcements.

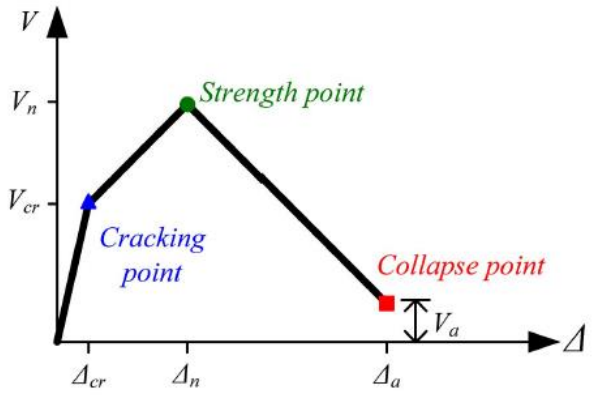

Figure 2-21 Trilinear shear strength-displacement curve (Weng et al 2017)

2.4. Empirical shear strength equations

Barda et al. (1977) tested eight squat walls with aspect ratio ranges from 0.25 to 1.0, the purpose of this study was to investigate effect of vertical, horizontal, boundary reinforcement ratios on wall shear strength. Results indicates the inefficient contribution of horizontal reinforcement on behavior of walls with aspect ratio 0.5 or less, rather it was efficient for 1.0-aspect-ratio walls. The longitudinal reinforcement was observed to significantly increase wall shear strength, this finding was difficult to predict by the ACI 1971 code equation, which constantly underestimate strength of walls with aspect ratio less than 1.0. Based on the results of this study, Barda et al. (1977) suggested the following equation, which gives more contribution credit for vertical reinforcement:

$$v_u = 8.3\sqrt{f_c'} - 3.4\sqrt{f_c'}\left(\frac{h_w}{l_w} - \frac{1}{2}\right) + \rho_n f_y$$

Where v_u is the wall shear strength (psi), ρ_n is the vertical reinforcement ratio, f'_c is the concrete compressive strength (psi) and h_w/l_w is the wall height to length ratio.

Wood (1990) investigated the results of tested143 squat walls in literature, based on the shear-friction model, he proposed the following empirical equation to estimate wall shear strength:

$$6\sqrt{f_c'}A_{cv} \le V_n = \frac{A_{vf}\, f_y}{4} \le 10\sqrt{f_c'}A_{cv}$$

Where V_n is the wall shear strength (Ib), f'_c is the concrete compressive strength (psi), A_{cv} is the wall web area (in.^{2}).

Similar to ACI 318-08 Chapter 21 equation, ACI 318-19 Chapter 18 section 18.10.4.3 requires vertical reinforcement at least equals to the horizontal reinforcement ratio for squat walls, the minimum reinforcement ratio for vertical and horizontal reinforcement is 0.25%. Wall shear strength (section 18.10.4.1) shall be estimated by:

$$V_n = A_{cv}\left(\alpha_c \lambda \sqrt{f_c'} + \rho_t f_y\right) \le 10\sqrt{f_c'}$$

$$\alpha_c = 3 \text{ for } h_w / l_w \le 1.5$$

$$\alpha_c = 2 \text{ for } h_w / l_w \ge 2.0$$

$$\alpha_c \text{ varies linearly between } 3.0 \text{ and } 2.0 \text{ for } 1.5 \le h_w / l_w \le 2.0$$

Where V_n is the wall shear strength (lb), ρ_t is the horizontal reinforcement ratio, f'_c is the concrete compressive strength (psi), A_{cv} is the wall web area (in.^{2}), h_w/l_w is the wall height to length ratio and λ is a reduction factor to reflect the reduced lightweight concrete strength.

The ACI 318-19 Chapter 18 equation only considers concrete compressive strength and the horizontal reinforcement to estimate wall shear strength, no credits are given for vertical reinforcement also wall aspect ratio is not significantly affect on shear strength.

Gulec et al. (2008) used 120 rectangular walls of the collected wall-database to evaluate the accuracy of previously mentioned equations; ACI 318-08 Chapter 21, ACI 318-08 Chapter 11, Barda et al. (1977), ASCE-43-05 and Wood (1990); the majority of walls had aspect ratio 0.25 to 1.0, web reinforcement ratio from 0.25% to 0.75%, and concrete compressive strength 2 to 5 ksi. The study showed that all predicting equations failed to accurately estimate wall shear strength, majority of walls were overestimated while lightly reinforced walls were underestimated. Wood's equation was found to be the most accurately predicting shear strength of rectangular walls. None of tested rectangular walls reached the limiting shear stress 20√fcm (psi) imposed by ASCE-43-05.

In addition, Gulec and Whittaker (2009) evaluated the test results of 150 rectangular squat walls reported in literature that failed in shear mode. The results show that shear strength predicted by Wood (1990) have the most accurate estimation

compared to ACI, Barda, and ASCE 43-05 equations (Figure 2-22), while ASCE 43-05 found to be the best to predict shear strength of walls with boundaries.

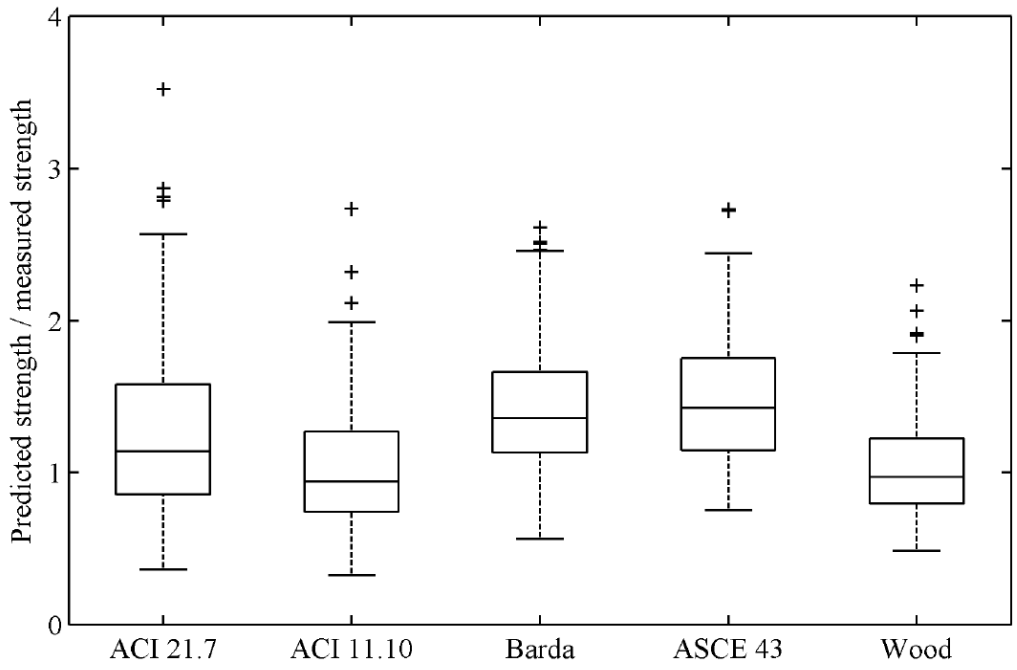

Figure 2-22 Predicted to measured shear strength ratio for rectangular squat walls (Gulec and Whittaker 2009)

Gulec et al. (2009) evaluated 247 squat walls having flanged or barbell. Most walls have web thickness from 2 to 4 inches, concrete compressive strength from 2 to 6 ksi, vertical and horizontal reinforcement ratio from 0 to 1%. The study revealed that ASCE 43-05 equation has the best average predicted to the experimental shear strength ratio. However, it considerably overestimates and underestimates several tested walls. On the other hand, the other equations by ACI 318-08, Wood (1990), and Barda (1977) are incapable to precisely estimate the wall shear strength of flange and barbell sections.

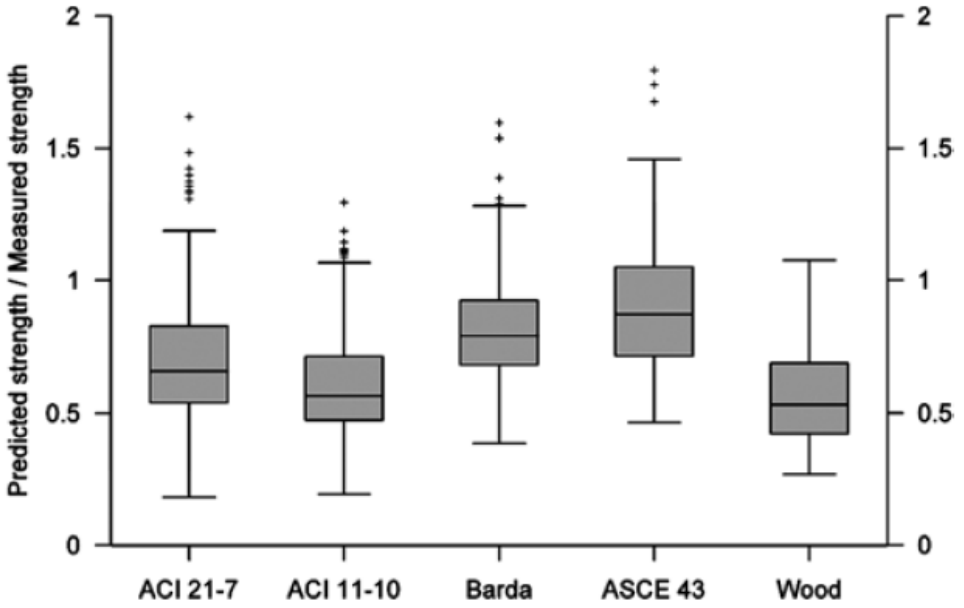

Figure 2-23 Predicted to measured shear strength ratio for rectangular squat walls (Gulec et al. 2009)

However, Luna et al. (2015) tested NSF-funded twelve large scale squat shear walls with length of 10 ft and thickness 8 inches, the wall height varies based on the selected aspect ratios of 0.33, 0.54 and 0.94. They tested the specimens at NEES facility (Network for Earthquake Engineering Simulation) at the University at Buffalo. The results highlighted that all current equations (ACI 318-08 Chapter 21, ACI 318-08 Chapter 11, Barda et al. 1977, Wood 1990, and Gulec 2011) showed significant scatter predicted shear strength (Figure 2-24), this indicates the need to modify current equations to estimate squat wall shear strength.

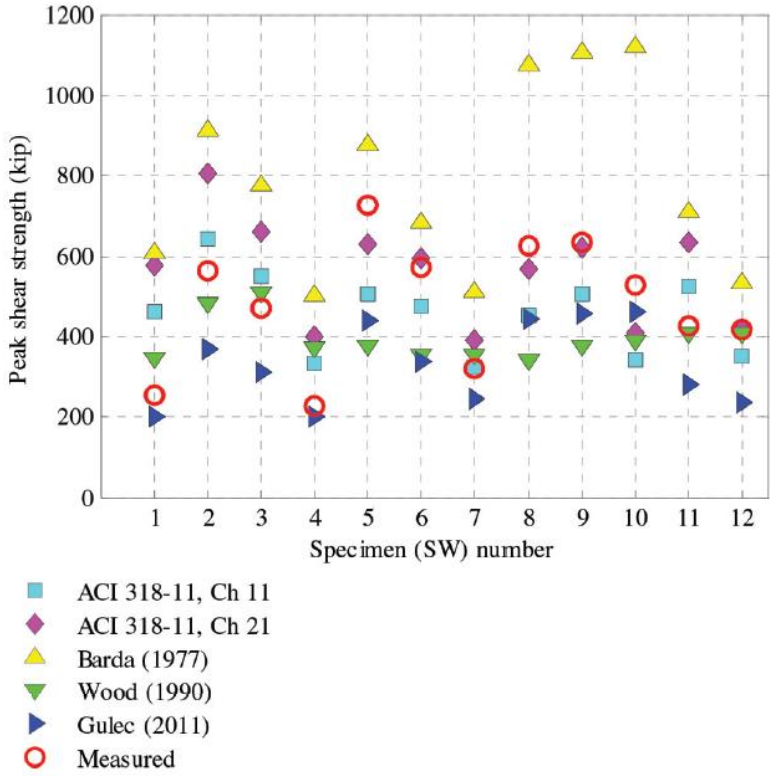

Figure 2-24 Predicted squat shear strength by various equations (Luna et al. 2015)

Ramos et al (2012) statistically evaluated the database of squat walls collected by Gulec and Whittaker (2009), the considered walls were 329 shear-critical walls that failed before reaching their nominal flexural strength, the walls have different cross sections – rectangular, flanged or barbell. The assessment criterion is to compare experimental shear strength to the predicted shear strength by the Mexican Code, Canadian Code, New Zealand Code and the Eurocode. The results showed that all four codes considerably inconsistent to predict the shear strength, especially walls with boundary elements. The Mexican and New Zealand codes are the best to estimate shear strength of rectangular walls and walls having boundary elements which was found to

have higher shear strength compared to walls do not have boundary elements. The Eurocode tends to underestimate shear strength of all shear-critical walls. For the same walls database, Gulec and Whittaker (2009) assessed the shear strength predicting equations of ACI 318-08 Chapter 21, ACI 318-08 Chapter 11, Barda et al. (1977), ASCE-43-05 and Wood (1990). In addition to the Mexican and New Zealand codes, the ACI 318-08 Chapter 11 are the best to predict strength of shear-critical walls, where the average predicted-to-experimental ratio is almost 1.0 with coefficient of variation about 0.43. The ASCE 43-05 is the best to estimate shear strength of walls with boundary elements.

Gulec et al. (2011) investigated the squat walls database to build a new predicting shear strength model for squat walls with aspect ratio 1.0 or less,

$$V_m = \frac{\beta_1 (f_c')^{\beta_2} A_{eff} + \beta_3 F_{vw} + \beta_4 F_{hw} + \beta_5 F_{vbe} + \beta_6 P}{(h_w / l_w)^{\beta_7}}$$

Where, β_1 to β_7 are the model unknowns; f'_c is the concrete compressive strength (psi); A_{eff} (in.^{2}) is the effective wall area; F_{vw}, F_{hw}, and F_{vbe} (lb) are the forces developed due to longitudinal, horizontal and boundary reinforcements, respectively; The forces are calculated by multiplying the reinforcement area by yielding steel stress; h_w (in.) is wall height; l_w (in.) is wall length; P (lb) is the applied external axial force.

While validating the model unknowns based on the walls database, the horizontal steel reinforcement found to have minor contribution on wall shear strength. Therefore, the force developed due to horizontal reinforcement, F_{hw}, was omitted from the model. The model unknowns are affected by the walls section; rectangular (V_{rec}) or flanged (V_{BE}), the equations are given by:

$$V_{rec} = \frac{1.5\sqrt{f_c'} A_w + 0.25 F_{vw} + 0.2 F_{vbe} + 0.4P}{\sqrt{h_w / l_w}} \le 10\sqrt{f_c'} A_w$$

$$V_{BE} = \frac{(0.04 f_c')A_{eff} + 0.4F_{vw} + 0.15F_{vbe} + 0.35P}{\sqrt{h_w / l_w}} \leq 15\sqrt{f_c'}A_t$$

The coefficient of variance (COV) are 0.13 and 0.11 for rectangular flanged walls, respectively, the average predicted-to-experimental shear strength ratio is almost 1.0 which gives better estimation accuracy compared to the other investigated equations in this study.

Teng and Chandra (2016) tested several 1.0 and 2.0-aspect-ratio walls with high strength concrete 100 MPa (14.5 ksi). Similar to normal concrete walls, horizontal reinforcement found to be more efficient for high wall aspect ratio, low aspect ratio walls and walls having flanges have higher shear strength than estimated values by the available building codes including the ACI 318-19 Chapter 18 equation.

Cheng et al. (2016) tested five walls, in particular, high strength steel bars were used in two specimens and the normal strength steel bars were used on the remaining walls. Compared to the equations predicting shear strength available in literature, the ACI 318-14 found to be adequately predict the shear strength while the equations of Wood (1990) and Gulec and Whittaker (2011) consistently underestimate shear strength with an average experimental-to-predict ratios of 1.92 and 1.54, respectively.

However, Baek et al. (2017a) observed that the ACI 318-14 Chapter 18 equation underestimates the shear strength of four critical-shear walls with reinforced by normal (60 ksi) or high (80 ksi) steel strength bars, where the tested-to-estimated strength ratio varies up to 1.46. The results also emphasized that no difference in wall behavior (mode failure, attained shear strength) for walls either reinforced by high or normal strength steel bars.

In other study, Baek et al. (2017) tested several walls with aspect ratio 0.5 or 1.0, high (80 ksi) or normal (60 ksi) steel strength bars were also considered. The results

showed that the ACI 318-14 underestimates the wall strength by tested-to-predicted shear strength ratio up to 1.9 for normal steel strength reinforced walls.

Moehle J. (2015) suggested an expression to estimate shear strength of squat walls, the model assumes shear forces to be transferred throughout the web diagonal struts like segment ab (Figure 2-25a), the developed stresses in diagonal struts shall be equilibrated by vertical web reinforcement only (Figure 2-25b), based on the model, horizontal reinforcement are needed to reduce crack opening and satisfy force equilibrium for segment cde (Figure 2-25c). The shear strength expression is given by:

$$V_n = \left(N_u + \rho_l f_y A_{cv} \right) \frac{1}{\tan\theta}$$

Where, ρ_l is the longitudinal steel ratio, N_u is the axial force, f_y is the yield steel stress, and V_n is the wall shear strength.

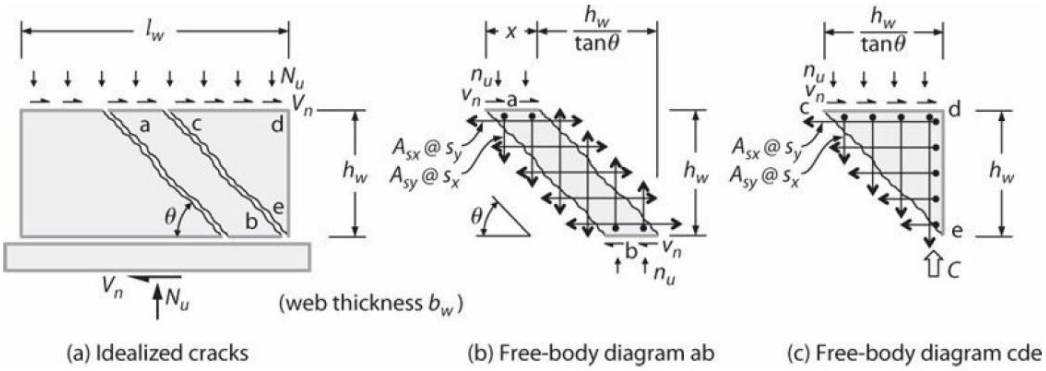

Figure 2-25 Squat shear walls force distribution (Moehle J. 2015)

Luna et al. (2019) modified Moehle's model by adding the contribution of aggregate interlock (F_s), assuming strut inclination angle to be 40 degrees, and introducing shear-friction factor of 0.5 that used at the base of segment A (Figure 2-26) to calculate the horizontal resisting-shear component. The shear strength of rectangular

squat walls without boundary elements are estimated by summation of all three segments shear contribution that illustrated in (Figure 2-27 and Figure 2-28), the final shear strength equation is given by:

$$V_n = 1.2\left(\rho_l A_{cv} f_{\bar{y}} + pl_w\right)\left(1 - 0.7\frac{h_w}{l_w} - \frac{c}{l_w}\right) + 0.25\rho_t \frac{h_w}{l_w} A_{cv} f_y + 0.5pc \le 10\sqrt{f_c'} A_{cv}$$

The shear strength of rectangular squat walls without boundary elements are estimated by:

$$V_{n,be} = 1.2\left(\rho_l A_{cv} f_y + p\right)\left(1 - 0.7\frac{h_w}{l_w} - 2\frac{l_{be}}{l_w}\right) + 1.75(pl_{be} + P) + 1.2\rho_{be} A_{s,be} f_{\bar{y}} + 0.25\rho_t A_{cv} \frac{h_w}{l_w} f_y \le 10\sqrt{f_c'} A_{cv}$$

Based on the shear force mechanism in this study, the authors modified the shear strength equation proposed by Gulec and Whittaker (2011), the updated shear strength for rectangular squat walls without boundaries is given by:

$$V_n = \frac{1.1\sqrt{f_c'} A_{eff} + 0.25F_{vw} + 0.2P}{\left(h_w / l_w\right)^{0.8}}$$

Where, f'_c is the concrete compressive strength (psi); A_{eff} (in.^{2}) is the effective wall area; A_{cv} (in.^{2}) is the gross section area; ρ_l, ρ_t, and ρ_{be} are vertical, horizontal, and boundary element reinforcement ratios, respectively; F_{vw} (lb) is the force developed due to longitudinal reinforcement, the force is calculated by multiplying the reinforcement area by yielding steel stress; h_w (in.) is wall height; l_w (in.) is wall length; P (lb) is the applied external axial force.

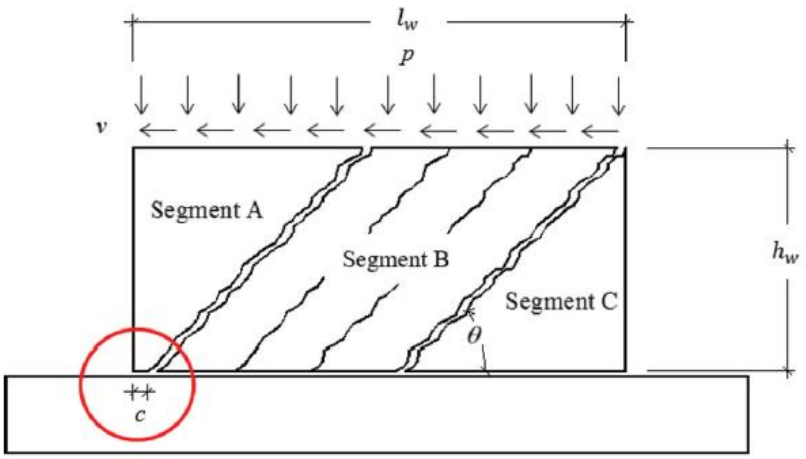

Figure 2-26 Shear force transfer for a wall without boundary elements (Luna et al. 2019)

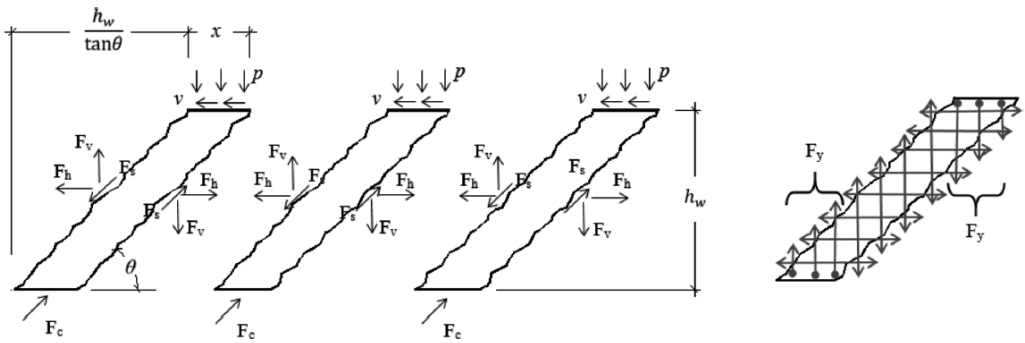

Figure 2-27 Force free-body diagram in segment B (Luna et al. 2019)

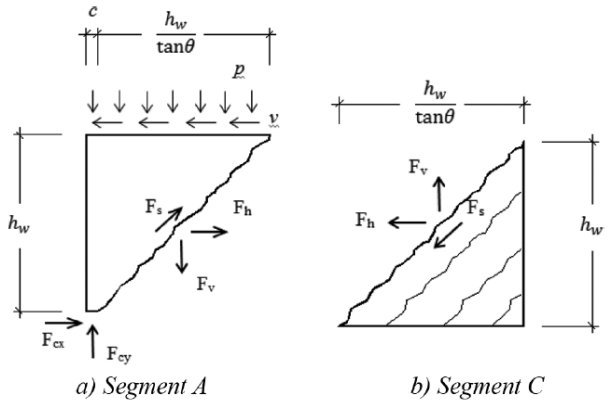

Figure 2-28 Force free-body diagram in segment A and C (Luna et al. 2019)

2.5. High strength rectangular squat shear walls

Squat walls with shear strength are needed in high seismic zones. Current ACI 314-19 limits the design strength of shear walls to be 10√fcm (psi) due to insufficient ductile behavior of high strength walls and high risks of sudden failure. Gulec and Whittaker (2008) collected results of 150 rectangular walls (Figure 2-29) but did not report any rectangular squat walls with shear strength more than 15√fcm (psi); fcm is the concrete compressive strength (psi). While they reported several barbell and flanged squat walls attained shear strength between 20 to 25√fcm (psi).

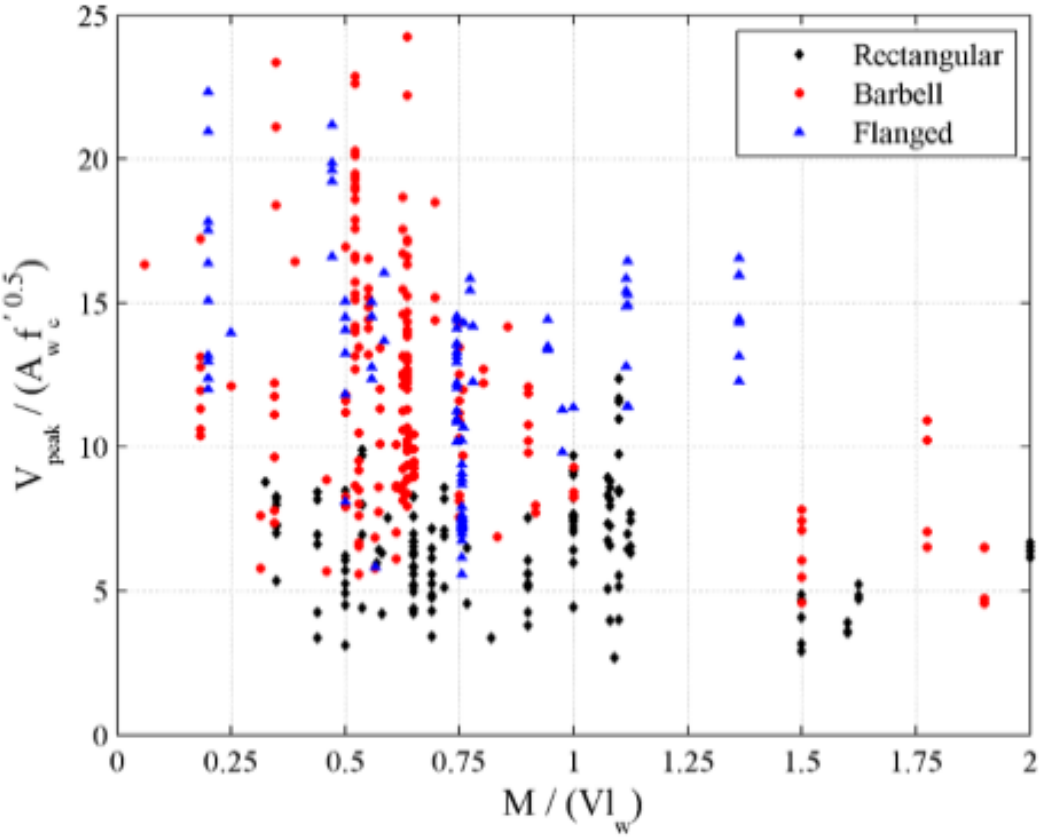

Figure 2-29 Summary of tested rectangular, barbell, and flanged squat walls (Gulec and Whittaker 2009)

2.6. Philosophy of concrete confinement

2.6.1. Plain concrete behavior under biaxial stress state

Figure 2-30 shows the general applied three principal stresses (f_1, f_2 and f_3) on a concrete specimen in x, y and z directions. Biaxial stress state can be defined when f_1 and f_2 have values, while $f_3 = 0$. Kupfer et al. tested concrete specimens in which stresses f_1 and f_2 were increased from zero until failure. Figure 2-30 illustrates the strength envelop for various ratios of f_1/f_2. Point (a) represents the ultimate uniaxial compressive stress in axis 1. Point (b) represents the uniaxial tensile failure stress in axis 1. Point (c) shows how a small tension in direction 2 causes significant reduction in the compressive stress for axis 1. Point (d) illustrates around 15% increase in ultimate compressive stresses for both directions 1 and 2 when $f_1 = f_2$, on other hand point (e) shows 25% increase when $f_1 = 2f_2$. It has been observed that the failure at points (d and e) is due to tensile splitting failure in direction 3. Therefore, in order to achieve higher concrete strength, the third direction must be restrained.

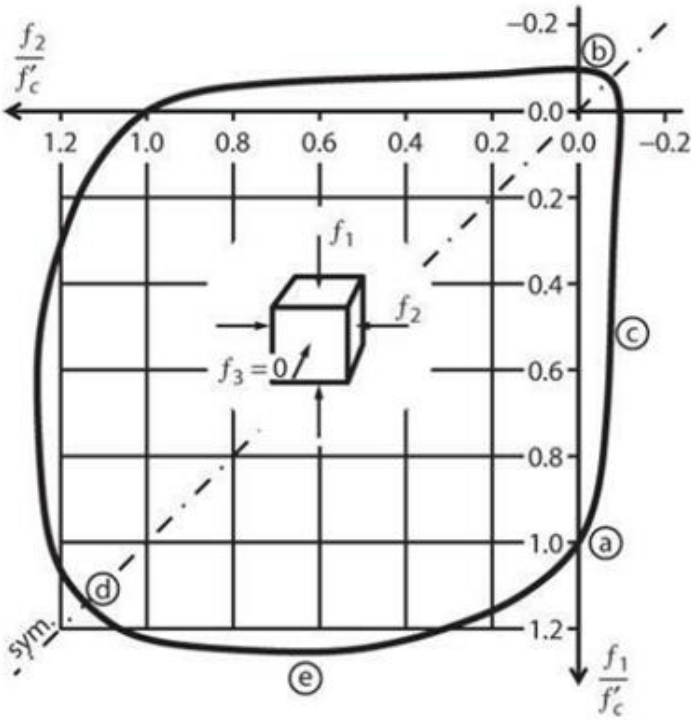

Figure 2-30 Concrete strength envelope under biaxial loading (Moehle J., 2015)

2.6.2. Plain concrete behavior under triaxial stress state

Plain concrete subjected to biaxial stresses shows slightly small strength enhancement as discussed in the previous section. However, many researchers observed a significant increase in concrete strength if it is confined in the third direction.

Figure 2-31 shows the stress – strain curves in direction 1 for concrete specimens having different amount of confining stresses in directions 2 and 3. The uniaxial concrete compressive strength is constant ($f_c' = 3660$ psi) for all curves.

Figure 2-31 clearly shows a small enhancement in both strength and maximum strain (ductility) if $f_2 = f_3 = 0.15 f_c'$.

On other hand, the ultimate concrete strength in direction 1 reaches four times the original strength and the area under stress-strain curve is very large; which means it has high capability to dissipate strain energy.

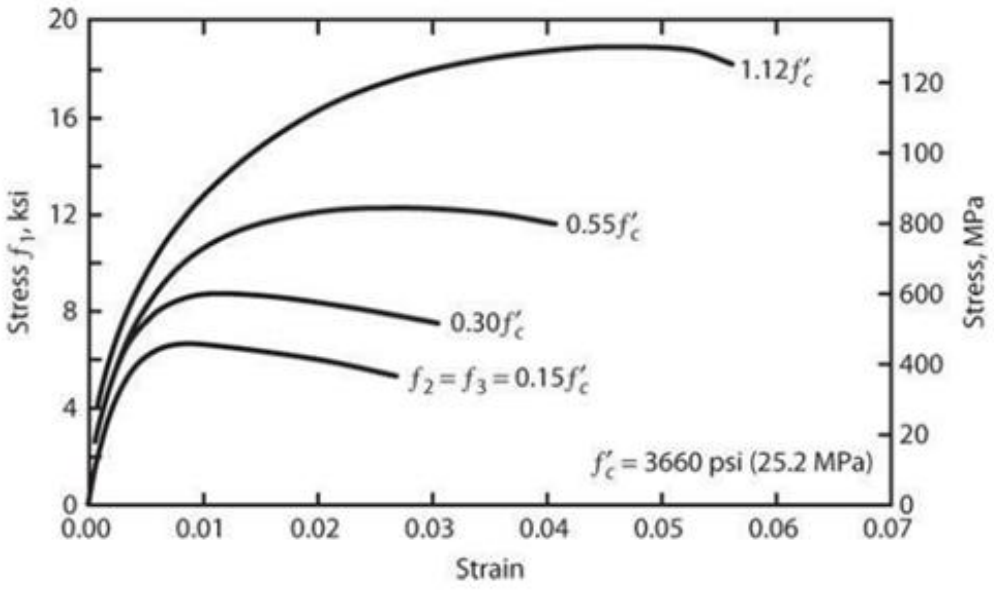

Figure 2-31 Stress-strain relationships for normal weight confined concrete by hydrostatic pressure and under axial compression force state (Moehle J., 2015)

Richart et al. (1928) tested large number of cylinder specimens; they proposed the following equation to predict the confined concrete strength:

$$f'_{cc} = f'_{co} + k_1 \, f_l \qquad \text{(Eq. 2-1)}$$

Where:

f'_{cc}: confined concrete strength.

f'_{co}: unconfied concrete strength.

k_1: coefficient depends on f_l.

$f_l = f_2 = f_3$: uniform confining pressure.

According to their results, the coefficient k_1 is given by:

$$k_1 = 6.7(f_l)^{-0.17} \qquad \text{(Eq. 2-2)}$$

They found that a constant value of $k_1 = 4.1$ gives a good prediction to their experimental results. Their model has been adopted in ACI building code (1989).

The uniform confining pressure depends on the column section and the spacing of hoops. Different column sections produce several reinforcement arrangements which have an effect on the uniformity of confining pressure. Lower spacing of hoops, makes the confining pressure more uniform.

For spiral columns, dilation due to axial forces results in spiral stress f_s and confining stresses f_2 and f_3; which can be found by satisfying equilibrium in Fig (2-26c), as following:

Compression in confined core = Tension in spiral hoops

$$f_2 Ds = 2 f_s A_{sp}$$

$$f_2 = f_3 = \frac{2 f_s A_{sp}}{Ds} = \frac{\rho_s f_s}{2} \qquad \text{(Eq. 2-3)}$$

Where:

D: is column diameter.

s : is hoops spacing.

ρ_s : is the volume of spiral reinforcement to the total volume of core confined by the spiral, calculated as following:

$$\rho_s = \frac{\pi D A_{sp}}{\frac{\pi}{4} D^2 s}$$

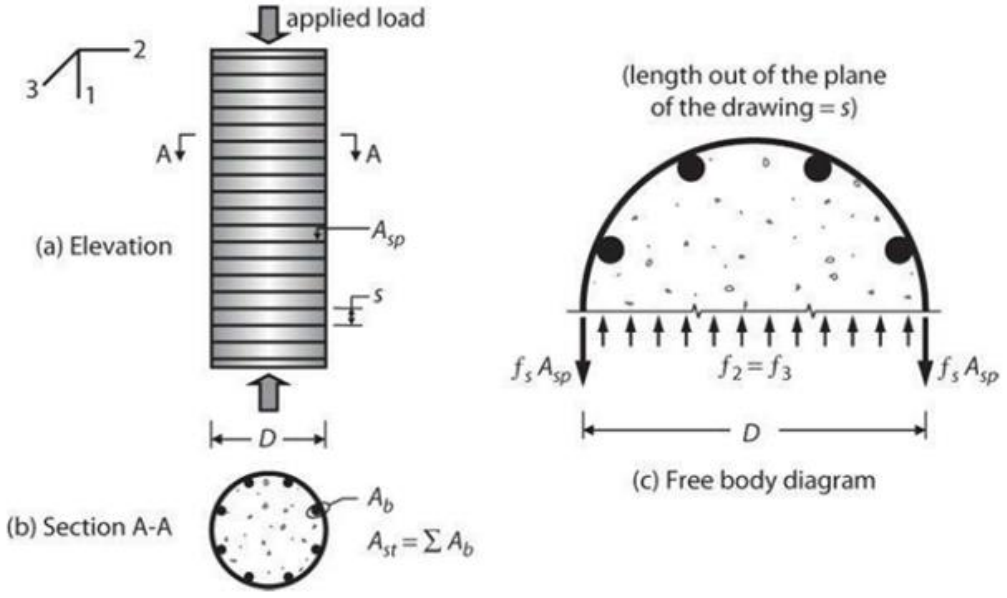

Figure 2-32 Concrete column confined by circular hoop: (a) elevation; (b) section A-A (c) free-body diagram of a slice at column core with thickness s (Moehle J., 2015)

2.6.3. Arching action and confinement effectiveness:

Providing small spacing between hoops, results in a uniform confining pressure in the column core. On the other hand, larger spacing causes poor confining pressure.

Figure 2-33a shows confinement action in circular columns, each circular hoop provides concentrated ring of confinement stresses acting radially inward at the locations of intersection between the hoop and longitudinal bars, making the column core confined at hoop level. The part of column core between two hoops, have free surface that is not confined by hoops, as shown in

Figure 2-33b).

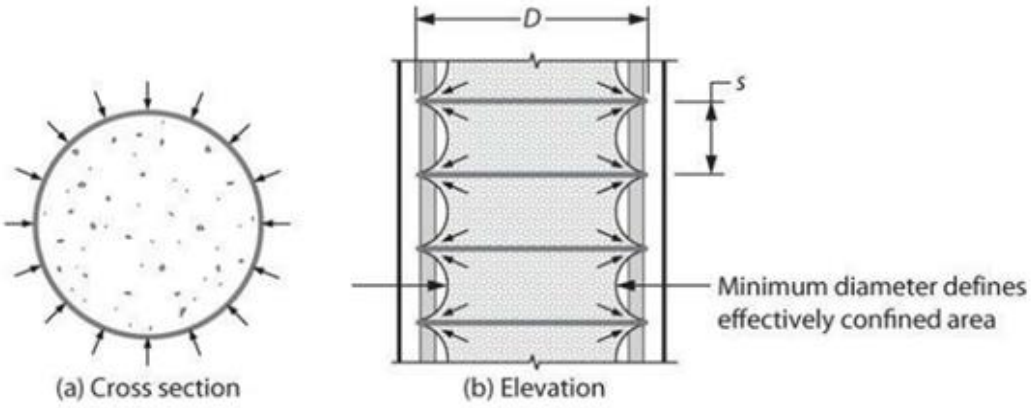

Figure 2-33 Concrete confinement of circular column: (a) radial pressures in circular hoop; (b) arch action concept and the effective concrete core confinement (Moehle J., 2015)

Figure 2-34 shows the three – dimensional arching in confined rectangular concrete columns. When column is subjected to axial forces, the core concrete dilates

outward horizontally. Concrete located near hoops, are well confined because hoops restrain the horizontal dilation of concrete core, as shown in Figure 2-34. However, concrete parts located between hoops, are not well confined since there is no hoops to restrain concrete dilation, so, unconfined concrete parts try to spall away of concrete core. This concept is called arching action, in which larger hoop spacing causes larger arch curvature resulting in reduction of confinement effectiveness and vice versa, as shown in

Figure 2-33b and Figure 2-34.

Arching action can be related by one parameter, s/D. a small value of s/D indicates higher confined concrete area. Confinement effectiveness factor, k_e, can be estimated by the following:

$$k_e = 1 - \frac{s}{D}$$

Therefore, the confining stress should be modified to consider the arching action effect, as following:

$$f_{2e} = k_e f_2 = k_e \frac{\rho_s f_s}{2} \qquad \text{(Eq. 2-4)}$$

Equation (2-1) must be updated to consider the effective confining pressure:

$$f'_{cc} = f'_{co} + 4.1\ f_l$$
$$f'_{cc} = f'_{co} + 4.1\left(k_e \frac{\rho_s f_s}{2}\right)$$
$$f'_{cc} = f'_{co} + 2.05 k_e \rho_s f_s \qquad \text{(Eq. 2-5)}$$

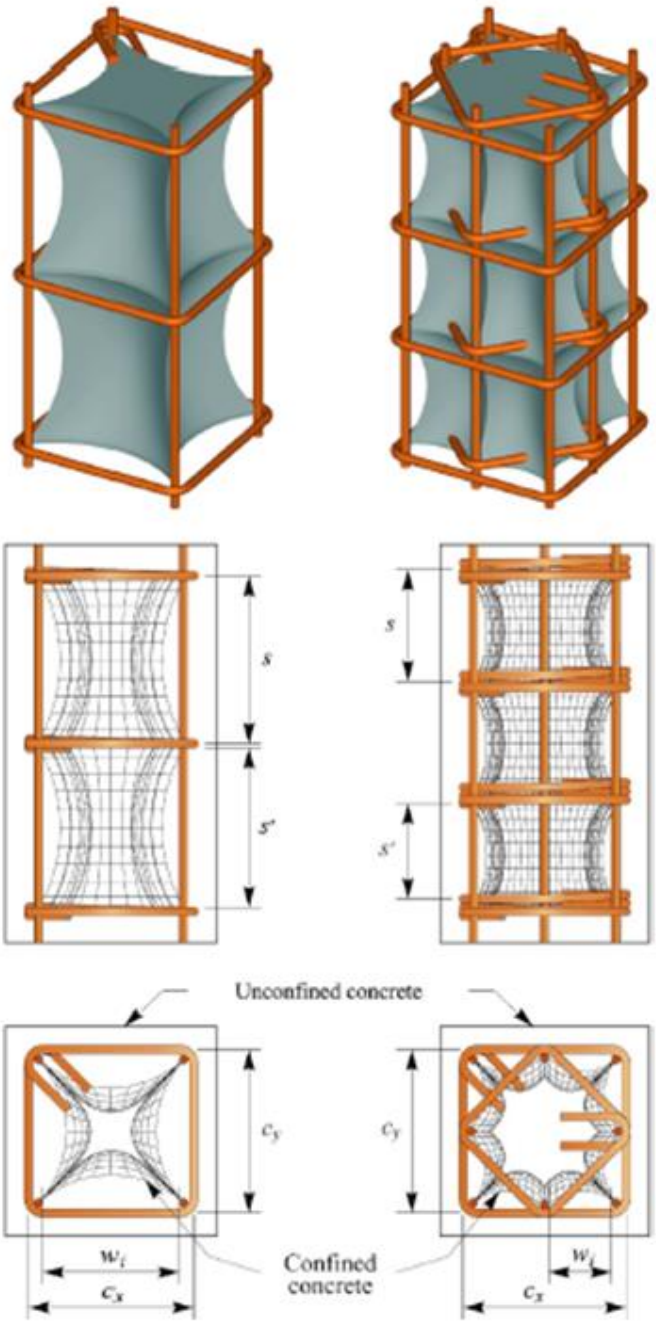

Figure 2-34 Arching effect (Paultre and legeron, 2008)

2.7. Normal concrete confinement models

2.7.1. Saatcioglu and razavi (1992)

Saatcioglu and razavi (1992) analyzed large number of columns tests, including confined and poorly confined concrete columns. They proposed an analytical model to predict the stress-strain relationship for confined concrete. The model consists of two parts; ascending and descending parts. Ascending part is parabolic while the descending part is two linear lines. This model is applicable for circular, square and rectangular column section. The only parameter to distinguish the confined concrete among those sections is the effective lateral confining pressure, because the confining pressure for circular section behaves in a different way compared to square or rectangular sections.

a) Circular sections:

Equation (2-1) can be used to estimate the concrete confining pressure for circular section. Figure 2-35 demonstrates how to find the uniform confining pressure in circular section.

The ultimate confined concrete strength can be derived from the following equation:

$$f_{cc}^{'} = f_{co}^{'} + k_1 \, f_l \qquad \text{(Eq. 2-6)}$$

Where:

$$f_l = \frac{2A_s f_{yt}}{b_c s}$$

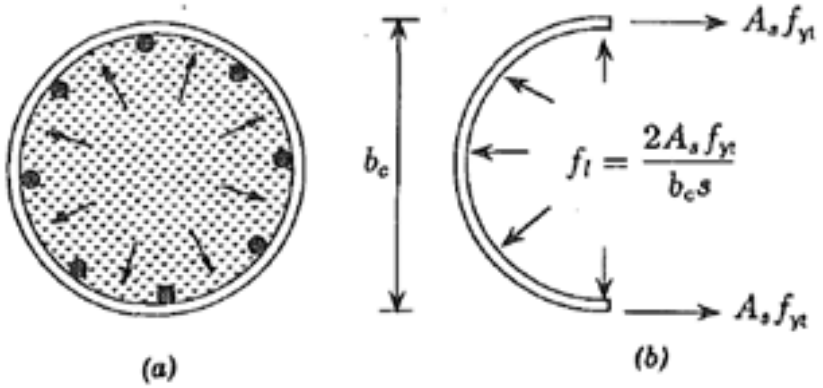

Figure 2-35 Lateral pressure in circular columns: (a) uniform distribution of pressure; and (b) computation of lateral pressure from hoop tension (Saatcioglu and razavi 1992)

b) Square columns:

Uniform confining pressure for circular columns can be easily found, but it is difficult to determine the confining pressure for square columns. However, an equivalent lateral pressure can be employed, instead.

Confining pressure in square columns comes from the restraining force developed in the hoop steel. The highest restraining force is developed at the corners because it is supported laterally by transverse legs, and the lowest restraining forces can be observed in locations between the corners. The restraining forces at corners depend on area and strength of steel hoops, but forces developed between corners depend on the flexural rigidity of the steel hoop.

Once the concrete dilates due to compressive forces, the hoops counteract this dilation by creating lateral pressure distribution, as shown in Figure 2-36a.

Reinforcement arrangement has an effect on the lateral pressure distribution. Increasing the number of ties between hoop corners, will make the lateral pressure distribution more uniform, because additional points of high lateral restraint are created, as shown in Figure 2-36b.

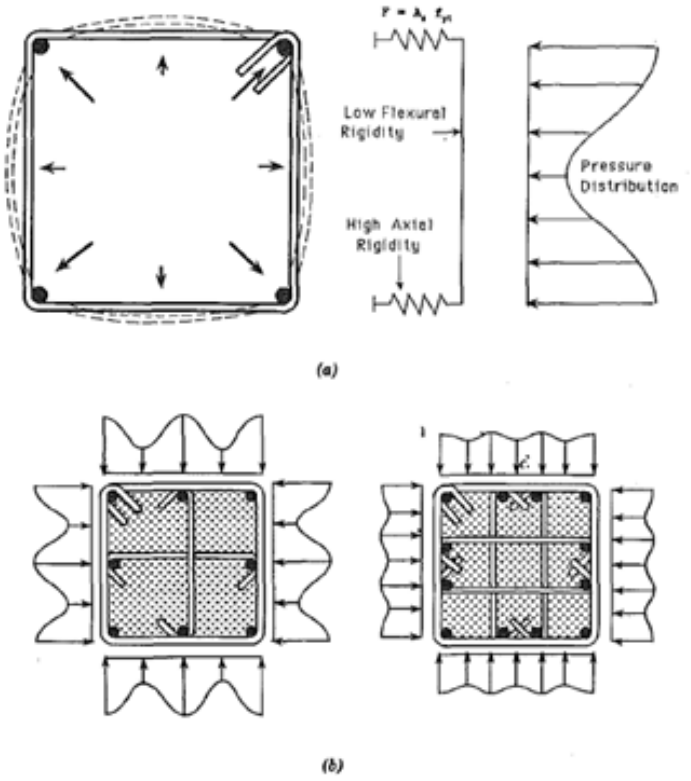

Figure 2-36 Lateral pressure in square columns: (a) lateral pressure distribution in square columns; and (b) pressure distributions resulting from different reinforcement arrangements (Saatcioglu and razavi 1992)

The ultimate confined concrete strength can be calculated by the following:

$$f_{cc}^{'} = f_{co}^{'} + k_1 \, f_{le} \qquad \text{(Eq. 2-7)}$$

Where

$$f_{le} = k_2 f_l$$

$$f_l = \frac{\sum A_s f_{yt} \sin\alpha}{s b_c}$$

$$k_1 = 6.7(f_{le})^{-0.17}$$

$$k_2 = 0.26\sqrt{\left(\frac{b_c}{s}\right)\left(\frac{b_c}{s_l}\right)\left(\frac{1}{f_l}\right)} \le 1.0$$

s_l is the spacing of laterally supported longitudinal reinforcement.

α is the angle between the transverse reinforcement and b_c.

c) Rectangular sections:

Since the rectangular section has different reinforcement distribution in two orthogonal directions, as shown in Figure 2-37, the lateral pressure distribution for each side shall be calculated following same procedure for square sections, and then the overall equivalent lateral pressure is calculated using the following equation:

$$f_{le} = \frac{f_{lex} b_{cx} + f_{ley} b_{cy}}{b_{cx} + b_{cy}} \qquad \text{(Eq. 2-8)}$$

Where f_{lex} and f_{ley} are effective lateral pressures acting perpendicular to core dimensions b_{cx} and b_{cy}, respectively.

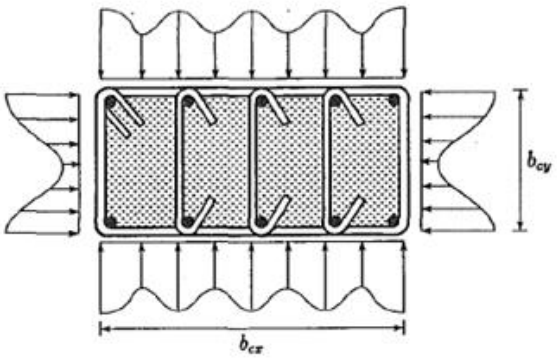

Figure 2-37 Lateral pressure distribution in rectangular columns (Saatcioglu and razavi 1992)

d) Confined concrete models:

Figure 2-38 shows a proposed model for confined concrete strength by Saatcioglu and razavi, it is described as following:

$$\varepsilon_1 = \varepsilon_{01}(1+5K)$$

$$\varepsilon_{85} = 260\rho\varepsilon_1 + \varepsilon_{085}$$

$$f_c = f'_{cc}\left[2\left(\frac{\varepsilon_c}{\varepsilon_1}\right) - \left(\frac{\varepsilon_c}{\varepsilon_1}\right)^2\right]^{1/(1+2K)} \leq f'_{cc}$$

Where:

$$K = \frac{k_1 f_{le}}{f'_{co}}$$

ε_{01} = strain corresponding to peak stress of unconfined concrete ($\varepsilon_{01} \approx 0.002$)

ε_{085} = strain at 85% of the maximum strength beyond the peak stress of unconfined concrete ($\varepsilon_{085} \approx 0.0038$)

$$\rho = \frac{\sum A_s}{s(b_{cx} + b_{cy})}$$

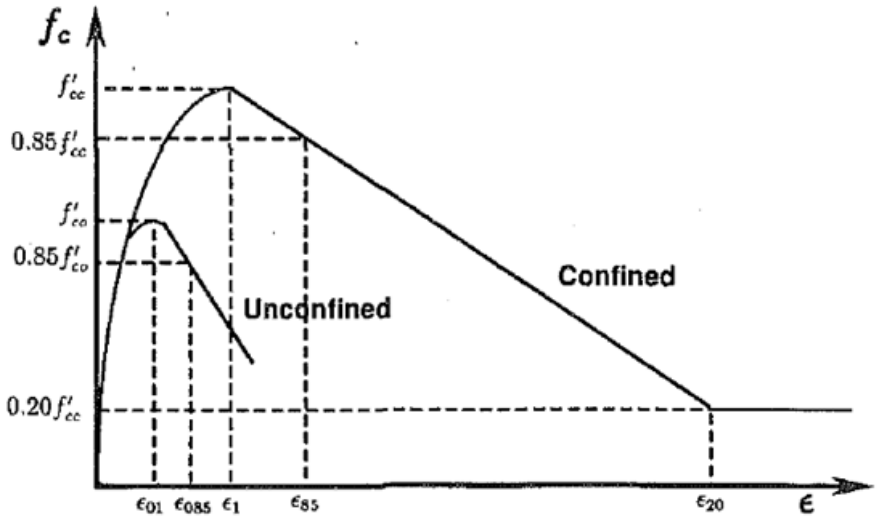

Figure 2-38 Proposed stress-strain relationship (Saatcioglu and razavi 1992)

2.7.2. Mander et al. model:

Mander et al. 1988 tested several large-scale reinforced concrete columns confined by spirals, circular and rectangular hoops. They observed a state of triaxle compression in the core concrete due to lateral confining pressure exerted by hoops, thus enhancing the compression strength and making a more ductile post-peak stress-strain behavior, as shown in Figure 2-39, this model consists of only one part that represents the stress-strain relationship for confined concrete columns.

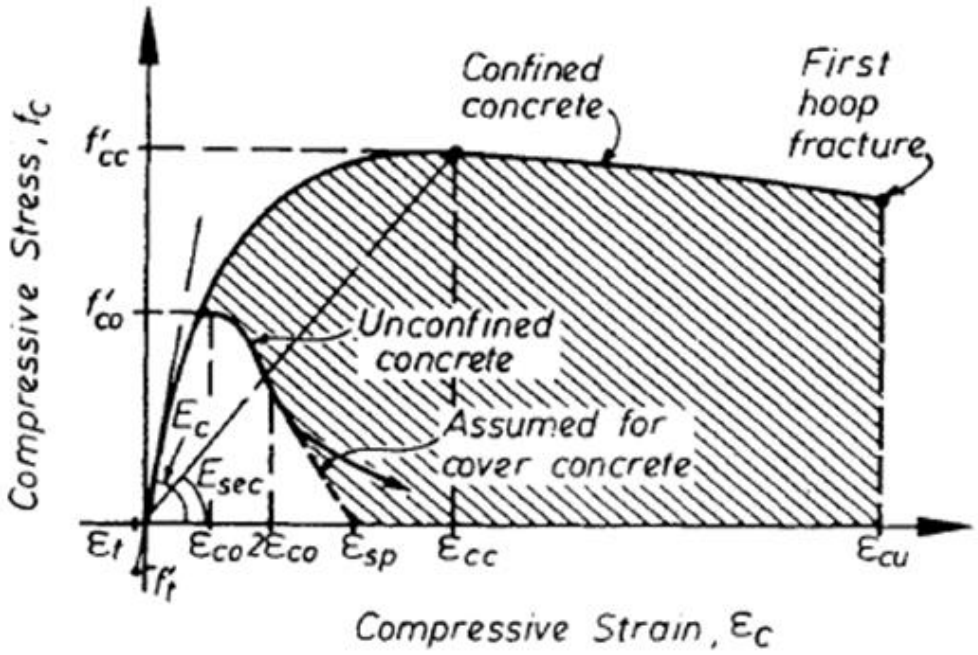

Figure 2-39 Concrete compressive stress-strain model proposed by Mander et al. 1988

The model that Mander et al. proposed is:

$$\frac{f'_{cc}}{f'_{co}} = 2.25\sqrt{1+7.94\frac{f'_l}{f'_{co}}} - 2.0\frac{f'_l}{f'_{co}} - 1.25 \qquad \text{(Eq. 2-9)}$$

Where:

f'_{cc} is the confined concrete compressive strength.

f'_{co} is the unconfined concrete compressive strength.

$f'_l = k_e f_l$

k_e is a confinement effectiveness coefficient, calculated as the ratio of the effective confined core area to concrete area within the hoop centerlines.

f_l confining stress calculated as shown in Fig (2-40).

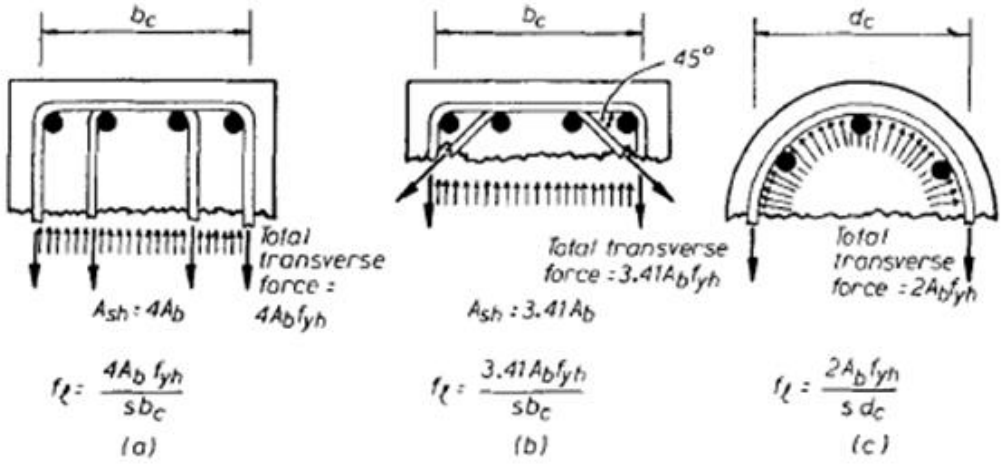

Figure 2-40 Confining stresses provided by different arrangements (Mander et al. 1988)

2.8. High-strength concrete confinement models

1. Behavior of confined high-strength concrete columns:

Razavi et al. (1994) investigated the strength and deformability of confined high-strength concrete columns based on available experimental data up to 250 columns. They drew up the following conclusions:

a) The main confinement parameters are volumetric ratio of longitudinal steel, hoop spacing, arrangement and strength of transverse reinforcement, concrete strength, and axial load.

b) High-strength concrete columns require significantly higher lateral confinement pressure compared to normal strength concrete columns.

c) Using high strength steel, increases confinement of high-strength concrete.

d) High applied axial loads reduce the deformability of high-strength concrete columns.

e) Strength and deformability of confined high-strength concrete can be enhanced by reducing hoop spacing and spacing of laterally supported longitudinal reinforcement.

2. Confinement models for high-strength concrete:

2.1 Razavi and Saatcioglu (1999)

A total of 46 near full –size columns were tested by Razavi and Saatcioglu (1994) with concrete strength between (60 to 124 MPa), also they collected results of 124 high strength concrete tests conducted by other researchers. Based on these data, Razavi and Saatcioglu (1999) proposed a confinement model for high-strength concrete, as

shown in Figure 2-41. Basically, this is a modified normal strength concrete which was proposed in (1992) by Razavi and Saatcioglu.

$$\varepsilon_1 = \varepsilon_{01}(1+5k_3K)$$

$$\varepsilon_{85} = 260k_3\rho_c\varepsilon_1\left[1+0.5k_2\left(k_4-1\right)\right]+\varepsilon_{085}$$

$$f_c = \frac{f_{cc}^{'}\left(\frac{\varepsilon_c}{\varepsilon_1}\right)r}{r-1+\left(\frac{\varepsilon_c}{\varepsilon_1}\right)^r}$$

Where:

$$k_3 = \frac{40}{f_{co}^{'}} \le 1.0$$

$$k_4 = \frac{f_{yt}}{500} \ge 1.0$$

$$K = \frac{k_1 f_{le}}{f_{co}^{'}}$$

$$\varepsilon_{01} = 0.0028 - 0.0008k_3$$

$$\varepsilon_{085} = \varepsilon_{01} + 0.0018(k_3)^2$$

$$\rho = \frac{\sum_{i=1}^{n}(A_{sx})_i + \sum_{j=1}^{m}(A_{sy})_j}{s(b_{cx}+b_{cy})}$$

$$r = \frac{E_c}{E_c - E_{\sec}}$$

$$E_{\sec} = \frac{f_{cc}^{'}}{\varepsilon_1}$$

$$E_c = 3320\sqrt{f_c^{'}} + 6900$$

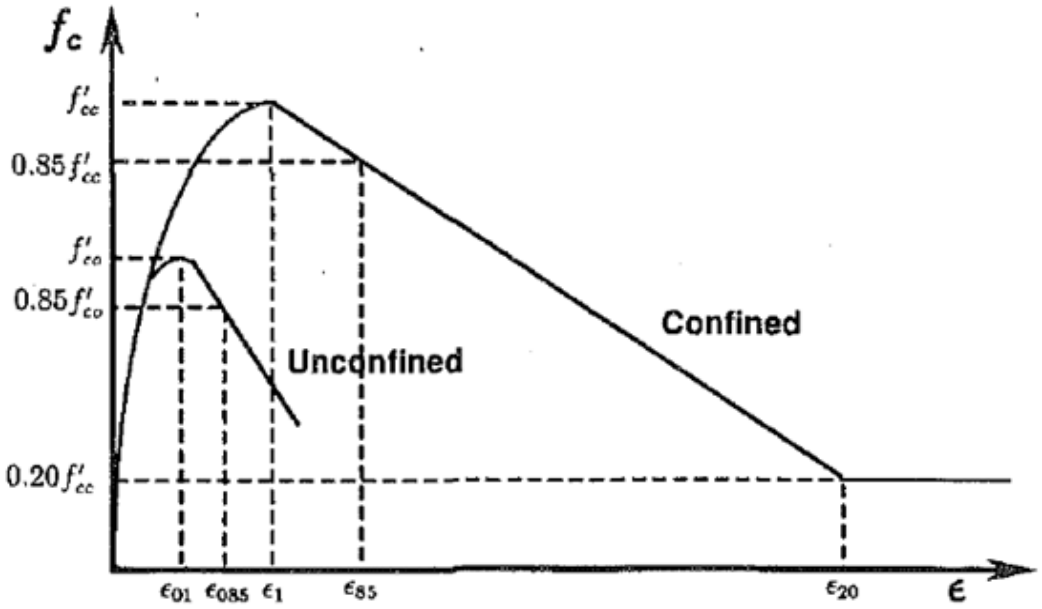

Figure 2-41 Proposed stress-strain relationship (Razavi and Saatcioglu 1999)

3. Confinement reinforcement design:

3.1 Paultre and legeron (1999)

Paultre and legeron (1999) proposed the required hoop volume ratio (ρ_s) for earthquake-resistant circular and rectangular columns having ultimate ductility of $\mu_\phi = \frac{\varphi_u}{\varphi_y} = 10$, Figure 2-42 shows the definition of concrete column ductility.

They considered the effect of applied axial load to axial column strength in their equations, since compressive stresses reduce the ultimate curvature, as a result, the concrete column ductility drops significantly. The required area of confining hoop steel for circular, square and rectangular column sections can be estimates as following:

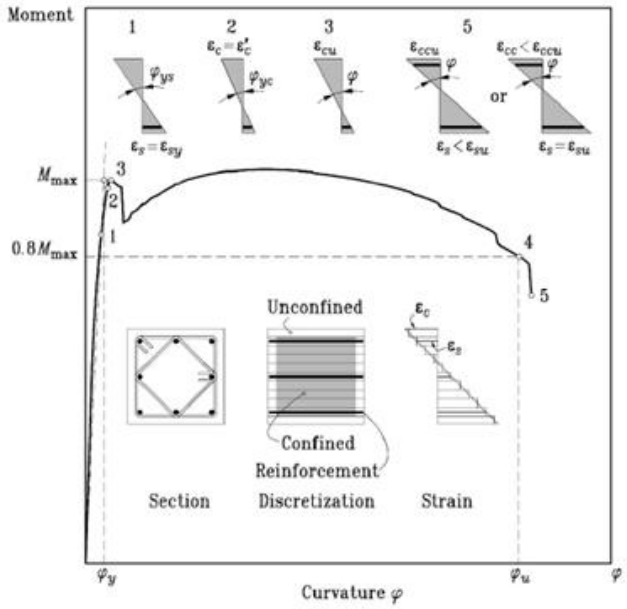

Figure 2-42 Ductility definition (Paultre and legeron 1999)

a) Circular columns:

$$\rho_s = 0.25 k_p \frac{f_c'}{f_{yh}} \qquad \text{(Eq. 2-10)}$$

Where:

$$k_p = \frac{P}{P_o}$$

$$P_o = 0.85(A_g - A_{st}) f_c' + A_{st} f_y$$

b) Square or rectangular columns:

$$A_{shy} = 0.17 k_p k_n \frac{f'_c}{f_{yh}} \frac{A_g}{A_{ch}} c_y s \qquad \text{(Eq. 2-11)}$$

Where

c_y is the confined column dimension in y-direction, as shown in Fig (2-43).

s is hoop spacing.

$$k_n = \frac{n_l}{n_l - 2}$$

$n_l =$ total number of longitudinal bars in the column cross section that are supported laterally the corners of hoops or by hooks.

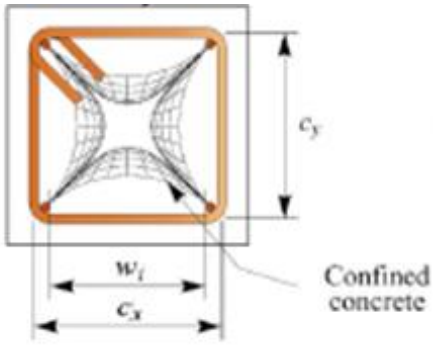

Figure 2-43 Definition of confined column dimensions (Paultre and legeron 1999)

3.2 Current design approach (ACI 318-19)

The confinement effectiveness k_n is adopted based on a proposed formula done by Paultre and legeron (2008). This factor takes into account the effect of closely spaced, laterally supported longitudinal steel bars n_l. Higher number of bars that are longitudinally supported (by seismic hooks or hoop corners), enhance the column confinement.

Concrete strength factor k_f depends on the uniaxial concrete compressive strength f_c'. High strength concrete is brittle in nature, so, it needs more hoop reinforcement to increase its confinement capacity. k_f and k_n can be calculated from the following two equations:

$$\mathrm{k}_f = \frac{f_c'}{25000} + 0.6 \geq 1.0$$

$$k_n = \frac{n_l}{n_l - 2}$$

According to ACI 318-19 section 18.7.5.4, the required amount of hoop reinforcement shall be calculated as following:

i) Rectilinear hoops:

Transverse Reinforcement	Conditions	Applicable expression	
$\frac{A_{sh}}{sb_c}$	$P_u \leq 0.3A_g f_c'$ and $f_c' \leq 10{,}000$ psi	Greater of (a) and (b)	$(a)\ 0.3\left(\frac{A_g}{A_{ch}} - 1\right)\frac{f_c'}{f_{yt}}$
	$P_u > 0.3A_g f_c'$ or $f_c' > 10{,}000$ psi	Greatest of (a), (b) and (c)	$(b)\ 0.9\frac{f_c'}{f_{yt}}$ $(c)\ 0.2\mathrm{k}_f k_n \frac{P_u}{f_{yt}A_{ch}}$

ii) Spiral or circular hoops:

Transverse Reinforcement	Conditions	Applicable expression	
$\frac{A_{sh}}{sb_c}$	$P_u \le 0.3A_g f_c'$ and $f_c' \le 10{,}000$ psi	Greater of (d) and (e)	$(d)\ 0.45\left(\frac{A_g}{A_{ch}}-1\right)\frac{f_c'}{f_{yt}}$
	$P_u > 0.3A_g f_c'$ or $f_c' > 10{,}000$ psi	Greatest of (d), (e) and (f)	$(e)\ 0.12\frac{f_c'}{f_{yt}}$ $(f)\ 0.35\mathrm{k}_f\ \frac{P_u}{f_{yt}A_{ch}}$

Equation (a), (b), (d) and (e) in the previous two tables were applied to ensure no axial column strength degradation due to column cover spalling. Equations (c) and (f) were adopted to make the column capable to reach a drift ratio of 3% with limited loss in column strength; also, equations (c) and (f) are intended to predict behavior of columns having axial load greater than $0.3A_g f_c'$.

Chapter 3

Proposed squat shear wall methodology

3.1. Research motivation

Extensive experimental works have been conducted to study the squat shear wall behavior. As summarized in the Literature Review at Chapter 2, Paulay et al. (1982), Barda (1977), and Cardenas et al. (1982) observed that the concrete crushing at wall web is common failure mode which leads to the sliding shear failure and sudden strength drop. In specific, the tested walls by Barda (1977) which were presented in Chapter 2 at Figure 2-6 and 2-7, show the concrete crushing at wall web. This highlights the insufficient wall web to resists the applied forces. The current study was devoted to tackle this problem by confining the concrete at wall web. Due to the lack information in this regard, the Vector2 software was used to simulate the confined wall at web.

3.2. Vector2 Analysis

At the first stage, SW-MA-1.0 and SW-MP-1.0-1 were constructed and tested, both specimens have same vertical reinforcement but the first specimen was designed according ACI 318-19 provisions which require horizontal steel bars in addition to the vertical bars, while the other specimen represents the proposed walls which have several steel cages of steel bars confined by hoops. The test results that presented in Chapter 4 and 5 reveals that ACI-compliant wall failed due to sliding failure mode, while the proposed wall specimen failed due to the diagonal tension failure mode because the gab between the steel cages was 5-inches which reduced the effective confined area of the wall.

For the second stage, the discussion started to investigate confining the wall web of the 0.5-aspect ratio located in high seismic zone to attain 18 to 24$\sqrt{f'_{cm}}$ (psi), and at the

same time, the gap between steel cages must be reduced as much as possible. Vecto2 software was involved to analyze the ACI and Proposed walls behavior. SW-HA-0.5 is an ACI compliant wall and SW-HP-1.0-1 is a Proposed wall consists of two wide cages at boundaries and four small cages at wall web, the design and more details of these two specimens are presented in Chapter 4.

The Vector2 model of both walls are shown in Figure 3-1 and Figure 3-4. The model consists of supporting block (Red color) and loading block (Yellow color) which are modeled to be well reinforced (15% steel ratio for vertical and horizontal reinforcement). The wall specimen is in between those two blocks. The material properties of both walls are shown in Table 3-2 and Table 3-3. The vertical and horizontal reinforcement were modeled by 2D link elements while the out-of-plane reinforcement were smeared. The default values of concrete and steel reinforcement parameters were selected, details of these parameters are shown in Table 3-1. Cyclic displacements were applied at the center of the loading block.

The cracks and mode failure of both specimens are shown in Figure 3-2 and Figure 3-5, were the ACI compliant wall failed due to sliding failure while the Proposed wall failed due to flexural mode failure. The model results revealed that the ACI compliant wall will lose it shear strength at drift ratio as half as what the proposed wall will attain as shown in Figure 3-3 and Figure 3-6. The ACI compliant wall strength dropped at drift ratio 0.5% while the Proposed wall reached 1% drift ratio. This result indicates that confining the wall web by closely spaced steel cages, would double the drift ductility of the squat wall. Shegay et al. (2017) observed that the Vector2 tends undermine the ultimate drift ratio capacity in some walls up to 45%. Therefore, the 0.5% and 1% of the modeled walls in this study were assumed to be equivalent to 0.73% and 1.45%, respectively.

After constructing and testing both walls, the results are shown in Chapter 5, specimen SW-MA-1.0 reached 276 kips at drift ratio 1% and specimen SW-MP-1.0-1 attained 210 kips with maximum drift ratio of 1.75% which is as twice as that attained by SW-MA-1.0. This an important step to enhance drift ductility of squat walls.

Table 3-1 Model material parameters

Concrete Models	
Compression Pre-Peak	Hogmestad (Parabpla)
Compression Post-Peak	Modified Park-Kent
Compression Softening	Vecchio 1992-A
Tension Stiffening	Modified Bentz 2003
Tension Softening	Linear
FRC Tension	Not Considered
Confined Strength	Kupfer / Richart
Dilation	Variable – Kupfer
Cracking Criteria	Mohr – Coulomb (Stress)
Crack Stress Calculation	Basic (DSFM/MCFT)
Crack Width Check	Agg/5 Max Crack Width
Crack Slip Calculation	Walraven (Monotonic)
Hysteretic Response	Nonlinear w/ Plastic Offsets
Concrete Bond	Eligehausen
Reinforcement Models	
Hysteretic Response	Bauschinger Effect (Seckin)
Dowel Action	Tassios (Crack Slip)
Buckling	Refined Dhakal-Maekaw

Table 3-2 Web and boundary reinforcement of specimen SW-HA-0.5

Material ID	**Vertical reinforcement**	**Horizontal reinforcement**	**Out-of-plane reinforcement ratio (%)**
2	4#7	#3@2.75 inches	0.92
3	#5@4 inches	#4@3.5 inches	0

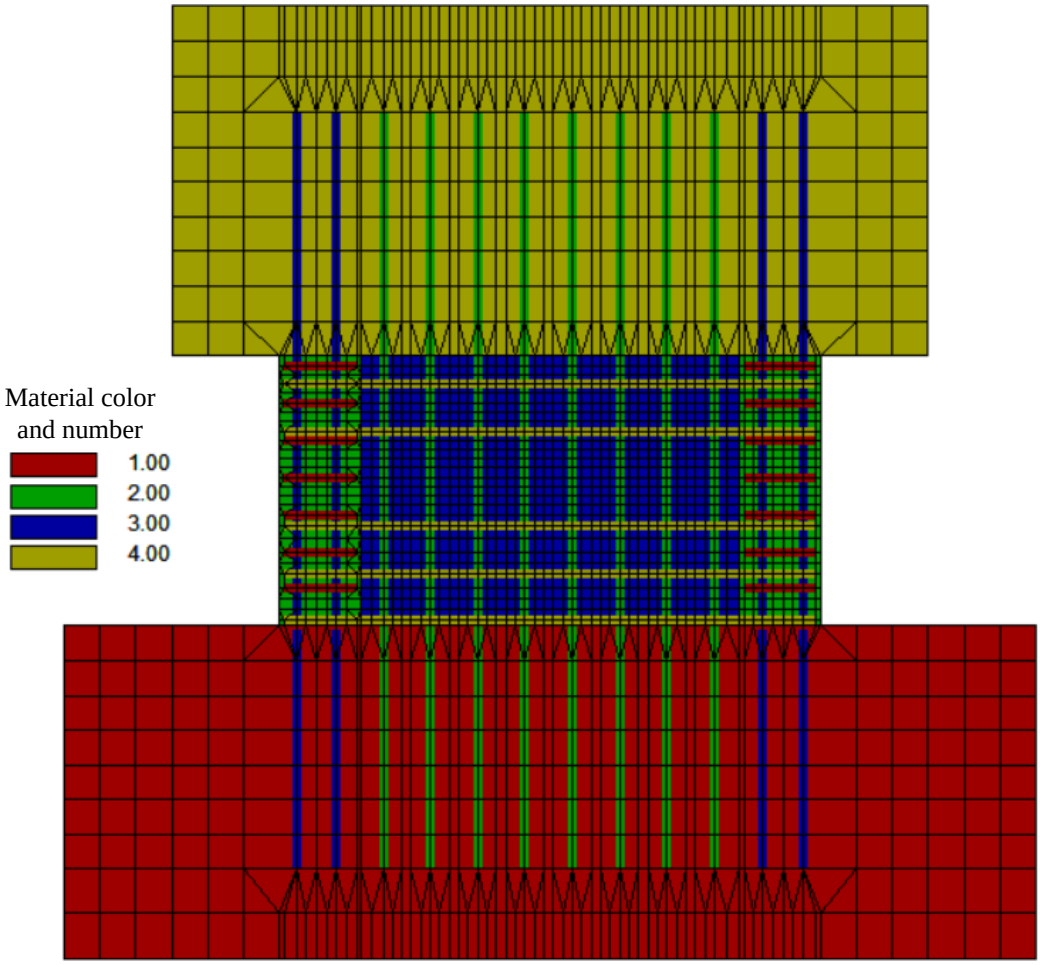

Figure 3-1 Vector2 model of specimen SW-HA-0.5

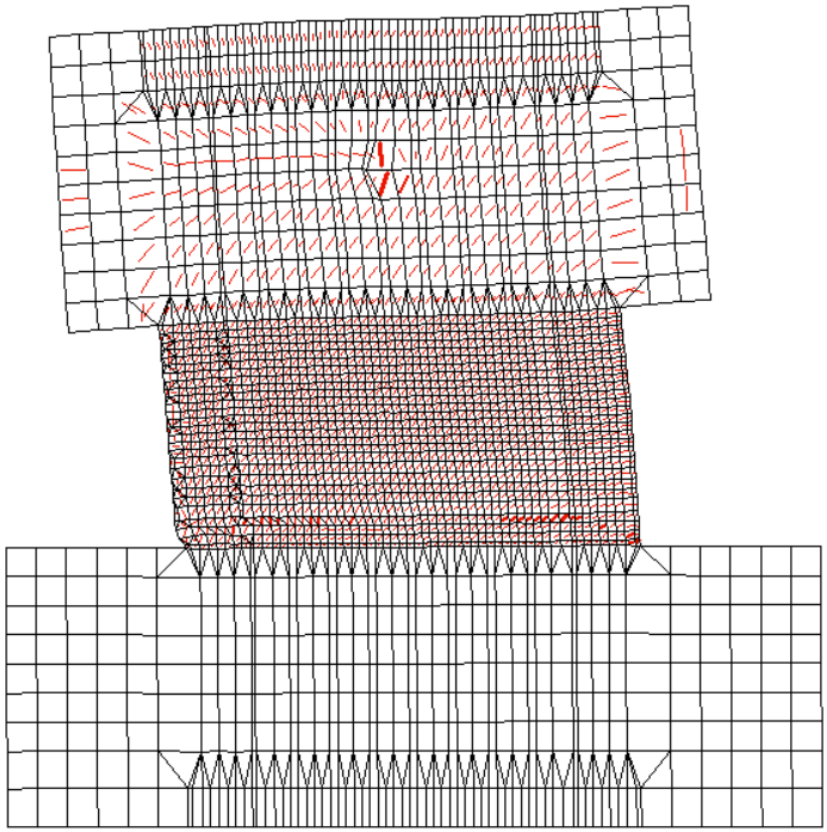

Figure 3-2 Sliding of specimen SW-HA-0.5 at the ultimate load

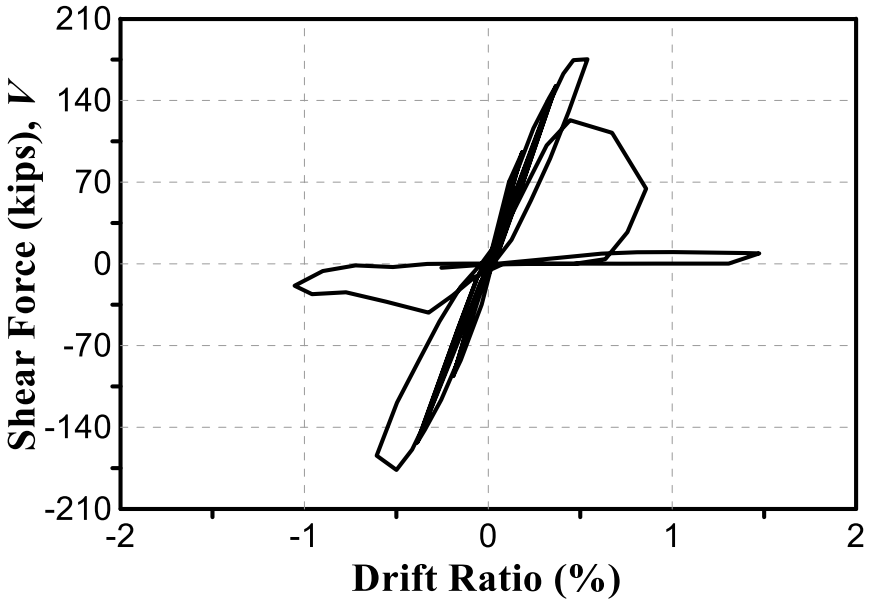

Figure 3-3 Shear force vs drift ratio for specimen SW-HA-0.5

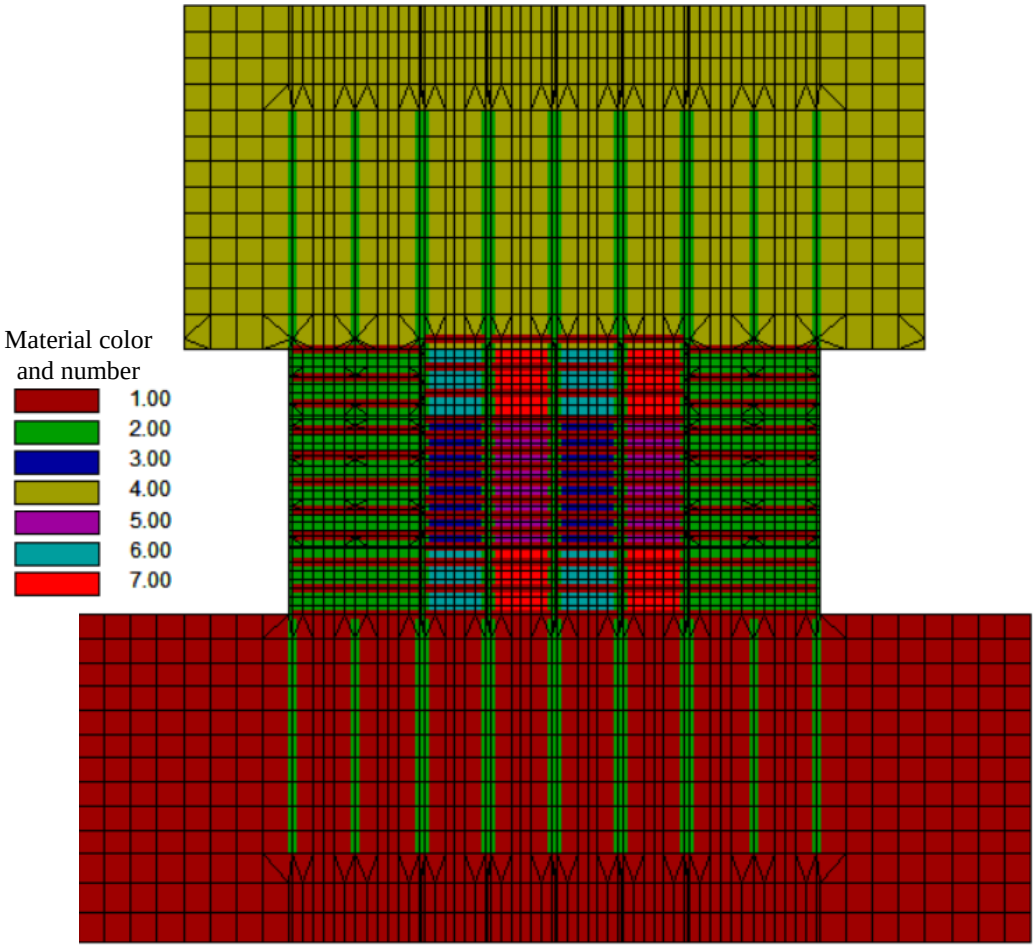

Figure 3-4 Vector2 model of specimen SW-HP-0.5-1

Table 3-3 Web and boundary reinforcement of specimen SW-HP-0.5-1

Material ID	Vertical reinforcement	Horizontal reinforcement	Out-of-plane reinforcement ratio (%)
2	6#5	#3@2 inches	1.1
3 and 4	4#5	#3@1.2 inches	3.67
5 and 6	4#5	#3@2 inches	2.2

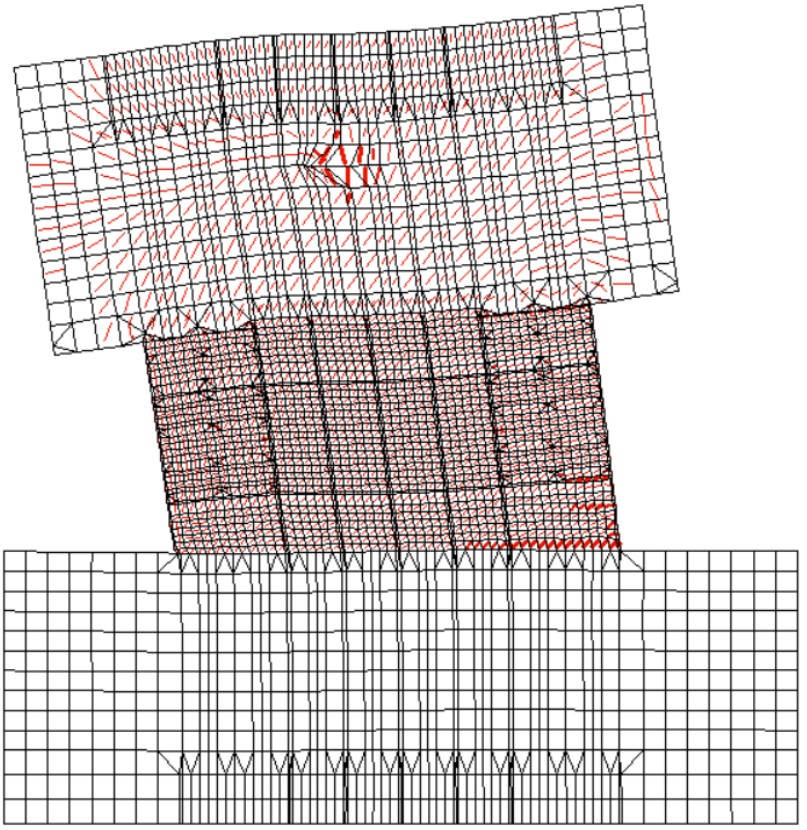

Figure 3-5 Flexural cracks of specimen SW-HP-0.5-1

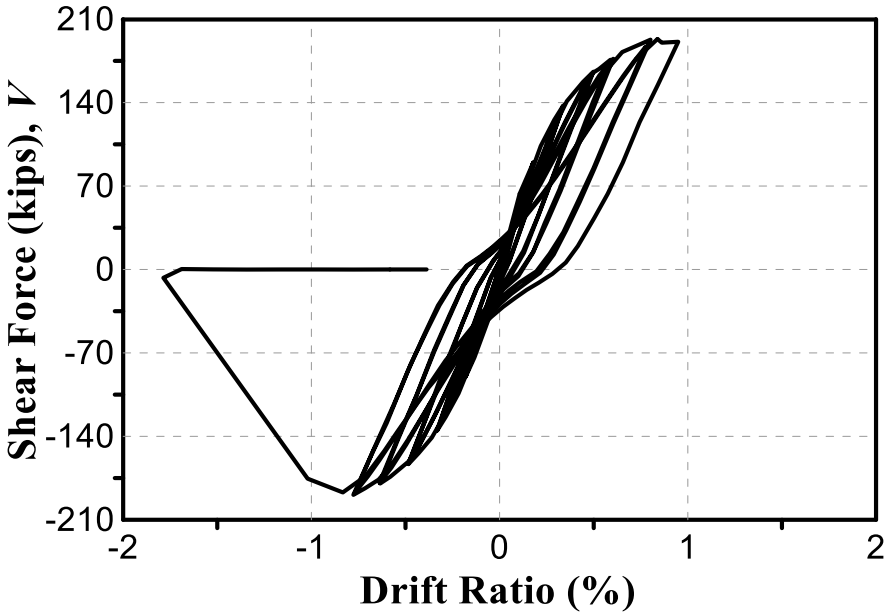

Figure 3-6 Shear force vs drift ratio for specimen SW-HP-0.5-1

The third stage was dedicated to further enhance drift ductility and increase the shear strength, at same time reducing the number of steel cages to make easier to construct and install the steel cages in practice. The modified proposed wall SW-MP-1.0-2 contains four-wide steel cages instead of 6 cages, the design and reinforcement layout were discussed in Chapter 4. The critical zone of the ACI compliant wall is the web as shown in Figure 3-7 up to the mid wall height, while concrete spalling was observed at both boundaries and the web in specimen SW-MP-1.0-1 as shown in Figure 3-8, but the web was still confined and contribute in resisting the shear forces. Therefore, the hoop spacing of steel cages were reduced to be 1.25 inches in all steel cages up to 2/3 wall height, this value of 1.25 in. was calculated by assuming the steel cages are column, and required hoop spacing are calculated based on Table 3-1, the final reinforcement layout of proposed walls is illustrated in Figure 3-9.

Figure 3-7 Failure mode of specimen SW-HA-0.5 at drift ratio 2%

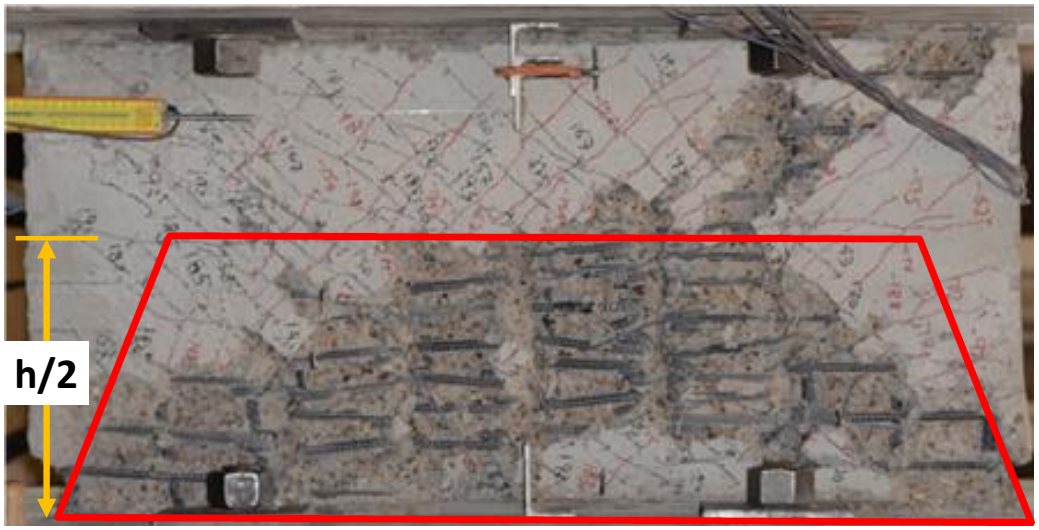

Figure 3-8 Failure mode of specimen SW-HP-0.5-1 at drift ratio 2.5%

Table 3-4 Quantifying the axial force in each steel cage to calculate hoops spacing

In proposed walls, consider Pu = (Aspect ratio)(Vu)

Transverse Reinforcement	Conditions	Applicable expression	
$\frac{A_{sh}}{sb_c}$ ACI 13.6.4.4	$P_u \le 0.3A_g f_c'$ and $f_c' \le 10{,}000$ psi	Greater of (a) and (b)	$(a)\ 0.3\left(\frac{A_g}{A_{ch}}-1\right)\frac{f_c'}{f_{yt}}$
	$P_u > 0.3A_g f_c'$ or $f_c' > 10{,}000$ psi	Greatest of (a), (b) and (c)	$(b)\ 0.09\frac{f_c'}{f_{yt}}$ $(c)\ 0.2k_f k_n \frac{P_u}{f_{yt}A_{ch}}$

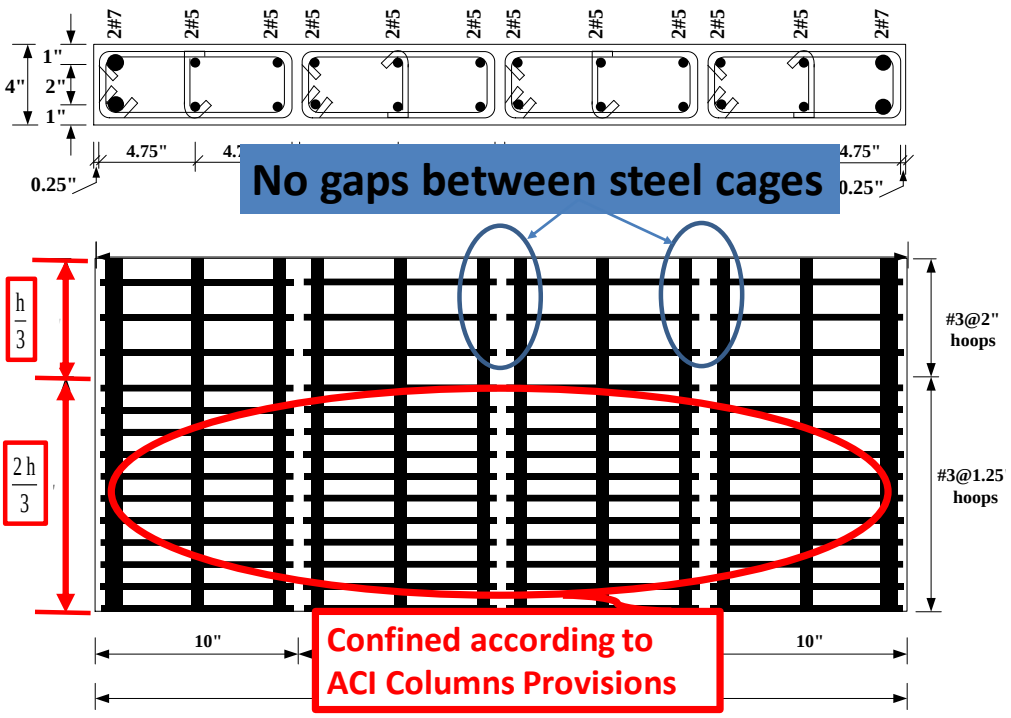

Figure 3-9 Final reinforcement layout of the proposed wall

Figure 3-10 and Table 3-5 contain the model and reinforcement properties, where each of the four cages have 6#5 longitudinal steel bars except the cages at boundaries that have 4#5 and 2#7 to increase the wall shear strength, it is worth to mention that the three walls SW-M!-0.5, SW-MP-1.0-1 and SW-MP-1.0-2 have almost similar of the total vertical steel reinforcement area but different horizontal reinforcement configuration.

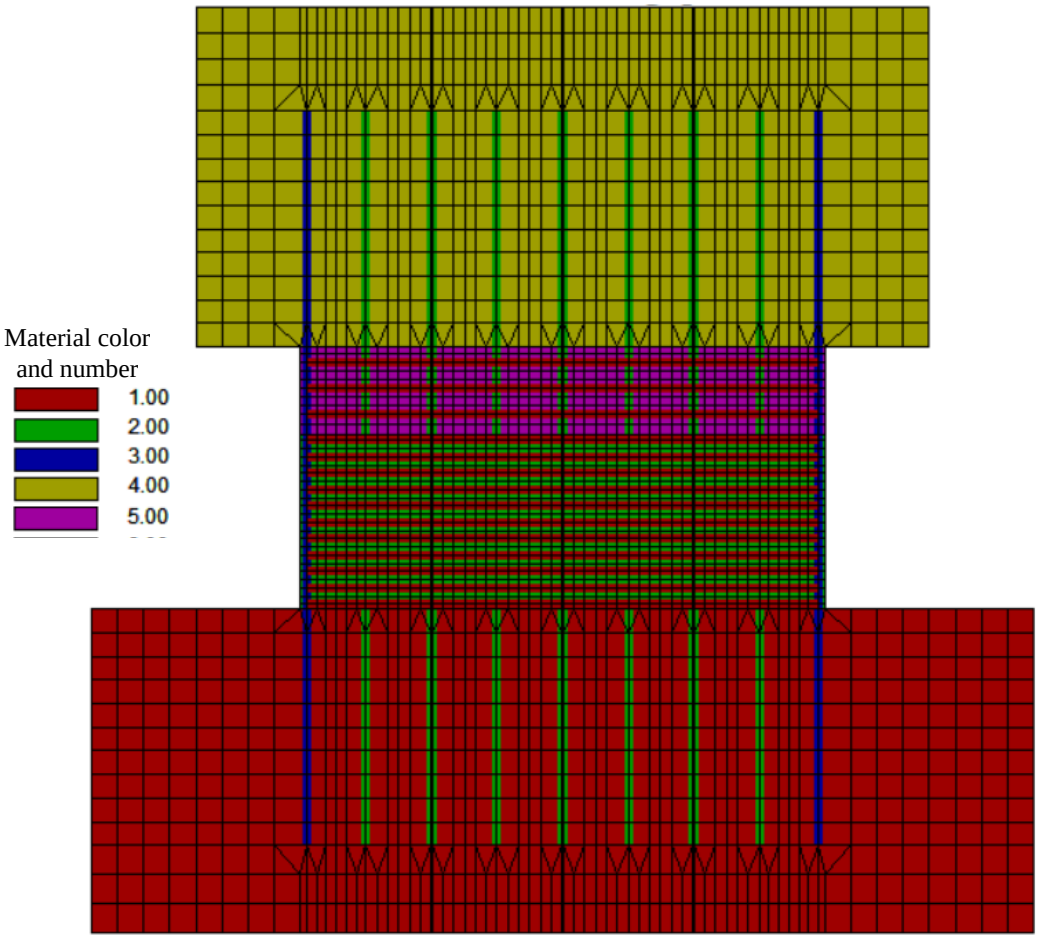

Figure 3-10 Vector2 model of specimen SW-HP-0.5-2

Table 3-5 Web and boundary reinforcement of specimen SW-HP-0.5-2

Material ID	Vertical reinforcement	Horizontal reinforcement	Out-of-plane reinforcement ratio (%)
2	2#7 and 4#5 at each boundary cages; 6#5 at each of the two web cages	#3@1.25 inches	1.1
5		#3@2 inches	3.67

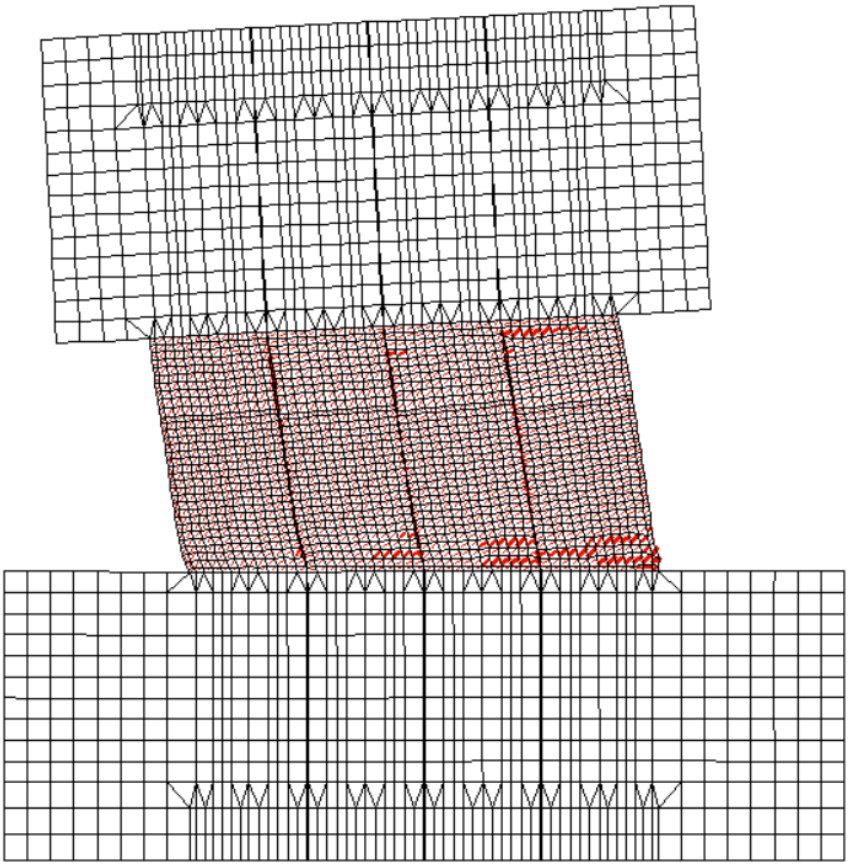

Figure 3-11 Flexural cracks of specimen SW-HP-0.5-2

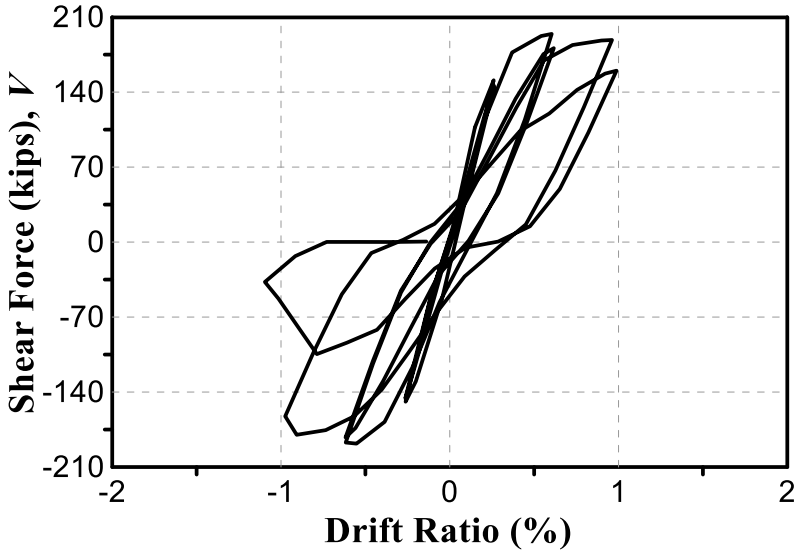

Figure 3-12 Shear force vs drift ratio for specimen SW-HP-0.5-2

The test results of specimen SW-MP-1.0-2 were as expected, having higher shear strength (257 kips) and higher drift ratio (1.75%). The concrete at wall web is well confined (Figure 3-13) and efficiently resists shear forces even after drift ratio 2%.

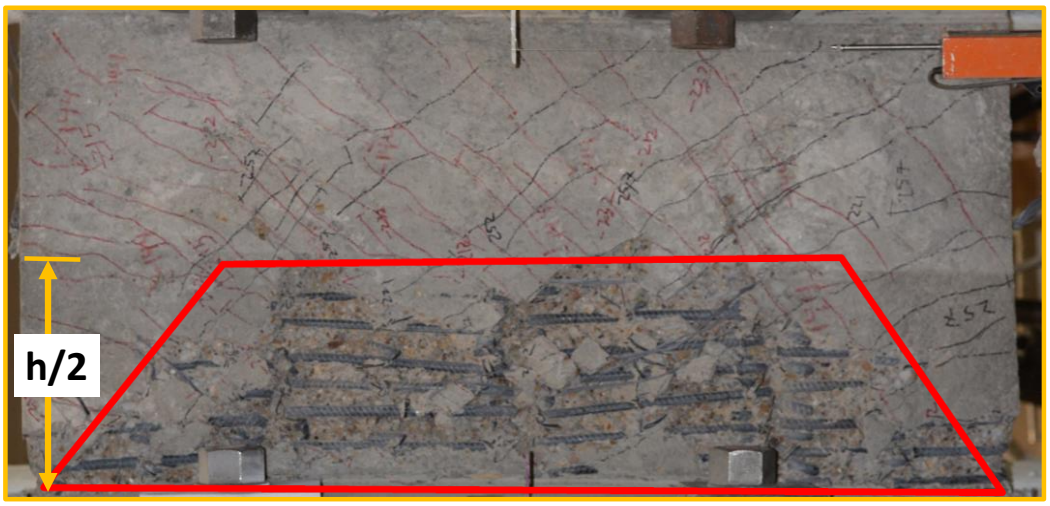

Figure 3-13 Failure mode of specimen SW-HP-0.5-2 at drift ratio 2%

Chapter 4

Experimental Program

4.1. Introduction

Seven squat shear walls with aspect ratio 0.5 or 1.0 were fabricated and tested under reversed cyclic loads. The information of each specimen is shown in Table 4-1. Each specimen name was designated according to test variables. Primary test variables were reinforcement configuration (ACI or Proposed), wall aspect ratio of 0.5 or 1.0, and design shear stress (High: 18 to 24√fcm (psi); or Medium: 10 to 12√fcm (psi)). For instance, Specimen SW-HA-0.5 represents a Squat Wall (SW) designed to reach High (H) shear stress between 18 to 24√fcm (psi), reinforcement configuration according to ACI 318-19 (A) provisions, wall high to length ratio is 0.5. For SW-HP-0.5-1 and SW-HP-0.5-2, labels of 1 and 2 were added to emphasis that the second specimen is the updated reinforcement configuration of the first specimen. Shear strength of ACI 318-19 compliant walls designed according to the equation:

$$V_n = A_{cv}(\alpha_c \lambda \sqrt{f_c'} + \rho_t f_y)$$

While the Proposed walls were designed by strut and tie model which is explained in Chapter 8, basically the tie strength controls wall strength as the proposed walls are well-confined and struts are stronger than the tie.

ACI 318-19 requires providing boundary elements at both ends of shear walls, these boundaries have high number of longitudinal bars confined with very closely hoops. If ACI limitations are applied to reinforce SW-HA-0.5 boundaries hoops, it ends up with using #3@1.33 inch hoops which is believed too conservative, instead scaling of equivalent amount of hoops was suggested, the scaling procedure was to find required amount of hoops for a full scale squat wall and calculate the volumetric steel hoops ratio.

Accordingly, this ratio was used to determine the equivalent number of hoops needed for SW-HA-0.5 boundaries, the required hoops at boundaries was calculated to be #3@2.75".

Table 4-1 Specimen information

Specimen [1]	f_{cm}[2] ksi	Web reinforcement		Boundary reinforcement	
		Horizontal, ρ_t (%)	Vertical, ρ_l (%)	Horizontal, ρ_t (%)	Vertical, ρ_l (%)
SW-HA-0.5	5.3	2.85 (#4@3.5 in.)	4.4 (#5@3.5 in.)	2.0 (#3@2.75 in.)	11.6 (4#7)
SW-HP-0.5-1	4.5	2.75[3] (#3@2 in.)	6.2 (4#5 per cage)	2.75 (#3@2 in.)	4.65 (6#5)
SW-HP-0.5-2	4.7	4.4[4] (#3@1.25 in.)	4.65 (6#5 per cage)	4.4[4] (#3@1.25 in.)	6.1 (4#5; 2#7)
SW-MA-0.5	5.0	1.38 (#3@4 in.)	1.38 (#3@4 in.)	4.4 (#3@1.25 in.)	2.47 (4#4; 2#3)
SW-MP-0.5	5.0	4.4[4] (#3@1.25 in.)	1.65 (6#3 per cage)	4.4[4] (#3@1.25 in.)	2.55 (4#4; 2#3)
SW-MA-1.0	4.13	1.1 (#3@5 in.)	1.1 (#3@5 in.)	2.0 (#3@2.75 in.)	5.6 (#4@3.5 in.)

[1]: SW refers to Shear Walls; H denotes to High design shear stress (18 to 24 $\sqrt{f_c'}$); M refers to Medium design shear stress (10 to 12 $\sqrt{f_c'}$); A refers to ACI provisions-based design walls; P represents Proposed walls, 0.5 or 1.0 is the wall height to length ratio.
[2]: f_{cm} is measured concrete compressive strength.
[3]: ρ_t =2.75% (#3@2 in.) from wall base to $h_w/4$ and from $3h_w/4$ to h_w. ρ_t =4.6% (#3@1.2 in.) from $h_w/4$ to $3h_w/4$.
[4]: ρ_t =4.4% (#3@1.25 in.) from wall base to $2h_w/3$. ρ_t =2.75% (#3@2 in.) from $2h_w/3$ to h_w.
Note: 1 in. = 25.4 mm and 1kip = 4.45 kN.

Another reason of scaling number of boundary hoops is that the failure of squat walls does not involve sever boundaries damage, instead the common squat walls failures types are due to shear sliding, so relaxing amount of boundaries hoops does not effect on behavior of squat walls. On the other hand, the provided hoops spacing in

specimen SW-MA-0.5 was #3@1.33 inch as was required by ACI because horizontal reinforcements are less congested compared to specimen SW-HA-0.5. Longitudinal steel reinforcement in SW-HA-0.5, SW-HP-0.5-1 and SW-HP-0.5-2 are almost same. SW-HP-0.5-1 was reinforced by uniformly distributed longitudinal steel bars, while SW-HP-0.5-2 was designed to have some concentrated steel bars at boundaries to increase the shear strength. In SW-HP-0.5-1, it was believed that the middle region in wall web is the critical zone, therefore hoop spacing was selected to be 1.25 inch and relaxed to 2 inches in all other wall regions. Based on the test results of SW-HP-0.5-1, the critical zone is observed to be within the wall web and boundaries up to ½ of wall height, so hoop spacing of SW-HP-0.5-2 and SW-MP-0.5 is provided to be 1.25 inch up to 2/3 of wall height and relaxed spacing of 2 inches in the remaining wall height. Specimens SW-MA-0.5 and SW-MP-0.5 were reinforced by identical size and number of longitudinal steel bars, to experimentally investigate drift ductility capacity of ACI compliant and proposed walls.

4.2. Squat reinforced concrete walls with aspect ratio 1.0

SW-MA-1.0 is a squat wall designed according to ACI 318-19 criteria, and SW-MP-1.0-1 is a proposed squat wall consists of multiple steel cages, both walls (dimensions 40 in.x 40 in. x 4 in.) are one-third of full scale walls having dimensions (120 in.x120 in. x4 in.) . The aim of testing SW-MA-1.0 and SW-MP-1.0-1 walls is to compare behavior of Proposed squat walls with the walls designed according to ACI 318-19 provisions, both walls have the same amount of longitudinal and horizontal steel rebars ratios but the major difference is that ACI code reinforces walls with horizontal and vertical bars whereas Proposed walls provides multiple steel cages to confine web region due to existence of confining hoops.

4.2.1. SW-MA-1.0

4.2.1.1. Specimen Design

Original Specimen Design:

The target wall shear strength is $V_n = 10 A_{cw} \sqrt{f_c'}$, with concrete compressive strength ($f_c' = 5 \ ksi$), aspect ratio ($\frac{h_w}{l_w} = \frac{40}{40} = 1$), and wall thickness ($t_w = 4''$).

1) Width limitation (ACI 18.10.6.4 b):

$$b > \frac{h_u}{16}$$

$$4 > \frac{40}{16}$$

$$4'' > 2.5'' \qquad (Ok)$$

2) Number of curtains (ACI 18.10.4.4):

$$V_n = 10A_{cw}\sqrt{f_c'}$$
$$V_n = 10(40)(4)\sqrt{5000}$$
$$V_n = 113.1\ kip$$

$$V_u = \phi V_n$$
$$V_u = 0.75(113.1)$$
$$V_u = 84.8\ kip$$

Because $V_u = 84.8\ kip > 2A_{cv}\lambda\sqrt{f_c'} = 2(40)(4)(1)\sqrt{5000} = 22.6\ kip$, two curtains are required

$$M_u = V_u l_u$$
$$M_u = 84.8(40)$$
$$M_u = 282.7\ \text{kip.ft}$$

3) Minimum distributed web reinforcement ratios (ACI 18.10.2.1):

The provided transverse and longitudinal reinforcements are (#3@4"), so:

$$\rho_t = \rho_l = \frac{A_s}{bs} = \frac{2(0.11)}{4(4)} = 0.0138 > 0.0025 \qquad (Ok)$$

4) Shear Design (ACI 18.10.4.1):

$$\phi V_n = \phi A_{cv}(\alpha_c \lambda\sqrt{f_c'} + \rho_t f_y)$$
$$\alpha_c = 3\ for\ \frac{h_w}{l_w} = 1$$
$$\phi V_n = 0.75(4)(40)\left[3(1)\sqrt{5000} + 0.0138(60000)\right]$$
$$\phi V_n = 124.8\ kip > V_u = 84.8\ kip \qquad (Ok)$$

5) Length of the Special Boundary Element (ACI 18.10.6.4 a):

The proposed geometry was modeled using spColumn software; the neutral axis depth (c) for the wall section is (6.98 in).

$$\text{Length of SBE} = \text{max. of} \begin{cases} c - 0.1 l_w = 6.98 - 0.1(40) = 2.98 \ in \\ \dfrac{c}{2} = \dfrac{6.98}{2} = 3.49 \ in \qquad (Controls) \end{cases}$$

As shown in Fig (1), use length of SBE = $5.5 \ in > 3.49 \ in$ $\qquad (Ok)$

6) Height of Special Boundary Element (18.10.6.2 b):

$$\text{Height of SBE} = \text{max. of} \begin{cases} l_w = 40 in \qquad (Controls) \\ \dfrac{M_u}{4V} = \dfrac{282.7(12)}{4(84.8)} = 10 \ in \end{cases}$$

$$\text{Height of SBE} = 40 \ in$$

7) Vertical Spacing of hoops in SBE:

$$h_x = \text{maximum spacing of supported bars} < \min \begin{cases} 14 \ in \\ \dfrac{2}{3} b = \dfrac{2(4)}{3} = 2.67 \ in \qquad (Controls) \end{cases}$$

As shown in Fig (4-1), use $h_x = 2.5 \ in < 2.67 \ in$ $\qquad (Ok)$

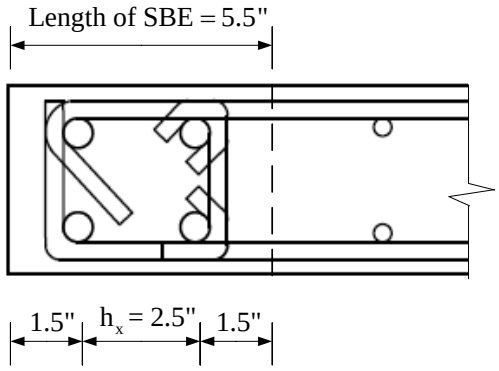

Figure 4-1 Illustration of h_x and length of SBE.

$$s = \min \begin{cases} b/3 = 4/3 = 1.33\ in & (Controls) \\ 6d_b = 6(5/8) = 3.75\ in & \\ 4 + \left(\frac{14 - h_x}{3}\right) = 4 + \left(\frac{14 - 2.5}{3}\right) = 7.83\ in & \\ 6\ in & \end{cases}$$

$$use\ s = 1.25\ in < 1.33\ in \qquad (Ok)$$

8) Limitations for the amount of transverse reinforcement (18.10.6.4 f):

$$b_{c1} = 2.5 + \frac{5}{8} + 2\left(\frac{3}{8}\right) = 3.88 \ in \qquad [\text{As shown in Fig (4-2)}]$$

$$b_{c2} = 2 + \frac{5}{8} + 2\left(\frac{3}{8}\right) = 3.38 \ in \qquad [\text{As shown in Fig (4-2)}]$$

$$A_{ch} = b_{c1} b_{c2}$$

$$A_{ch} = 3.88(3.38) = 13.1 \ in^2$$

$$A_g = 5.5(4) = 22 \ in^2$$

(*a*) Check minimum reinforcement for (b_{c1}) direction:

$$A_{sh1} = \max \text{ of } \begin{cases} 0.09 \dfrac{f_c^{'}}{f_{yt}} s b_{c1} \\ 0.3\left(\dfrac{A_g}{A_{ch}} - 1\right) \dfrac{f_c^{'}}{f_{yt}} s b_{c1} \end{cases}$$

$$A_{sh1} = \max \text{ of } \begin{cases} 0.09 \dfrac{5}{60}(1.25)(3.88) = 0.036 \\ 0.3\left(\dfrac{22}{13.1} - 1\right) \dfrac{5}{60}(1.25)(3.88) = 0.08 \qquad (Controls) \end{cases}$$

Provided steel area $= 2(0.11) = 0.22 \ in^2 > 0.08 \ in^2 \qquad (Ok)$

(*b*) Check minimum reinforcement for (b_{c2}) direction:

$$A_{sh2} = \max \text{ of} \begin{cases} 0.09\dfrac{f_c'}{f_{yt}} s b_{c2} \\ 0.3\left(\dfrac{A_g}{A_{ch}} - 1\right)\dfrac{f_c'}{f_{yt}} s b_{c2} \end{cases}$$

$$A_{sh2} = \max \text{ of} \begin{cases} 0.09\dfrac{5}{60}(1.25)(2.98) = 0.028 \\ 0.3\left(\dfrac{22}{13.1} - 1\right)\dfrac{5}{60}(1.25)(3.38) = 0.07 \quad (Controls) \end{cases}$$

Provided steel area $= 2(0.11) = 0.22\ in^2 > 0.07\ in^2$ (*Ok*)

use #3 *hoops* @1.25" spacing.

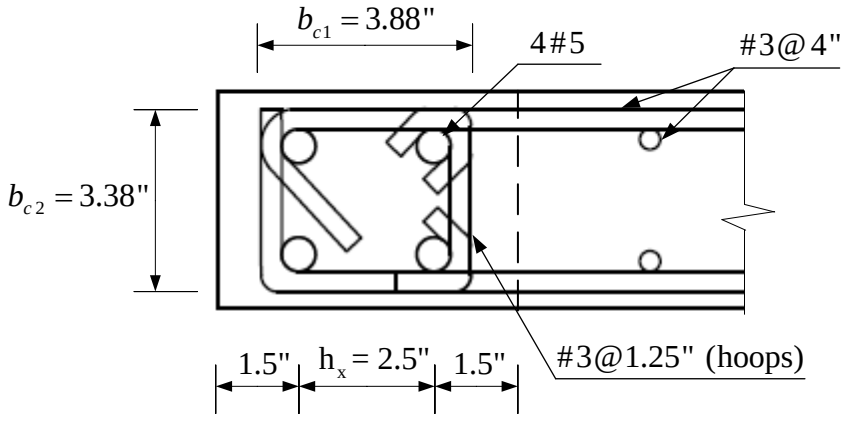

Figure 4-2 Definition of b_{c1} and b_{c2}

The final specimen reinforcement layout for SW-MA-1.0 is shown in Figure 4-5.

Scaled Specimen Design (Three times of original specimen):

$f_c^{'} = 5\ ksi,\ \frac{h_w}{l_w} = \frac{120}{120} = 1 < 2$ (Squat Shear Wall), $t_w = 12"$

1) Vertical Spacing of hoops in SBE:

$$h_x = \max \text{ spcing of supported bars} < \min \begin{cases} 14\ in \\ \frac{2}{3}b = \frac{2(12)}{3} = 8\ in \end{cases} \quad (Controls)$$

As shown in Fig (4-3), use $h_x = 4\ in < 8\ in$ (Ok)

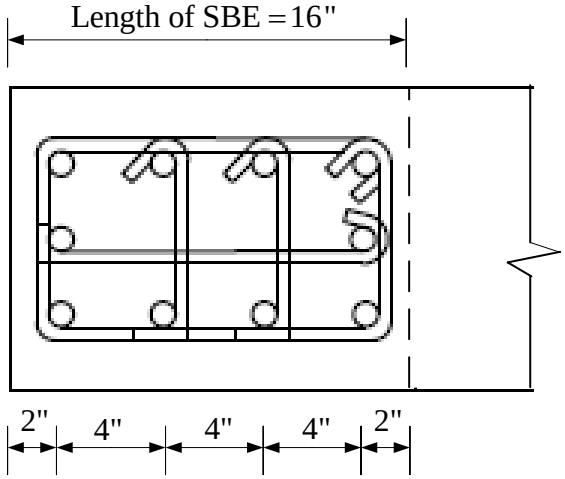

Figure 4-3 Illustration of h_x and length of SBE.

$$s = \min \begin{cases} b/3 = 12/3 = 4\ in \quad (Controls) \\ 6d_b = 6(9/8) = 6.75\ in \\ 4 + \left(\frac{14 - h_x}{3}\right) = 4 + \left(\frac{14-8}{3}\right) = 6\ in \\ 6\ in \end{cases}$$

$use\ s = 3\ in < 4\ in \quad (Ok)$

2) Limitations for the amount of transverse reinforcement (18.10.6.4 f):

$$b_{c1} = 12 + \frac{9}{8} + 2\left(\frac{4}{8}\right) = 14.13 \ in \qquad \left[\text{As shown in Fig (4-4)}\right]$$

$$b_{c2} = 6 + \frac{9}{8} + 2\left(\frac{4}{8}\right) = 8.13 \ in \qquad \left[\text{As shown in Fig (4-4)}\right]$$

$$A_{ch} = b_{c1} b_{c2}$$

$$A_{ch} = 14.13(8.13) = 114.9 \ in^2$$

$$A_g = 16(12) = 192 \ in^2$$

(*a*) Check minimum reinforcement for (b_{c1}) direction:

$$A_{sh1} = \max \text{ of } \begin{cases} 0.09 \dfrac{f_c^{'}}{f_{yt}} s b_{c1} \\ 0.3\left(\dfrac{A_g}{A_{ch}} - 1\right) \dfrac{f_c^{'}}{f_{yt}} s b_{c1} \end{cases}$$

$$A_{sh1} = \max \text{ of } \begin{cases} 0.09 \dfrac{5}{60}(3)(14.13) = 0.32 \\ 0.3\left(\dfrac{192}{114.9} - 1\right) \dfrac{5}{60}(3)(14) = 0.71 \qquad (\textit{Controls}) \end{cases}$$

Provided steel area $= 4(0.2) = 0.8 \ in^2 > 0.71 \ in^2$ (*Ok*)

(*b*) Check minimum reinforcement for (b_{c2}) direction:

$$A_{sh2} = \max \text{ of} \begin{cases} 0.09\dfrac{f_c^{'}}{f_{yt}} s b_{c2} \\ 0.3\left(\dfrac{A_g}{A_{ch}} - 1\right)\dfrac{f_c^{'}}{f_{yt}} s b_{c2} \end{cases}$$

$$A_{sh2} = \max \text{ of} \begin{cases} 0.09\dfrac{5}{60}(3)(8.13) = 0.18 \\ 0.3\left(\dfrac{192}{114.9} - 1\right)\dfrac{5}{60}(3)(8.13) = 0.41 \quad (\textit{Controls}) \end{cases}$$

Provided steel area $= 3(0.2) = 0.6\ in^2 > 0.41\ in^2$ (*Ok*)

use #4 *hoops* @3" spacing.

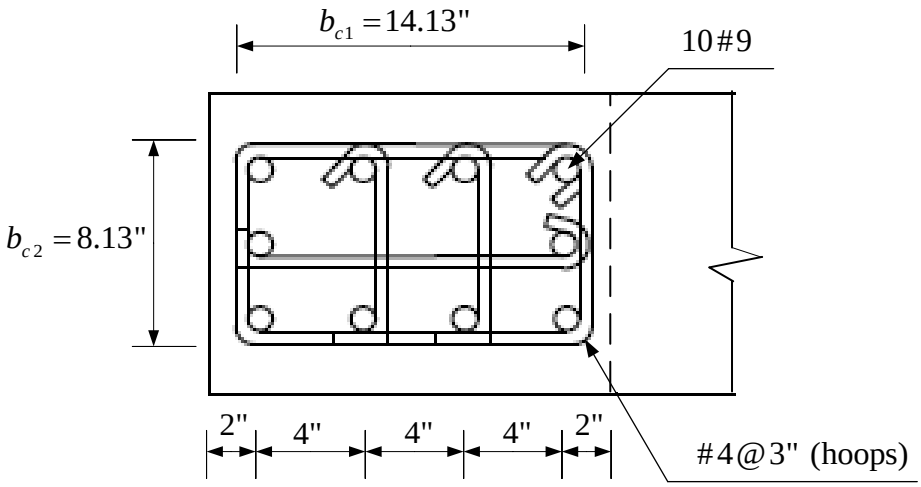

Figure 4-4 Definition of b_{c1} and b_{c2}

Scaling assumptions:

1) Same amount of confined core ratio (A_{ch}/A_g):

Original specimen:

$$\frac{A_{ch}}{A_g} = \frac{13.1}{22} = 59.5\%$$

Scaled specimen:

$$\frac{A_{ch}}{A_g} = \frac{114.9}{192} = 59.8\%$$

2) Same amount of longitudinal steel ratio in the SBE (A_s/A_g):

Original specimen (4#5):

$$\frac{A_s}{A_g} = \frac{4(0.31)}{22} = 5.6\%$$

Scaled specimen (10#9):

$$\frac{A_s}{A_g} = \frac{10(1)}{192} = 5.2\%$$

Scaling the hoop steel ratio and spacing:

Scaled specimen:

Four #4 legs in b_{c1} direction, and Three #4 legs in b_{c2} direction, as shown in Fig. (4-4), then the steel hoop volume ratio (ρ_v) is:

$$\rho_v = \frac{A_{s\,(hoop)}}{A_{ch}\,s} = \frac{4(0.2)+3(0.2)}{114.9(3)} = 1.22\%$$

Original specimen:

Two #3 legs in b_{c1} direction, and Two #3 legs in b_{c2} direction, as shown in Fig. (4-2). We need to get the spacing (s) that makes ρ_v for scaled specimen is equivelant to ρ_v for original specimen:

$$\rho_v = \frac{A_{s\,(hoop)}}{A_{ch}\,s}$$

$$1.22\% = \frac{2(0.11)+2(0.11)}{13.1\ (s)}$$

$$s = 2.75"$$

So, we can use spacing up to 2.75" for small scale specimen.

For current spacing (s = 1.33"), then:

$$\rho_v = \frac{A_{s\,(hoop)}}{A_{ch}\,s}$$

$$\rho_v = \frac{2(0.11)+2(0.11)}{13.1\,(1.33)} = 2.53\%$$

Table 4-2 shows a scaling summary for small- and large-scale specimens.

Table 4-2 Scaling Summary.

Specimen Scale	Hoop spacing in the SBE	Hoop steel volume ratio, ρ_v
Large Scale	3"	1.22%
Small Scale (1/3 scale)	1.33"	2.53%
	2.75"	1.22%

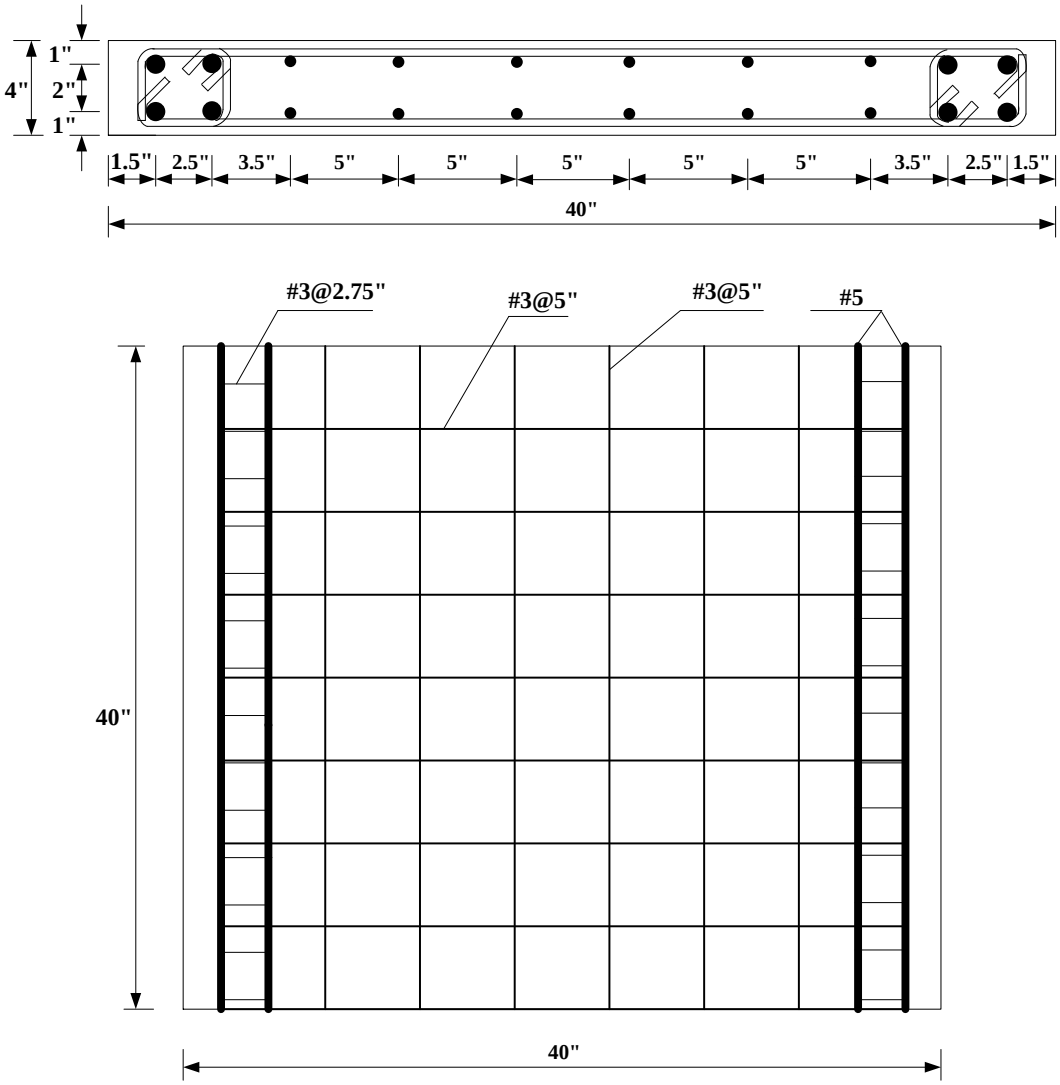

Figure 4-5 Reinforcement layout for specimen SW-MA-1.0

4.2.1.2. Strain gauge locations

Twelve strain gauges were attached to the vertical steel rebars which are labeled by the orange color and have designation L1 to L12 as shown in Figure 4-6. Strain gauges were also attached to the boundary hoops and horizontal steel bars which are labeled by blue colors and have designation of S12 to S16.

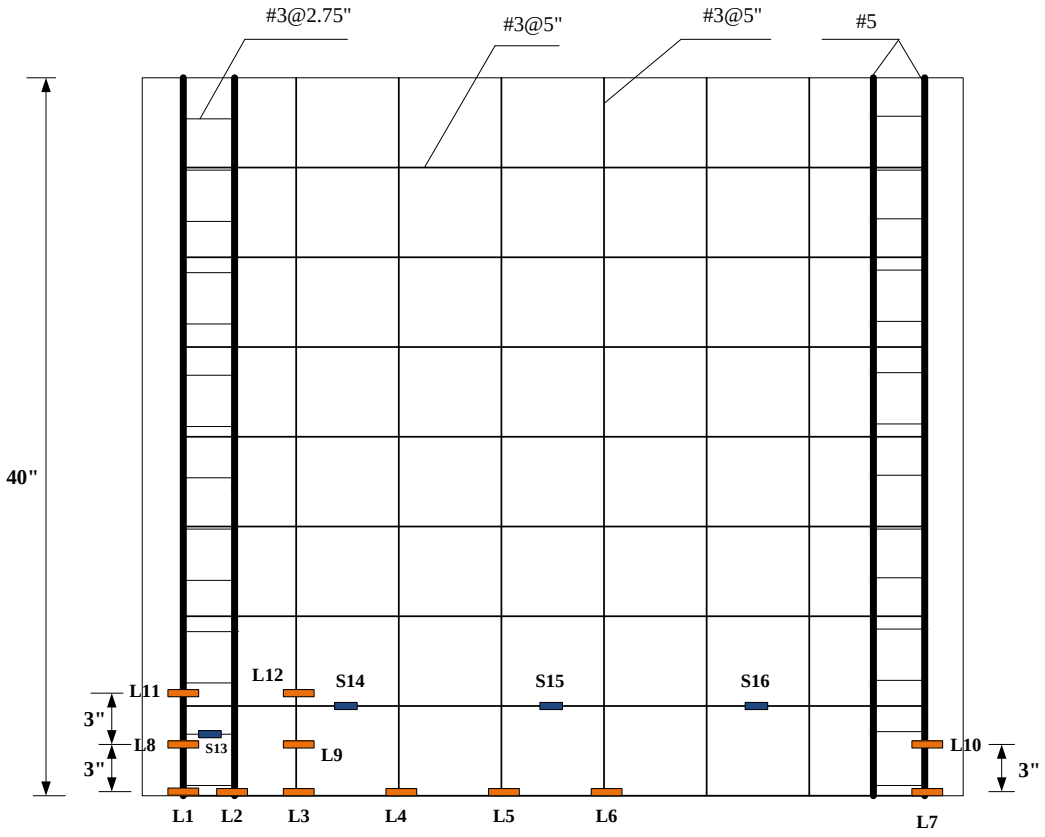

Figure 4-6 Strain gauges layout for specimen SW-MA-1.0

4.2.1.3. Specimen Construction

Plywood of 2 in. (51 mm) by 4 in. (102 mm) were used to make specimen formwork, the wall dimensions are 40 in. (1016 mm) length by 20 in. (508 mm) by 4 in. (102 mm) thickness, the supporting block is 64 in. (1626 mm) length by 72 in. (1829 mm) height by 43 in. (1092 mm) thickness. The formwork of wall and the blocks are connected to monolithically cast the specimen components. Ready-mix concrete was used. The ordered concrete compressive and steel yield strength were 5000 (34.5 MPa) and 60,000 psi (414 MPa), respectively.

Figure 4-7 to Figure 4-18 show the process of specimen preparation and steel fabrication. The specimen consists of supporting and loading blocks linked by the shear wall. The purpose of the supporting block is to provide fixed support to the wall specimen during the test, while the loading block purpose is to transfer the cyclic loading from the actuator to the wall specimen. The supporting block steel reinforcement consists of six #11 steel bars at top and bottom faces and two #11 bars at the vertical sides (Figure 4-9), the #3 steel stirrups were provided at 5 inch spacing. The loading block (Figure 4-10) consists of four #5 steel bars at top and bottom faces, and one #5 steel bar at the cage mid height of each face. The stirrups are #3@5 inches.

Strain gauge (Figure 4-11) are attached at longitudinal and horizontal steel bars. The process starts by grinding the steel bar face, cleaning the face by acidic neutralizing agents, then attaching the strain gauge to smoothed bar face using the glue. M-coat A should be spread on top of the strain gauge and wait for at least 15 minutes to add M-coat B. After two hours, electrical tap and liquid sealant should be used to cover and preserve the coated strain gauges.

The complete prepared specimen before concrete casting is shown in Figure 4-14. The specimen consists of the supporting (Big) block and the loading (small) block, where the wall is embedded between the two blocks. The supporting block contains of a steel cage, six 2-1/2 diameter non pressurized plastic pipes with length 76 inches each, the pipes are running from East to the West sides of the supporting block, the purpose of these pipes is to post-tension the supporting block to the strong floor using threaded rods of 2-1/2 inch diameter, the spacing of these pipes or rods is 24 inches in both directions because the typical strong floor holes spacing is 24 inches in both directions. the ends of plastic pipes are confined by several 4-inch by 4-inch stirrups as shown in Figure 4-18.

There are also four 2-inch diameter plastic pipes running from the South to the North faces of the supporting and loading blocks, the aim of these pipes is to hold and tighten the supporting and loading blocks together while flipping the specimen and to prevent any protentional external stress on the wall during overturning the specimen.

The loading block contains four 2-inch diameter plastic pipes spaced by 16 inches in both directions. These pipes are used later to connect the actuator head to the loading block by four post-tensioned rods with 1.5-inch threaded rods diameter.

Concrete casting process is shown in Figure 4-19 to Figure 4-22. First, concrete was poured up to mid height of the supporting block, then up to mid height of the loading block, after that, the wall part is cast and its face smoothed. We do the same of this process for the other specimen, then we come back to the first specimen and fill up both blocks as shown in Figure 4-22. The reason of this process is to give the concrete a time

to harden and reduce pressure on the formwork sides of the supporting block, for additional safety, two ropes were used to tighten all sides of the formwork.

Figure 4-7 Picking up the steel reinforcement order from Commercial Metals Company (CMC), Dallas, TX.

Figure 4-8 Preparing the steel cage of supporting block

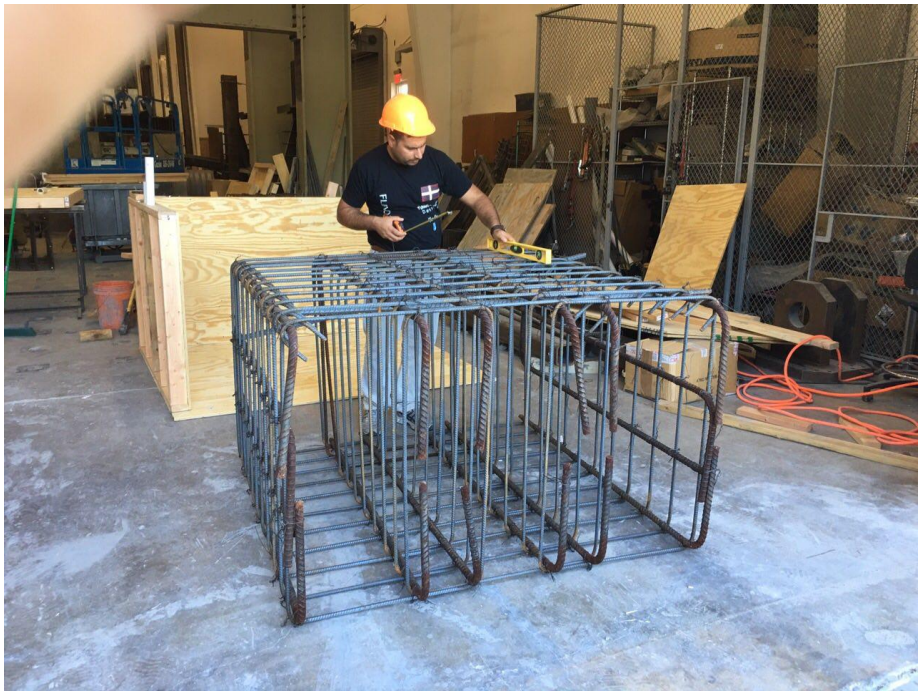

Figure 4-9 The fabricated cage of supporting block.

Figure 4-10 The fabricated cage of loading block.

Figure 4-11 Process to attach strain gages to the longitudinal steel bars.

Figure 4-12 The fabricated wall reinforcement

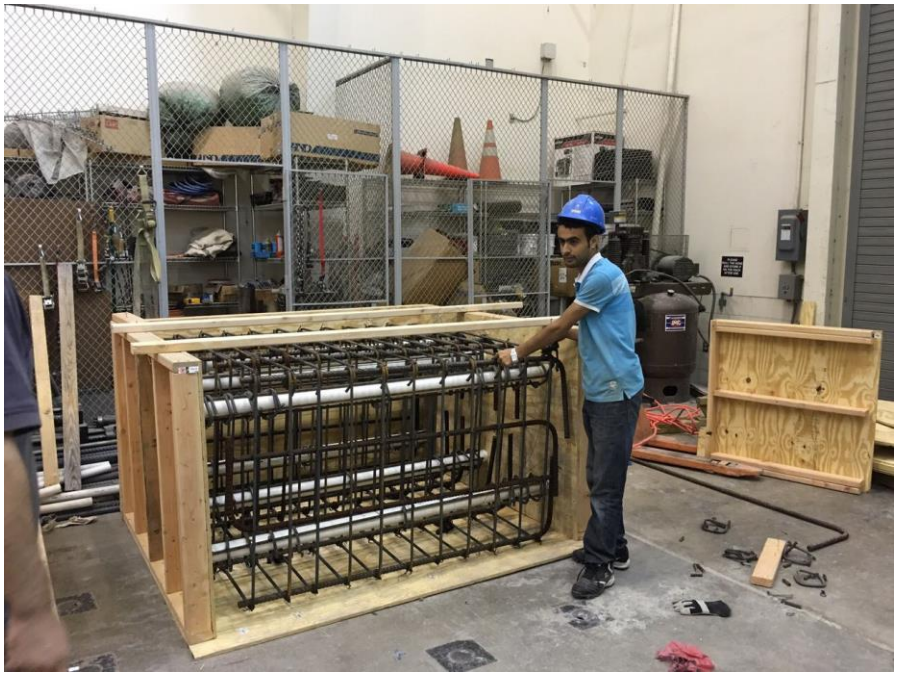

Figure 4-13 Preparing the supporting block (formwork, plastic pipes and steel cage)

Figure 4-14 Complete specimen components before concrete casting.

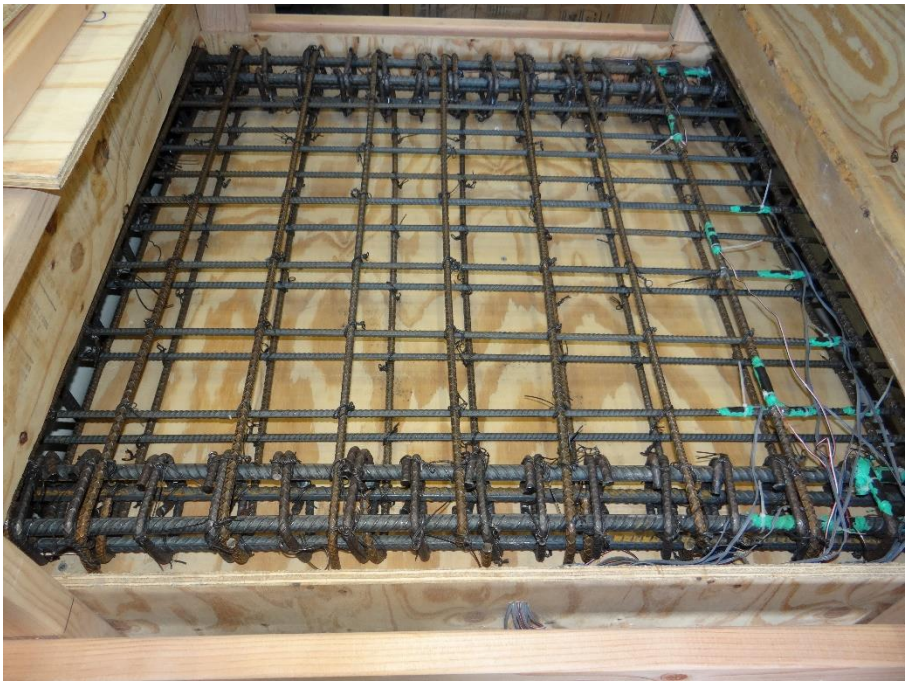

Figure 4-15 The steel reinforcement of wall

Figure 4-16 The steel reinforcement of loading block

Figure 4-17 The steel reinforcement of supporting block

Figure 4-18 Confining hoops around the plastic pipes

Figure 4-19 Concrete casting of supporting block

Figure 4-20 Concrete casting of the wall

Figure 4-21 Smoothening the wall face after concrete casting

Figure 4-22 Finishing the blocks surfaces.

Flipping the specimen process starts at least 28 days after casting the concrete as shown in Figure 4-23 to Figure 4-32. Four ¾-inch diameter used to connect the supporting (big) block to the loading (small) block as shown in Figure 4-23 to Figure 4-26. Another four 2-1/2 inch diameter rods were inserted in the supporting (big) block as shown in Figure 4-23, Figure 4-26, and Figure 4-27. The flipping process starts by connecting the crane chain to the 2-1/2-inch rods located in the supporting block as shown in Figure 4-27.

The forklift is used to simultaneously lift the loading block with supporting block as shown in Figure 4-28. The process gradually overturns the supporting and the loading block until the whole specimen is flipped 90 degrees as shown in Figure 4-29. Later, the specimen is moved to be underneath the actuator frame and the supporting block is post-tensioned to the strong floor by six 2-1/2 inch threaded rods diameter using super bolts as shown in Figure 4-30, at this point the actuator is hooked by two steel chains to the actuator frame (i.e. the actuator head stroke is almost zero inch), the aim of this action is to have enough space to move the specimen under the actuator.

After post-tensioning the super bolts, the chains of the actuator are removed and lowered down until the head touches the top face of the loading block. The head is square already has four 2-inch holes spaced by 16 inches in both directions. The actuator head is tightened to the loading block by four 1.5-inch diameter rods. Two lateral bracing frames are positioned at each face of the loading block as shown in Figure 4-32. Each frame is post-tensioned to the strong floor by two 1.5-inch rods, the post-tensioning force is 60 kips. The frame consists of two 10-inch by 20-inch steel plates to provide lateral bracing for the loading block as shown in Figure 4-33. A general use grease was spread at the contact between lateral bracing frame steel plates and both sides of the loading block to eliminate any frictional forces which might affect on the precise loading value.

Figure 4-23 The West side view of the specimen while preparing to flip the specimen, four rods with 2-1/2 inch diameter were inserted in the supporting block

Figure 4-24 The North side view of the specimen while preparing to flip the specimen, four rods with ¾- inch diameter were inserted to connect the supporting to loading blocks

Figure 4-25 The South side view of the specimen while preparing to flip the specimen, four rods with ¾- inch diameter were inserted to connect the supporting to loading blocks

Figure 4-26 The East side view of the specimen while preparing to flip the specimen, four rods with ¾- inch diameter were inserted to connect the supporting to loading blocks plus four rods with 2-1/2 inch diameter were inserted to flip the supporting block by crane.

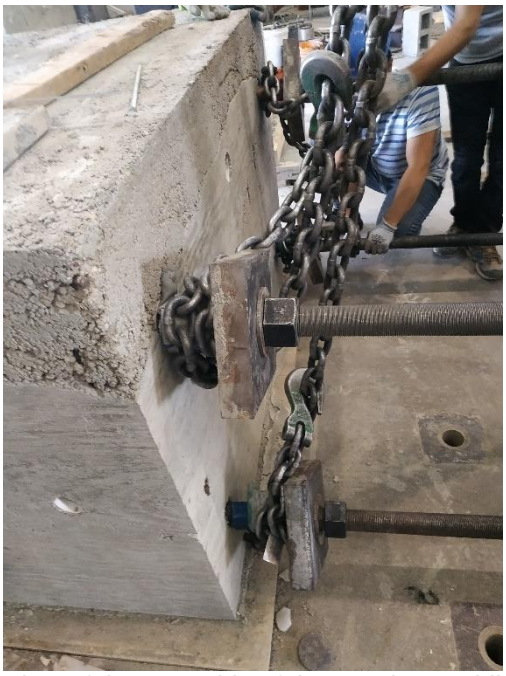

Figure 4-27 A close view of the East side of the specimen while preparing to flip it.

Figure 4-28 Gradually flipping the specimen. The supporting block lifted by crane and the loading block by the forklift, both blocks are connected by ¾-inch diameter rods

Figure 4-29 The specimen after flipping process was completed.

Figure 4-30 The supporting block was post-tensioned to the strong floor by six 2-1/2 inch diameter threaded rods, super bolts where used to apply 130 kips in each threaded rod.

Figure 4-31 Super bolts to apply post-tensioning force on the supporting block rods.

Figure 4-32 Two lateral bracing were used to prevent out-of-plane displacement for both sides of the loading block.

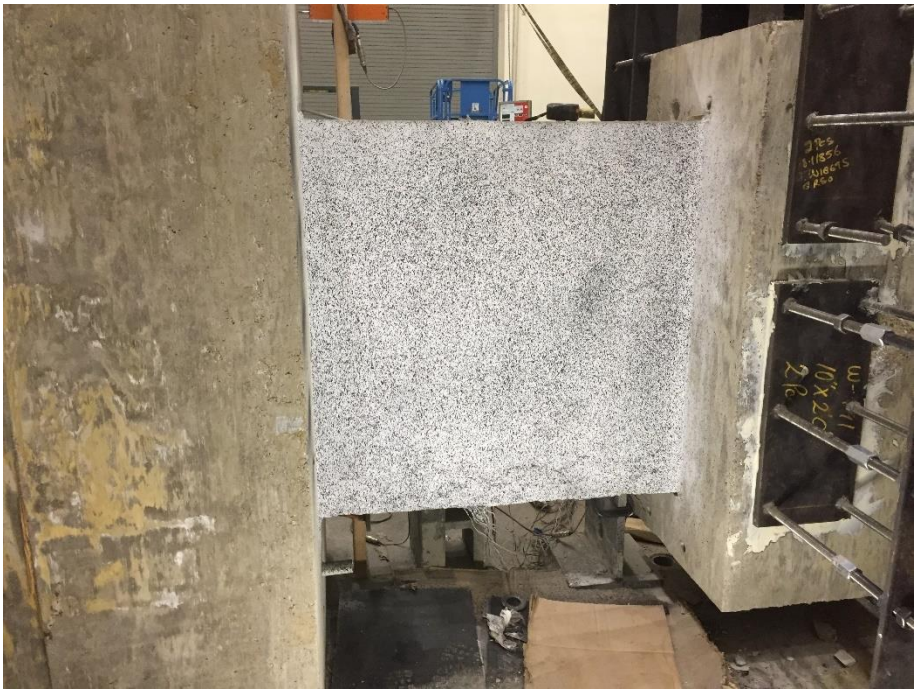

Figure 4-33 The lateral bracing consists of two10-inch by 20-inch steel plates

4.2.2. SW-MP-1.0-1

4.2.2.1. Specimen Design

The vertical reinforcement of specimen SW-MP-1.0-1 is similar to what was provided in specimen SW-MA-1.0, but different horizontal reinforcement layout, where 5-inch-spacing hoops used to confine the vertical reinforcement instead of the horizontal rebars that required by ACI 318-19 provisions. The wall consists of Three small cages at boundaries confined by 2.5-inch-spacing hoops as shown in Figure 4-34, while the wall web contained three wider cages with 5-inch-spacing hoops. The gab between web cages was 5 inches.

The boundaries spacing of 2.75 inches was selected to be consistent to the confinement that provided in specimen SW-MA-1.0, this value was derived based on the scaling of full wall dimensions that are commonly used in practice. The 5-inch spacing of

hoops at wall web was selected to have similar horizontal spacing of specimen SW-MA-1.0.

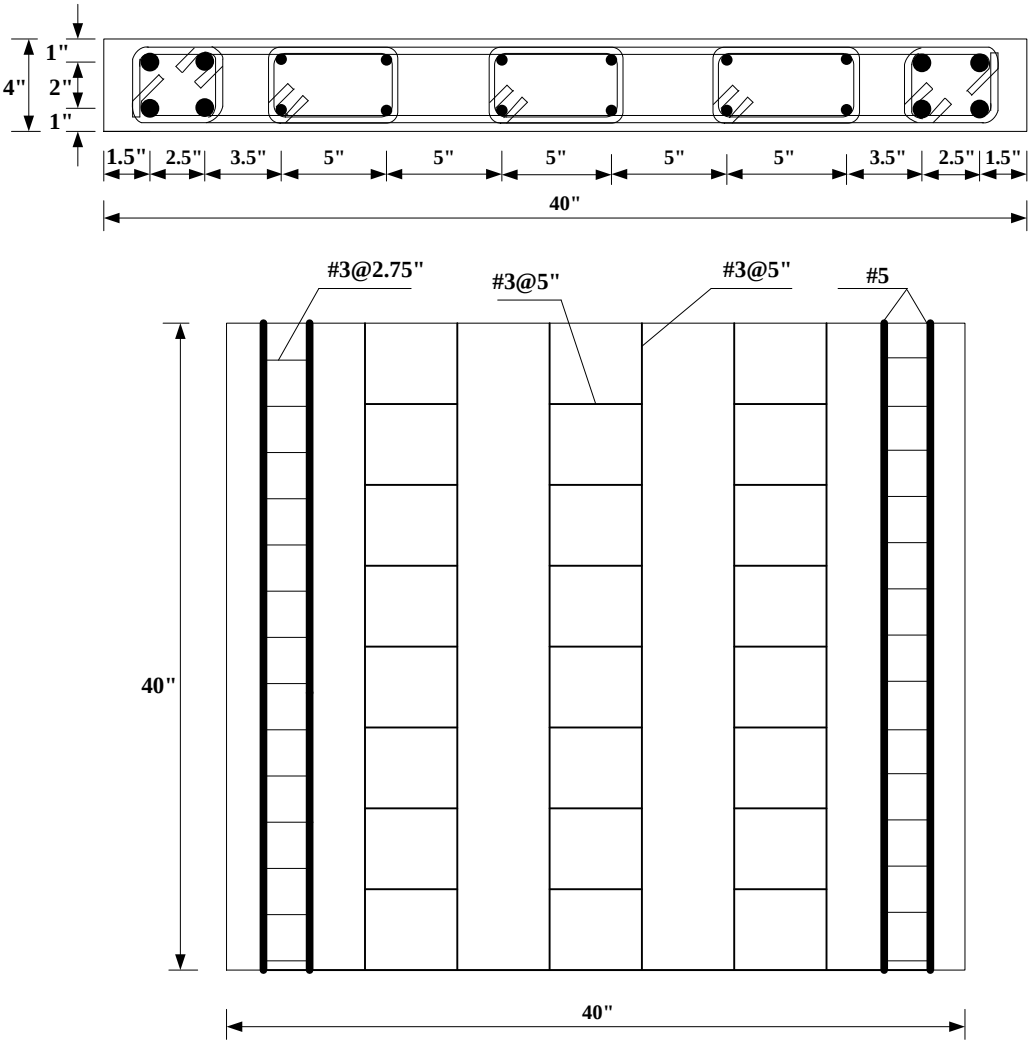

Figure 4-34 Reinforcement layout for specimen SW-MP-1.0-1

4.2.2.2. Strain gauge layout

Twelve strain gauges were attached to the vertical steel rebars which are labeled by the orange color and have designation L1 to L12 as shown in Figure 4-35. Strain gauges were also attached to the hoops which are labeled by blue colors and have designation of S12 to S16.

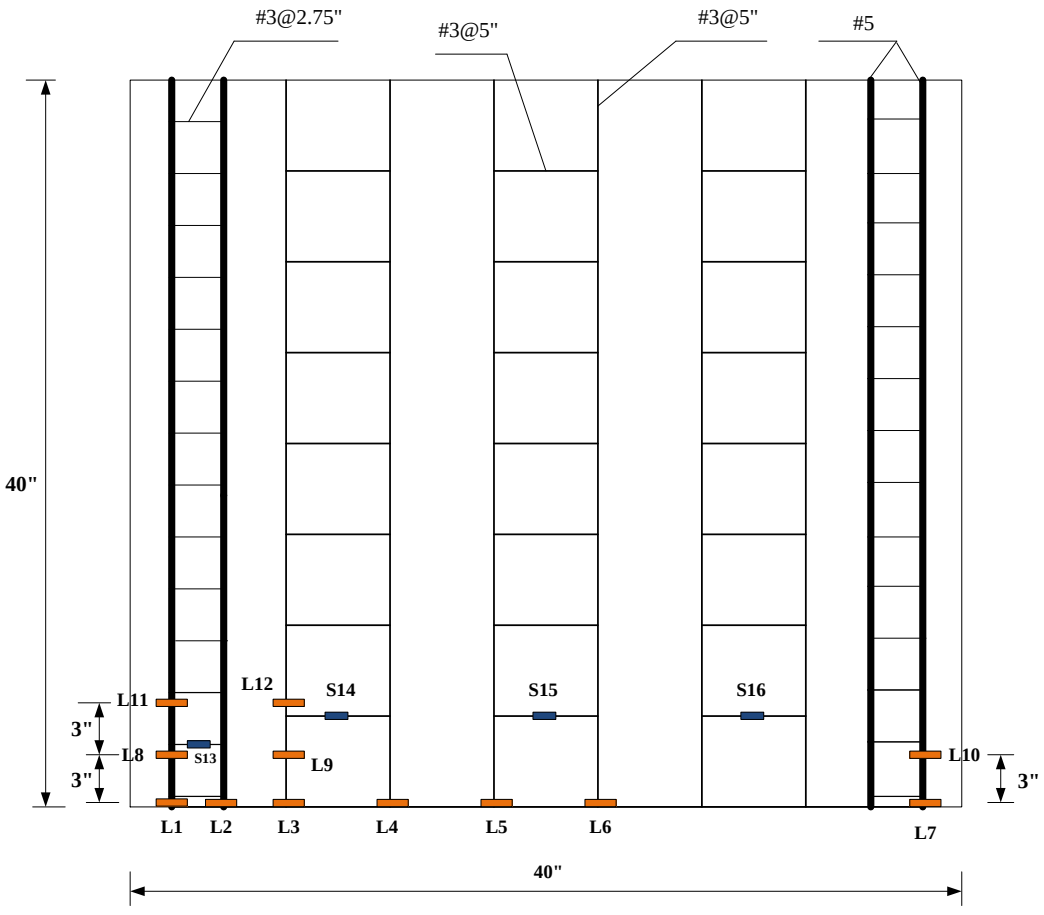

Figure 4-35 Strain gauges layout for specimen SW-MP-1.0-1

4.2.2.3. Specimen preparation

Preparing the web and boundary steel cages are shown in Figure 4-36 and Figure 4-37. The completed framework and reinforcements just before concrete casting are illustrated in Figure 4-38. Concrete casting process is summarized in Figure 4-39 to

Figure 4-42. Basically, both supporting and loading blocks were cast up to the mid height then cast the wall part. After casing the wall, all blocks are filled by concrete. A conical concrete bucket hooked to the crane chain, was utilized to move the concrete to the far parts where the mixer cannot reach. Six concrete cylinders were taken from the same concrete batch that used to cast the wall part.

After overturning the specimen and moving it under the actuation, the supporting block was post-tensioned to the strong floor by six 2-1/2-inch threaded rods diameter. The actuator head was lowered down and tighten it to the loading block. Two latera bracing frames were used to prevent the lateral displacements (Figure 4-43).

Figure 4-36 Preparing the web cages


Figure 4-37 Preparing the boundary cages

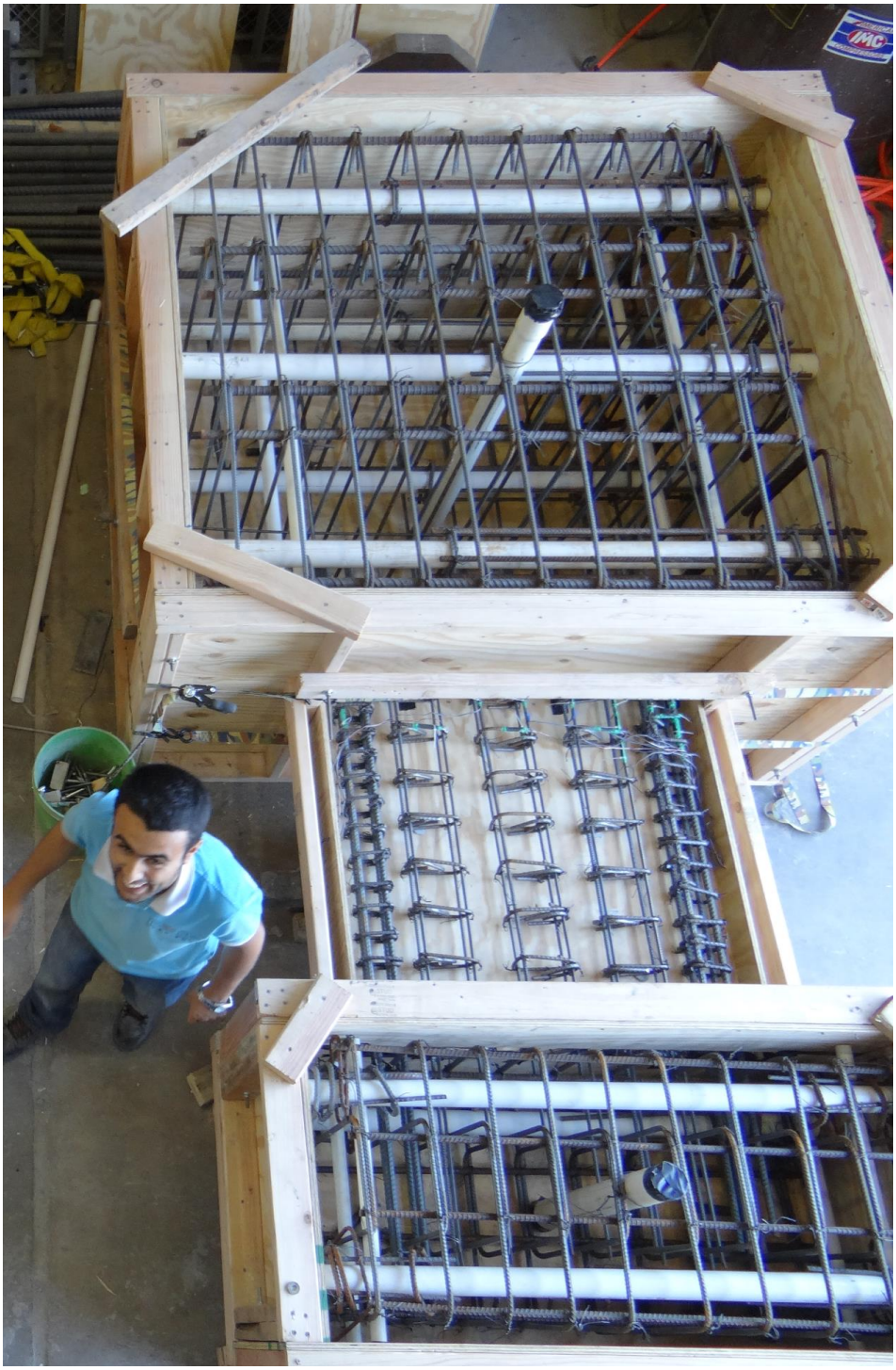

Figure 4-38 Completed construction work, just before casting the concrete

Figure 4-39 Concrete casting of the loading block up to mid height.

Figure 4-40 Concrete casting of the supporting and loading blocks up to mid height and wall casting.

Figure 4-41 Concrete conical bucket to cast concrete

Figure 4-42 Concrete cylinders for test quality control

Figure 4-43 Fully prepared specimen for testing.

4.3. Squat reinforced shear walls with aspect ratio 0.5

Specimens SW-MA-0.5 and SW-MP-0.5 have same amount of vertical steel rebars but different horizontal reinforcement. They were constructed and designed to reach medium shear stress 10 to $12\sqrt{f_{cm}}$; f_{cm} is the measured concrete compressive strength. On the other hand specimen SW-HA-0.5 was designed to reach high shear stress level 18 to $24\sqrt{f_{cm}}$ based on the ACI-compliant provisions, the two proposed walls SW-HP-0.5-1 and SW-HP-0.5-2 were constructed to have similar amount of vertical steel bars area to the ACI- compliant wall SW-HA-0.5 but have different horizontal reinforcement layout; vertical steel bars are uniformly distributed in SW-HP-0.5-1 while some vertical bars were lumped at boundaries of SW-HP-0.5-2.

4.3.1.SW-HA-0.5

4.3.1.1. Specimen Design

Original Specimen Design:

$$f_c' = 6\ ksi,\quad \frac{h_w}{l_w} = \frac{20"}{40"} = 0.5 < 2\ \text{(Squat Shear Wall)},\ t_w = 4"$$

1) Vertical Spacing of hoops in SBE:

$$h_x = \max \text{ spcing of supported bars} < \min \begin{cases} 14\ in \\ \frac{2}{3}b = \frac{2(4)}{3} = 2.67\ in \end{cases} \qquad (Controls)$$

As shown in Fig (1), use $h_x = 2.5\ in < 2.67\ in$ $\qquad (Ok)$

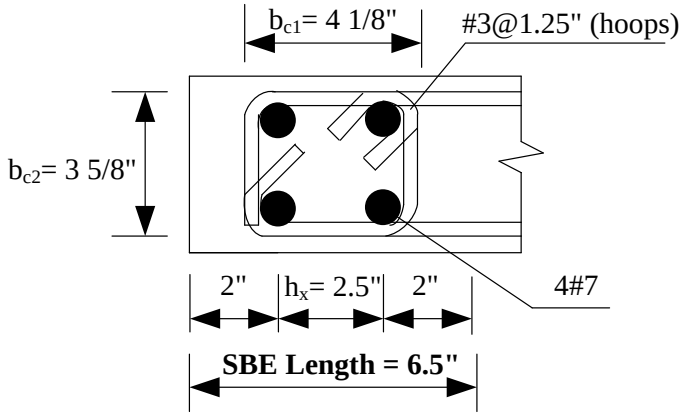

Figure 4-44 Illustration of h_x, length of SBE, b_{c1} and b_{c2}.

$$s = \min \begin{cases} b/3 = 4/3 = 1.33\ in & (Controls) \\ 6d_b = 6(7/8) = 5.25\ in & \\ 4 + \left(\frac{14 - h_x}{3}\right) = 4 + \left(\frac{14 - 2.5}{3}\right) = 7.83\ in & \\ 6\ in & \end{cases}$$

$$use\ s = 1.25\ in < 1.33\ in \quad (Ok)$$

2) Limitations for the amount of transverse reinforcement (18.10.6.4 f):

$$b_{c1} = 2.5 + \frac{7}{8} + 2\left(\frac{3}{8}\right) = 4\ 1/8\ in \quad \left[\text{As shown in Fig (4-44)}\right]$$

$$b_{c2} = 2 + \frac{5}{8} + 2\left(\frac{3}{8}\right) = 3\ 5/8\ in \quad \left[\text{As shown in Fig (4-44)}\right]$$

$$A_{ch} = b_{c1} b_{c2}$$

$$A_{ch} = 4.125(3.625) = 14.95\ in^2$$

$$A_g = 6.5(4) = 26\ in^2$$

(a) Check minimum reinforcement for (b_{c1}) direction:

$$A_{sh1} = \max \text{ of } \begin{cases} 0.09\dfrac{f_c'}{f_{yt}} s b_{c1} \\ 0.3\left(\dfrac{A_g}{A_{ch}} - 1\right)\dfrac{f_c'}{f_{yt}} s b_{c1} \end{cases}$$

$$A_{sh1} = \max \text{ of } \begin{cases} 0.09\dfrac{6}{60}(1.25)(4.125) = 0.046 \\ 0.3\left(\dfrac{26}{14.95} - 1\right)\dfrac{6}{60}(1.25)(4.125) = 0.11 \quad (Controls) \end{cases}$$

Provided steel area $= 2(0.11) = 0.22\ in^2 > 0.11\ in^2$ (Ok)

(*b*) Check minimum reinforcement for (b_{c2}) direction:

$$A_{sh2} = \max \text{ of } \begin{cases} 0.09\dfrac{f_c'}{f_{yt}} sb_{c2} \\ 0.3\left(\dfrac{A_g}{A_{ch}} - 1\right)\dfrac{f_c'}{f_{yt}} sb_{c2} \end{cases}$$

$$A_{sh2} = \max \text{ of } \begin{cases} 0.09\dfrac{6}{60}(1.25)(3.625) = 0.04 \\ 0.3\left(\dfrac{26}{14.95} - 1\right)\dfrac{6}{60}(1.25)(3.625) = 0.1 \quad (\textit{Controls}) \end{cases}$$

Provided steel area $= 2(0.11) = 0.22\ in^2 > 0.1\ in^2$ (*Ok*)

use #3 *hoops*@1.25" spacing.

3) Ultimate shear force (18.10.4.4):

We will use $V_n = 20A_{cw}\sqrt{f_c'}$ instead of using $V_n = 10A_{cw}\sqrt{f_c'}$

$V_n = 20(4)(40)\sqrt{6000}$

$V_n = 247.9$ kips

$V_u = \phi V_n$ (we will drop the value of ϕ)

$V_u = V_n = 247.9$ kips

4) Minimum distributed web reinforcement ratios (18.10.2.1):

a) Longitudinal rebars are #5@3.5" at the web, so:

$$\rho_l = \frac{A_s}{bs} = \frac{2(0.31)}{4(3.5)} = 0.04429 \quad \text{(as shown in Fig 4-45)}$$

b) Horizontal rebars are #4@3.5", so:

$$\rho_t = \frac{A_s}{bs} = \frac{2(0.2)}{4(3.5)} = 0.0285 \quad \text{(as shown in Fig 4-45)}$$

5) Shear Design (18.10.4.1):

$$\phi V_n = \phi A_{cv}(\alpha_c \lambda \sqrt{f_c'} + \rho_t f_y)$$

$$\alpha_c = 3 \text{ for } \frac{h_w}{l_w} = 0.5$$

$$\phi V_n = 0.75(4)(40)\left[3(1)\sqrt{6000} + 0.0285(60000)\right]$$

$$\phi V_n = 233 \text{ kips} < V_u = 247.9 \text{ kips}$$

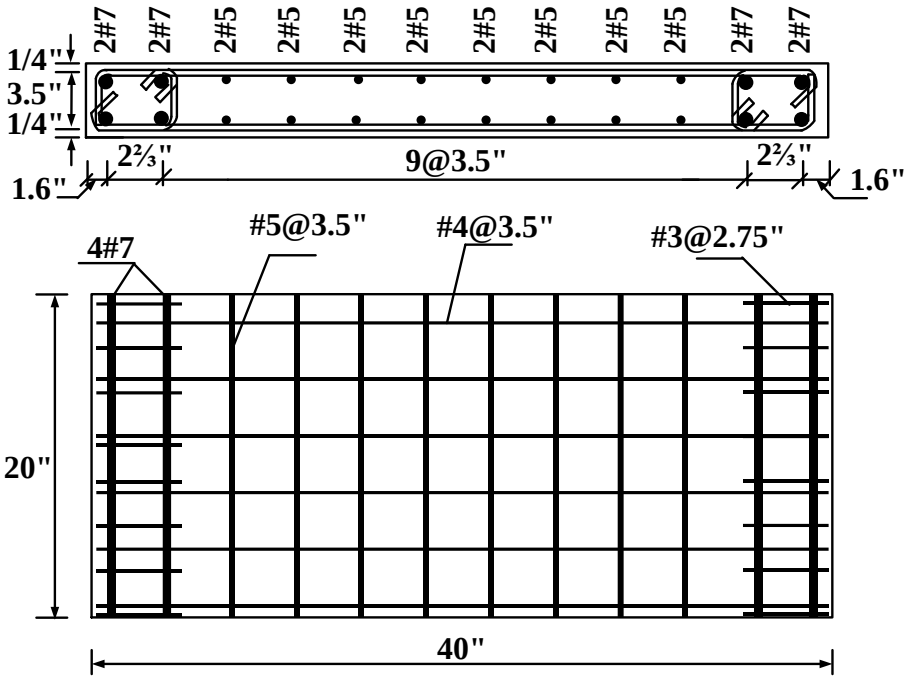

Figure 4-45 Top and side views of shear wall reinforcement for SW-HA-0.5.

Scaled Specimen Design (Six times of original specimen):

A full-scale squat shear wall was used to scale down the required confinement ratio at boundaries, the wall dimensions are 10 ft height, 19 ft length and 2 ft thickness.

$$f_c' = 6\ ksi,\quad \frac{h_w}{l_w} = \frac{10\text{ ft}}{19\text{ ft}} = 0.53 < 2\ \text{(Squat Shear Wall)},\ t_w = 2\text{ ft}$$

1) Vertical Spacing of hoops in SBE:

$$h_x = \max\ \text{spcing of supported bars} < \min\begin{cases} 14\ in \\ \frac{2}{3}b = \frac{2(24)}{3} = 16\ in \end{cases} \qquad (Controls)$$

$$\text{use } h_x = 10\ in < 16\ in \qquad (Ok)$$

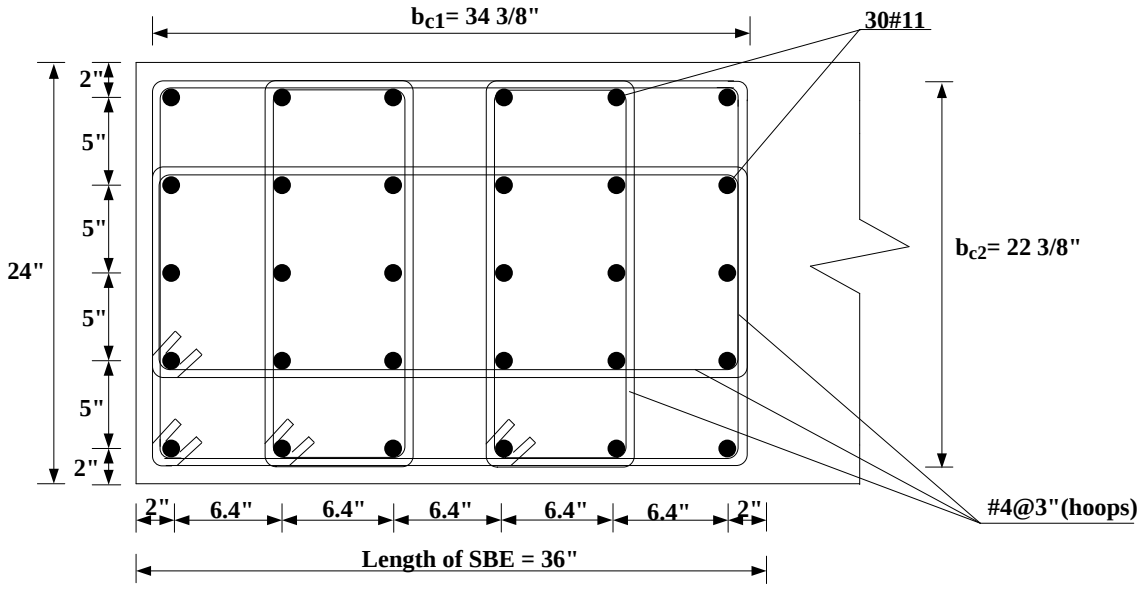

Figure 4-46 Illustration of SBE length.

$$s = \min \begin{cases} b/3 = 24/3 = 8 \ in \\ 6d_b = 6(11/8) = 8.25 \ in \\ 4 + \left(\dfrac{14 - h_x}{3}\right) = 4 + \left(\dfrac{14 - 10}{3}\right) = 5.3 \ in \ (\text{controls}) \\ 6 \ in \end{cases}$$

$$use \ s = 3 \ in < 5.3 \ in \qquad (Ok)$$

2) Limitations for the amount of transverse reinforcement (18.10.6.4 f):

$$b_{c1} = 6.4(5) + \frac{11}{8} + 2\left(\frac{4}{8}\right) = 34.375 \ in \qquad \left[\text{As shown in Fig (4-46)}\right]$$

$$b_{c2} = 5(4) + \frac{11}{8} + 2\left(\frac{4}{8}\right) = 22.375 \ in \qquad \left[\text{As shown in Fig (4-46)}\right]$$

$$A_{ch} = b_{c1} b_{c2}$$

$$A_{ch} = 34.375(22.375) = 769.1 \ in^2$$

$$A_g = 24(36) = 864 \ in^2$$

(*a*) Check minimum reinforcement for (b_{c1}) direction:

$$A_{sh1} = \max \text{ of } \begin{cases} 0.09 \dfrac{f_c'}{f_{yt}} s b_{c1} \\ 0.3\left(\dfrac{A_g}{A_{ch}} - 1\right) \dfrac{f_c'}{f_{yt}} s b_{c1} \end{cases}$$

$$A_{sh1} = \max \text{ of } \begin{cases} 0.09 \dfrac{6}{60}(3)(34.375) = 0.93 \qquad (Controls) \\ 0.3\left(\dfrac{864}{769.1} - 1\right) \dfrac{6}{60}(3)(34.375) = 0.38 \end{cases}$$

Provided steel area $= 6(0.2) = 1.2 \ in^2 > 0.93 \ in^2$ (*Ok*)

(*b*) Check minimum reinforcement for (b_{c2}) direction:

$$A_{sh2} = \max \text{ of } \begin{cases} 0.09\dfrac{f_c^{'}}{f_{yt}} sb_{c2} \\ 0.3\left(\dfrac{A_g}{A_{ch}} - 1\right)\dfrac{f_c^{'}}{f_{yt}} sb_{c2} \end{cases}$$

$$A_{sh2} = \max \text{ of } \begin{cases} 0.09\dfrac{6}{60}(3)(22.375) = 0.61 \ \ (Controls) \\ 0.3\left(\dfrac{864}{769.1} - 1\right)\dfrac{6}{60}(3)(22.375) = 0.25 \end{cases}$$

Provided steel area $= 4(0.2) = 0.8 \ in^2 > 0.61 \ in^2$ (*Ok*)

use #4 *hoops* @ 3" spacing.

Scaling the hoop steel ratio and spacing:

Scaled specimen:

Six #4 legs in b_{c1} direction, and Four #4 legs in b_{c2} direction, as shown in Fig. (4-46), then the steel hoop area ratio (ρ) is:

$$\rho = \frac{A_{s(hoop)}}{b_{c1}s + b_{c2}s} = \frac{6(0.2) + 4(0.2)}{34.375(3) + 22.375(3)} = 1.17\%$$

Original specimen:

Two #3 legs in b_{c1} direction, and Two #3 legs in b_{c2} direction, as shown in Fig. (4-44). We need to get the spacing (s) that makes ρ for scaled specimen is equivelant to ρ for original specimen:

$$\rho = \frac{A_{s(hoop)}}{b_{c1}s + b_{c2}s}$$

$$1.17\% = \frac{2(0.11) + 2(0.11)}{4.125(s) + 3.625(s)}$$

$s = 4.85"$

So, we can use spacing up to 4.85" for small scale specimen.

we willl use s = 2.75"

4.3.1.2. Strain gauge layout

Eight strain gauges were attached to the vertical steel rebars which are labeled by L1 to L8 as shown in Figure 4-47. Strain gauges were also attached to the hoops and horizontal steel bars which are labeled by S9 to S17.

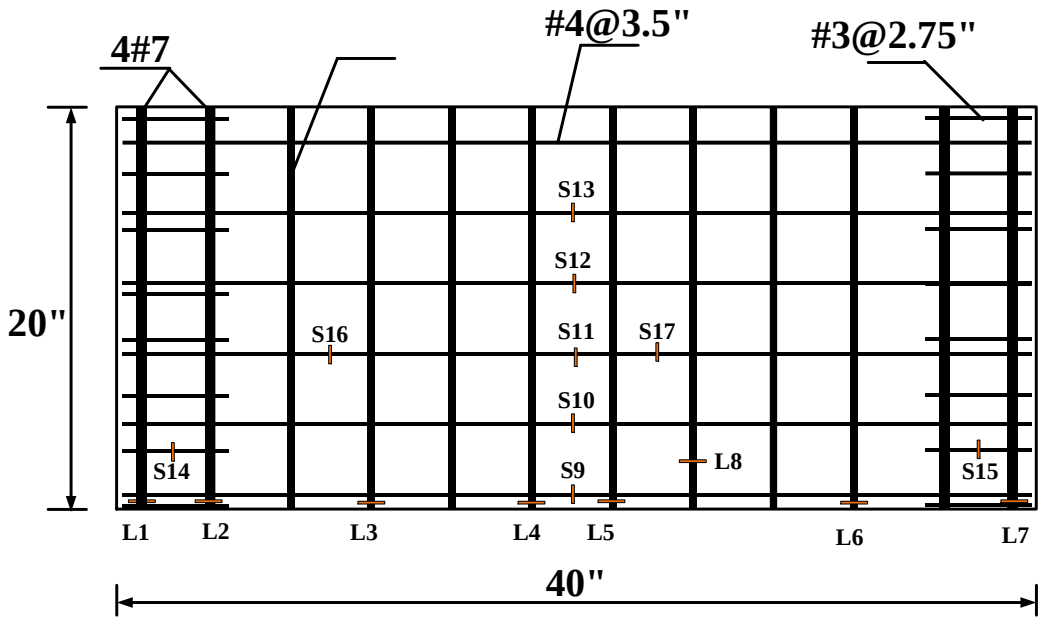

Figure 4-47 Strain gauges layout for specimen SW-HA-0.5

4.3.1.3. Specimen Preparation

Figure 4-48 to Figure 4-58 present the specimen preparation process. Fabrication the boundary cages, horizontal and vertical steel bars are shown in Figure 4-48 to Figure 4-52. After completing the supporting block formwork, the wall and loading block formwork are monolithically connected together as shown in Figure 4-53, the wall reinforcement is inserted from the loading block side since it still has two unclosed sides, then the loading block steel cages is inserted inside the loading block formwork and all remaining sides are closed. Figure 4-54 to Figure 4-58 illustrate the completed specimen right before and after casting the concrete.

Figure 4-48 preparing the boundary steel cages

Figure 4-49 Connecting the horizontal steel bars to the boundaries

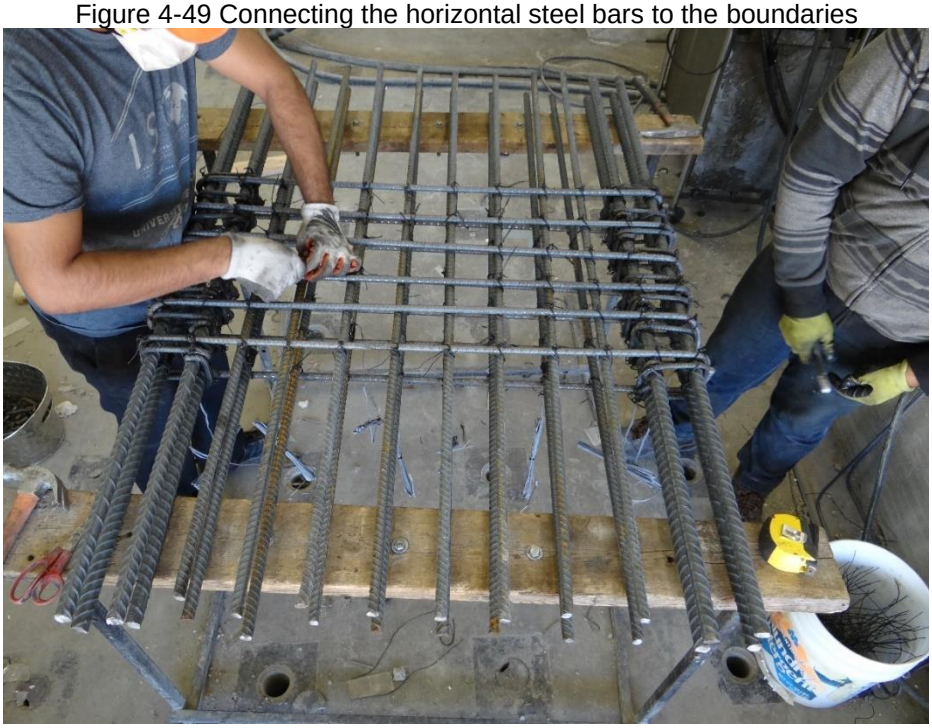

Figure 4-50 Fabricating the wall cage

Figure 4-51 Fully prepared cage reinforcement including the attached strain gauges.

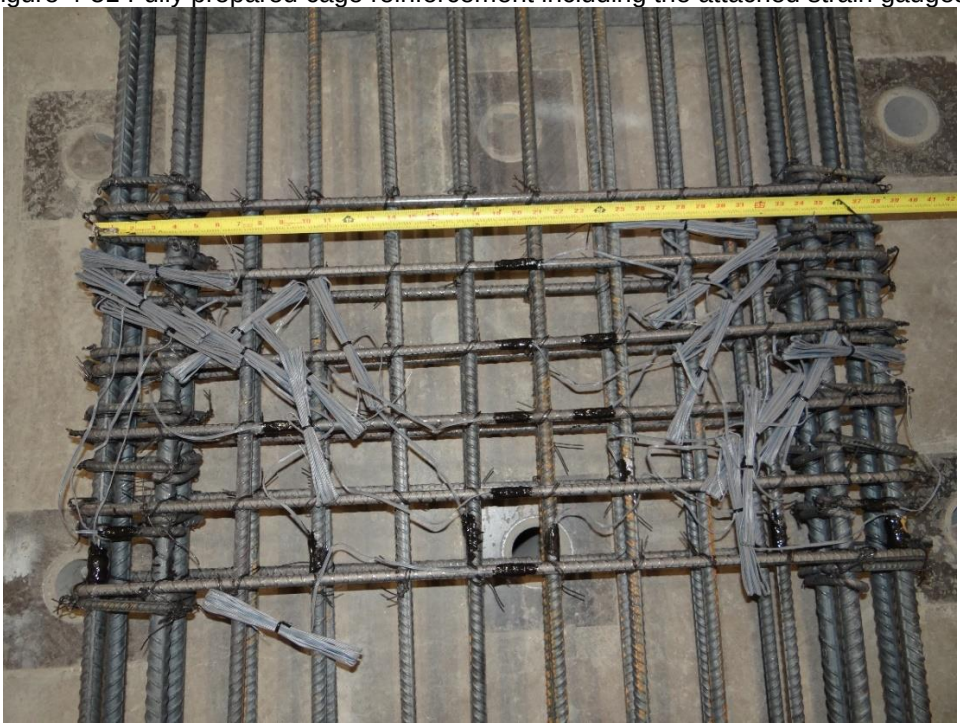

Figure 4-52 Wall length is 40 inches.

Figure 4-53 Specimen formwork

Figure 4-54 Formworks of Supporting and loading blocks

Figure 4-55 Overall steel reinforcement of specimen

Figure 4-56 Wall length is 40 inches.

Figure 4-57 Wall height is 20 inches.

Figure 4-58 Concrete finishing

4.3.2.SW-HP-0.5-1

4.3.2.1. Specimen Design

SW-HP0.5-1 was constructed with closely spaced steel cages at the middle part of the web. The purpose of this modification is to increase the wall confinement capacity, at same time, reinforcements at boundaries are relaxed since forces are believed not critical based on results of Barda (1977) where the concrete at wall web crushes before the boundaries. The wall consists of four cages at wall web and two wider steel cages at boundaries as shown in Figure 4-59.

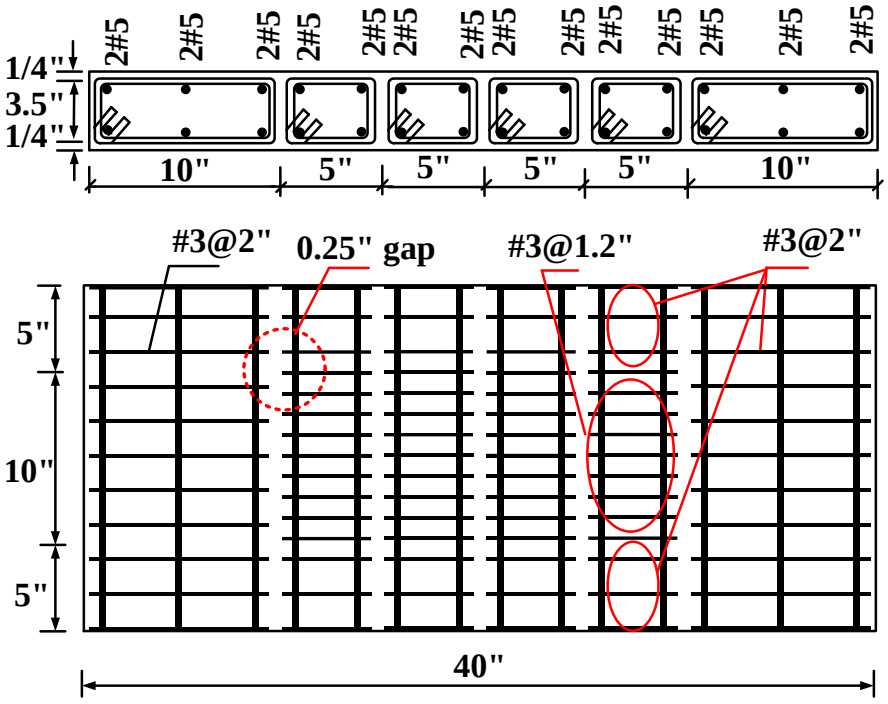

Figure 4-59 Top and side views of shear wall reinforcement for SW-HP-0.5-1.

4.3.2.2. Strain gauge layout

Fourteen strain gauges were attached to the vertical steel rebars which are labeled by L1 to L14 as shown in Figure 4-60. Strain gauges were also attached to the hoops which are labeled by S15 to S19.

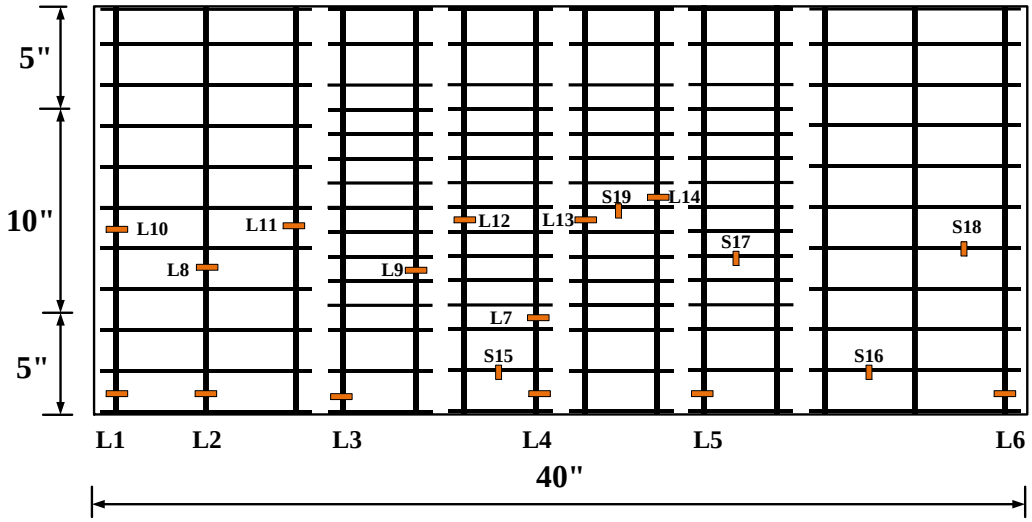

Figure 4-60 Strain gauges layout for specimen SW-MP-1.0-1

4.3.3.SW-HP-0.5-2

4.3.3.1. Specimen Design

After testing SW-HP-0.5-1 which consists of 6 steel cages; the results which explained in Chapter 5 it reached high strength and ductility. However, it is believed that 6 cages will require more efforts to construct the wall on field. Therefore, SW-HP-0.5-2 consists of 4 steel cages to make it easy to construct. Additionally, failure on SW-HP-0.5-1 started at both boundary cages because the number of hoops is not enough to resist shear stresses which were developed at wall boundaries. To avoid this problem, all cages on SW-HP-0.5-2 were provided with closely spaced hoops up to the first 2/3 of wall height. Shear stresses on the top part of wall are minor, so the hoops spacing was

relaxed on the top third of wall. SW-HP-0.5-2 reinforcement layout is shown in Figure 4-61.

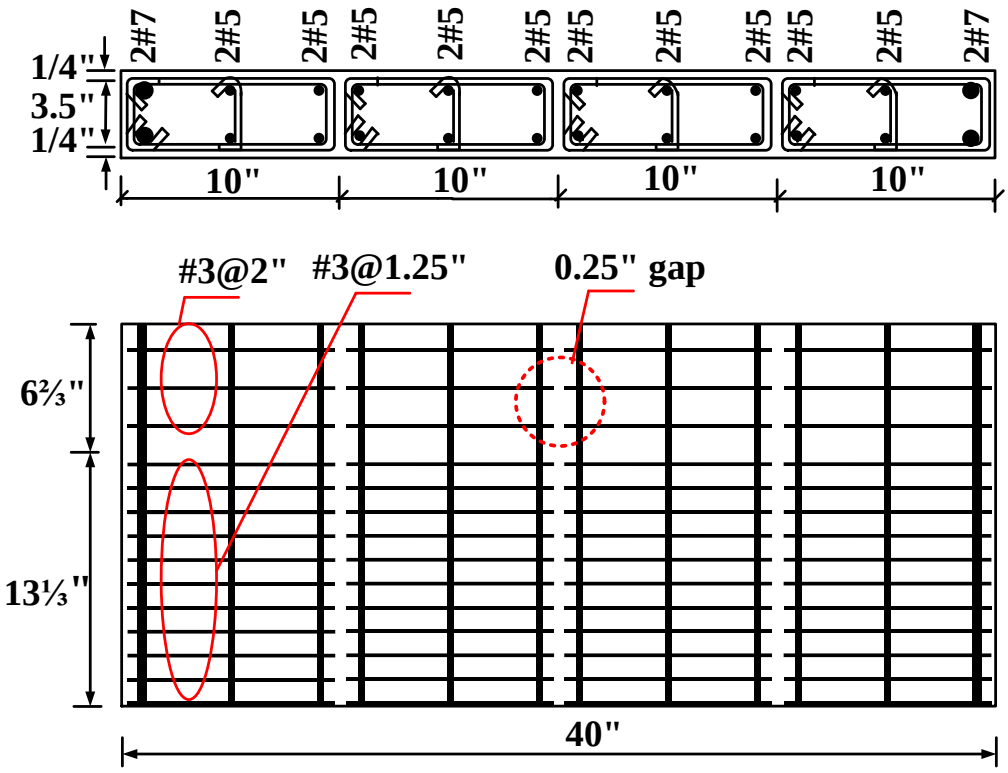

Figure 4-61 Reinforcement layout for specimen SW-HP-0.5-2

4.3.3.2. Strain gauge layout

Six strain gauges were attached to the vertical steel rebars which are labeled by L1 to L6 as shown in Figure 4-62. Strain gauges were also attached to the hoops which are labeled by S7 to S13.

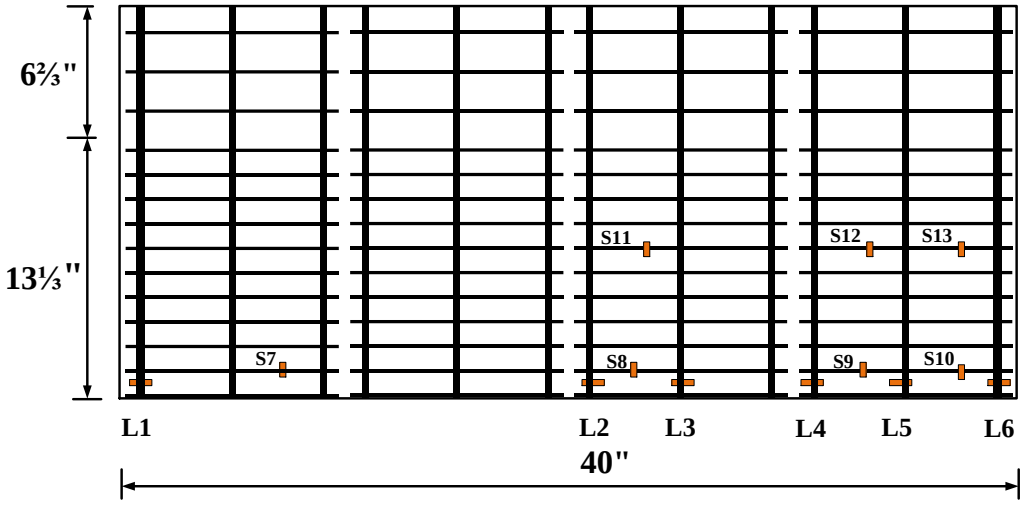

Figure 4-62 Strain gauges layout for specimen SW-MP-1.0-2

4.3.3.3. Specimen preparation

Specimen construction, fabrication, concrete casting and experimental setup before testing are show in Figure 4-63 to Figure 4-71. Strain gauges were attached to the longitudinal steel bars before constructing the steel cages as shown in Figure 4-63.The wall reinforcement consists of four wide steel cages confined by steel hoops with 2- spacing as shown in Figure 4-66. Specimen construction and concrete casting are illustrated in Figure 4-67 to Figure 4-70.

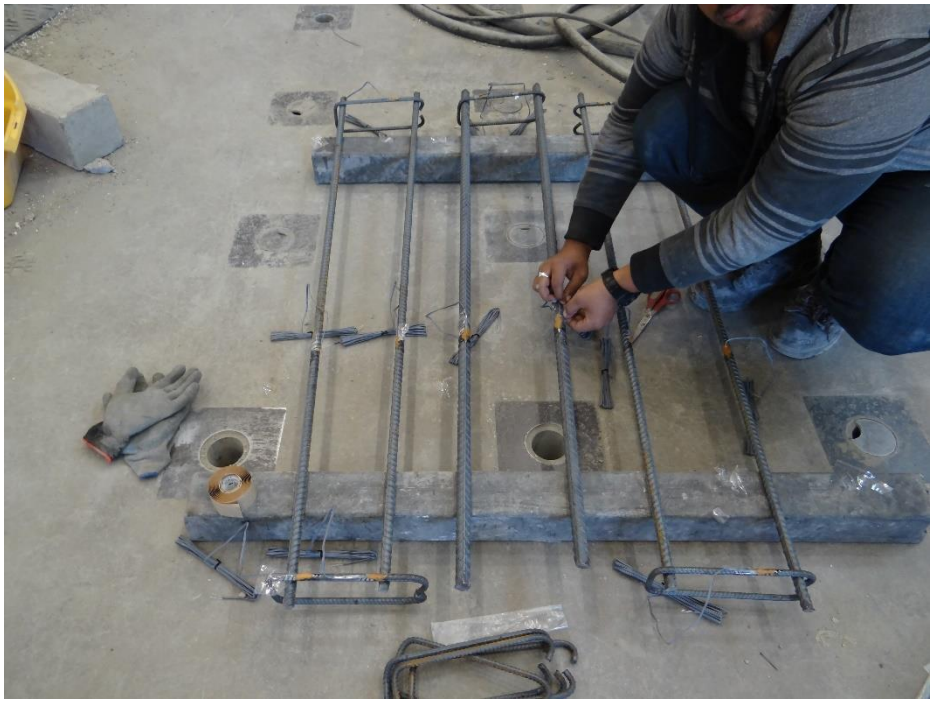

Figure 4-63 Strain gauge attachment process

Figure 4-64 Steel cages to create a wall length of 40 inches.

Figure 4-65 Wall height is 20 inches.

Figure 4-66 Wall thickness is 4 inches.

Figure 4-67 Formwork of the completed specimen

Figure 4-68 Wall length of 40 inches.

Figure 4-69 Wall height of 20 inches.

Figure 4-70 Concrete casting.

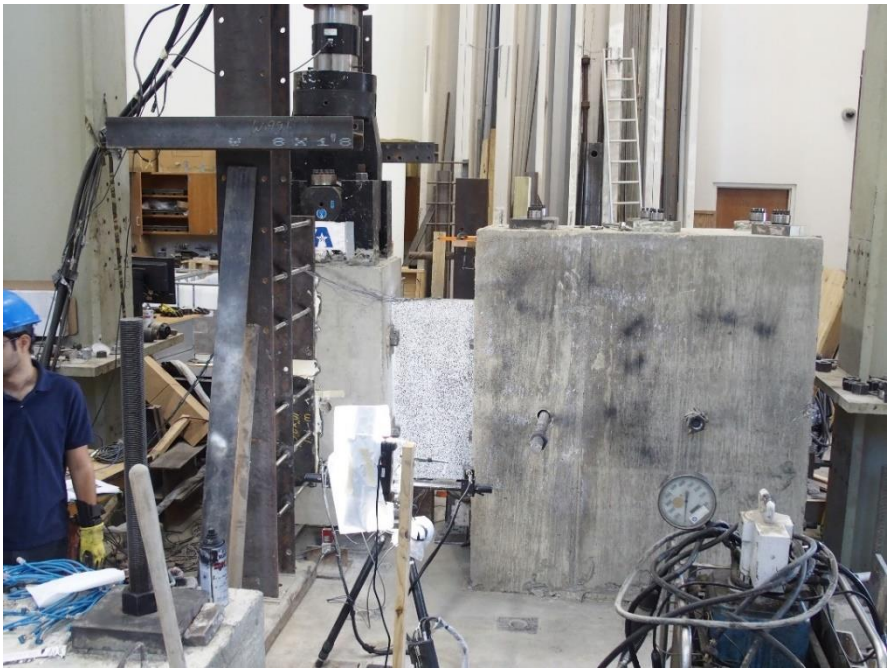

Figure 4-71 Experimental setup before testing

4.3.4.SW-MA-0.5

4.3.4.1. Specimen Design

$$f_c' = 5\ ksi,\quad \frac{h_w}{l_w} = \frac{20"}{40"} = 0.5 < 2\ \text{(Squat Shear Wall)},\ t_w = 4"$$

1) Vertical Spacing of hoops in SBE (18.10.6.4 e):

$$h_x = \max \text{ spcing of supported bars} < \min \begin{cases} 14\ in \\ \frac{2}{3}b = \frac{2(4)}{3} = 2.67\ in \end{cases} \qquad (Controls)$$

As shown in Fig (4-72), use $h_x = 2.67\ in$

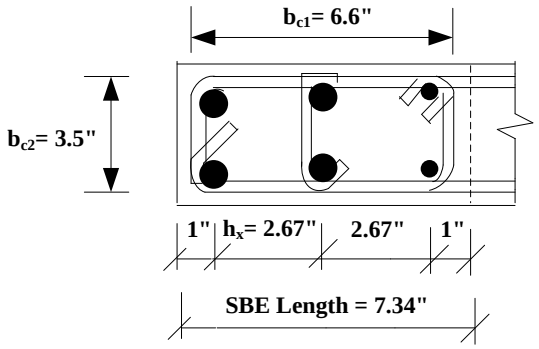

Figure 4-72 Illustration of h_x, length of SBE, b_{c1} and b_{c2}.

$$s = \min \begin{cases} b/3 = 4/3 = 1.33\ in & (Controls) \\ 6d_b = 6(4/8) = 3\ in & \\ 4 + \left(\dfrac{14 - h_x}{3}\right) = 4 + \left(\dfrac{14 - 2.67}{3}\right) = 7.78\ in & \\ 6\ in & \end{cases}$$

$$use\ s = 1.33\ in$$

2) Limitations for the amount of transverse reinforcement (18.10.6.4 f):

$$b_{c1} = 2.67 + 2.67 + \frac{4}{8} + 2\left(\frac{3}{8}\right) = 6.6 \ in \qquad [\text{As shown in Fig (4-72)}]$$

$$b_{c2} = 2.25 + \frac{4}{8} + 2\left(\frac{3}{8}\right) = 3.5 \ in \qquad [\text{As shown in Fig (4-72)}]$$

$$A_{ch} = b_{c1} b_{c2}$$

$$A_{ch} = 6.6(3.5) = 23.1 \ in^2$$

$$A_g = 7.34(4) = 29.4 \ in^2$$

(a) Check minimum reinforcement for (b_{c1}) direction:

$$A_{sh1} = \max \text{ of } \begin{cases} 0.09 \dfrac{f_c'}{f_{yt}} s b_{c1} \\ 0.3\left(\dfrac{A_g}{A_{ch}} - 1\right)\dfrac{f_c'}{f_{yt}} s b_{c1} \end{cases}$$

$$A_{sh1} = \max \text{ of } \begin{cases} 0.09 \dfrac{5}{60}(1.33)(6.6) = 0.066 \\ 0.3\left(\dfrac{29.4}{23.1} - 1\right)\dfrac{5}{60}(1.33)(6.6) = 0.06 \qquad (Controls) \end{cases}$$

Provided steel area $= 3(0.11) = 0.33 \ in^2 > 0.066 \ in^2 \qquad (Ok)$

(*b*) Check minimum reinforcement for (b_{c2}) direction:

$$A_{sh2} = \max \text{ of } \begin{cases} 0.09\dfrac{f_c'}{f_{yt}} s b_{c2} \\ 0.3\left(\dfrac{A_g}{A_{ch}} - 1\right)\dfrac{f_c'}{f_{yt}} s b_{c2} \end{cases}$$

$$A_{sh2} = \max \text{ of } \begin{cases} 0.09\dfrac{5}{60}(1.33)(3.5) = 0.035 \quad (\textit{Controls}) \\ 0.3\left(\dfrac{29.4}{23.1} - 1\right)\dfrac{5}{60}(1.33)(3.5) = 0.032 \end{cases}$$

Provided steel area $= 2(0.11) = 0.22\ in^2 > 0.035\ in^2$ (*Ok*)

use #3 *hoops*@1.33" spacing.

3) Minimum distributed web reinforcement ratios (18.10.2.1):

Horizontal and vertical rebars are #3@4", so:

$\rho_{minimum} = 0.25\%$

$\rho_t = \rho_l = \dfrac{A_s}{bs} = \dfrac{2(0.11)}{4(4)} = 1.375\%$ (as shown in Fig 4-73)

$\rho_t \geq \rho_{minimum}$ (okay)

4) Shear Design (18.10.4.1):

$$V_n = A_{cv}(\alpha_c \lambda \sqrt{f_c'} + \rho_t f_y)$$

$$\alpha_c = 3 \text{ for } \frac{h_w}{l_w} = 0.5$$

$$V_n = 4(40)\left[3(1)\sqrt{5000} + 0.01375(60000)\right]$$

$$V_n = 165 \text{ kips } (14.6A_{cv}\sqrt{f_c'})$$

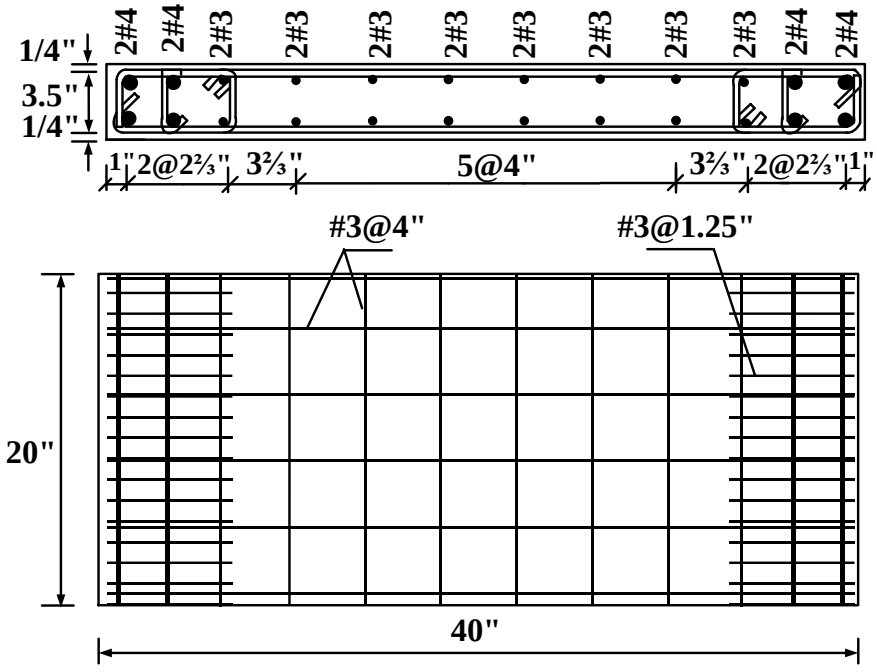

Figure 4-73 Top and side views of shear wall SW-MA-0.5.

Design of SW-MA-0.5 based on the proposed strut and tie model:

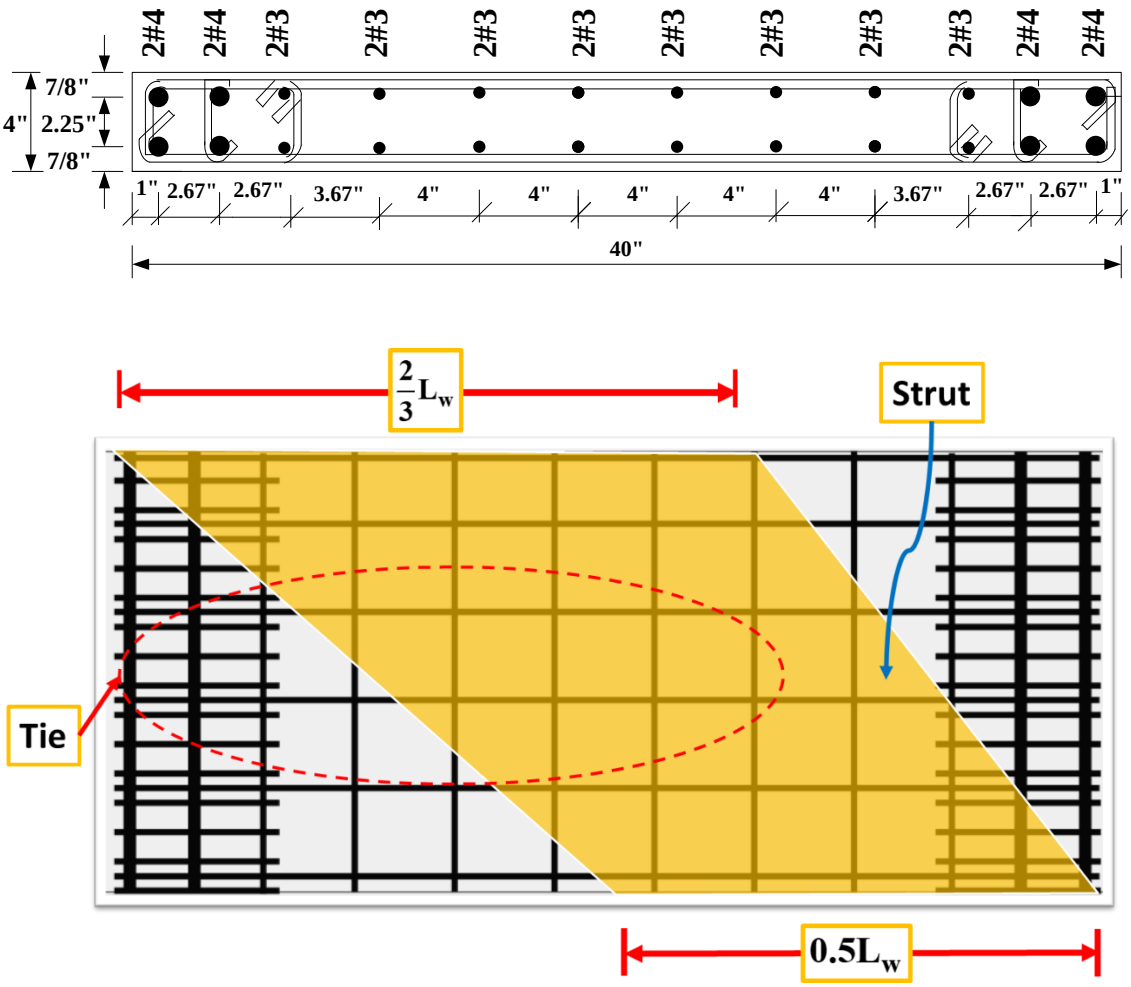

Figure 4-74 Proposed strut and tie model for SW-MA-0.5.

1- Tie strength (Figure 4-74)

$V_{tie} = 2/3A_{sv}F_{yv}$

$2/3A_{sv} = 4\#4 + 12\#3 = 4(0.2)+12(0.11) = 2.12\ in^2$

$V_{tie} = 2.12(60) = 127.2$ kips

2- Strut strength (Figure 4-74)

$V_{strut} = 0.6(0.85)(A_w/2)(f'_c)\cos(45) + 0.5A_{sh}F_{yh}$

$V_{strut} = 0.6(0.85)(40(4)/2)(5)\cos(45) + 0.5(6)(2)(0.11)(60)$

$V_{strut} = 183$ kips

3- Expected SW-MA-0.5 shear strength

The strut strength is 183 kips, and the tie strength is 127.2 kips. The expected strength of the shear wall is the minimum of 183 and 127.2 kips, so the wall shear strength is 127.2 kips. Although the strut is stronger than the tie, the wall will reach the tie strength, 127.2 kips and the strut would deteriorate quickly which leads to reduce the wall drift ductility.

4.3.4.2. Strain gauge layout

Thirteen strain gauges were attached to the vertical steel rebars which are labeled by L1 to L3 as shown in Figure 4-75. Strain gauges were also attached to the hoops and horizontal steel bars which are labeled by S14 to S20.

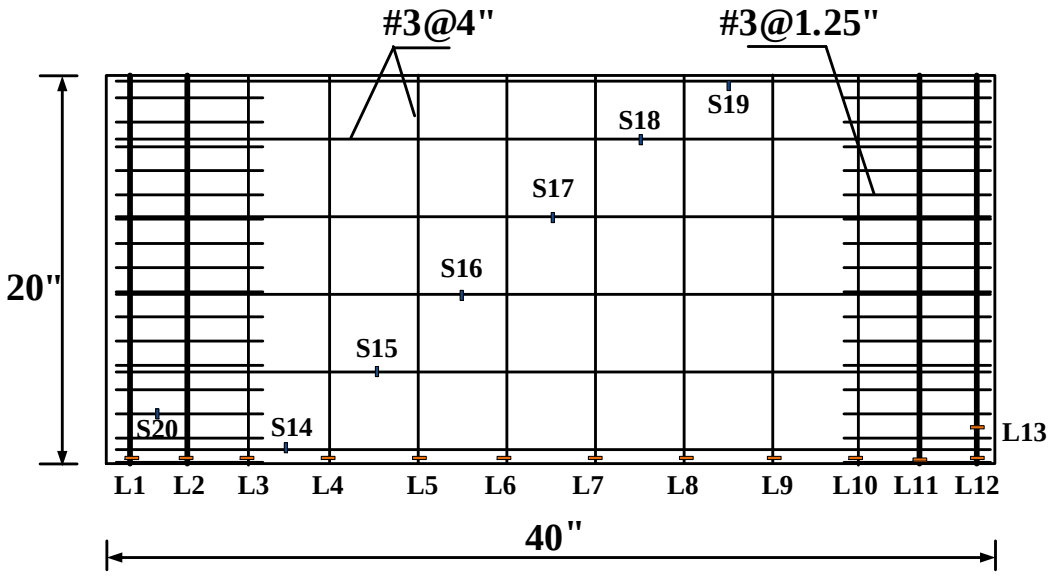

Figure 4-75 Strain gauges layout for specimen SW-MA-0.5

4.3.4.3. Specimen preparation

Specimen preparation, concrete casting and test setup are shown in Figure 4-76 to Figure 4-83. Supporting block components of steel and plastic pipes are shown in Figure 4-77 to Figure 4-78 where six 2-1/2-inch diameter plastic pipes running from north to the south of Figure 4-78 and 4 2-inch diameter plastic pipes running from the east to the west to hold the supporting and loading blocks together while flipping the specimen. Figure 4-79 shows rope used as extra safety to prevent the supporting block to open during concrete casting.

Figure 4-76 Completed formwork and reinforcement fabrication

Figure 4-77 Supporting block reinforcement cages and plastic pipes

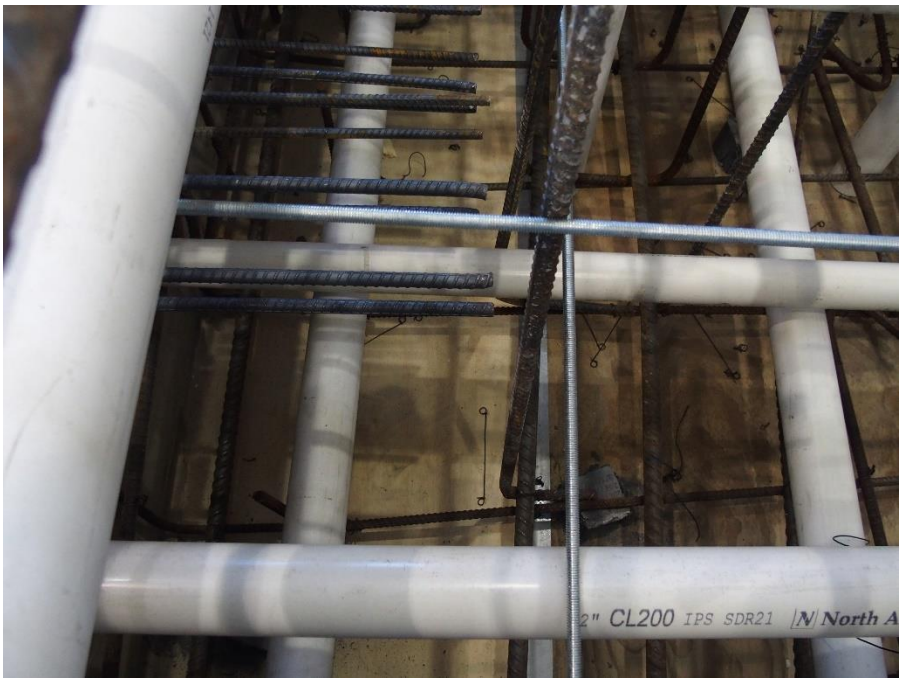

Figure 4-78 A close view of plastic pipe inside the supporting block

Figure 4-79 Rope used as extra safety to prevent the supporting block to open during concrete casting

Figure 4-80 Concrete casting

Figure 4-81 Moving the specimen

Figure 4-82 Specimen near to the actuator.

Figure 4-83 Specimen setup

4.3.5.SW-MP-0.5

4.3.5.1. Specimen Design

Specimen Design:

SW-MP-0.5 is reinforced by four cages, the number of vertical bars is same as that provided in SW-MA-0.5 (ACI compliant) wall, as shown in Figure 4-84. The vertical bars are enclosed by #3@1.25” hoops up to two thirds of the wall height, the hoops spacing is relaxed on the remaining wall height (#3@2” hoops).

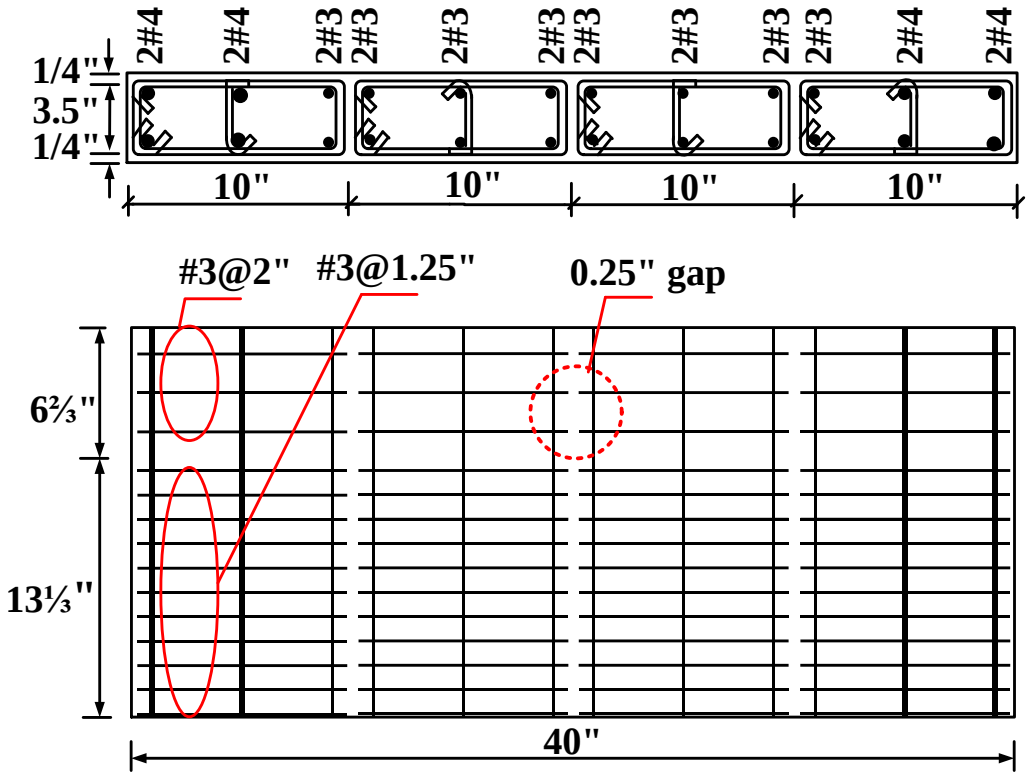

Figure 4-84 Top and side views of shear wall SW-MP-0.5.

Design of SW-MP-0.5 based on the proposed strut and tie model:

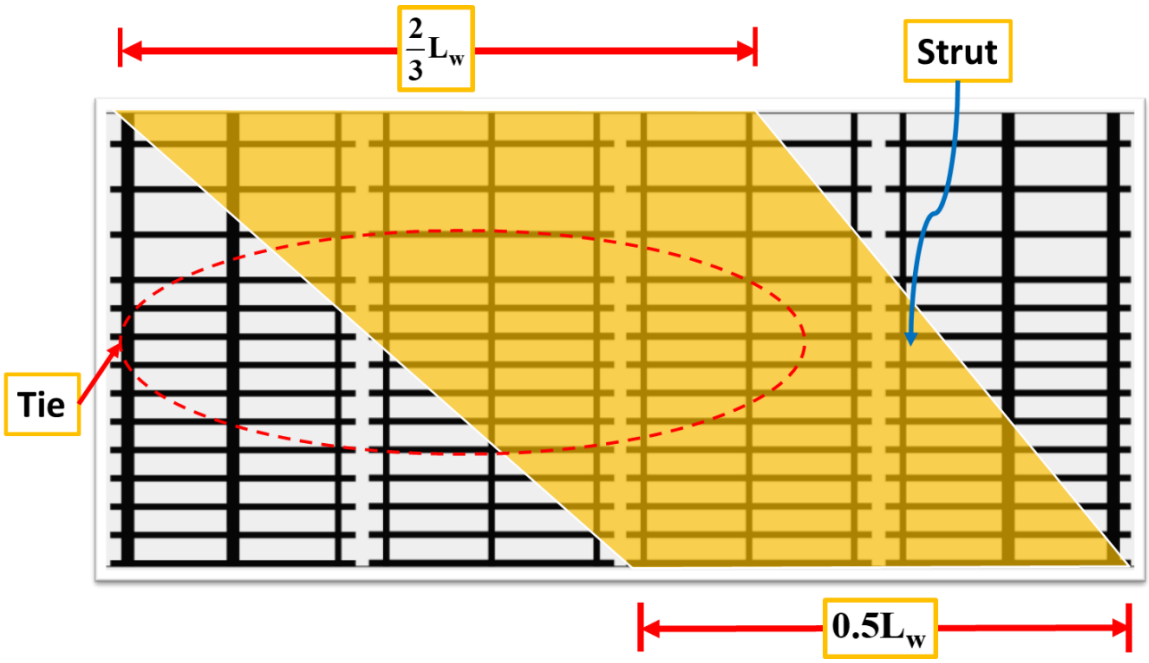

Figure 4-85 Proposed strut and tie model for SW-MP-0.5.

1- Tie strength (Figure 4-85)

$V_{tie} = 2/3A_{sv}F_{yv}$

$2/3A_{sv}$ = 4#4 + 12#3 = 4(0.2) + 12(0.11) = 2.12 in^2

V_{tie} = 2.12(60) = 127.2 kips

2- Strut strength:

Figure 4-85 shows that the strut width is 0.5 L_w, two cages are devoted to carry compressive forces in the strut at a certain drift ratio, and they should be designed by ACI columns limitations. Therefore, steel cages shall be confined by hoops according to section ACI 18.7.5.4:

K_f = f'c/25000+0.6 ≥1.0 , where f'c = 5000 psi

K_f = 5000/25000+0.6 = 0.8 ≥1.0, so k_f = 1.0

$K_n = n_l/(n_l-2)$, where n_l is the number of longitudinal steel bars that are supported by hoops or ties, n_l =6

K_n = 6/(6-2) = 1.5

Two cages will carry the shear forces at a certain drift ratio. Since the tie strength is 127.2 kips, the total compressive forces on struts are equal the tie strength, 127.2 kips, because the angle between the strut and the tie is almost 45 degrees. Therefore, each cage will carry a compressive force (P_u) of 127.2/2 =63.6 kips.

$$b_{c1} = 4.75 + 4.75 = 9 \text{ in. as shown in Fig (4-86)}$$

$$b_{c2} = 2.25 + \frac{4}{8} + 2\left(\frac{3}{8}\right) = 3.5 \text{ in. as shown in Fig (4-86)}$$

$$A_{ch} = b_{c1} b_{c2}$$

$$A_{ch} = 9(3.5) = 31.5 \text{ in}^2$$

$$A_g = 10(4) = 40 \text{ in}^2$$

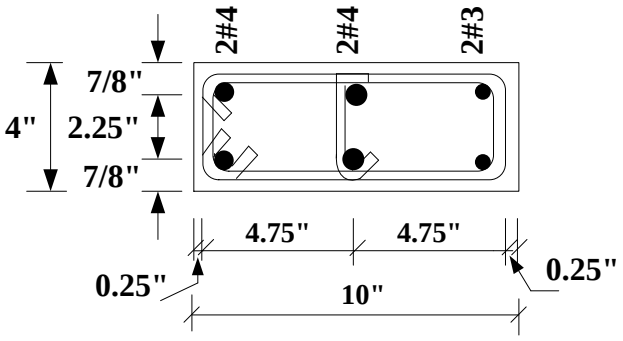

Figure 4-86 Dimensions of a typical steel cage.

(*a*) Check minimum reinforcement for (b_{c1}) direction:

$$A_{sh1} = \max \text{ of } \begin{cases} 0.09\dfrac{f_c'}{f_{yt}} sb_{c1} \\ 0.3\left(\dfrac{A_g}{A_{ch}} - 1\right)\dfrac{f_c'}{f_{yt}} sb_{c1} \\ 0.2k_f k_n \dfrac{P_u}{f_{yt} A_{ch}} \end{cases}$$

$$A_{sh1} = \max \text{ of } \begin{cases} 0.09\dfrac{5}{60}(2.5)(9.5) = 0.18 \\ 0.3\left(\dfrac{40}{31.5} - 1\right)\dfrac{5}{60}(2.5)(9.5) = 0.16 \\ 0.2(1)(1.5)\dfrac{63.6}{60(31.5)}(2.5)(9.5) = 0.24 \text{ in}^2 \text{ (controls)} \end{cases}$$

Provided steel area $= 3(0.11) = 0.33\ in^2 > 0.24\ in^2$ (*Ok*)

(*b*) Check minimum reinforcement for (b_{c2}) direction:

$$A_{sh2} = \max \text{ of } \begin{cases} 0.09\dfrac{f_c'}{f_{yt}} sb_{c2} \\ 0.3\left(\dfrac{A_g}{A_{ch}} - 1\right)\dfrac{f_c'}{f_{yt}} sb_{c2} \\ 0.2k_f k_n \dfrac{P_u}{f_{yt} A_{ch}} \end{cases}$$

$$A_{sh2} = \max \text{ of } \begin{cases} 0.09\dfrac{5}{60}(2.5)(3.5) = 0.07 \\ 0.3\left(\dfrac{40}{31.5} - 1\right)\dfrac{5}{60}(2.5)(3.5) = 0.06 \\ 0.2(1)(1.5)\dfrac{63.6}{60(31.5)}(2.5)(3.5) = 0.09 \text{ in}^2 \text{ (controls)} \end{cases}$$

$$\text{Provided steel area} = 2(0.11) = 0.22 \ in^2 > 0.09 \ in^2 \qquad (Ok)$$

$$use \ \#3 \ hoops @ 2.5" \text{ spacing.}$$

Although the required hoop reinforcement is #3@2.5", the authors decided to reduce hoop spacing to be #3@1.25" to see how much improvement on drift ductility, and if the wall could reach a drift ratio more than 2% without significant deterioration on shear strength.

There is no need to calculate V_{strut} as long as hoops of steel cages satisfy ACI confinement provisions in section ACI 18.7.5.4, which already has been calculated on this section.

3- Expected SW-MP-0.5 shear strength

The strength of SW-MP-0.5 is controlled by tie strength, 127.2 kips, but it is expected to reach a higher drift ratio compared to SW-MA-0.5, because the strut is well-confined and capable to sustain shear strength at high drift ratios.

4.3.5.2. Strain gauge layout

Thirteen strain gauges were attached to the vertical steel rebars which are labeled by L1 to L3 as shown in Figure 4-87. Strain gauges were also attached to the hoops which are labeled by S14 to S20.

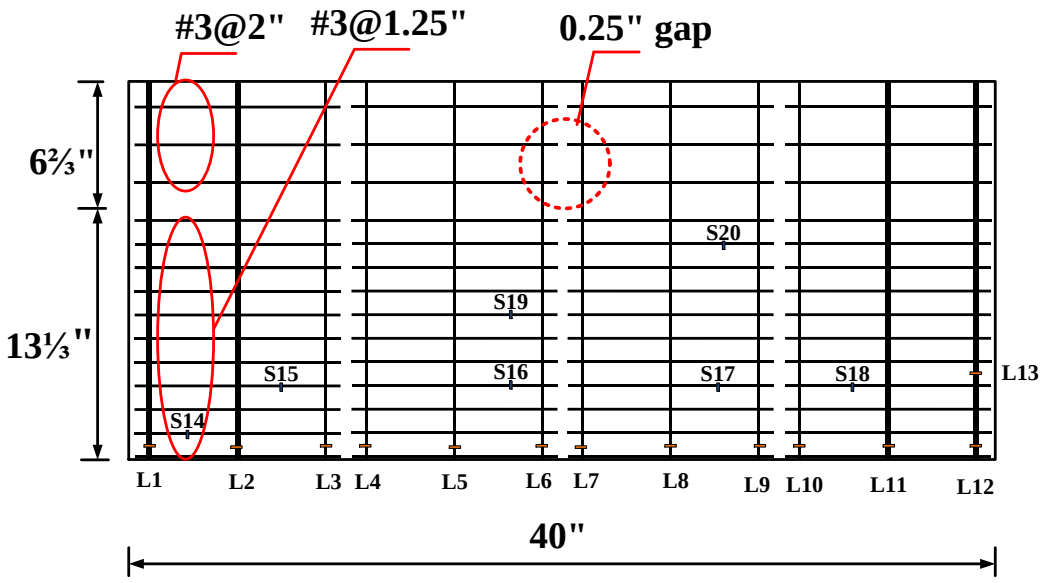

Figure 4-87 Strain gauges layout for specimen SW-MP-0.5

4.3.5.3. Specimen preparation

Plywood of 2 in. (51 mm) by 4 in. (102 mm) were used to make specimen formwork, the wall dimensions are 40 in. (1016 mm) length by 20 in. (508 mm) by 4 in. (102 mm) thickness, the supporting block is 64 in. (1626 mm) length by 72 in. (1829 mm) height by 43 in. (1092 mm) thickness. The formwork of wall and the blocks are connected to monolithically cast the specimen components. Ready-mix concrete was used. The ordered concrete compressive and steel yield strength were 5000 (34.5 MPa) and 60,000 psi (414 MPa), respectively. Figure 4-88 to Figure 4-91 show the construction of

specimen. The wall consist of four wide steel cages confined by stirrups with spacing 1.25 inch up to 2/3 wall length and spacing relaxed to 2 inches at the remaining wall height as shown in Figure 4-88, the bottom side of Figure 4-88 is the supporting block while the top side is the loading block. Concrete casting process is shown in Figure 4-89 to Figure 4-91. The connection between head of the actuator and the loading block is illustrated in Figure 4-92, while the lateral bracing frames are shown in Figure 4-93 to prevent the out-of-plane displacement of loading block while testing. Test setup is shown in Figure 4-94.

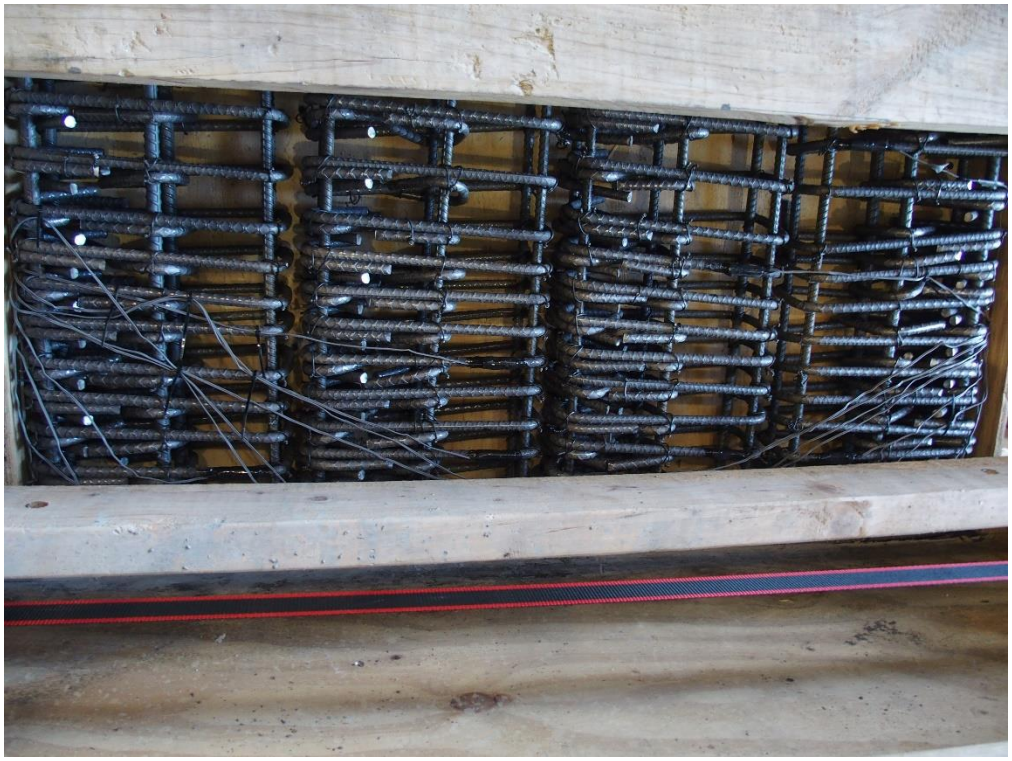

Figure 4-88 Wall reinforcement

Figure 4-89 Concrete flowing from the loading block toward the wall

Figure 4-90 Casting the supporting block

Figure 4-91 Interface between the loading block and the wall

Figure 4-92 Connected actuator head to the loading block

Figure 4-93 Lateral bracing frame

Figure 4-94 Test setup and DIC system

4.4. Specimen setup and instrumentation

The specimens were cast horizontally, then flipped and positioned in the test setup, the supporting block was posttensioned to the strong floor by six threaded rods (Figure 4-95), the loading block was posttensioned to the actuator by four threaded rods, two lateral bracing frames were used to prevent any out-of-plane displacements as shown in Figure 4-96. The walls were tested by single curvature using a vertical actuator to apply displacement reversals at the centroid of loading block which transmits uniform shear forces to the wall. The loading block is laterally supported at both sides to prevent any out-of-plane rotations during the test.

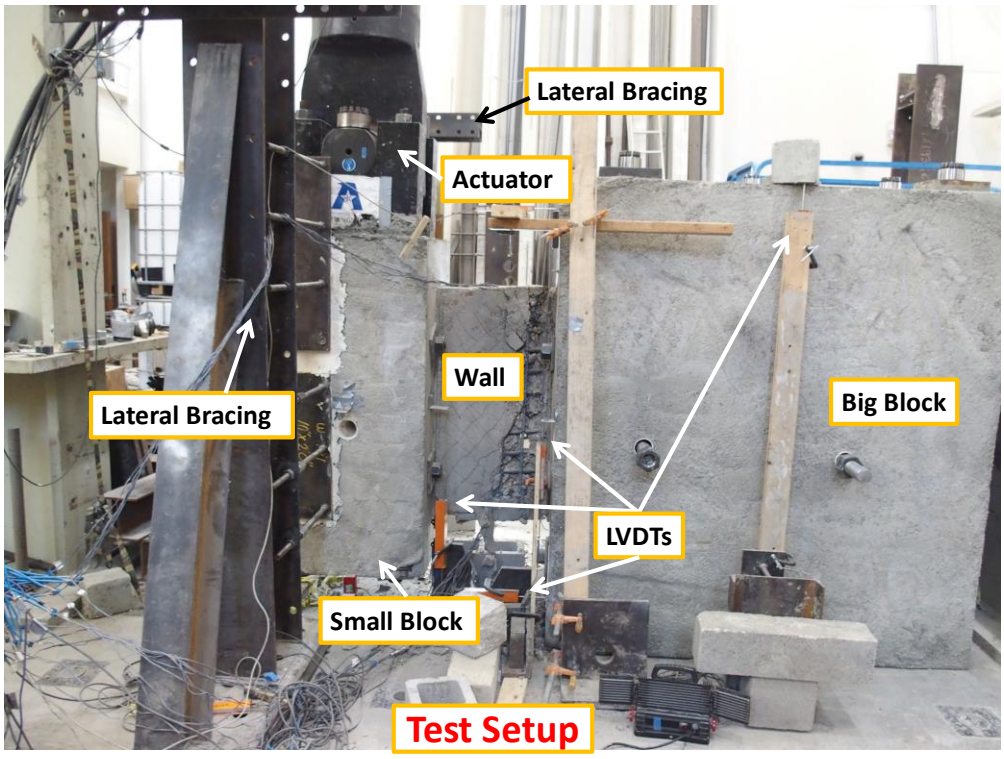

Figure 4-95 Specimen setup

Figure 4-96 Specimen setup Overview

Deformation of the specimens were measured by Digital Image Correlation (DIC) and Linear variable differential transformers (LVDTs). One face of each wall was painted by white color then black dots to allow the DIC to compute strain distribution during the test.

The LVDTs were attached at the other face of each wall, the displacement at the line of force action equals the average of LVDT displacement at wall-to-loading block interface (LVDT 1) and the LVDT displacement at the outer face of loading block LVDT 2. To deduct the supporting block movement during the test, the net deformation of walls equals the displacement at line of force action minus the wall-to-supporting block displacement (LVDT 3). LVDT 4 and LVDT 5 are at attached at top and bottom sides of the supporting block to measure the block rotation during the test. LVDT 6 was provided to measure the displacement at center of supporting block, this LVDT displacement

provided as a backup results in case of crushing the supporting block-to-wall interface which might result of inaccurate wall movement during the test, both LVDT 3 and LVDT 6 shall have the same displacement results. The wall drift ratio was calculated as the wall net deformation divided by distance from wall-to-supporting face to the line of force action (equals 20 inch plus 13 inch, equals to 33 inches for 0.5 aspect ratio walls and 40 inch plus 13 inch, equals 53 inches for 1.0 aspect ratio walls; the 13 inches represents half of the 26-inch-loading block width). The drift ratio of the wall is calculated by the following equation.

$$\text{Drift ratio} = \left[\frac{\frac{\text{LVDT1} + \text{LVDT2}}{2} - \text{LVDT3}}{L_w} - \frac{\text{LVDT4} - \text{LVDT5}}{\text{Distance between LVDT4 and LVDT5}} \right] \times 100\%$$

Where L_w is the distance between the wall-to-supporting interface and the center of the head of actuator. This value equals 20 inches plus 13 inches, equals to 33 inches for 0.5 aspect ratio walls and 40 inches plus 13 inches, equals 53 inches for 1.0 aspect ratio walls; the 13 inches represents half of the 26-inch-loading block width.

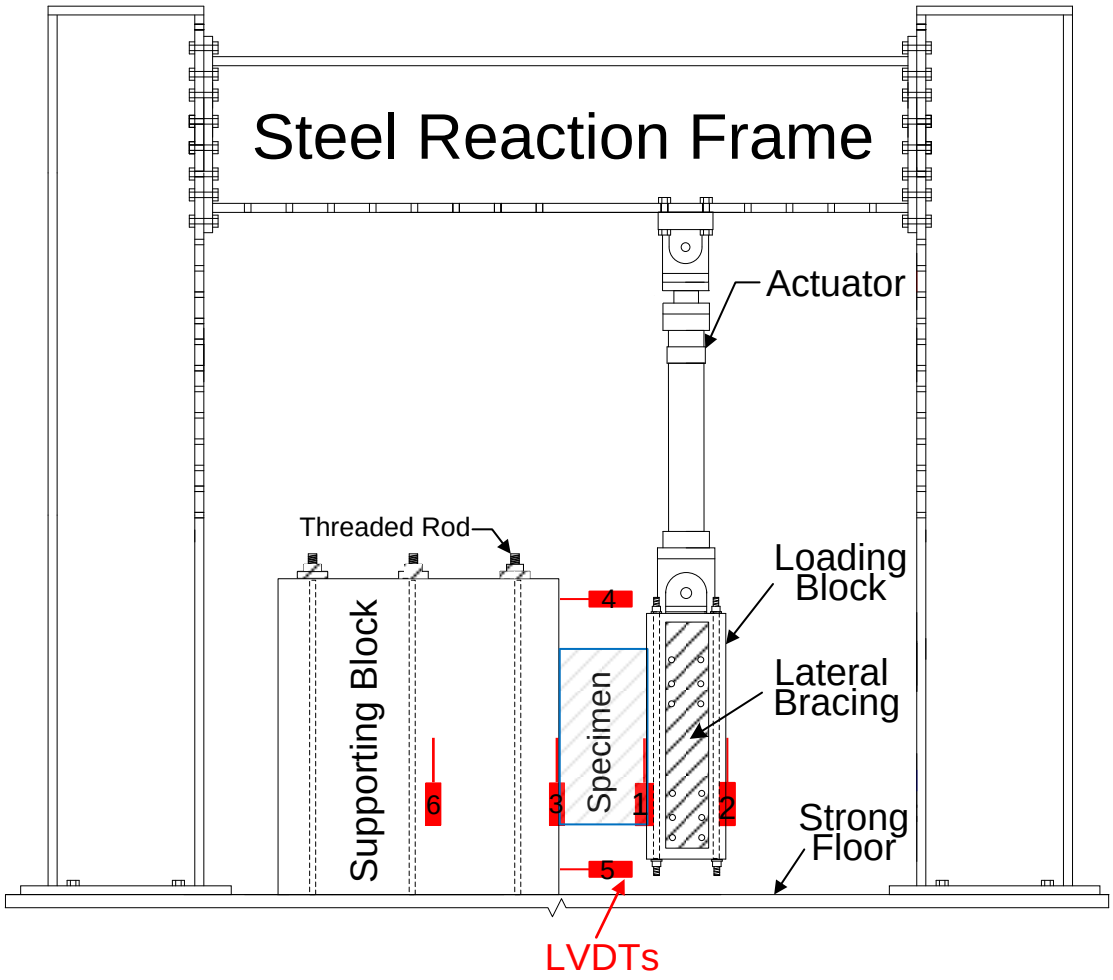

Figure 4-97 Specimen setup and LVDTs location

One of the smooth wall faces was used for the DIC. The face was painted by White color, at least one day later, black dots were spread so that 50% of the wall face is White and 50% of the wall face is Black dots as shown in Figure 4-98. The DIC system consists of two cameras supported by a tripod and connected to a computer which has sensor box, the left and right cameras are connected to the sensor on the specified ports which labeled as left and right. On the night of the test, the cameras must be calibrated to

the accurately cover the wall dimensions, the calibration takes at least two hours to complete, basically the cameras resolution and precision are adjusted to capture the black dots on the wall face, the distance between the cameras to the object center was selected 132 cm which is the same distance between the cameras tripods to the center of wall face as shown in Figure 4-99 and Figure 4-100. The height of the cameras is the same height of wall face center (36 inches from the floor level to the center of cameras).

Just before starting the test, the cameras shuttering time is adjusted to have suitable degree of lightening, extra bulbs are used to provide some light on the wall face. There is tow reasons of this, first the calibration was executed over the night witch has less resolution compared to the light on the morning (time of testing). Second, the black dots are not 100% uniform, therefore the lightening over the wall face varies.

The cameras capture one photo per five seconds, which precisely tracks the movement and deformation of all Black dots over the wall face while testing the wall specimen. After completing the test, the pictures are post-processed to analyze the displacement and strain distribution of the wall face. In this study, the major and minor strain were used extensively to track the shear force distribution from the wall tip to the supporting block and to precisely quantify the critical and highly stressed zones.

Figure 4-98 Wall face painted by White and Black dots.

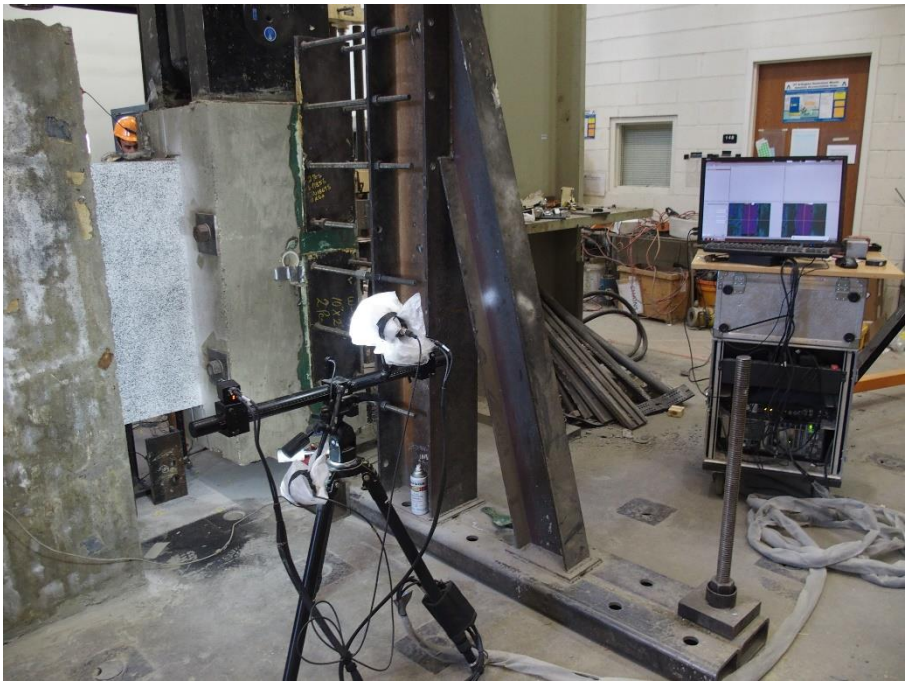

Figure 4-99 DIC system

Figure 4-100 Symmetric cameras distance relative to the wall center.
a

Strains of longitudinal and horizontal steel rebars were measured by strain gauges attached to the reinforcement. The strain gauges and LVDTs wires are attached to the blue wires which connected to four Data Acquisition (DAQ) sensors (version 8000) as shown in Figure 4-101. The four sensors connected together by an adaptor which has a port to connect to the laptop that have the DAQ software installed in, as shown in Figure 4-102.

Figure 4-101 DAQ sensors

Figure 4-102 Adaptor to connect the four DAQ sensors

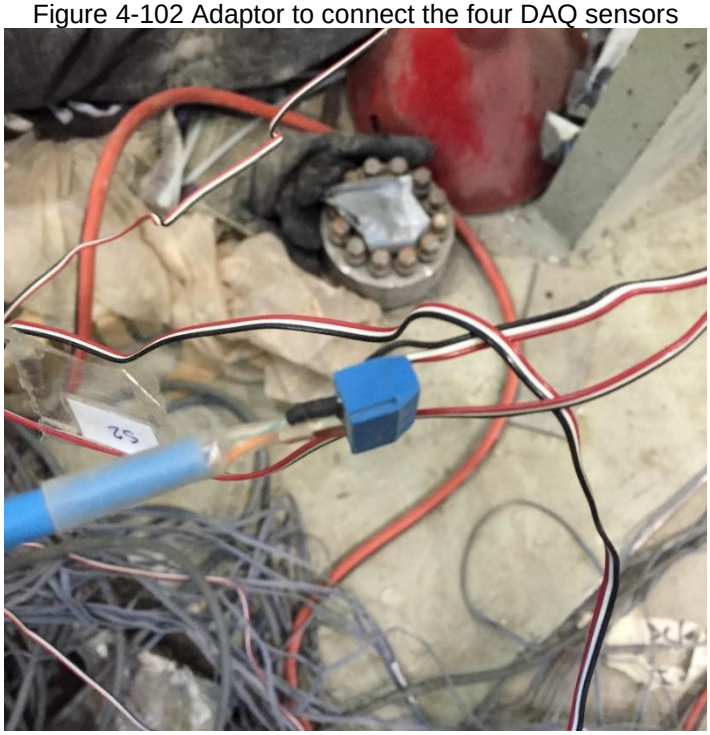

Figure 4-103 Strain gauge wire to the blue wire connection

4.5. Loading Protocol

The applied loading protocol consists of symmetric cyclic displacements as shown in Figure 4-104

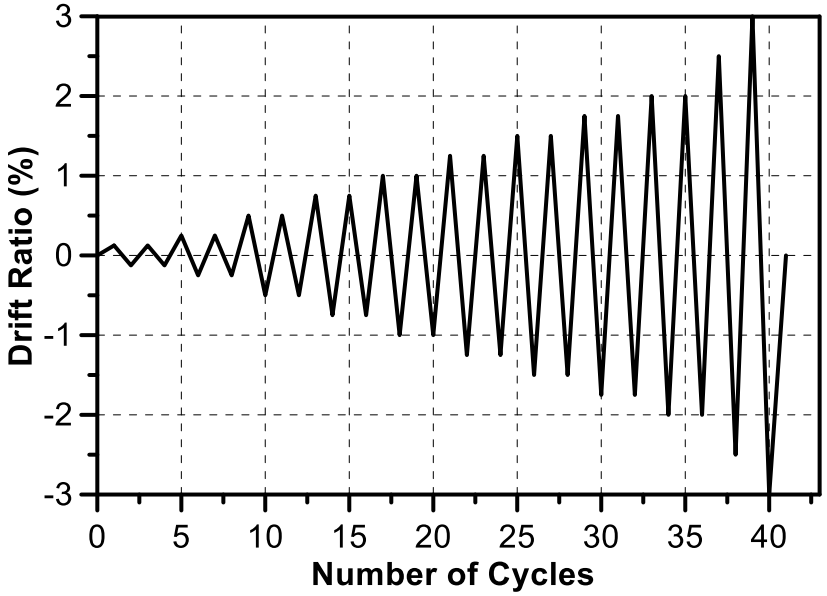

Figure 4-104 Loading protocol

Chapter 5

Experimental Results

5.1. Introduction

Seven squat shear walls were experimentally tested to investigate the effect of wall web concrete confinement on overall squat walls behavior. The walls were carefully confined to eliminate the unpleasable sliding shear failure mode that most of current walls suffer from. Generally, sliding shear failure prevents squat walls to reach sufficient drift ductility and dissipated energy due to softening then crushing of the diagonal struts commences at low drift ratios, consequently, wall shear strength drops suddenly. Therefore, it is hard to precisely predict either the wall peak drift or strength.

Specifically, five of the tested walls have 0.5 aspect ratio and two walls with 1.0 aspect ratio. The walls designated by SW-HA-0.5, SW-HP-0.5-1, SW-HP-0.5-2, SW-MA-0.5, SW-MP-0.5, and SW-MA-1.0. Each of the wall designation letters were discussed in Chapter 3.

The following sections discusses testing results of wall cracking and damage pattern, attained shear force and drift ratio, and stresses of horizontal and vertical steel reinforcement

5.2. SW-MA-0.5

5.2.1 Cracking and Damage Pattern

Shear and flexural cracks propagation at drift ratio 0.125%, 0.25%, 0.5%, 0.75%, 1%, 1.25%, 1.5%, 1.75% and 2% are shown in Figure 2-1. Cracks developed along the diagonal compressive struts until 1% drift ratio (Figure 2-1). Base of web struts started crushing at drift ratio 1.25% due to insufficient concrete confinement at the web

compared to the well-confined boundaries, thereby the wall shear strength sharply dropped. Consequently, struts crushing propagated toward wall boundaries due to reversed loading which initiated the sliding plane and the wall deformed as a rigid block. At this point, concrete struts are no longer resisting shear forces, instead the longitudinal steel rebar are only resisting shear forces by dowel action (by kinking the steel rebars).

5.2.2 Shear strength response

Shear force versus drift ratio response of specimen SW-MA-0.5 is shown in Figure 5-2. The maximum attained shear force was 133 kips ($11.8\sqrt{f_{cm}}$) at drift ratio 1.25%. However, sudden drop in shear strength commenced at this drift level due to sliding shear failure, where the diagonal concrete struts crushed and no longer resist shear forces, the shear forces are resisted by dowel action (kinking the longitudinal steel rebars).

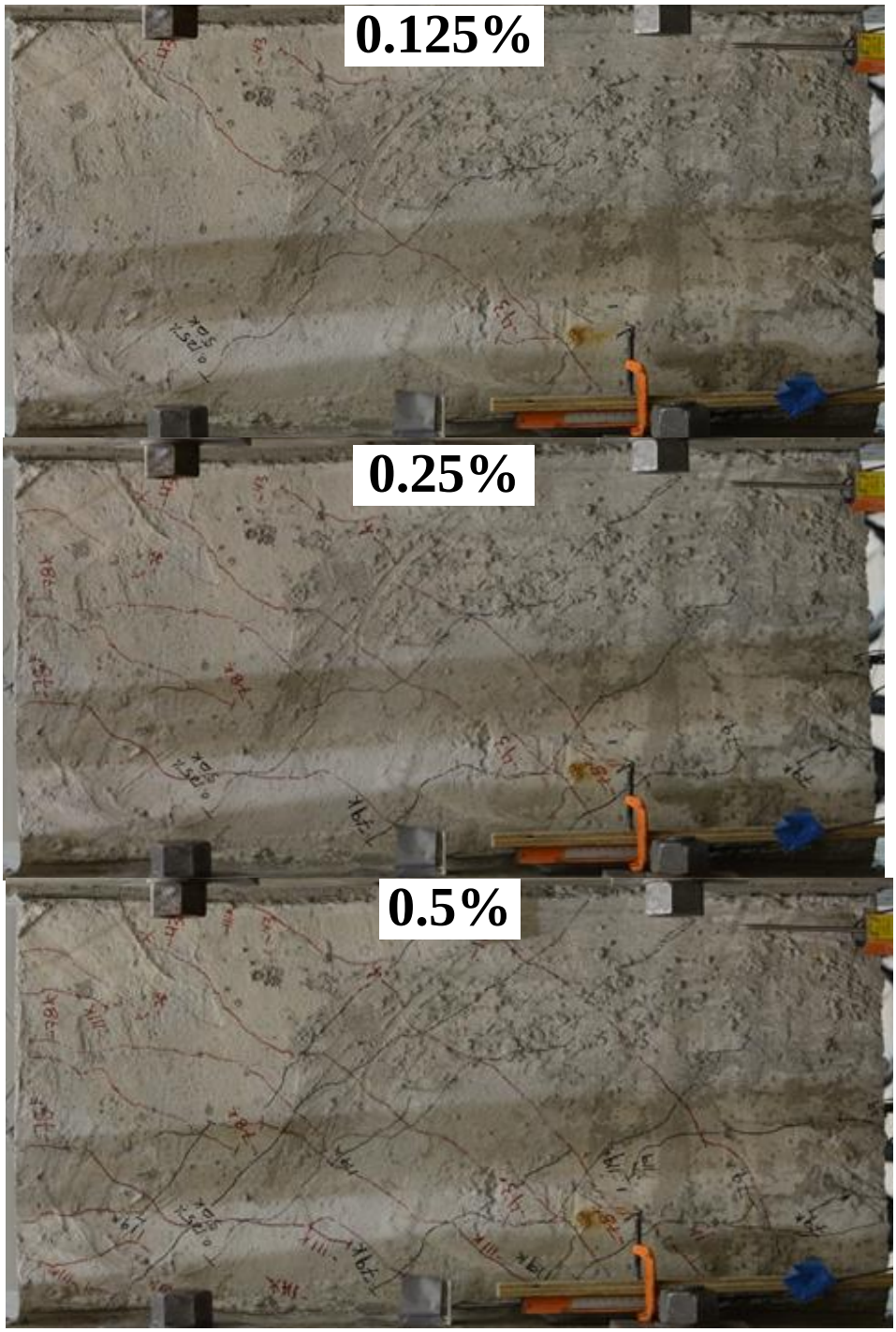

Figure 5-1 Test results of specimen SW-MA-0.5 at drift ratio 0.125%, 0.25%, 0.5%, 0.75%, 1%, 1.25%, 1.5%, 1.75% and 2% (continued)

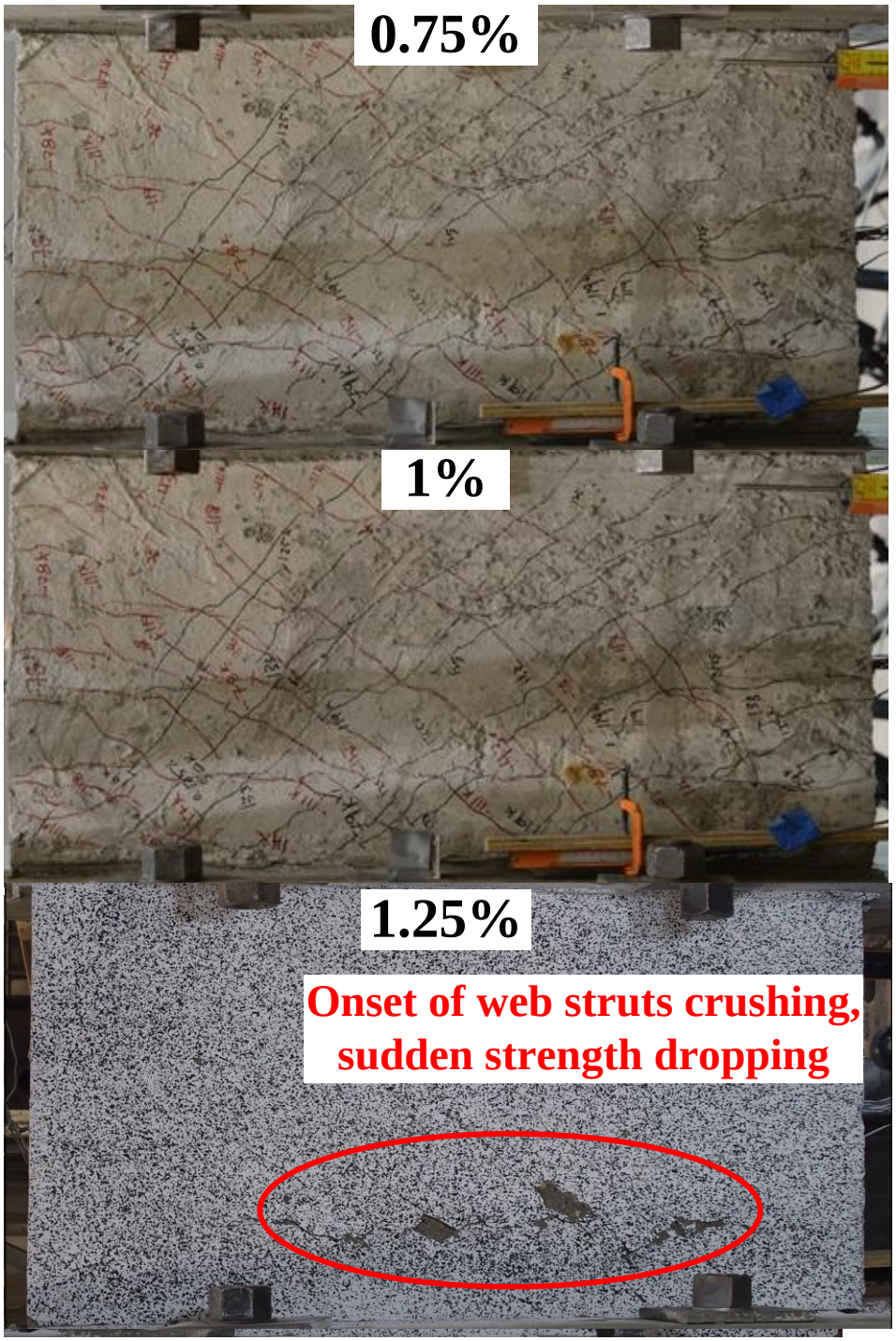

Figure 5-1 Test results of specimen SW-MA-0.5 at drift ratio 0.125%, 0.25%, 0.5%, 0.75%, 1%, 1.25%, 1.5%, 1.75% and 2% (continued)

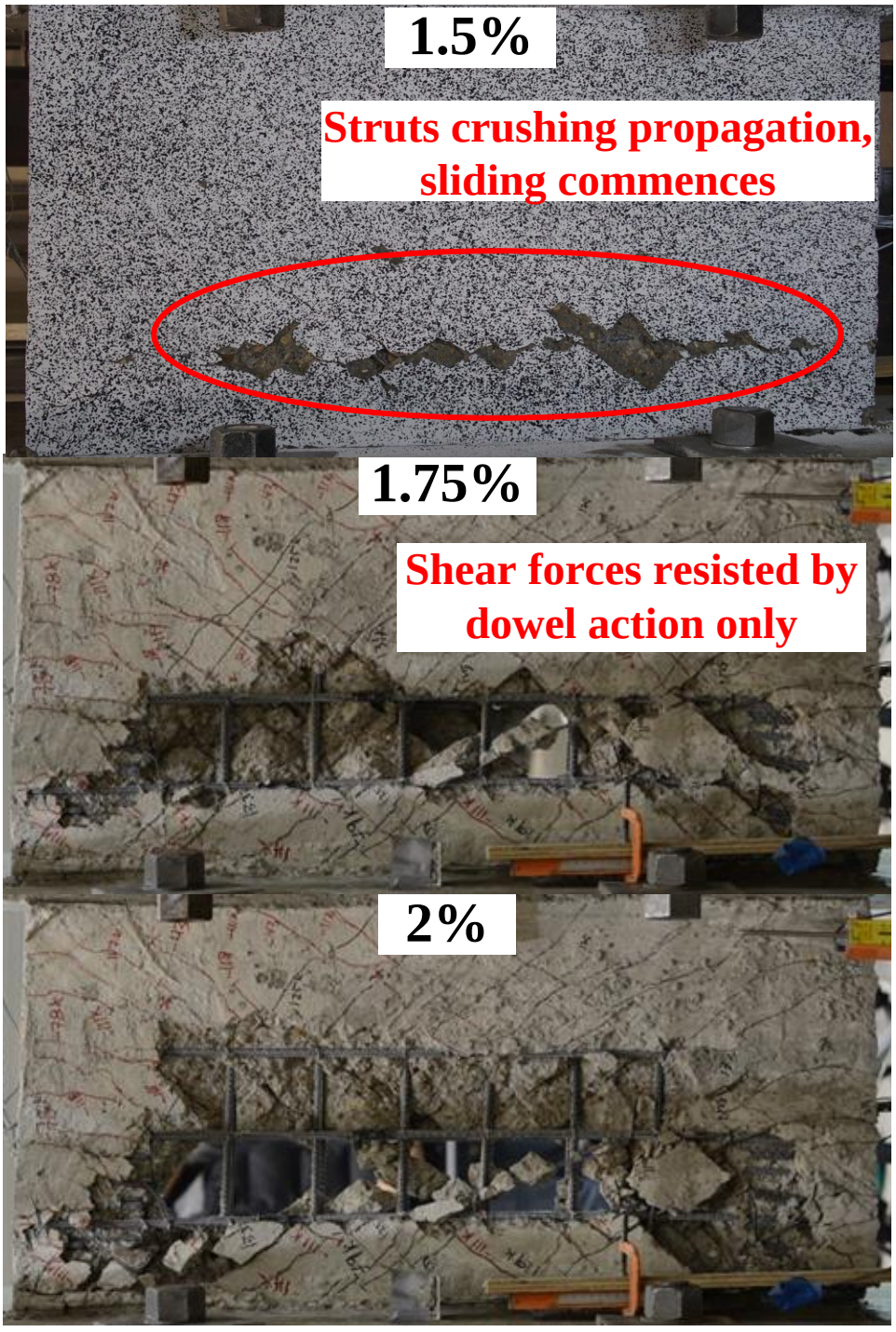

Figure 5-1 Test results of specimen SW-MA-0.5 at drift ratio 0.125%, 0.25%, 0.5%, 0.75%, 1%, 1.25%, 1.5%, 1.75% and 2% (continued)

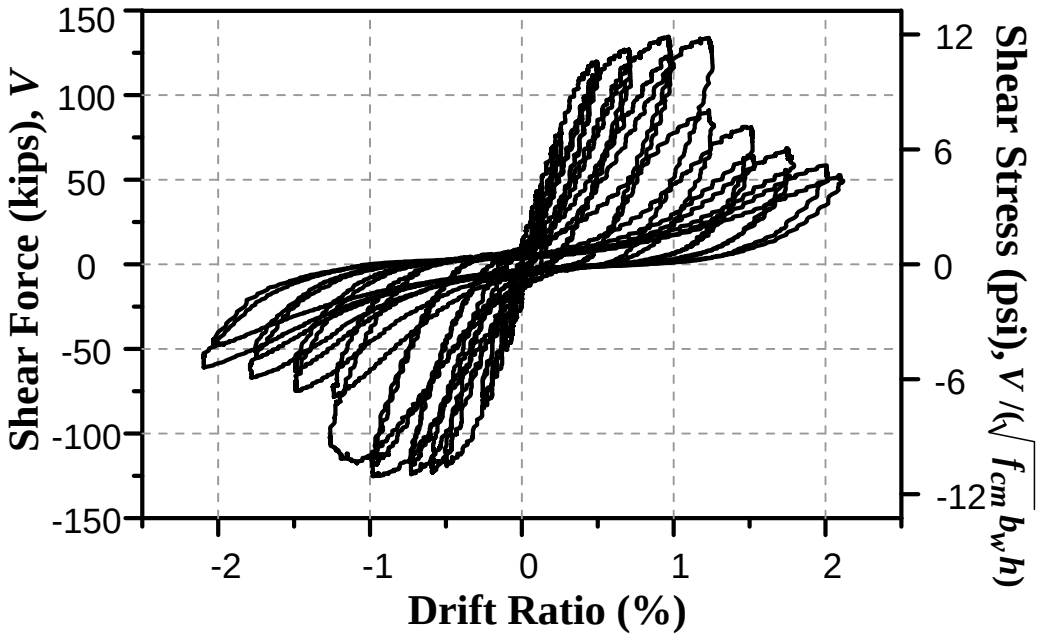

Figure 5-2 Shear strength hysteresis curve of specimen SW-MA-0.5

5.2.3 Steel reinforcement stresses

Strain gauges were attached at boundaries, longitudinal and horizontal steel bars as shown in Figure 5-3. Strain gauges L1 to L13 are attached at vertical steel bars, while S14 to S20 are attached at boundaries and horizontal steel bars. Results of drift ratio and the attained steel stress in strain gauges L1 to S20 are shown in Figure 5-4 to Figure 5-23. All vertical steel bars yielded (reached the yielding strength of (60 ksi) and S15 to S17 yielded but all other strain gauges did not reach the yielding strength.

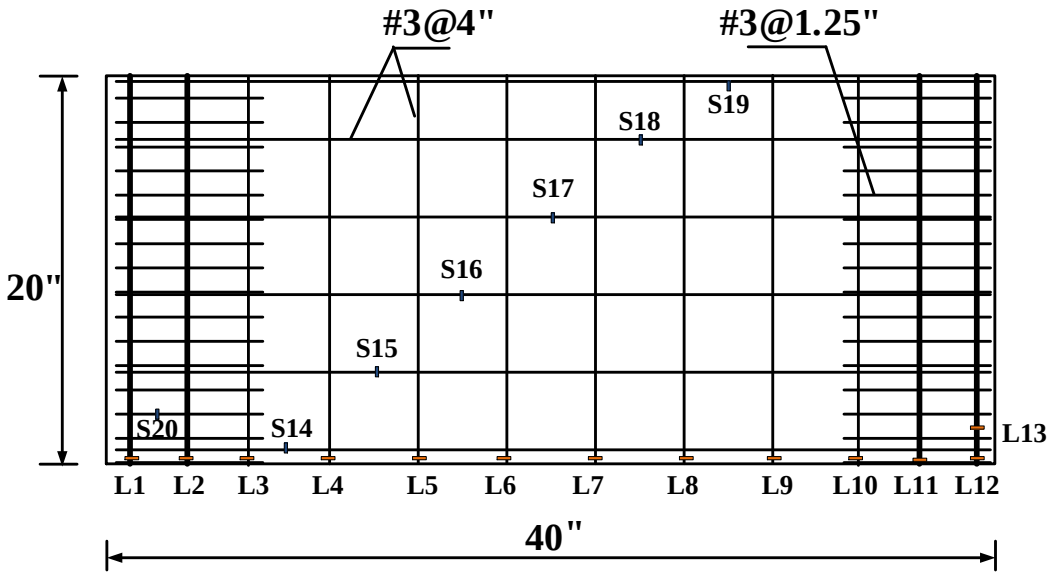

Figure 5-3 Locations of strain gauges at boundaries, vertical and horizontal steel bars for specimen SW-MA-0.5

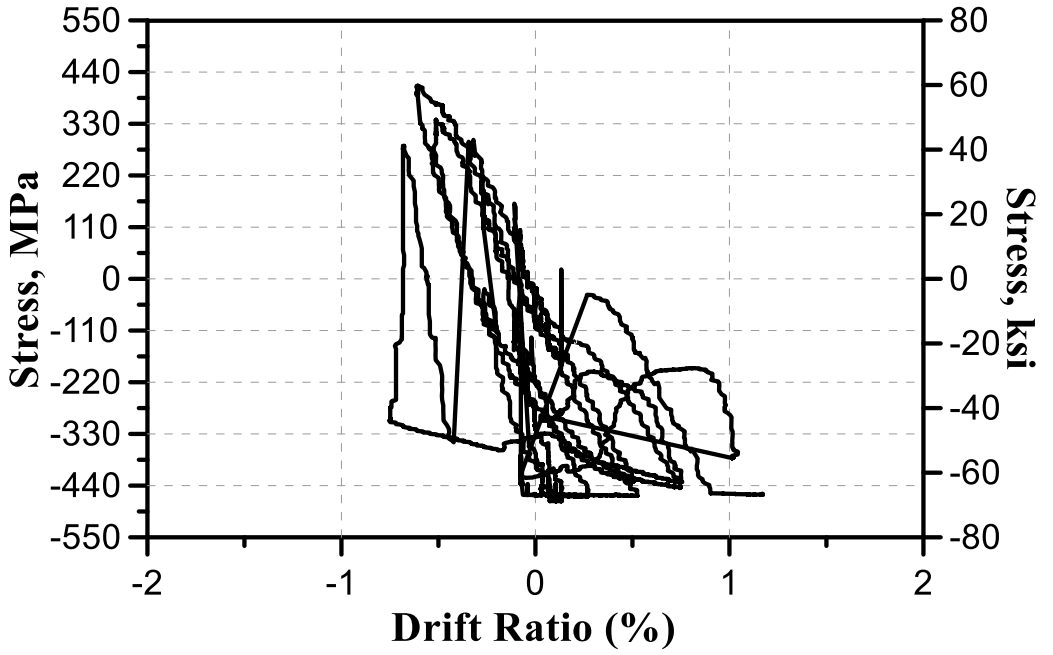

Figure 5-4 Measured stresses of strain gauge (L1) for specimen SW-MA-0.5

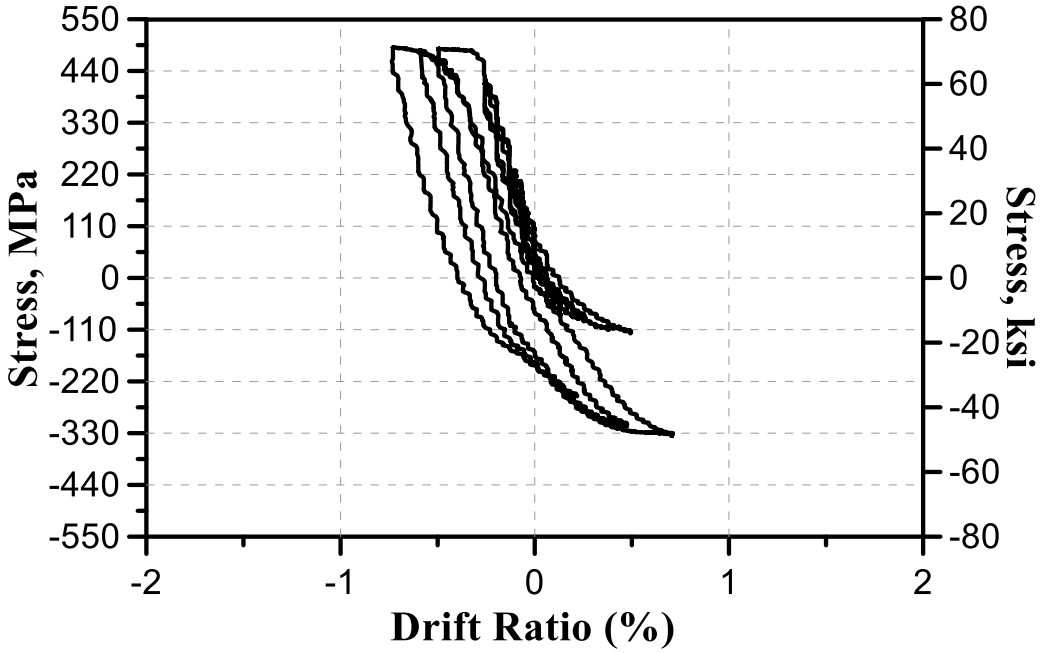

Figure 5-5 Measured stresses of strain gauge (L2) for specimen SW-MA-0.5

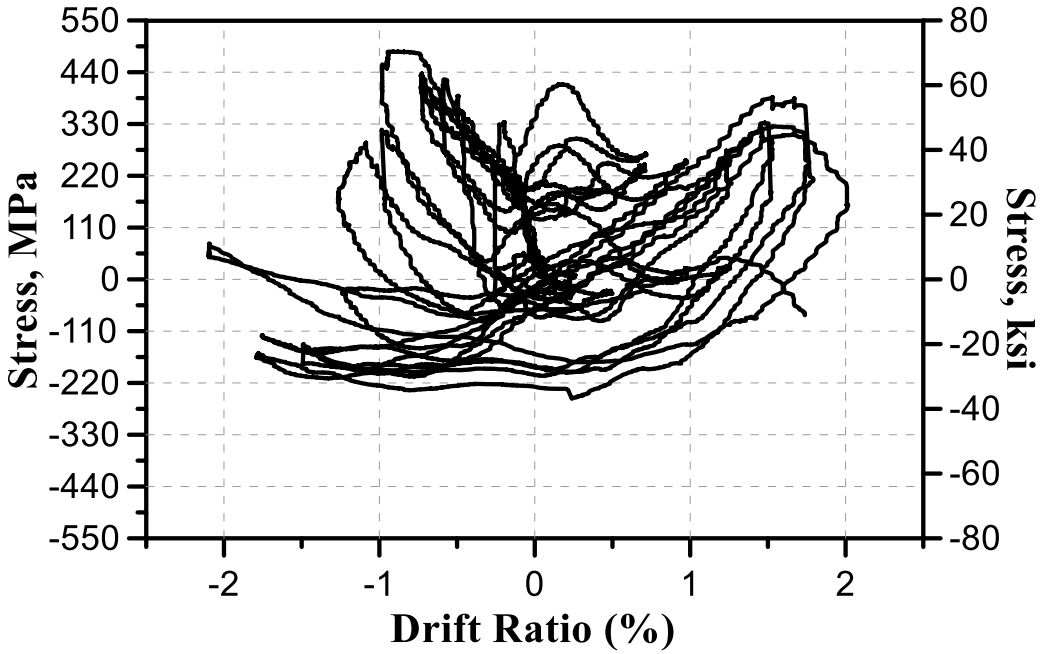

Figure 5-6 Measured stresses of strain gauge (L3) for specimen SW-MA-0.5

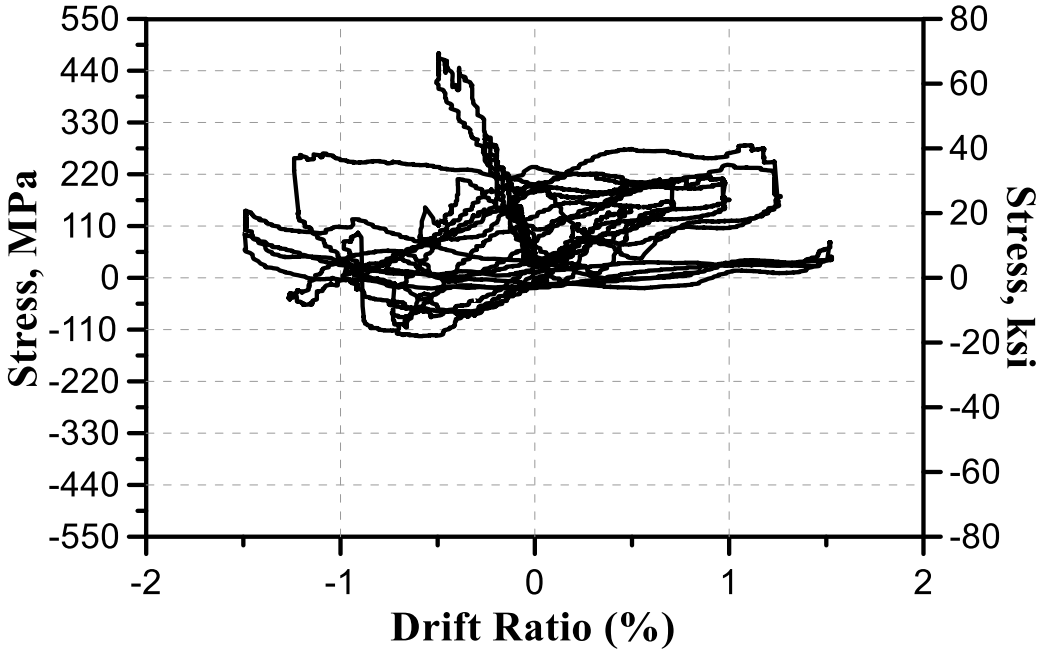

Figure 5-7 Measured stresses of strain gauge (L4) for specimen SW-MA-0.5

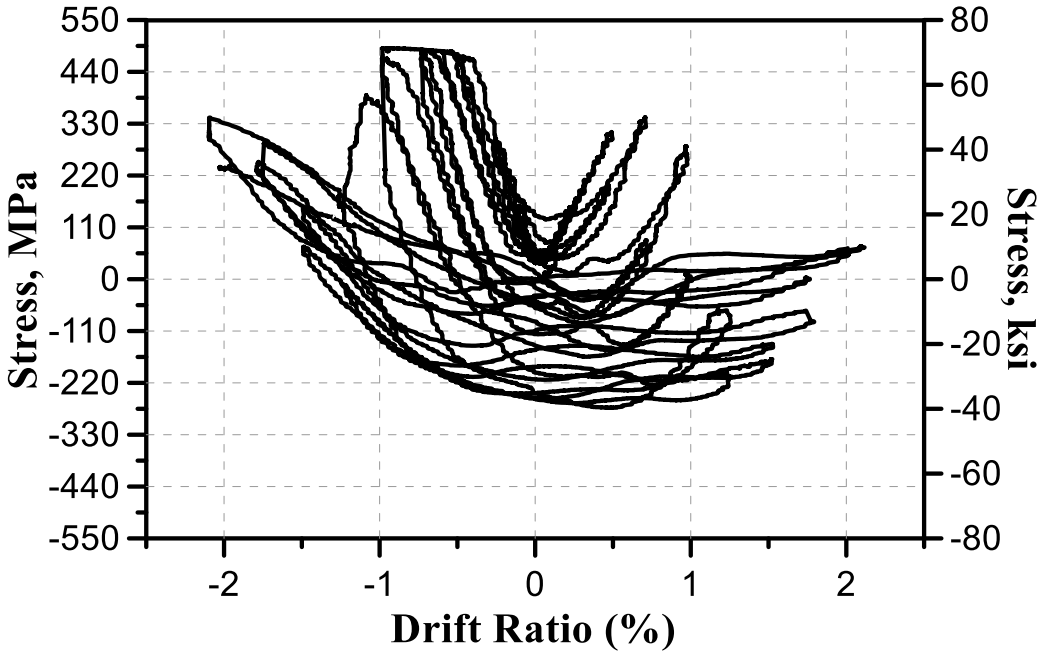

Figure 5-8 Measured stresses of strain gauge (L5) for specimen SW-MA-0.5

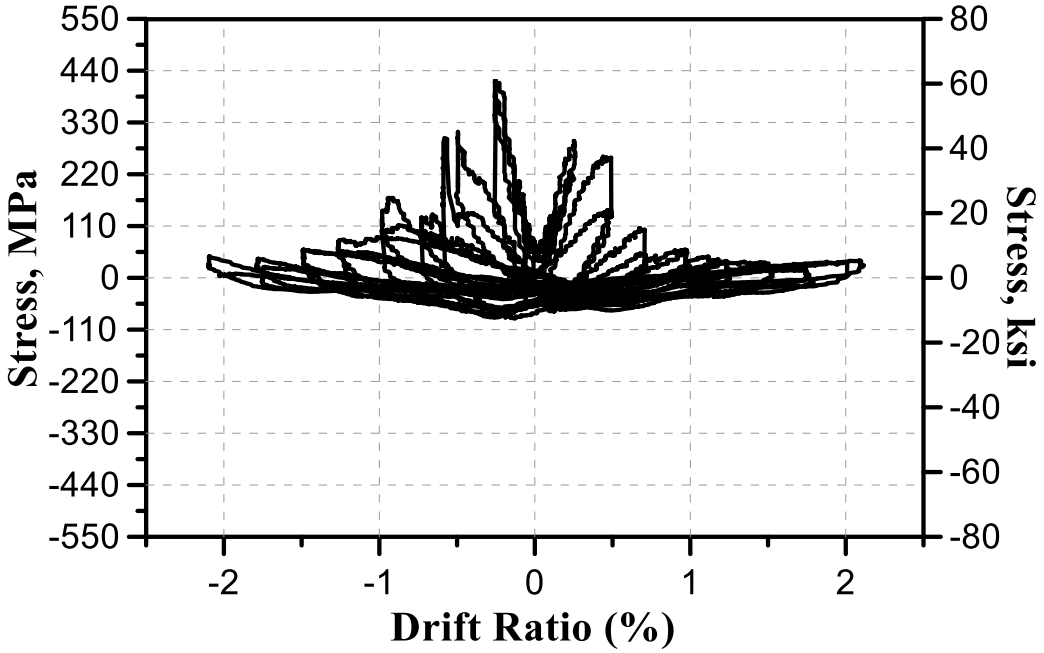

Figure 5-9 Measured stresses of strain gauge (L6) for specimen SW-MA-0.5

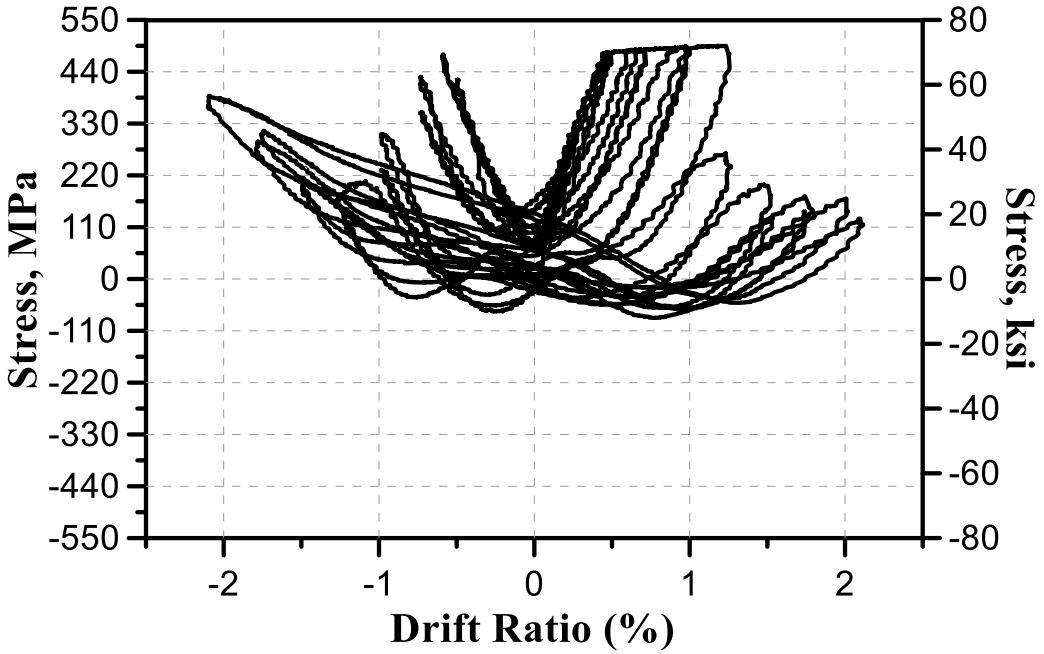

Figure 5-10 Measured stresses of strain gauge (L7) for specimen SW-MA-0.5

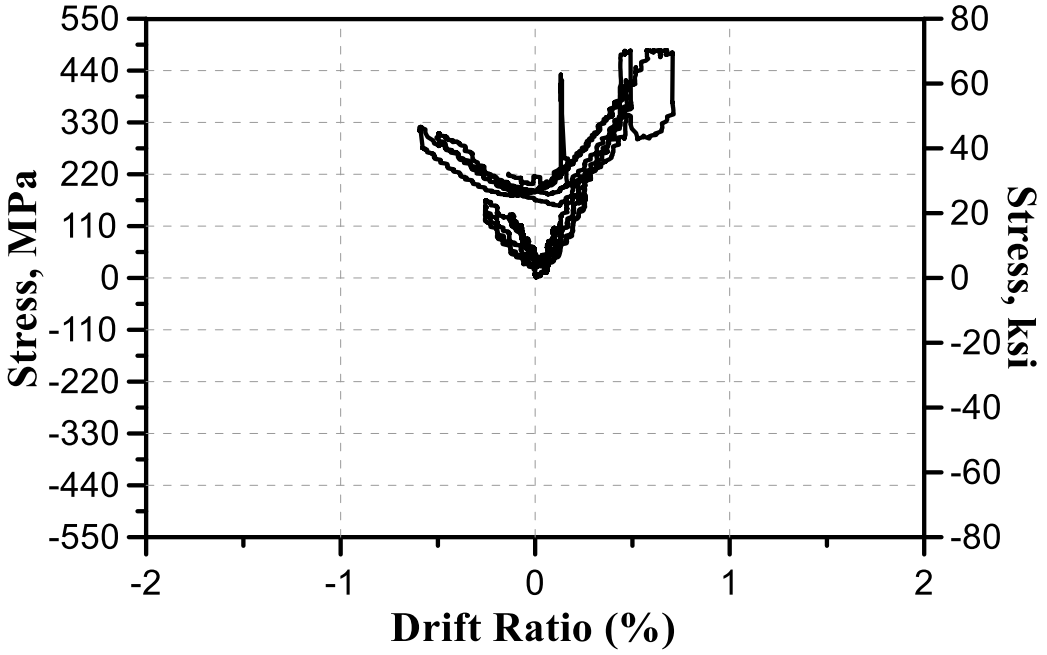

Figure 5-11 Measured stresses of strain gauge (L8) for specimen SW-MA-0.5

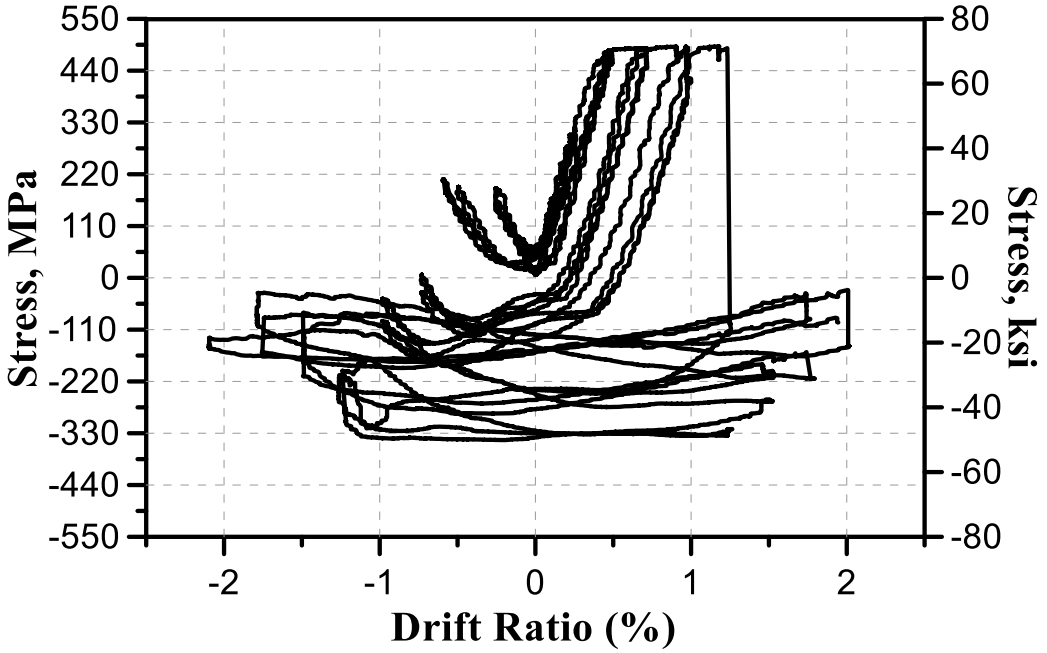

Figure 5-12 Measured stresses of strain gauge (L9) for specimen SW-MA-0.5

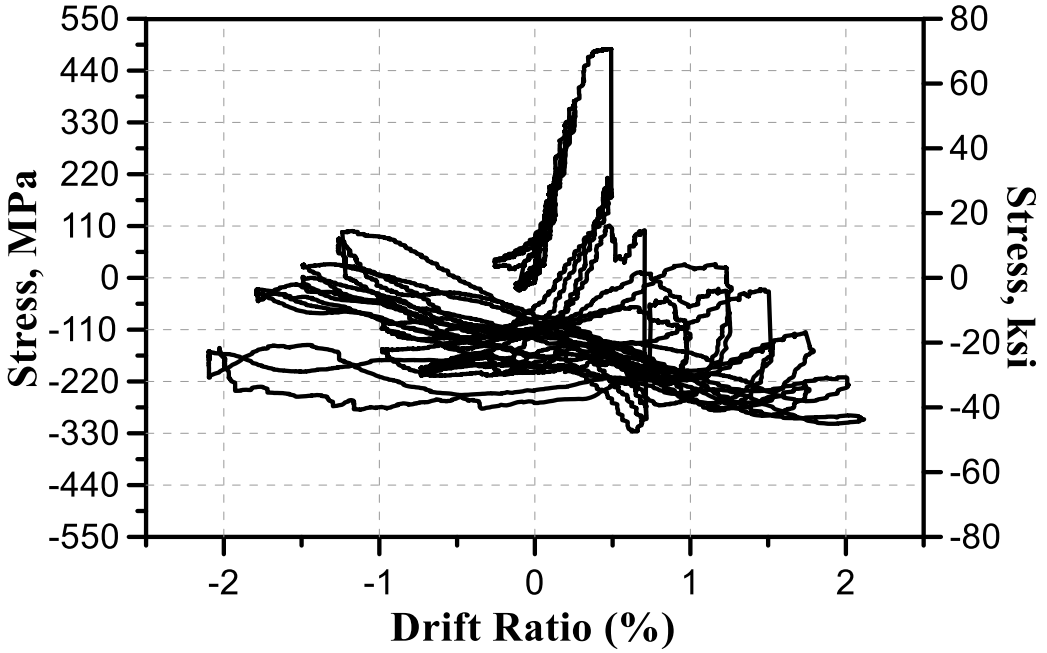

Figure 5-13 Measured stresses of strain gauge (L10) for specimen SW-MA-0.5

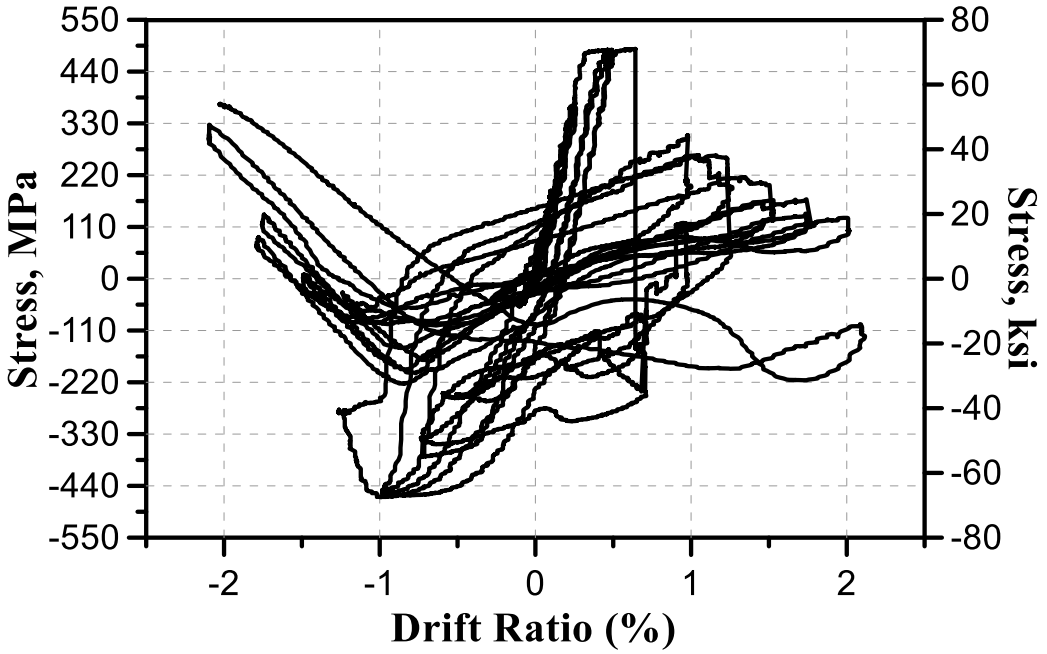

Figure 5-14 Measured stresses of strain gauge (L11) for specimen SW-MA-0.5

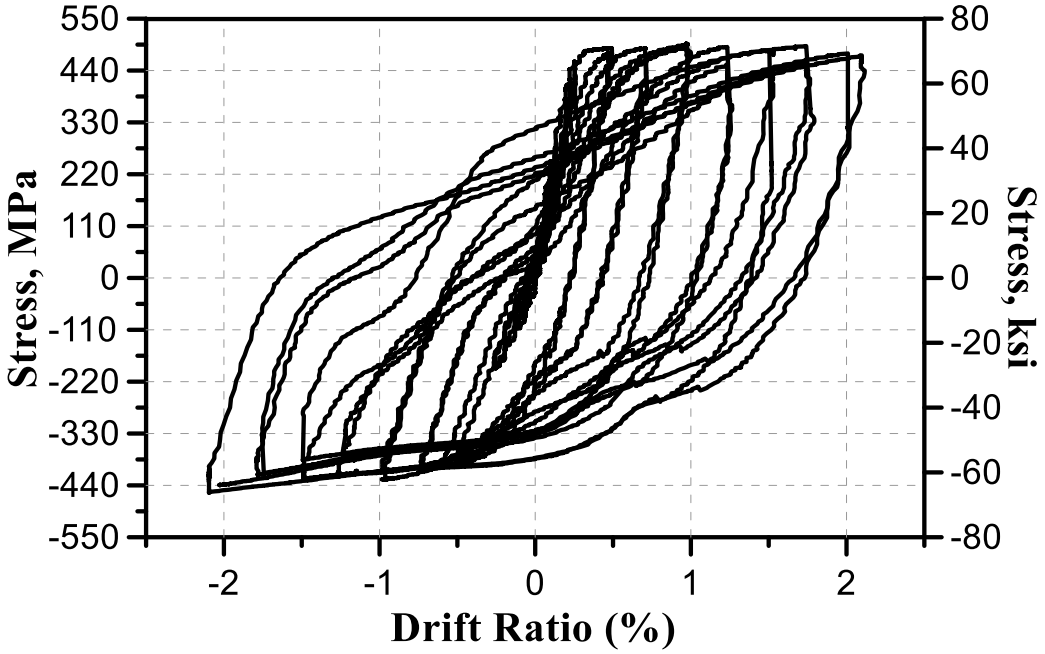

Figure 5-15 Measured stresses of strain gauge (L12) for specimen SW-MA-0.5

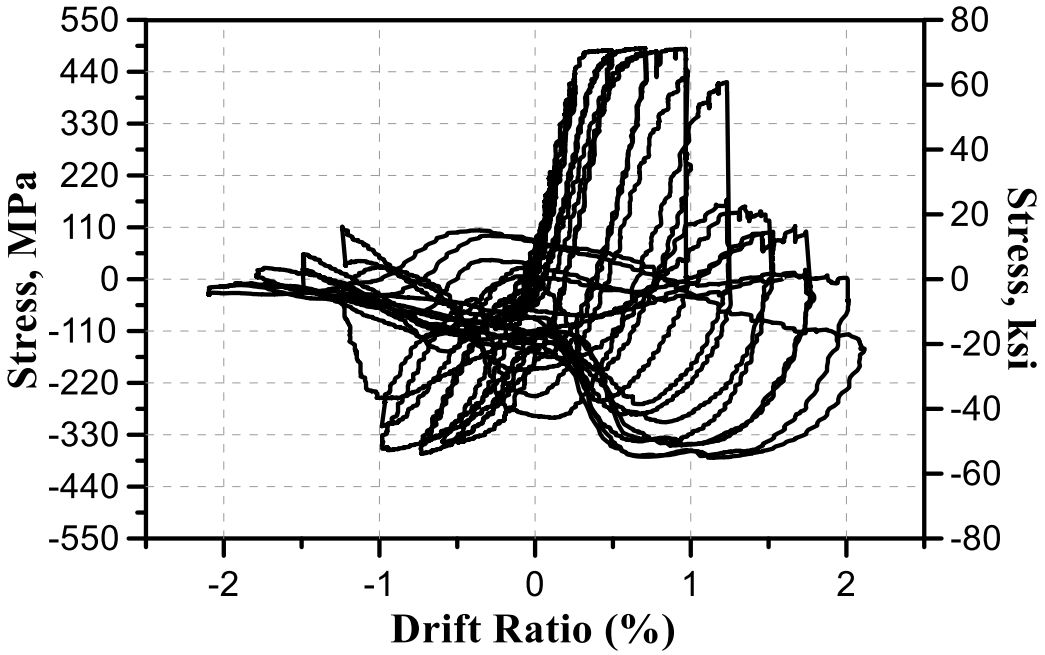

Figure 5-16 Measured stresses of strain gauge (L13) for specimen SW-MA-0.5

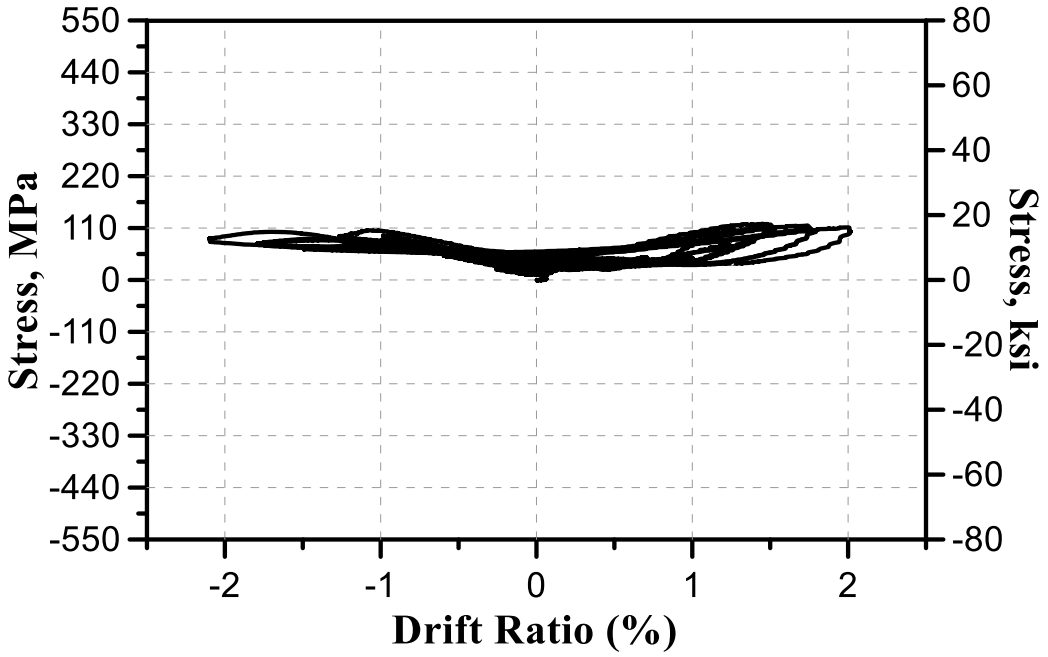

Figure 5-17 Measured stresses of strain gauge (S14) for specimen SW-MA-0.5

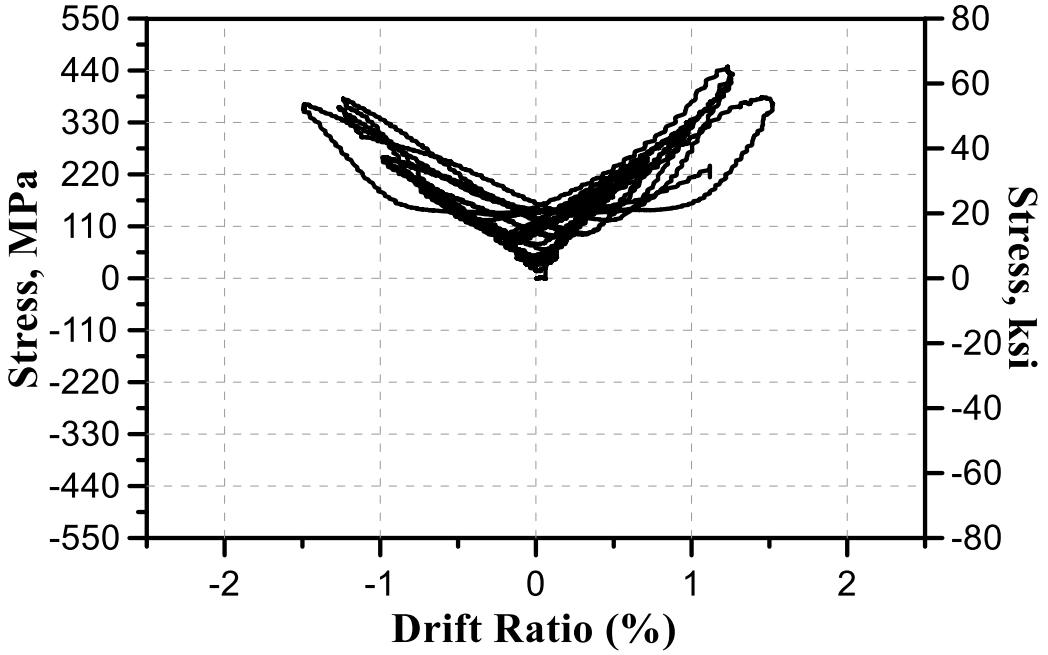

Figure 5-18 Measured stresses of strain gauge (S15) for specimen SW-MA-0.5

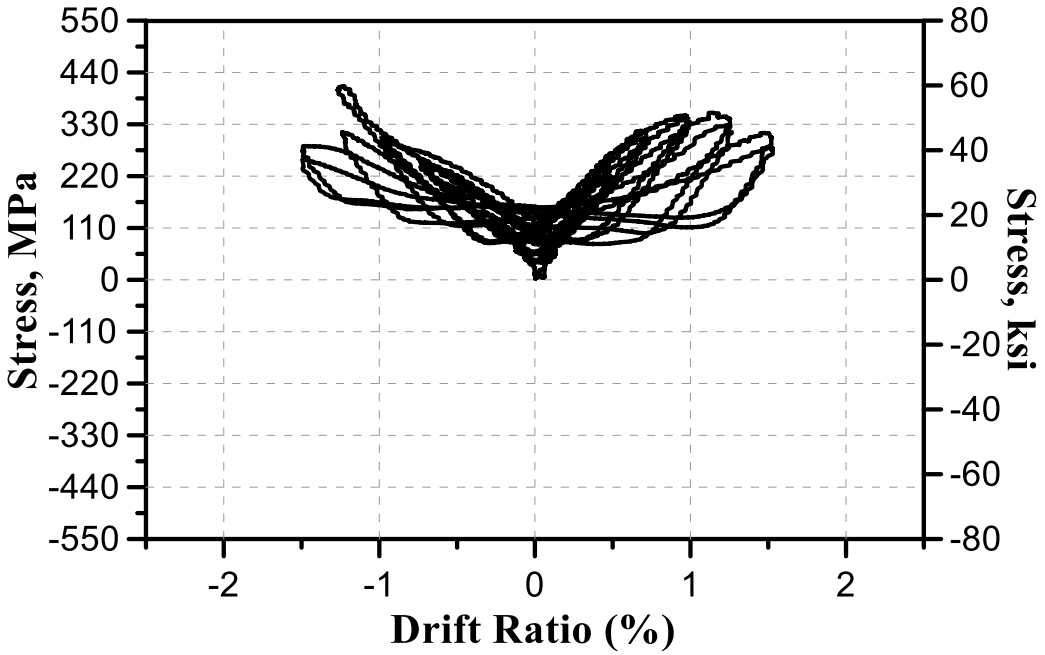

Figure 5-19 Measured stresses of strain gauge (S16) for specimen SW-MA-0.5

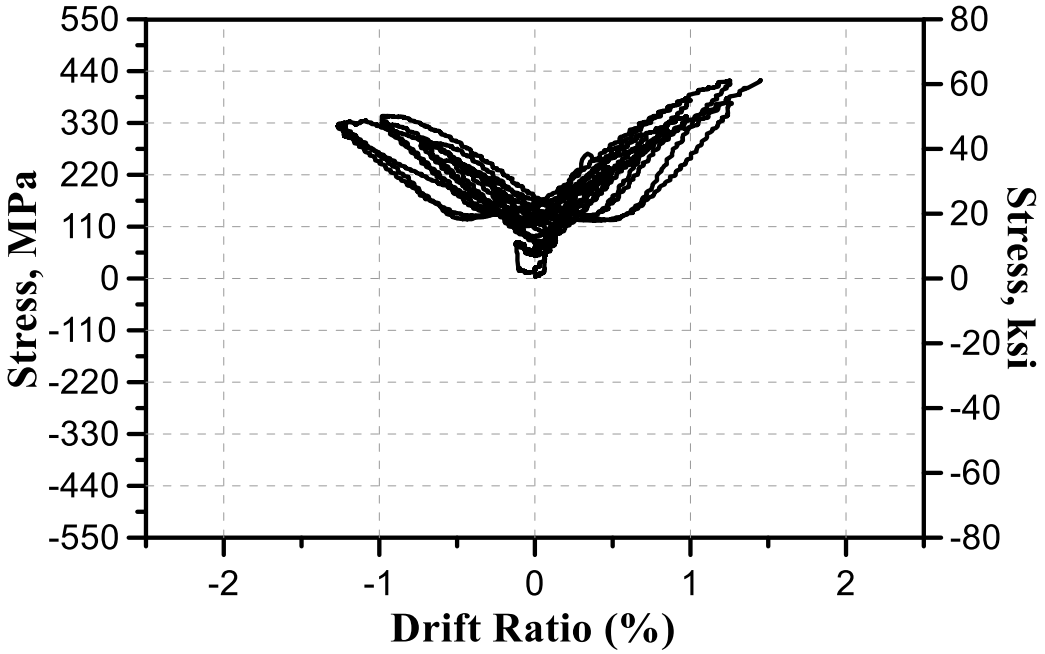

Figure 5-20 Measured stresses of strain gauge (S17) for specimen SW-MA-0.5

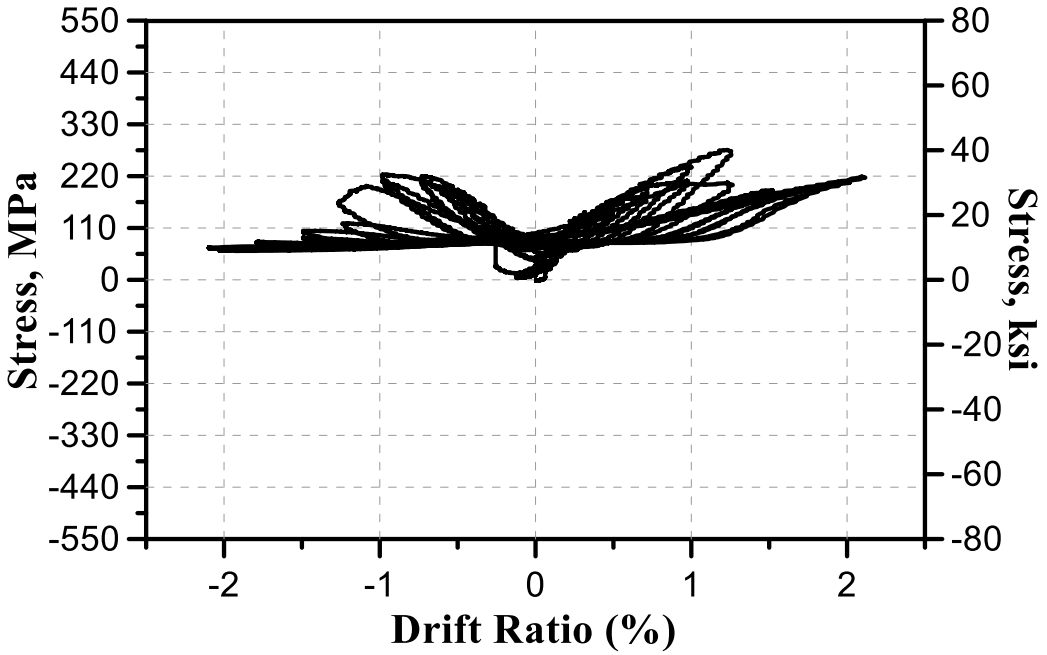

Figure 5-21 Measured stresses of strain gauge (S18) for specimen SW-MA-0.5

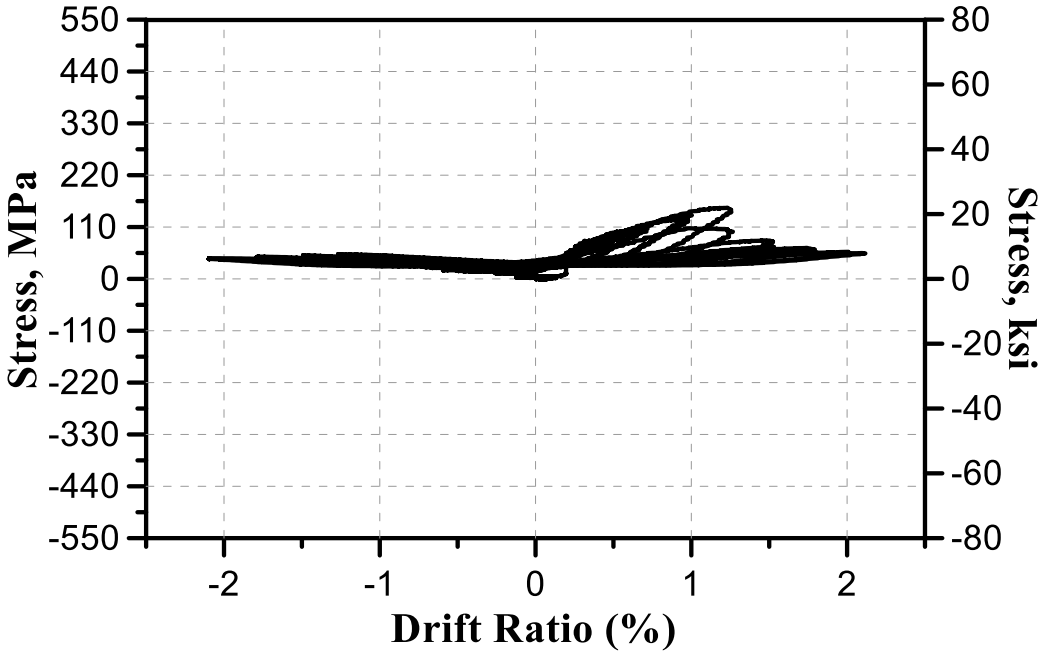

Figure 5-22 Measured stresses of strain gauge (S19) for specimen SW-MA-0.5

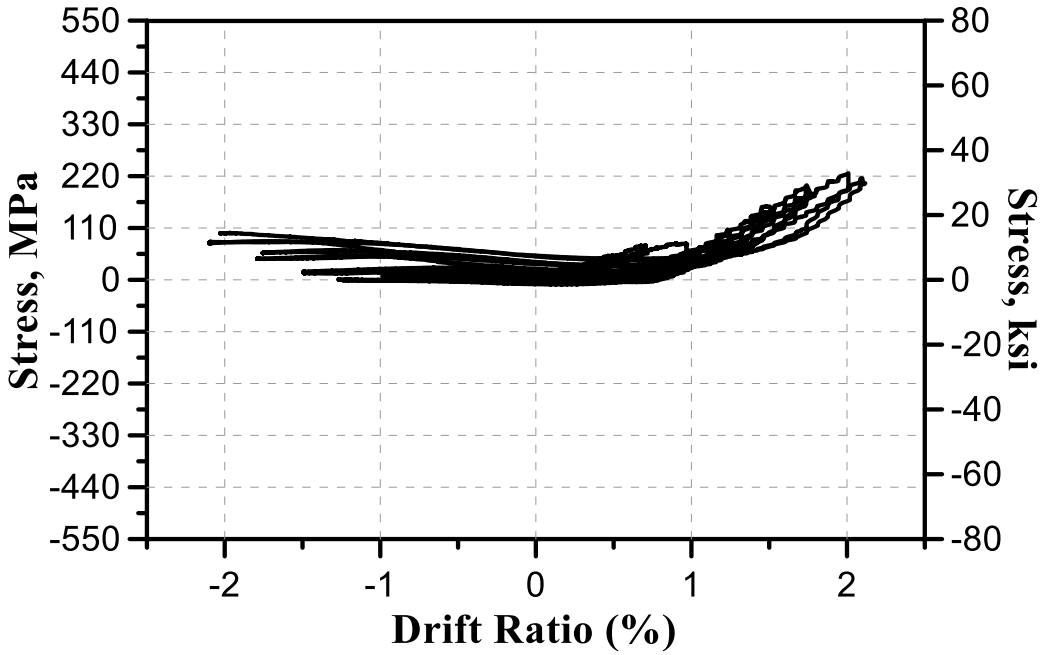

Figure 5-23 Measured stresses of strain gauge (S20) for specimen SW-MA-0.5

5.3 SW-MP-0.5

5.3.1 Cracking and Damage Pattern

Shear and flexural cracks propagation at drift ratio 0.125%, 0.25%, 0.5%, 0.75%, 1%, 1.25%, 1.5%, 1.75%, 2%, 2.5% and 3% are shown in Figure 5-24. No struts crushing, or shear strength drop was observed in specimen SW-MP-0.5 up to drift ratio 2.5% (Figure 5-24), which represents as twice as the drift ratio at onset of sudden shear strength drop in SW-MA-0.5. Concrete cover spalling while confined core concrete was observed in the proposed wall after drift ratio 2.5%. Thus, shear strength drop was gradual, and no sudden drop was reported.

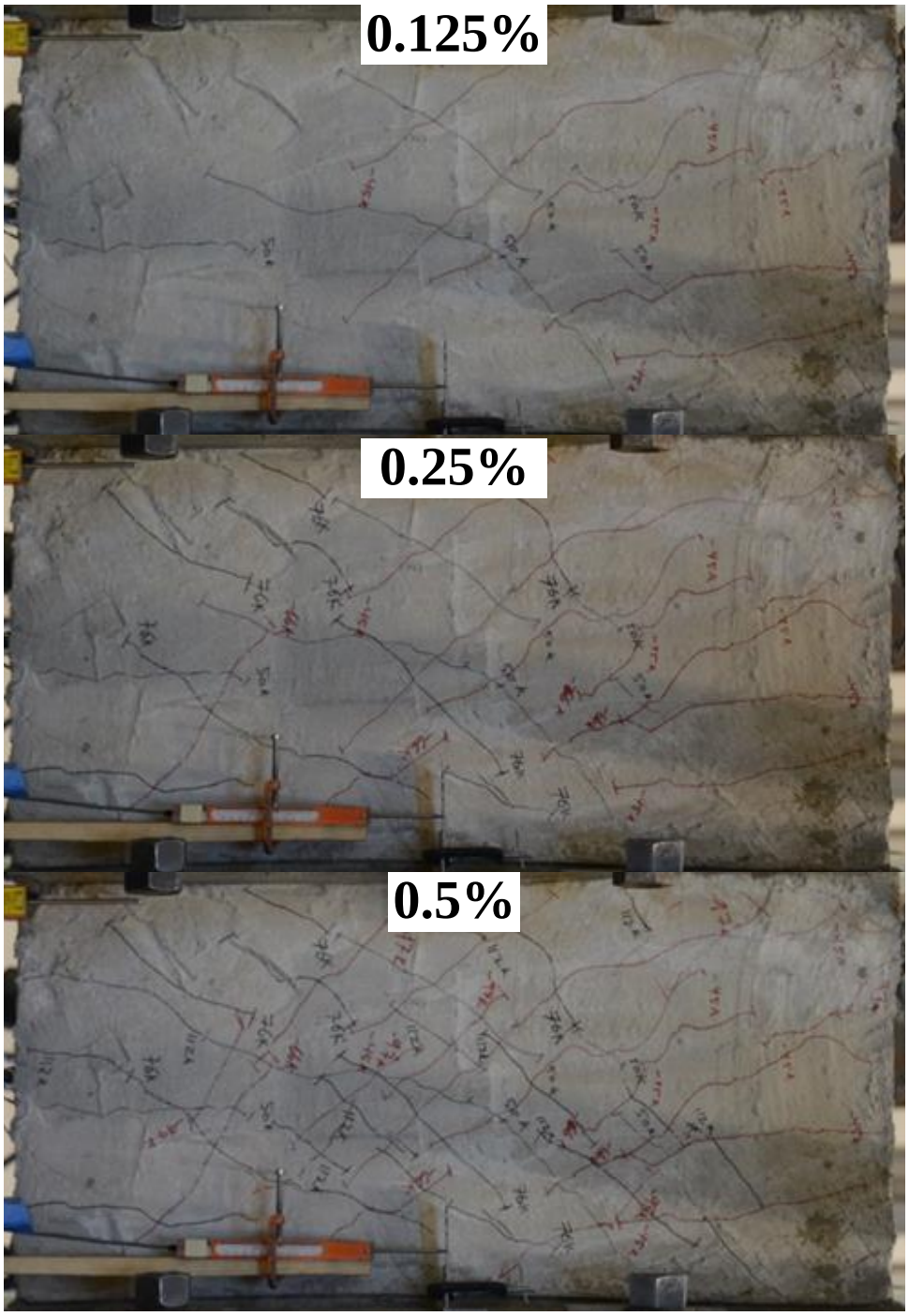

Figure 5-24 Test results of specimen SW-MP-0.5 at drift ratio 0.125%, 0.25%, 0.5%, 0.75%, 1%, 1.25%, 1.5%, 1.75%, 2%, 2.5%, and 3% (continued)

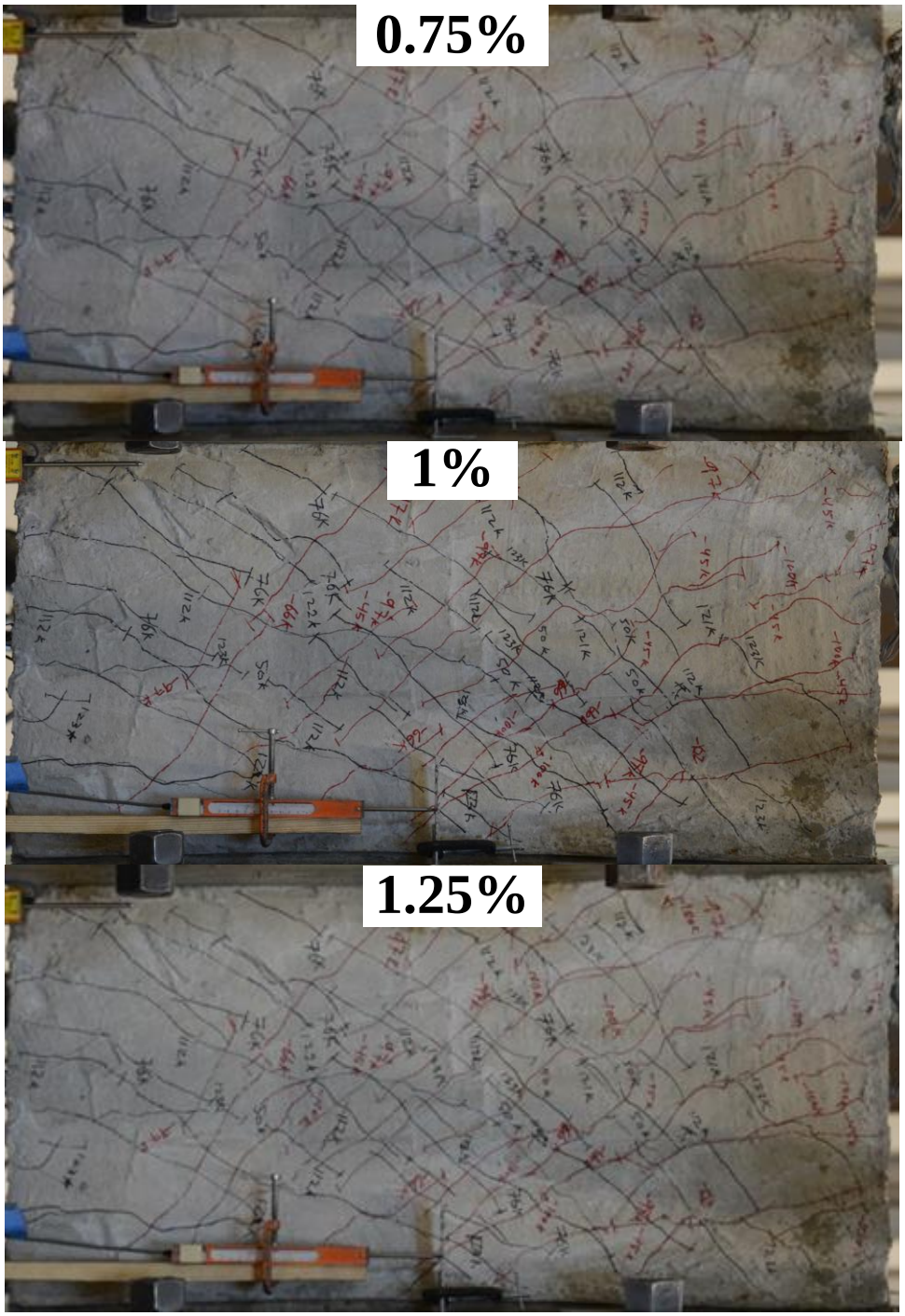

Figure 5-24 Test results of specimen SW-MP-0.5 at drift ratio 0.125%, 0.25%, 0.5%, 0.75%, 1%, 1.25%, 1.5%, 1.75%, 2%, 2.5%, and 3% (continued)

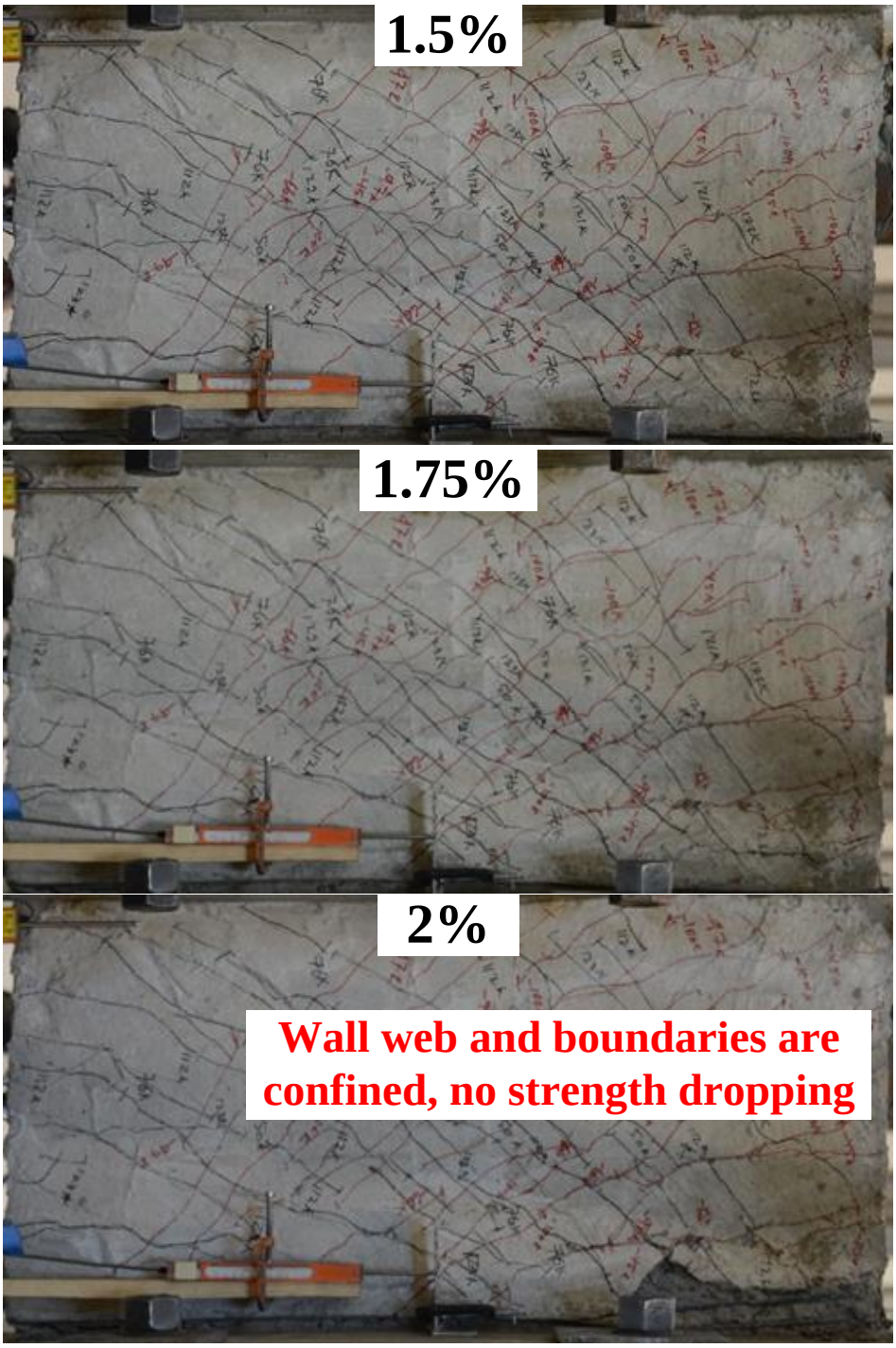

Figure 5-24 Test results of specimen SW-MP-0.5 at drift ratio 0.125%, 0.25%, 0.5%, 0.75%, 1%, 1.25%, 1.5%, 1.75%, 2%, 2.5%, and 3% (continued)

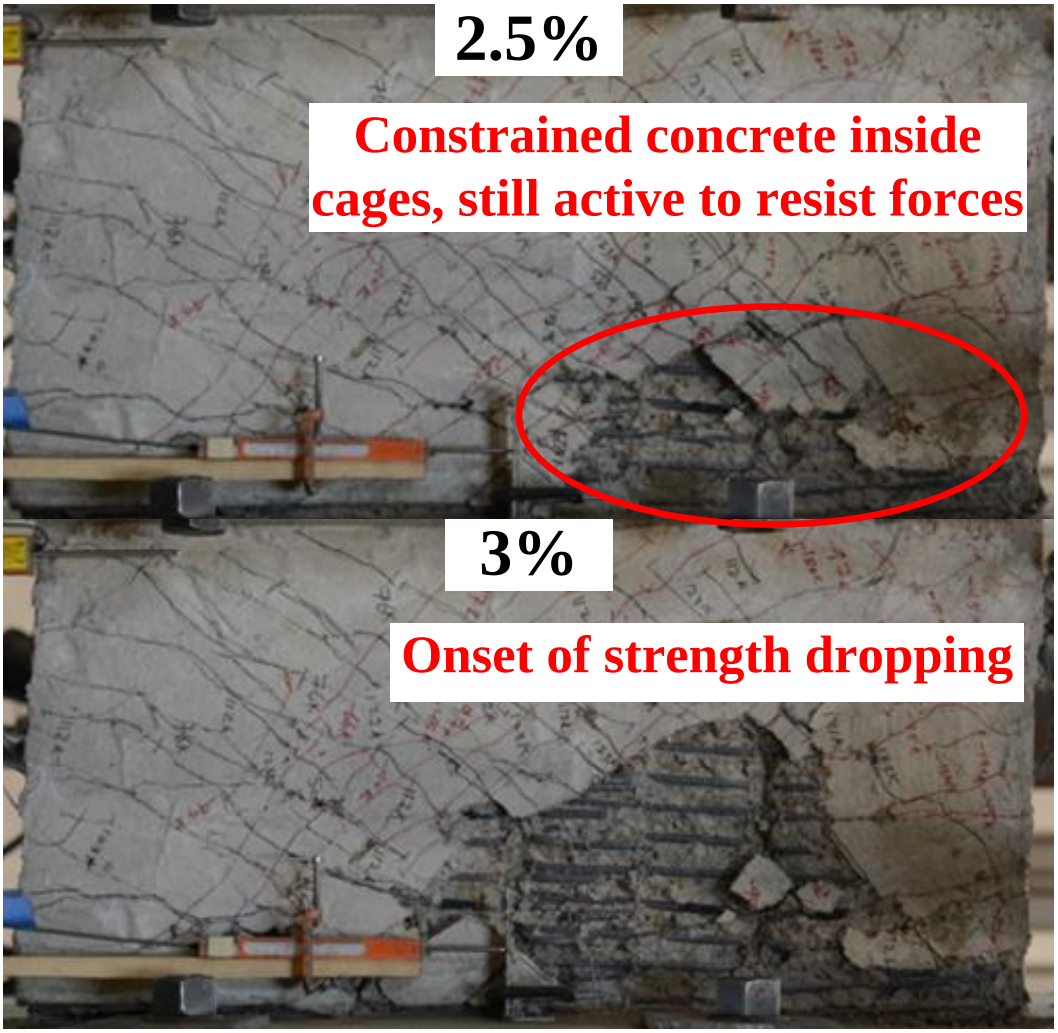

Figure 5-24 Test results of specimen SW-MP-0.5 at drift ratio 0.125%, 0.25%, 0.5%, 0.75%, 1%, 1.25%, 1.5%, 1.75%, 2%, 2.5%, and 3% (continued)

5.3.2 Shear strength response

Shear force versus drift ratio response of specimen SW-MP-0.5 is shown in Figure 5-25. The maximum attained shear force was 123 kips ($10.9\sqrt{f_{cm}}$) at drift ratio 0.75% and remained at plateau up to drift ratio 2.5%. Shear strength and stiffness

gradually decreased after drift ratio 2.5% which equivalent to a drift ratio as twice as that attained in specimen SW-MA-0.5.

Figure 5-25 Shear strength hysteresis curve of specimen SW-MP-0.5

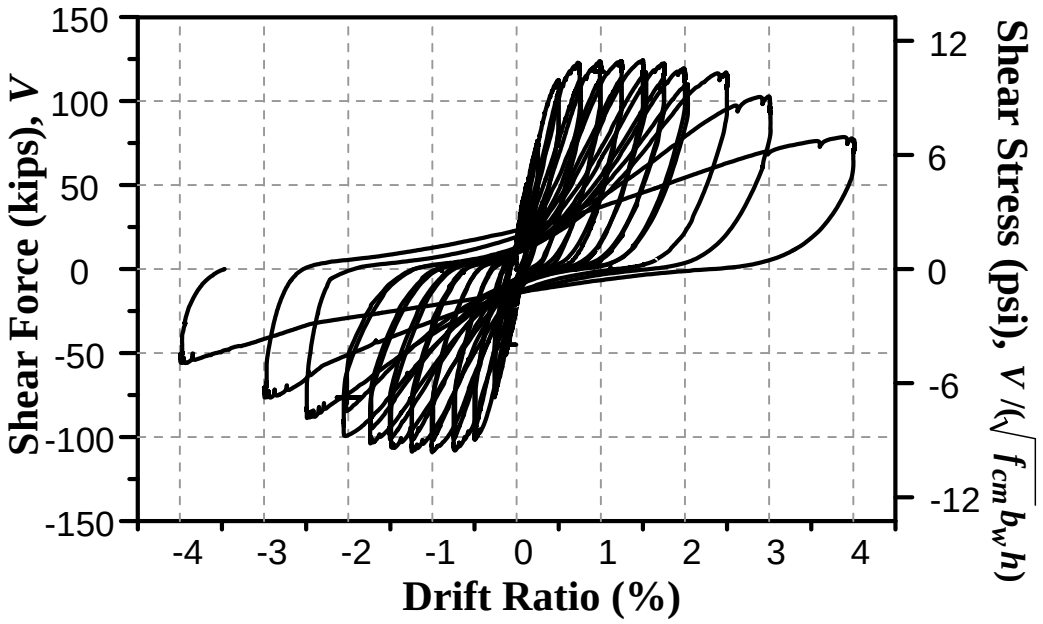

5.3.3 Steel reinforcement stresses

Strain gauges were attached at boundaries, longitudinal and horizontal steel bars as shown in Figure 5-26. Strain gauges L1 to L13 are attached at vertical steel bars, while S14 to S20 are attached at boundaries and horizontal steel bars. Results of drift ratio and the attained steel stress in strain gauges L1 to S20 are shown in Figure 5-27 to Figure 5-46. All vertical steel bars yielded (reached the yielding strength of (60 ksi) except strain gauge L11 which reached stress of 43 ksi. None of the boundaries or horizontal strain gauges reached the yielding strength.

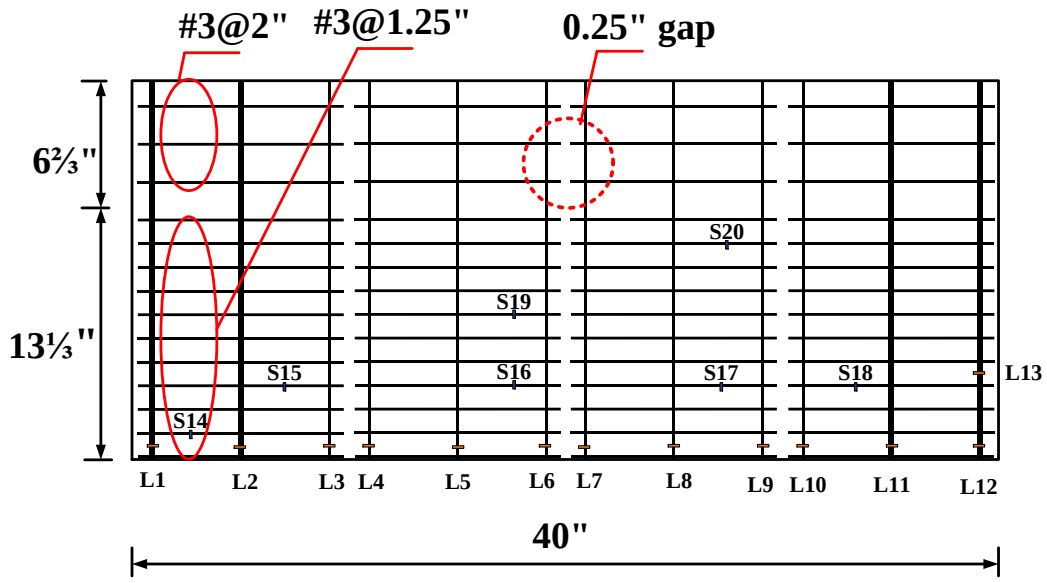

Figure 5-26 Locations of strain gauges at boundaries, vertical and horizontal steel bars for specimen SW-MA-0.5

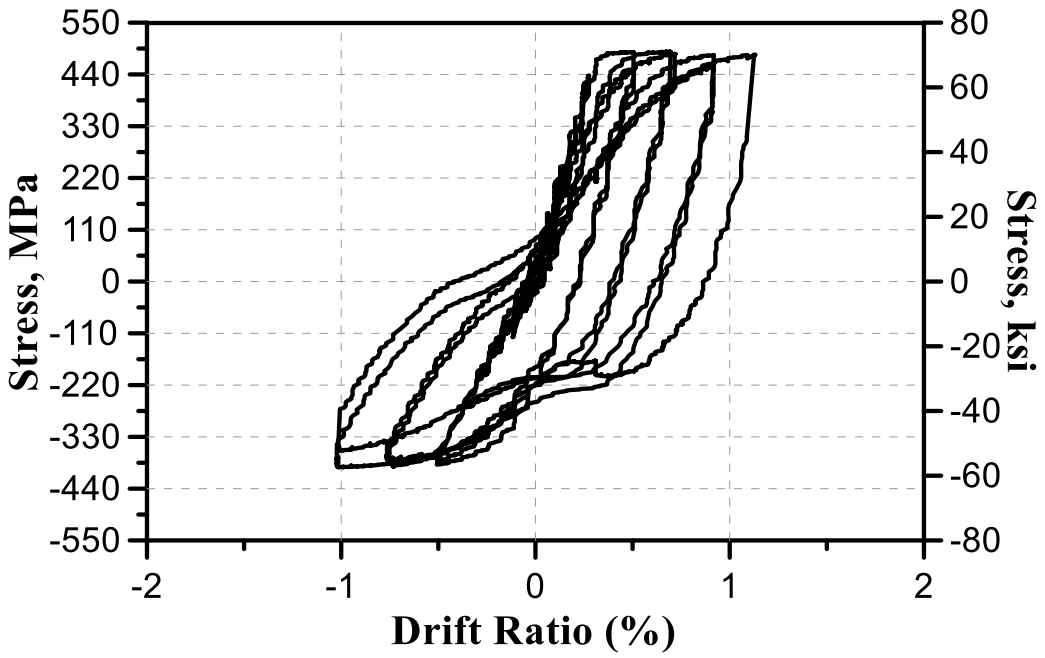

Figure 5-27 Measured stresses of strain gauge (L1) for specimen SW-MP-0.5

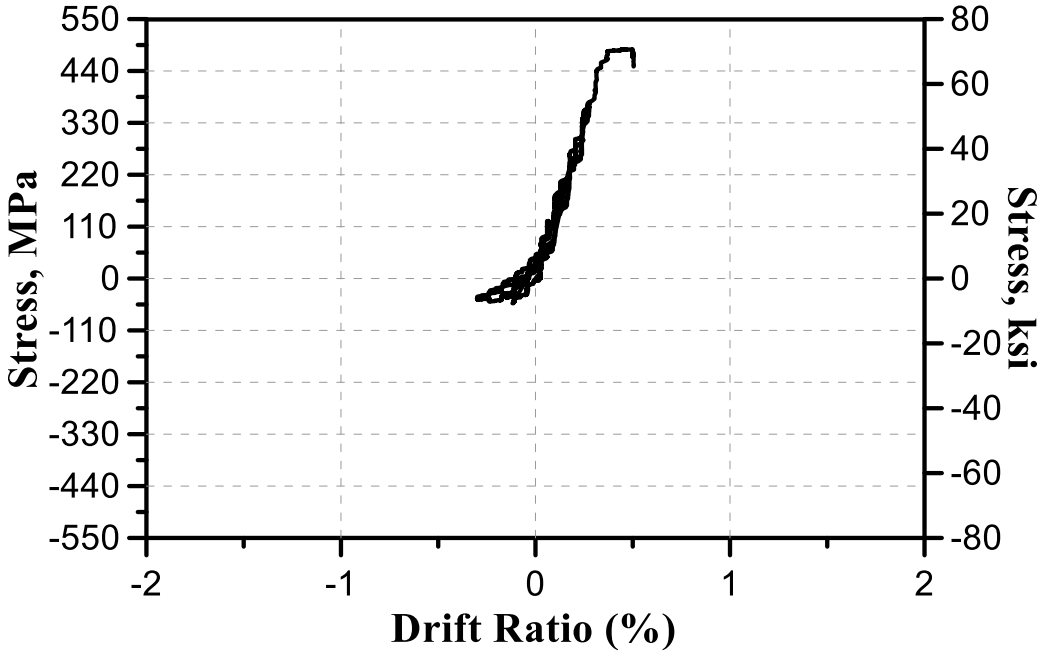

Figure 5-28 Measured stresses of strain gauge (L2) for specimen SW-MP-0.5

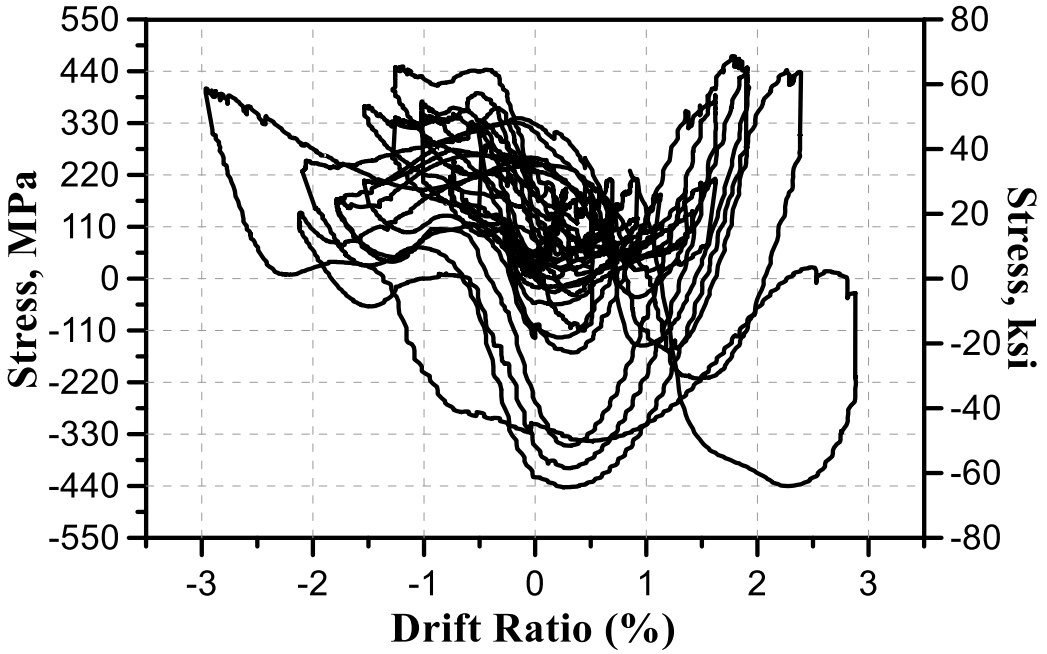

Figure 5-29 Measured stresses of strain gauge (L3) for specimen SW-MP-0.5

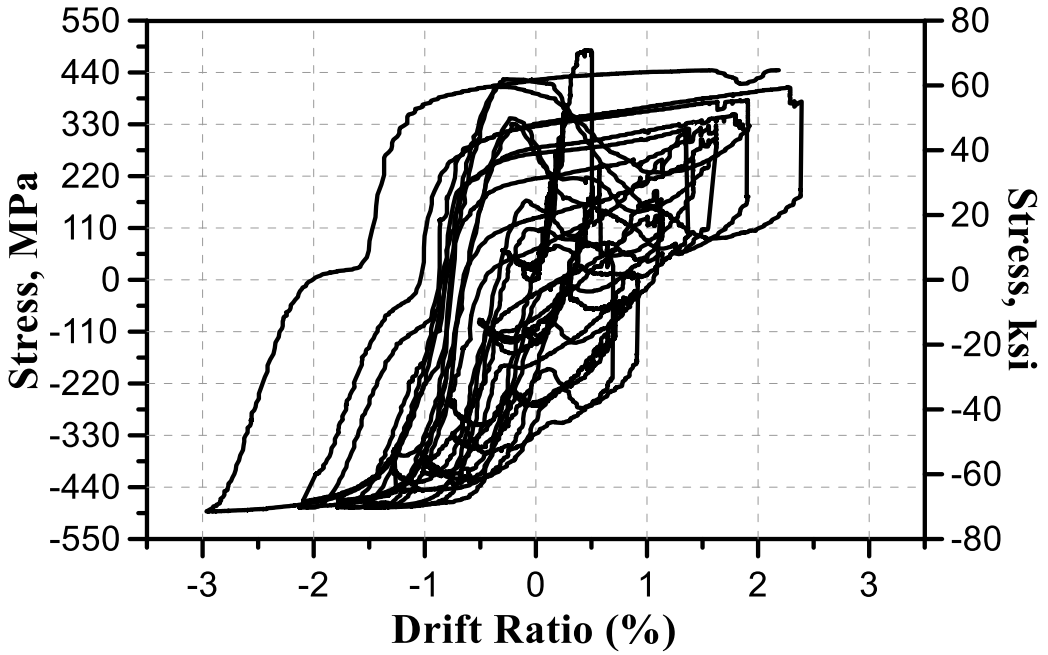

Figure 5-30 Measured stresses of strain gauge (L4) for specimen SW-MP-0.5

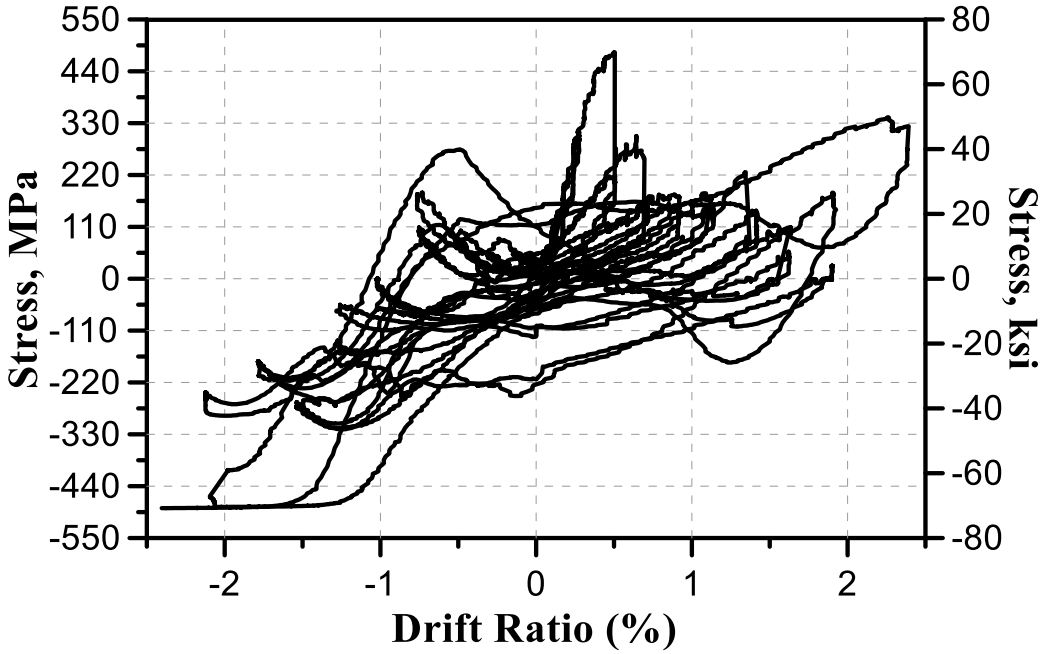

Figure 5-31 Measured stresses of strain gauge (L5) for specimen SW-MP-0.5

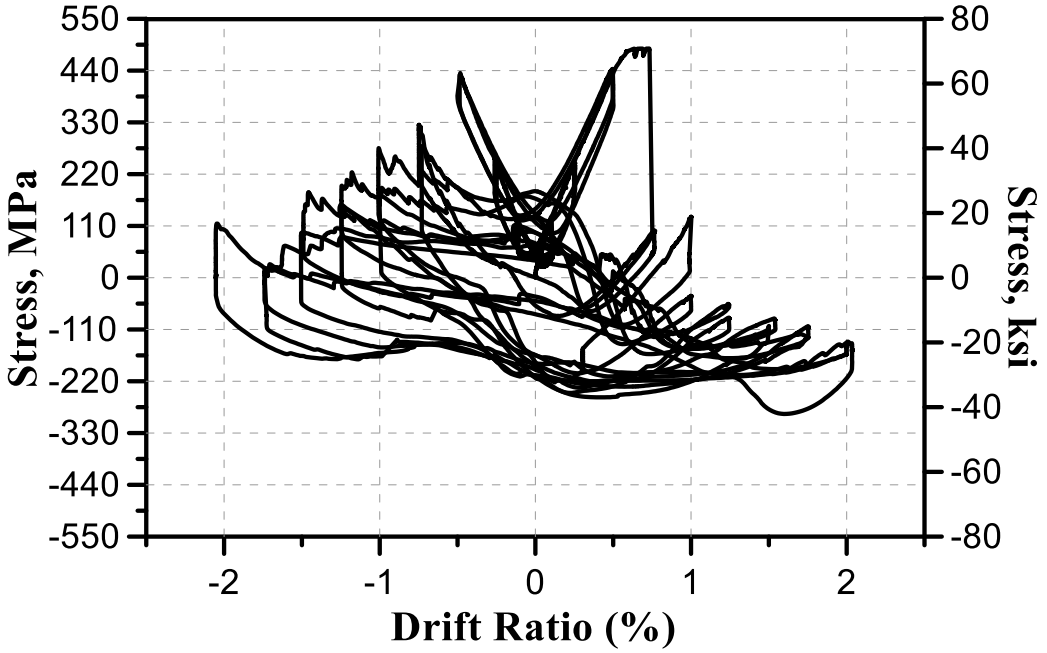

Figure 5-32 Measured stresses of strain gauge (L6) for specimen SW-MP-0.5

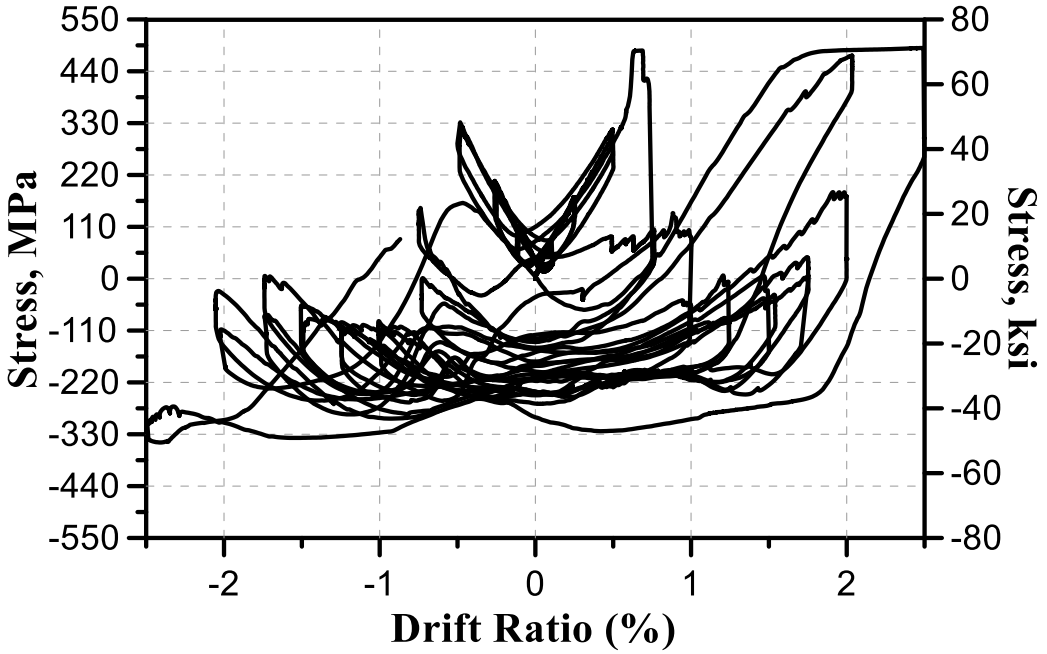

Figure 5-33 Measured stresses of strain gauge (L7) for specimen SW-MP-0.5

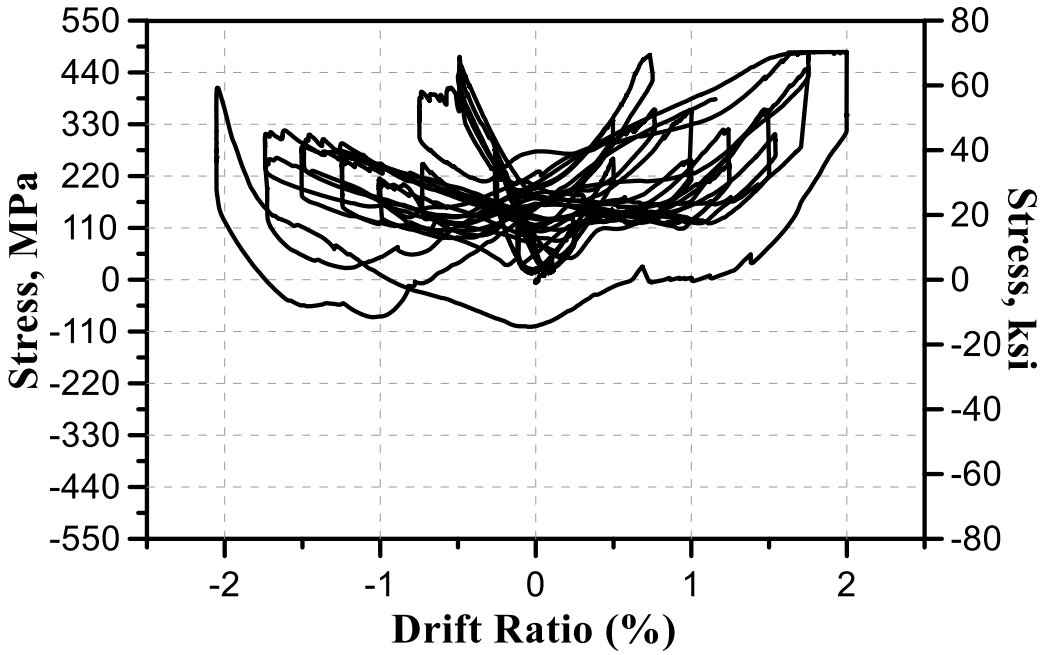

Figure 5-34 Measured stresses of strain gauge (L8) for specimen SW-MP-0.5

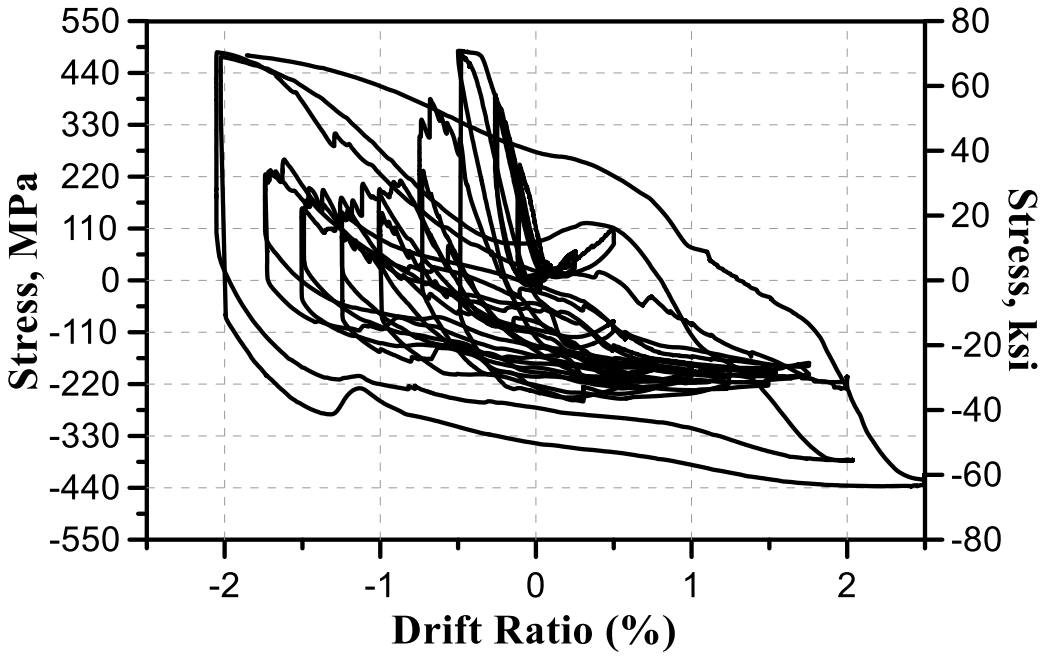

Figure 5-35 Measured stresses of strain gauge (L9) for specimen SW-MP-0.5

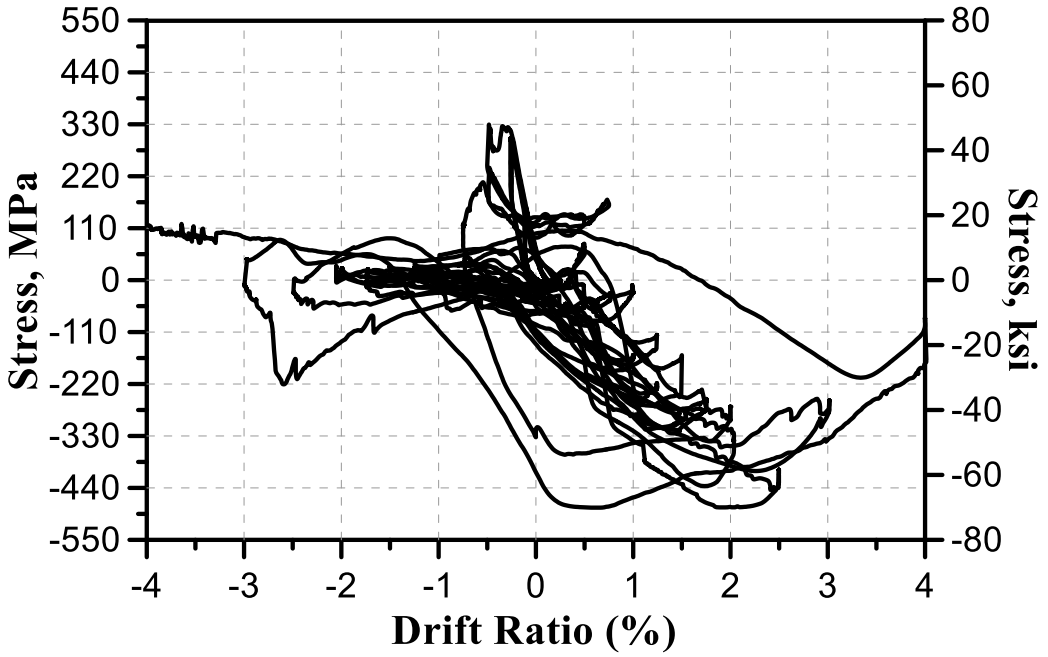

Figure 5-36 Measured stresses of strain gauge (L10) for specimen SW-MP-0.5

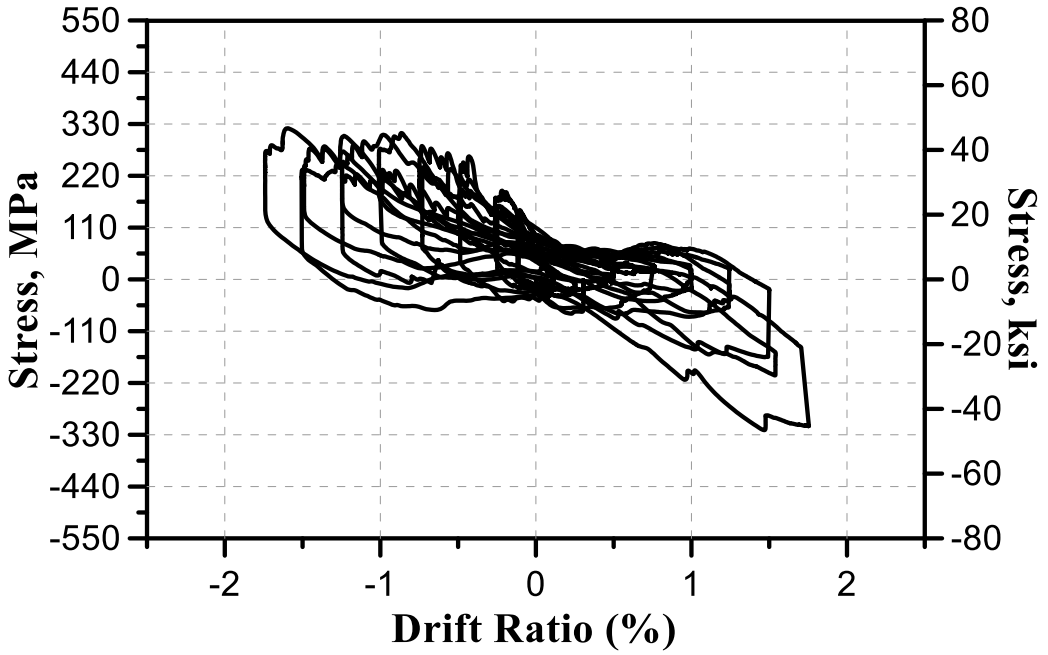

Figure 5-37 Measured stresses of strain gauge (L11) for specimen SW-MP-0.5

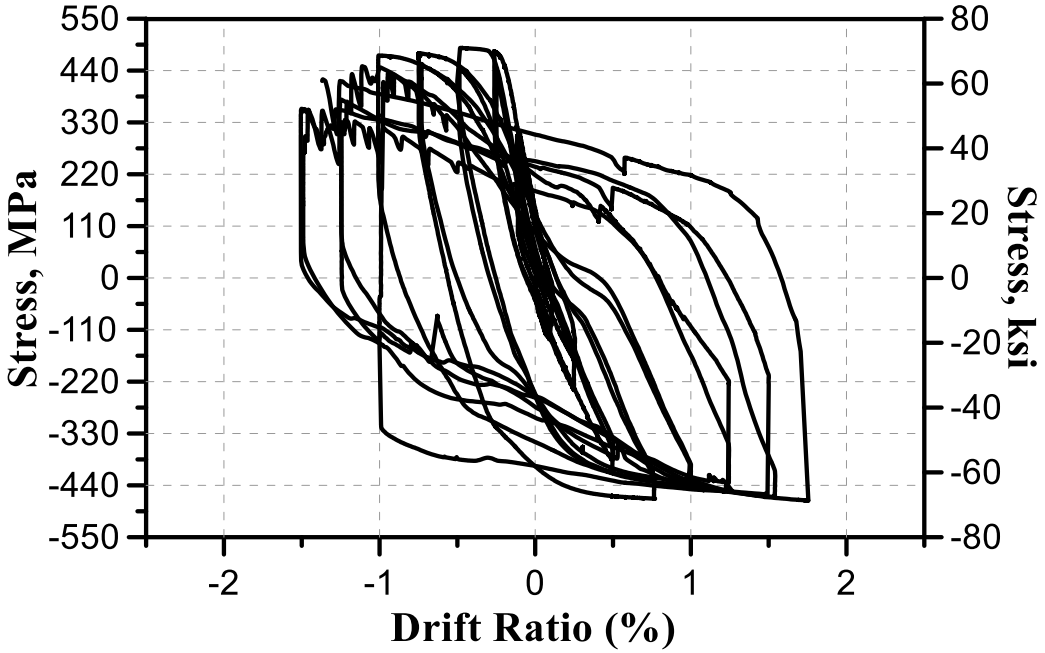

Figure 5-38 Measured stresses of strain gauge (L12) for specimen SW-MP-0.5

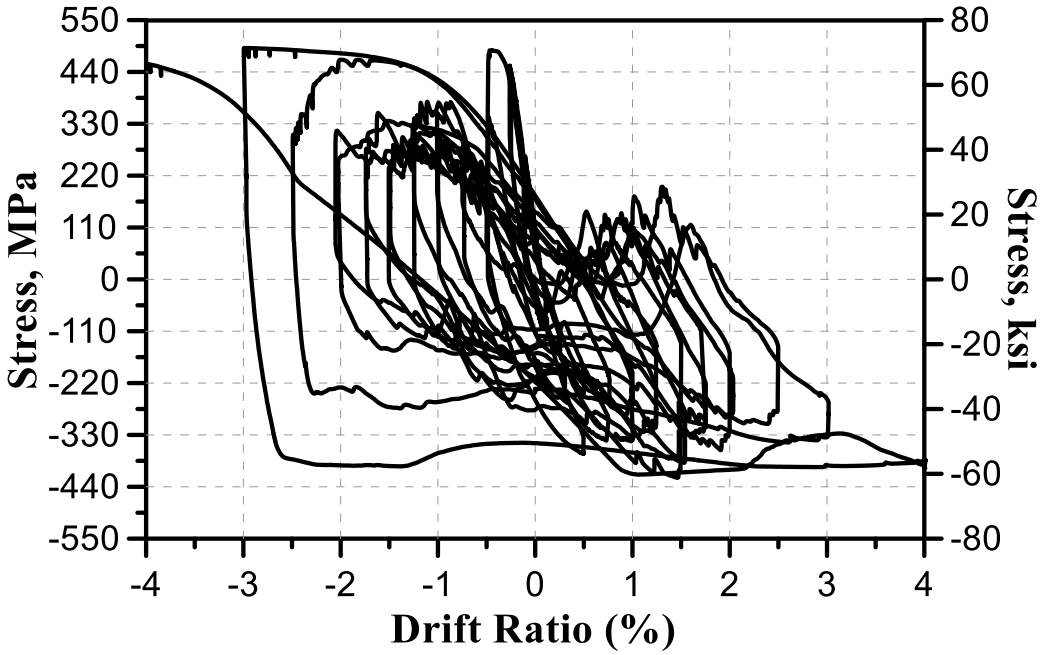

Figure 5-39 Measured stresses of strain gauge (L13) for specimen SW-MP-0.5

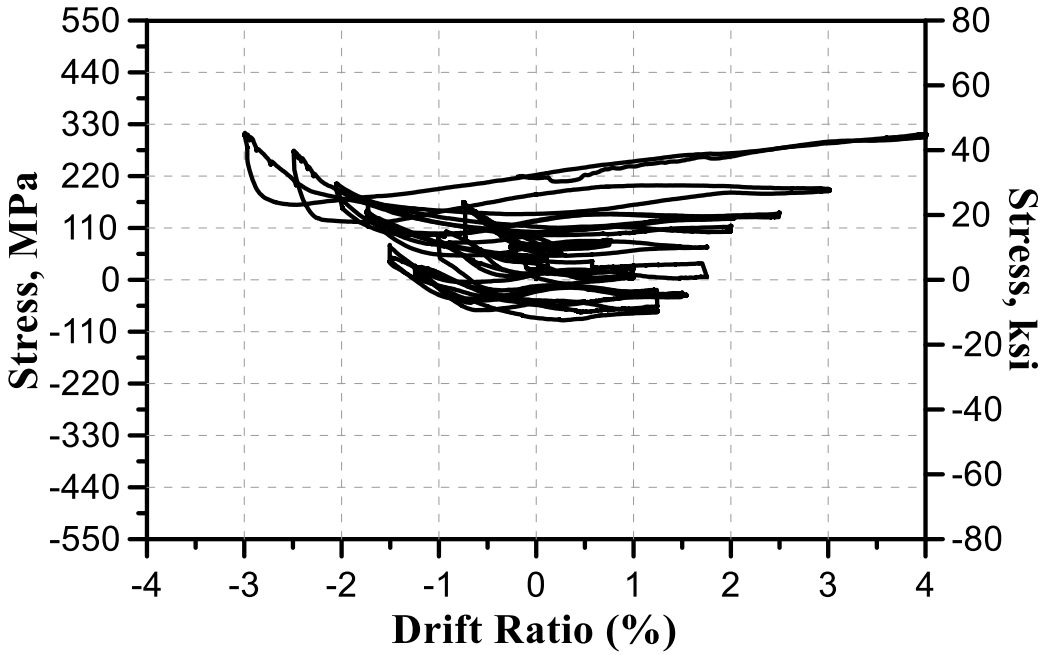

Figure 5-40 Measured stresses of strain gauge (S14) for specimen SW-MP-0.5

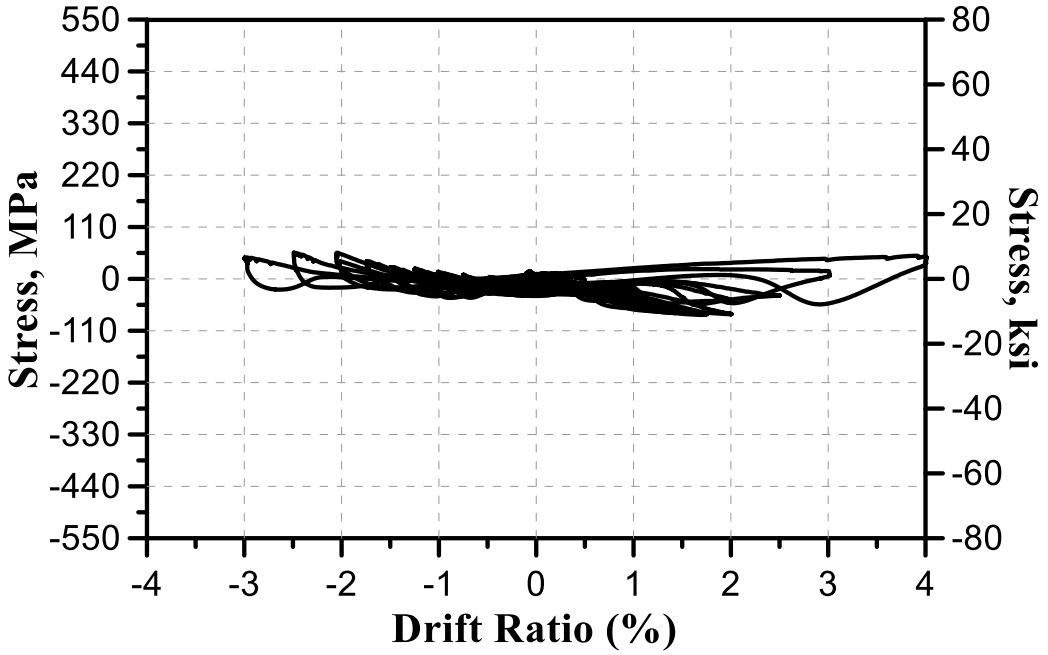

Figure 5-41 Measured stresses of strain gauge (S15) for specimen SW-MP-0.5

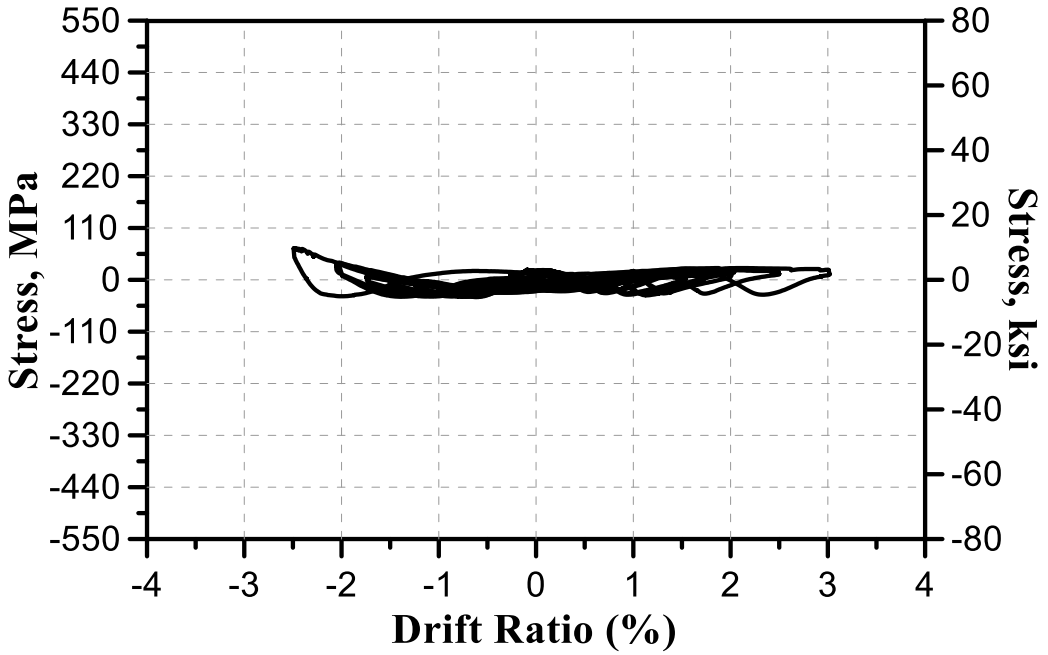

Figure 5-42 Measured stresses of strain gauge (S16) for specimen SW-MP-0.5

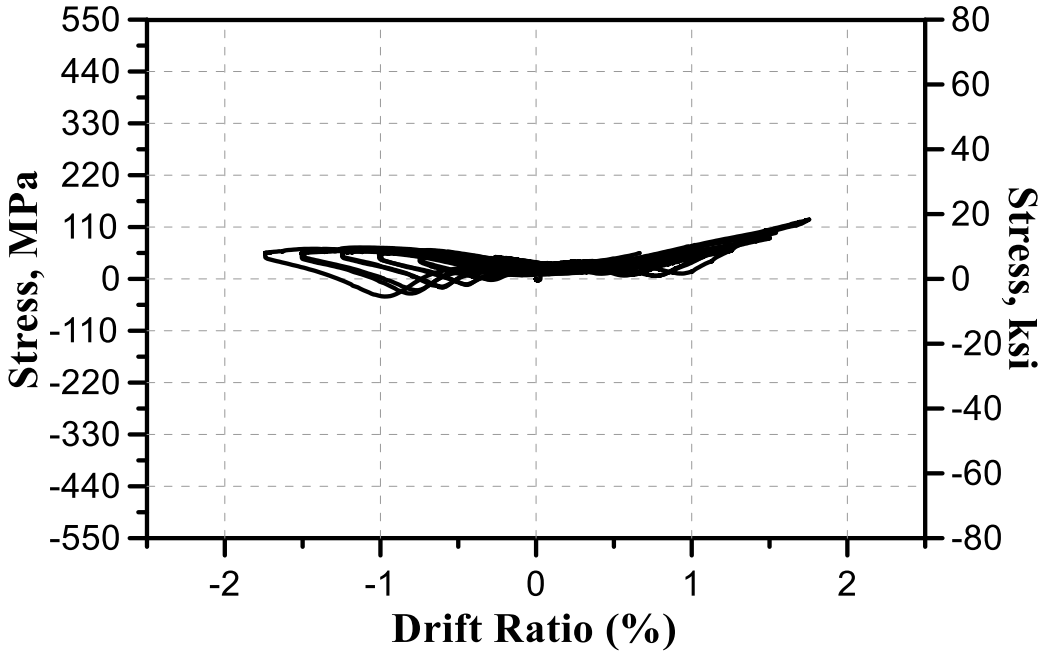

Figure 5-43 Measured stresses of strain gauge (S17) for specimen SW-MP-0.5

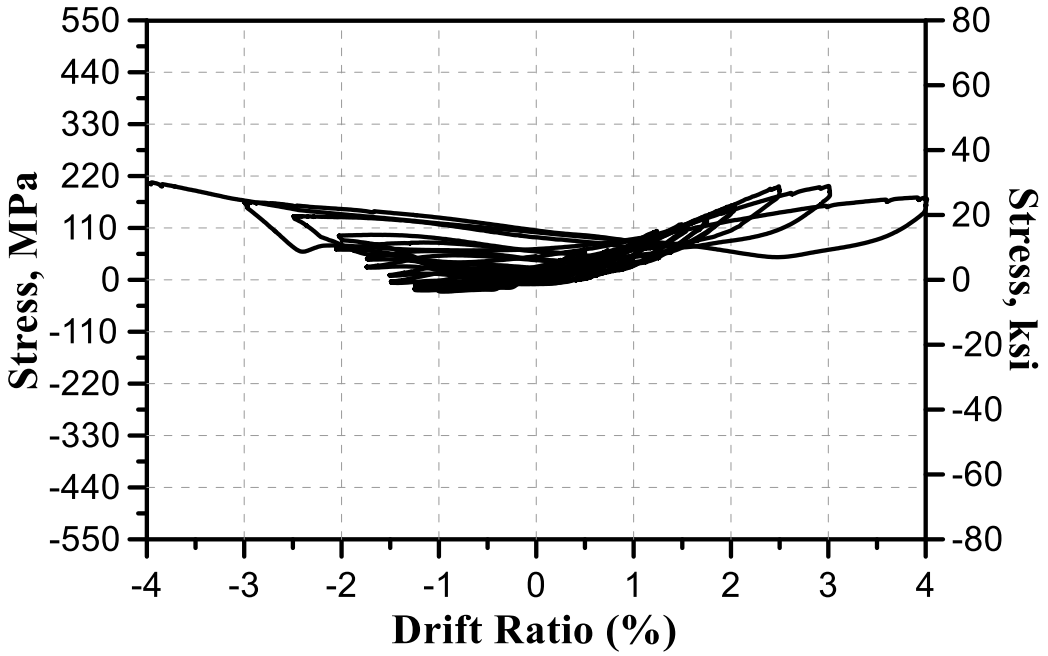

Figure 5-44 Measured stresses of strain gauge (S18) for specimen SW-MP-0.5

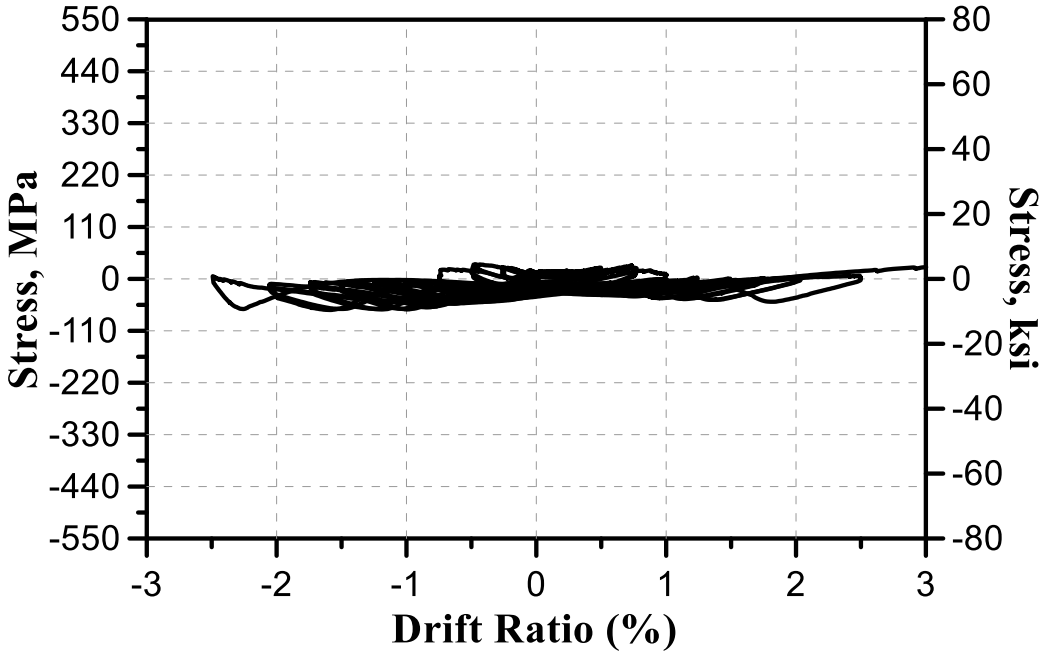

Figure 5-45 Measured stresses of strain gauge (S19) for specimen SW-MP-0.5

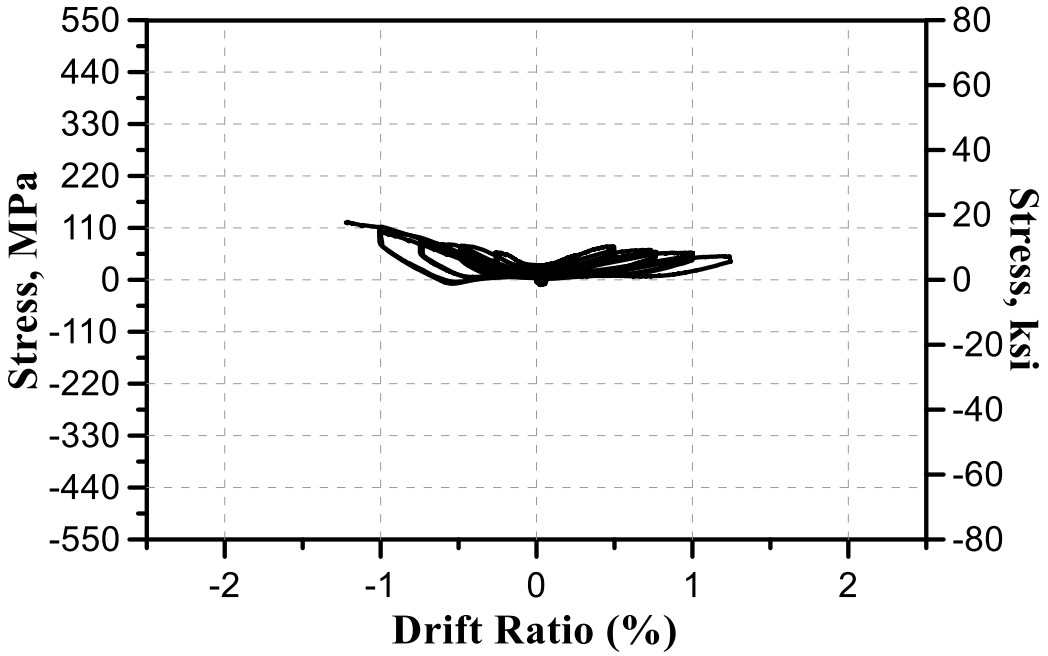

Figure 5-46 Measured stresses of strain gauge (S20) for specimen SW-MP-0.5

5.4 SW-HA-0.5

5.4.1 Damage and Cracking Pattern

Shear and flexural cracks propagation at drift ratio 0.125%, 0.25%, 0.5%, 0.75%, 1%, 1.25%, 1.5%, 1.75%, and 2% are shown in Figure 5-47. A drastic explosive struts crushing was observed over testing the ACI-compliant wall, SW-HA-0.5, at the first cycle of 1% drift ratio (Figure 5-47), resulting in sharp shear strength drop from 275 kips to 70 kips. Afterwards, struts crushing spread toward wall boundaries, forming sliding shear failure along the wall length, and shear forces are only resisted by dowel action.

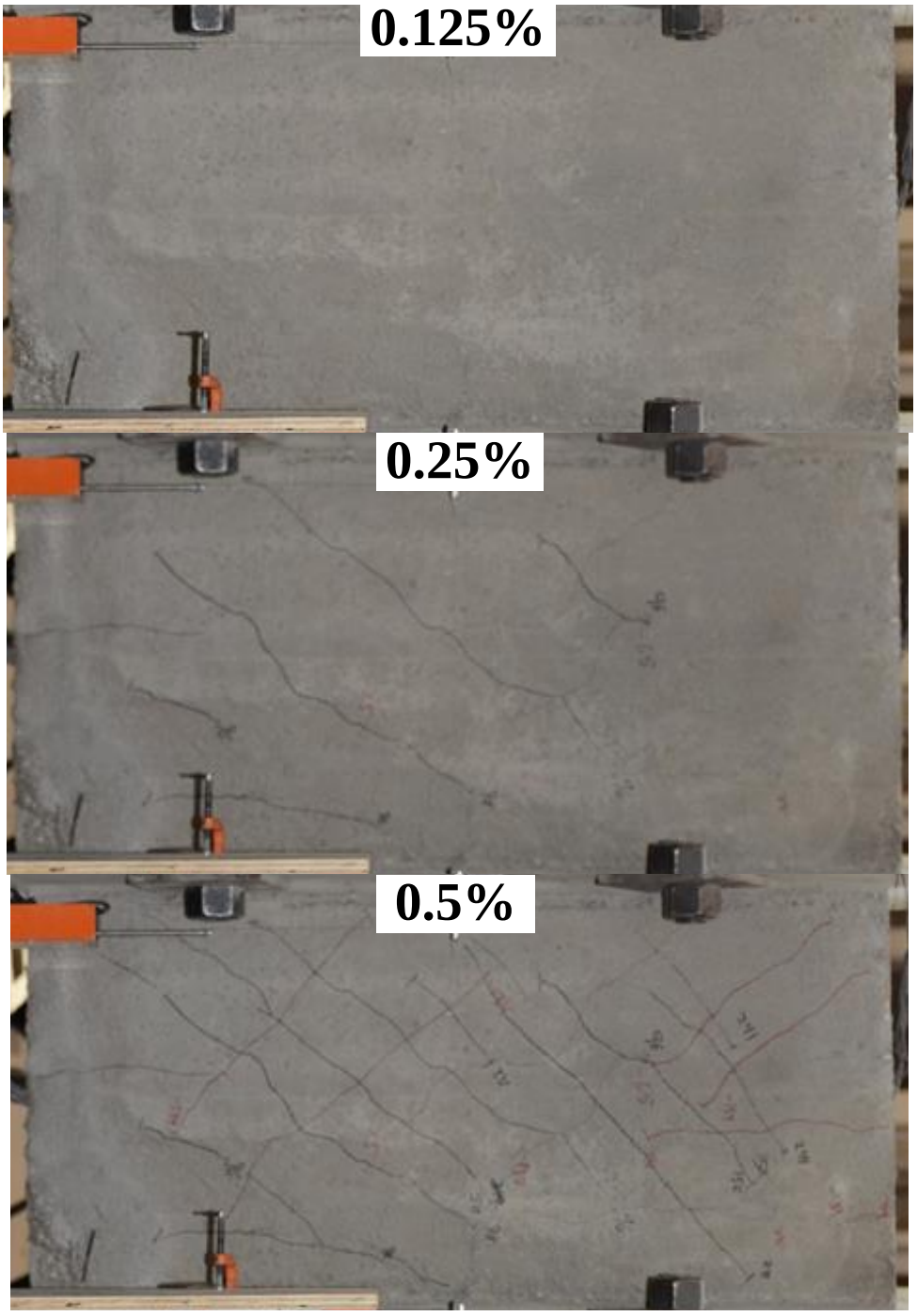

Figure 5-47 Test results of specimen SW-HA-0.5 at drift ratio 0.125%, 0.25%, 0.5%, 0.75%, 1%, 1.25%, 1.5%, 1.75%, and 2% (continued)

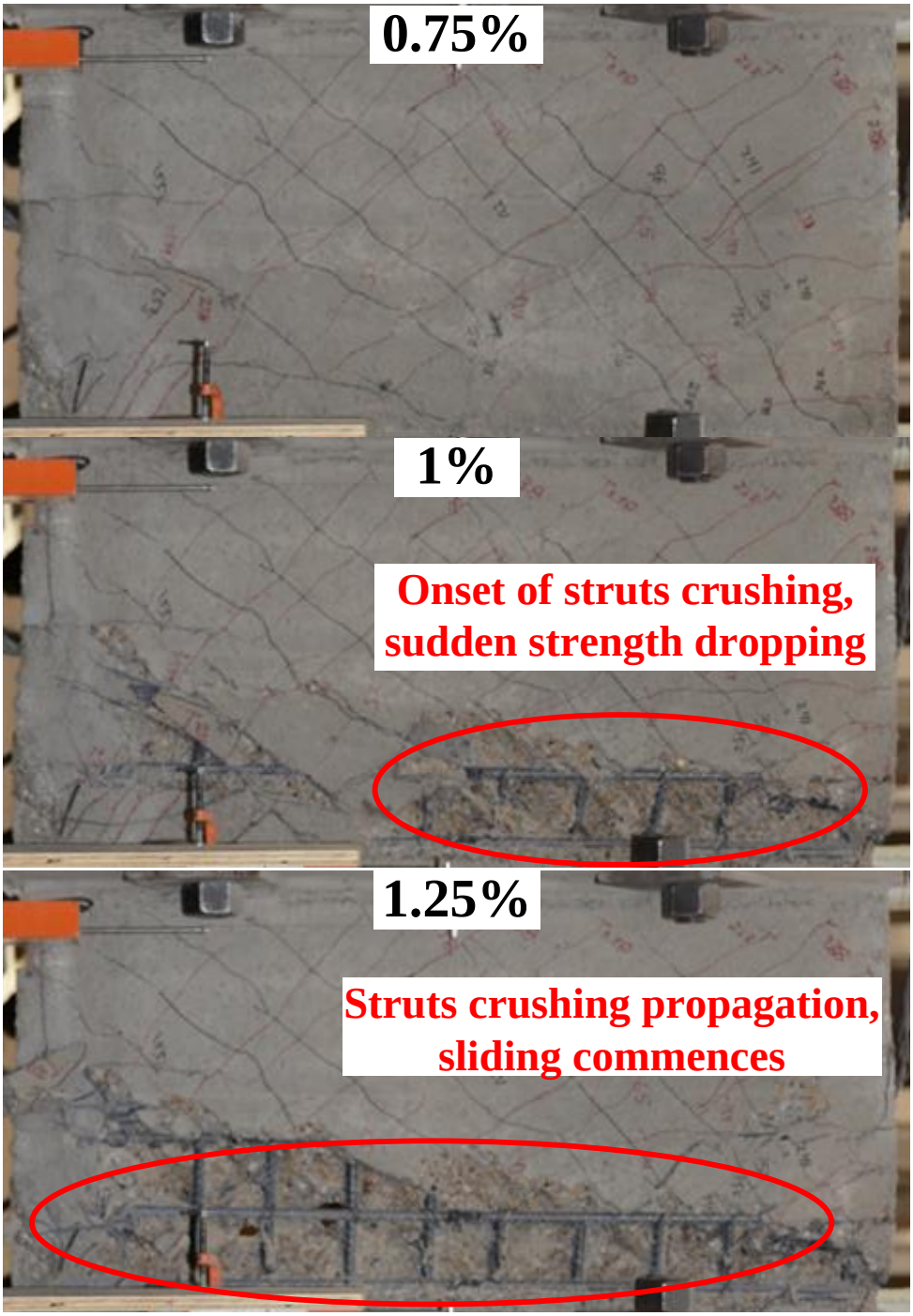

Figure 5-47 Test results of specimen SW-HA-0.5 at drift ratio 0.125%, 0.25%, 0.5%, 0.75%, 1%, 1.25%, 1.5%, 1.75%, and 2% (continued)

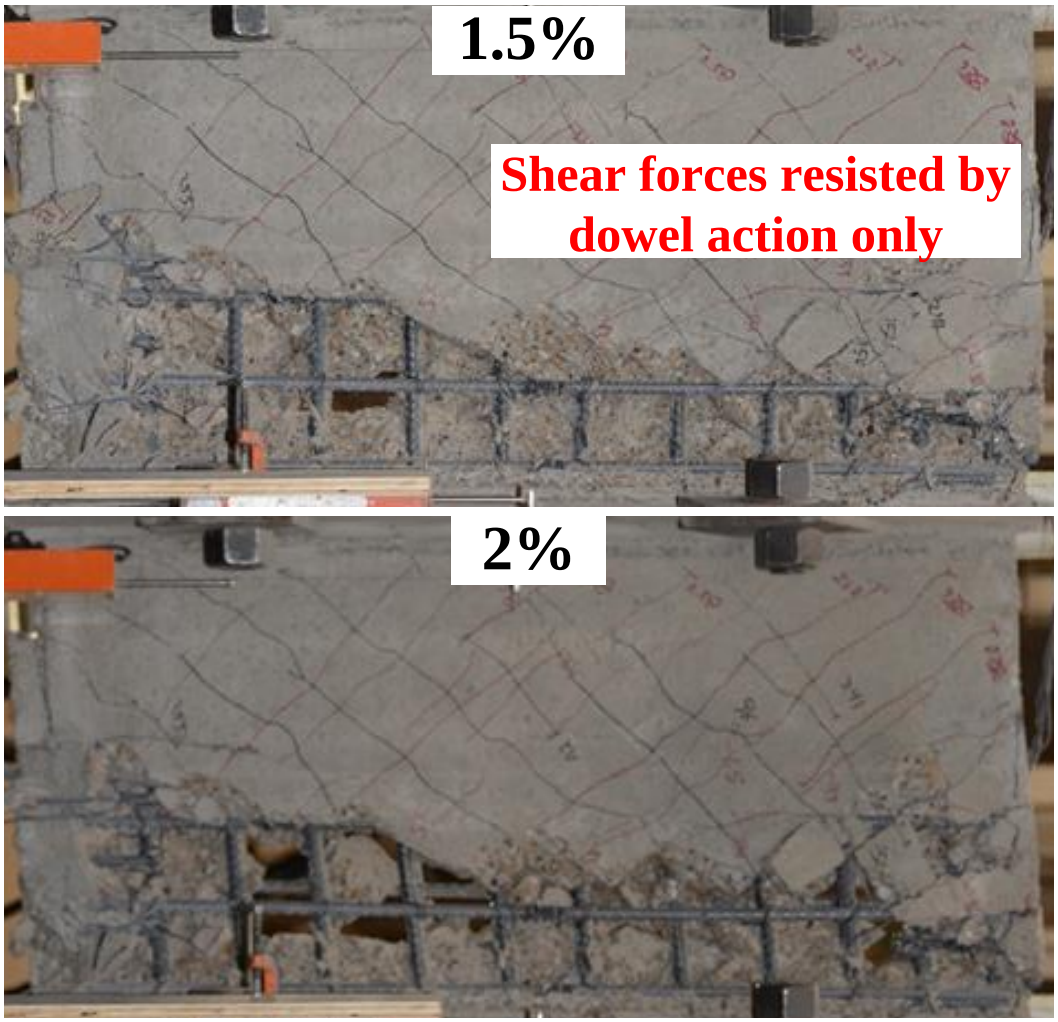

Figure 5-47 Test results of specimen SW-HA-0.5 at drift ratio 0.125%, 0.25%, 0.5%, 0.75%, 1%, 1.25%, 1.5%, 1.75%, and 2% (continued)

5.4.2 Shear strength response

Shear force versus drift ratio response of specimen SW-HA-0.5 is shown in Figure 5-48. The maximum achieved shear force was 275 kips ($23.6\sqrt{f_{cm}}$) at drift ratio 1%. However, sudden drop in shear strength commenced at this drift level due to sliding shear failure, where the diagonal concrete struts at boundaries crushed and no longer

resist shear forces, the shear forces are resisted by dowel action (kinking the longitudinal steel rebars).

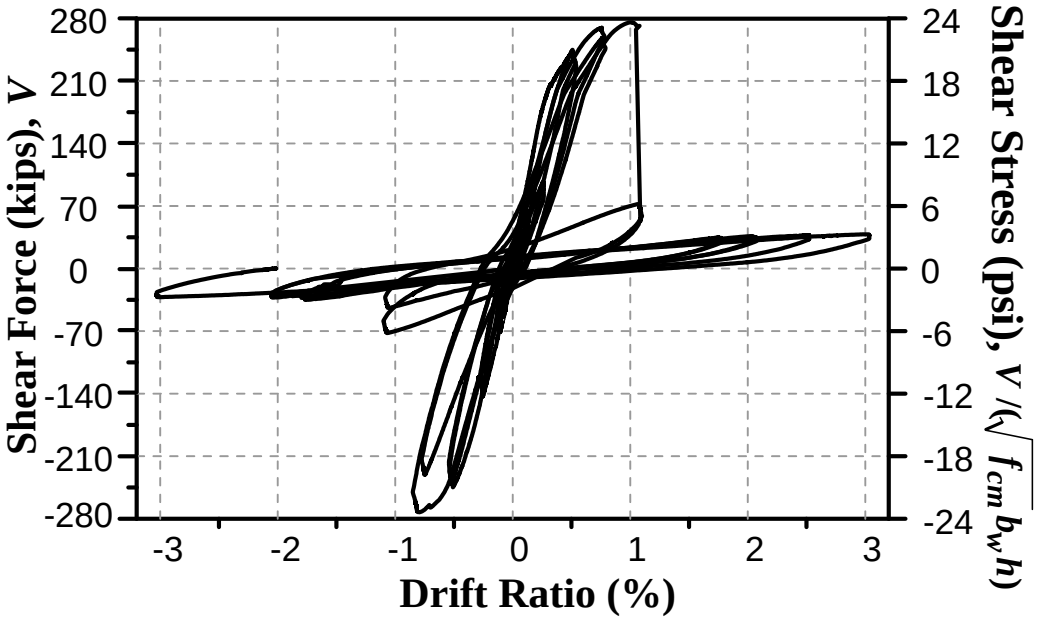

Figure 5-48 Shear strength hysteresis curve of specimen SW-HA-0.5

5.3.4 Steel reinforcement stresses

Strain gauges were attached at boundaries, longitudinal and horizontal steel bars as shown in Figure 5-49. Strain gauges L1 to L8 are attached at vertical steel bars, while S9 to S17 are attached at boundaries and horizontal steel bars. The results of drift ratio and the attained steel stress in strain gauges L1 to S17 are shown in Figure 5-50 to Figure 5-66. All vertical steel bars yielded (reached the yielding strength of (60 ksi). Also, almost at drift ratio 1%, all strain gauges at boundaries and horizontal steel bars yielded except S9, S10, and S15 which did not yield. The reason of yielding horizontal bars that sudden sliding shear failure started at 1%.

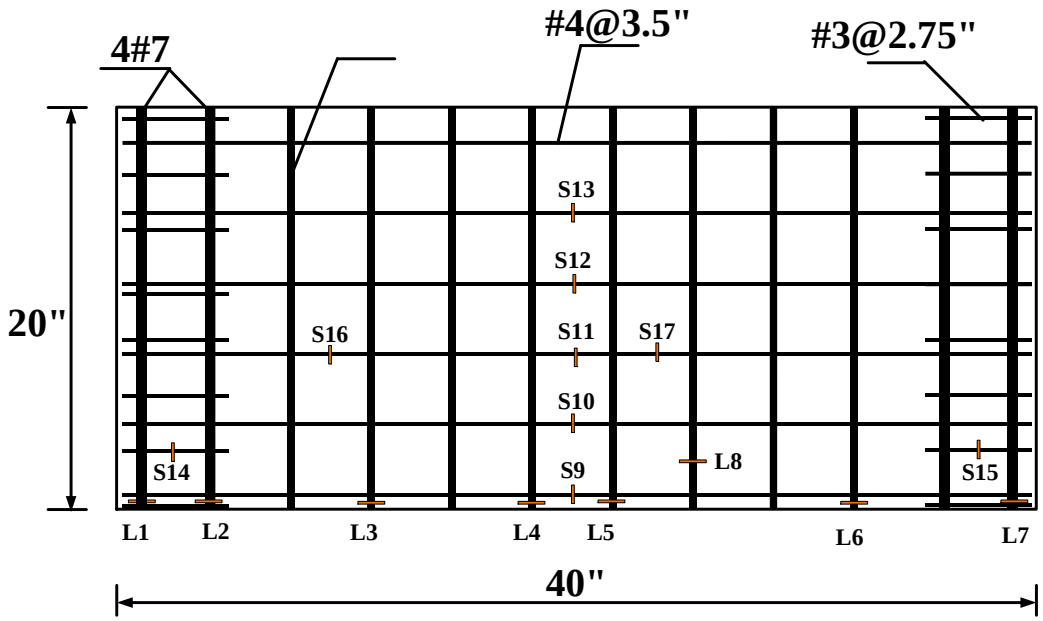

Figure 5-49 Locations of strain gauges at boundaries, vertical and horizontal steel bars for specimen SW-HA-0.5

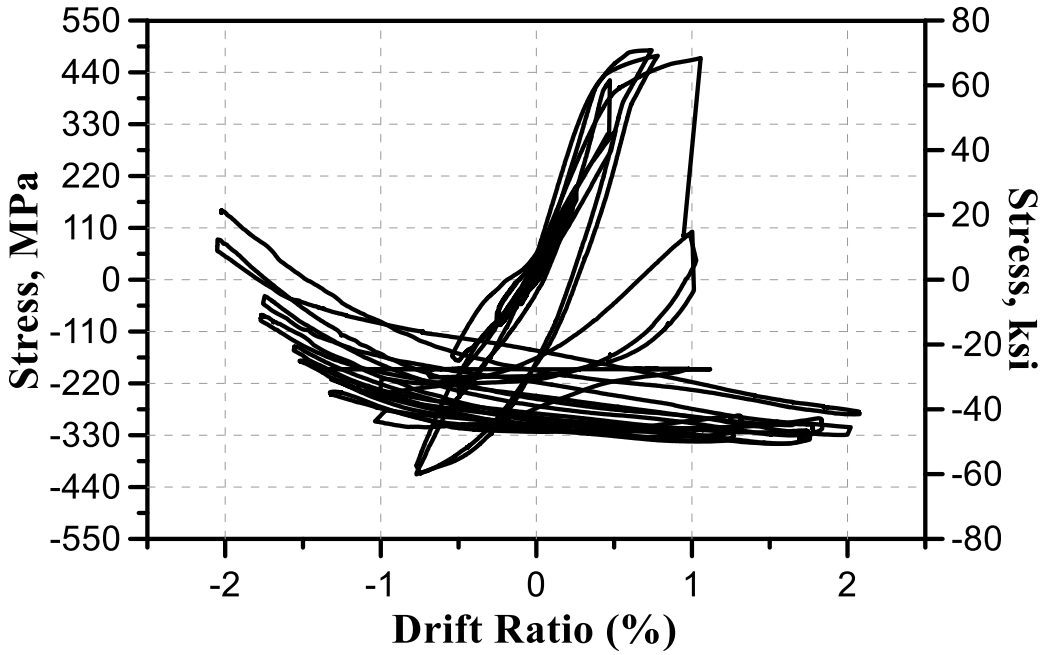

Figure 5-50 Measured stresses of strain gauge (L1) for specimen SW-HA-0.5

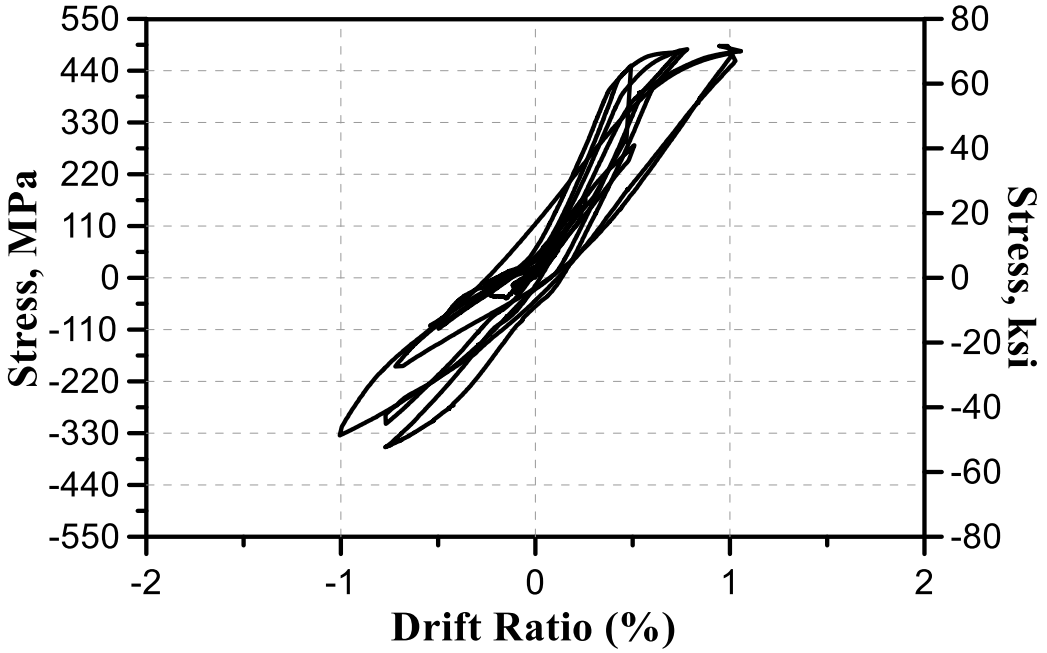

Figure 5-51 Measured stresses of strain gauge (L2) for specimen SW-HA-0.5

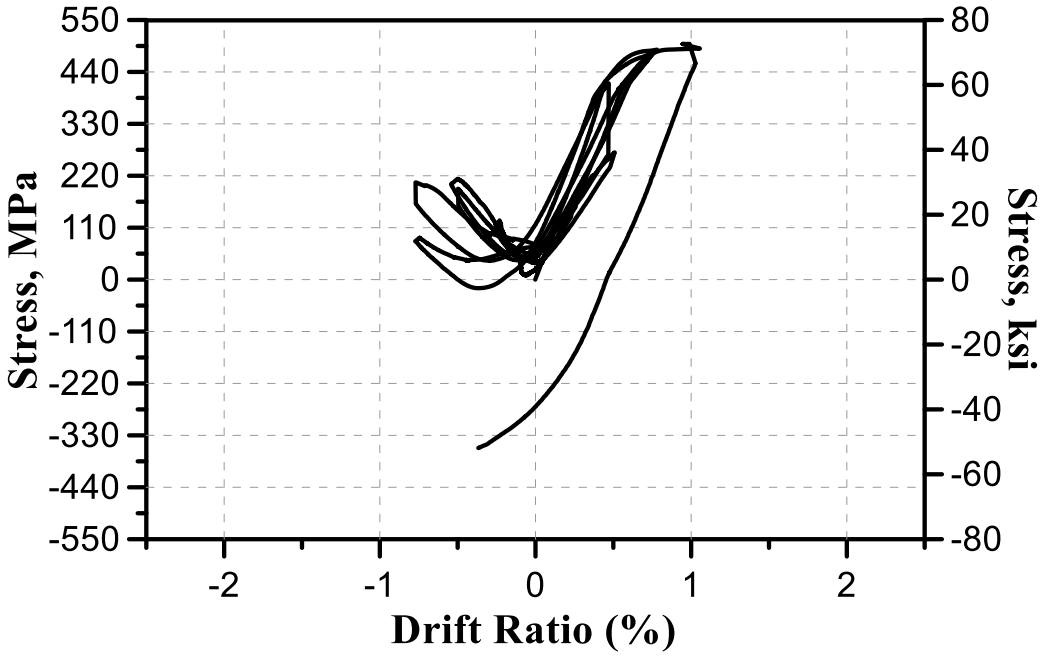

Figure 5-52 Measured stresses of strain gauge (L3) for specimen SW-HA-0.5

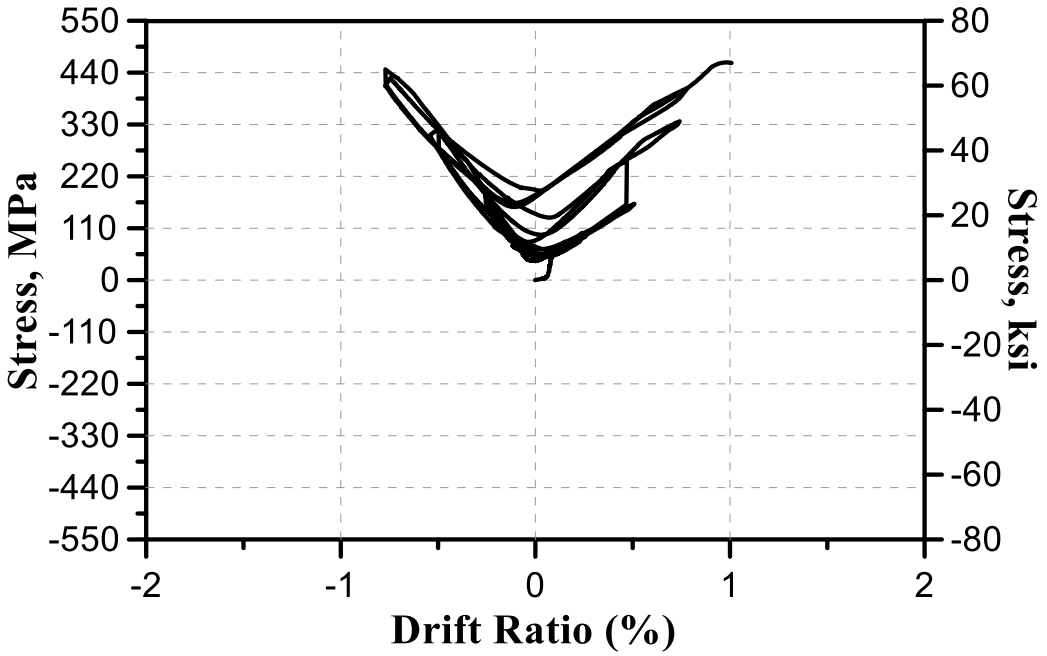

Figure 5-53 Measured stresses of strain gauge (L4) for specimen SW-HA-0.5

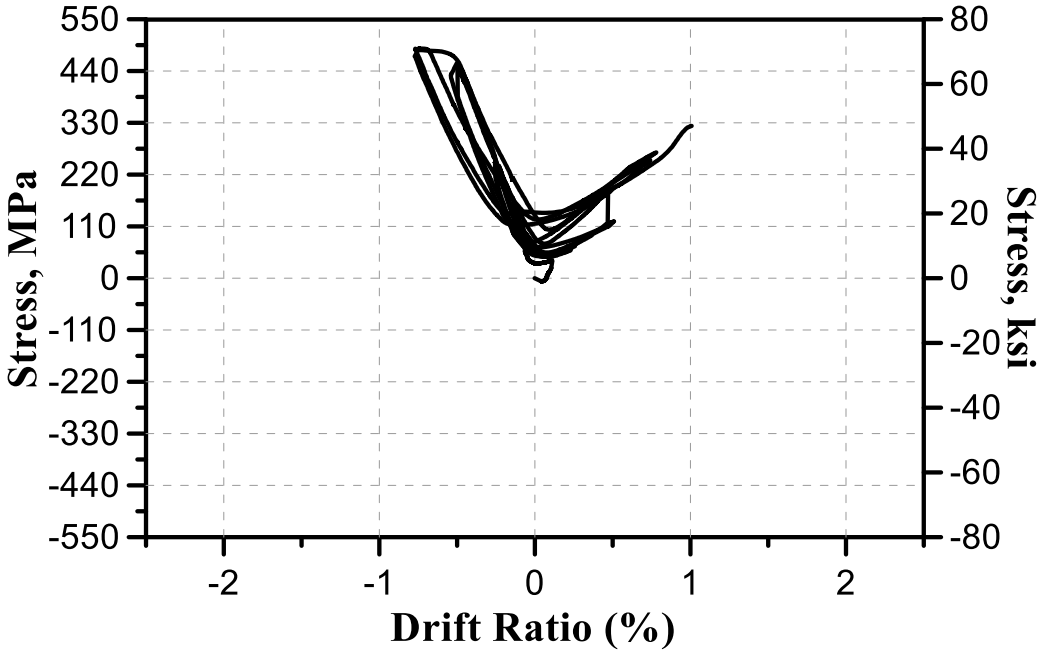

Figure 5-54 Measured stresses of strain gauge (L5) for specimen SW-HA-0.5

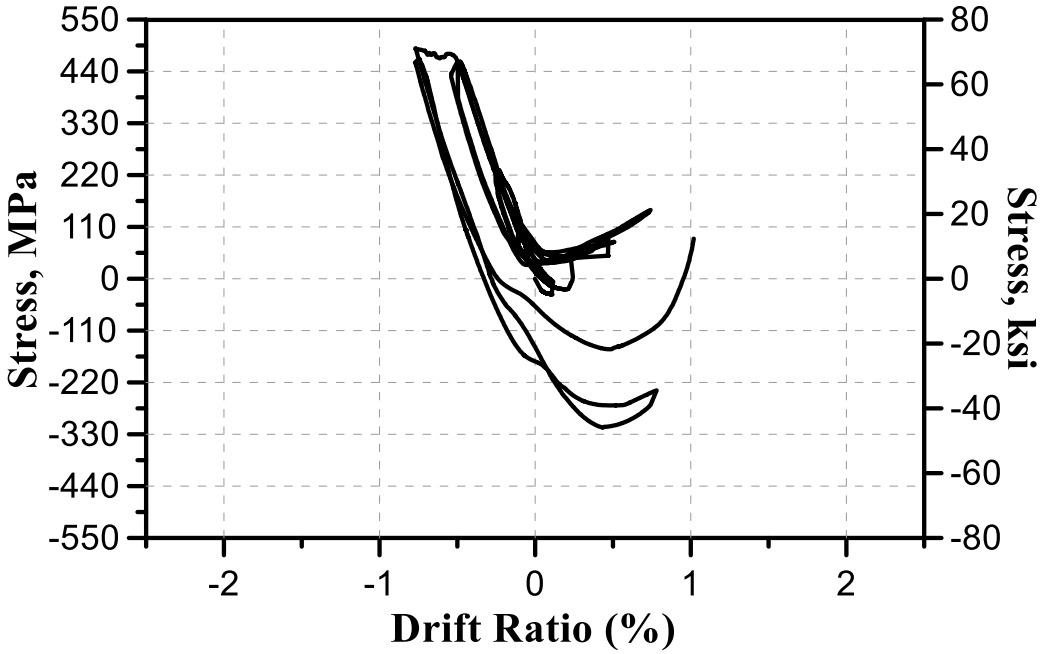

Figure 5-55 Measured stresses of strain gauge (L6) for specimen SW-HA-0.5

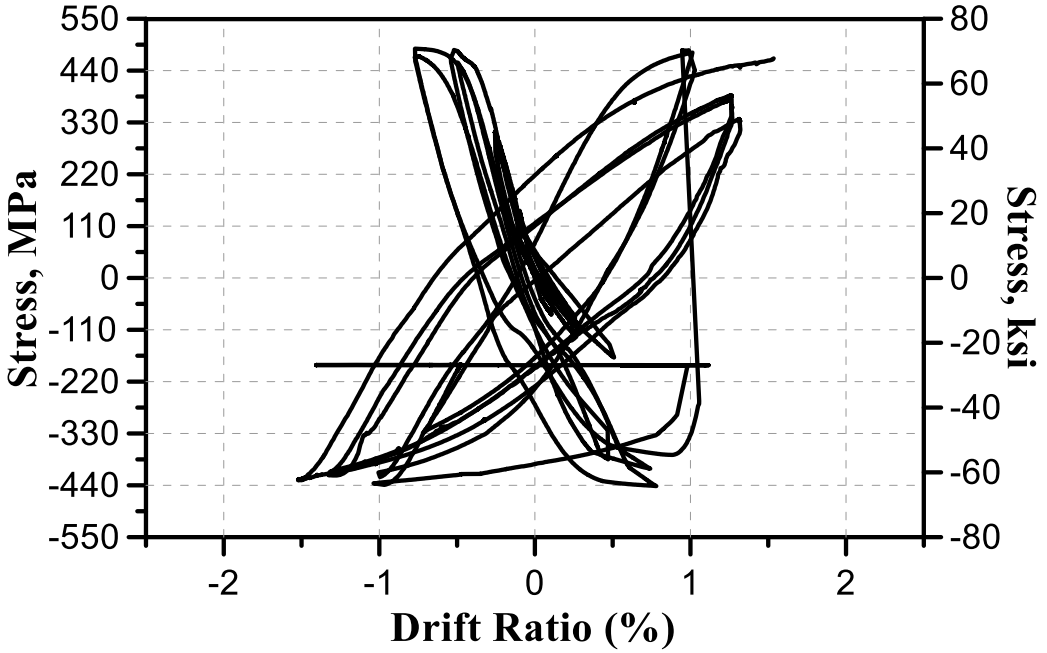

Figure 5-56 Measured stresses of strain gauge (L7) for specimen SW-HA-0.5

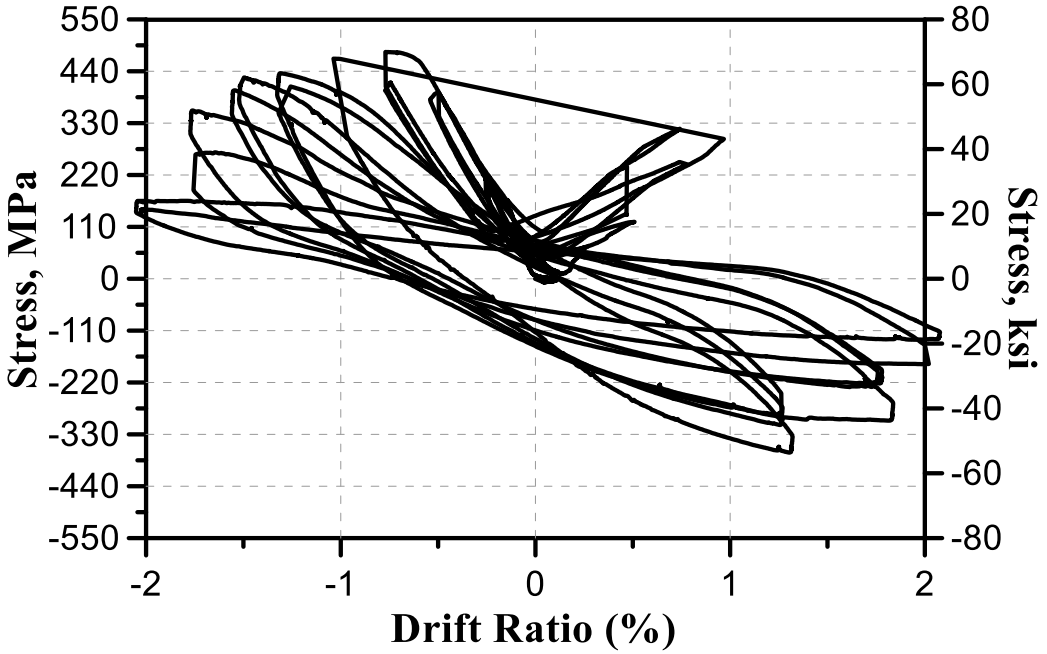

Figure 5-57 Measured stresses of strain gauge (L8) for specimen SW-HA-0.5

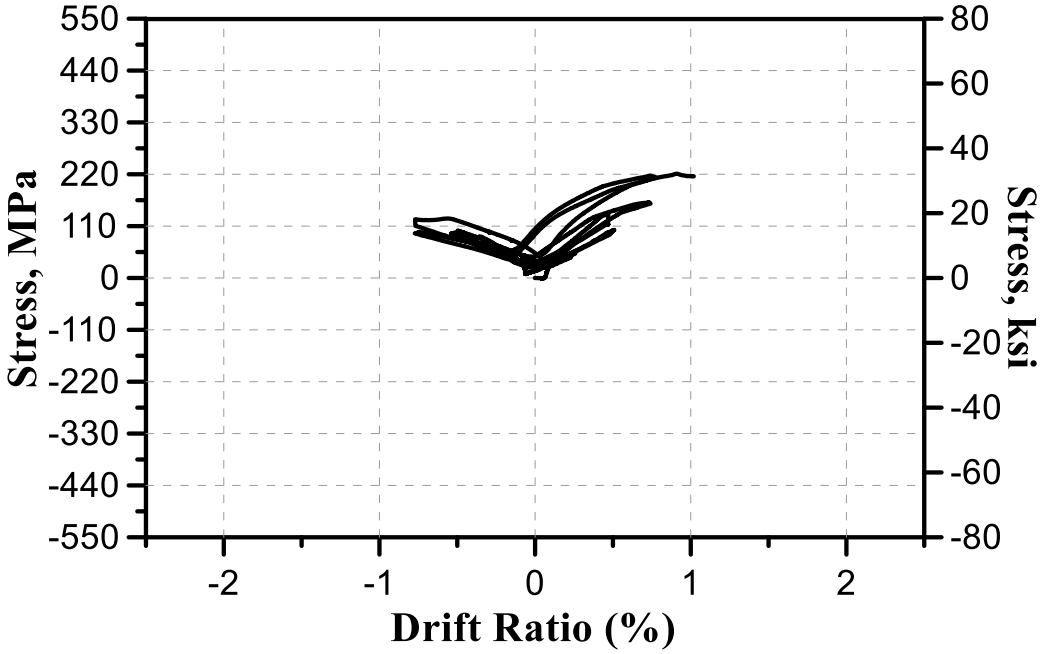

Figure 5-58 Measured stresses of strain gauge (S9) for specimen SW-HA-0.5

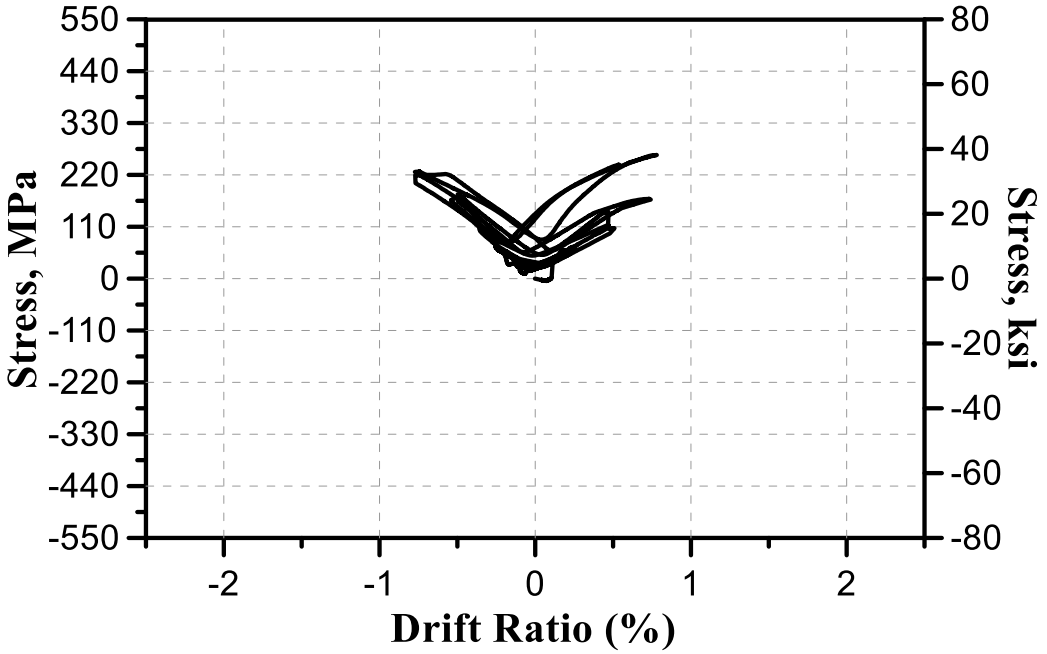

Figure 5-59 Measured stresses of strain gauge (S10) for specimen SW-HA-0.5

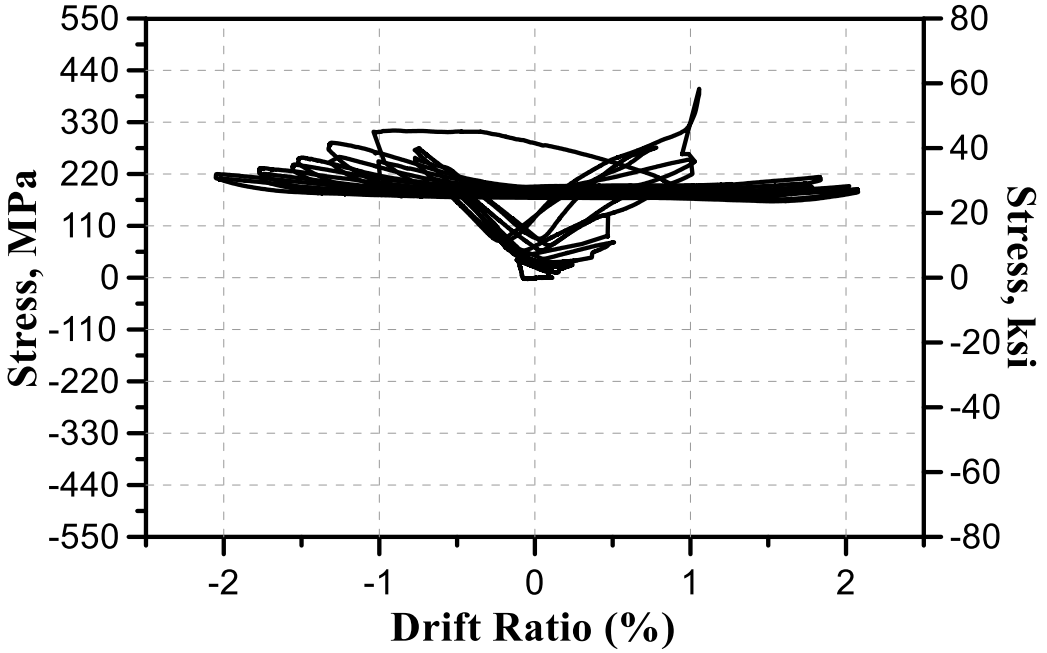

Figure 5-60 Measured stresses of strain gauge (S11) for specimen SW-HA-0.5

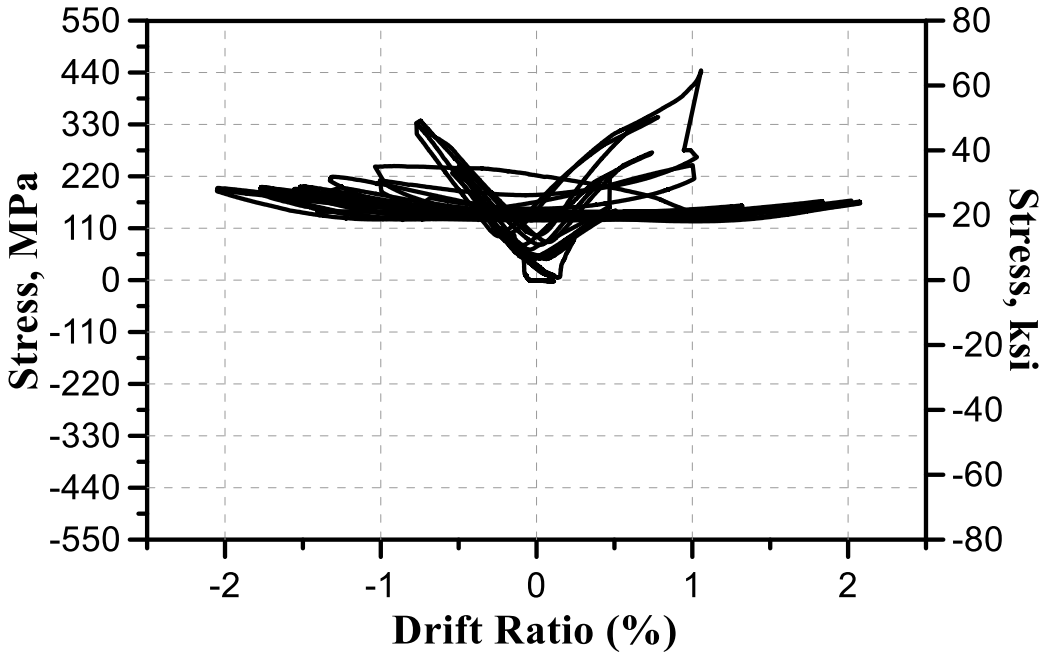

Figure 5-61 Measured stresses of strain gauge (S12) for specimen SW-HA-0.5

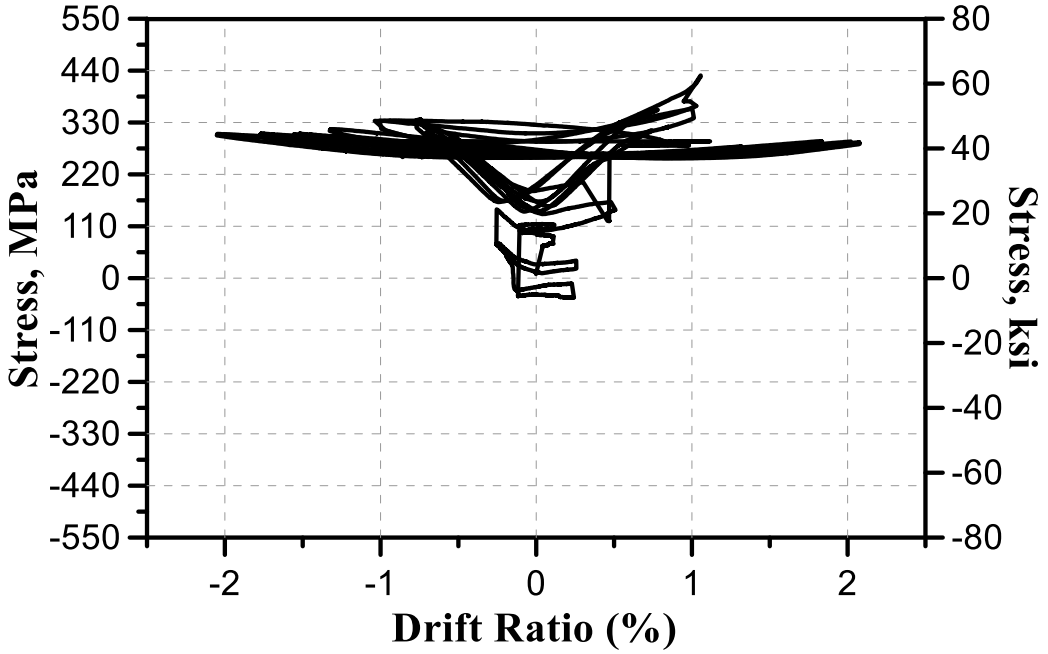

Figure 5-62 Measured stresses of strain gauge (S13) for specimen SW-HA-0.5

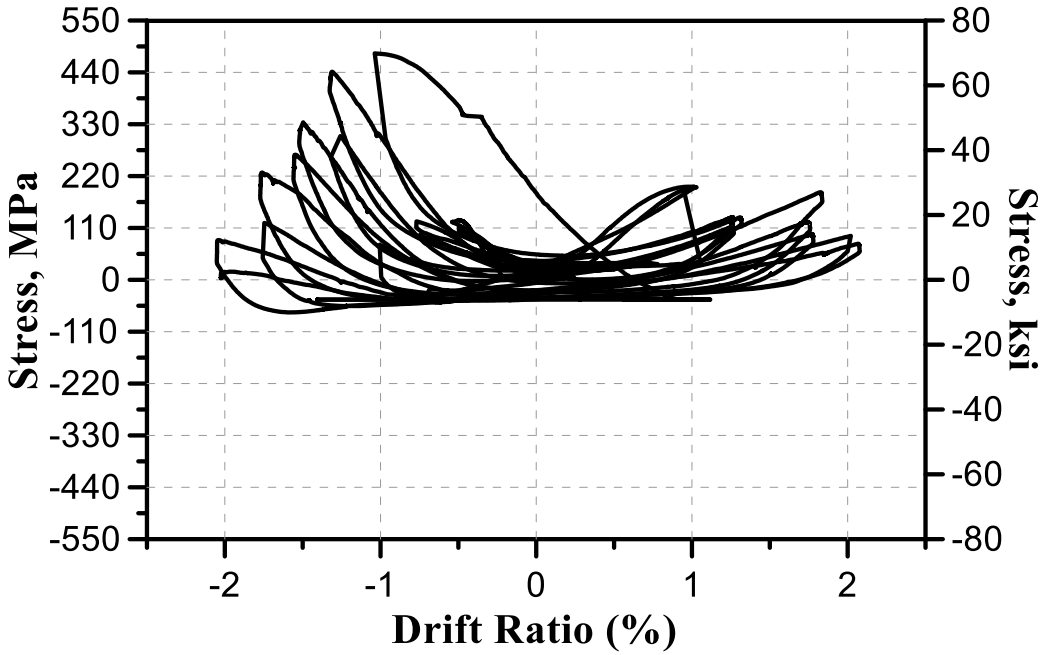

Figure 5-63 Measured stresses of strain gauge (S14) for specimen SW-HA-0.5

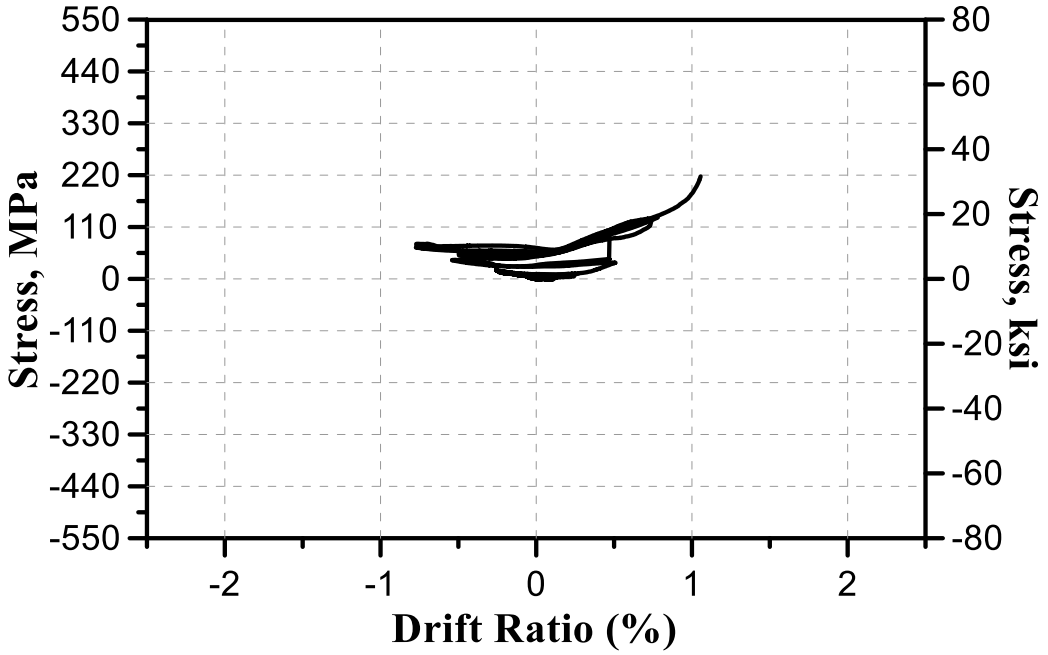

Figure 5-64 Measured stresses of strain gauge (S15) for specimen SW-HA-0.5

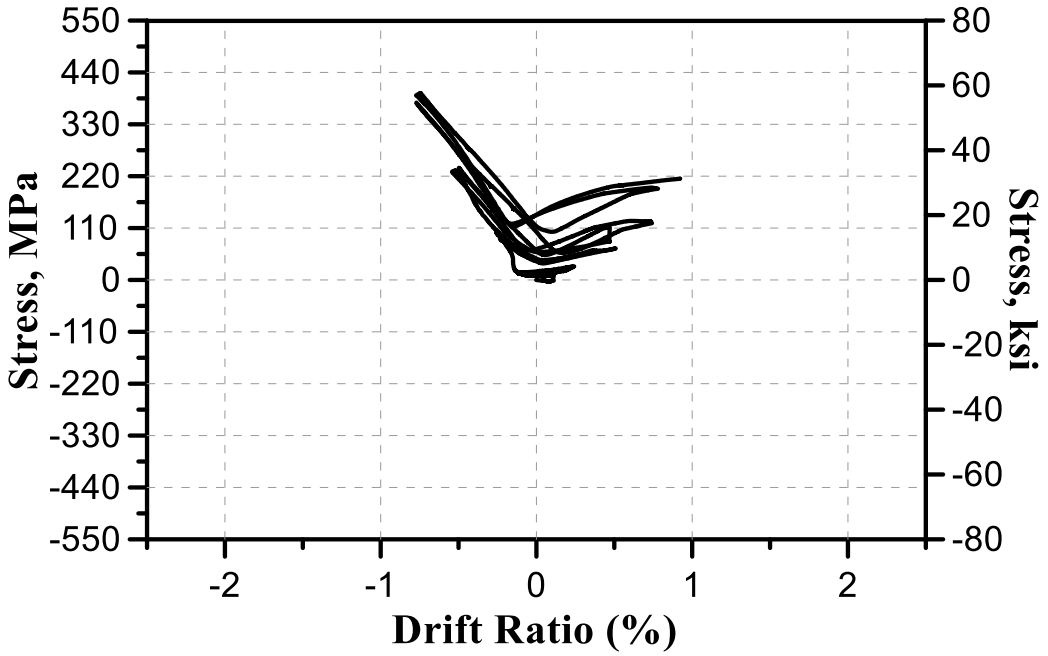

Figure 5-65 Measured stresses of strain gauge (S16) for specimen SW-HA-0.5

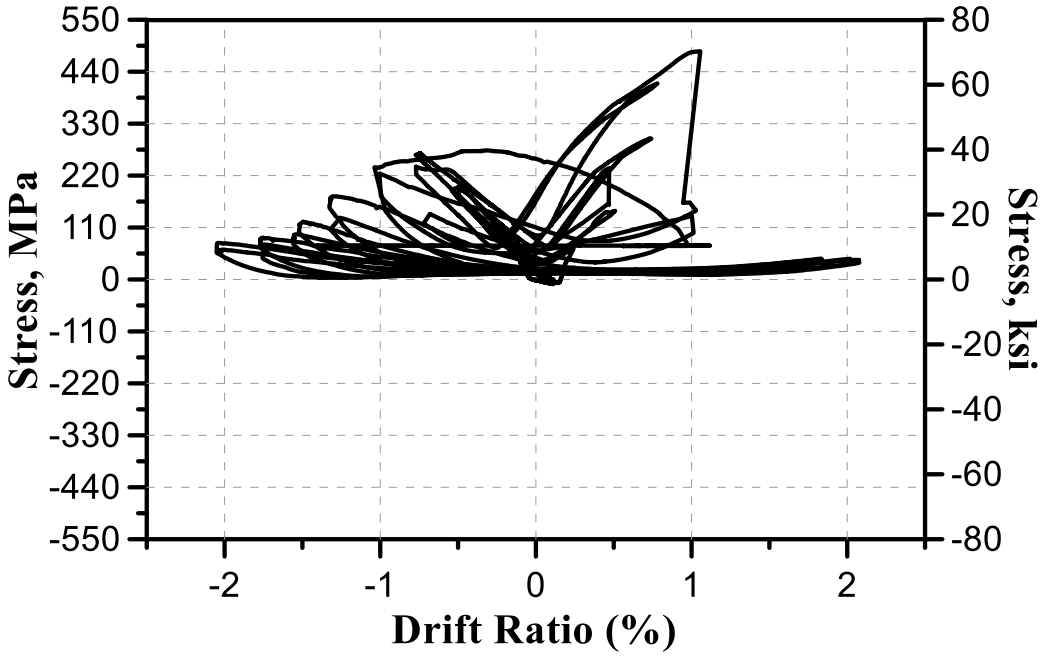

Figure 5-66 Measured stresses of strain gauge (S17) for specimen SW-HA-0.5

5.5 SW-HP-0.5-1

5.5.1 Damage and cracking pattern

Shear and flexural cracks propagation at drift ratio 0.125%, 0.25%, 0.5%, 0.75%, 1%, 1.25%, 1.5%, 1.75%, 2% and 2.5% are shown in Figure 5-67. The two proposed walls SW-HP-0.5-1 and SW-HP-0.5-2 were constructed to have similar amount of vertical steel bars area to the ACI- compliant wall SW-HA-0.5 but different horizontal reinforcement layout; vertical steel bars are uniformly distributed in SW-HP-0.5-1 while some vertical bars lumped at boundaries of SW-HP-0.5-2. Concrete cover spalled at 1.75% and 2% drift ratio in SW-HP-0.5-1 (Figure 5-67). The core concrete is well-confined and still resist shear forces. The reported maximum drift ratio at onset of wall strength deterioration is 1.75%, with maximum attained shear forces was 210 kips.

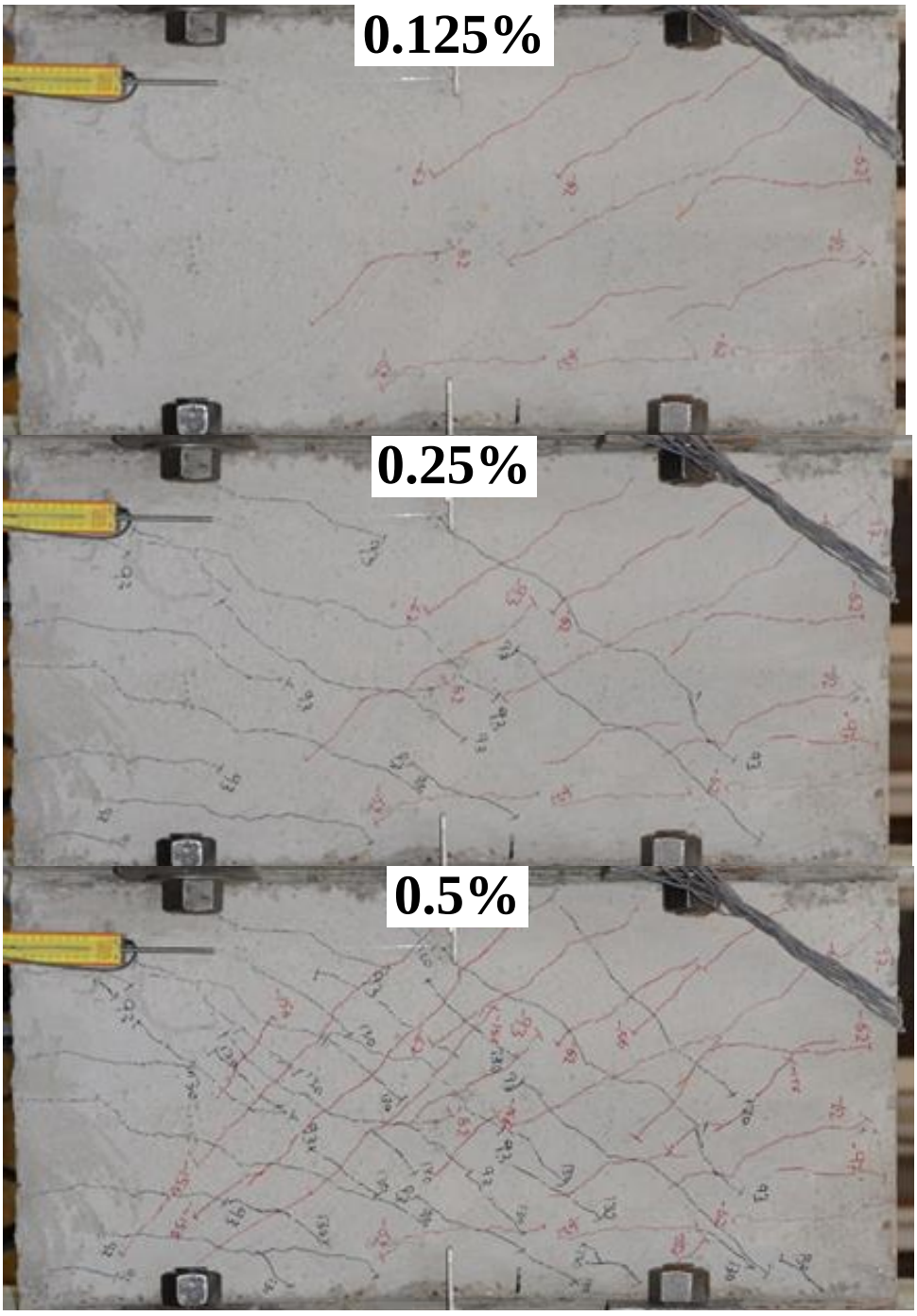

Figure 5-67 Test results of specimen SW-HP-0.5-1 at drift ratio 0.125%, 0.25%, 0.5%, 0.75%, 1%, 1.25%, 1.5%, 1.75%, 2%, and 2.5% (continued)

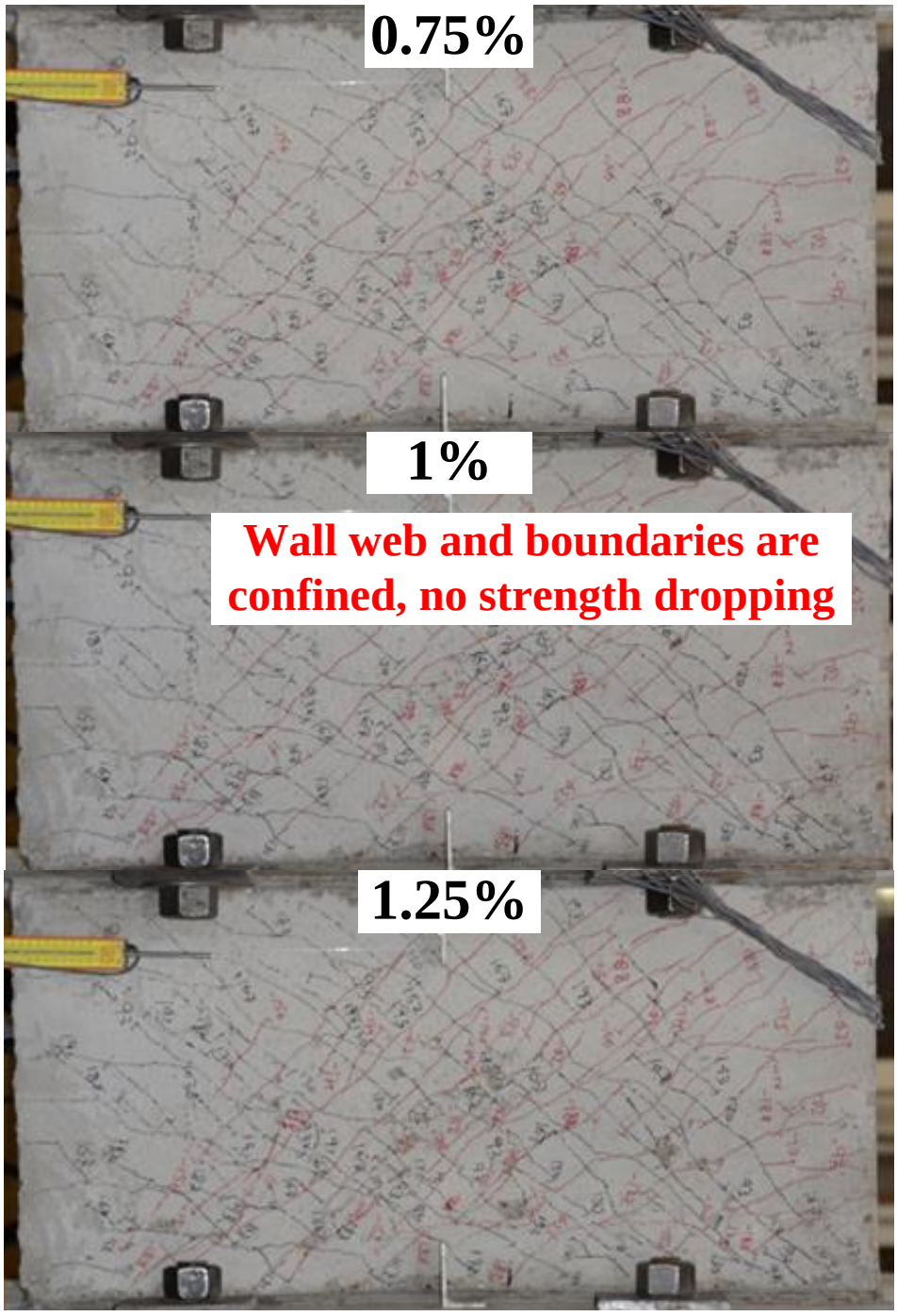

Figure 5-67 Test results of specimen SW-HP-0.5-1 at drift ratio 0.125%, 0.25%, 0.5%, 0.75%, 1%, 1.25%, 1.5%, 1.75%, 2%, and 2.5% (continued)

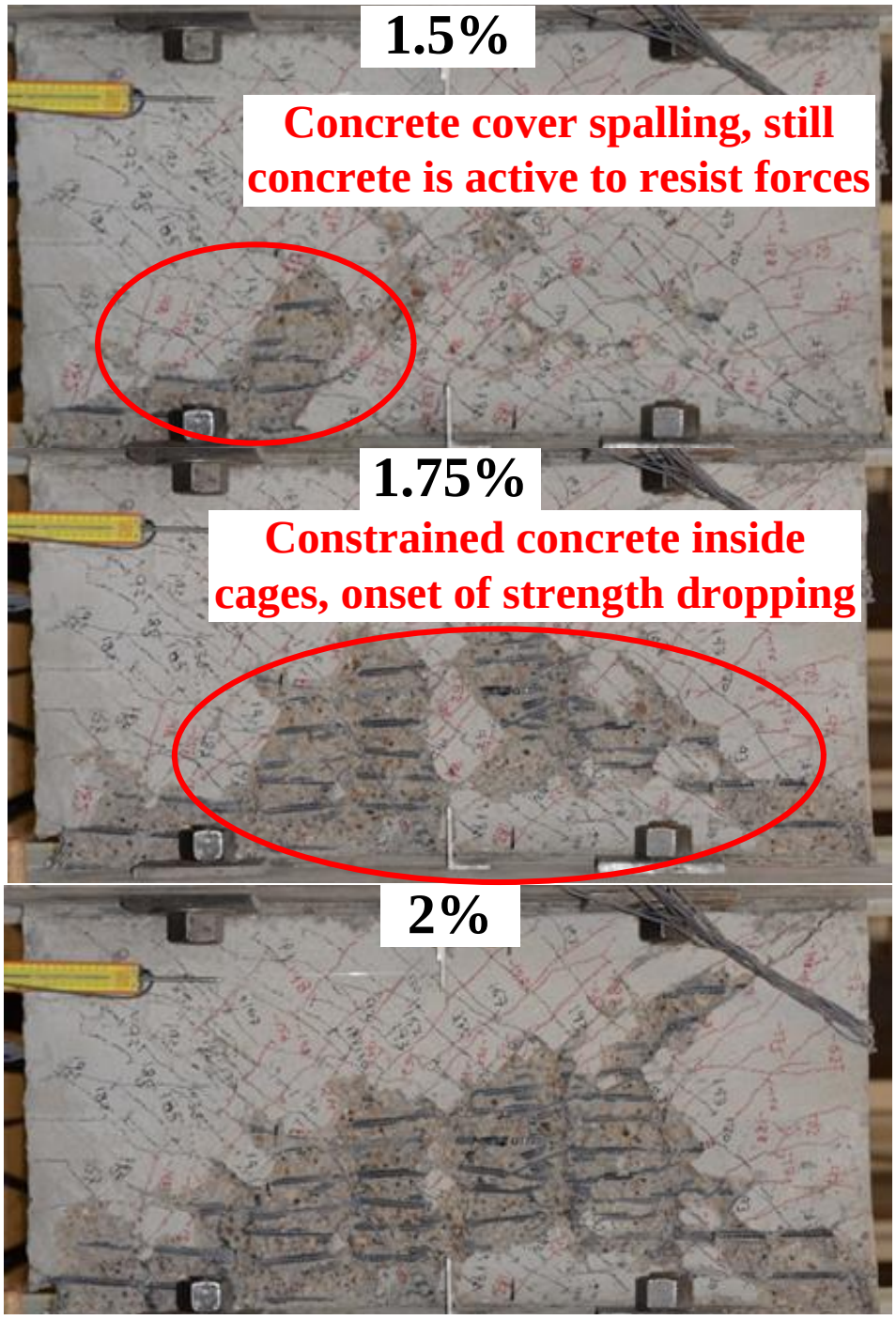

Figure 5-67 Test results of specimen SW-HP-0.5-1 at drift ratio 0.125%, 0.25%, 0.5%, 0.75%, 1%, 1.25%, 1.5%, 1.75%, 2%, and 2.5% (continued)

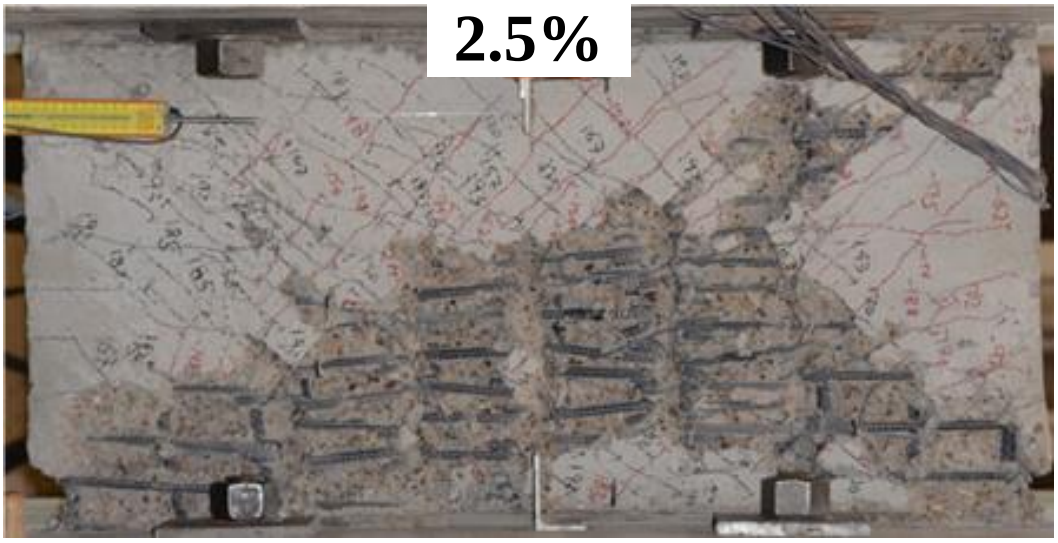

Figure 5-67 Test results of specimen SW-HP-0.5-1 at drift ratio 0.125%, 0.25%, 0.5%, 0.75%, 1%, 1.25%, 1.5%, 1.75%, 2%, and 2.5% (continued)

5.5.2 Shear strength response

Shear force versus drift ratio response of specimen SW-HP-0.5-1 is shown in Figure 5-68. The maximum attained shear force was 210 kips ($19.6\sqrt{f_{cm}}$) at drift ratio 0.75% and remained at plateau up to drift ratio 1.75%. Shear strength and stiffness gradually decreased after drift ratio 1.75% which equivalent to a drift ratio as twice as that attained in specimen SW-HA-0.5.

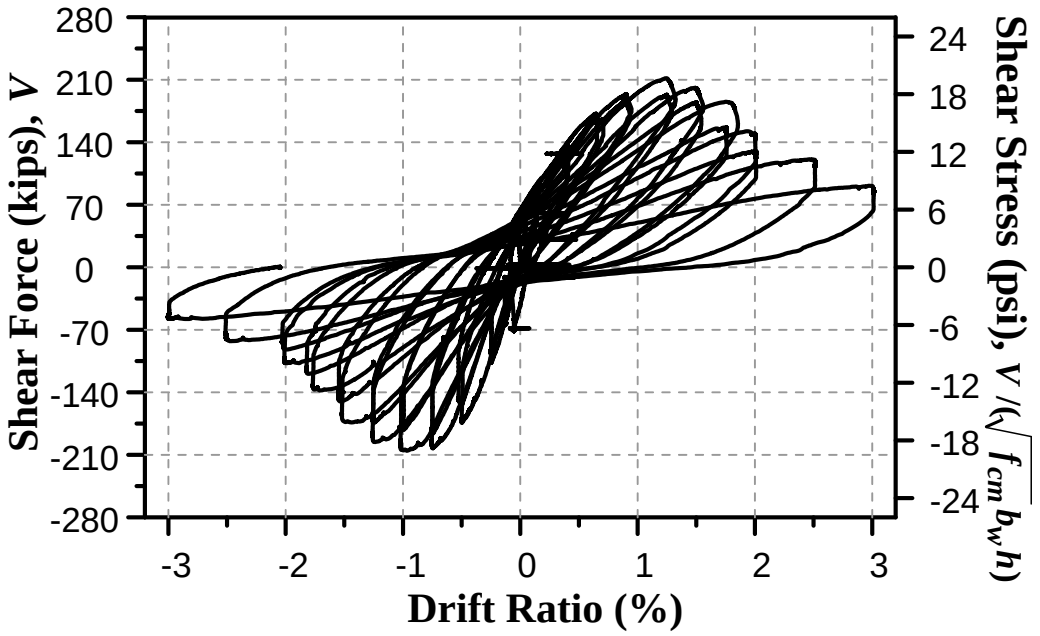

Figure 5-68 Shear strength hysteresis curve of specimen SW-HP-0.5-1

5.3.5 Steel reinforcement stresses

Strain gauges were attached at boundaries, longitudinal and horizontal steel bars as shown in Figure 5-69. Strain gauges L1 to L14 are attached at vertical steel bars, while S15 to S19 are attached at boundaries and horizontal steel bars. The results of drift ratio and the attained steel stress in strain gauges L1 to S19 are shown in Figure 5-70 to Figure 5-88. All vertical steel bars yielded (reached the yielding strength of (60 ksi). None of strain gauges at boundaries or horizontal steel bars yielded.

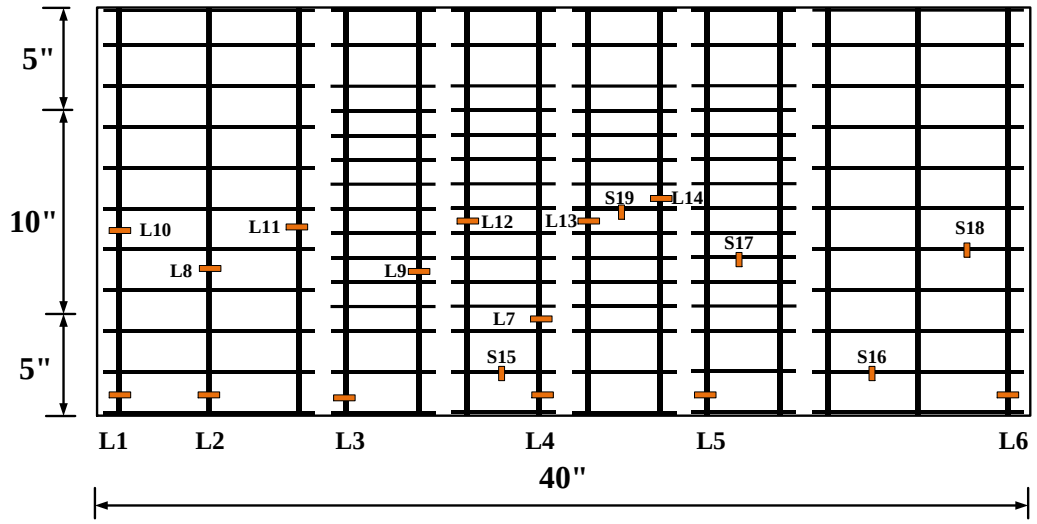

Figure 5-69 Locations of strain gauges at boundaries, vertical and horizontal steel bars for specimen SW-HP-0.5-1

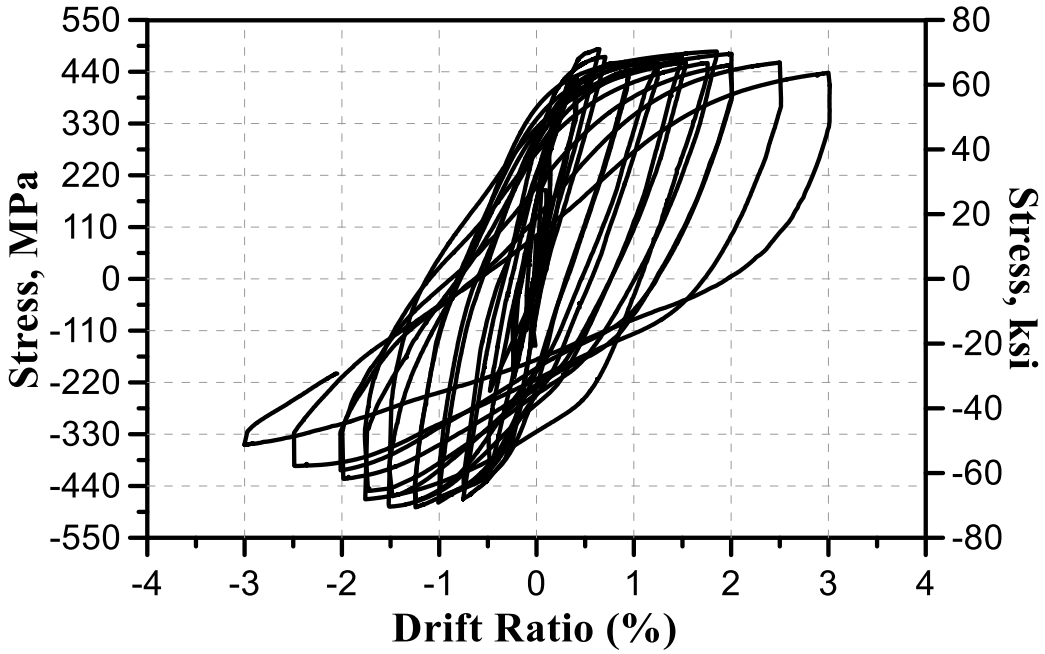

Figure 5-70 Measured stresses of strain gauge (L1) for specimen SW-HP-0.5-1

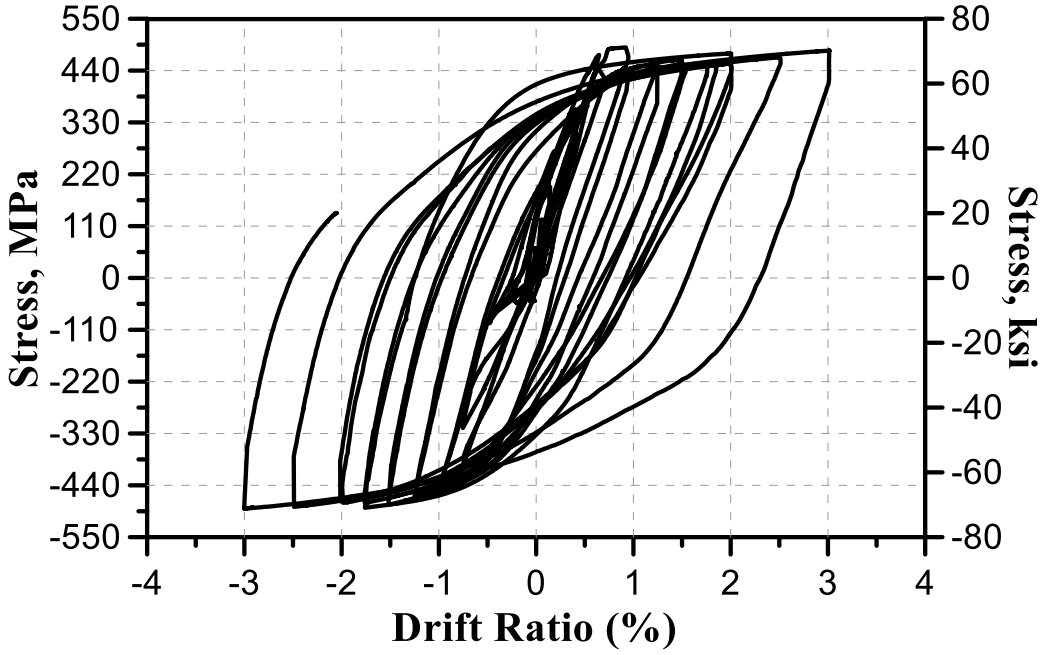

Figure 5-71 Measured stresses of strain gauge (L2) for specimen SW-HP-0.5-1

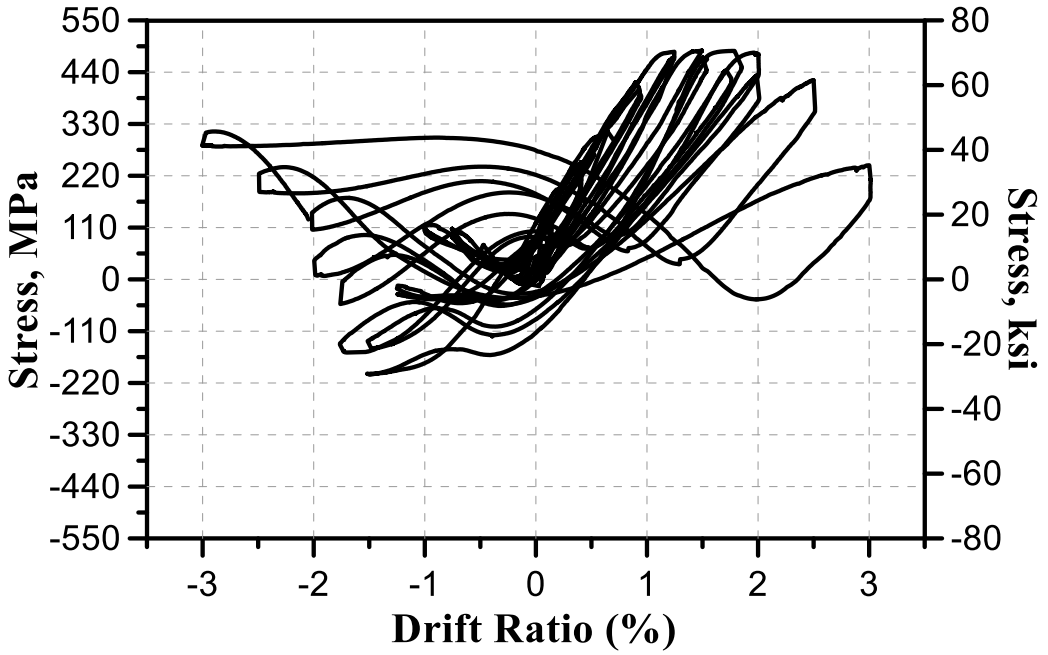

Figure 5-72 Measured stresses of strain gauge (L3) for specimen SW-HP-0.5-1

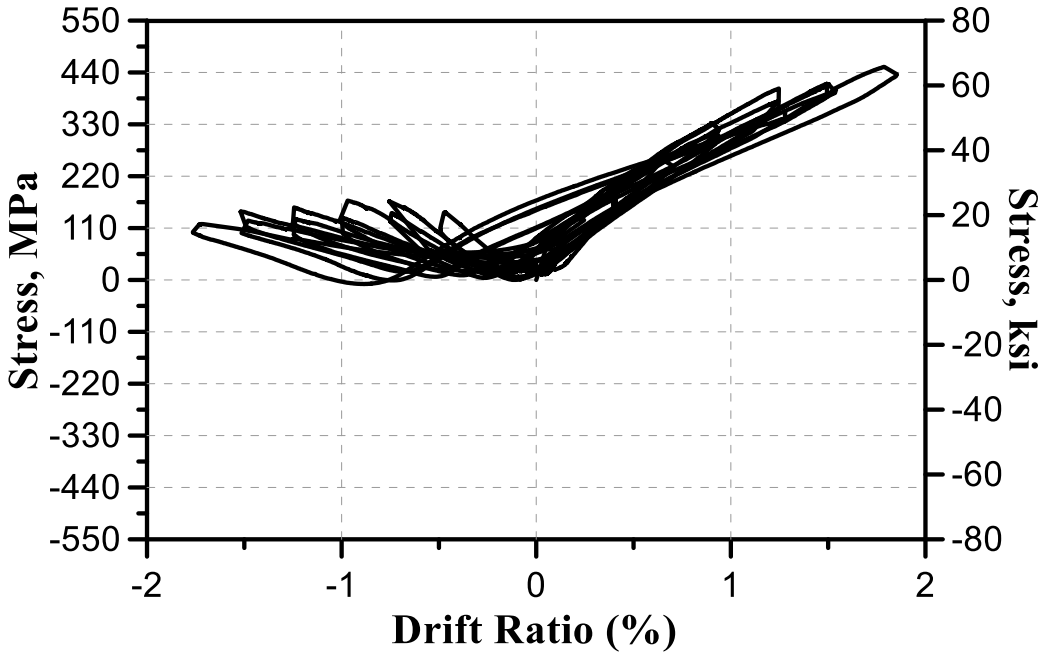

Figure 5-73 Measured stresses of strain gauge (L4) for specimen SW-HP-0.5-1

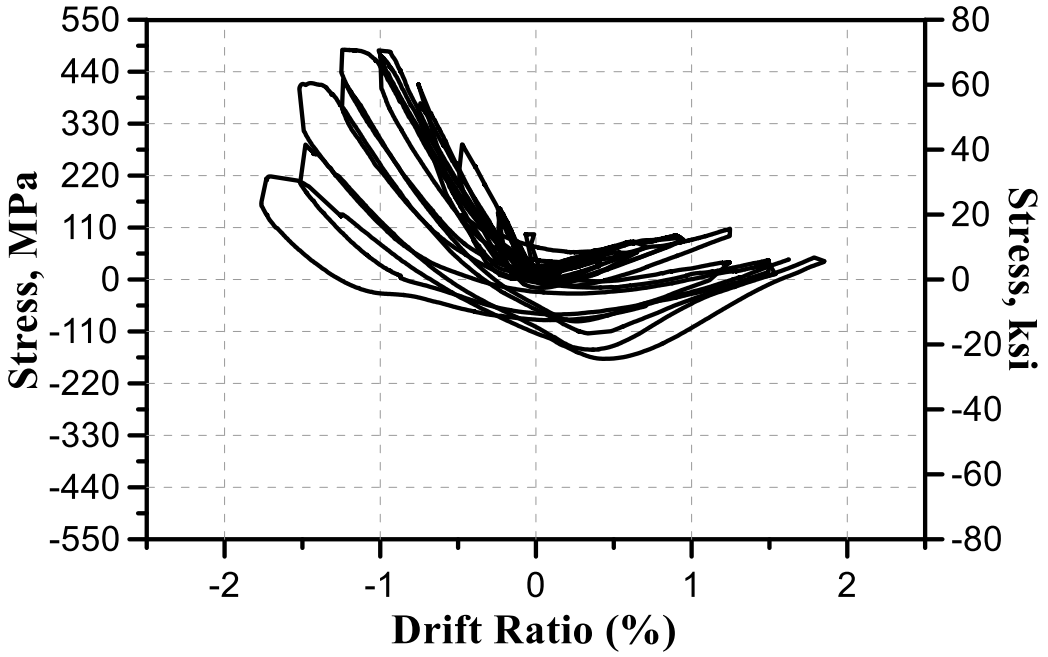

Figure 5-74 Measured stresses of strain gauge (L5) for specimen SW-HP-0.5-1

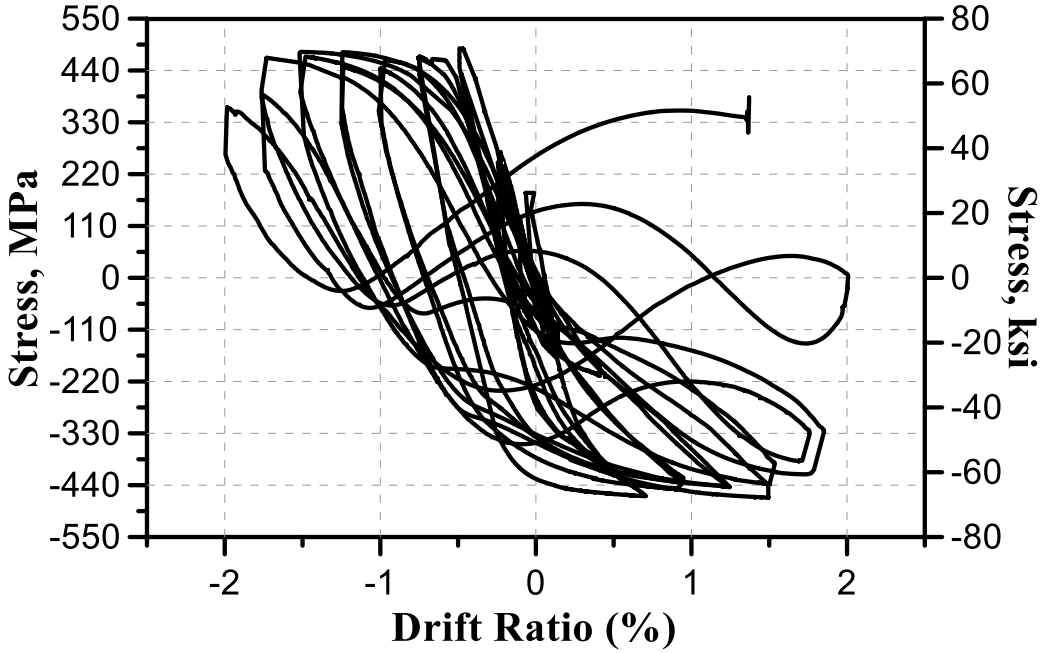

Figure 5-75 Measured stresses of strain gauge (L6) for specimen SW-HP-0.5-1

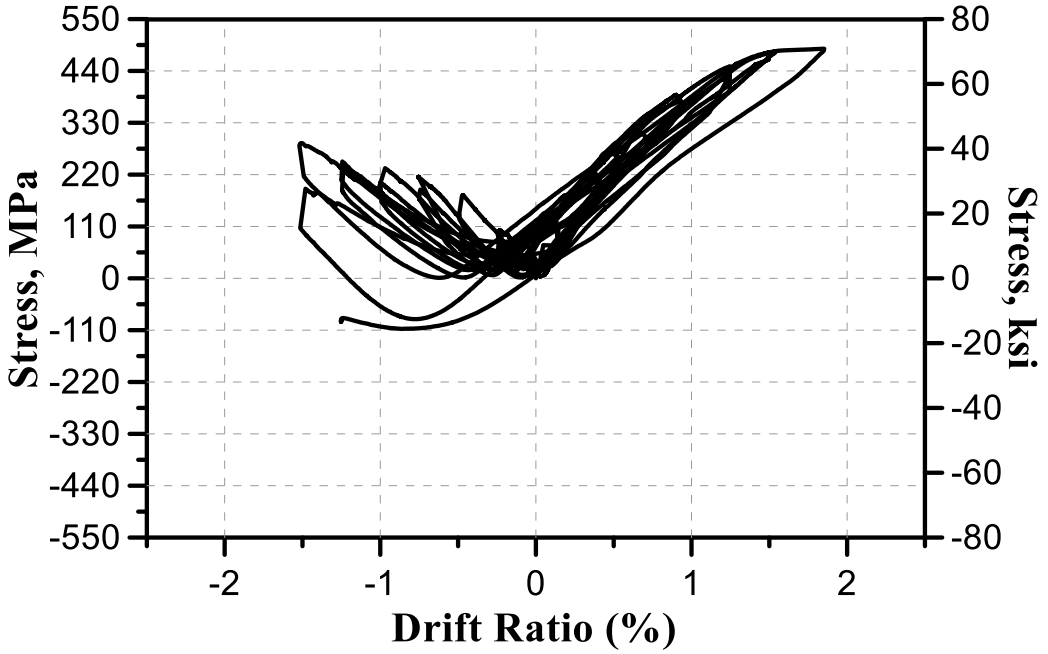

Figure 5-76 Measured stresses of strain gauge (L7) for specimen SW-HP-0.5-1

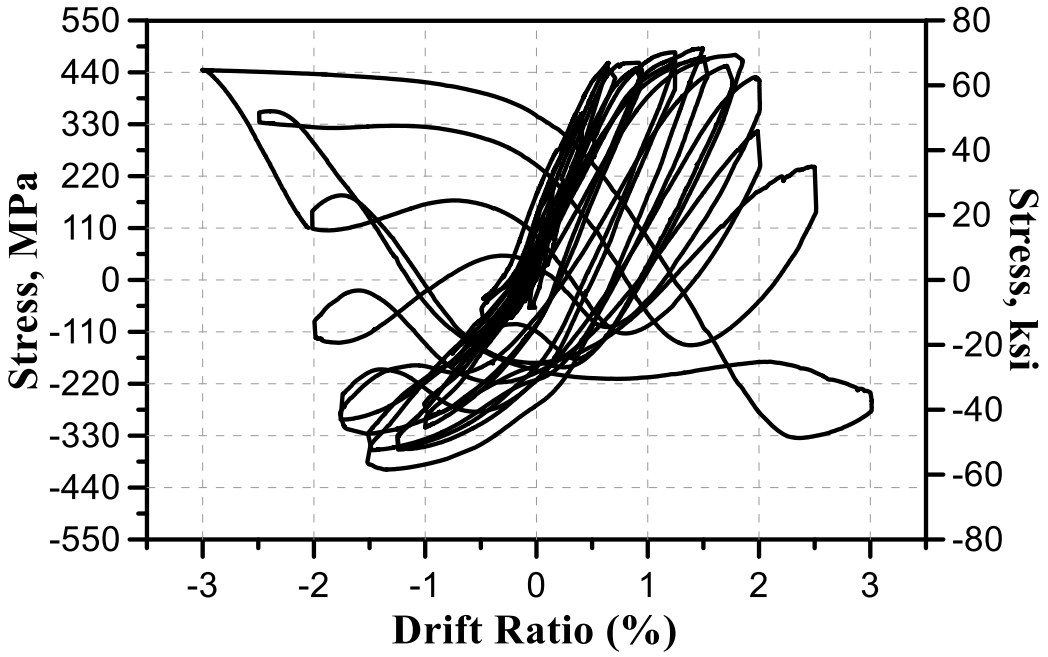

Figure 5-77 Measured stresses of strain gauge (L8) for specimen SW-HP-0.5-1

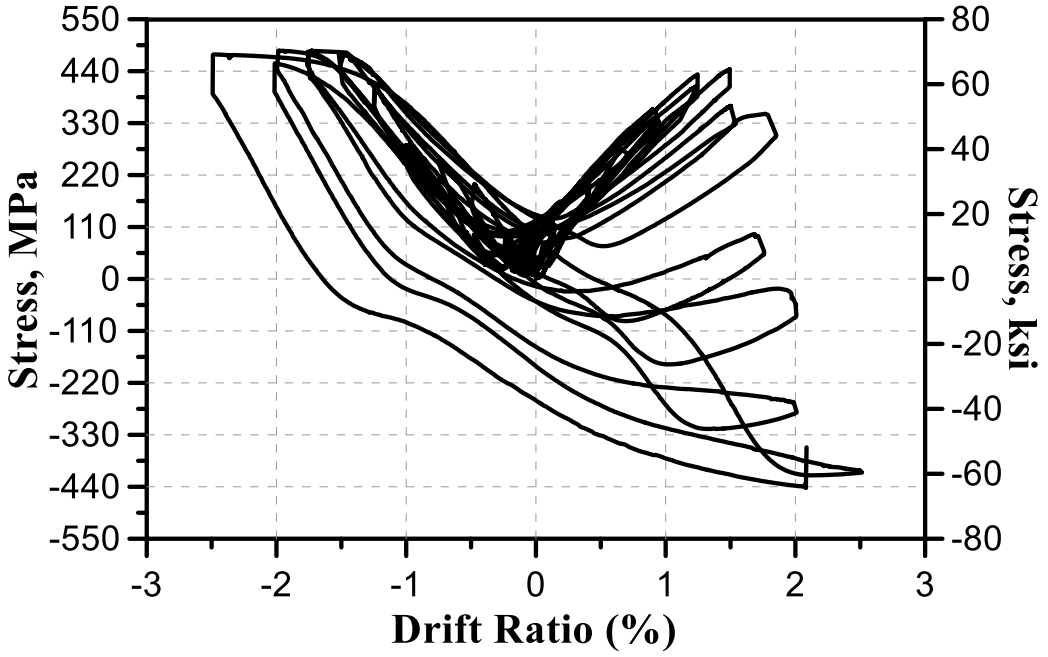

Figure 5-78 Measured stresses of strain gauge (L9) for specimen SW-HP-0.5-1

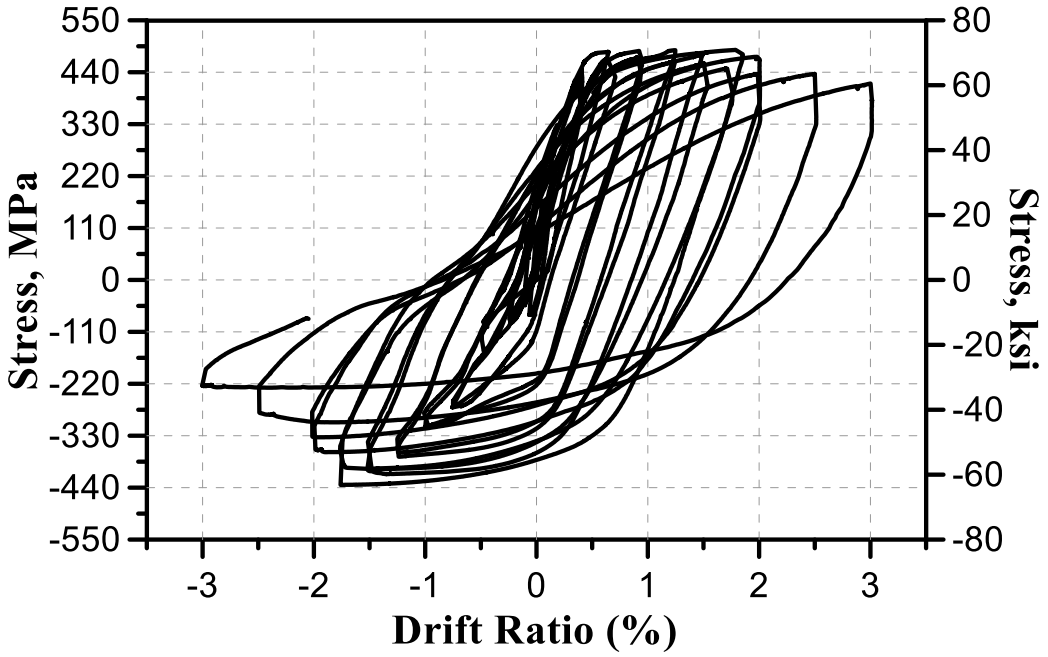

Figure 5-79 Measured stresses of strain gauge (L10) for specimen SW-HP-0.5-1

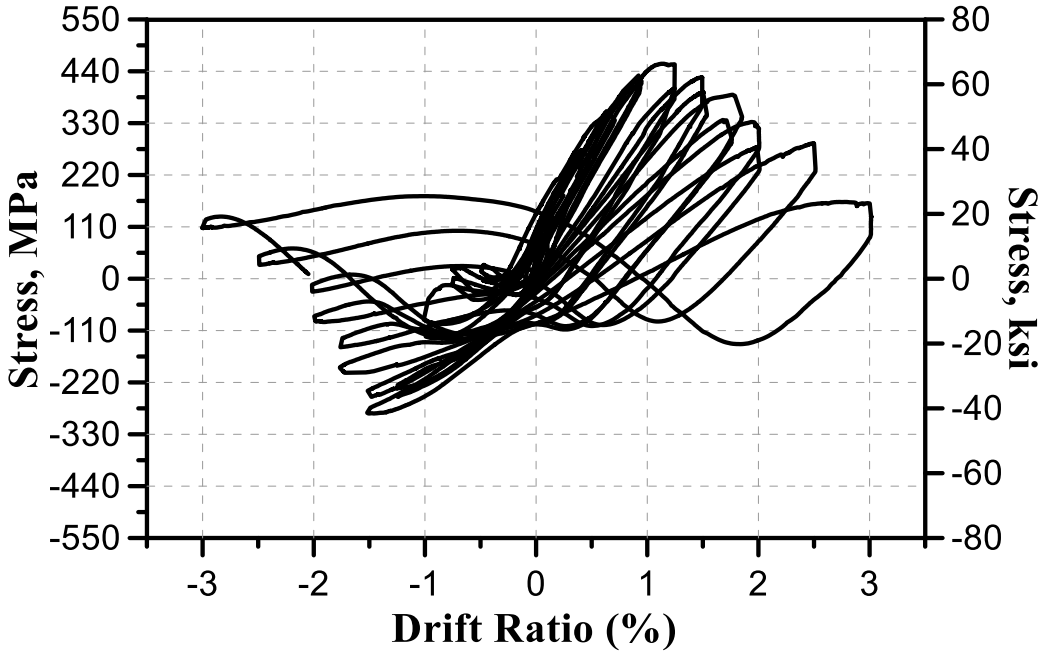

Figure 5-80 Measured stresses of strain gauge (L11) for specimen SW-HP-0.5-1

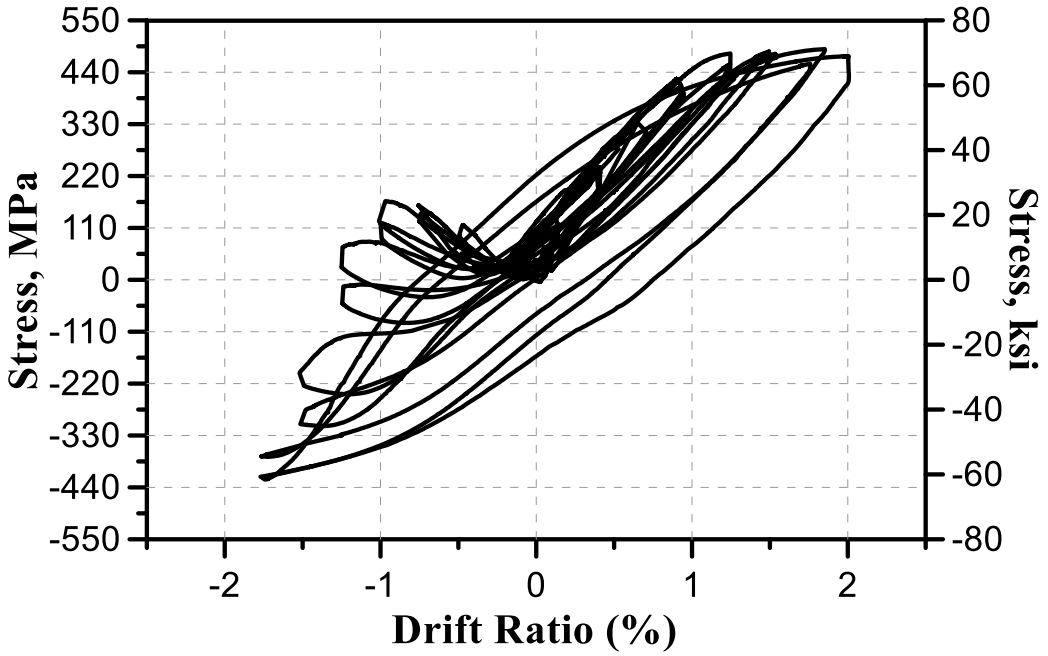

Figure 5-81 Measured stresses of strain gauge (L12) for specimen SW-HP-0.5-1

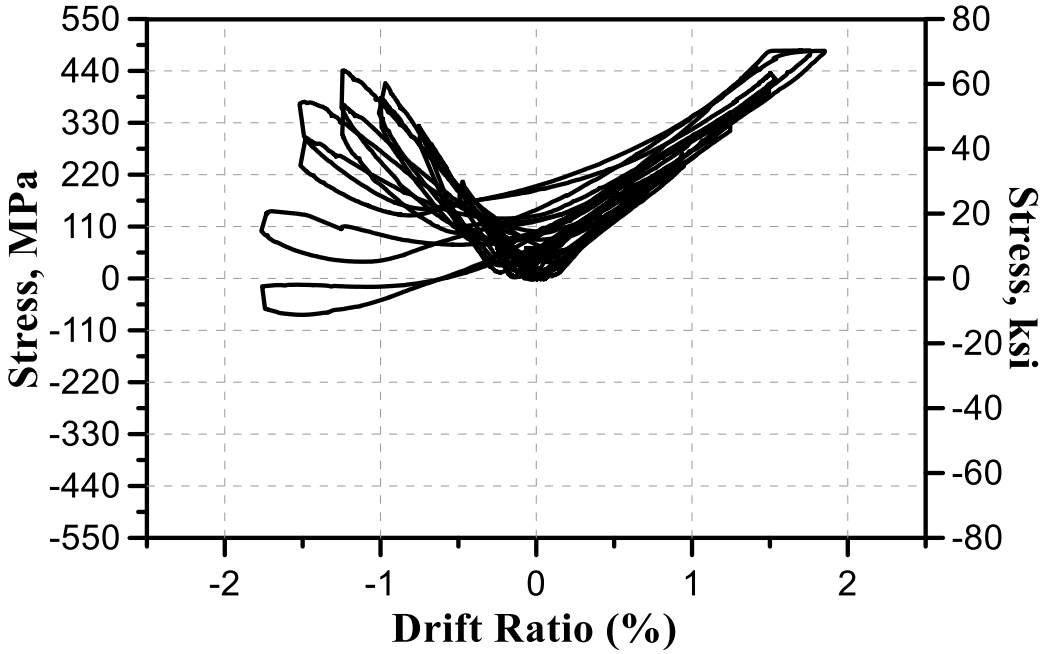

Figure 5-82 Measured stresses of strain gauge (L13) for specimen SW-HP-0.5-1

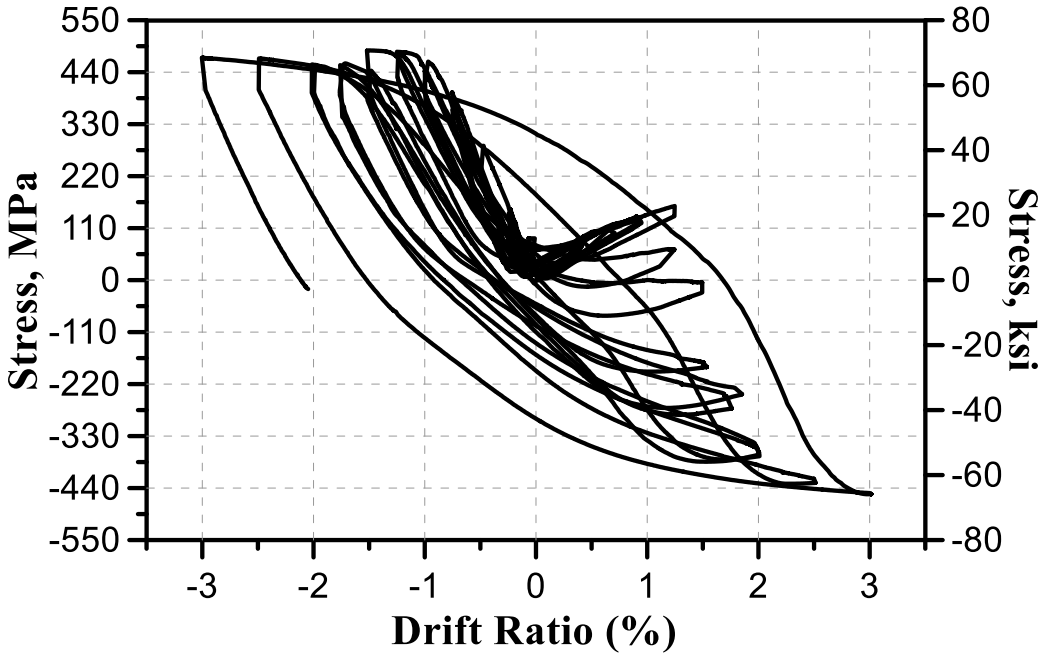

Figure 5-83 Measured stresses of strain gauge (L14) for specimen SW-HP-0.5-1

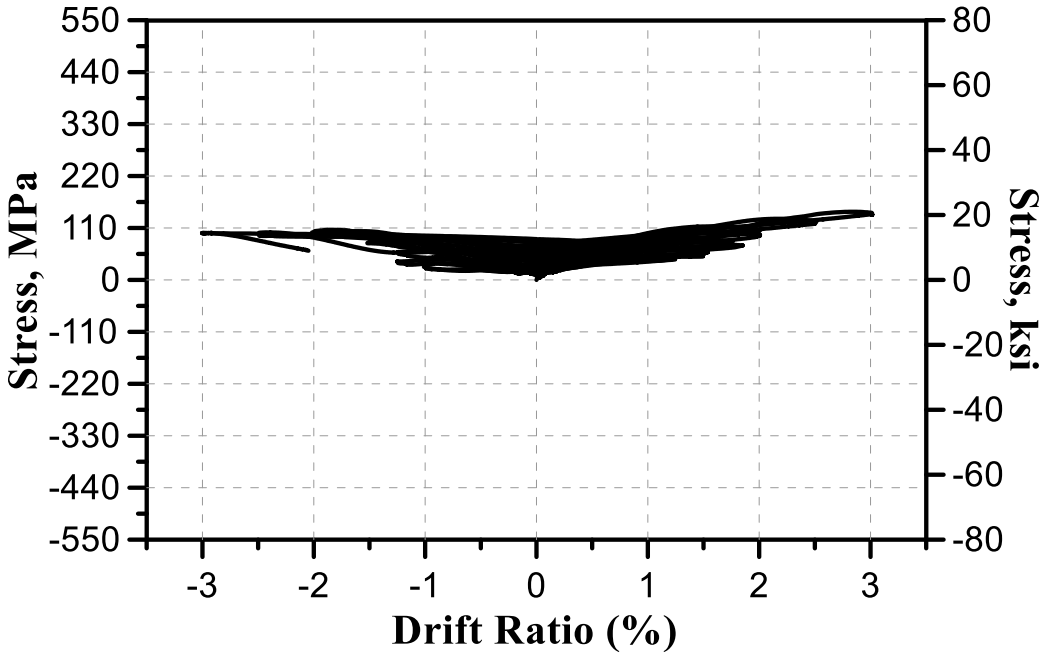

Figure 5-84 Measured stresses of strain gauge (S15) for specimen SW-HP-0.5-1

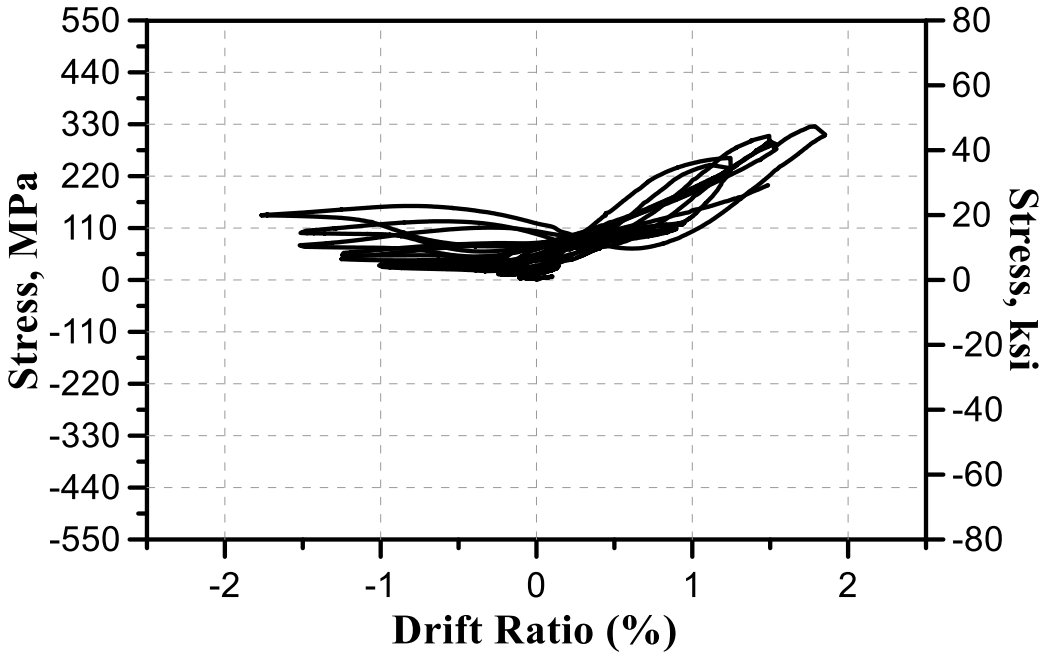

Figure 5-85 Measured stresses of strain gauge (S16) for specimen SW-HP-0.5-1

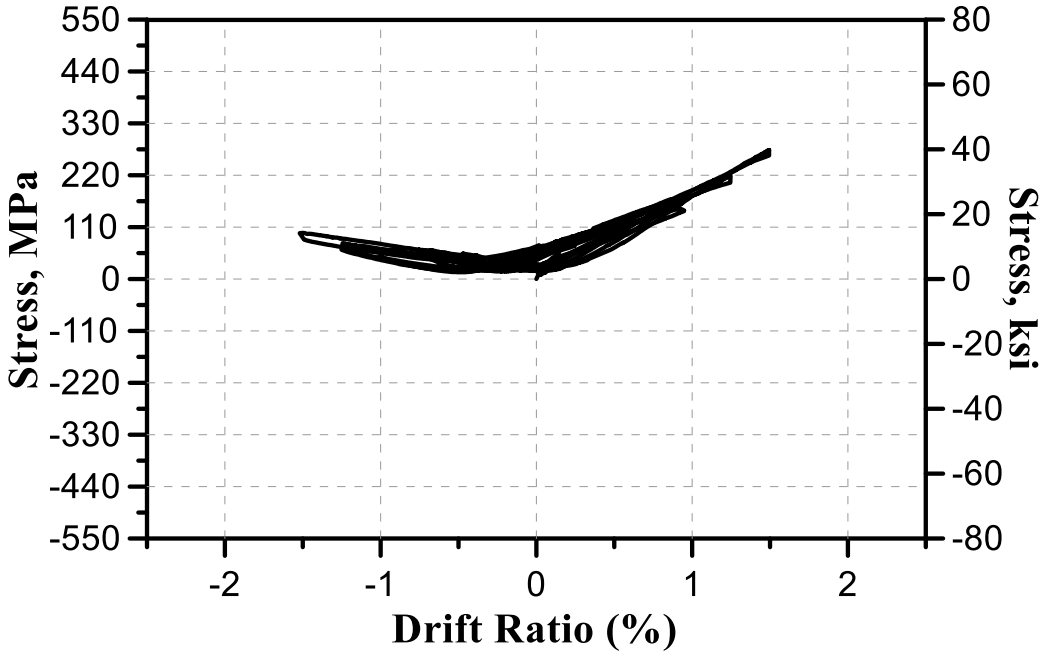

Figure 5-86 Measured stresses of strain gauge (S17) for specimen SW-HP-0.5-1

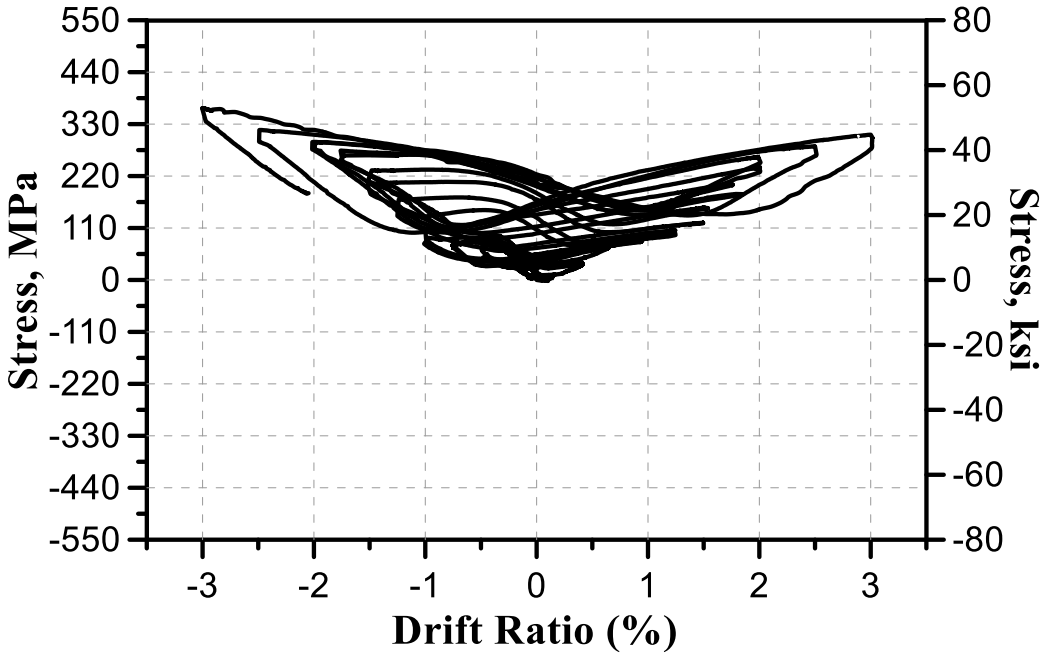

Figure 5-87 Measured stresses of strain gauge (S18) for specimen SW-HP-0.5-1

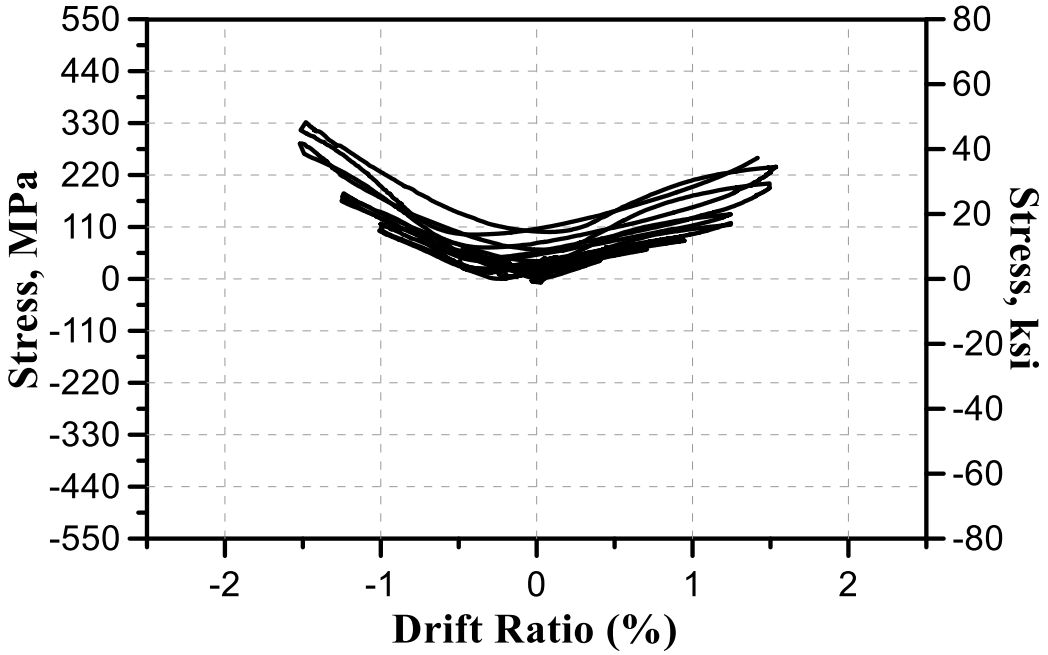

Figure 5-88 Measured stresses of strain gauge (S19) for specimen SW-HP-0.5-1

5.6 SW-HP-0.5-2

5.6.1 Damage and cracking pattern

Shear and flexural cracks propagation at drift ratio 0.125%, 0.25%, 0.5%, 0.75%, 1%, 1.25%, 1.5%, 1.75%, 2% and 2.5% are shown in Figure 5-89. The proposed wall SW-HP-0.5-2 was designed to have similar amount of vertical steel reinforcement to specimen SW-HP-0.5-2 but some vertical bars were lumped at boundaries. Concrete cover spalled at 2% drift ratio (Figure 5-89). Core concrete is well-confined and still resist shear forces. The reported maximum drift ratio at onset of wall strength deterioration is 1.75%, specimen SW-HP-0.5-2 reached shear strength of 257 kips compared to 210 kips for SW-HP-0.5-1. This observation indicates the importance of lumped steel bars at boundaries on maximum attained shear strength, at the same time the wall web shall be well-confined to strengthen the concrete struts.

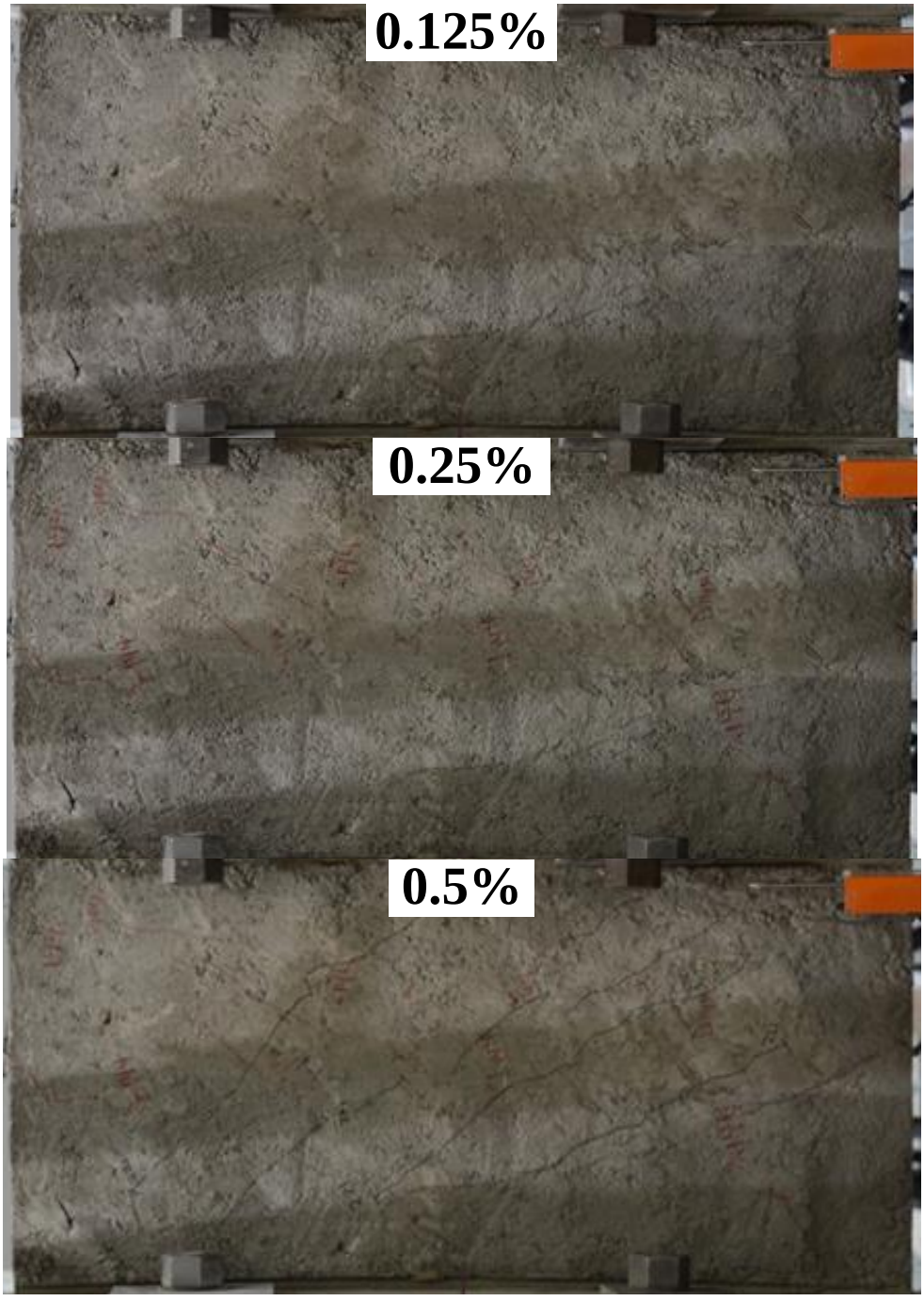

Figure 5-89 Test results of specimen SW-HP-0.5-2 at drift ratio 0.125%, 0.25%, 0.5%, 0.75%, 1%, 1.25%, 1.5%, 1.75%, 2% and 2.5%

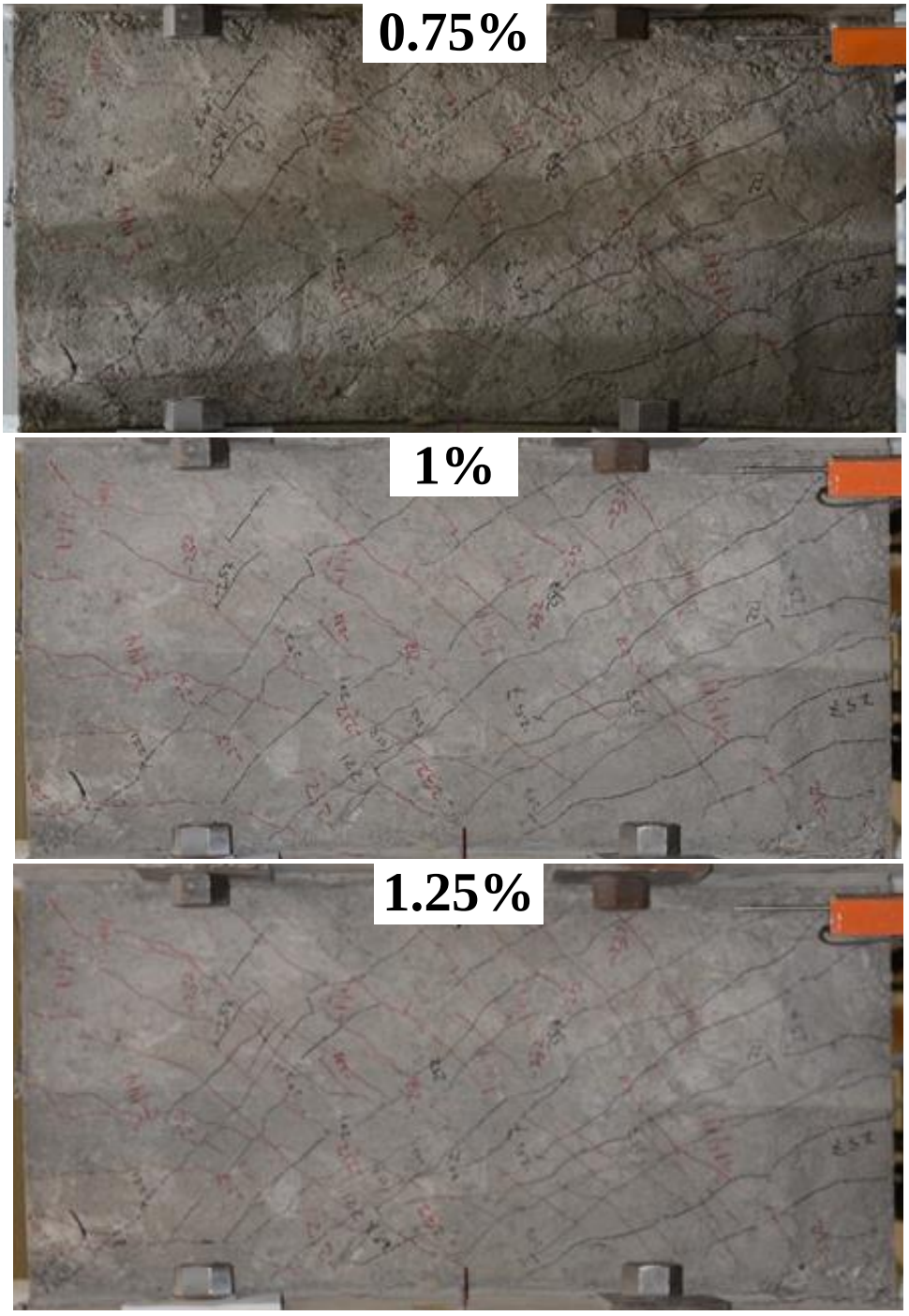

Figure 5-89 Test results of specimen SW-HP-0.5-2 at drift ratio 0.125%, 0.25%, 0.5%, 0.75%, 1%, 1.25%, 1.5%, 1.75%, 2% and 2.5% (continued)

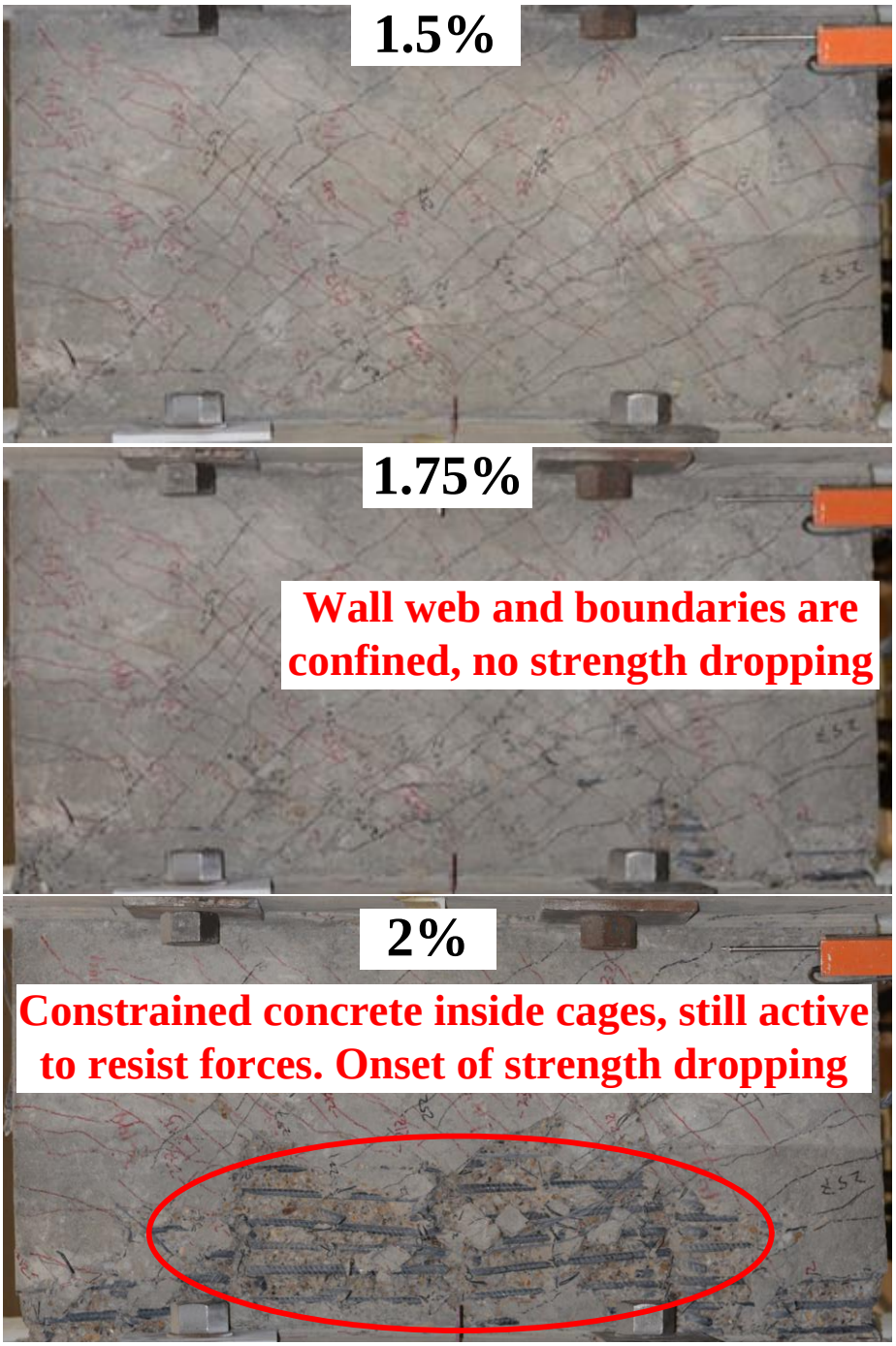

Figure 5-89 Test results of specimen SW-HP-0.5-2 at drift ratio 0.125%, 0.25%, 0.5%, 0.75%, 1%, 1.25%, 1.5%, 1.75%, 2% and 2.5% (continued)

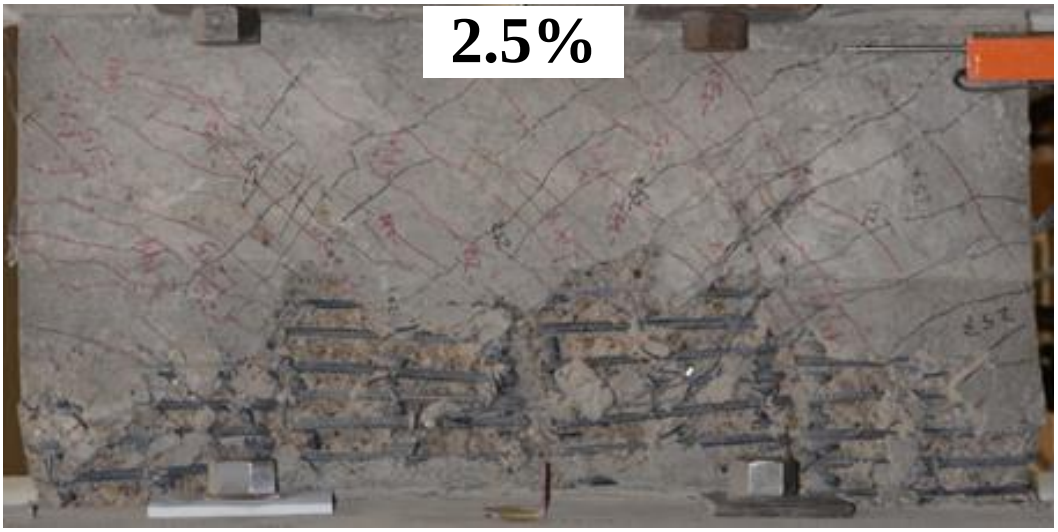

Figure 5-89 Test results of specimen SW-HP-0.5-2 at drift ratio 0.125%, 0.25%, 0.5%, 0.75%, 1%, 1.25%, 1.5%, 1.75%, 2% and 2.5% (continued)

5.6.2 Shear strength response

Shear force versus drift ratio response of specimen SW-HP-0.5-2 is shown in Figure 5-90. The maximum attained shear force was 257 kips ($23.4\sqrt{f_{cm}}$) at drift ratio 0.75% and remained at plateau up to drift ratio 1.75%. Shear strength and stiffness gradually decreased after drift ratio 1.75% which equivalent to a drift ratio as twice as that attained in specimen SW-HA-0.5.

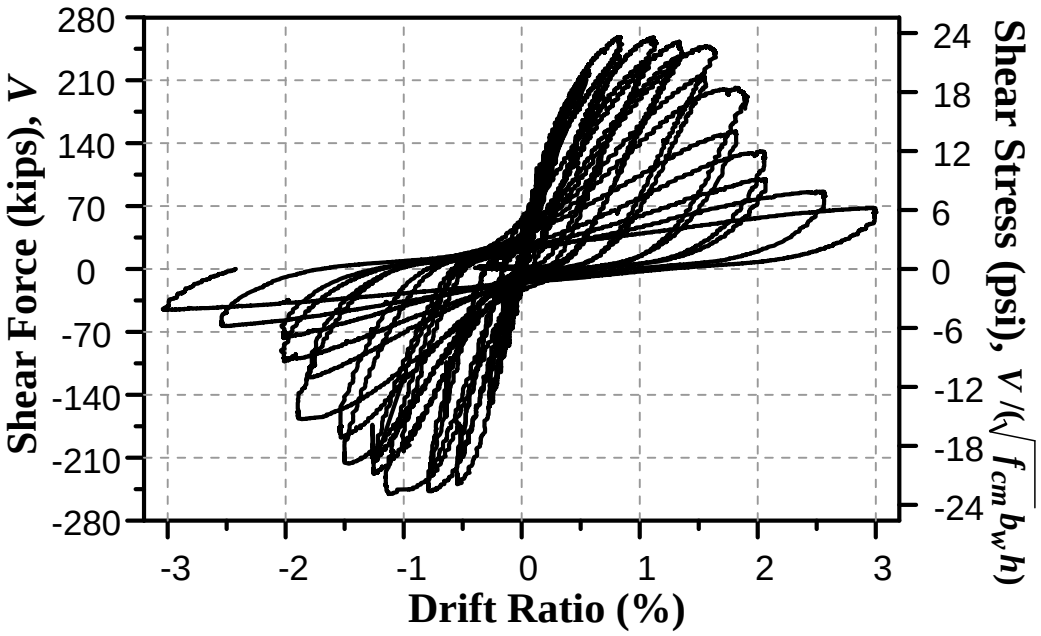

Figure 5-90 Shear strength hysteresis curve of specimen SW-HP-0.5-2

5.6.3 Steel reinforcement stresses

Strain gauges were attached at boundaries, longitudinal and horizontal steel bars as shown in Figure 5-91. Strain gauges L1 to L6 are attached at vertical steel bars, while S7 to S13 are attached at boundaries and horizontal steel bars. The results of drift ratio and the attained steel stress in strain gauges L1 to S13 are shown in Figure 5-92 to Figure 5-104. All vertical steel bars yielded (reached the yielding strength of (60 ksi). None of strain gauges at boundaries or horizontal steel bars yielded except S7 and S10.

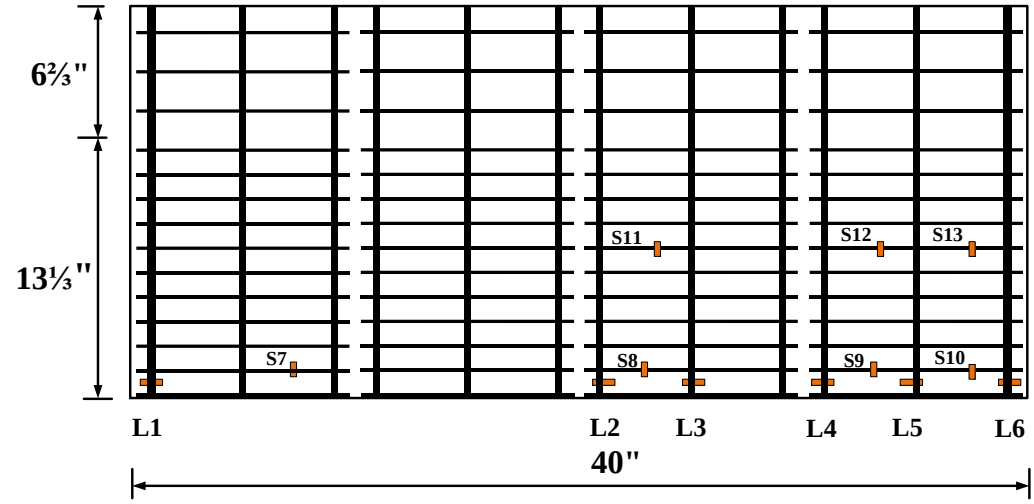

Figure 5-91 Locations of strain gauges at boundaries, vertical and horizontal steel bars for specimen SW-HP-0.5-2

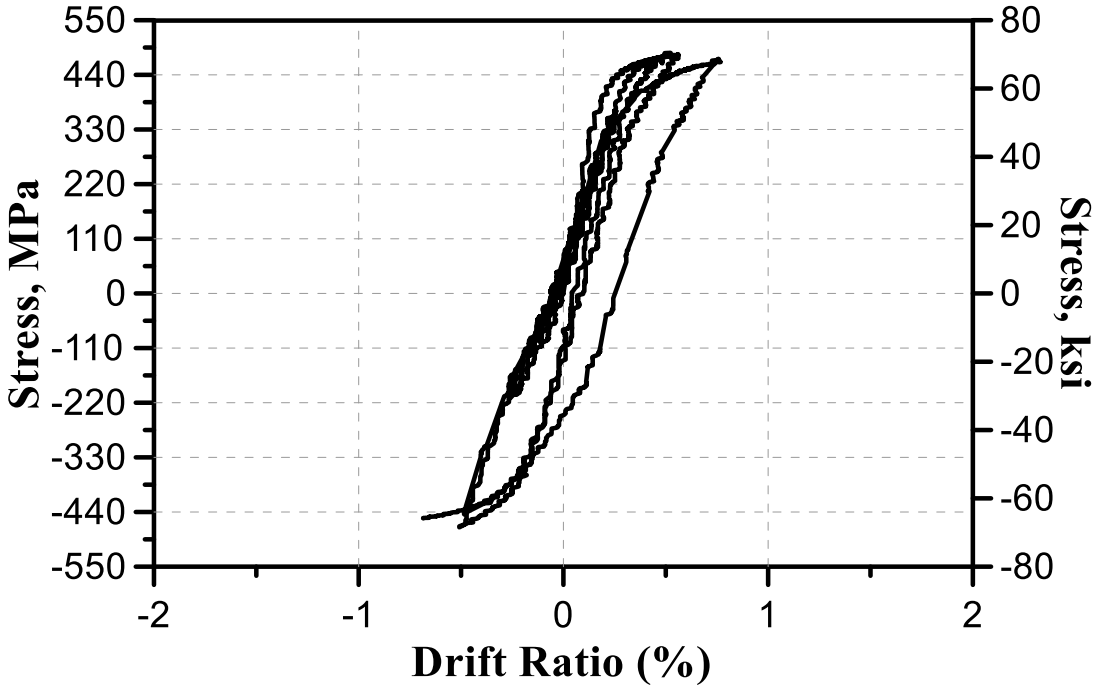

Figure 5-92 Measured stresses of strain gauge (L1) for specimen SW-HP-0.5-2

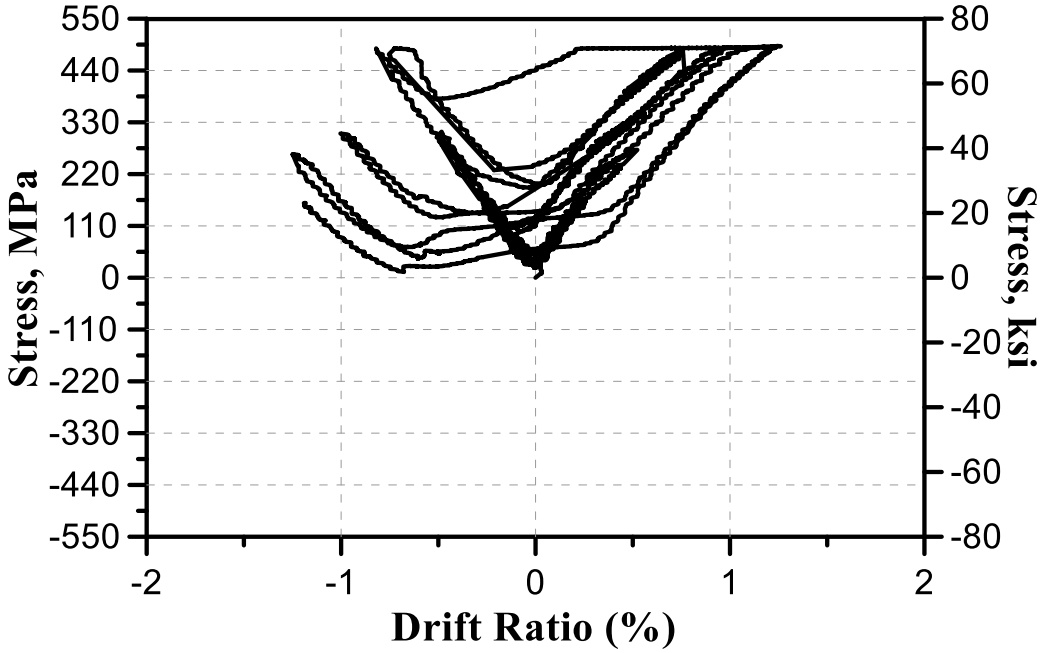

Figure 5-93 Measured stresses of strain gauge (L2) for specimen SW-HP-0.5-2

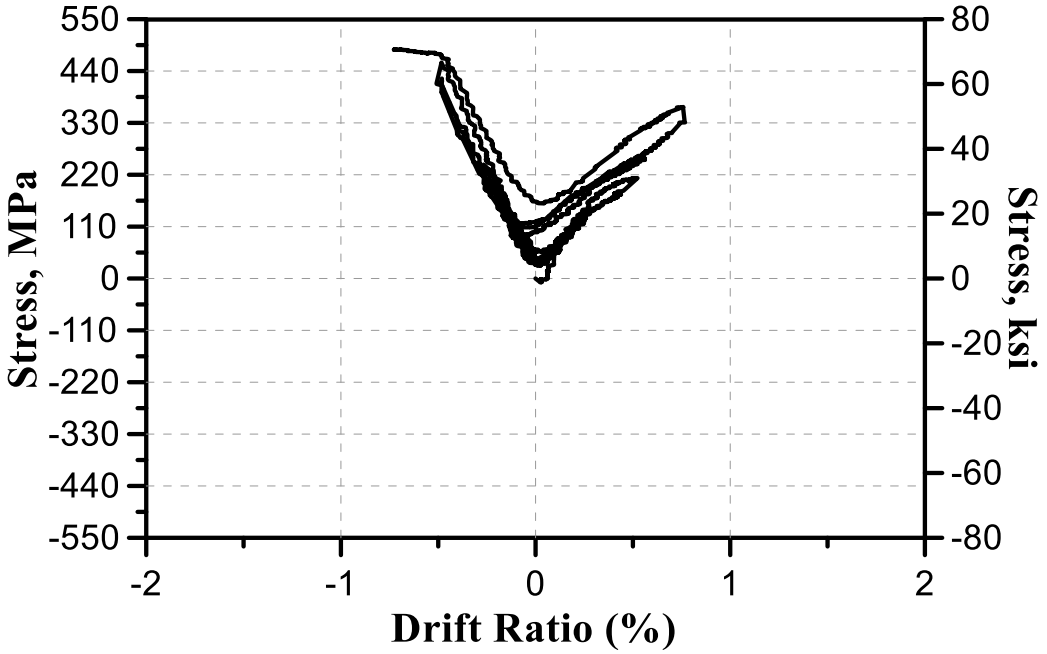

Figure 5-94 Measured stresses of strain gauge (L3) for specimen SW-HP-0.5-2

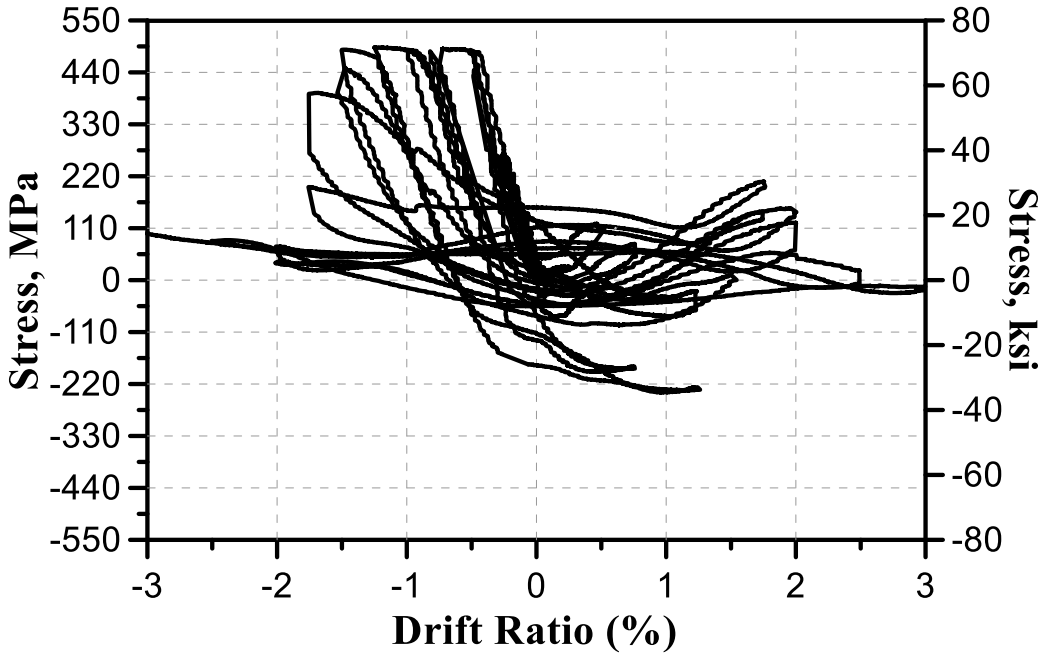

Figure 5-95 Measured stresses of strain gauge (L4) for specimen SW-HP-0.5-2

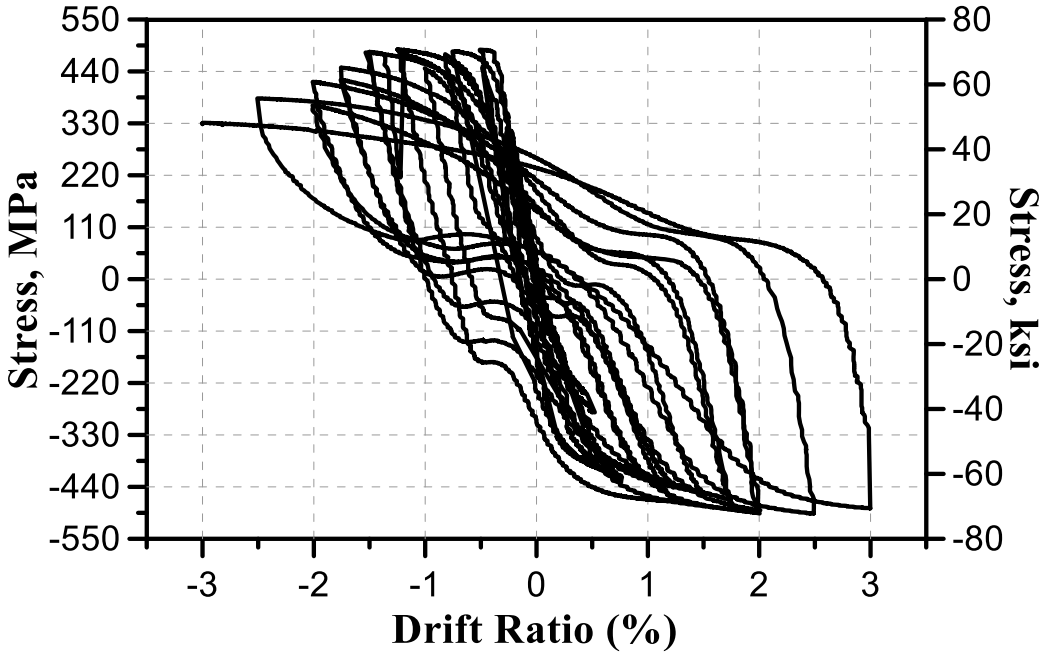

Figure 5-96 Measured stresses of strain gauge (L5) for specimen SW-HP-0.5-2

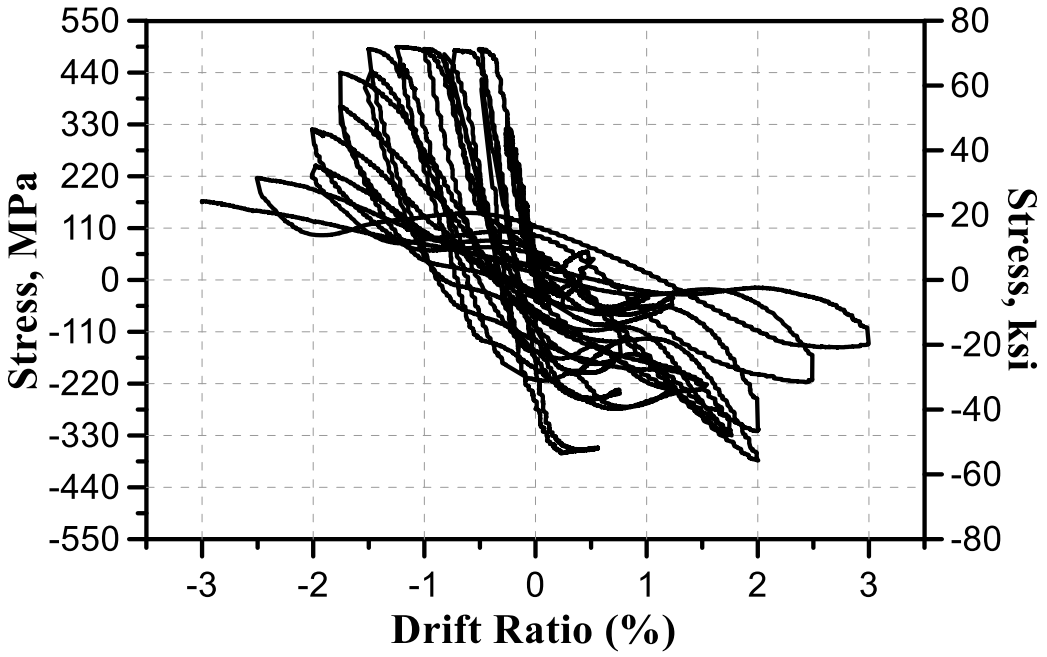

Figure 5-97 Measured stresses of strain gauge (L6) for specimen SW-HP-0.5-2

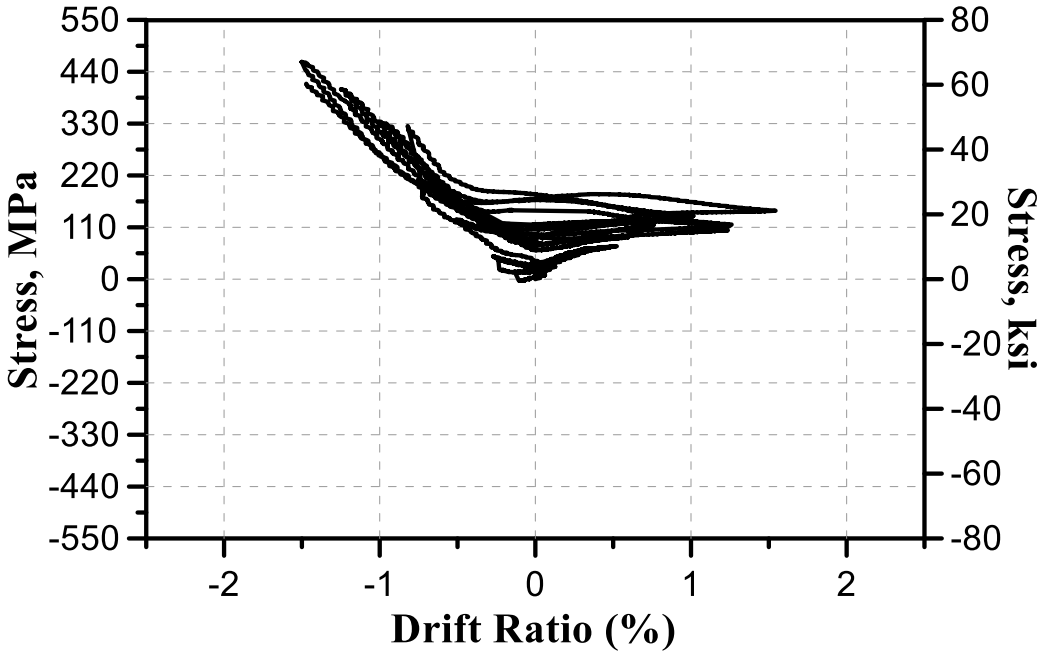

Figure 5-98 Measured stresses of strain gauge (S7) for specimen SW-HP-0.5-2

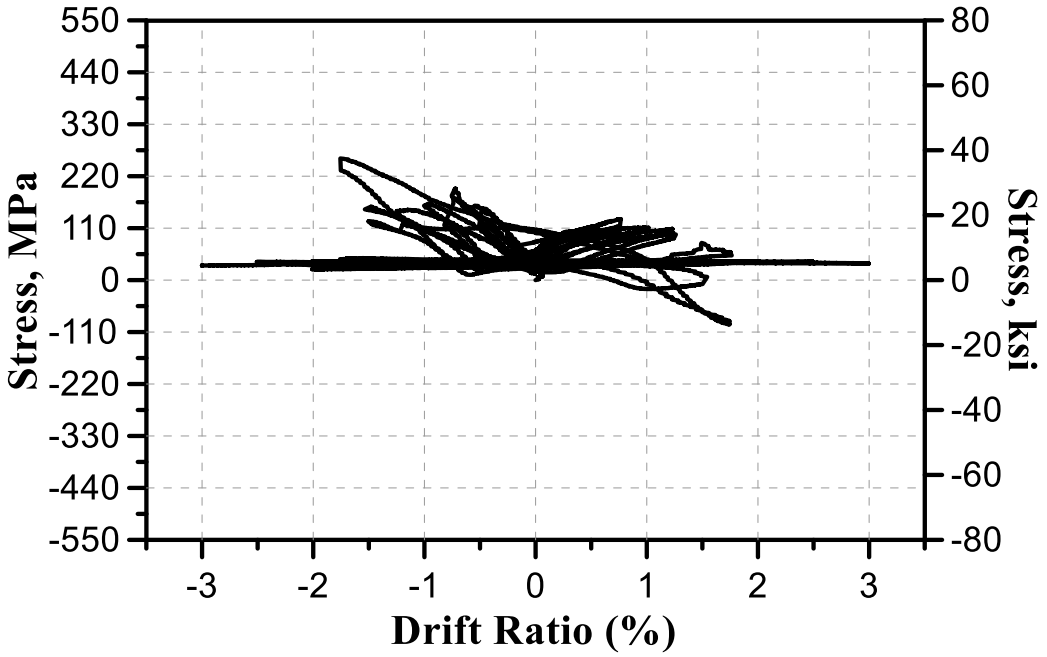

Figure 5-99 Measured stresses of strain gauge (S8) for specimen SW-HP-0.5-2

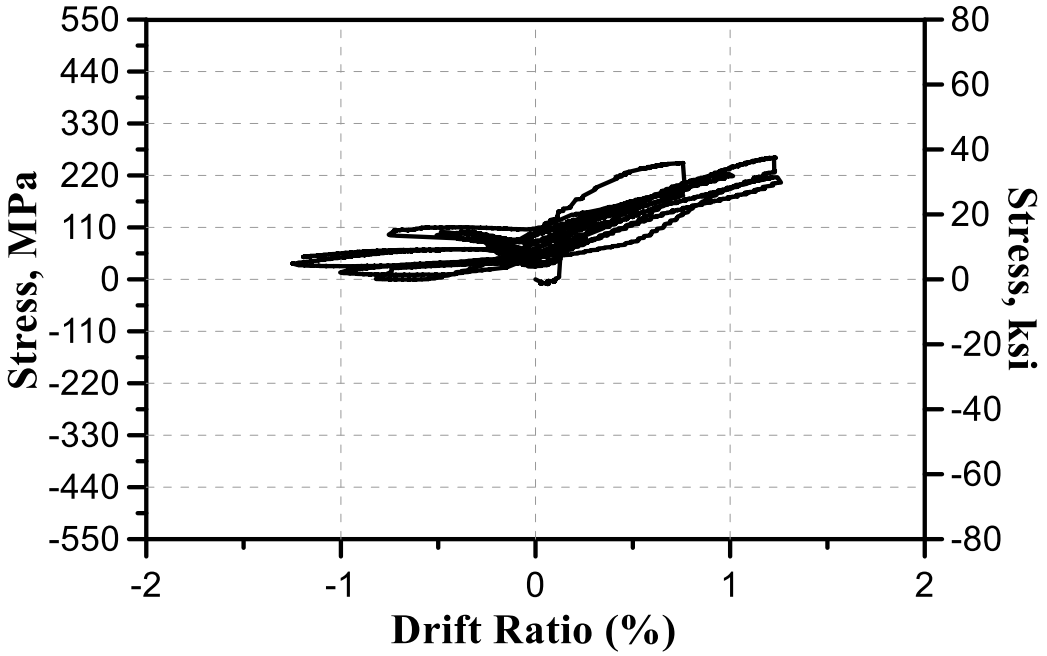

Figure 5-100 Measured stresses of strain gauge (S9) for specimen SW-HP-0.5-2

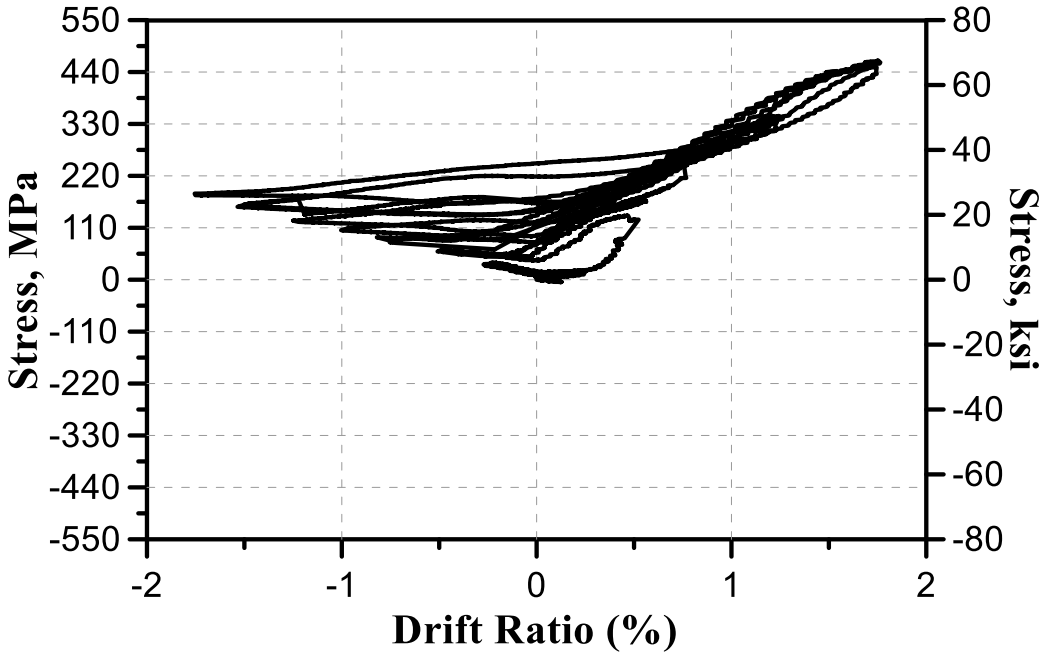

Figure 5-101 Measured stresses of strain gauge (S10) for specimen SW-HP-0.5-2

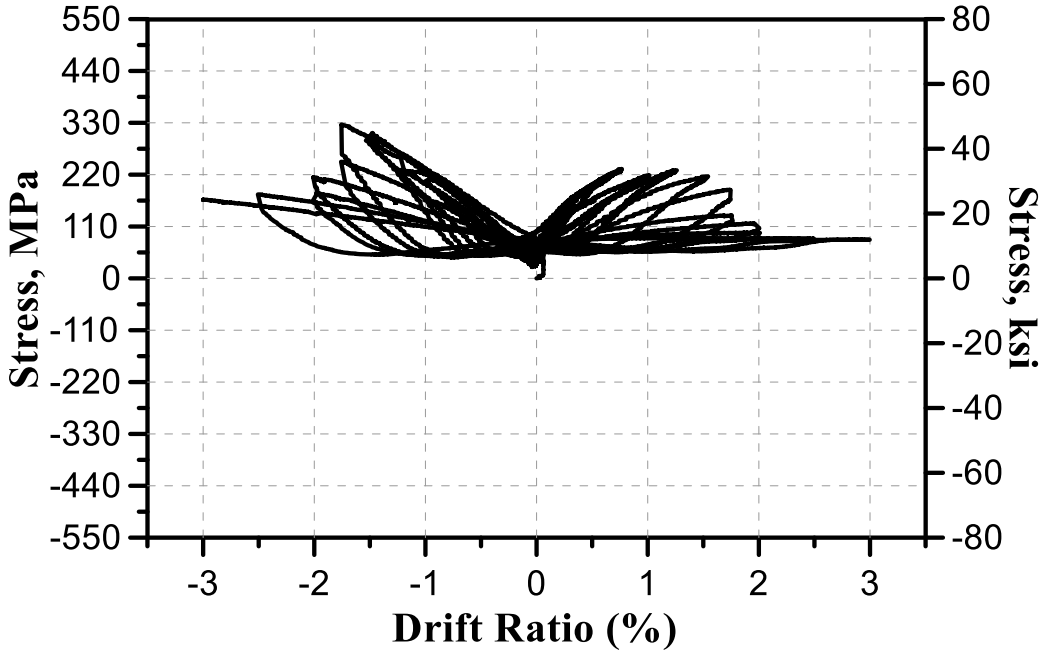

Figure 5-102 Measured stresses of strain gauge (S11) for specimen SW-HP-0.5-2

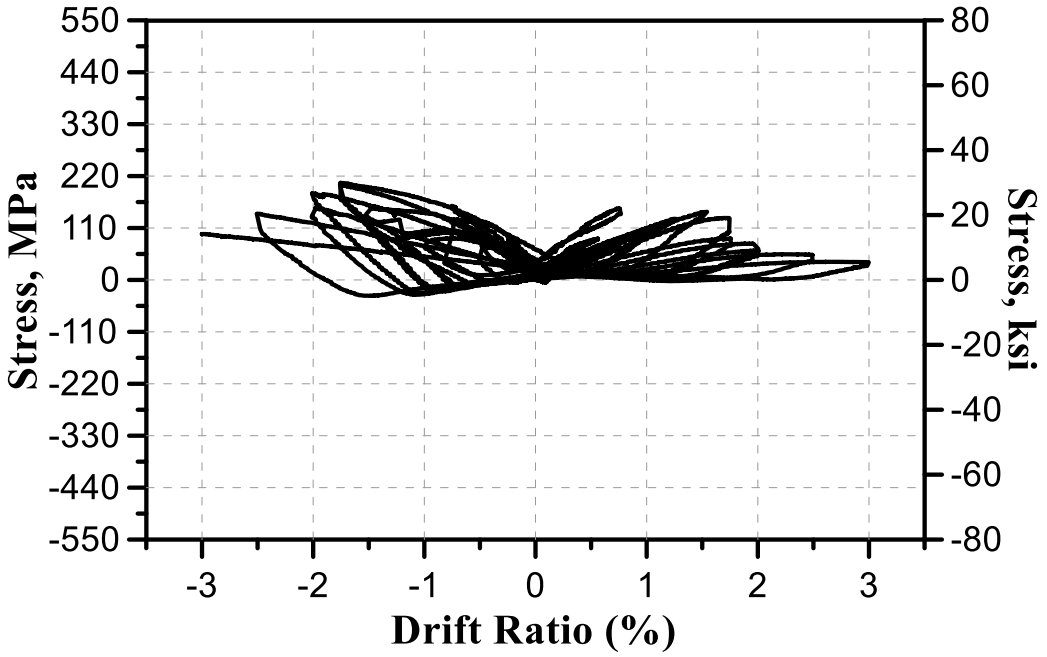

Figure 5-103 Measured stresses of strain gauge (S12) for specimen SW-HP-0.5-2

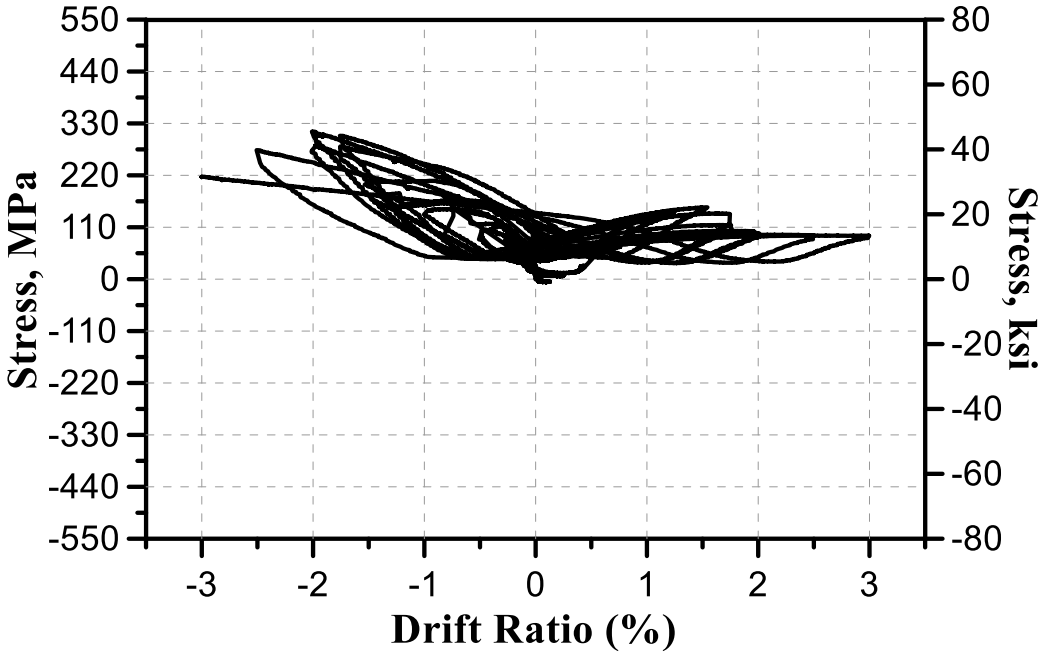

Figure 5-104 Measured stresses of strain gauge (S13) for specimen SW-HP-0.5-2

5.7 SW-MA-1.0

5.7.1 Damage and cracking propagation

Shear and flexural cracks propagation at drift ratio 0.125%, 0.25%, 0.5%, 0.75%, 1%, 1.25%, and 1.5% are shown in Figure 5-105. Cracks developed along the diagonal compressive struts until 0.75% drift ratio. For walls of aspect ratio 1:1, it was observed that one inclined strut was responsible to carry forces from the tip of wall to its base, the base width is 0.25 wall length. The boundaries are the critical zones where the flexural and compressive stresses concentrated. Therefore, a sudden shear strength drop observed at drift ratio 1% due sliding shear failure.

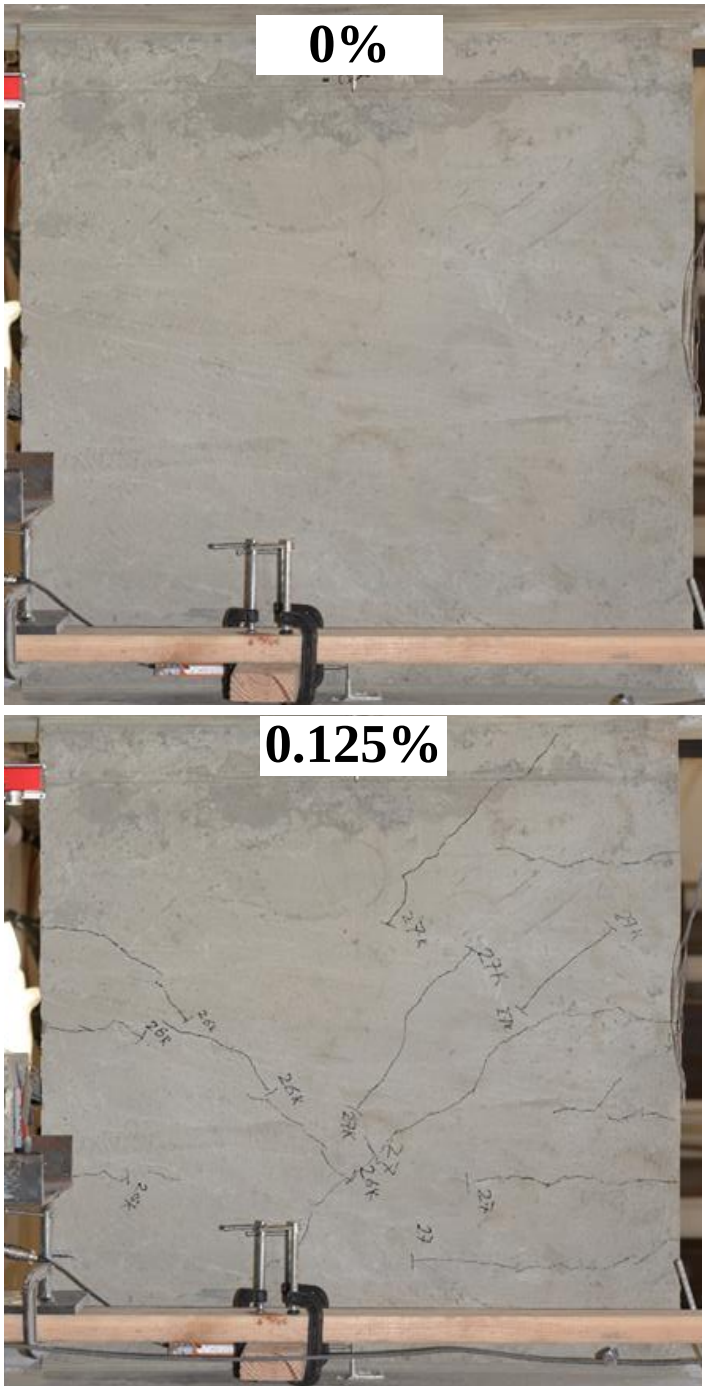

Figure 5-105 Test results of specimen SW-MA-1.0 at drift ratio 0.125%, 0.25%, 0.5%, 0.75%, 1%, 1.25%, and 1.5% (continued)

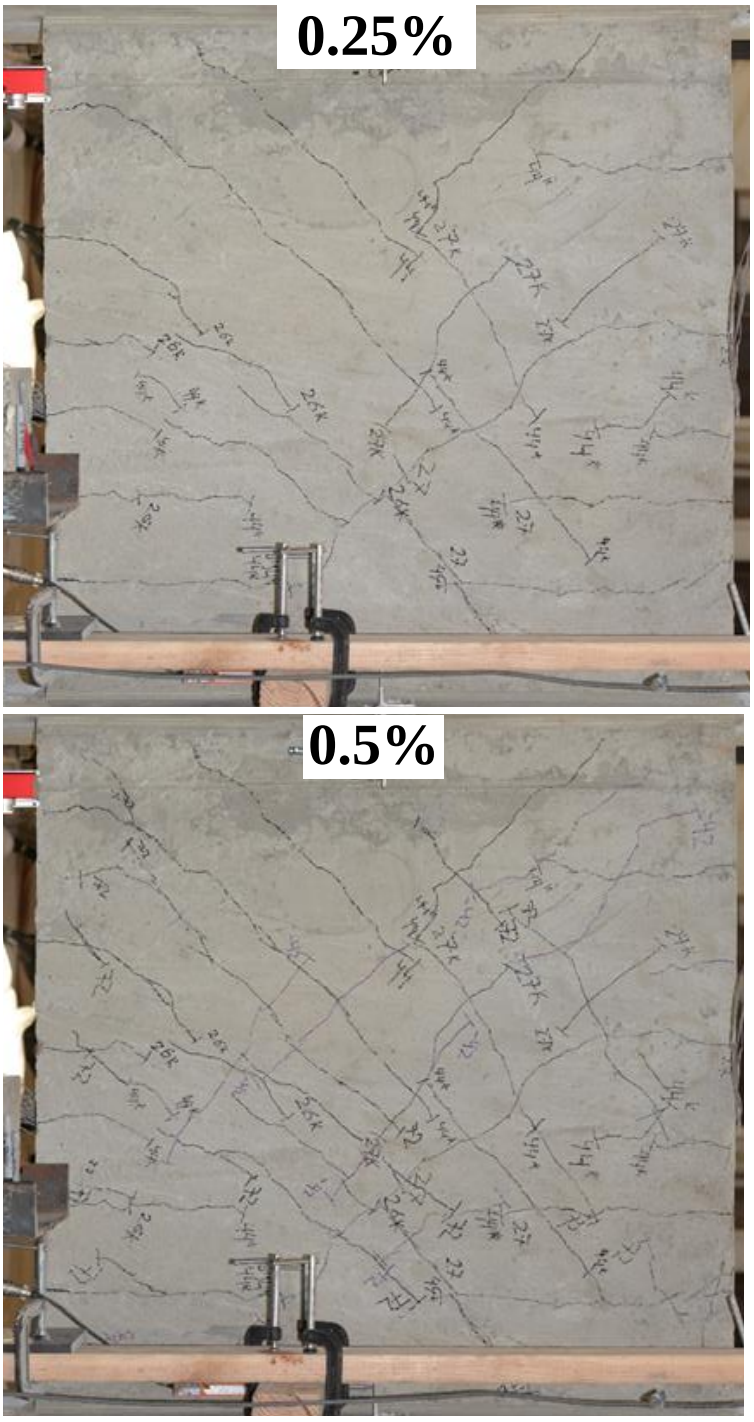

Figure 5-105 Test results of specimen SW-MA-1.0 at drift ratio 0.125%, 0.25%, 0.5%, 0.75%, 1%, 1.25%, and 1.5% (continued)

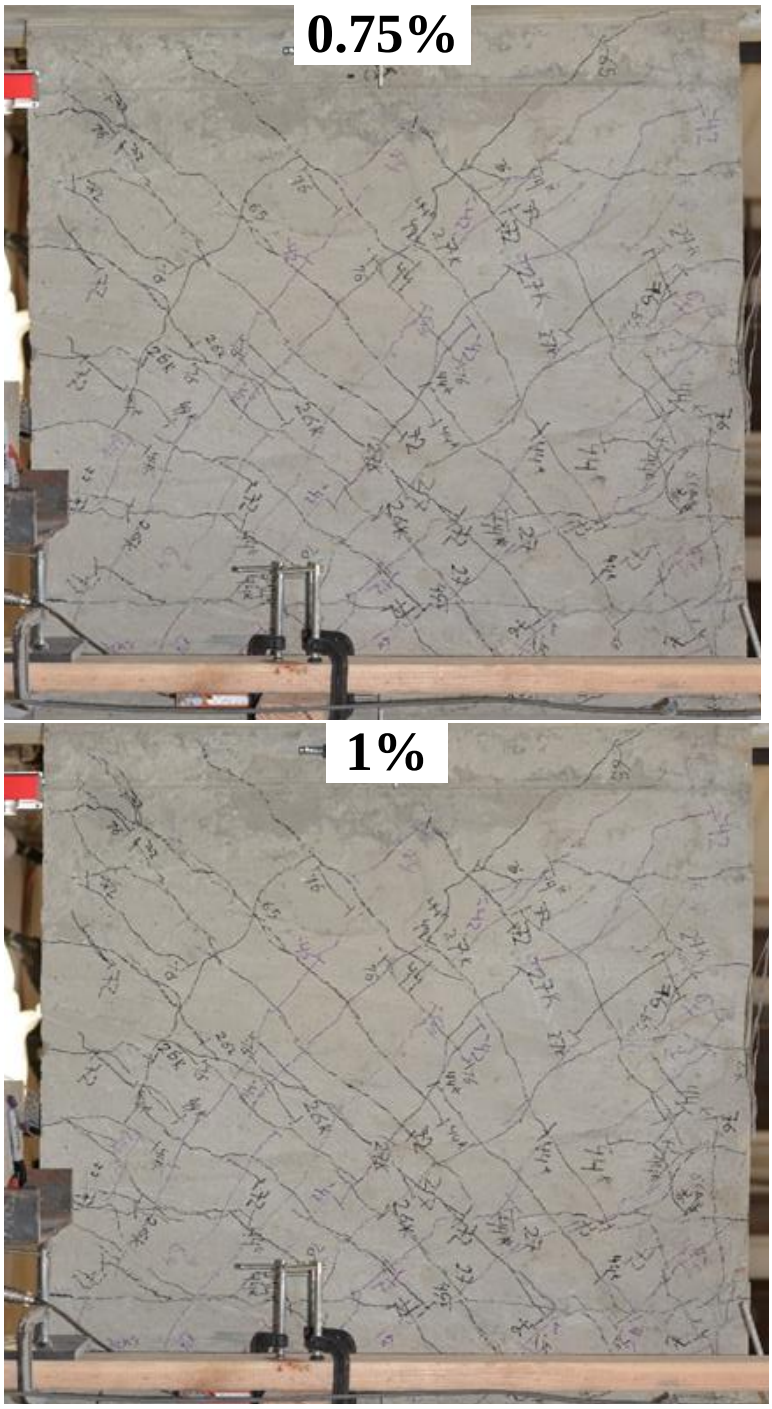

Figure 5-105 Test results of specimen SW-MA-1.0 at drift ratio 0.125%, 0.25%, 0.5%, 0.75%, 1%, 1.25%, and 1.5% (continued)

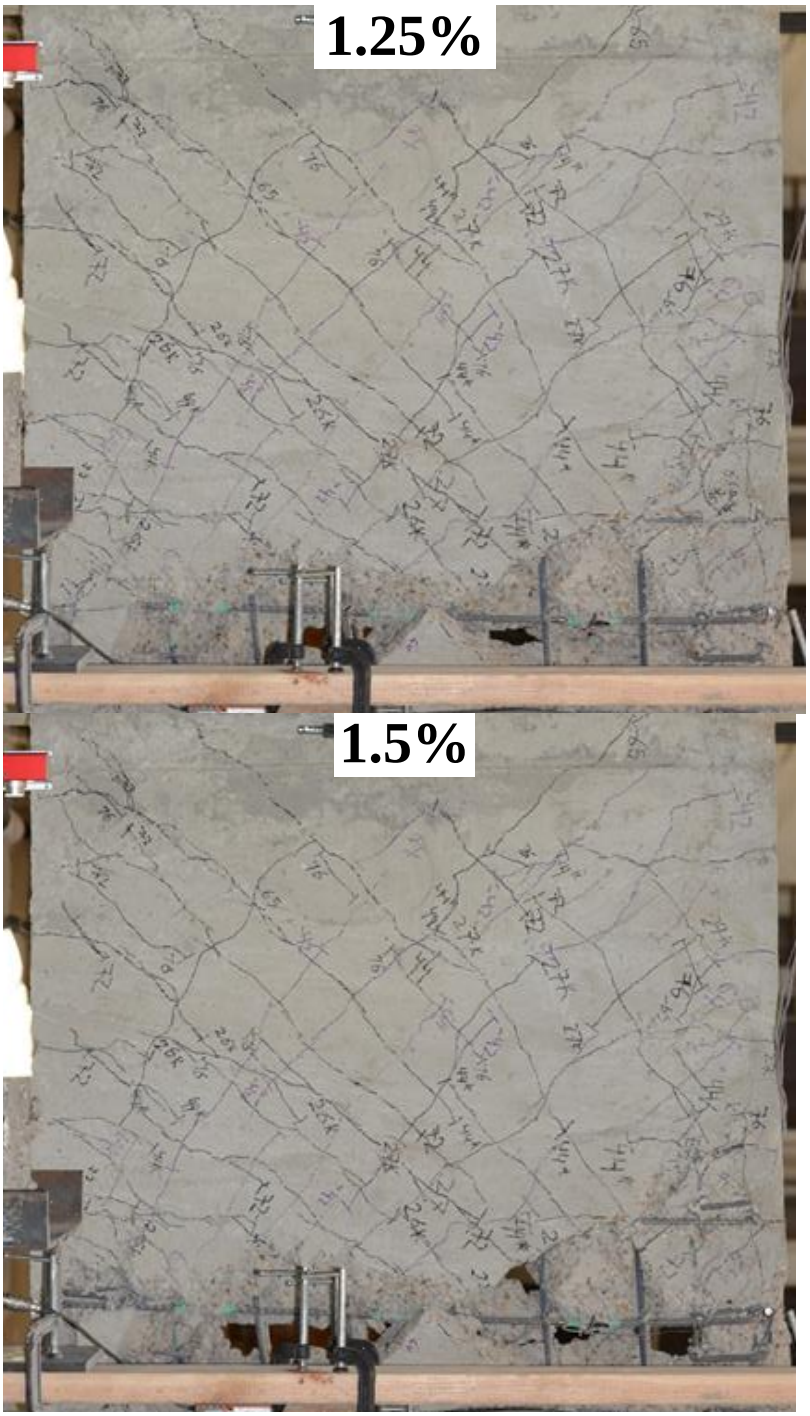

Figure 5-105 Test results of specimen SW-MA-1.0 at drift ratio 0.125%, 0.25%, 0.5%, 0.75%, 1%, 1.25%, and 1.5% (continued)

5.7.2 Shear strength response

Shear force versus drift ratio response of specimen SW-MA-1.0 is shown in

Figure 5-106. The maximum attained shear force was 76 kips (7.4√fcm) at drift ratio 1.0%. However, sudden drop in shear strength commenced at this drift level due to sliding shear failure, where the diagonal concrete struts crushed and no longer resist shear forces, the shear forces are resisted by dowel action (kinking the longitudinal steel rebars).

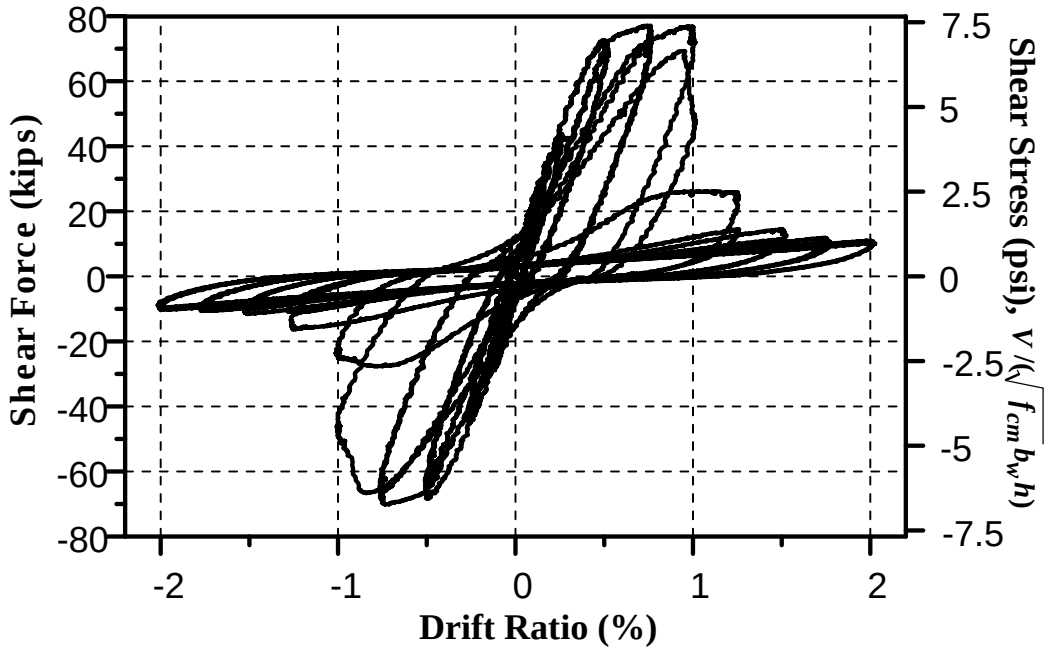

Figure 5-106 Shear strength hysteresis curve of specimen SW-MA-1.0

5.7.3 Steel reinforcement stresses

Strain gauges were attached at boundaries, longitudinal and horizontal steel bars as shown in Figure 5-107. Strain gauges L1 to L12 are attached at vertical steel bars,

while S13 to S16 are attached at boundaries and horizontal steel bars. The results of drift ratio and the attained steel stress in strain gauges L1 to S16 are shown in Figure 5-108 to Figure 5-123. All vertical steel bars yielded (reached the yielding strength of (60 ksi). None of strain gauges at boundaries or horizontal steel bars yielded.

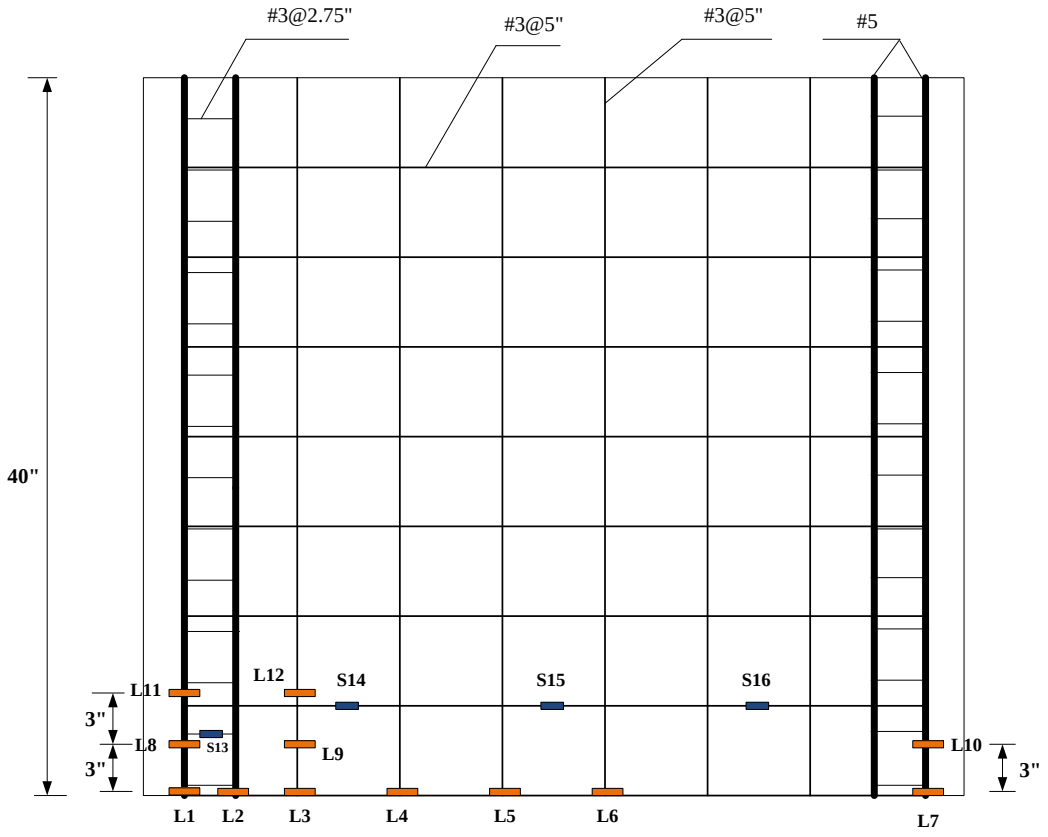

Figure 5-107 Locations of strain gauges at boundaries, vertical and horizontal steel bars for specimen SW-MA-1.0

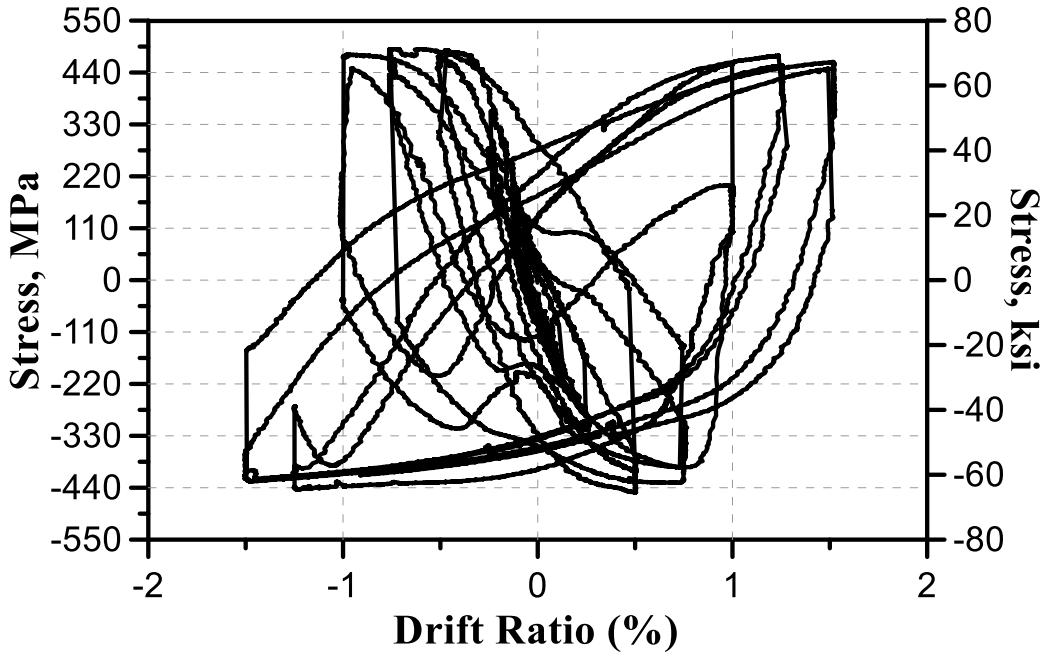

Figure 5-108 Measured stresses of strain gauge (L1) for specimen SW-MA-1.0

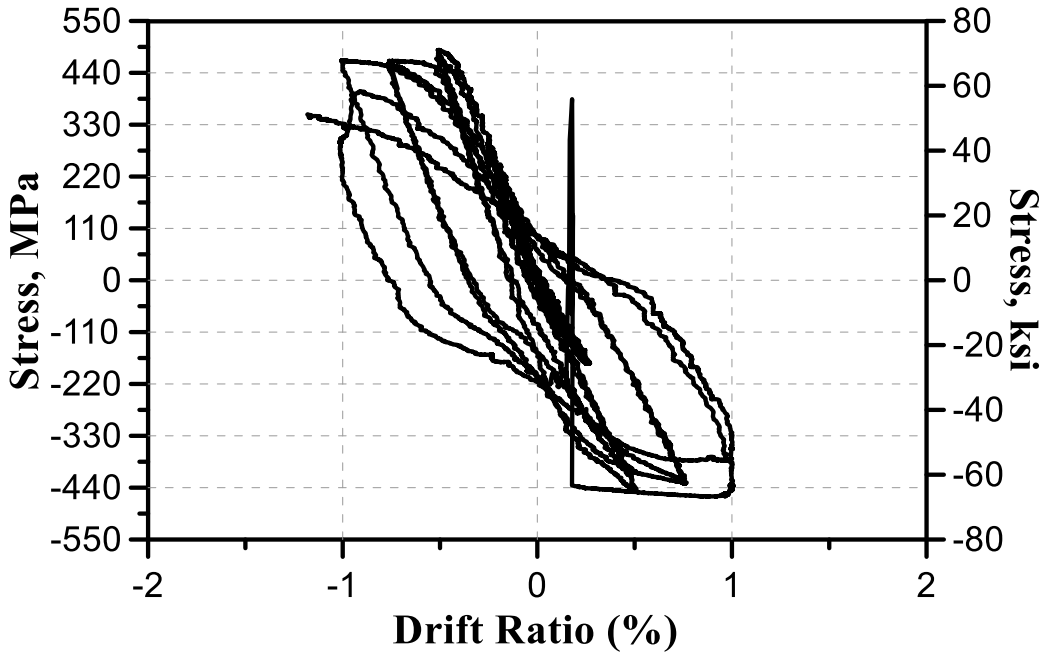

Figure 5-109 Measured stresses of strain gauge (L2) for specimen SW-MA-1.0

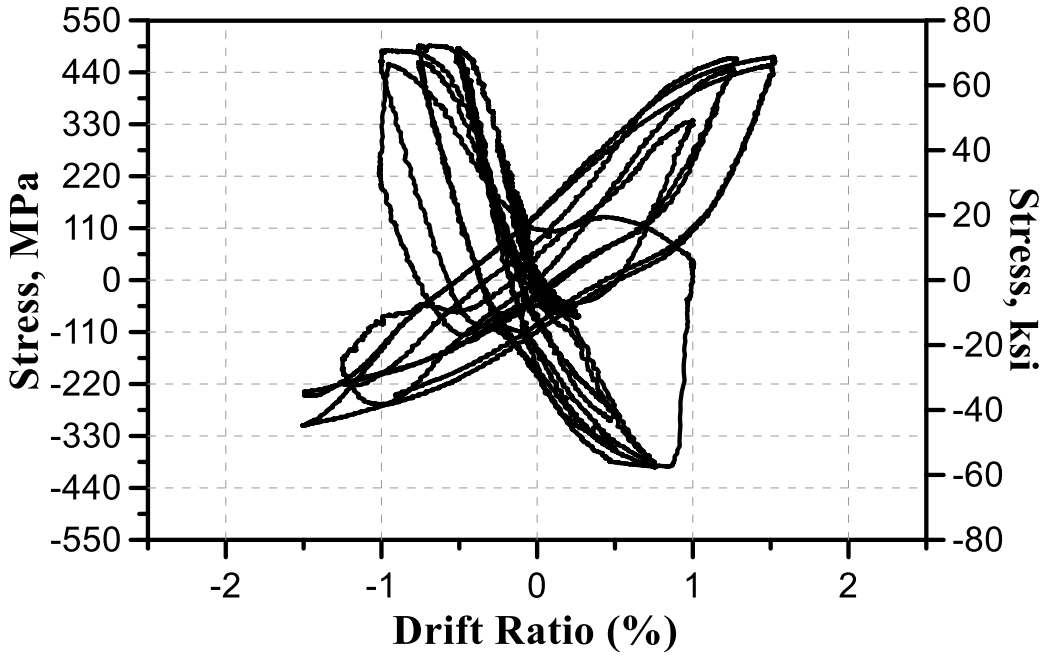

Figure 5-110 Measured stresses of strain gauge (L3) for specimen SW-MA-1.0

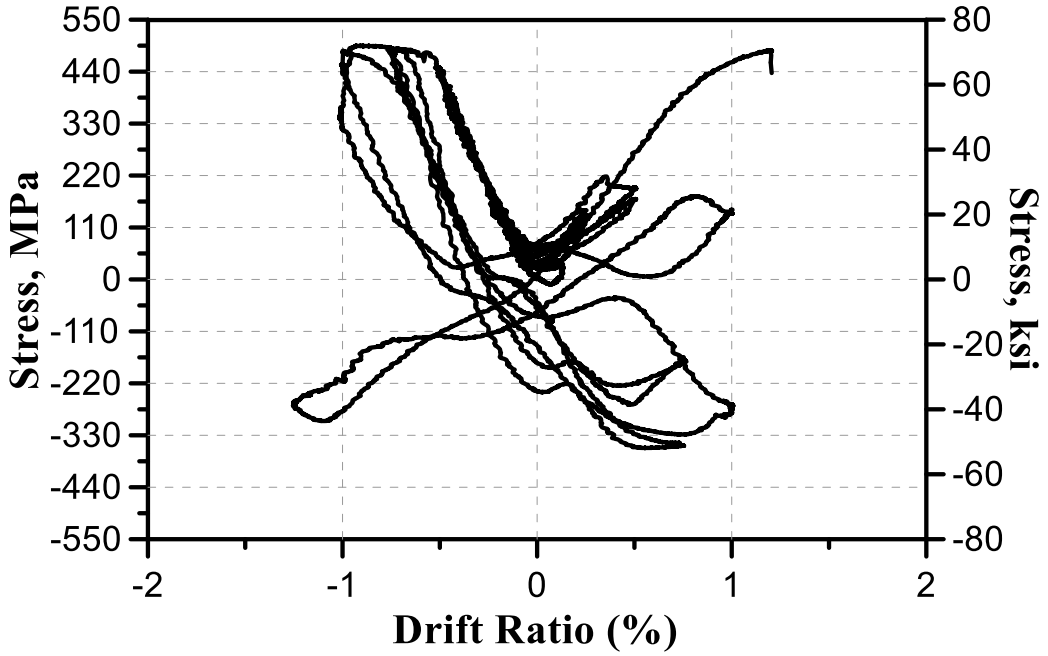

Figure 5-111 Measured stresses of strain gauge (L4) for specimen SW-MA-1.0

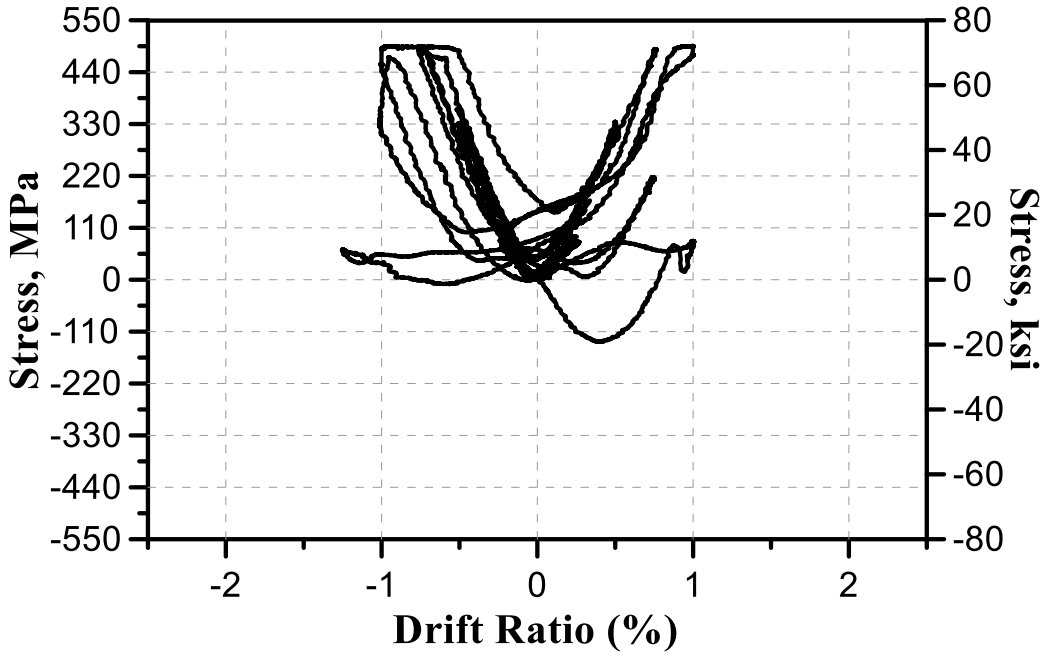

Figure 5-112 Measured stresses of strain gauge (L6) for specimen SW-MA-1.0

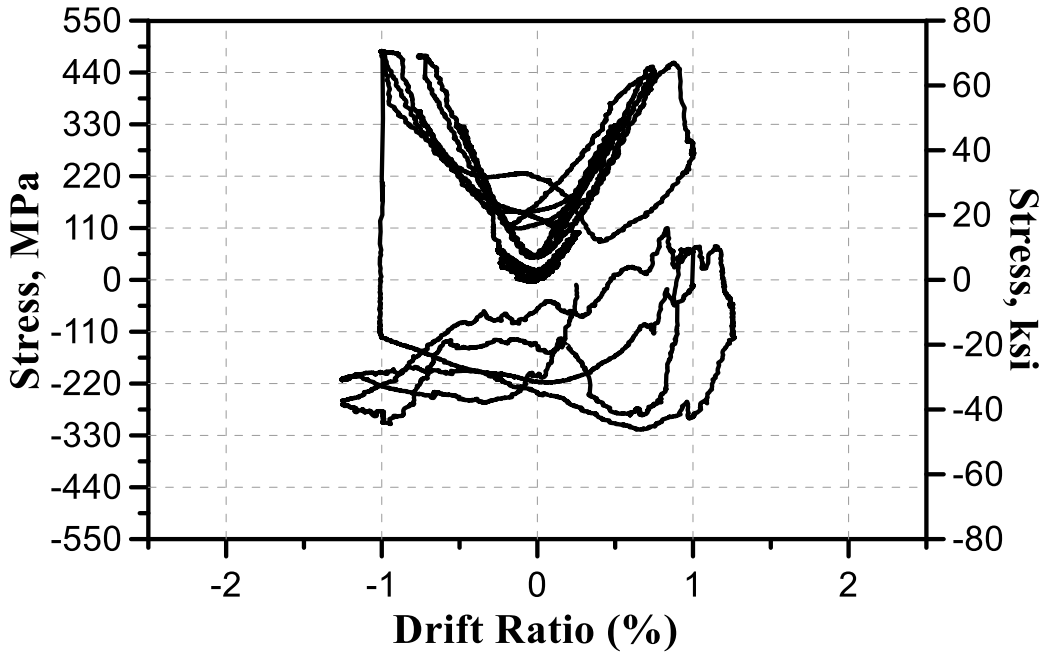

Figure 5-113 Measured stresses of strain gauge (L6) for specimen SW-MA-1.0

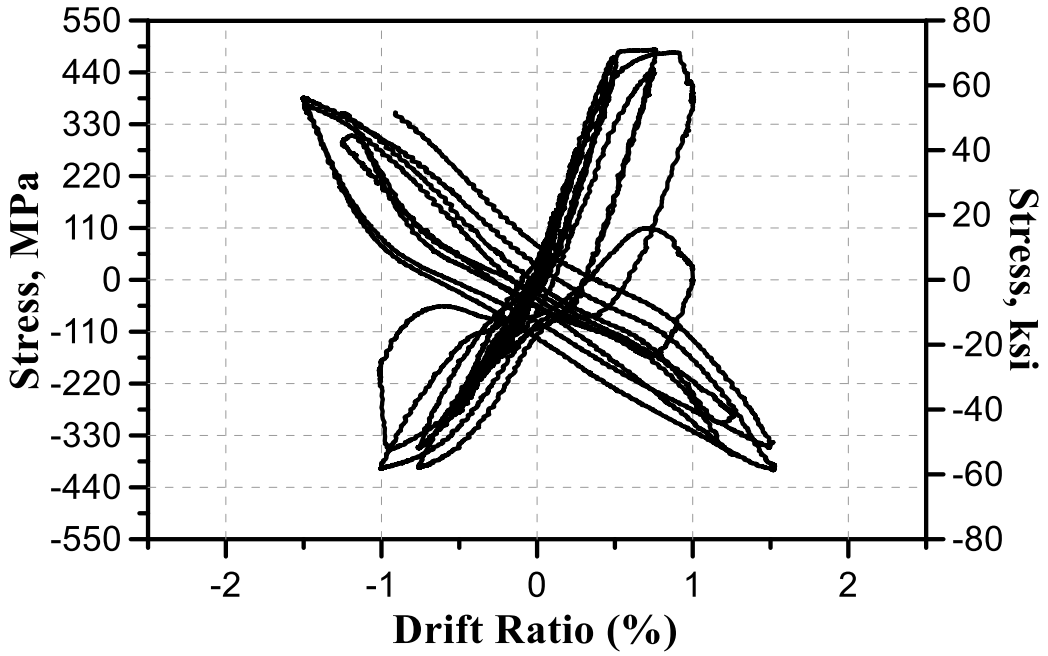

Figure 5-114 Measured stresses of strain gauge (L7) for specimen SW-MA-1.0

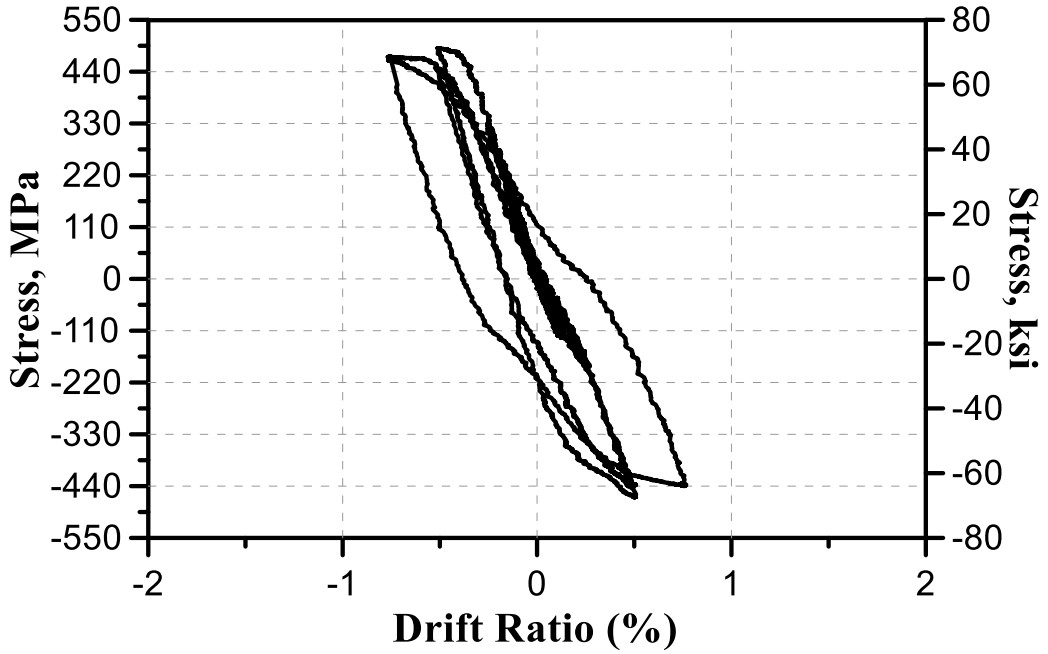

Figure 5-115 Measured stresses of strain gauge (L8) for specimen SW-MA-1.0

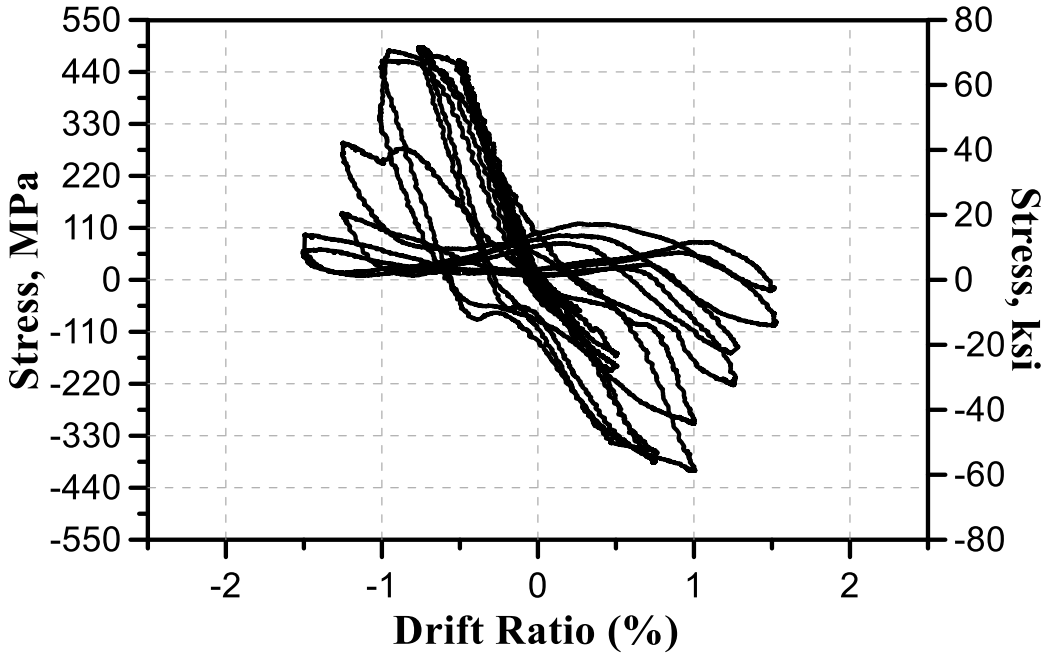

Figure 5-116 Measured stresses of strain gauge (L9) for specimen SW-MA-1.0

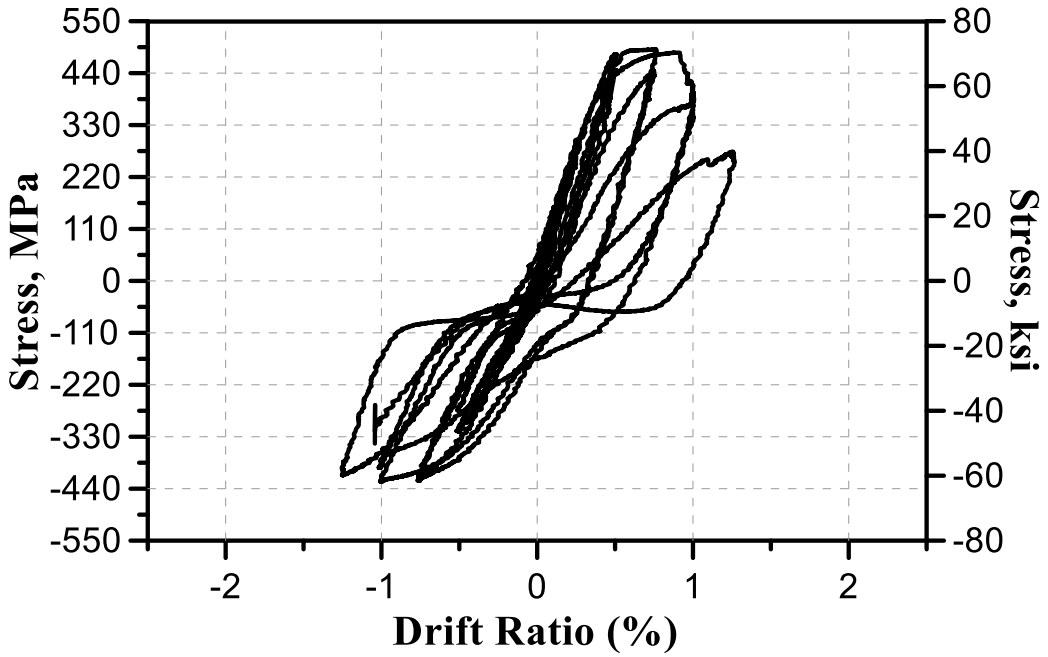

Figure 5-117 Measured stresses of strain gauge (L10) for specimen SW-MA-1.0

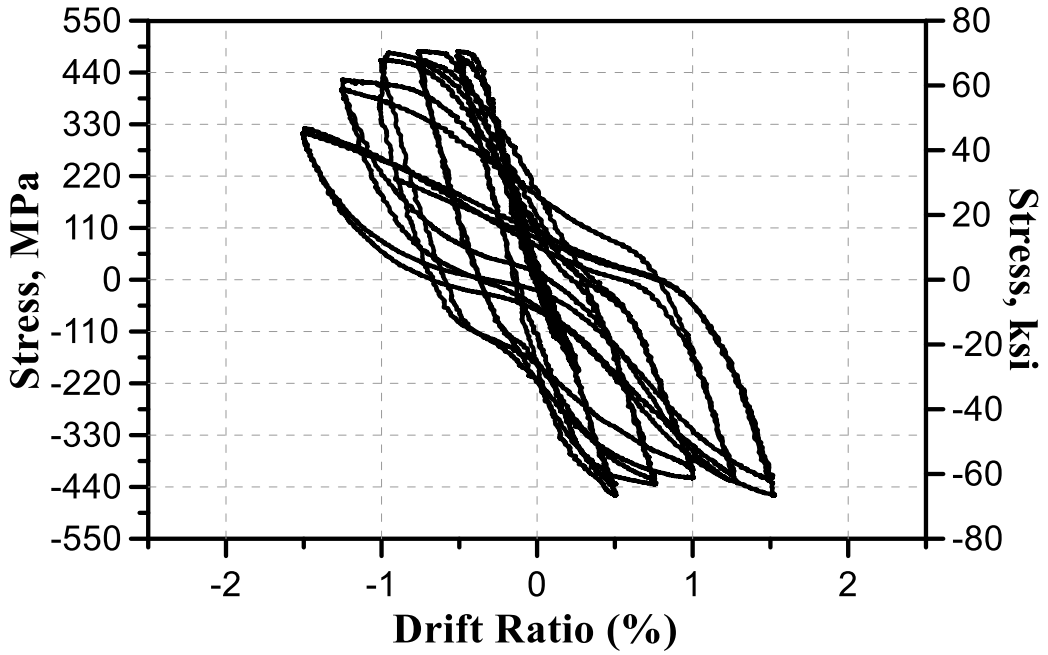

Figure 5-118 Measured stresses of strain gauge (L11) for specimen SW-MA-1.0

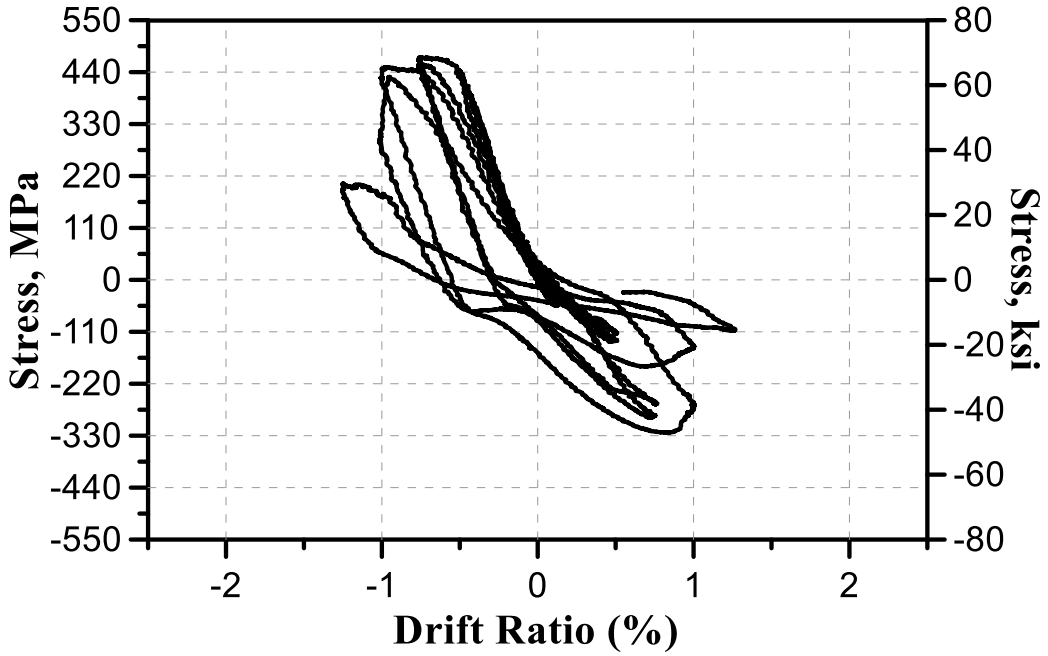

Figure 5-119 Measured stresses of strain gauge (L12) for specimen SW-MA-1.0

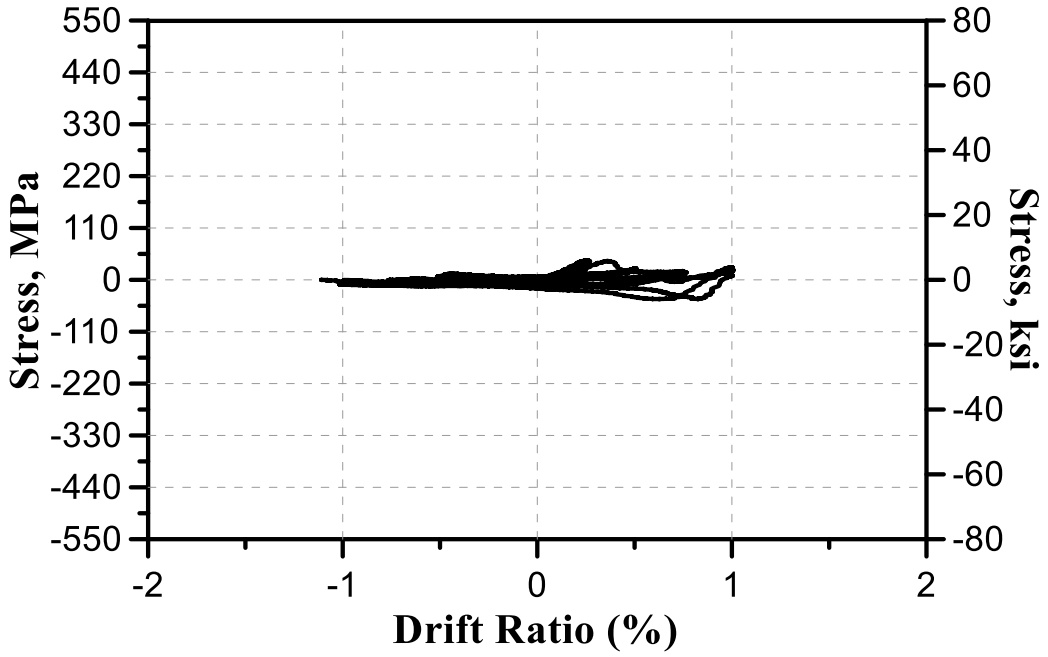

Figure 5-120 Measured stresses of strain gauge (S13) for specimen SW-MA-1.0

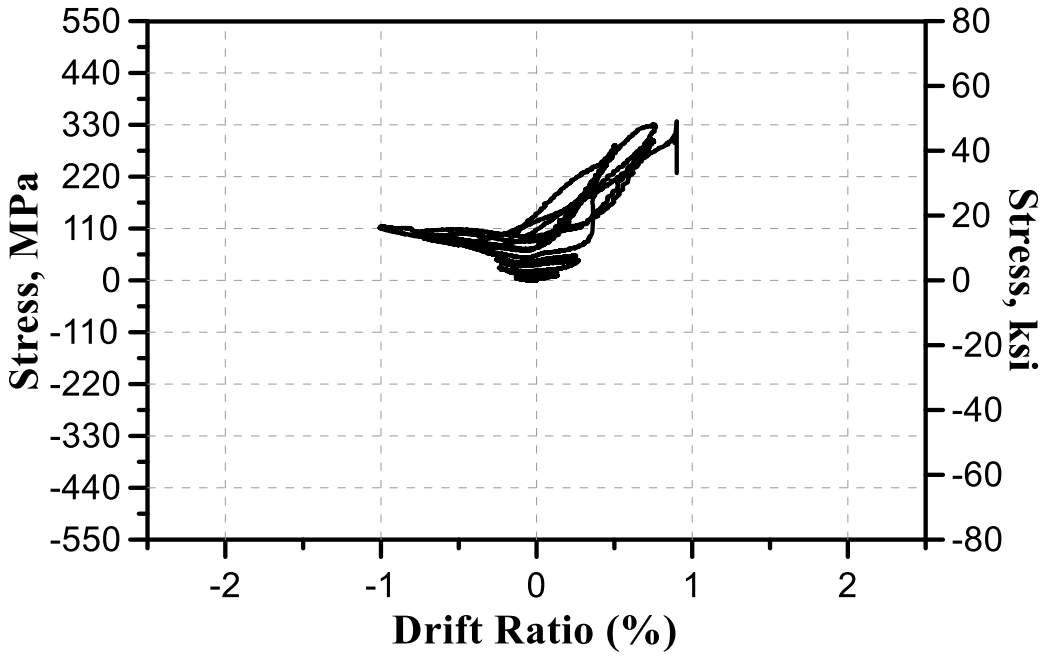

Figure 5-121 Measured stresses of strain gauge (S14) for specimen SW-MA-1.0

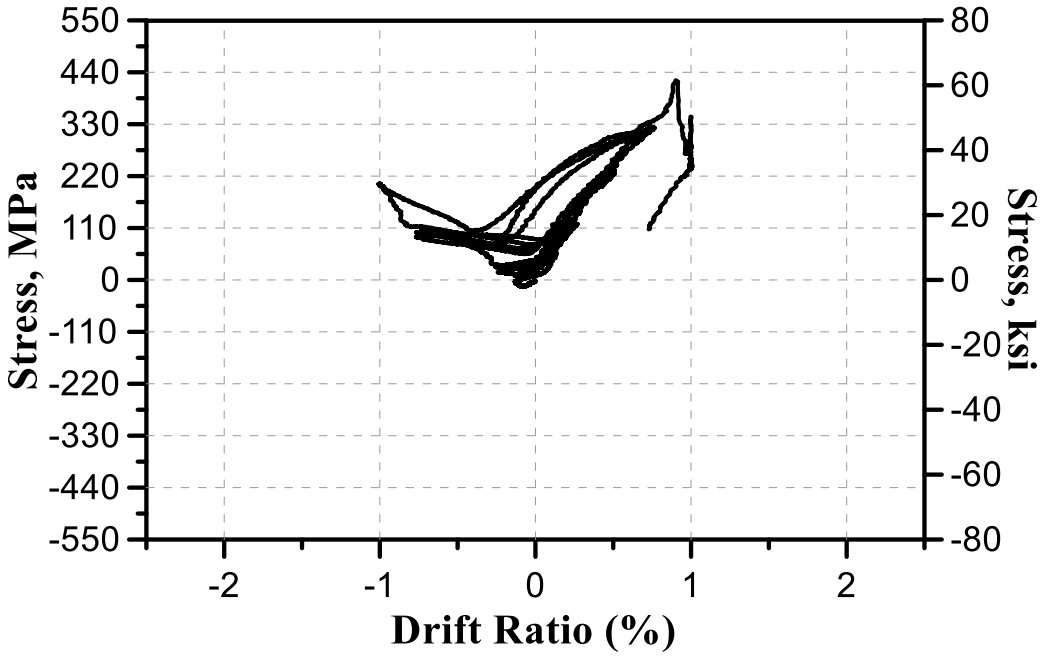

Figure 5-122 Measured stresses of strain gauge (S15) for specimen SW-MA-1.0

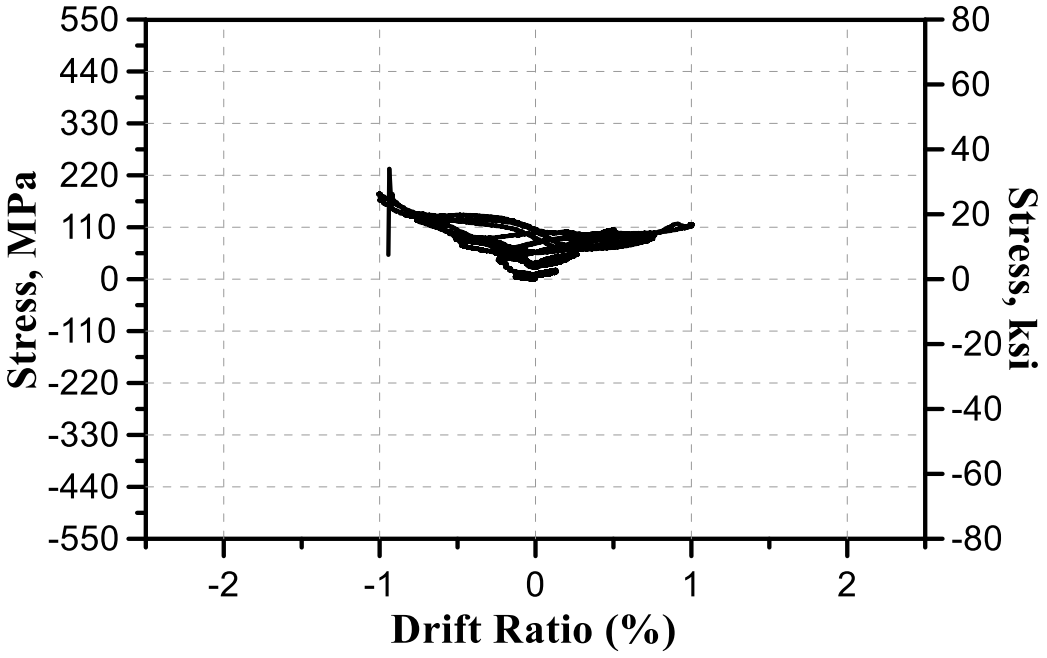

Figure 5-123 Measured stresses of strain gauge (S16) for specimen SW-MA-1.0

5.8 SW-MP-1.0-1

5.8.1 Damage and cracking propagation

Shear and flexural cracks propagation at drift ratio 0.125%, 0.25%, 0.5%, 0.75%, 1%, 1.25%, and 1.5% are shown in Figure 5-124. Cracks developed along the diagonal compressive struts until 0.75% drift ratio. For walls of aspect ratio 1:1, it was observed that one inclined strut was responsible to carry forces from the tip of wall to its base, the base width is 0.25 wall length. The gap between steel cages was 5 inches which was not sufficient to confine the concrete at wall web. Therefore, a sudden shear strength drop observed at drift ratio 0.75% due to diagonal tension failure.

Figure 5-124 Test results of specimen SW-MA-1.0 at drift ratio 0.125%, 0.25%, 0.5%, 0.75%, 1%, 1.25%, and 1.5% (continued)

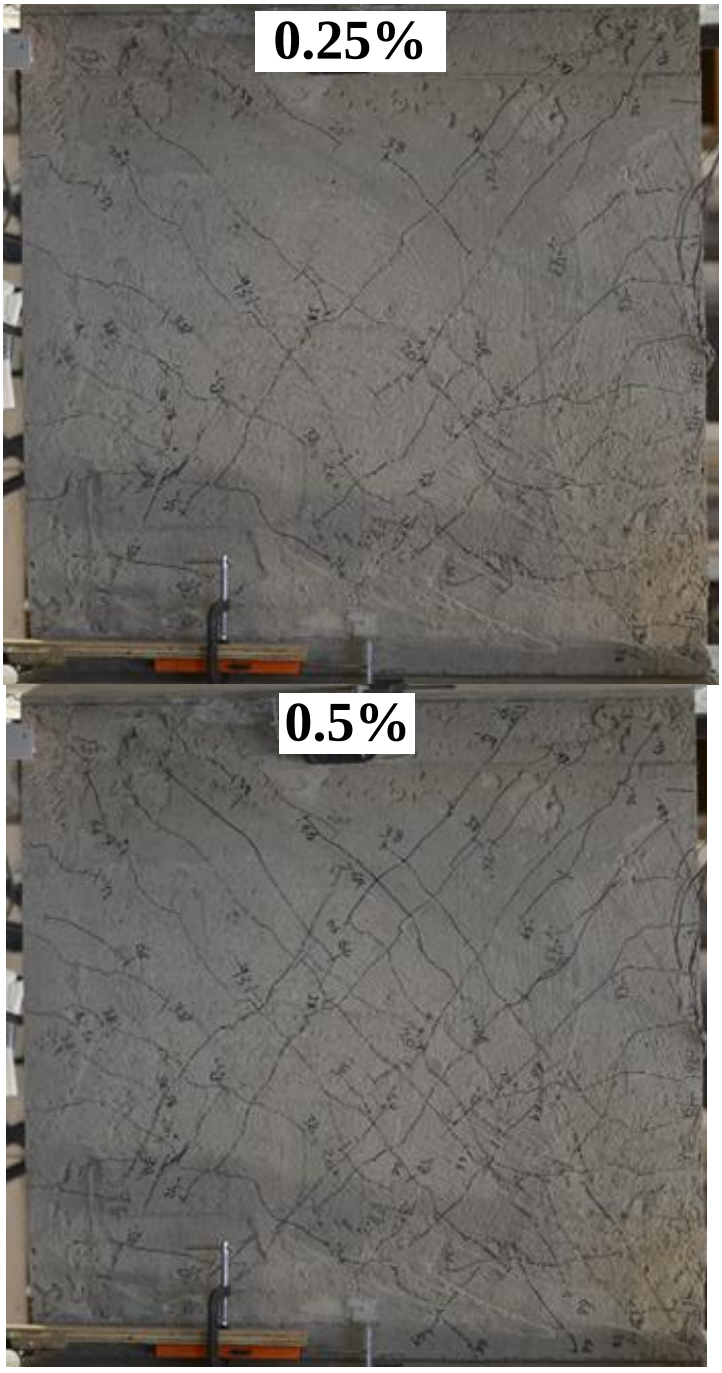

Figure 5-124 Test results of specimen SW-MA-1.0 at drift ratio 0.125%, 0.25%, 0.5%, 0.75%, 1%, 1.25%, and 1.5% (continued)

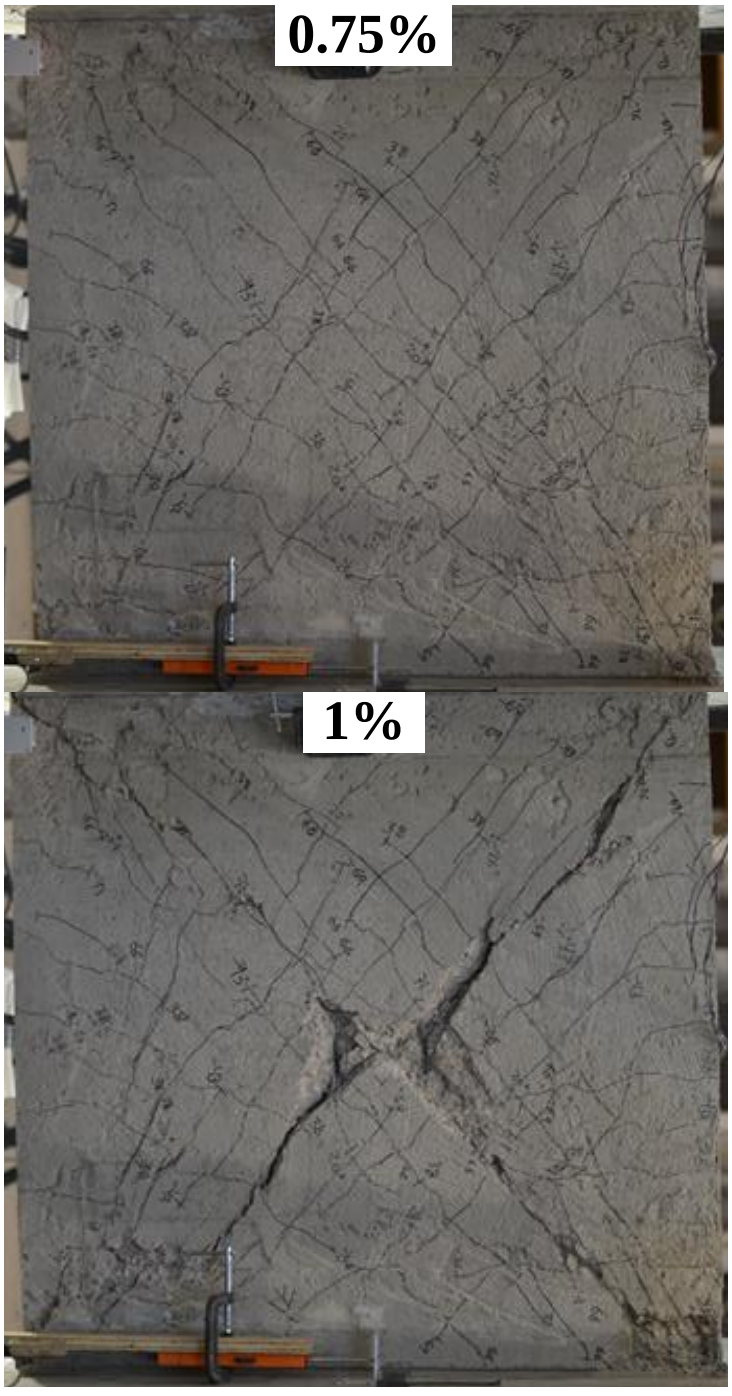

Figure 5-124 Test results of specimen SW-MA-1.0 at drift ratio 0.125%, 0.25%, 0.5%, 0.75%, 1%, 1.25%, and 1.5% (continued)

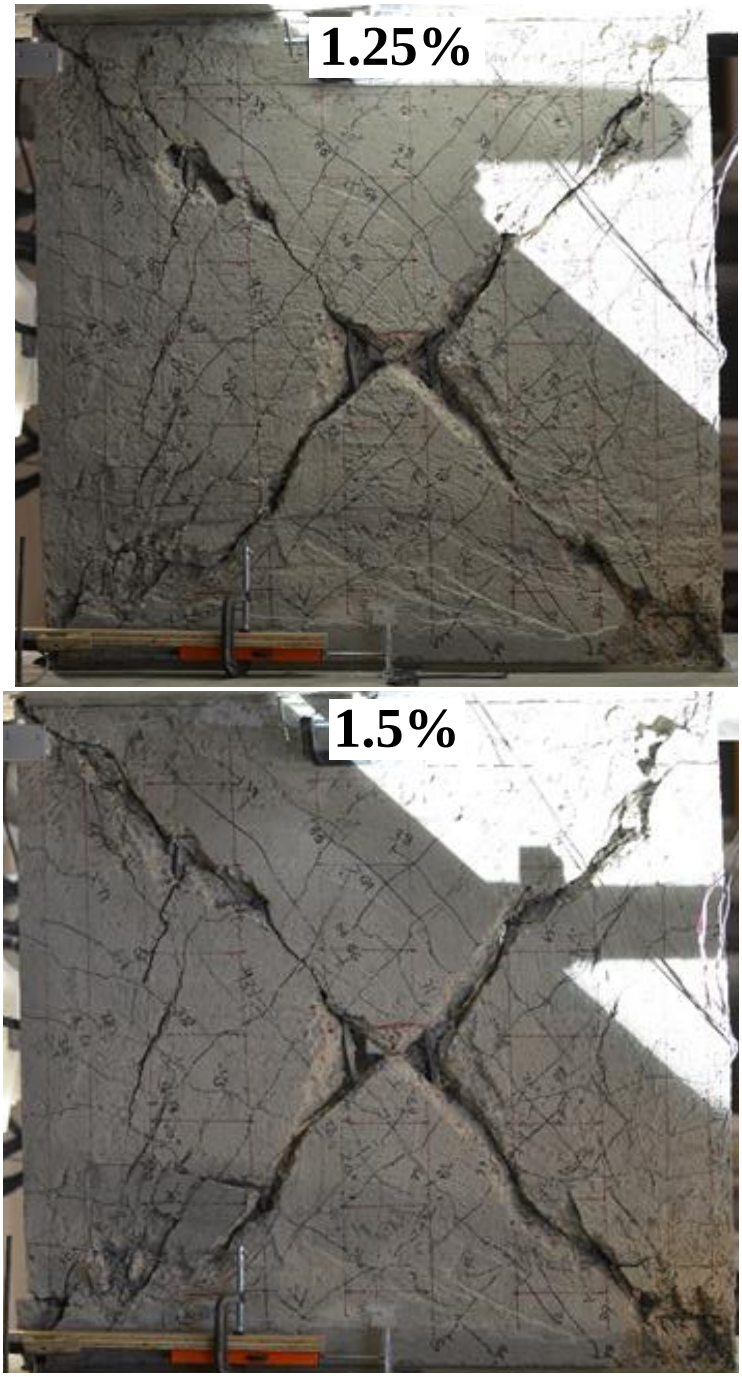

Figure 5-124 Test results of specimen SW-MA-1.0 at drift ratio 0.125%, 0.25%, 0.5%, 0.75%, 1%, 1.25%, and 1.5%

5.8.2 Shear strength response

Shear force versus drift ratio response of specimen SW-MP-1.0-1 is shown in Figure 5-125. The maximum attained shear force was 76 kips ($7.3\sqrt{f_{cm}}$) at drift ratio 0.75%. However, sudden drop in shear strength commenced at this drift level due to diagonal tension failure, where the diagonal concrete strut split at 45-degree angle, the wide gap between steel cages was the main reason of this type of failure, where the concrete was insufficiently confined.

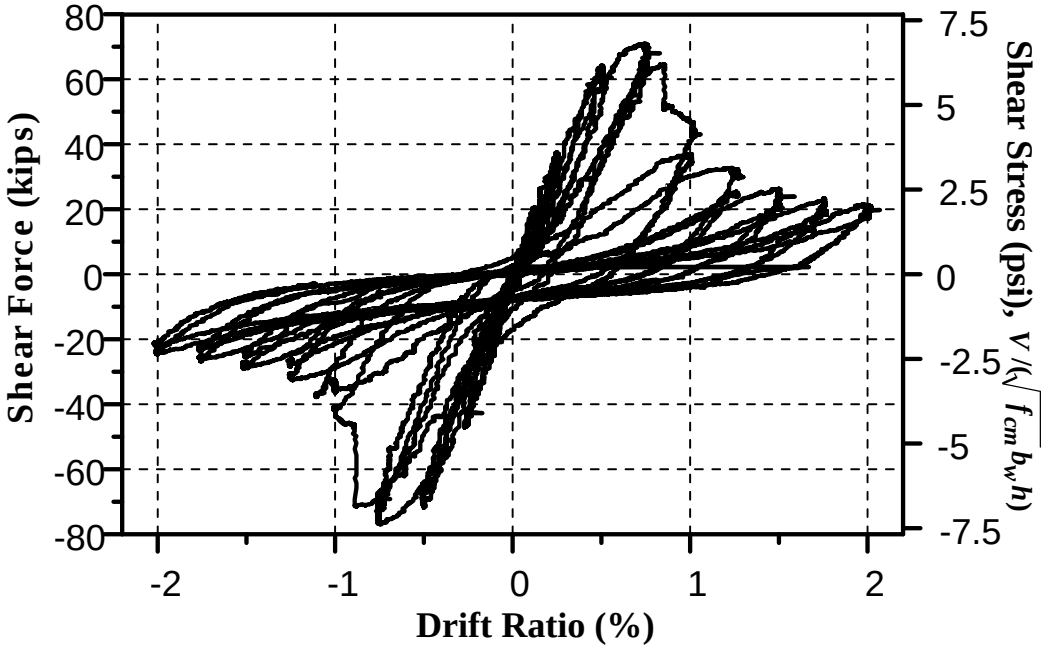

Figure 5-125 Shear strength hysteresis curve of specimen SW-MP-1.0-1

5.8.3 Steel reinforcement stresses

Strain gauges were attached at boundaries, longitudinal and horizontal steel bars as shown in Figure 5-126. Strain gauges L1 to L12 are attached at vertical steel bars, while S13 to S16 are attached at boundaries and horizontal steel bars. The results of drift ratio and the attained steel stress in strain gauges L1 to S16 are shown in Figure 5-127

to Figure 5-142. All vertical steel bars yielded (reached the yielding strength of (60 ksi) except L9. None of strain gauges at boundaries or horizontal steel bars yielded.

Figure 5-126 Locations of strain gauges at boundaries, vertical and horizontal steel bars for specimen SW-MA-1.0-1

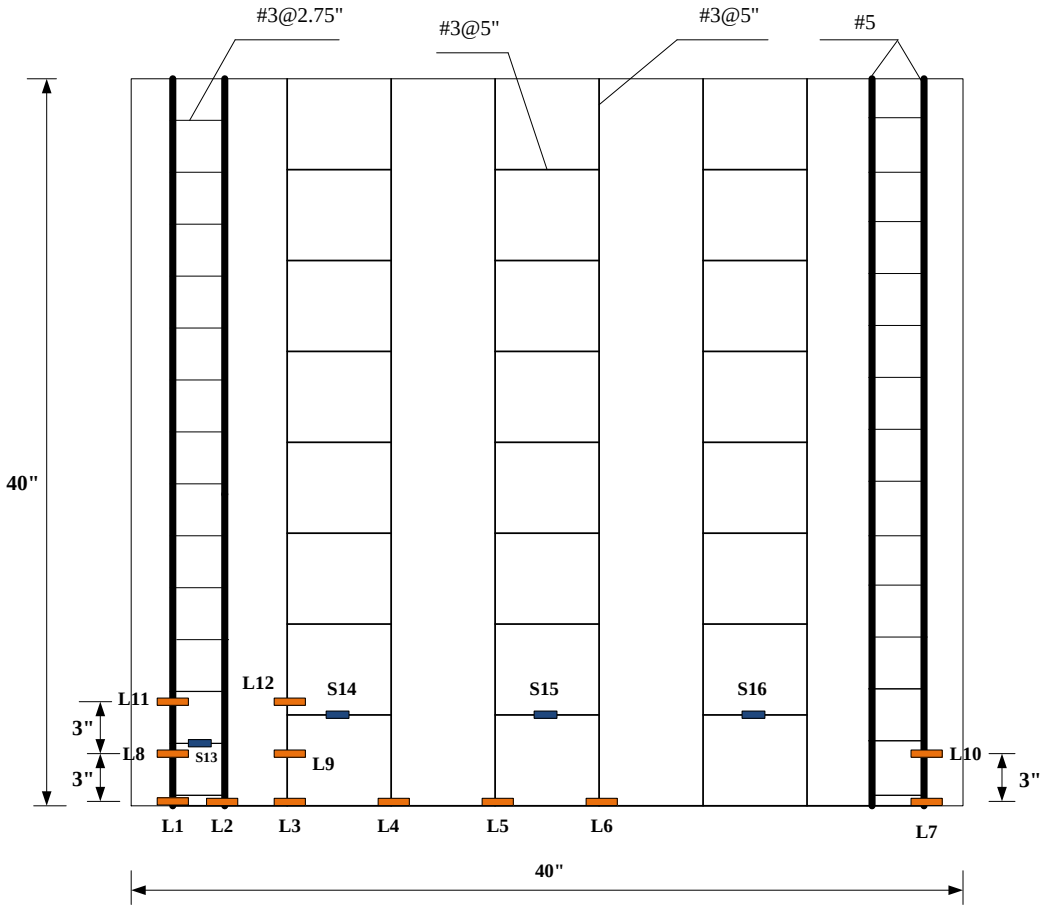

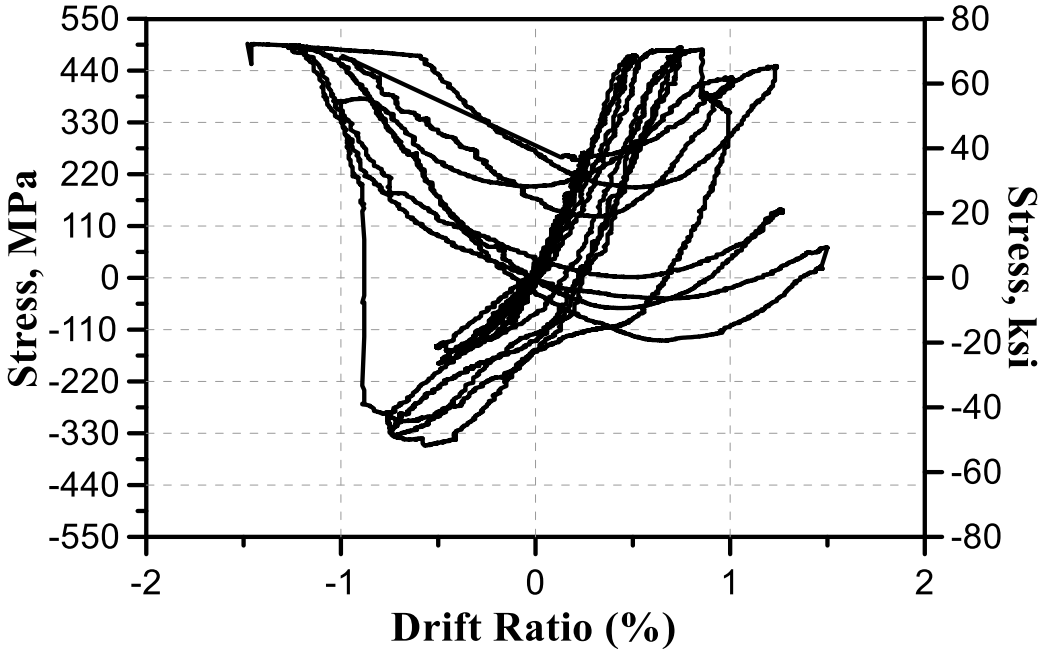

Figure 5-127 Measured stresses of strain gauge (L1) for specimen SW-MP-1.0-1

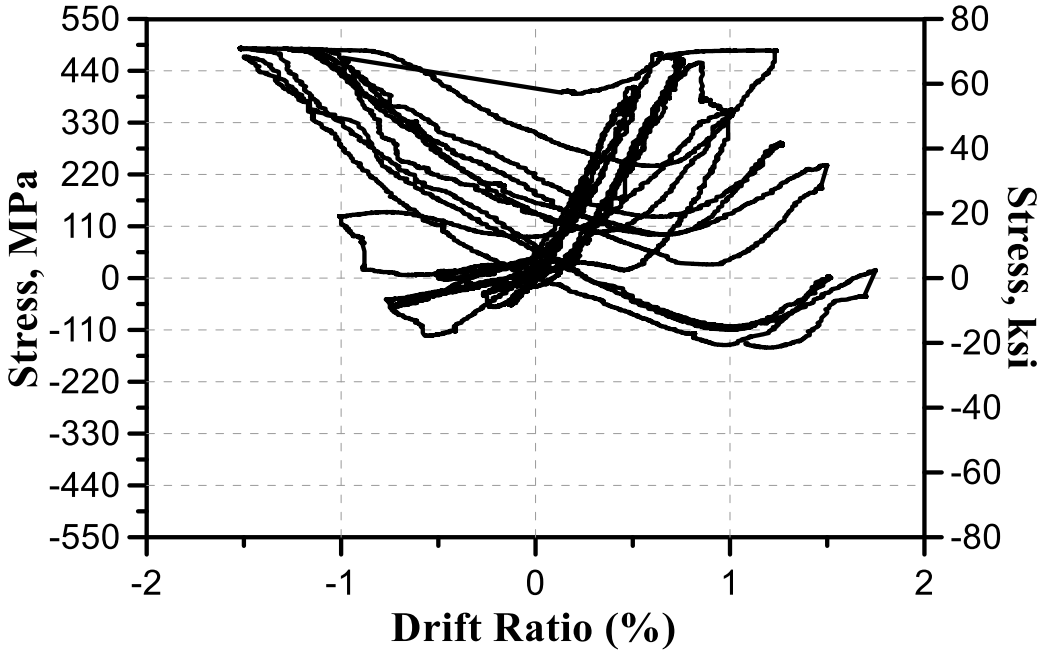

Figure 5-128 Measured stresses of strain gauge (L2) for specimen SW-MP-1.0-1

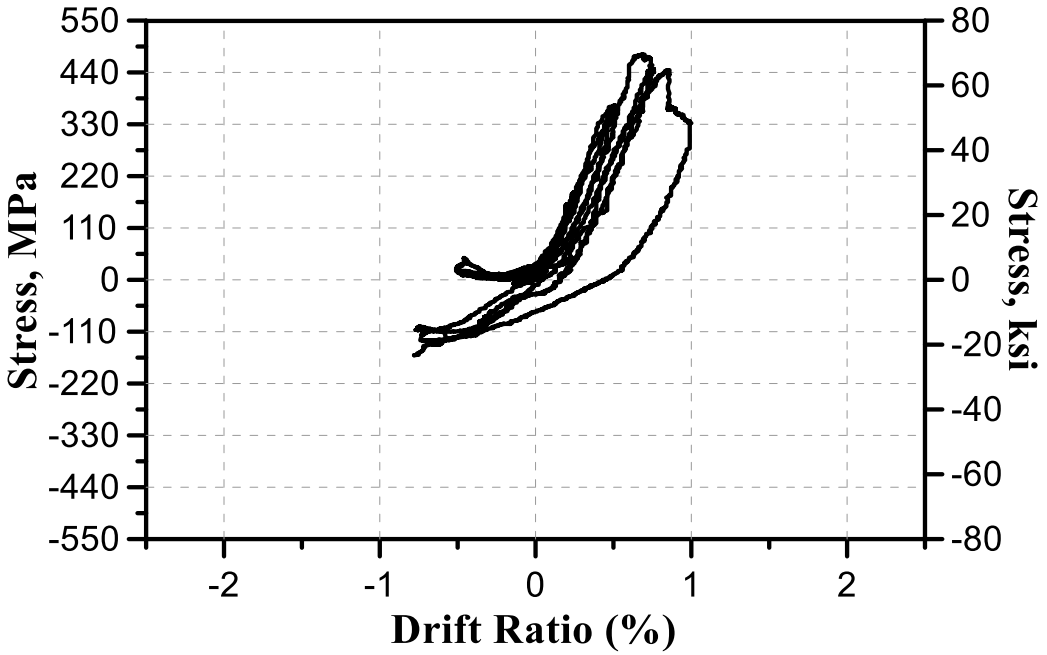

Figure 5-129 Measured stresses of strain gauge (L3) for specimen SW-MP-1.0-1

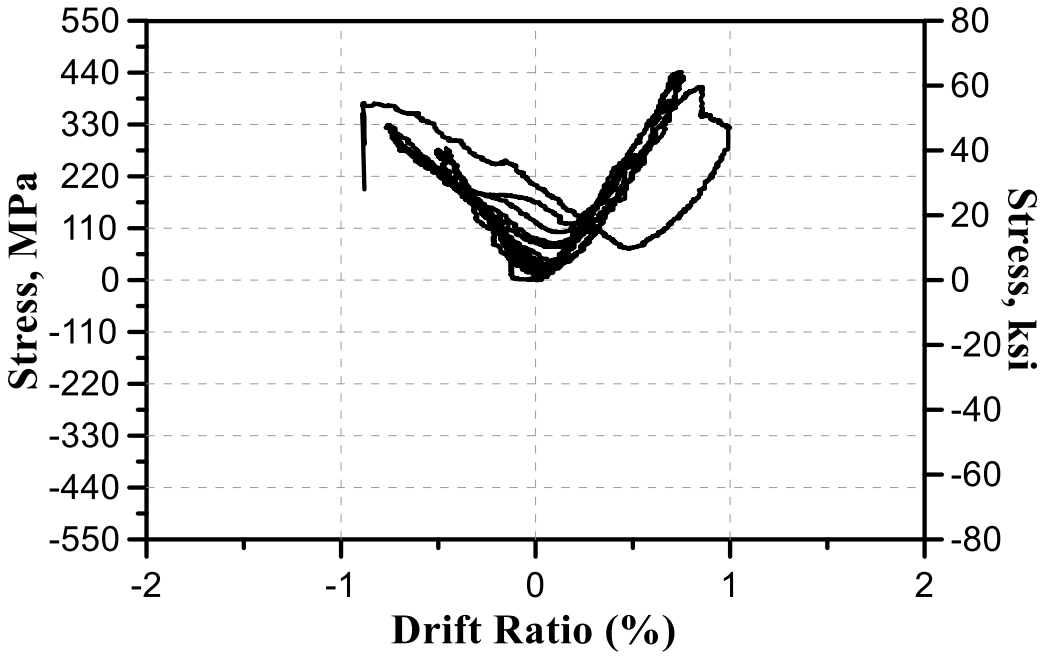

Figure 5-130 Measured stresses of strain gauge (L4) for specimen SW-MP-1.0-1

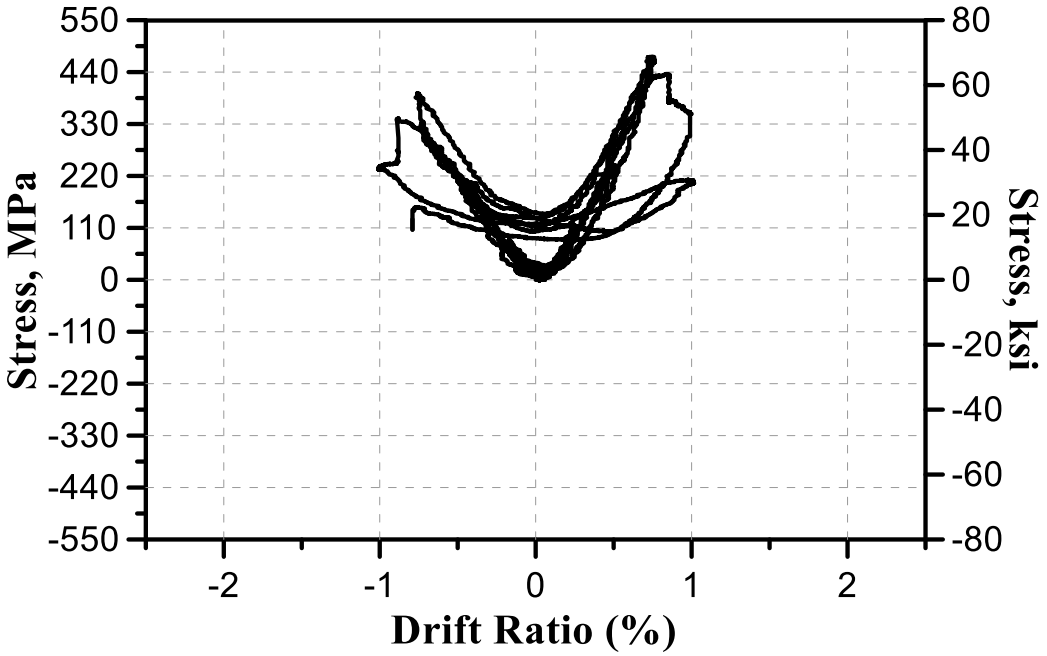

Figure 5-131 Measured stresses of strain gauge (L5) for specimen SW-MP-1.0-1

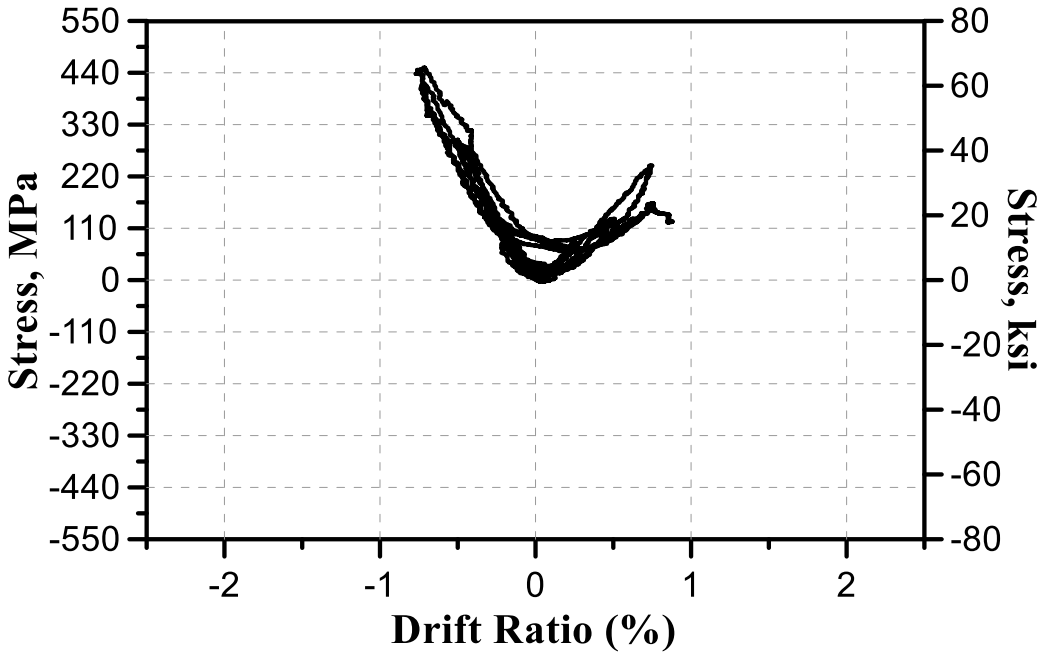

Figure 5-132 Measured stresses of strain gauge (L6) for specimen SW-MP-1.0-1

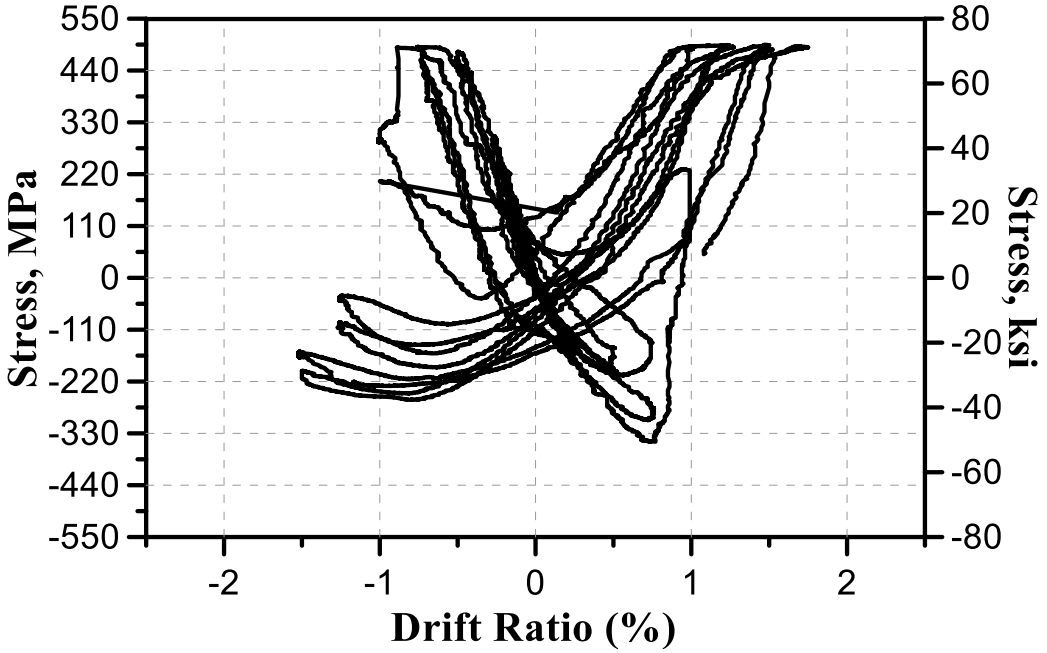

Figure 5-133 Measured stresses of strain gauge (L7) for specimen SW-MP-1.0-1

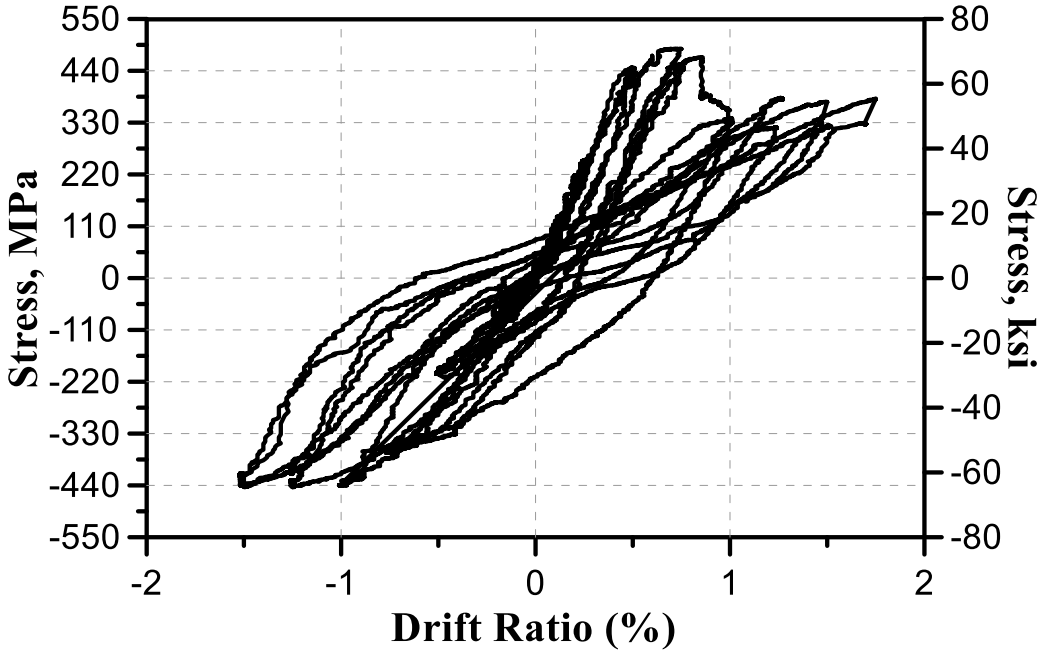

Figure 5-134 Measured stresses of strain gauge (L8) for specimen SW-MP-1.0-1

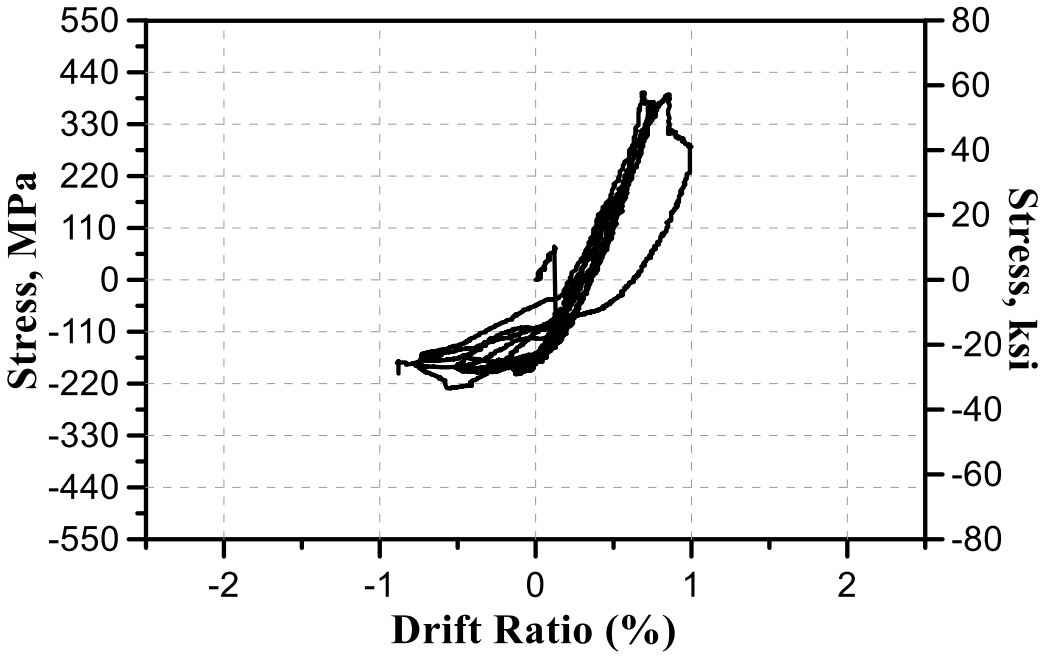

Figure 5-135 Measured stresses of strain gauge (L9) for specimen SW-MP-1.0-1

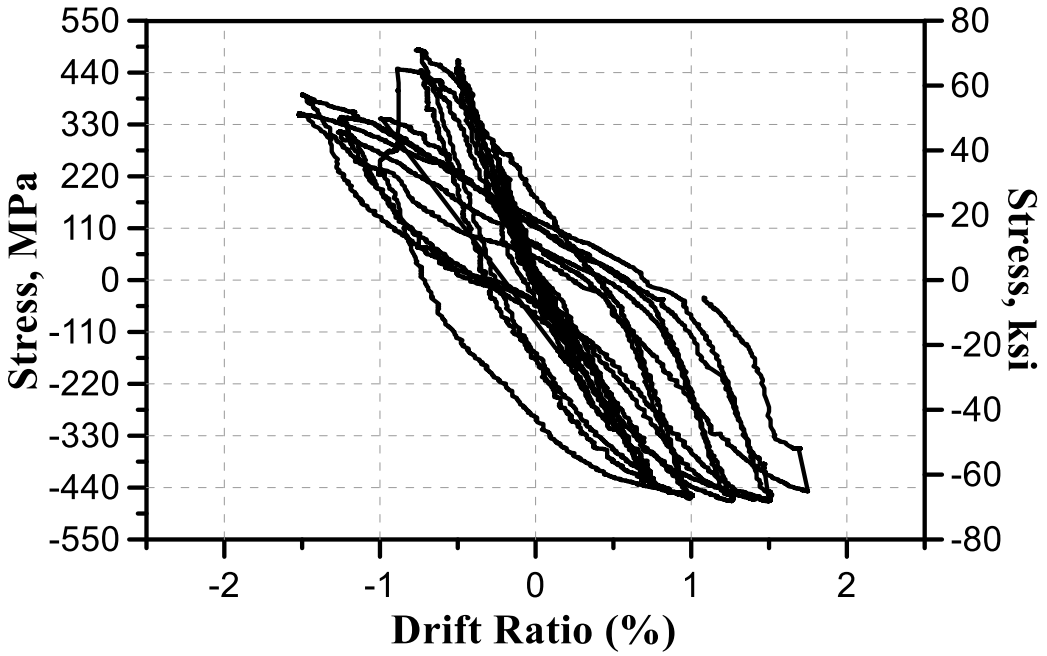

Figure 5-136 Measured stresses of strain gauge (L10) for specimen SW-MP-1.0-1

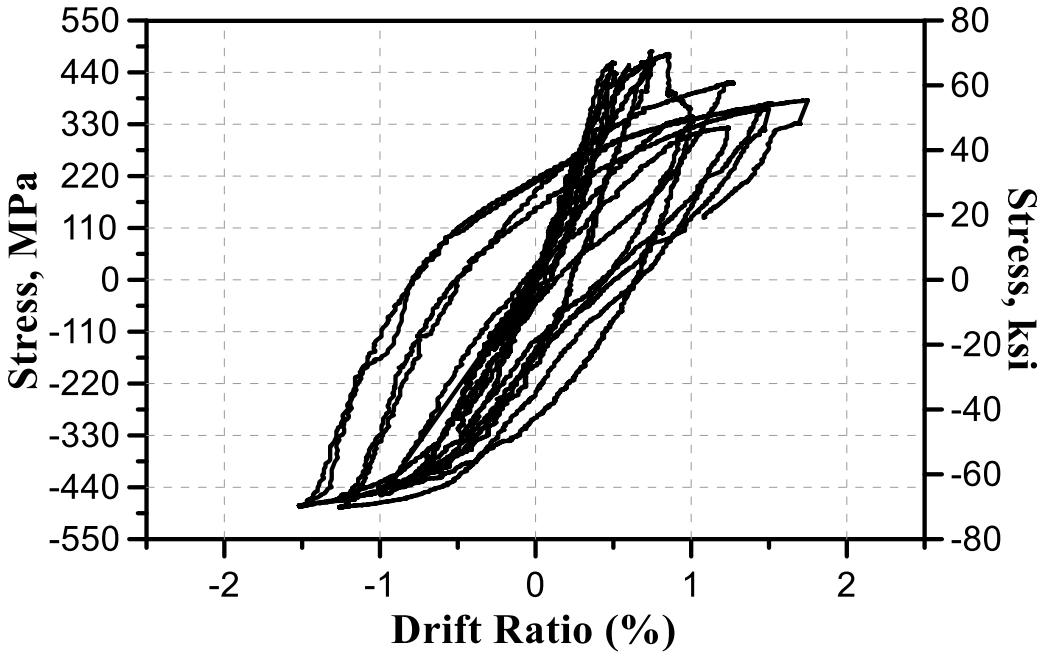

Figure 5-137 Measured stresses of strain gauge (L11) for specimen SW-MP-1.0-1

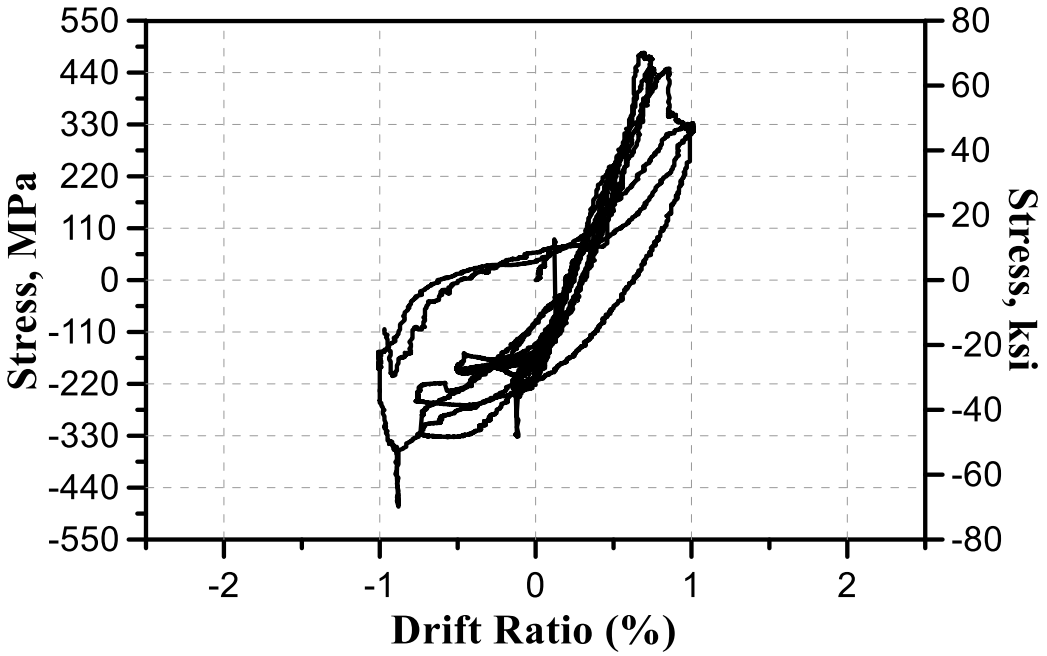

Figure 5-138 Measured stresses of strain gauge (L12) for specimen SW-MP-1.0-1

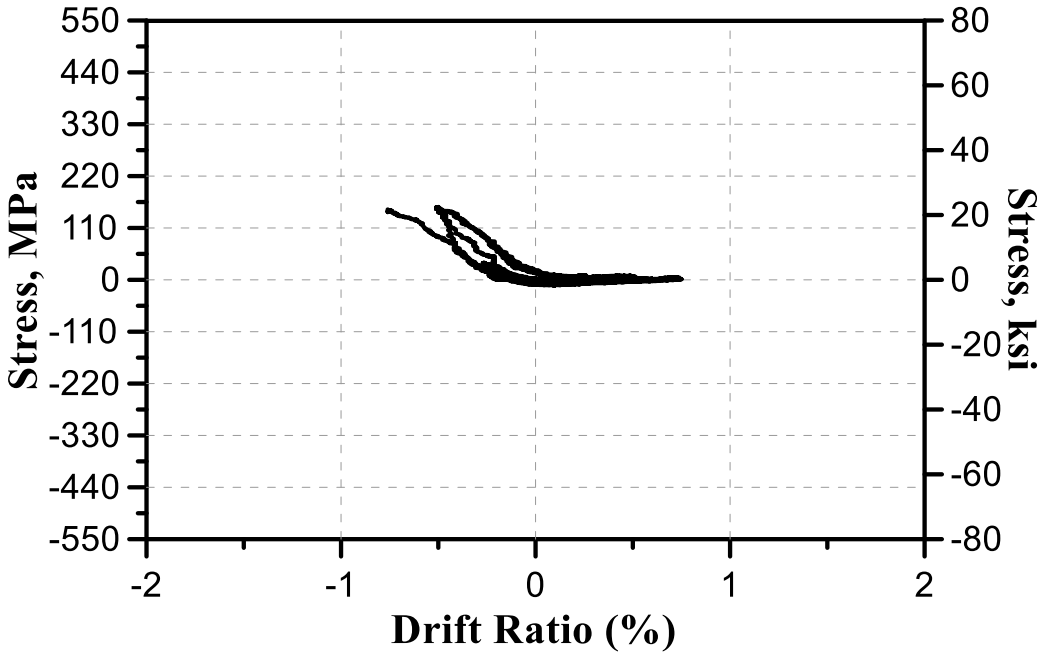

Figure 5-139 Measured stresses of strain gauge (S13) for specimen SW-MP-1.0-1

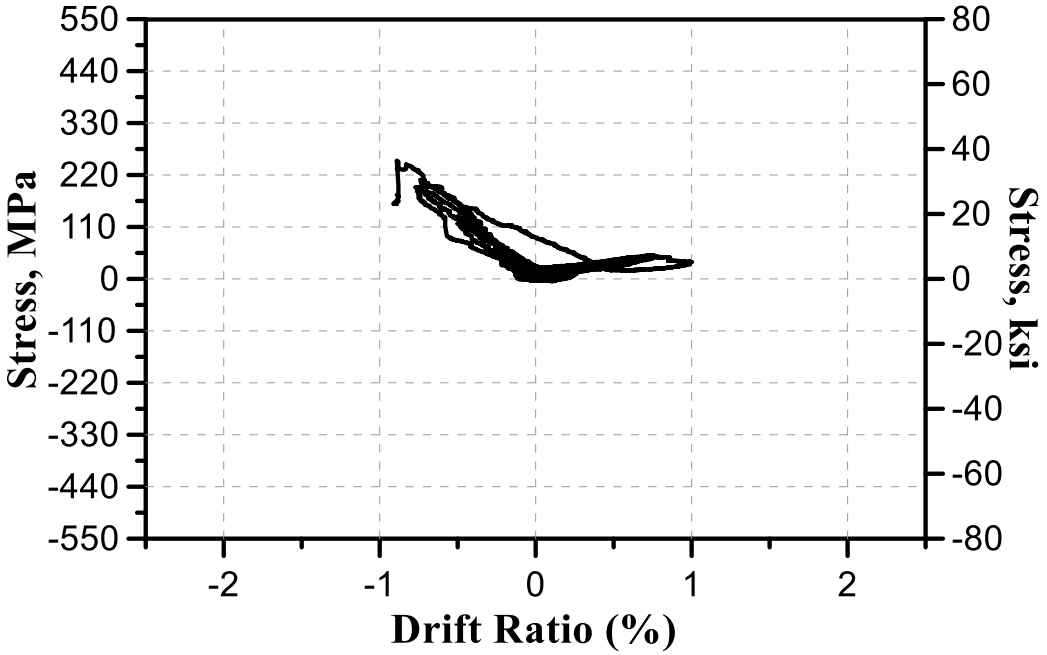

Figure 5-140 Measured stresses of strain gauge (S14) for specimen SW-MP-1.0-1

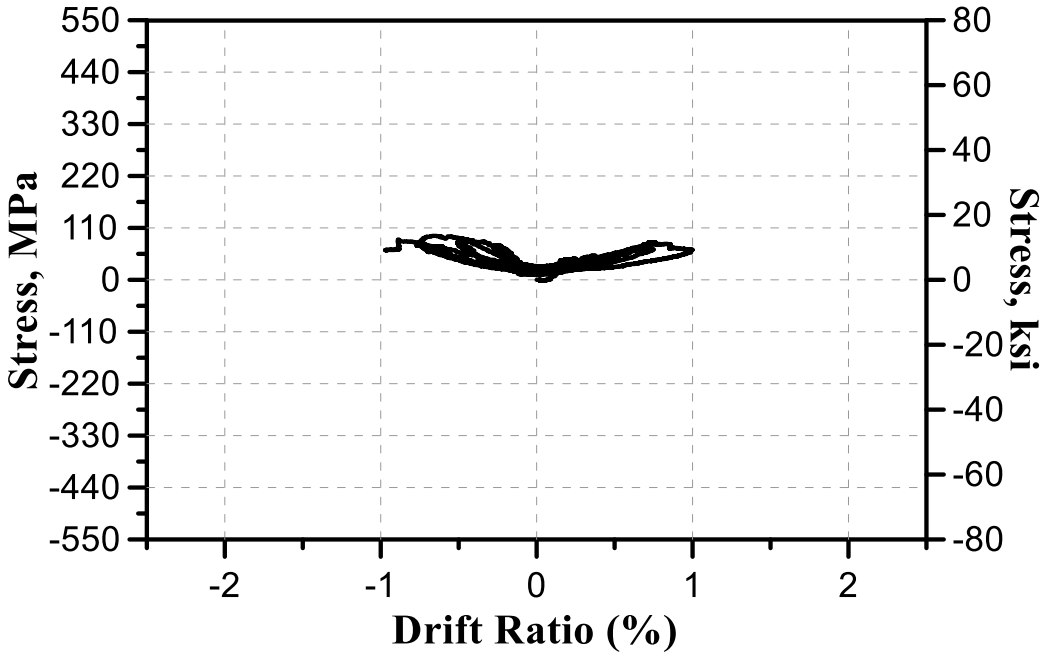

Figure 5-141 Measured stresses of strain gauge (S15) for specimen SW-MP-1.0-1

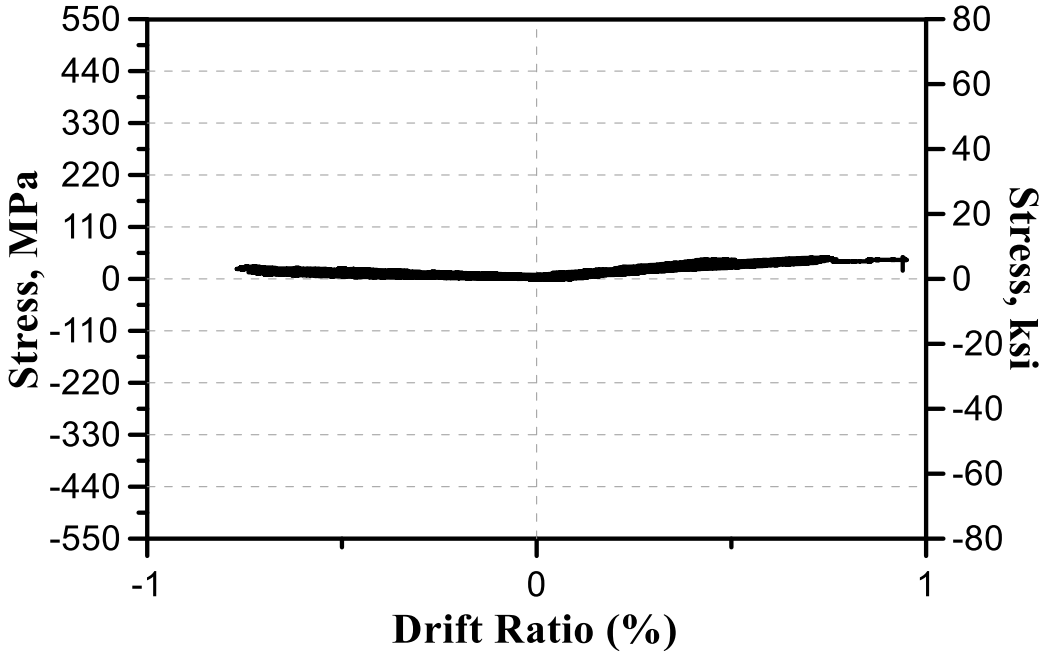

Figure 5-142 Measured stresses of strain gauge (S16) for specimen SW-MP-1.0-1

Chapter 6

DIC Results

6.1. Introduction

The Digital Image Correlation (DIC) technique was utilized to trace the displacement and deformation of the squat walls during the test. In details, one of the smoothest wall faces was painted by white color then uniformly small size dots were sprayed, the final color of wall face should show nearly 50% White and 50% black. Two calibrated cameras used to capture photos of the painted wall face during the test, the rate was a picture per five seconds. The photos were postprocessed later on after the test, where extraction of displacement and strain distribution over the wall face are obtained.

The following sections presents the postprocessed results of DIC pictures, which includes major strain and minor strain distributions for the tested squat wall specimens.

6.2. Specimen SW-MA-0.5

6.2.1. DIC major strain distribution

Cracks development at drift ratio 0.125%, 0.25%, 0.5%, 0.75%, 1%, 1.25%, 1.5% and 1.75% are shown in Figure 6-1 to Figure 6-7. The diagonal red lines refer to the axis of struts developed to transfer shear forces from wall's tip to the base, while the horizontal red lines represent the flexural cracks due to bending stresses. Diagonal struts remained intact until drift ratio +1.25%. Due to insufficient concrete confinement at the web, the struts started crushing at -1.25% and the shear strength suddenly dropped. Although the highest compressive stresses at wall boundaries, struts crushing started at the web as the concrete at wall boundaries are well confined. Afterward, the crushing of

diagonal struts propagated toward wall boundaries to form the sliding plan, therefore sliding shear failure commenced.

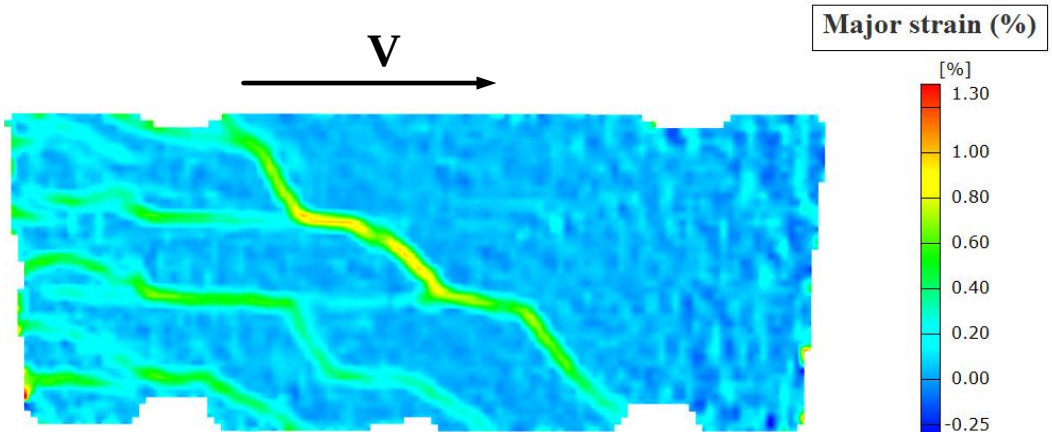

Drift ratio 0.125%

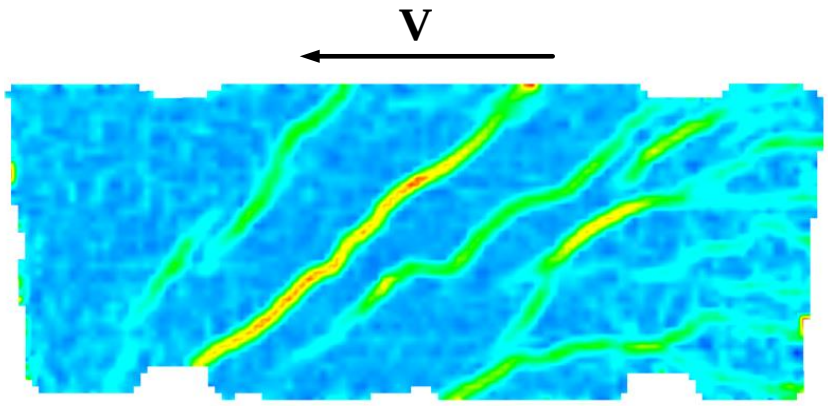

Drift ratio -0.125%

Figure 6-1 DIC major strain results of specimen SW-MA-0.5 at drift ratio 0.125% (positive strain is tension and negative strain is compression)

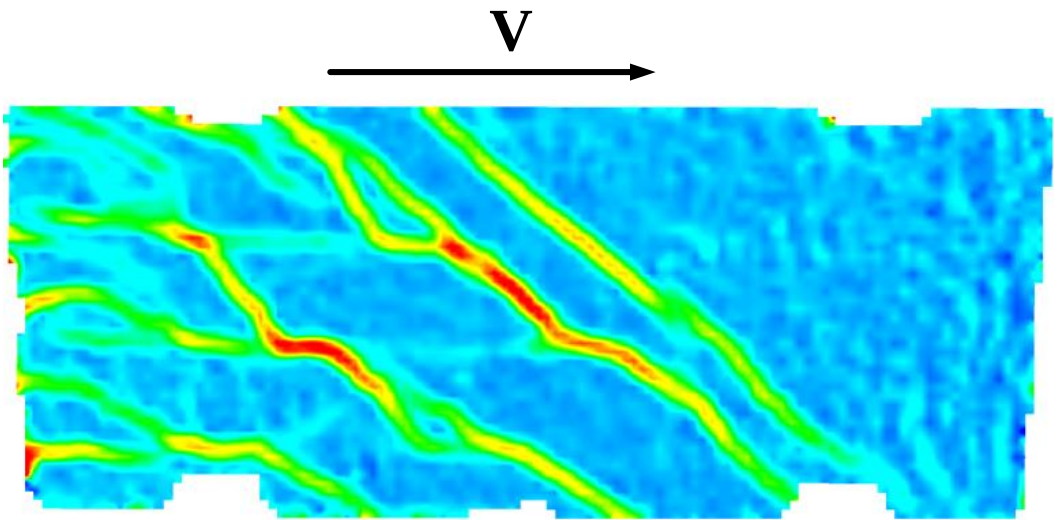

Drift ratio 0.25%

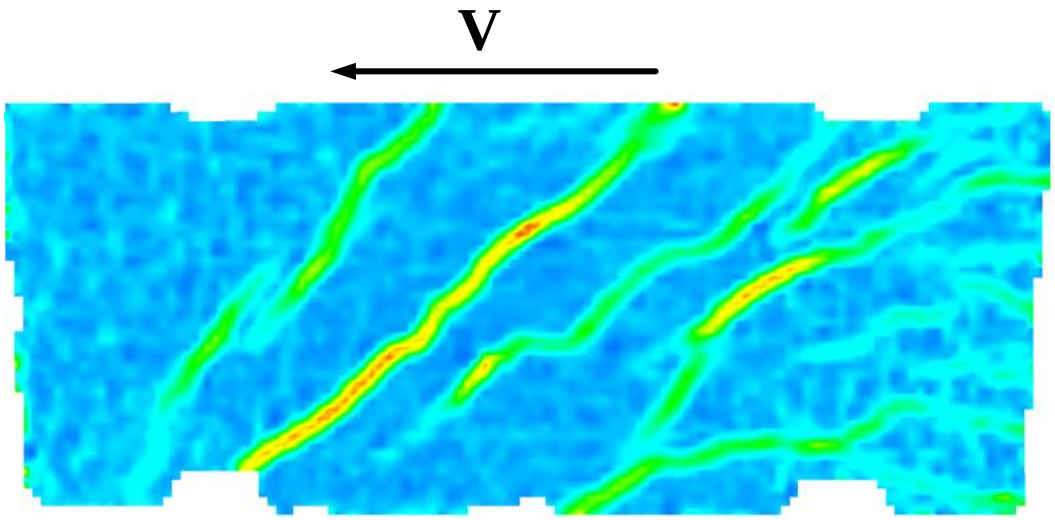

Drift ratio -0.25%

Figure 6-2 DIC major strain results of specimen SW-MA-0.5 at drift ratio 0.25%

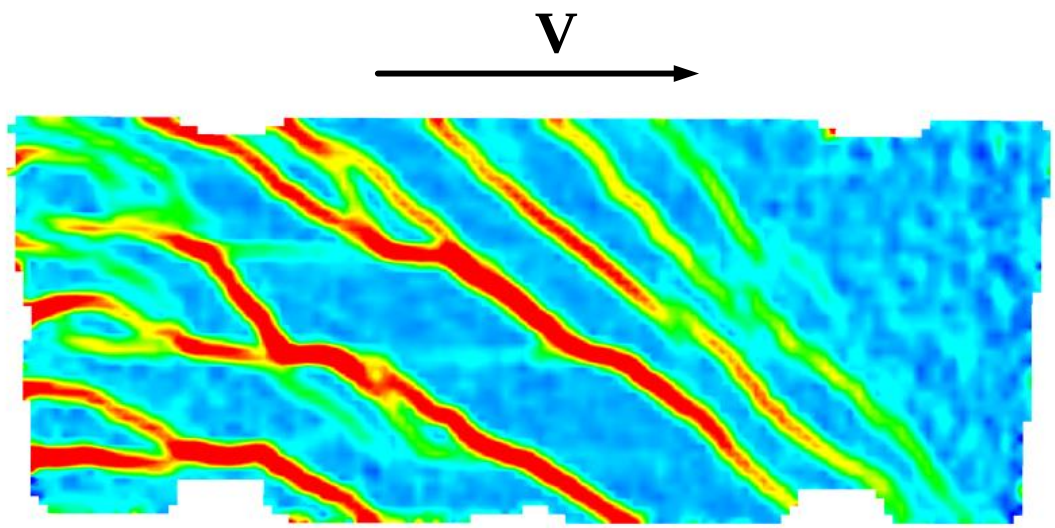

Drift ratio 0.5%

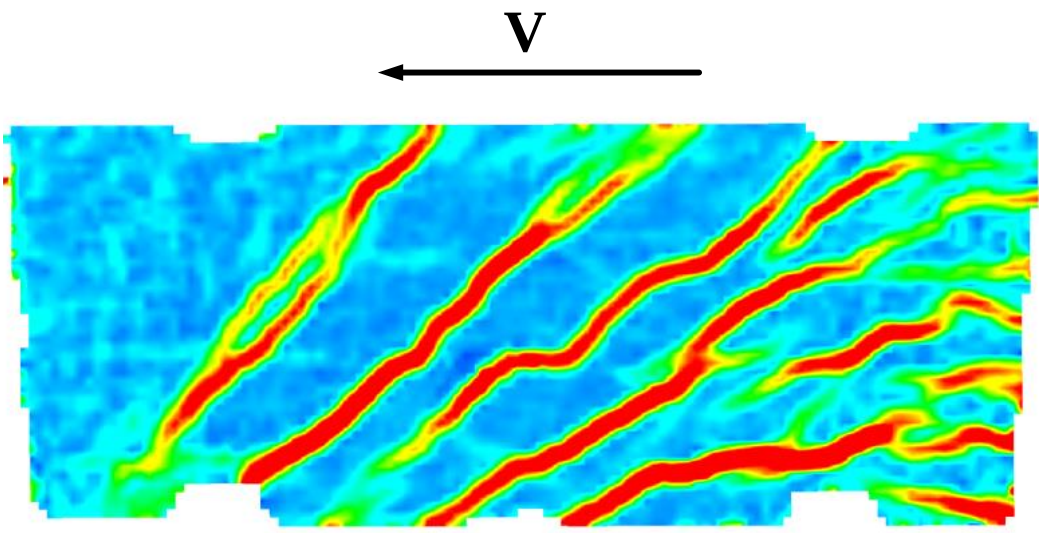

Drift ratio -0.5%

Figure 6-3 DIC major strain results of specimen SW-MA-0.5 at drift ratio 0.5%

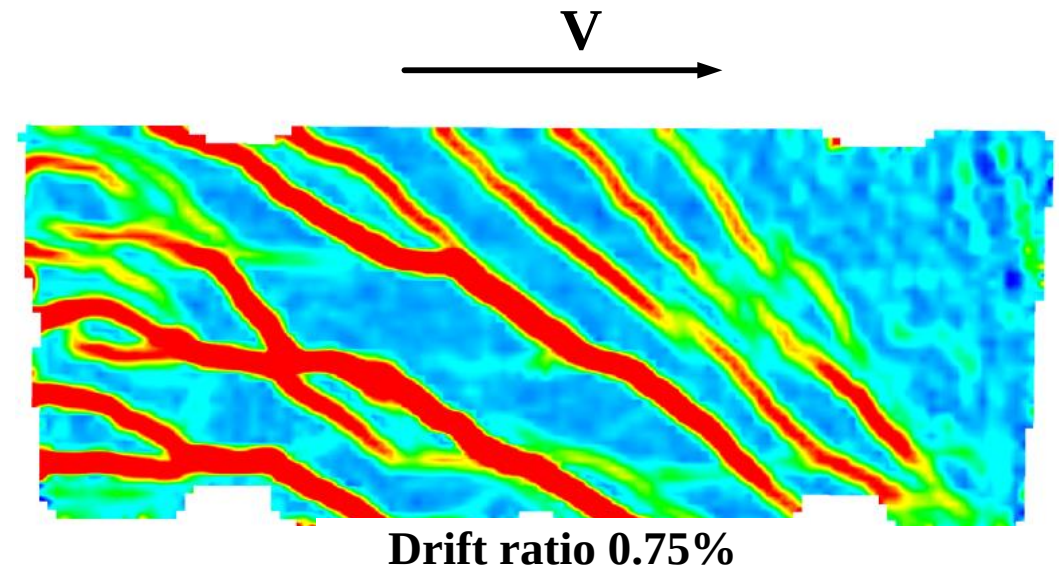

Figure 6-4 DIC major strain results of specimen SW-MA-0.5 at drift ratio 0.75%

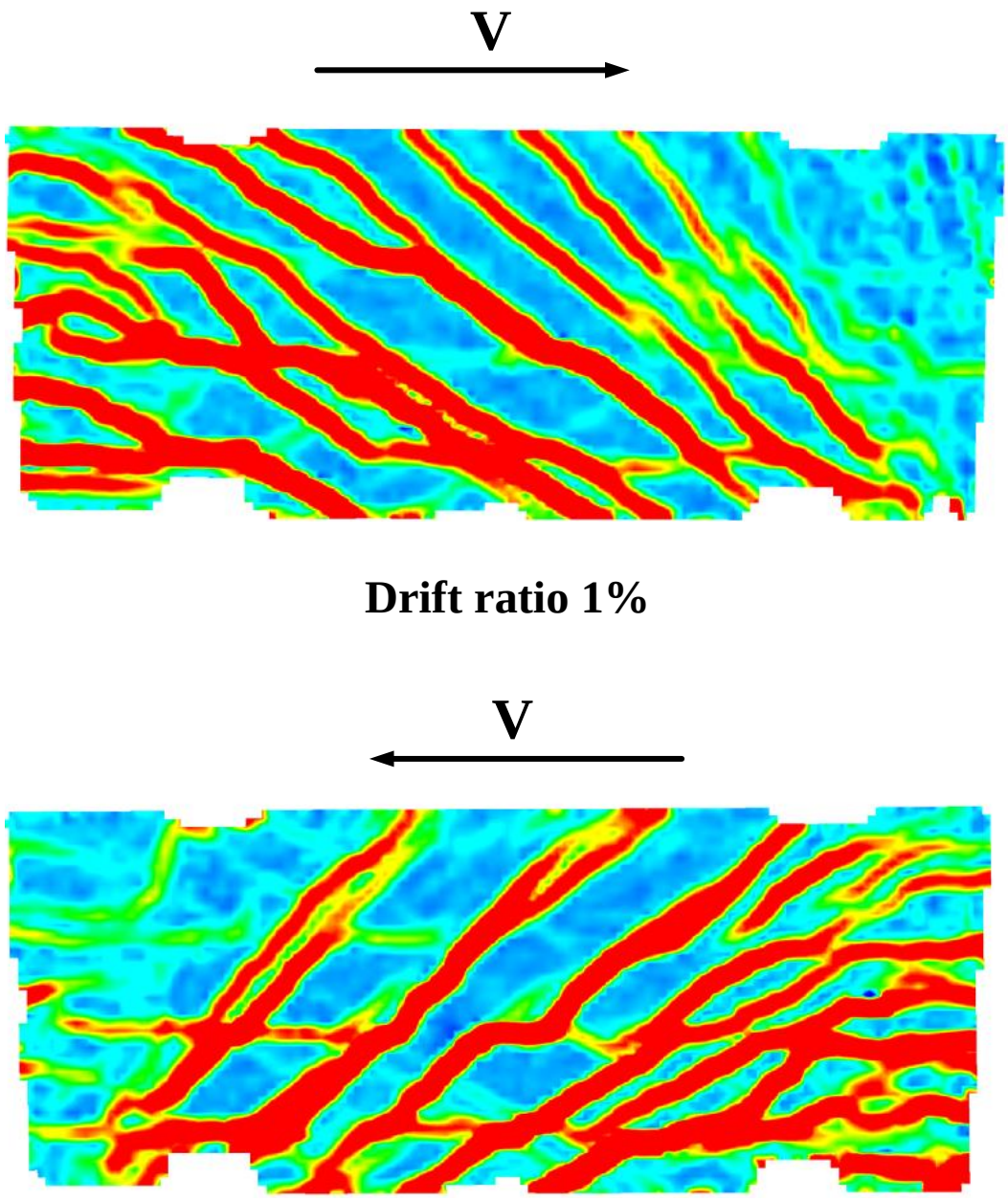

Figure 6-5 DIC major strain results of specimen SW-MA-0.5 at drift ratio 1%

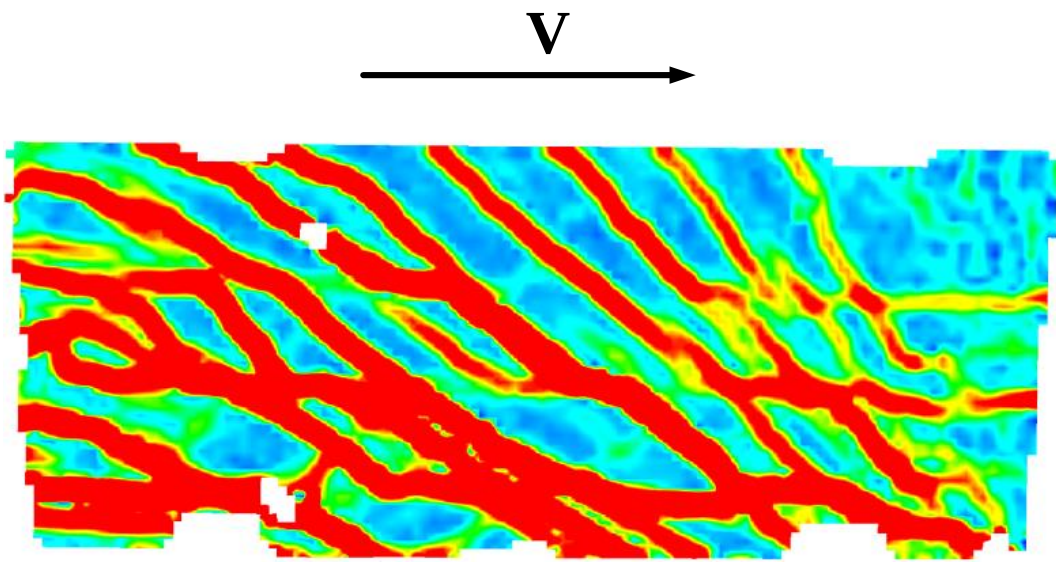

Drift ratio 1.25%

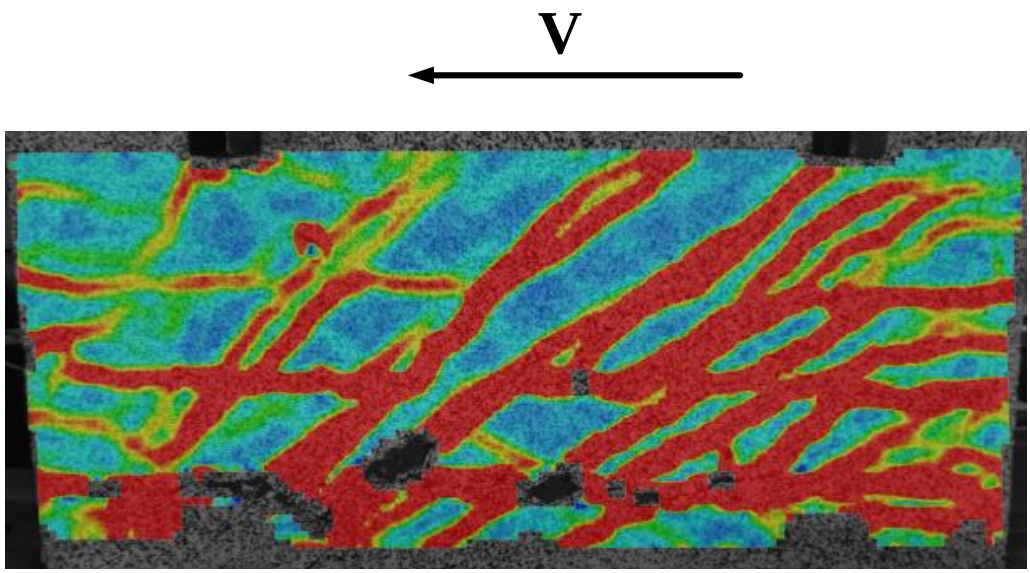

Drift ratio -1.25%

Figure 6-6 DIC major strain results of specimen SW-MA-0.5 at drift ratio 1.25%

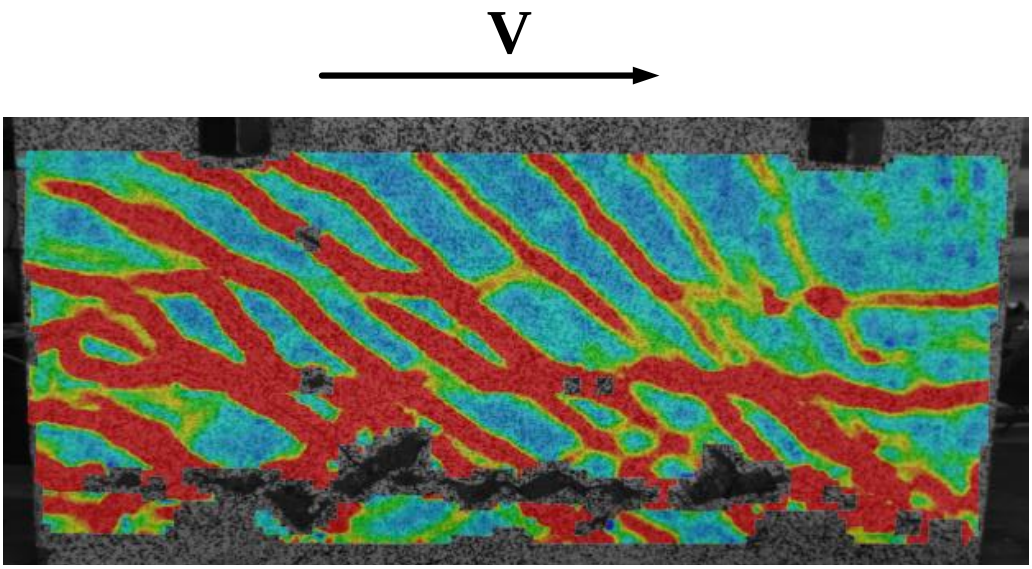

Drift ratio 1.5%

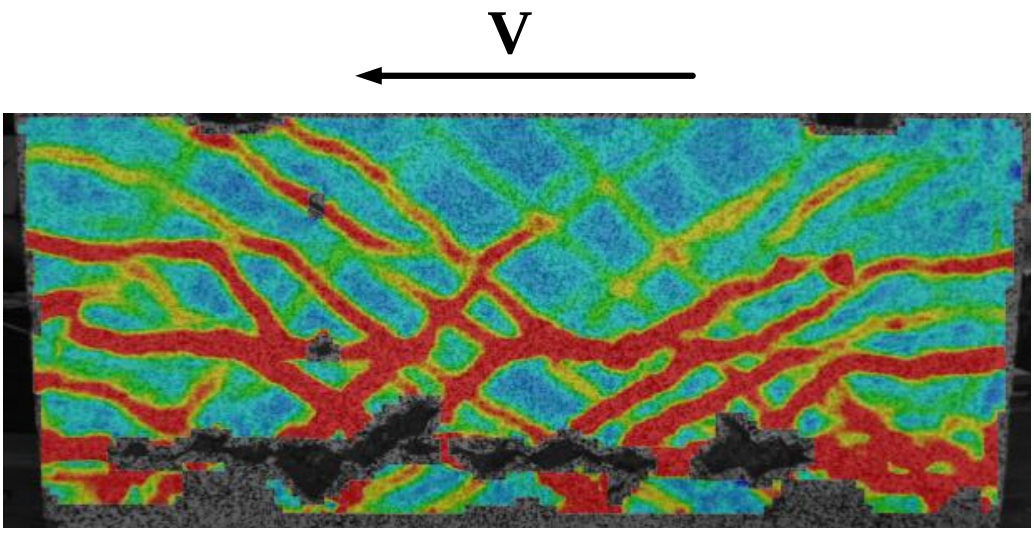

Drift ratio -1.5%

Figure 6-7 DIC major strain results of specimen SW-MA-0.5 at drift ratio 1.5%

6.2.2. DIC minor strain distribution

Cracks development at drift ratio 0.125%, 0.25%, 0.5%, 0.75%, 1%, and 1.25% are shown in Figure 6-8 to Figure 6-10. The diagonal blue lines refer to the axis of struts developed to transfer shear forces from wall's tip to the base. Diagonal struts remained intact until drift ratio 1.25%. All strain distributions have same legend values that shown at Drift ratio 0.125%.

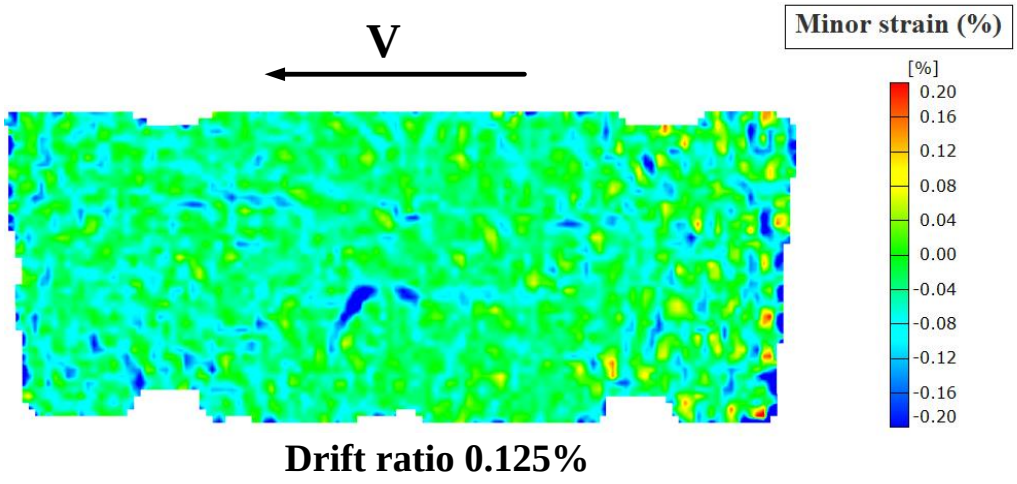

Figure 6-8 DIC minor strain results of specimen SW-MA-0.5 at drift ratio 0.125% and 0.25% (positive strain is tension and negative strain is compression)

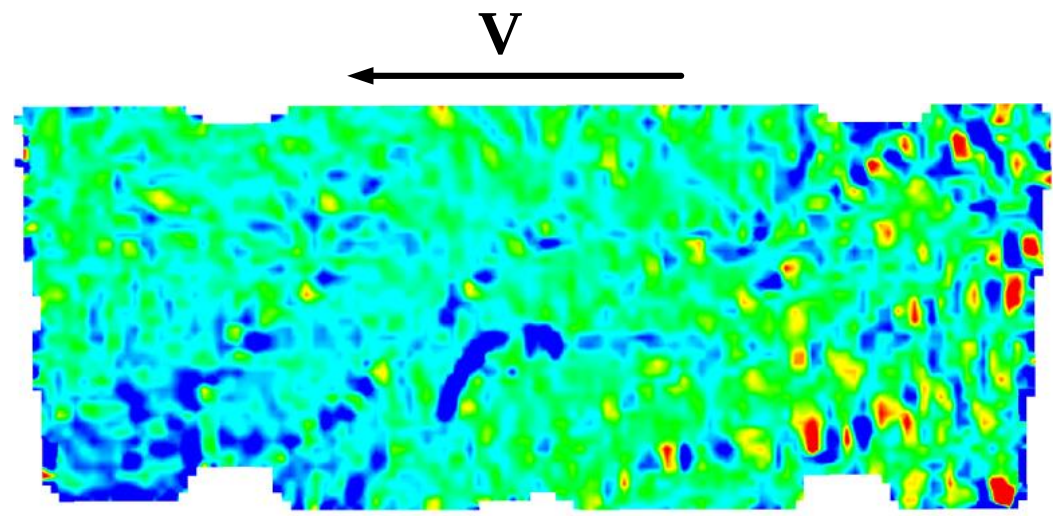

Drift ratio 0.5%

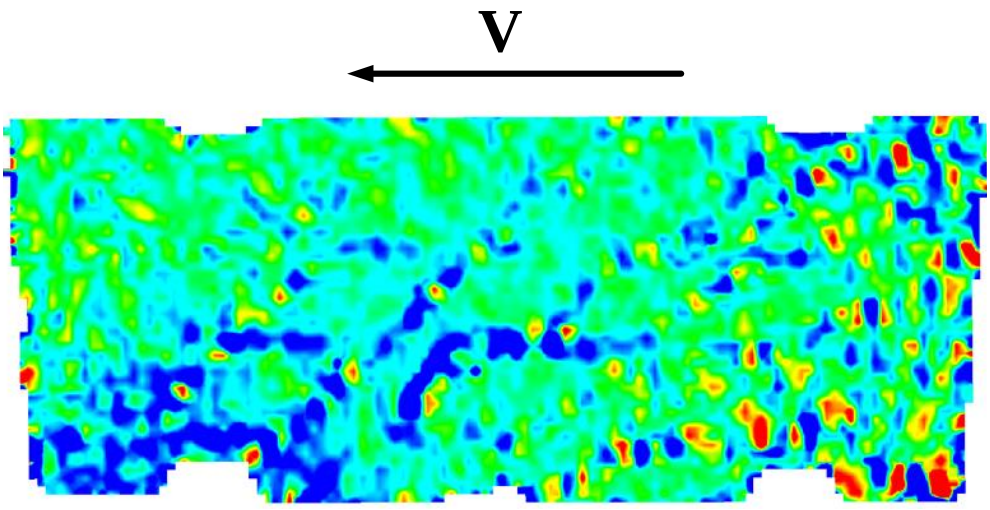

Drift ratio 0.75%

Figure 6-9 DIC minor strain results of specimen SW-MA-0.5 at drift ratio 0.5% and 0.75%

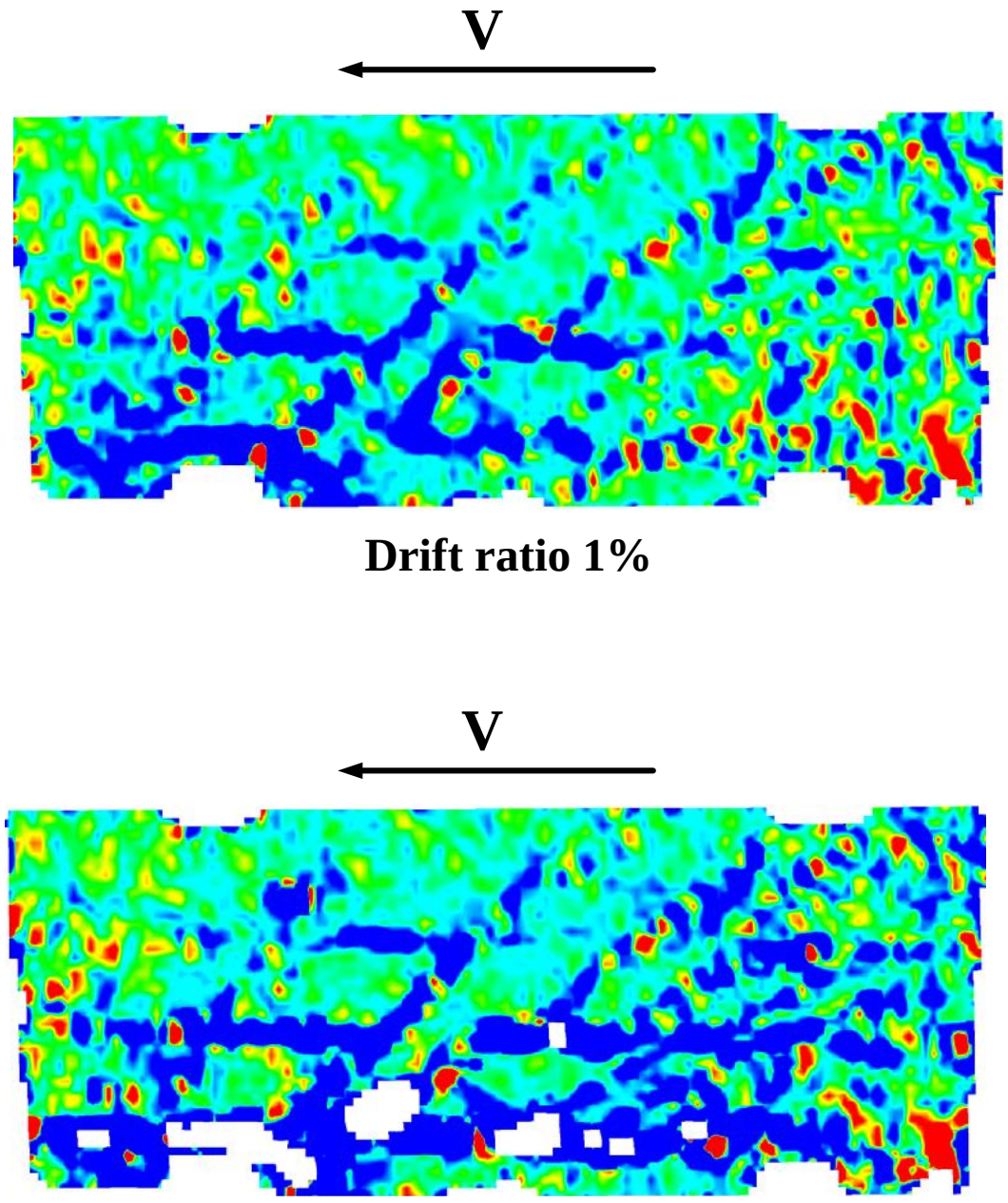

Figure 6-10 DIC minor strain results of specimen SW-MA-0.5 at drift ratio 1% and 1.25%

6.3 SW-MP-0.5

6.3.1 DIC major strain distribution

Cracks development at drift ratio 0.125%, 0.25%, 0.5%, 0.75%, 1%, 1.25%, 1.5% and 1.75% are shown in

Figure 6-11 to Figure 6-18. The diagonal red lines refer to the axis of struts developed to transfer shear forces from wall's tip to the base, while the horizontal red lines represent the flexural cracks due to bending stresses. Although diagonal struts remained undamaged until drift ratio 1.5%, shear strength gradually decreased after drift ratio 2.5% which equals as twice as what attained by ACI- compliant wall (SW-MA-0.5), and emphasis the ductile behavior of the proposed wall. The highest compressive stresses are located at wall boundaries due to compressive bending stresses and diagonal compressive struts. Due to reversed cyclic loading, the wall boundaries are vulnerable to the highest compressive and flexural stresses which weaken concrete at boundaries, thereby weakening zones at boundaries arise after drift ratio 1.5%, but this zone does not effect on shear strength where it remained plateaued until drift ratio 2.5%. All strain distributions have same legend values that shown at Drift ratio 0.125%.

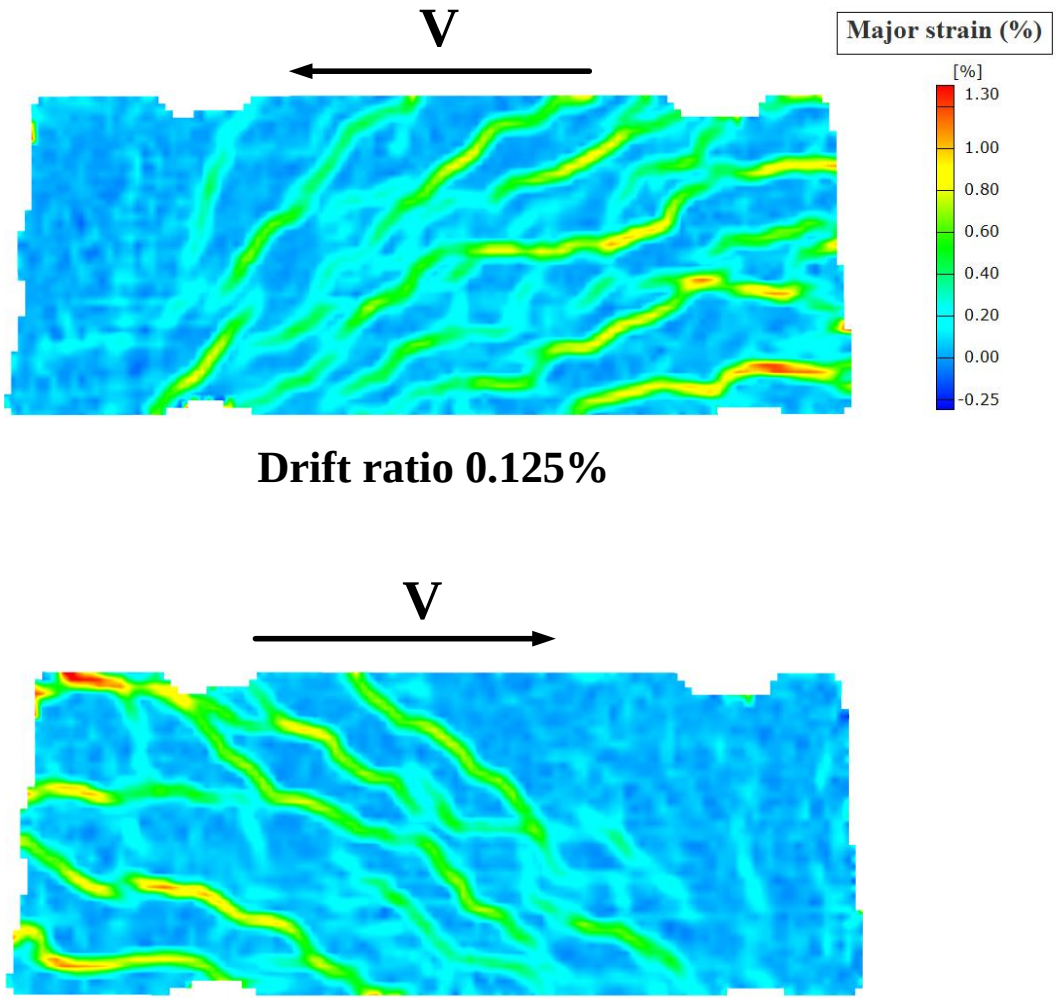

Figure 6-11 DIC major strain results of specimen SW-MP-0.5 at drift ratio 0.125%

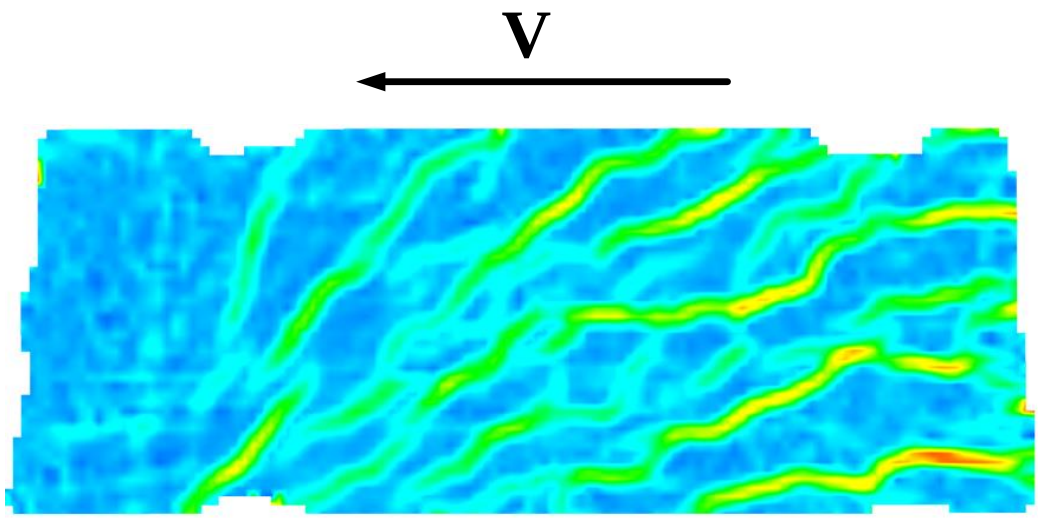

Drift ratio 0.25%

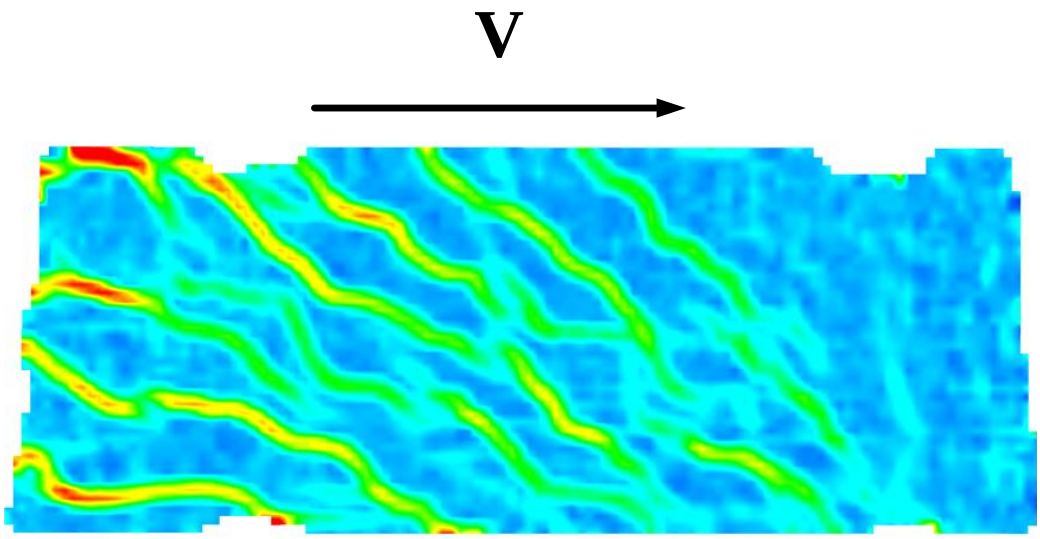

Drift ratio -0.25%

Figure 6-12 DIC major strain results of specimen SW-MP-0.5 at drift ratio 0.25%

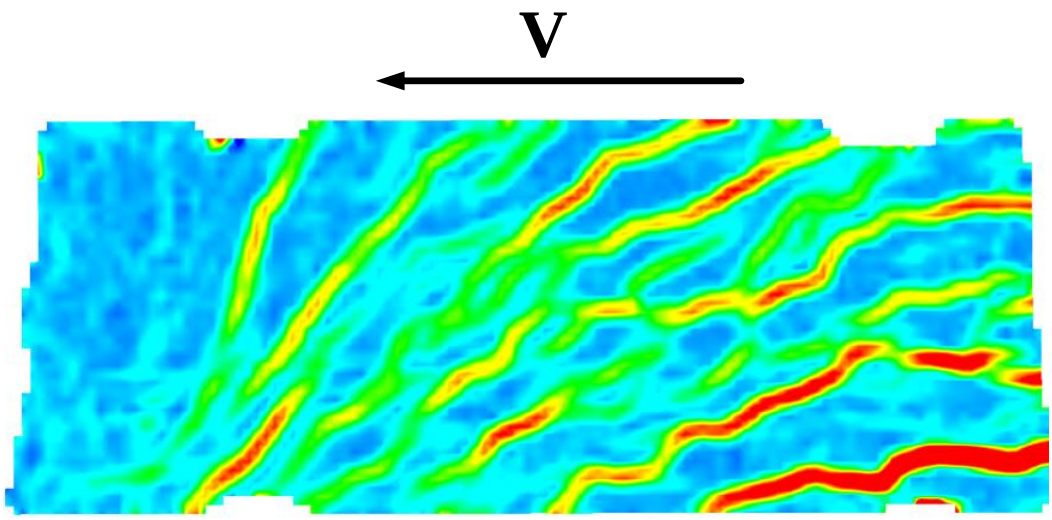

Drift ratio 0.5%

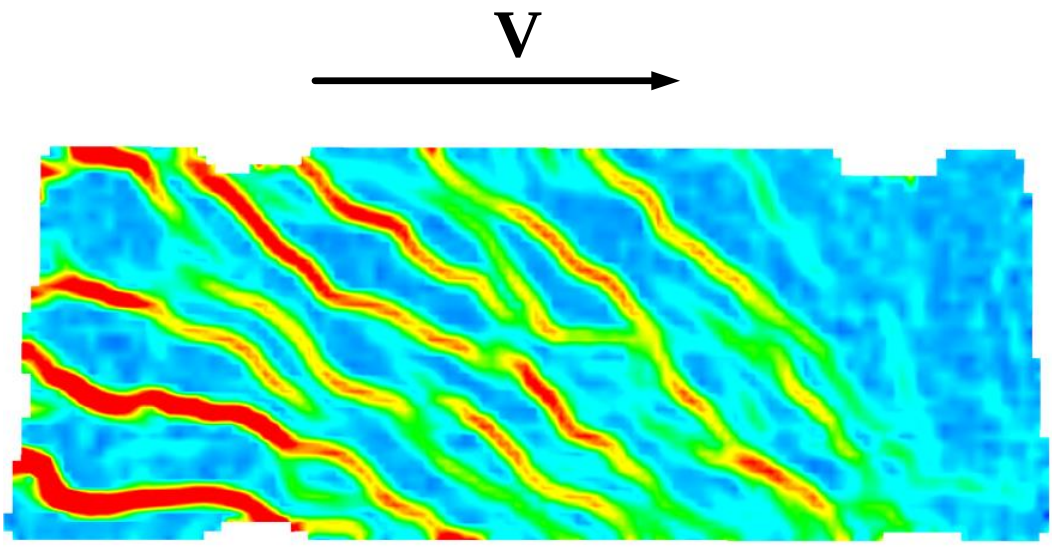

Drift ratio -0.5%

Figure 6-13 DIC major strain results of specimen SW-MP-0.5 at drift ratio 0.5%

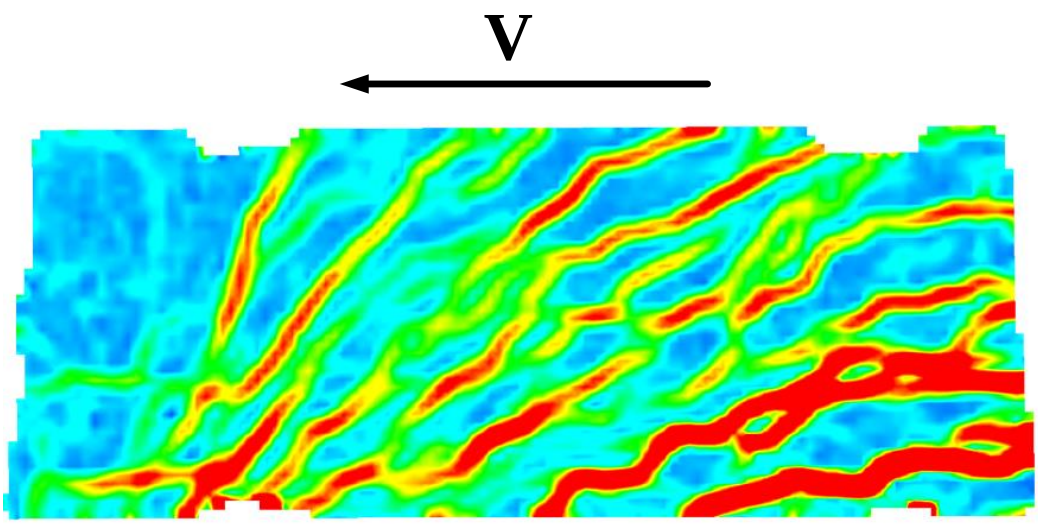

Drift ratio 0.75%

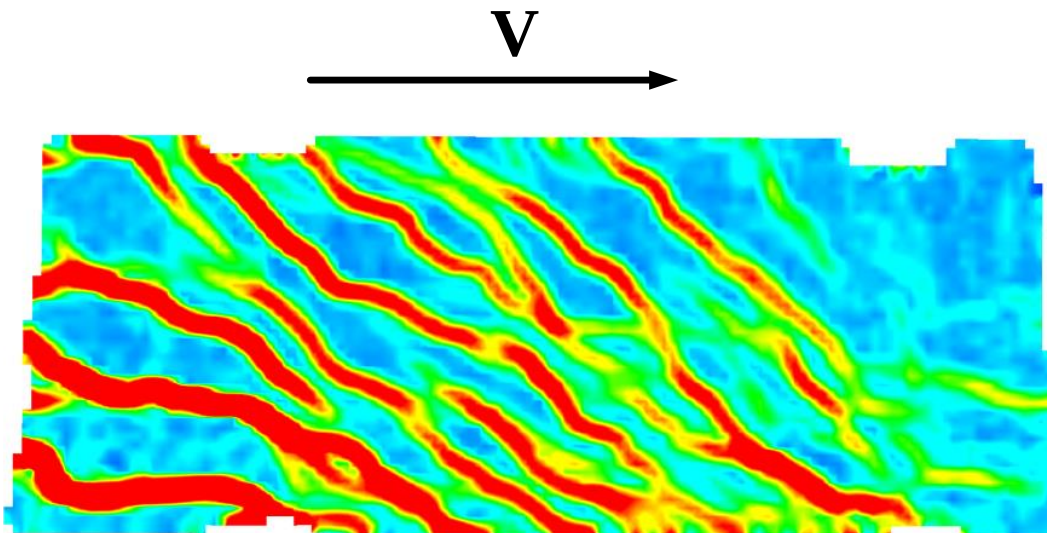

Drift ratio -0.75%

Figure 6-14 DIC major strain results of specimen SW-MP-0.5 at drift ratio 0.75%

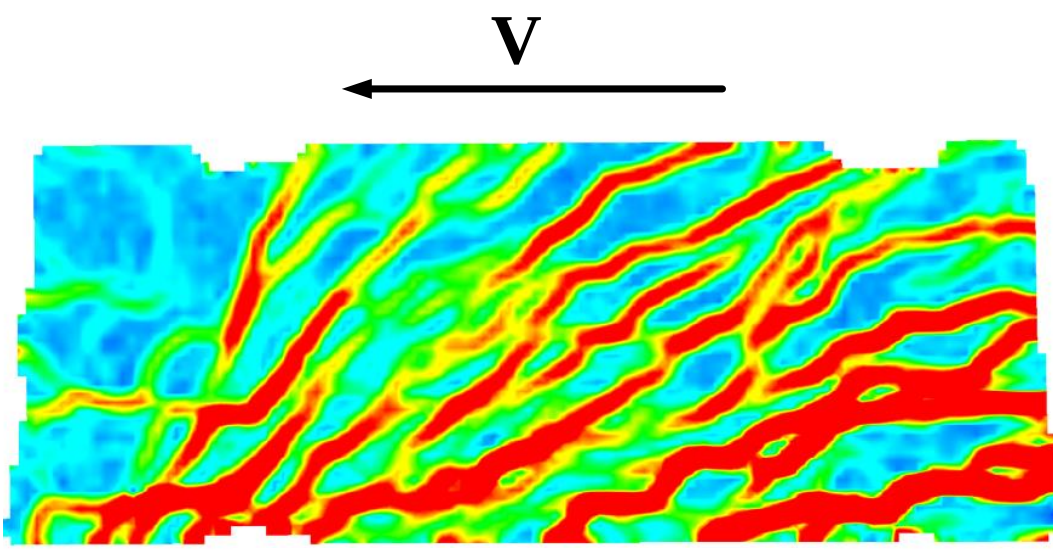

Drift ratio 1%

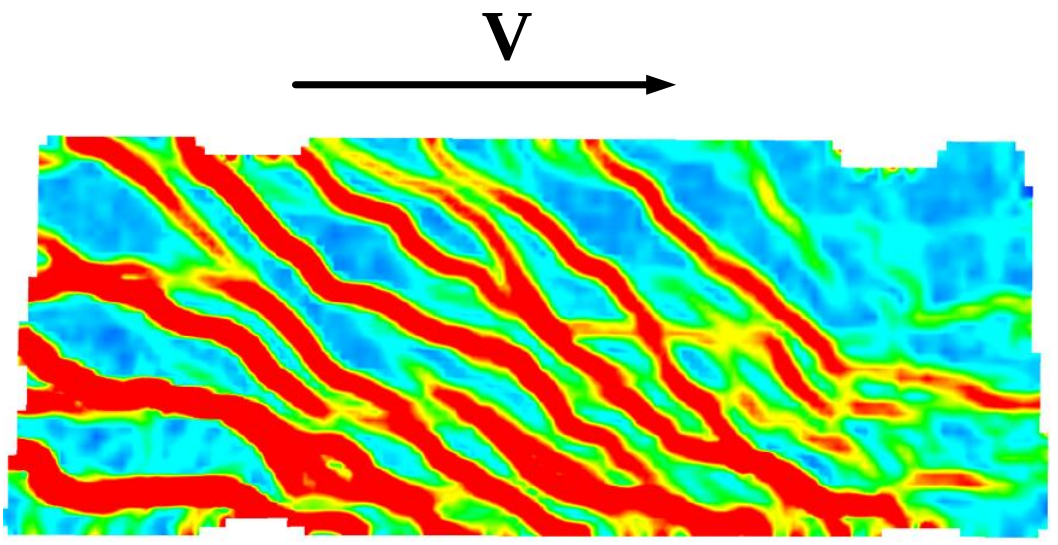

Drift ratio -1%

Figure 6-15 DIC major strain results of specimen SW-MP-0.5 at drift ratio 1%

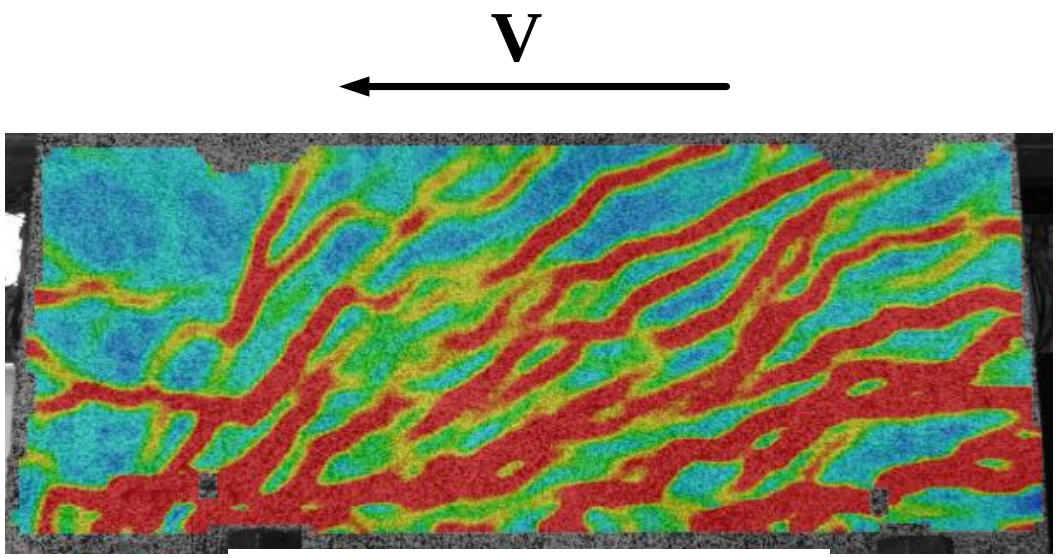

Drift ratio 1.25%

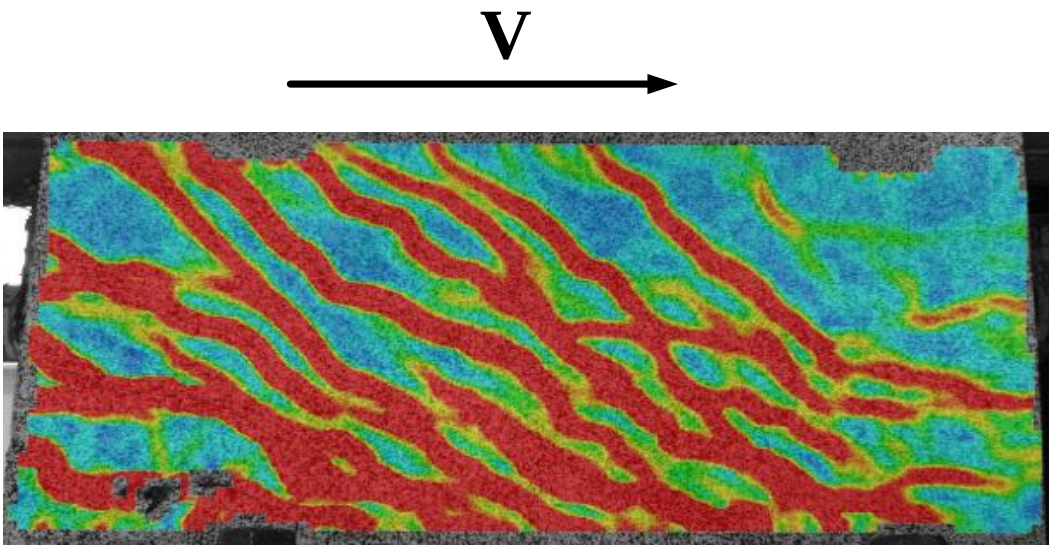

Drift ratio -1.25%

Figure 6-16 DIC major strain results of specimen SW-MP-0.5 at drift ratio 1.25%

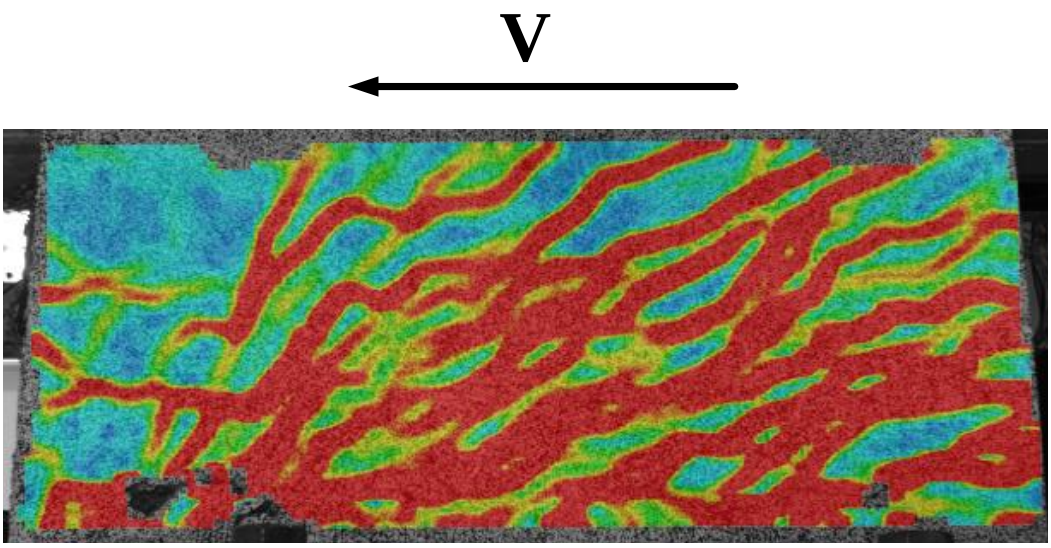

Drift ratio 1.5%

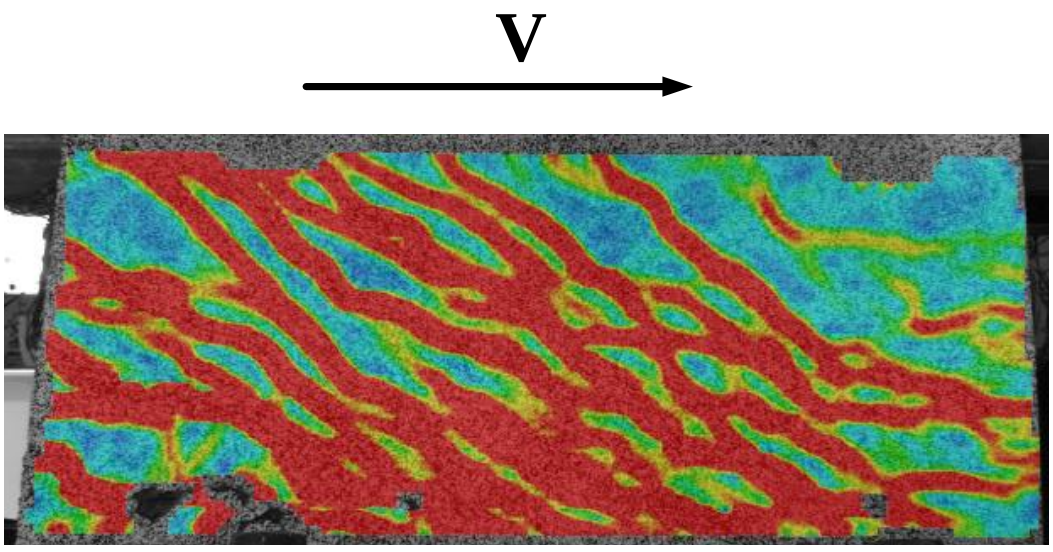

Drift ratio -1.5%

Figure 6-17 DIC major strain results of specimen SW-MP-0.5 at drift ratio 1.5%

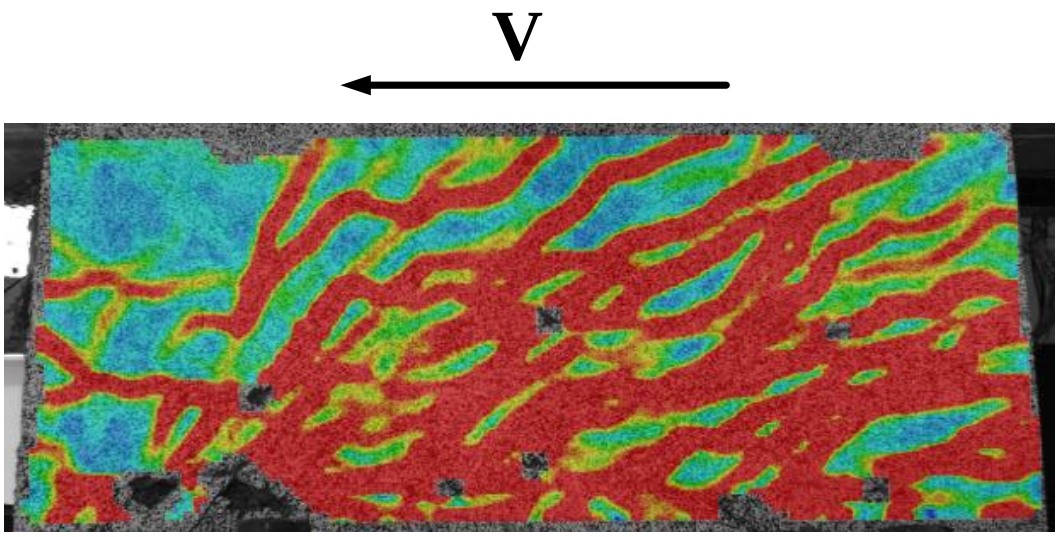

Drift ratio 1.75%

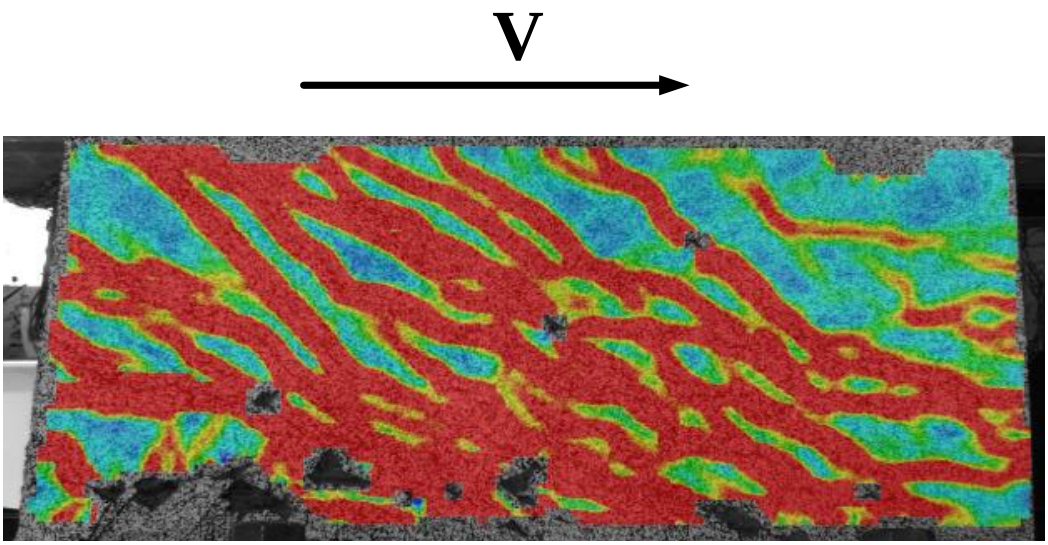

Drift ratio -1.75%

Figure 6-18 DIC major strain results of specimen SW-MP-0.5 at drift ratio 1.75%

6.3.2 DIC minor strain distribution

Cracks development at drift ratio 0.125%, 0.25%, 0.5%, 0.75%, 1%, and 1.25% are shown in

Figure 6-19 to Figure 6-26. The diagonal blue lines refer to the axis of struts developed to transfer shear forces from wall's tip to the base. Diagonal struts remained undamaged until drift ratio 1.5%. Spalling of concrete cover started at 1.75% which prevents the DIC to capture the deformation of black dots on the wall face. All strain distributions have same legend values that shown at Drift ratio 0.125%.

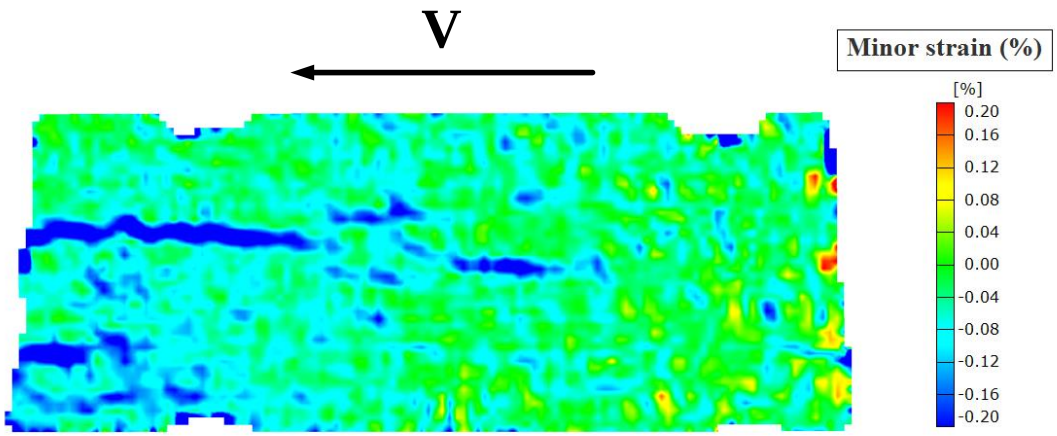

Drift ratio 0.125%

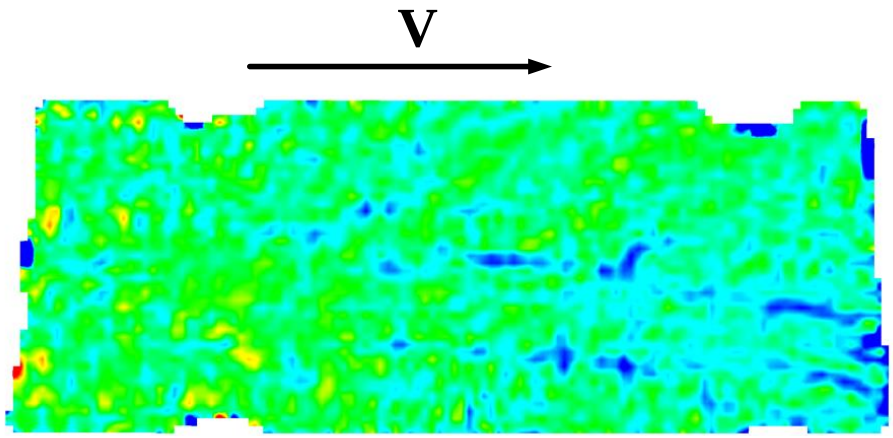

Drift ratio -0.125%

Figure 6-19 DIC minor strain results of specimen SW-MP-0.5 at drift ratio 0.125%

(positive strain is tension and negative strain is compression)

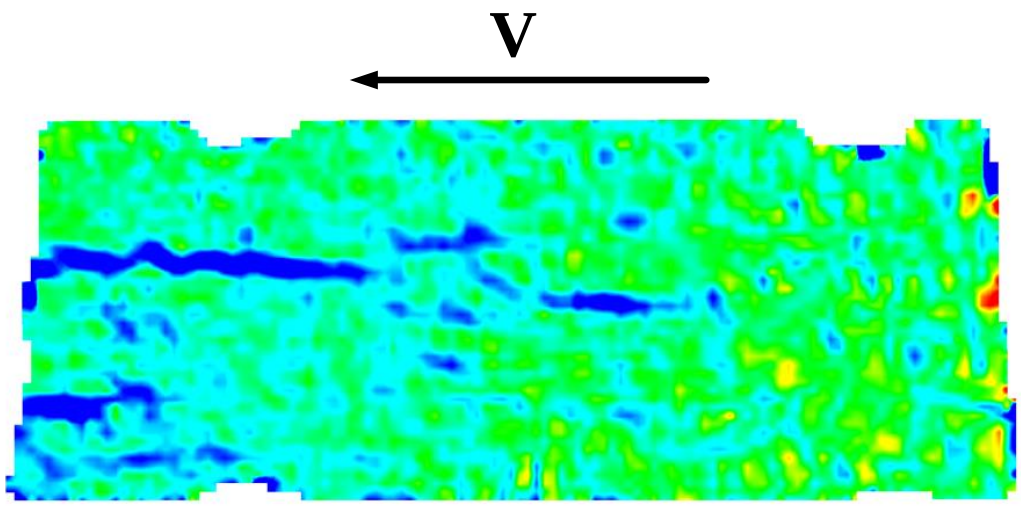

Drift ratio 0.25%

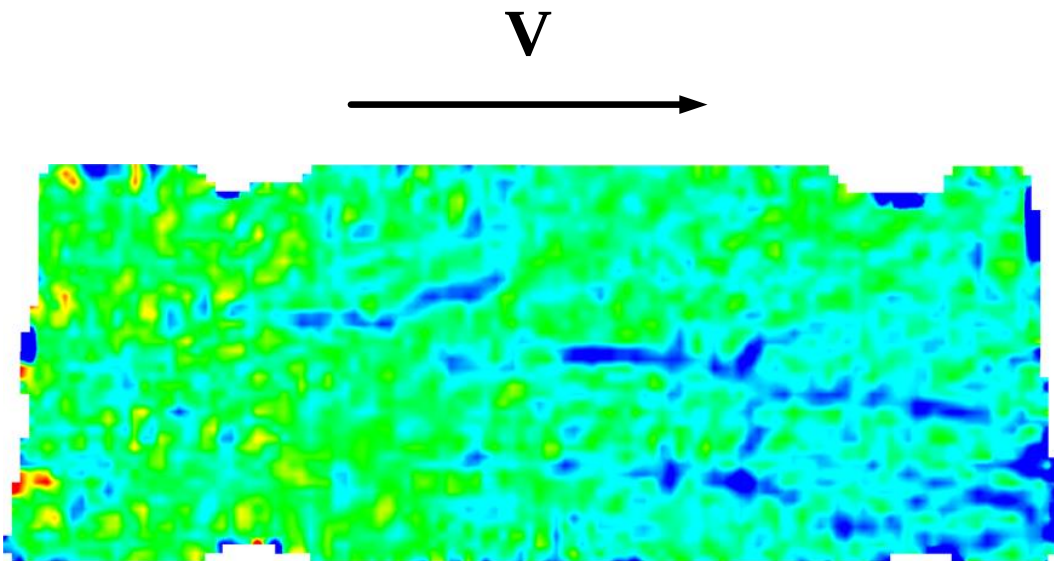

Drift ratio -0.25%

Figure 6-20 DIC minor strain results of specimen SW-MP-0.5 at drift ratio 0.25%

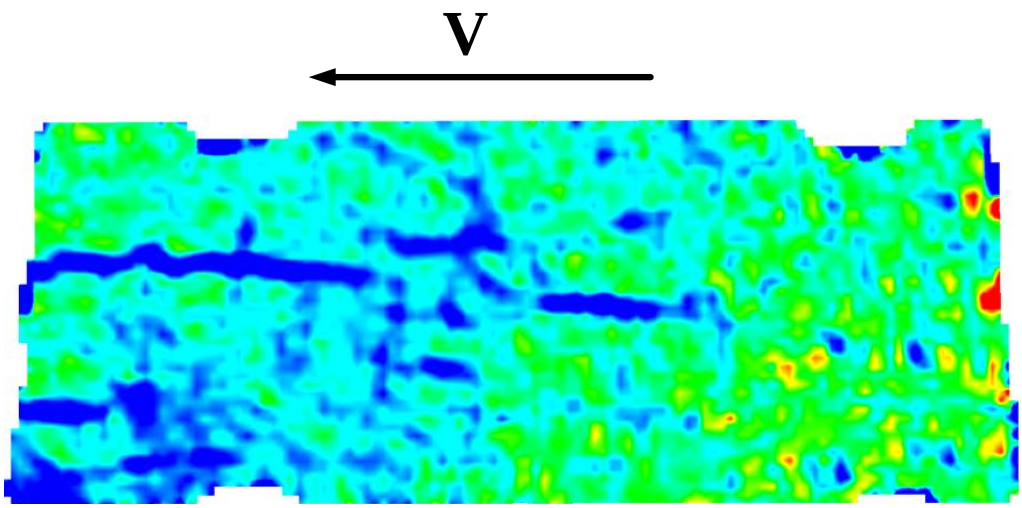

Drift ratio 0.5%

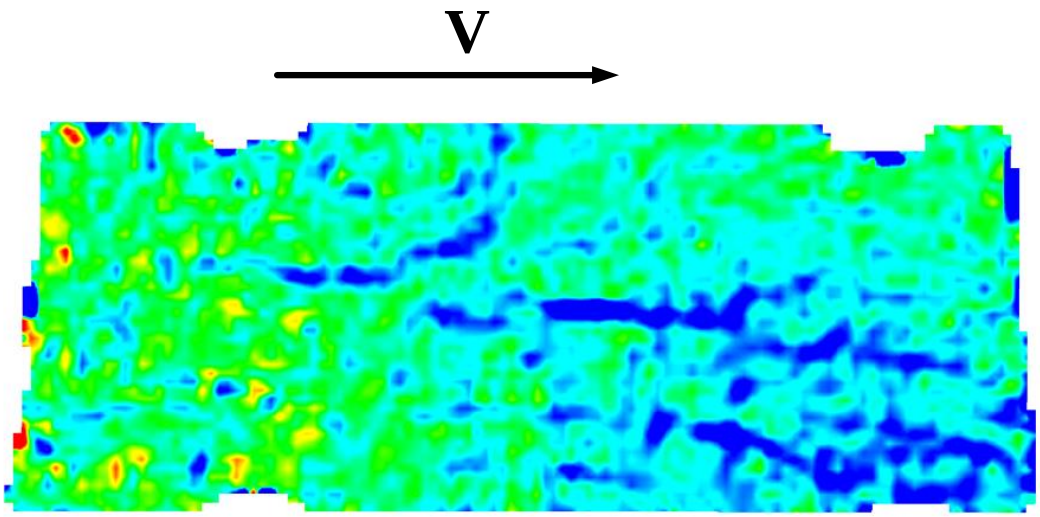

Drift ratio -0.5%

Figure 6-21 DIC minor strain results of specimen SW-MP-0.5 at drift ratio 0.5%

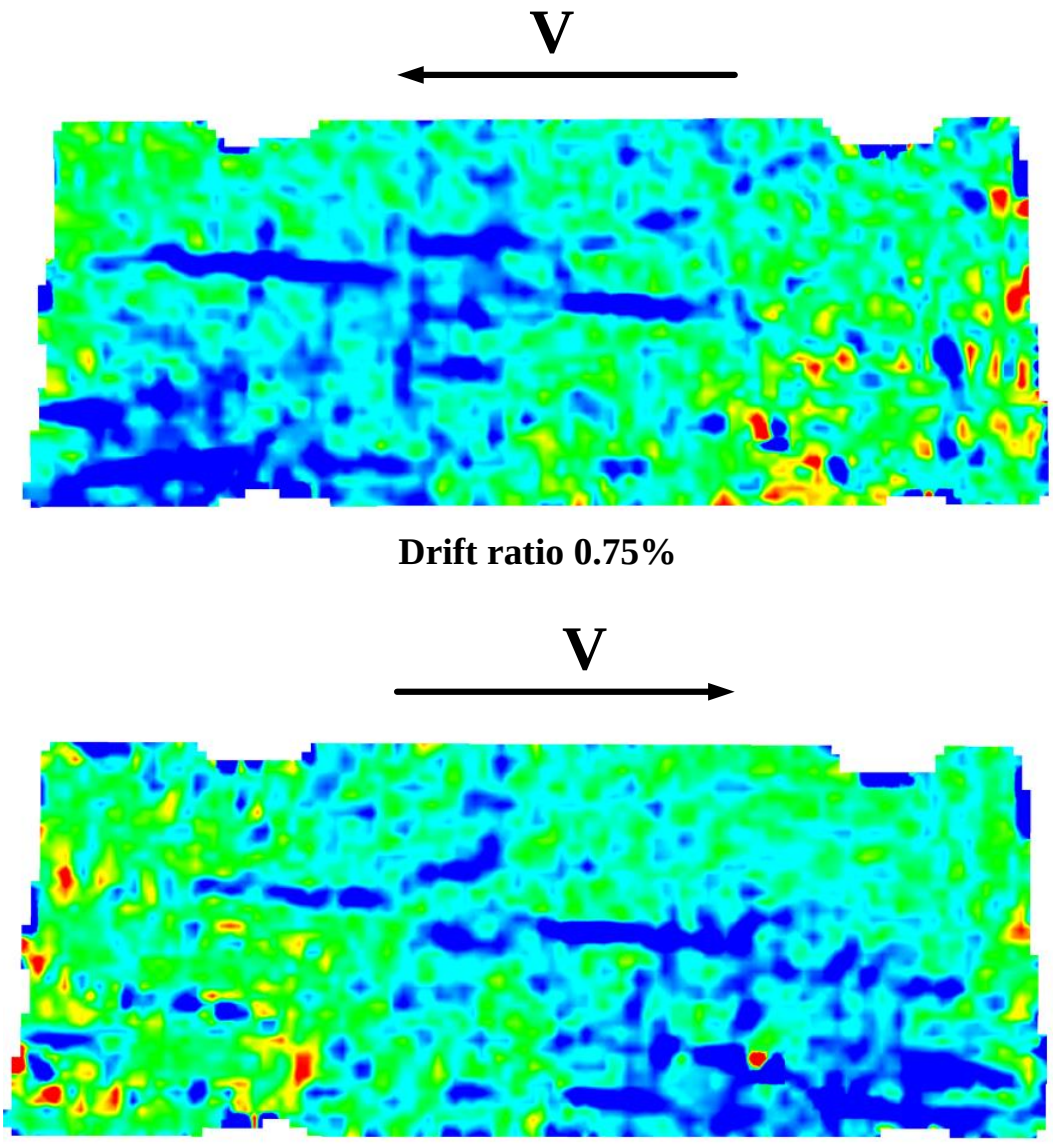

Figure 6-22 DIC minor strain results of specimen SW-MP-0.5 at drift ratio 0.75%

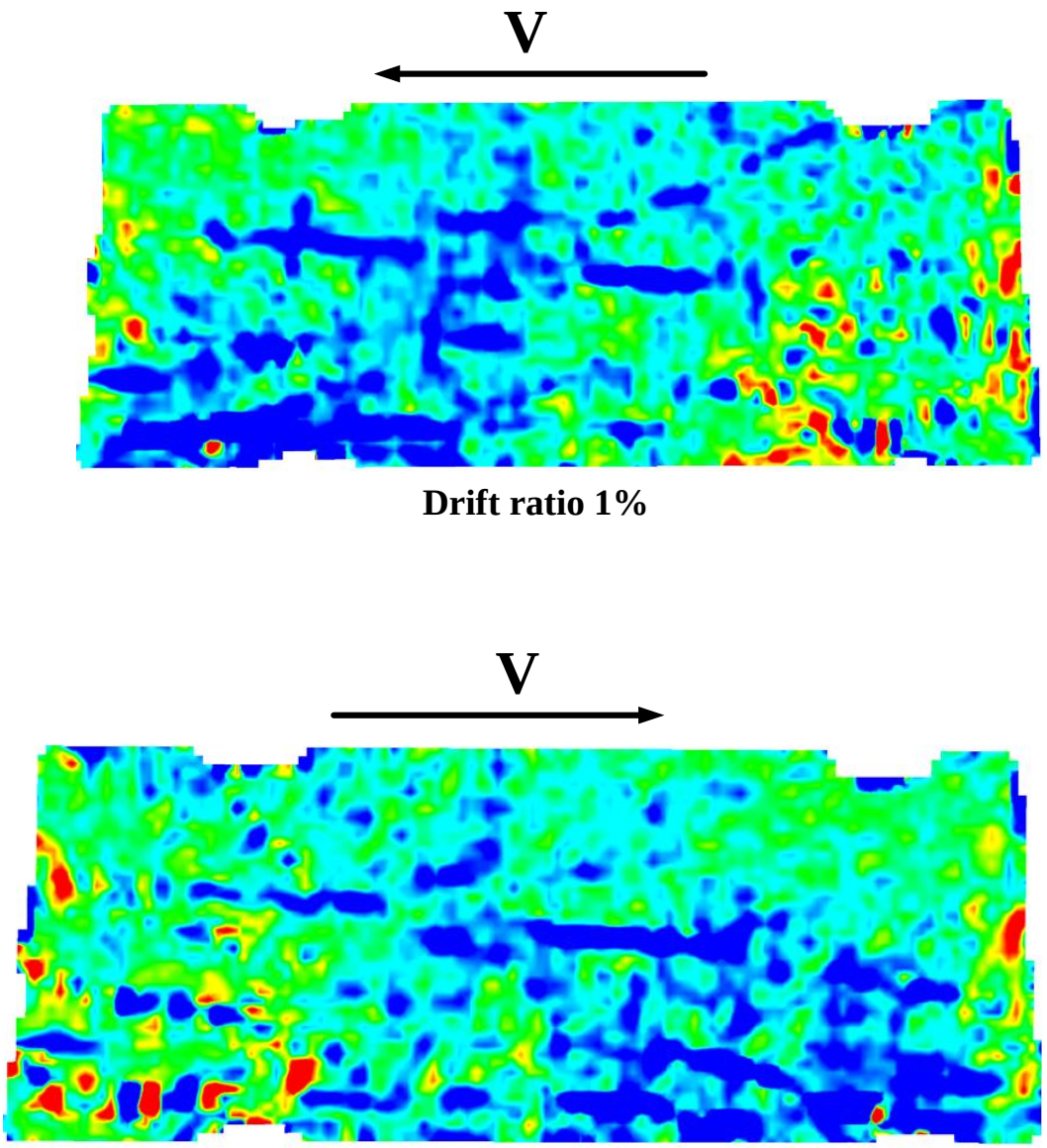

Figure 6-23 DIC minor strain results of specimen SW-MP-0.5 at drift ratio 1%

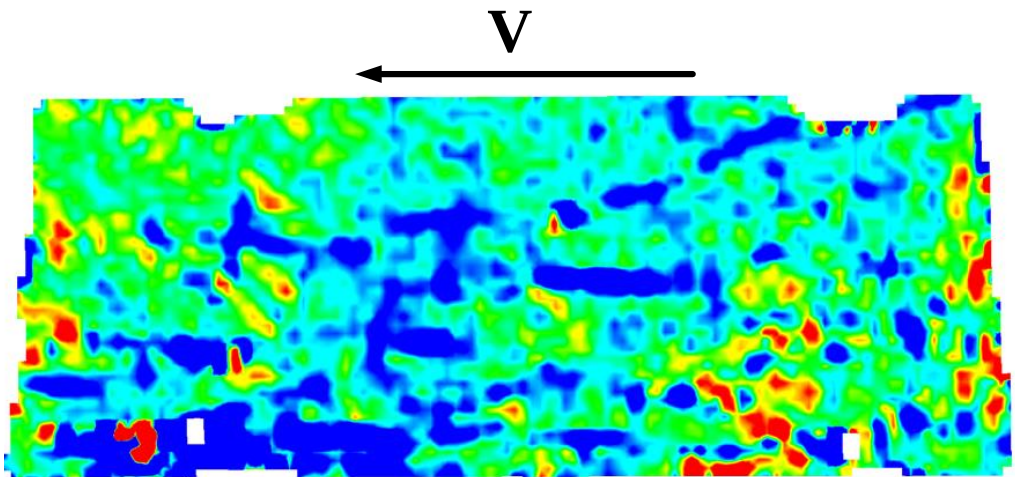

Drift ratio 1.25%

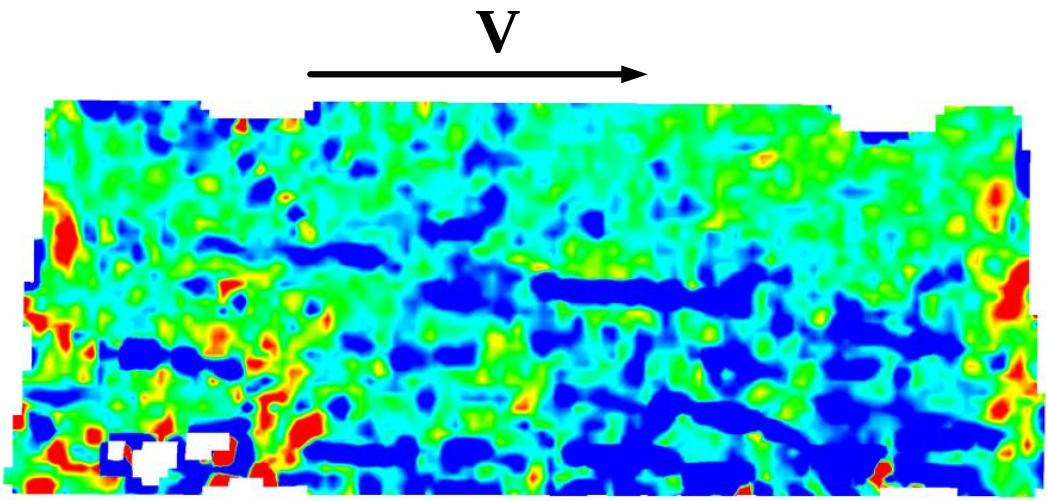

Drift ratio -1.25%

Figure 6-24 DIC minor strain results of specimen SW-MP-0.5 at drift ratio 1.25%

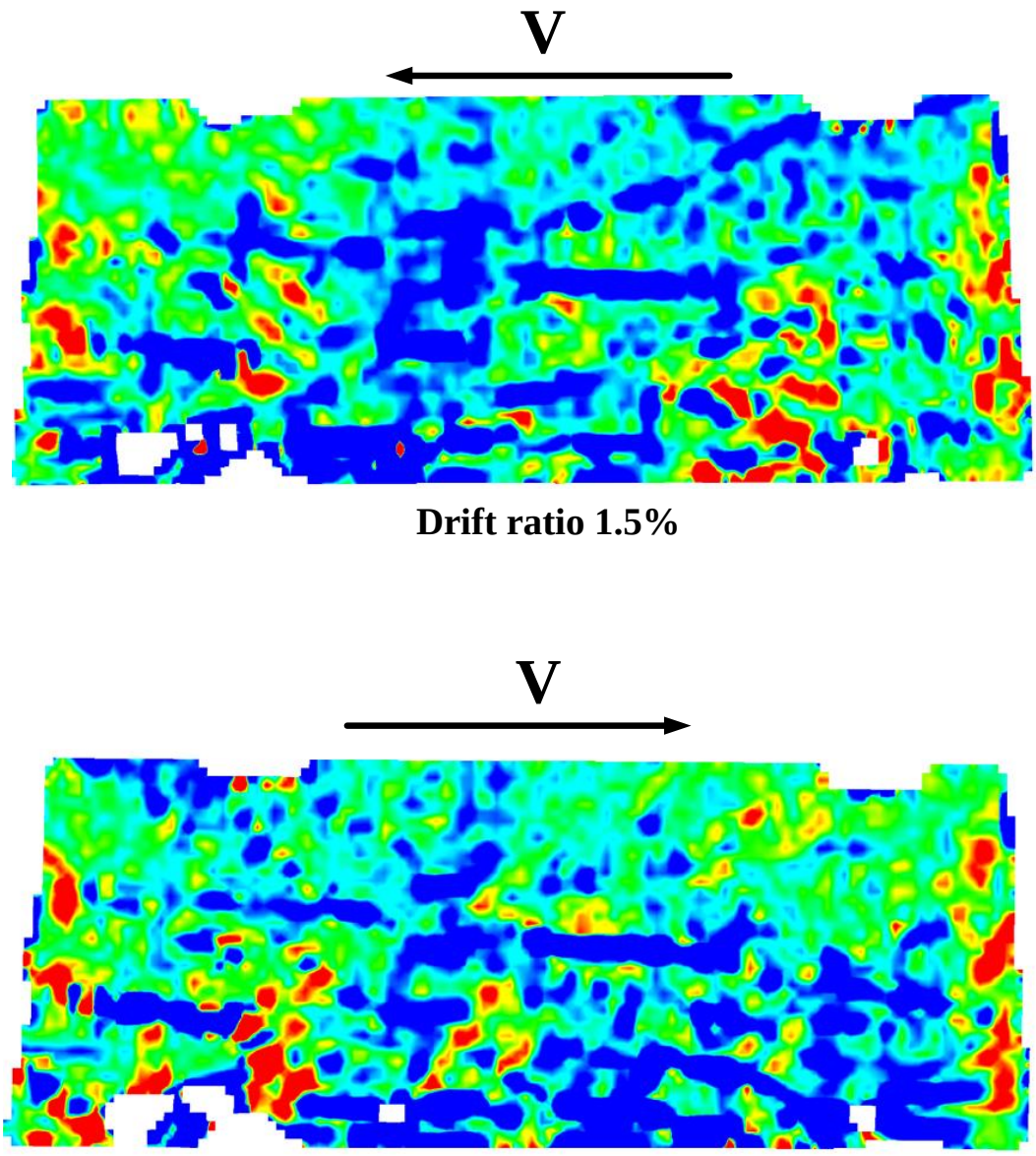

Figure 6-25 DIC minor strain results of specimen SW-MP-0.5 at drift ratio 1.5%

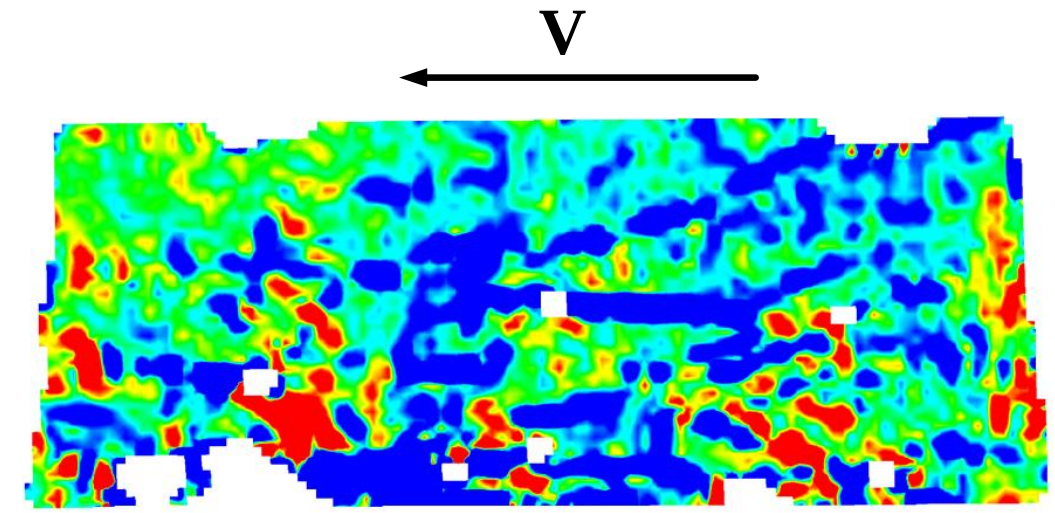

Drift ratio 1.75%

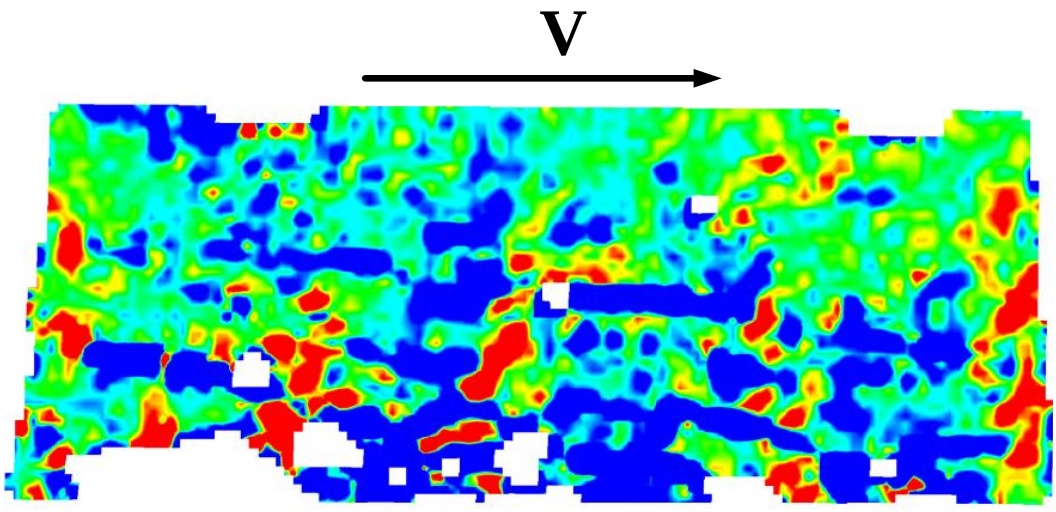

Drift ratio -1.75%

Figure 6-26 DIC minor strain results of specimen SW-MP-0.5 at drift ratio 1.75%

6.4 Specimen SW-HA-0.5

6.4.1 DIC major strain distribution

Cracks development at drift ratio 0.125%, 0.25%, 0.5%, 0.75%, and 1% are shown in Figure 6-27 to Figure 6-31. The diagonal red lines refer to the axis of struts developed to transfer shear forces from wall's tip to the base, while the horizontal red lines represent the flexural cracks due to bending stresses. Diagonal struts remained intact until drift ratio 0.75%. Due to insufficient concrete confinement at the web, the struts started crushing at +1% and the shear strength suddenly dropped. All strain distributions have same legend values that shown at Drift ratio 0.125%.

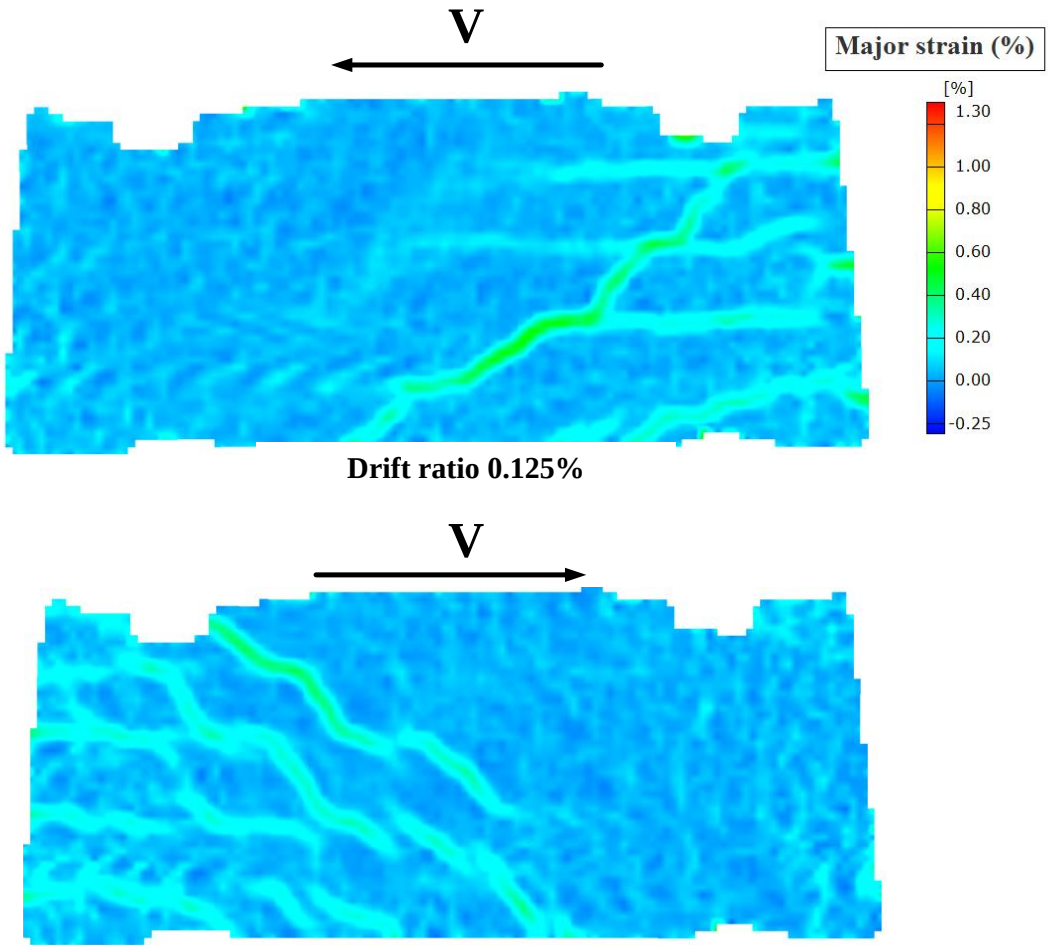

Figure 6-27 DIC major strain results of specimen SW-HA-0.5 at drift ratio 0.125%

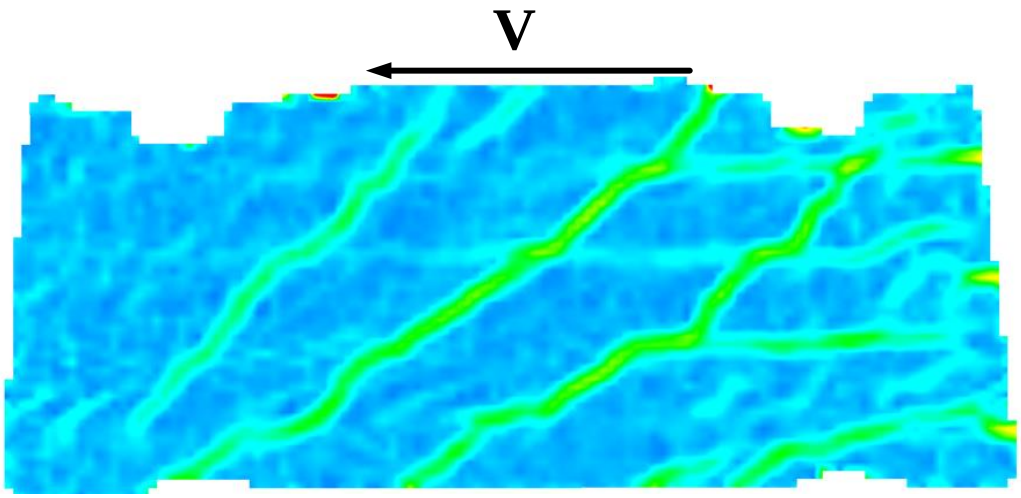

Drift ratio 0.25%

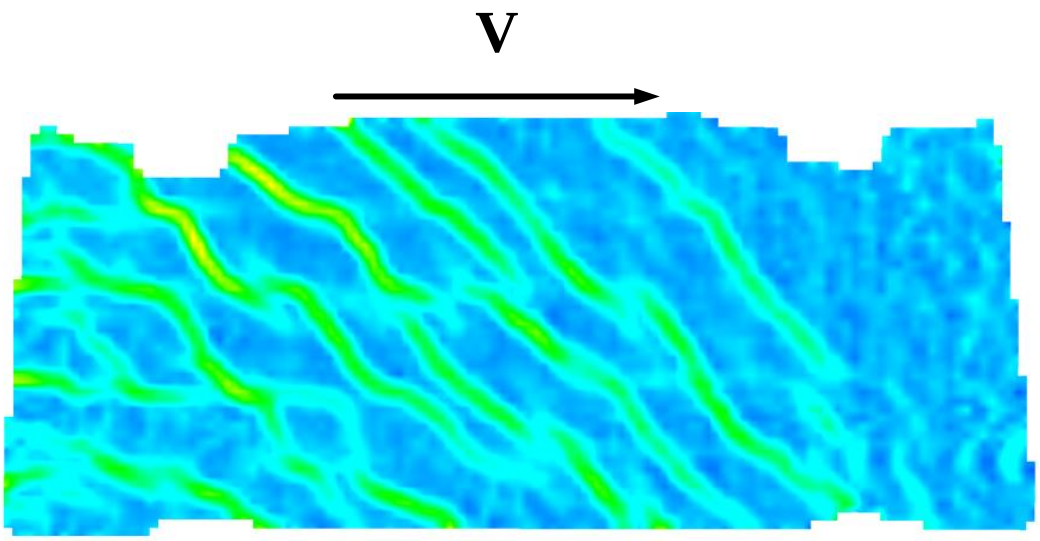

Drift ratio -0.25%

Figure 6-28 DIC major strain results of specimen SW-HA-0.5 at drift ratio 0.25%

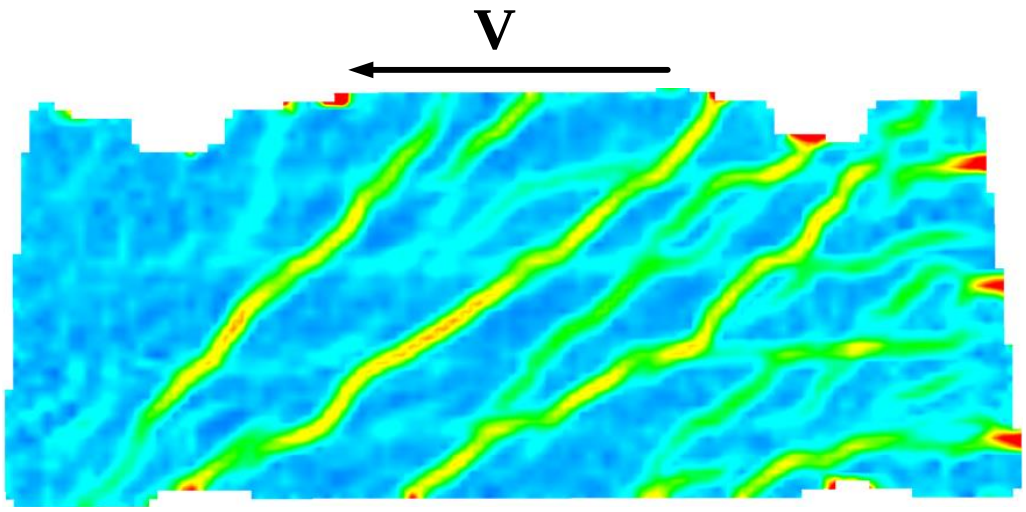

Drift ratio 0.5%

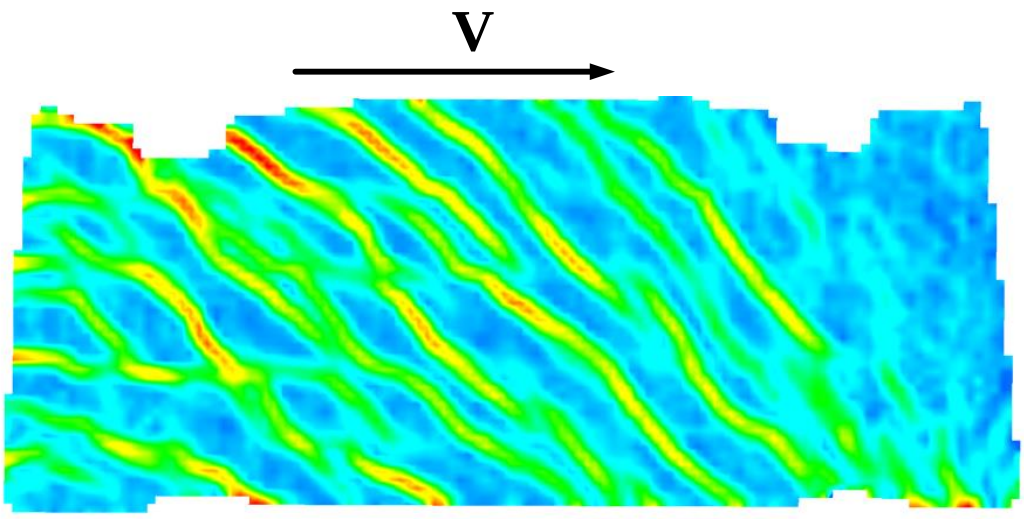

Drift ratio -0.5%

Figure 6-29 DIC major strain results of specimen SW-HA-0.5 at drift ratio 0.5%

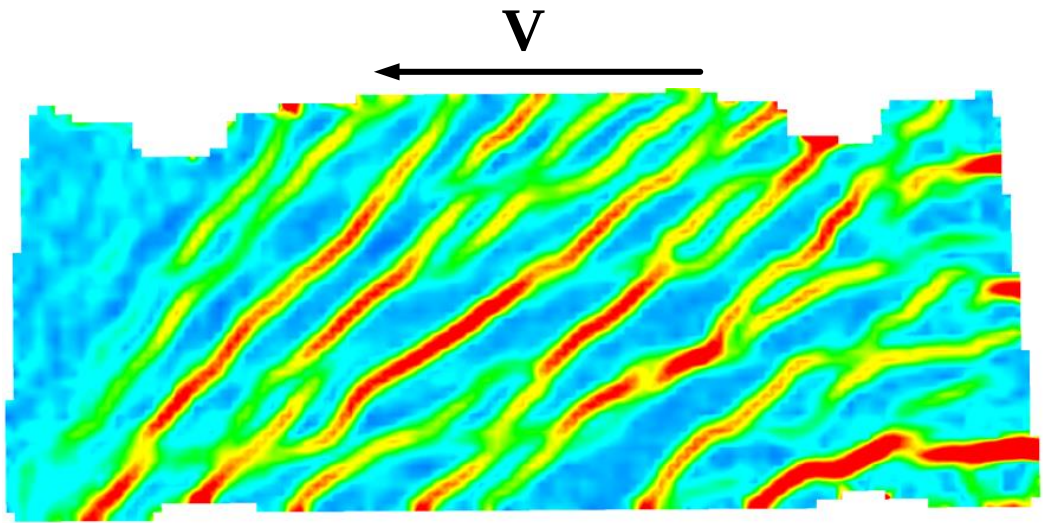

Drift ratio 0.75%

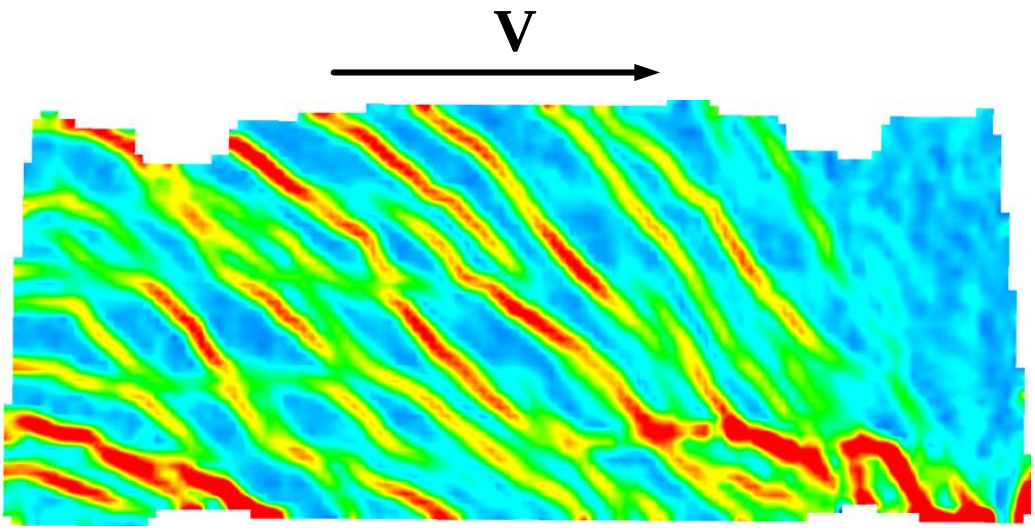

Drift ratio -0.75%

Figure 6-30 DIC major strain results of specimen SW-HA-0.5 at drift ratio 0.75%

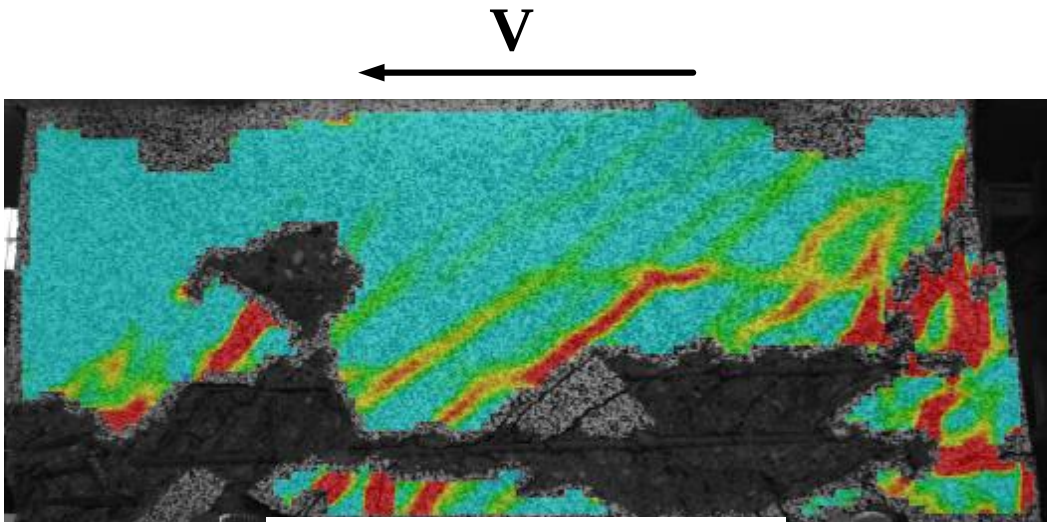

Drift ratio 1%

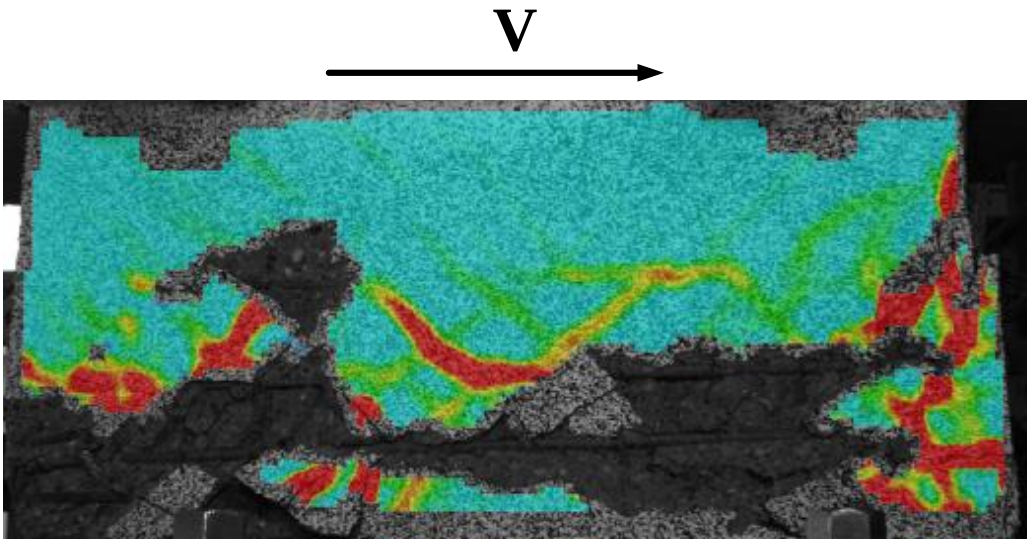

Drift ratio -1%

Figure 6-31 DIC major strain results of specimen SW-HA-0.5 at drift ratio 1%

6.4.2 DIC minor strain distribution

Cracks development at drift ratio 0.125%, 0.25%, 0.5%, 0.75%, 1%, and 1.25% are shown in Figure 6-32 to Figure 6-36. The diagonal blue lines refer to the axis of struts developed to transfer shear forces from wall's tip to the base. Diagonal struts remained undamaged until drift ratio +1%. Sudden sliding and crushing commenced at -1% which prevents the DIC to capture the deformation of black dots on the wall face. All strain distributions have same legend values that shown at Drift ratio 0.125%.

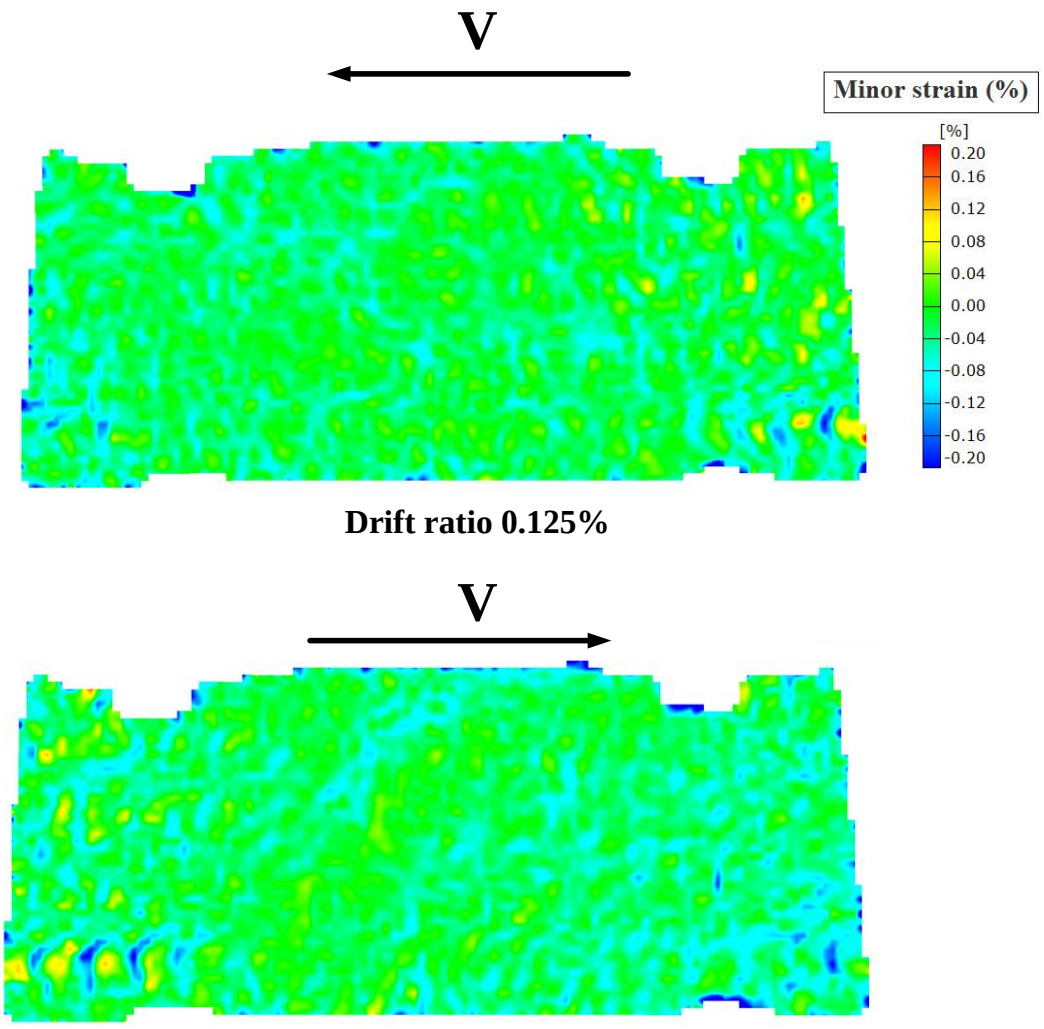

Figure 6-32 DIC minor strain results of specimen SW-HA-0.5 at drift ratio 0.125%

(positive strain is tension and negative strain is compression)

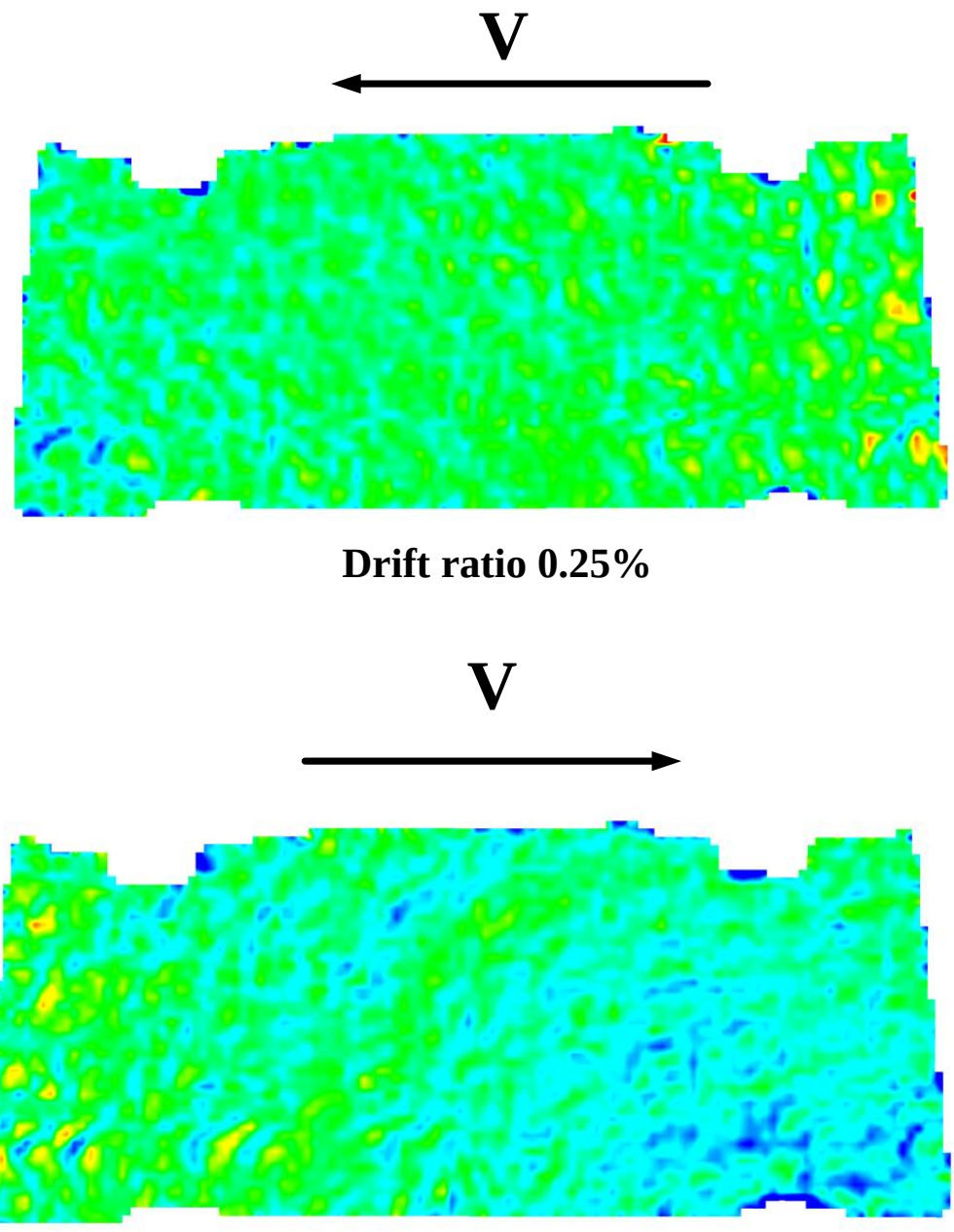

Figure 6-33 DIC minor strain results of specimen SW-HA-0.5 at drift ratio 0.25%

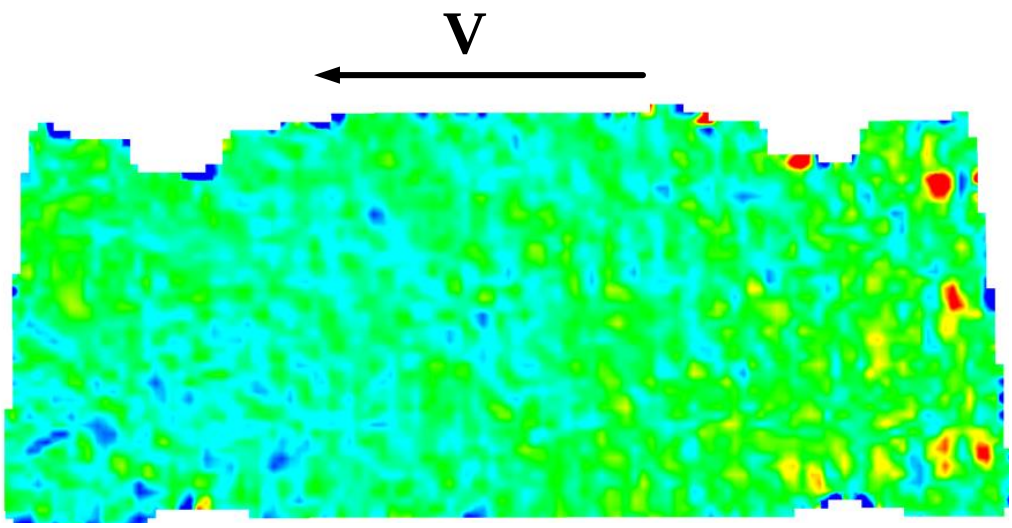

Drift ratio 0.5%

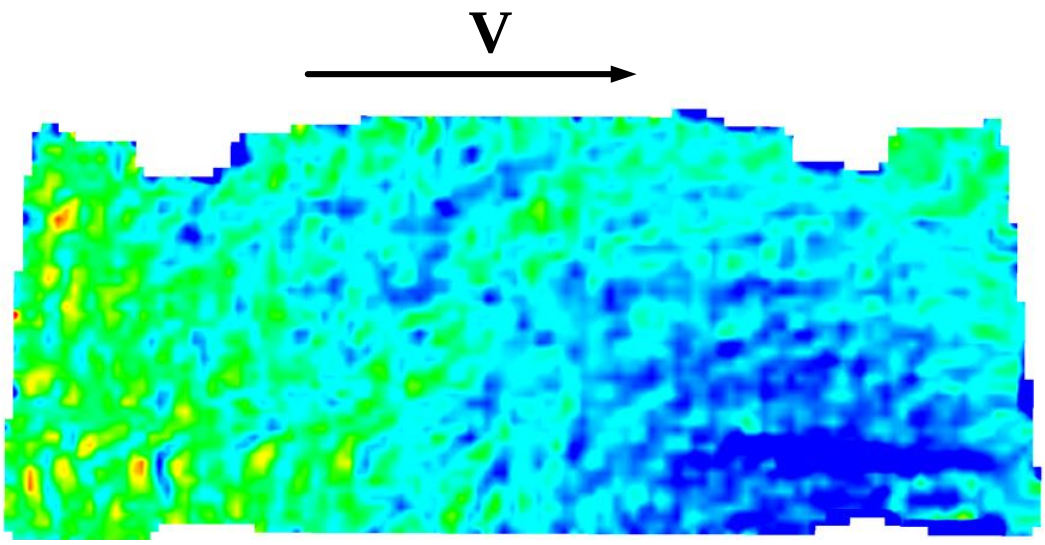

Drift ratio -0.5%

Figure 6-34 DIC minor strain results of specimen SW-HA-0.5 at drift ratio 0.5%

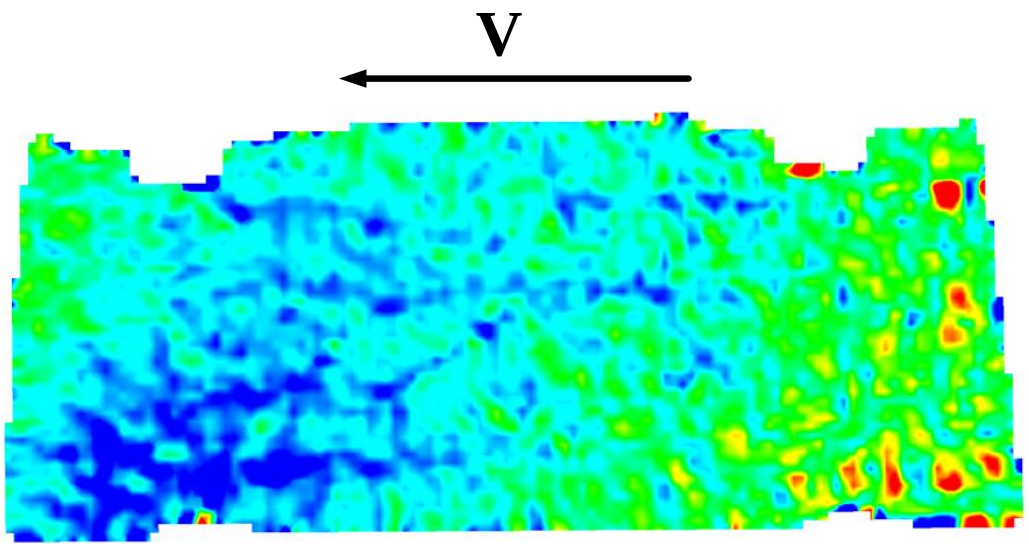

Drift ratio 0.75%

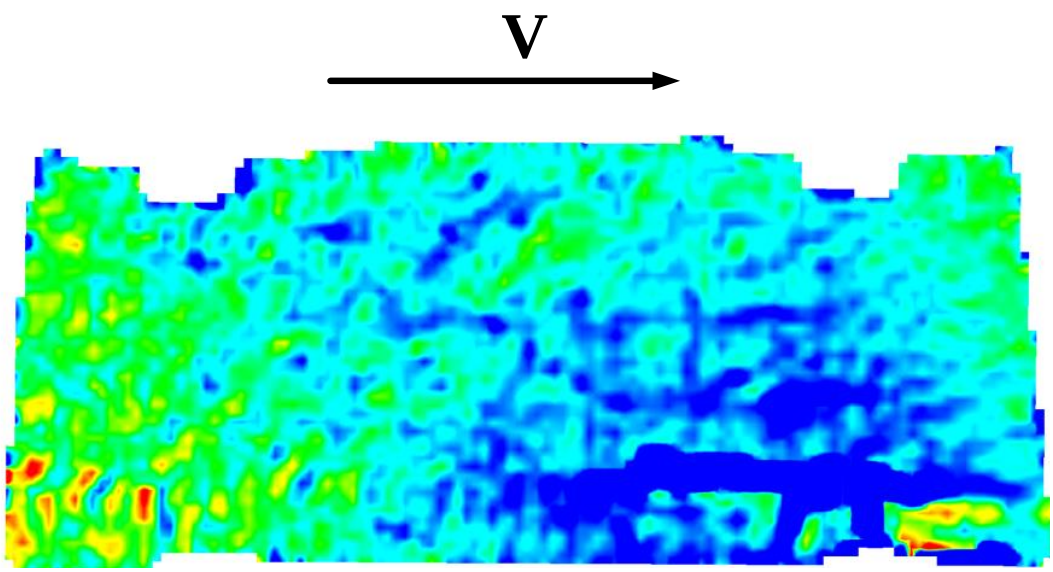

Drift ratio -0.75%

Figure 6-35 DIC minor strain results of specimen SW-HA-0.5 at drift ratio 0.75%

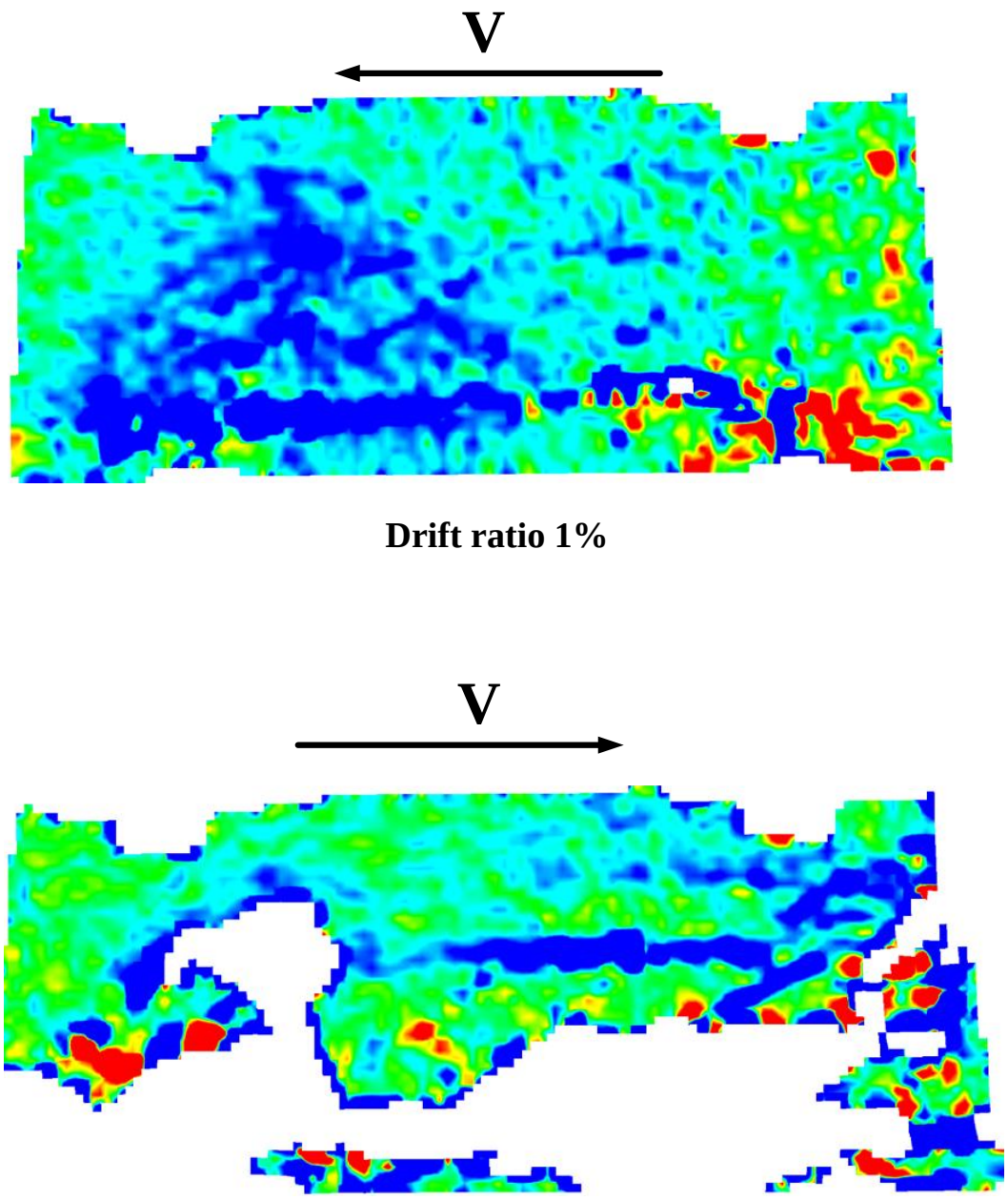

Figure 6-36 DIC minor strain results of specimen SW-HA-0.5 at drift ratio 1%

6.5 Specimen SW-HP-0.5-1

6.5.1 DIC major strain distribution

Cracks development at drift ratio 0.125%, 0.25%, 0.5%, 0.75%, 1%, 1.25%, 1.5%, and 1.75% are shown in Figure 6-37 to Figure 6-44. The diagonal red lines refer to the axis of struts developed to transfer shear forces from wall's tip to the base, while the horizontal red lines represent the flexural cracks due to bending stresses. Diagonal struts remained intact until drift ratio -1%. Flexural cracks concentrated at wall boundaries especially after drift ratio 0.75%, the reversed cyclic compressive and flexural stresses at boundaries caused stresses concentration and weakening zone. At drift ratio1.25%, concrete cover started spalling at boundaries, but the shear strength remained unaffected. The concrete cover spalling extended to the wall web at drift ratios 1.5% and 1.75%. However, shear strength gradually decreased after drift ratio 1.75% because the concrete core is well-confined and still resist shear stresses. All strain distributions have same legend values that shown at Drift ratio 0.125%.

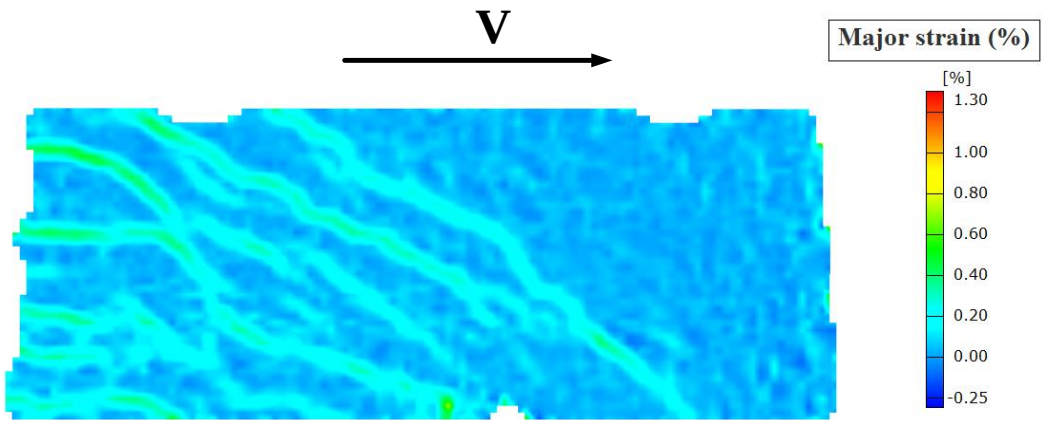

Drift ratio 0.125%

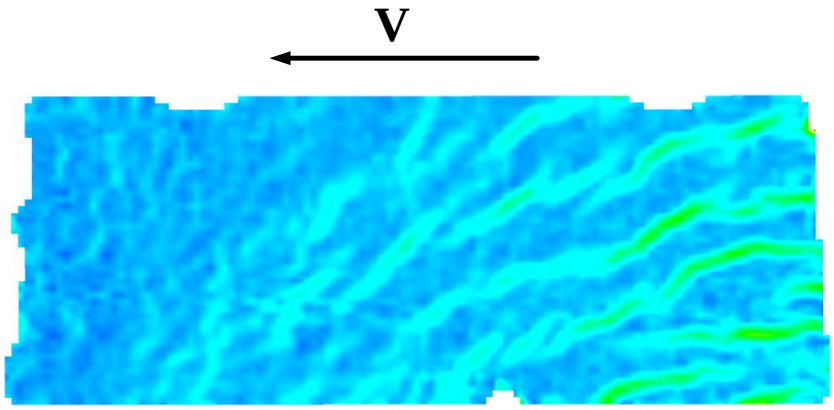

Drift ratio -0.125%

Figure 6-37 DIC major strain results of specimen SW-MP-0.5-1 at drift ratio 0.125%

(positive strain is tension and negative strain is compression)

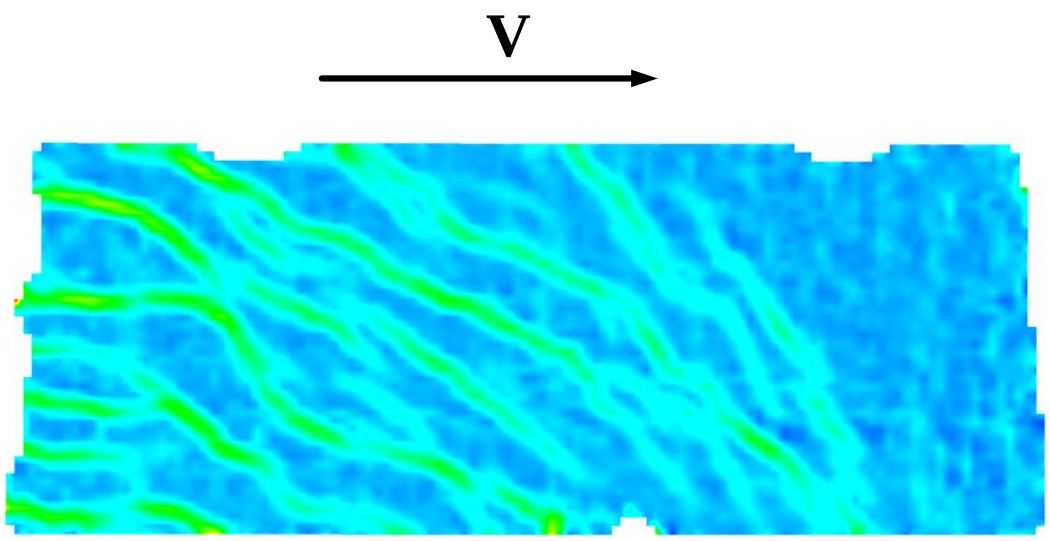

Drift ratio 0.25%

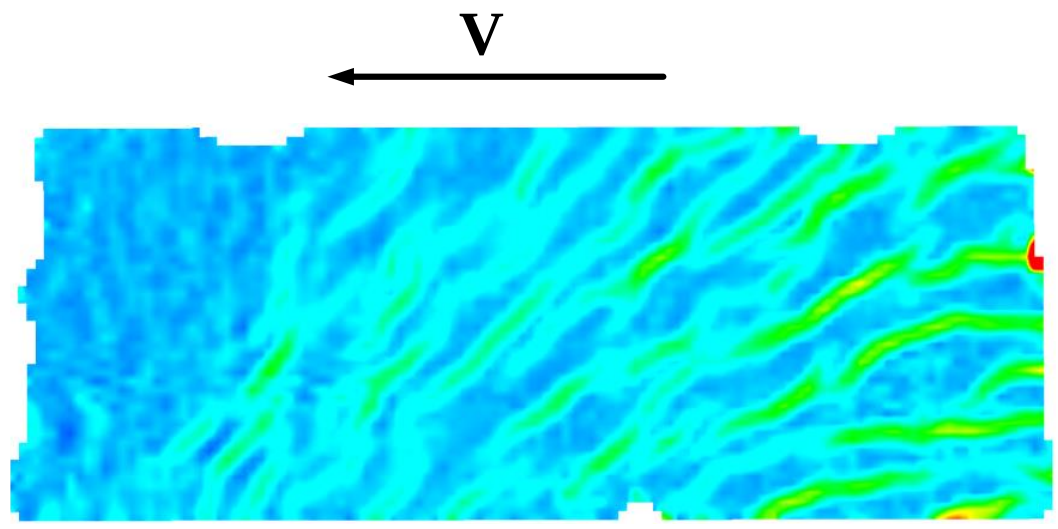

Drift ratio -0.25%

Figure 6-38 DIC major strain results of specimen SW-MP-0.5-1 at drift ratio 0.125%

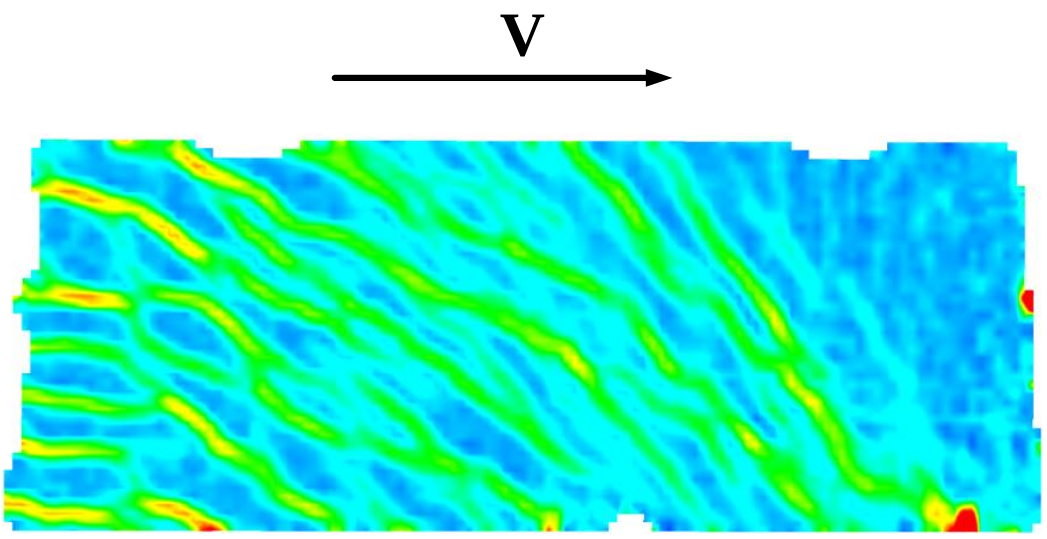

Drift ratio 0.5%

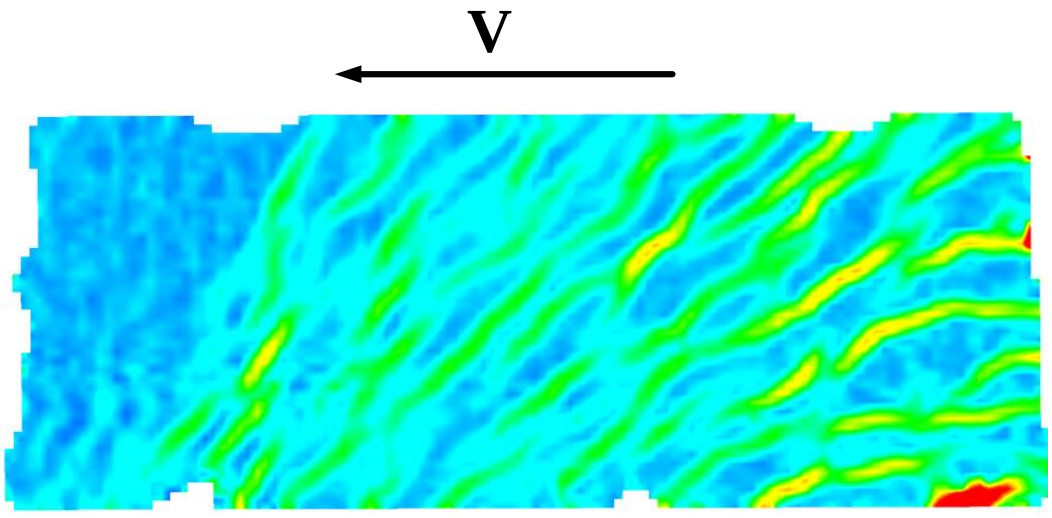

Drift ratio -0.5%

Figure 6-39 DIC major strain results of specimen SW-MP-0.5-1 at drift ratio 0.5%

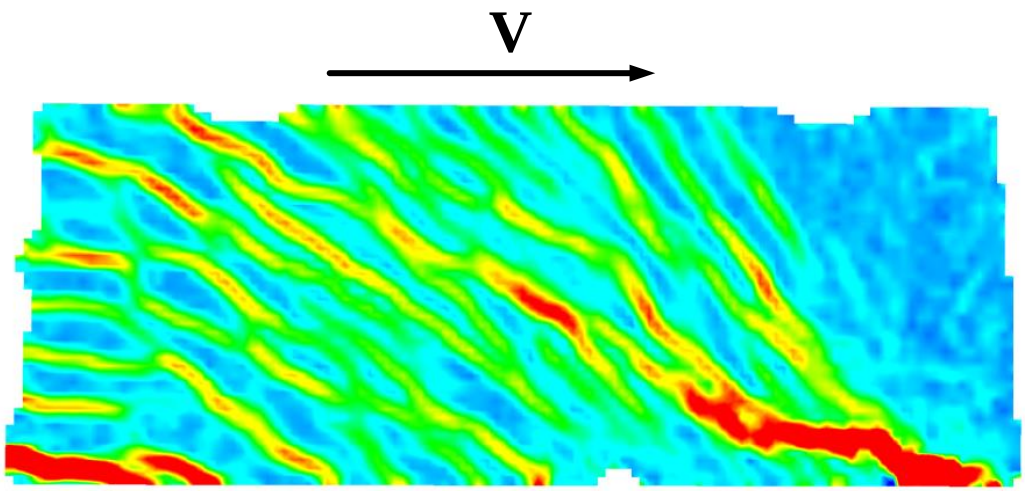

Drift ratio 0.75%

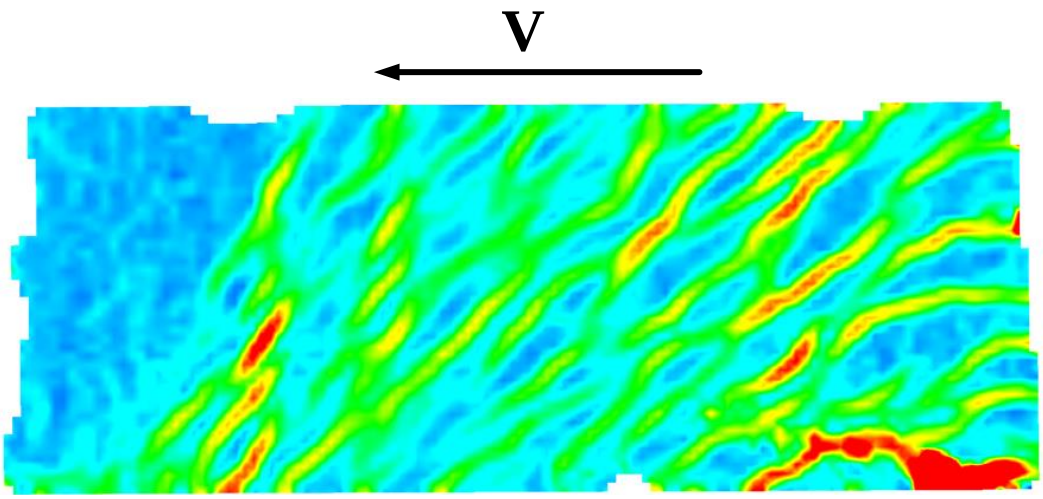

Drift ratio -0.75%

Figure 6-40 DIC major strain results of specimen SW-MP-0.5-1 at drift ratio 0.75%

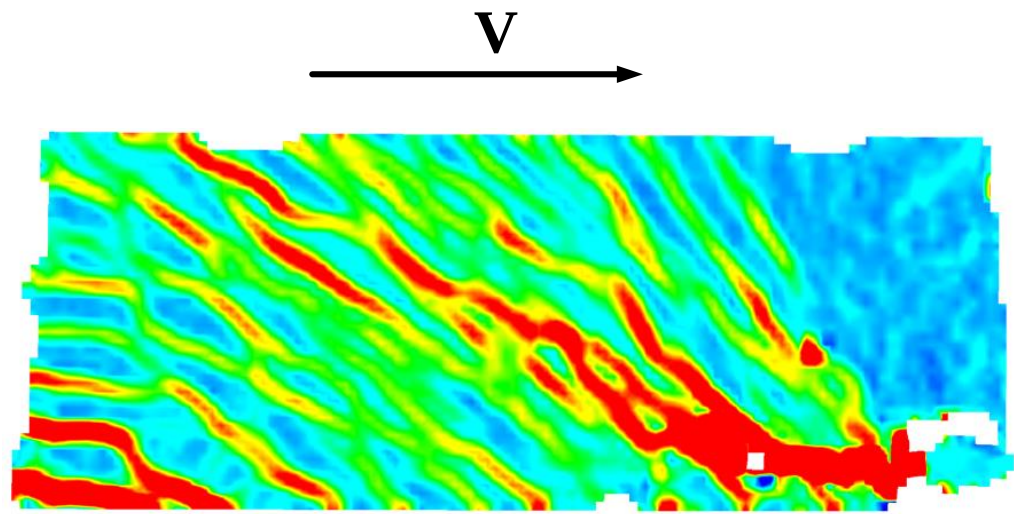

Drift ratio 1%

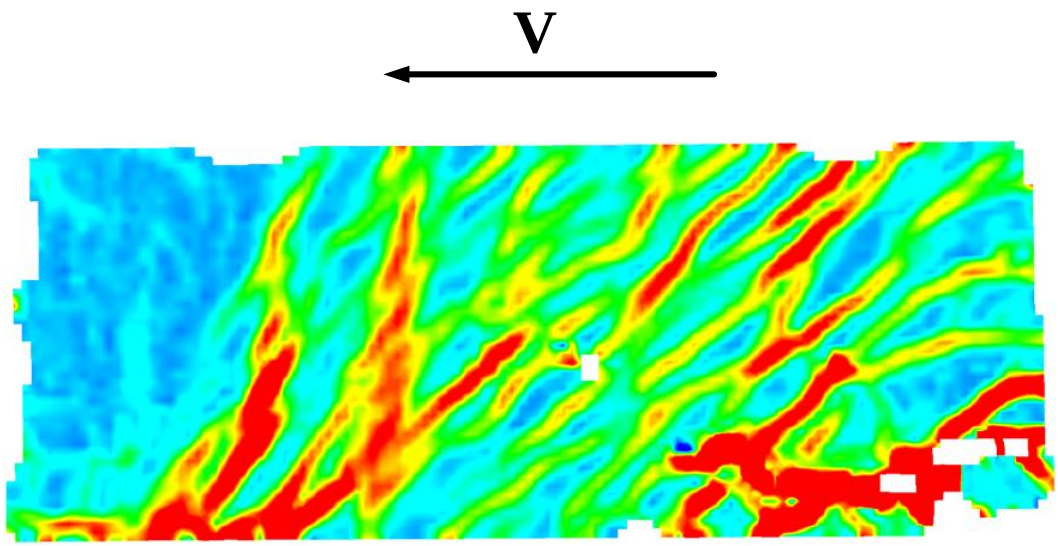

Drift ratio -1%

Figure 6-41 DIC major strain results of specimen SW-MP-0.5-1 at drift ratio 1%

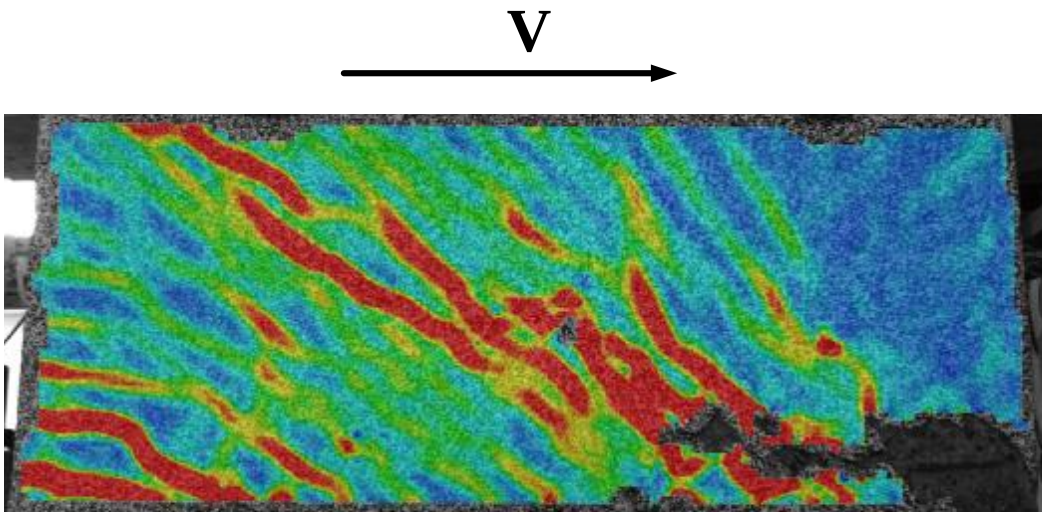

Drift ratio 1.25%

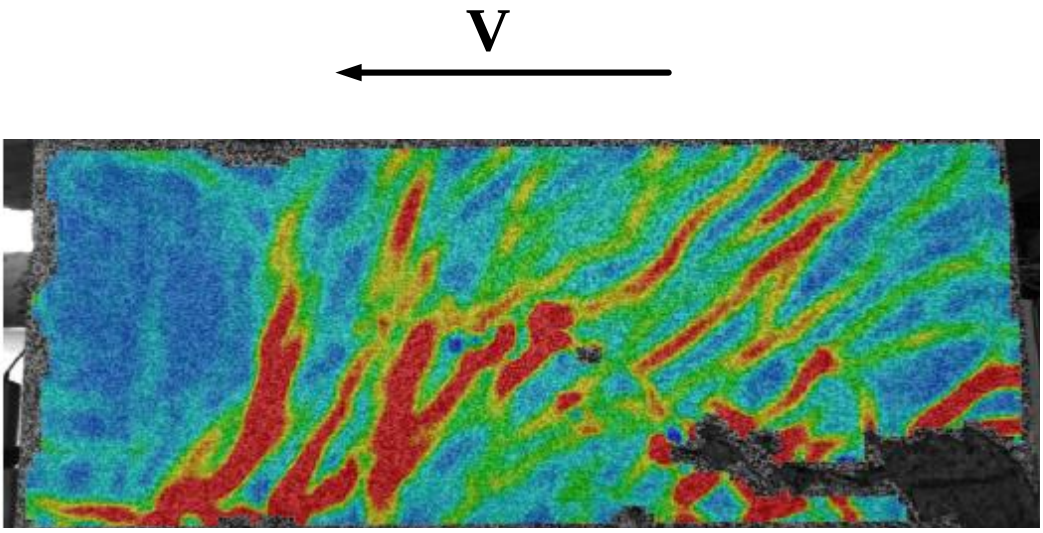

Drift ratio -1.25%

Figure 6-42 DIC major strain results of specimen SW-MP-0.5-1 at drift ratio 1.25%

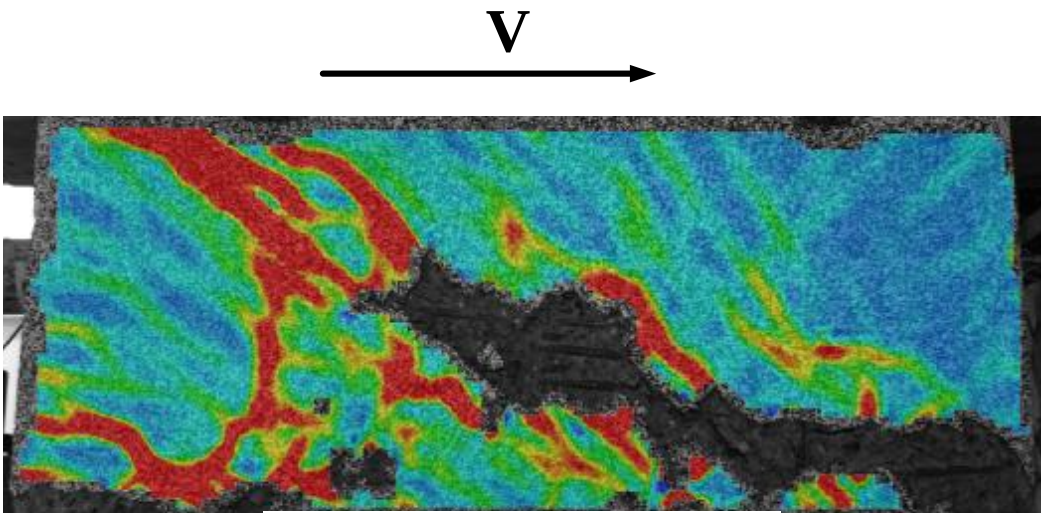

Drift ratio 1.5%

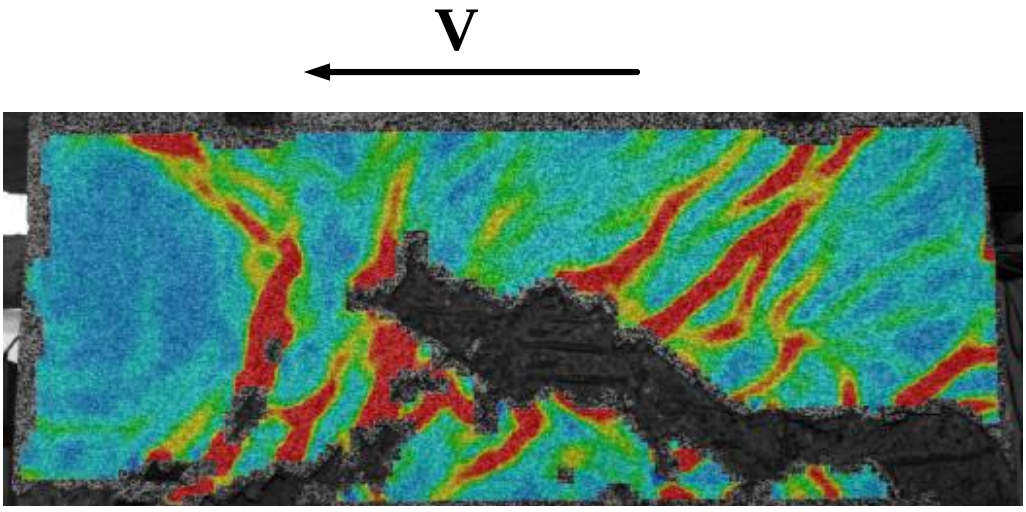

Drift ratio -1.5%

Figure 6-43 DIC major strain results of specimen SW-MP-0.5-1 at drift ratio 1.5%

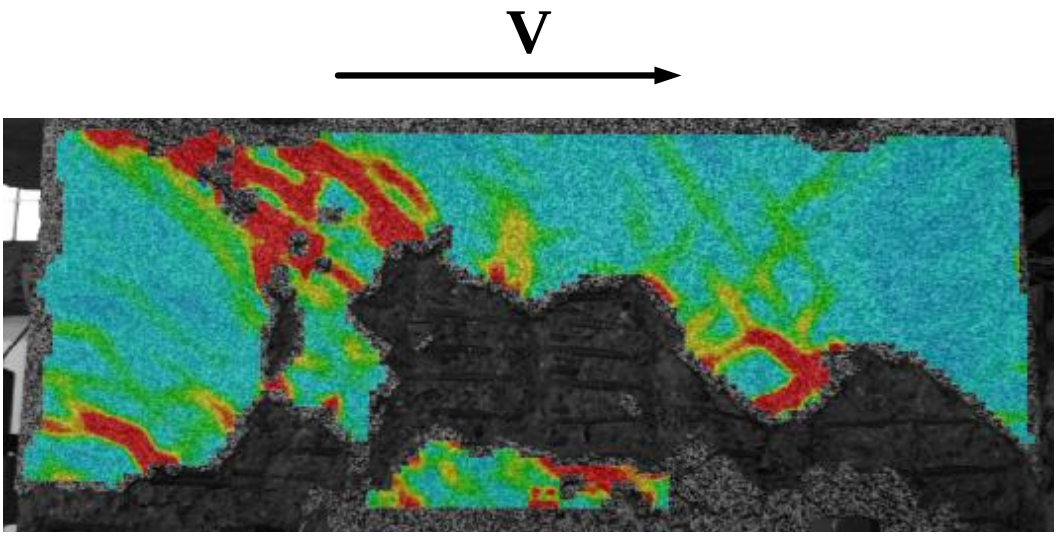

Drift ratio 1.75%

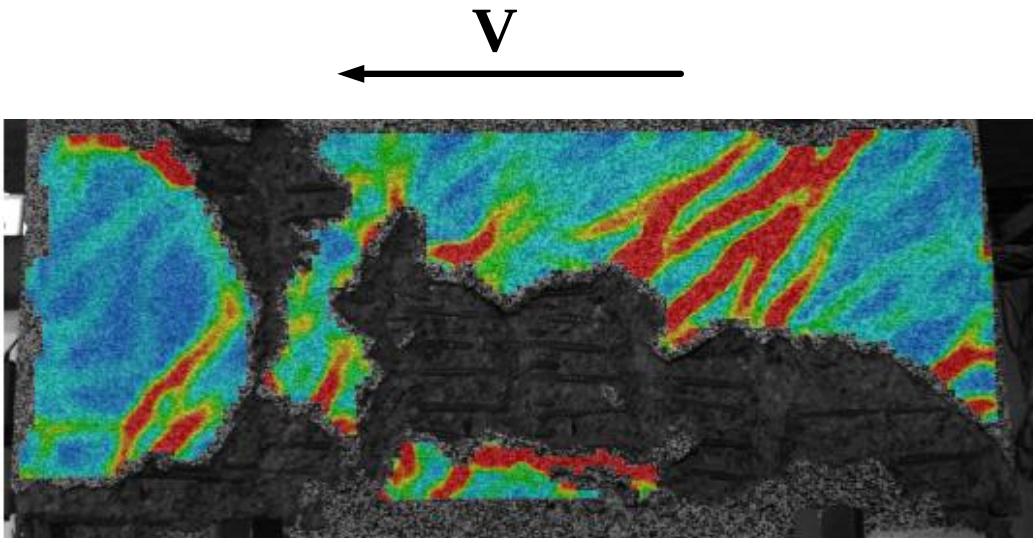

Drift ratio -1.75%

Figure 6-44 DIC major strain results of specimen SW-MP-0.5-1 at drift ratio 1.75%

6.5.2 DIC Minor strain distribution

Cracks development at drift ratio 0.125%, 0.25%, 0.5%, 0.75%, 1%, 1.25%, and 1.5% are shown in Figure 6-45 to Figure 6-51. The diagonal blue lines refer to the axis of struts developed to transfer shear forces from wall's tip to the base. Diagonal struts remained undamaged until drift ratio 1%. Spalling of concrete cover started at 1.25% which prevents the DIC to capture the deformation of black dots on the wall face. All strain distributions have same legend values that shown at Drift ratio 0.125%.

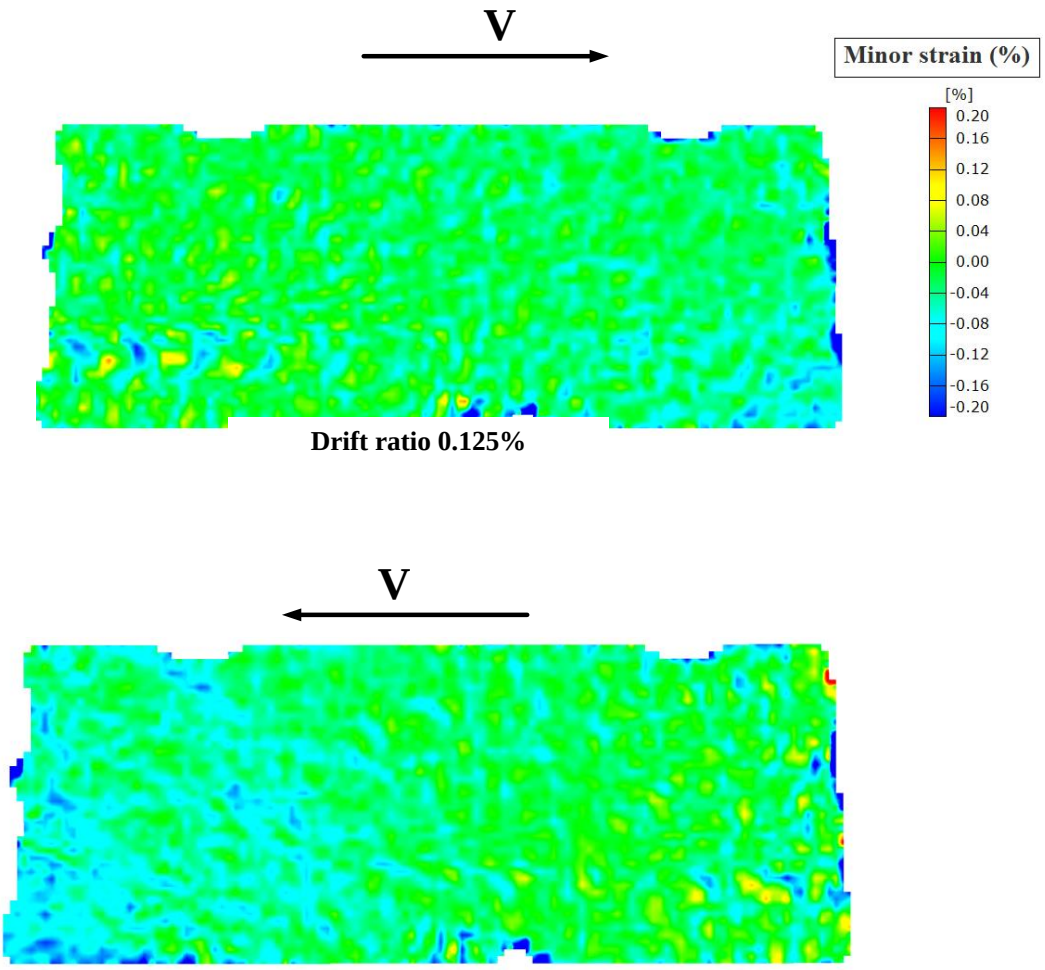

Figure 6-45 DIC minor strain results of specimen SW-MP-0.5-1 at drift ratio 0.125%

(positive strain is tension and negative strain is compression)

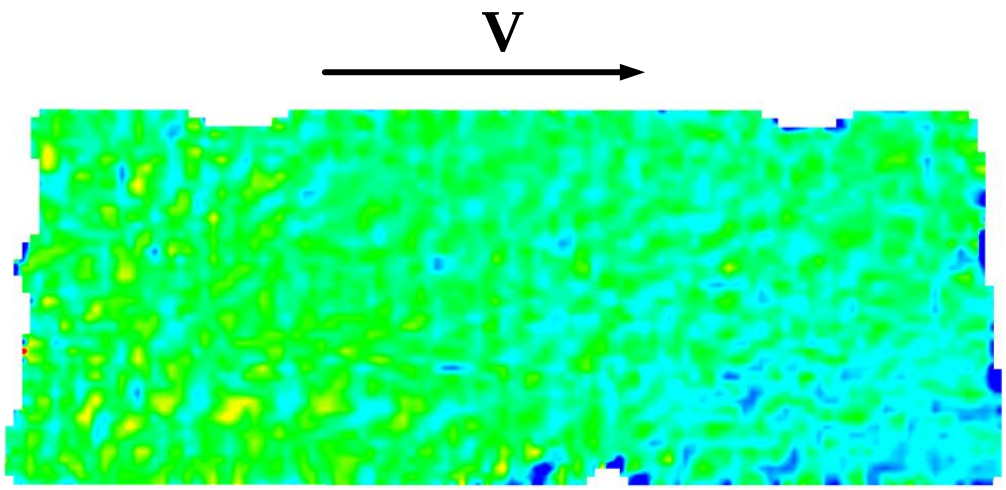

Drift ratio 0.25%

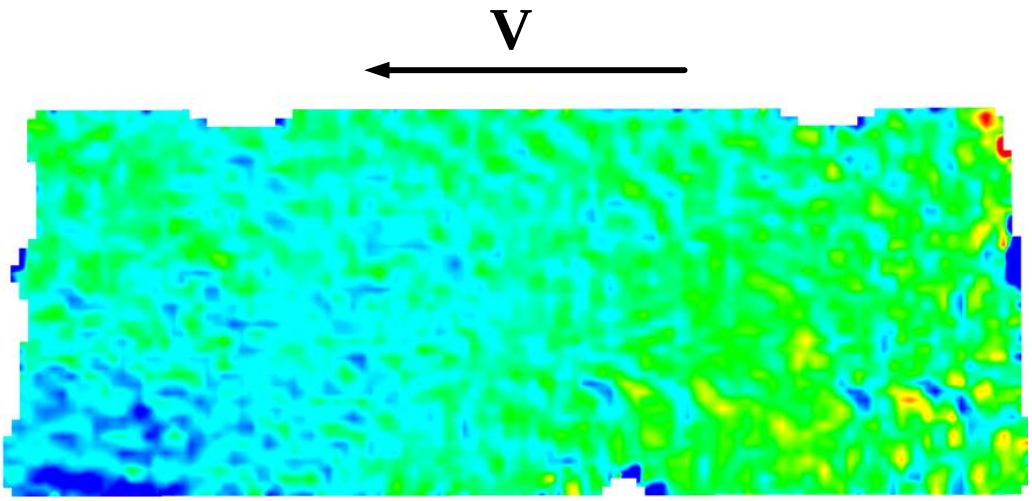

Drift ratio -0.25%

Figure 6-46 DIC minor strain results of specimen SW-MP-0.5-1 at drift ratio 0.25%

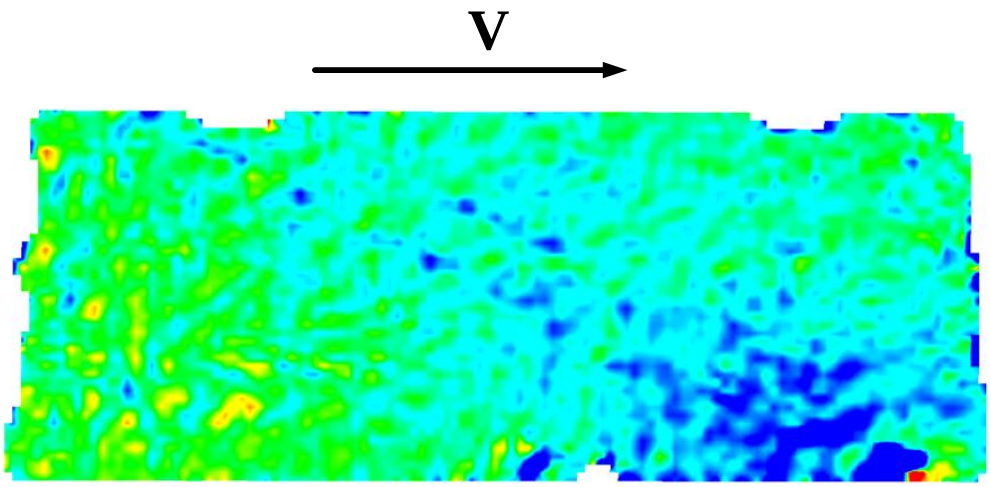

Drift ratio 0.5%

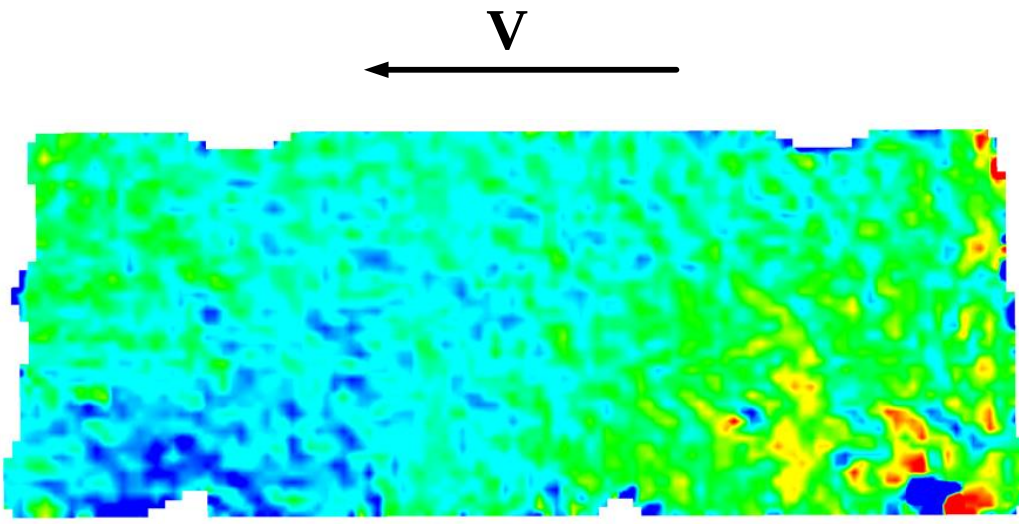

Drift ratio -0.5%

Figure 6-47 DIC minor strain results of specimen SW-MP-0.5-1 at drift ratio 0.5%

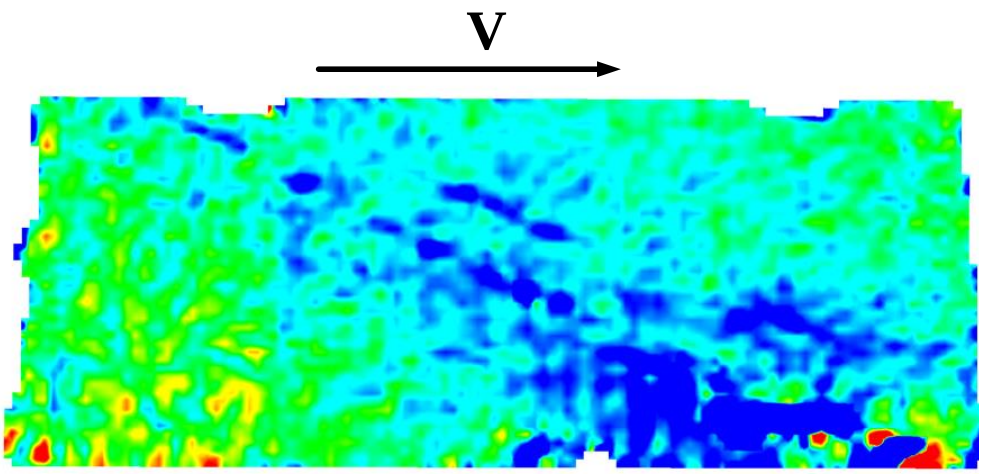

Drift ratio 0.75%

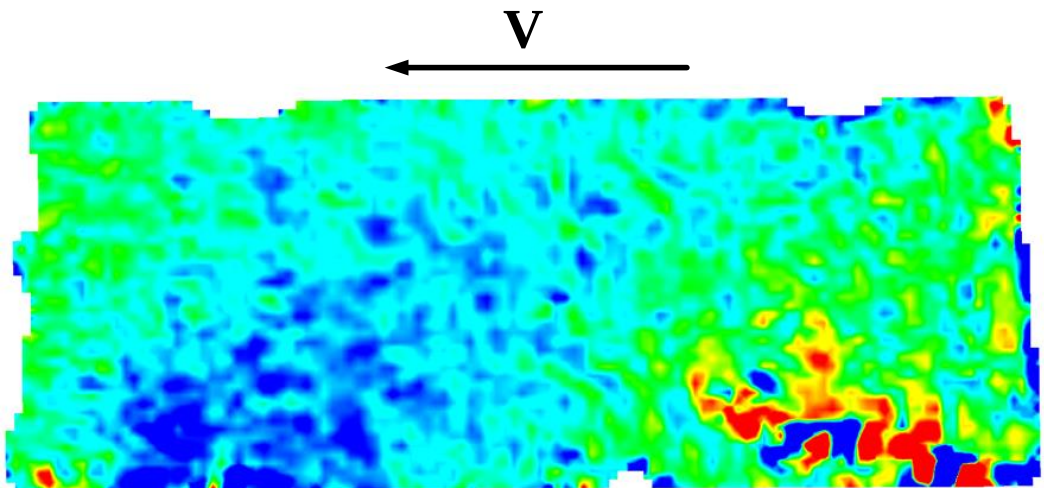

Drift ratio -0.75%

Figure 6-48 DIC minor strain results of specimen SW-MP-0.5-1 at drift ratio 0.75%

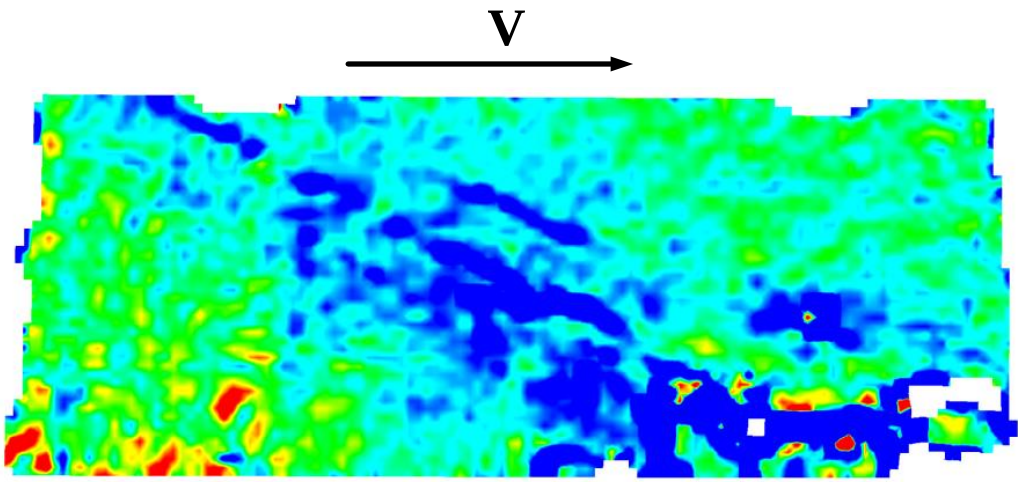

Drift ratio 1%

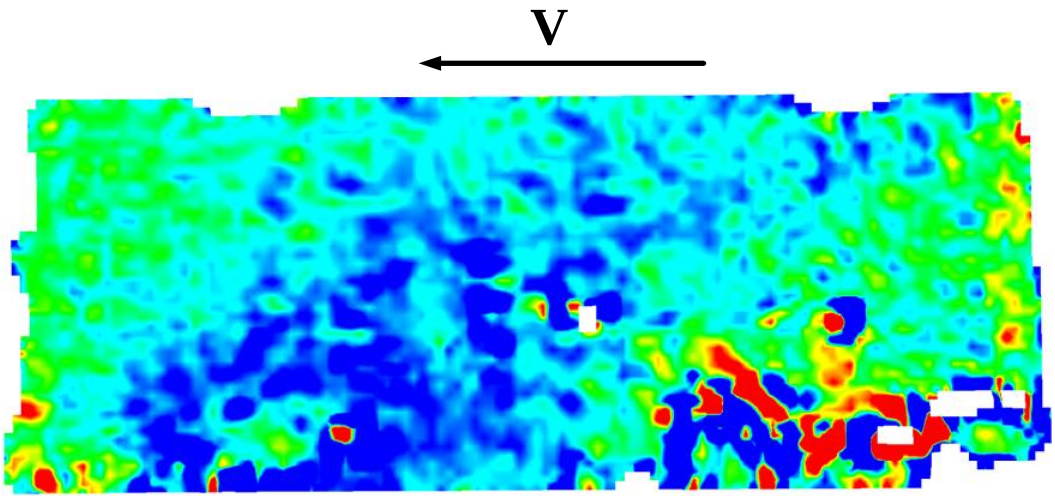

Drift ratio -1%

Figure 6-49 DIC minor strain results of specimen SW-MP-0.5-1 at drift ratio 1%

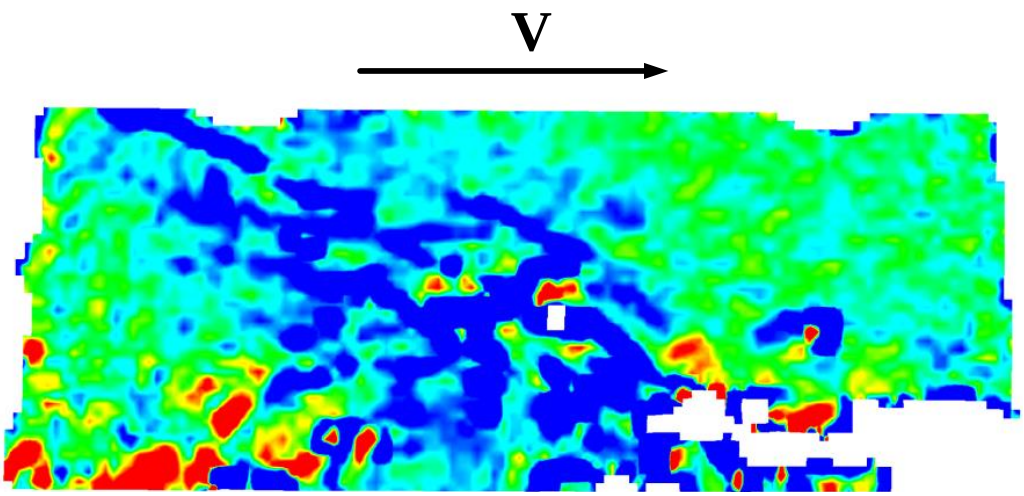

Drift ratio 1.25%

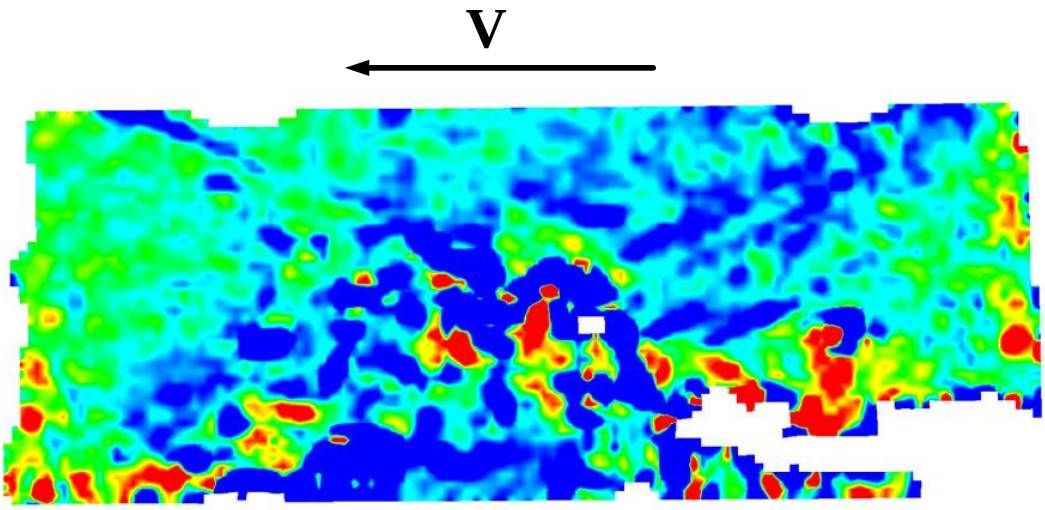

Drift ratio -1.25%

Figure 6-50 DIC minor strain results of specimen SW-MP-0.5-1 at drift ratio 1.25%

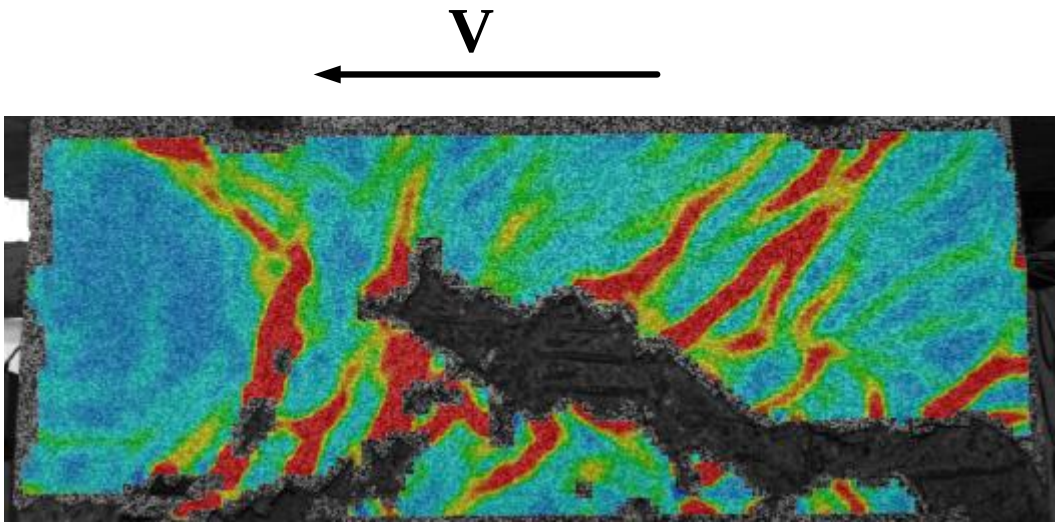

Drift ratio -1.5%

Figure 6-51 DIC minor strain results of specimen SW-MP-0.5-1 at drift ratio 1.5%

6.6 SW-HP-0.5-2

6.6.1 DIC major strain distribution

Cracks development at drift ratio 0.125%, 0.25%, 0.5%, 0.75%, 1%, 1.25%, 1.5%, and 1.75% are shown in Figure 6-52 to Figure 6-59. The diagonal red lines refer to the axis of struts developed to transfer shear forces from wall's tip to the base, while the horizontal red lines represent the flexural cracks due to bending stresses. Diagonal struts remained intact until drift ratio 1.25%. Flexural and diagonal cracks are uniformly distributed over wall web and boundaries indicating the benefit of increasing longitudinal reinforcement volume at boundaries. After drift ratio 1.25%, concrete cover spalling started at boundaries due to joining diagonal compressive struts to the flexural cracks, but the shear strength remained plateaued. Concrete cover spalling continued toward the wall web due to cyclic loading, while shear strength gradually decreased after drift ratio 1.75%. All strain distributions have same legend values that shown at Drift ratio 0.125%.

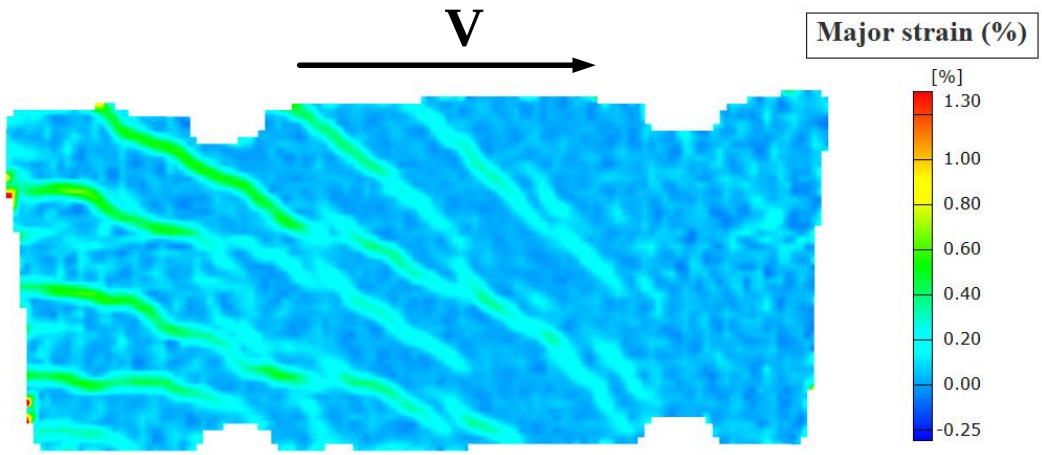

Drift ratio 0.125%

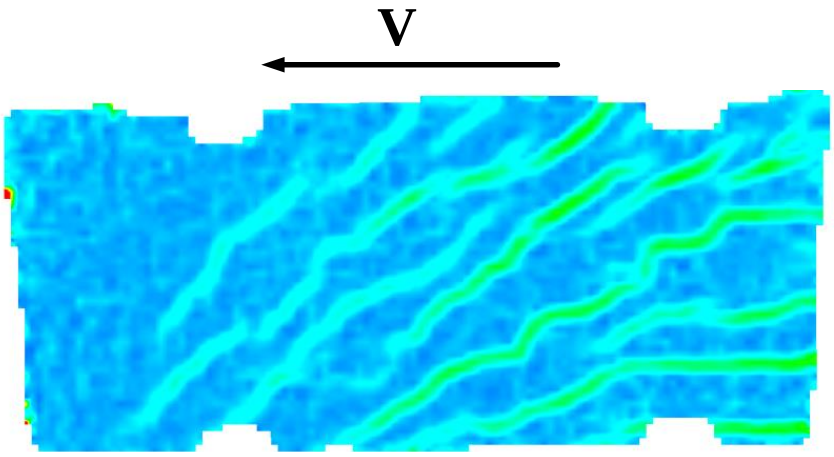

Drift ratio -0.125%

Figure 6-52 DIC major strain results of specimen SW-HP-0.5-2 at drift ratio 0.125%

(positive strain is tension and negative strain is compression)

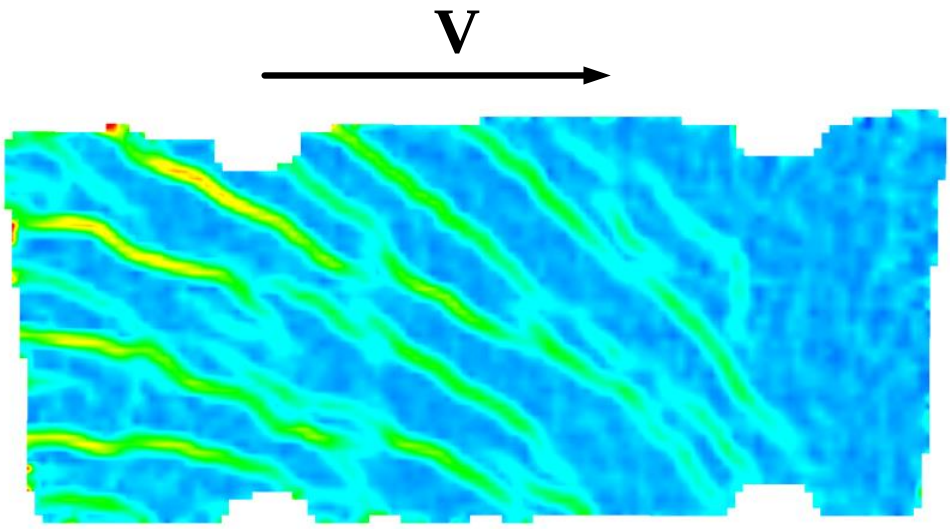

Drift ratio 0.25%

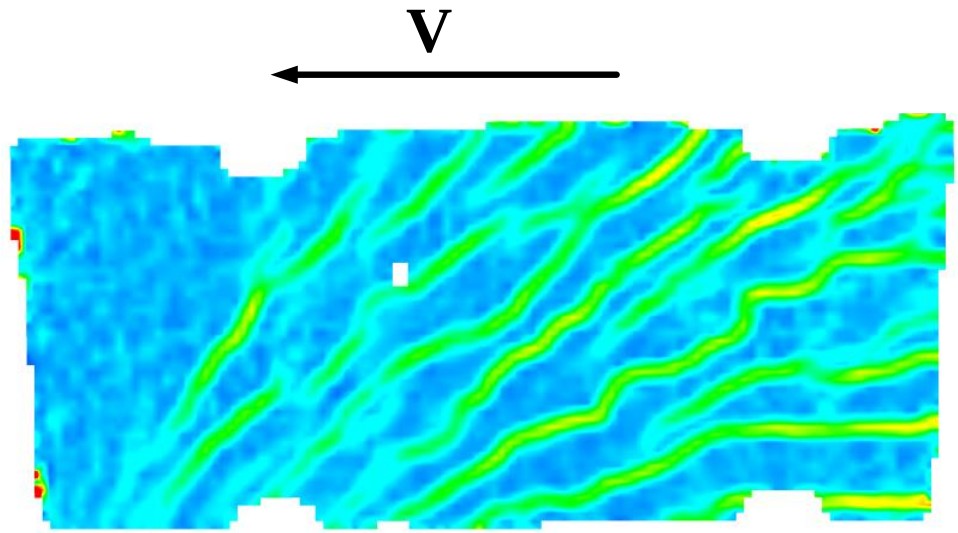

Drift ratio -0.25%

Figure 6-53 DIC major strain results of specimen SW-HP-0.5-2 at drift ratio 0.25%

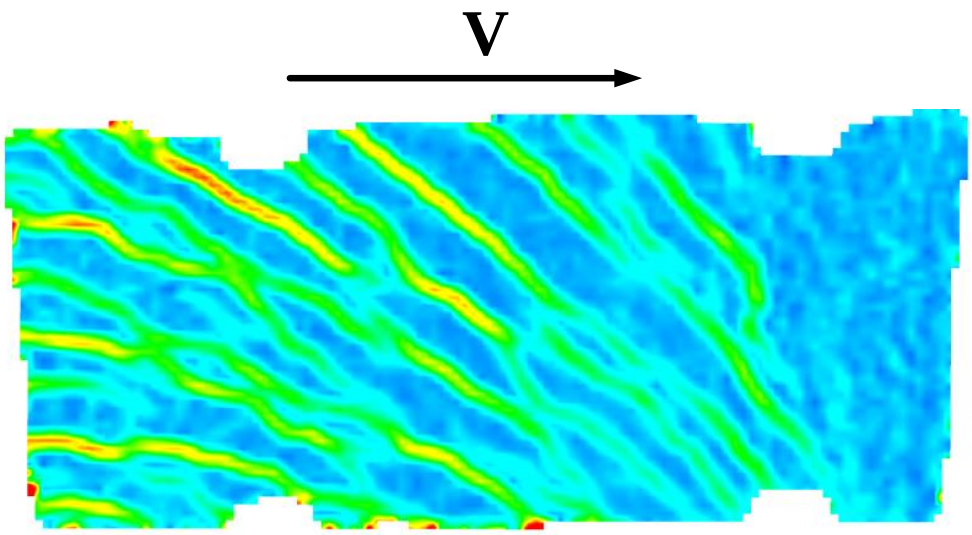

Drift ratio 0.5%

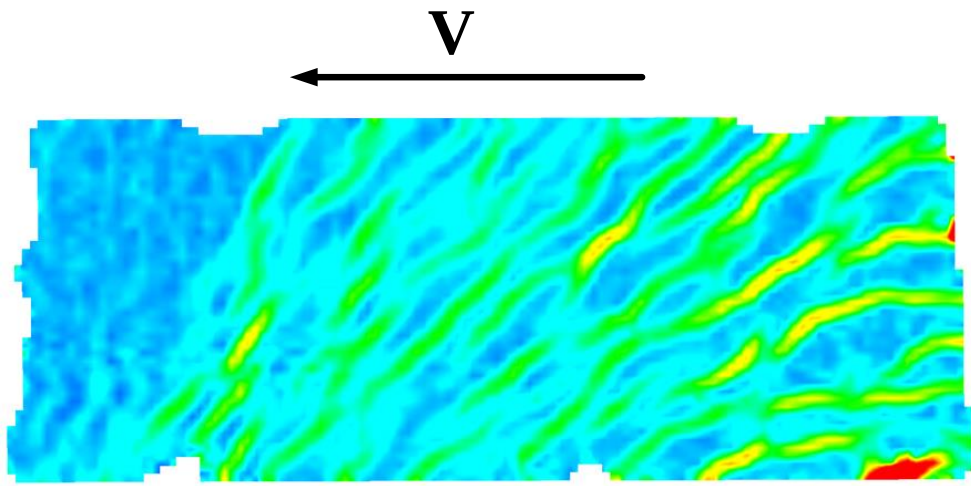

Drift ratio -0.5%

Figure 6-54 DIC major strain results of specimen SW-HP-0.5-2 at drift ratio 0.5%

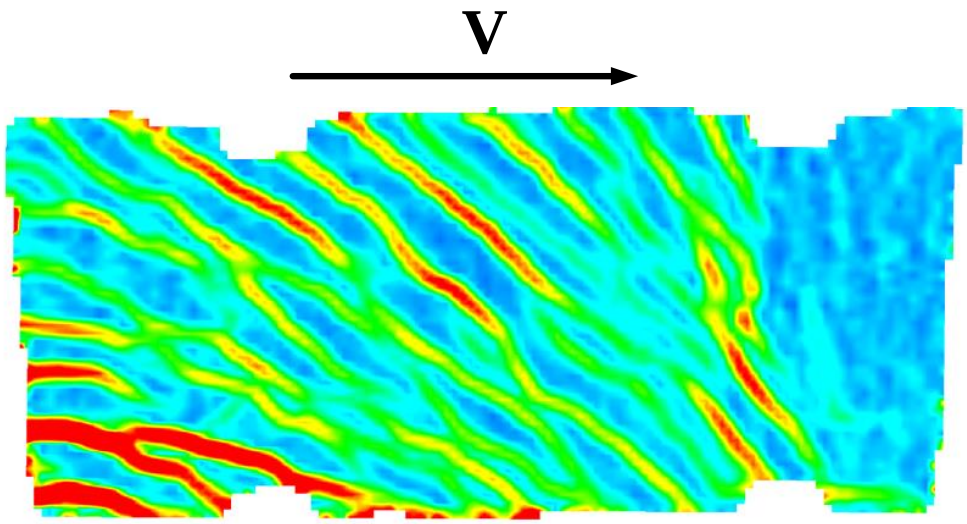

Drift ratio 0.75%

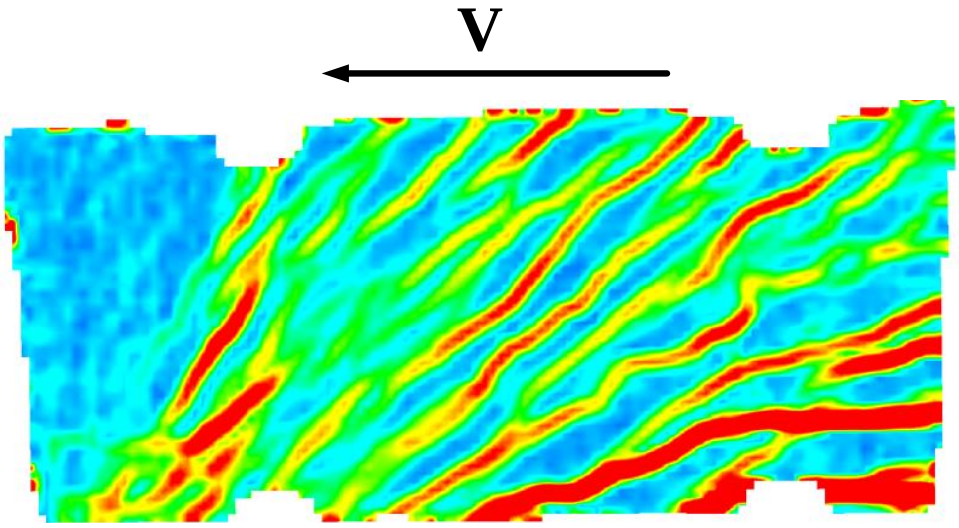

Drift ratio -0.75%

Figure 6-55 DIC major strain results of specimen SW-HP-0.5-2 at drift ratio 0.75%

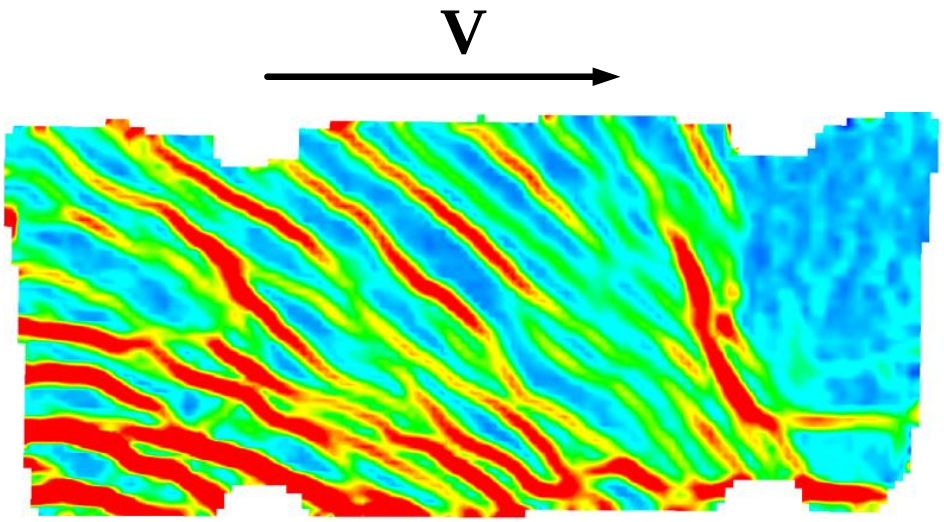

Drift ratio 1%

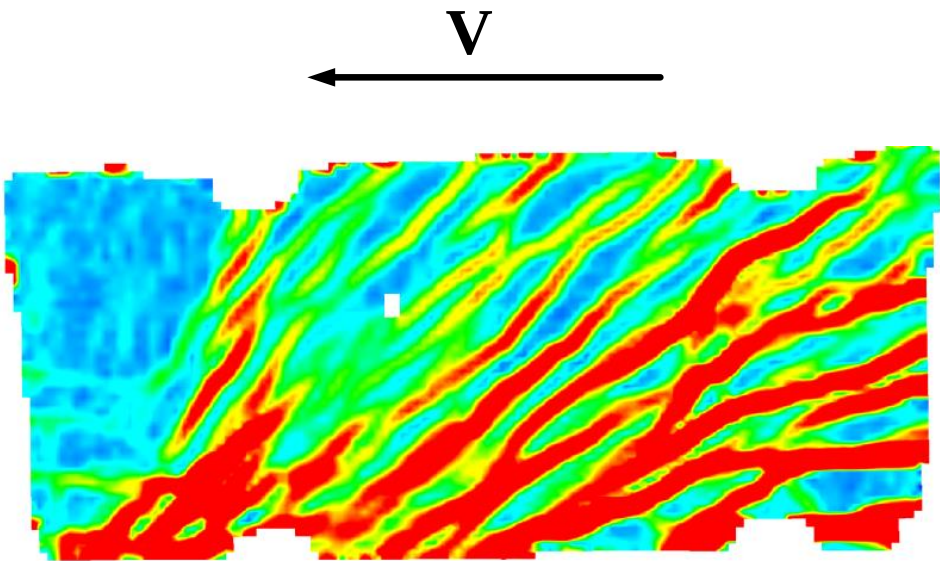

Drift ratio -1%

Figure 6-56 DIC major strain results of specimen SW-HP-0.5-2 at drift ratio 1%

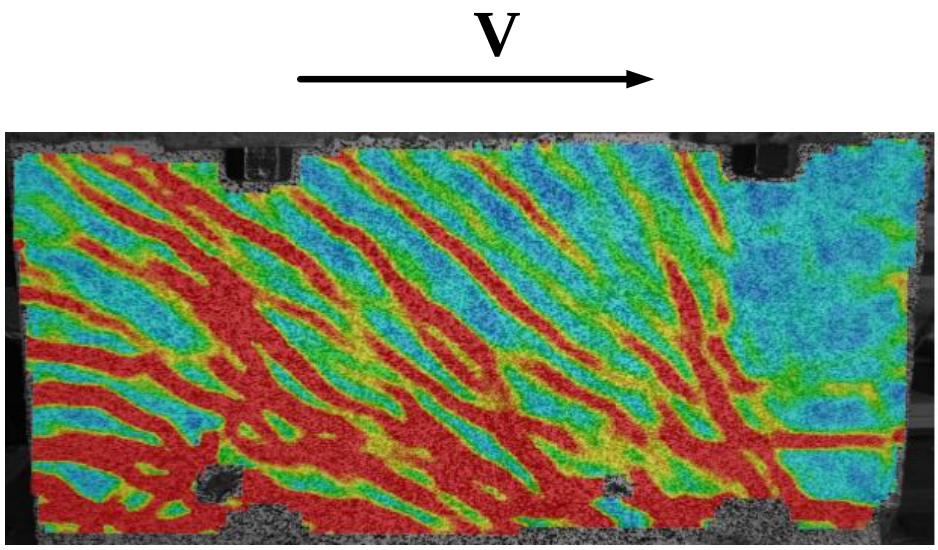

Drift ratio 1.25%

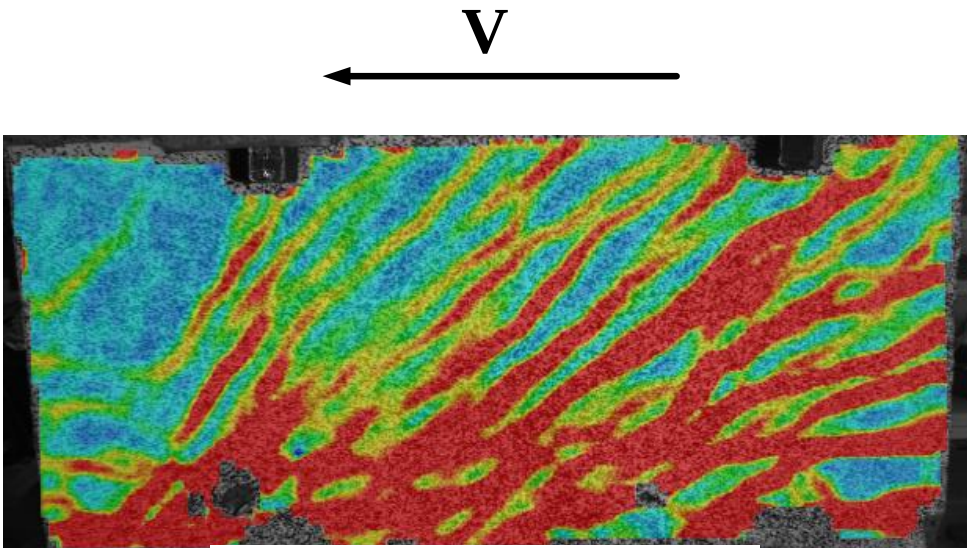

Drift ratio -1.25%

Figure 6-57 DIC major strain results of specimen SW-HP-0.5-2 at drift ratio 1.25%

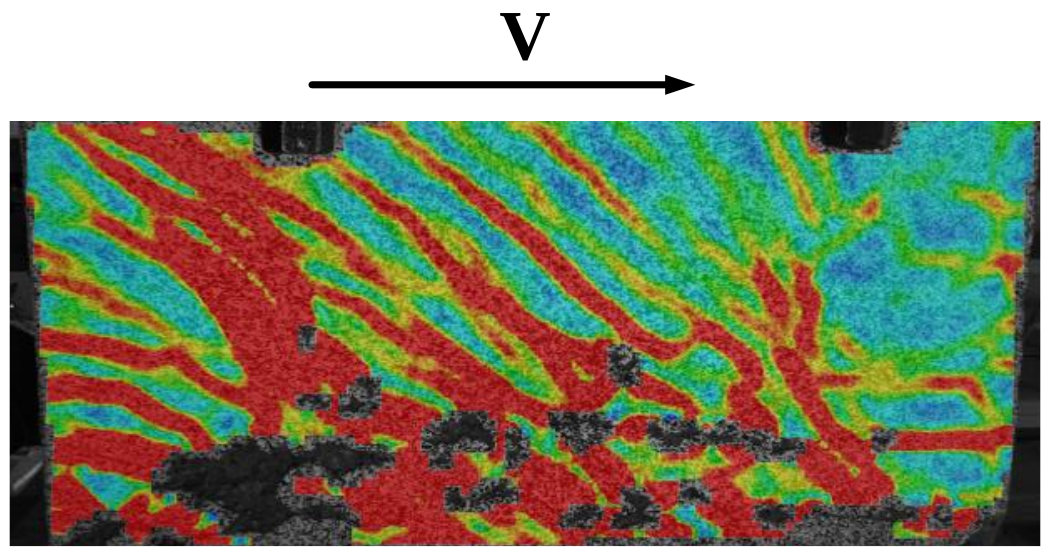

Drift ratio 1.5%

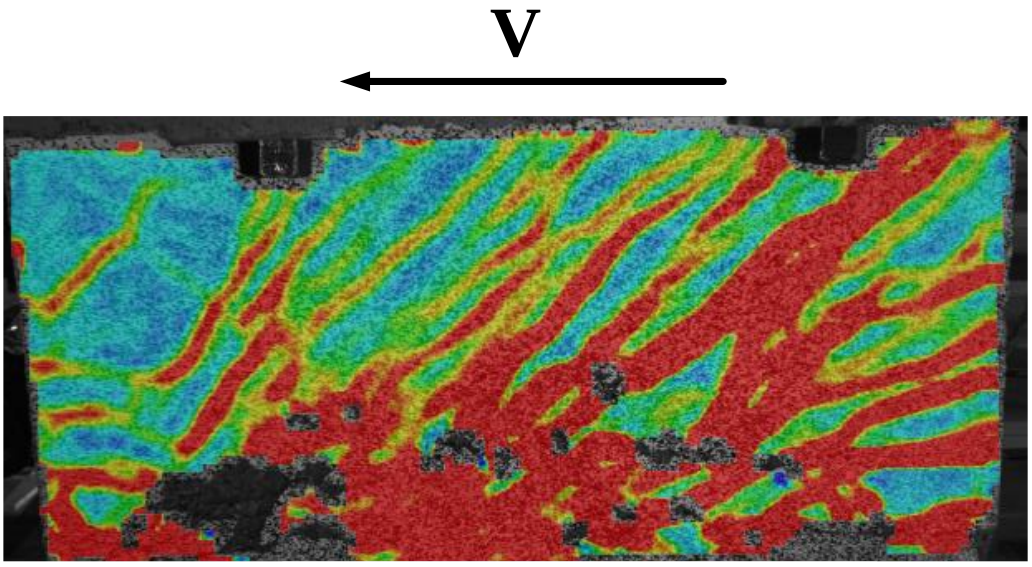

Drift ratio -1.5%

Figure 6-58 DIC major strain results of specimen SW-HP-0.5-2 at drift ratio 1.5%

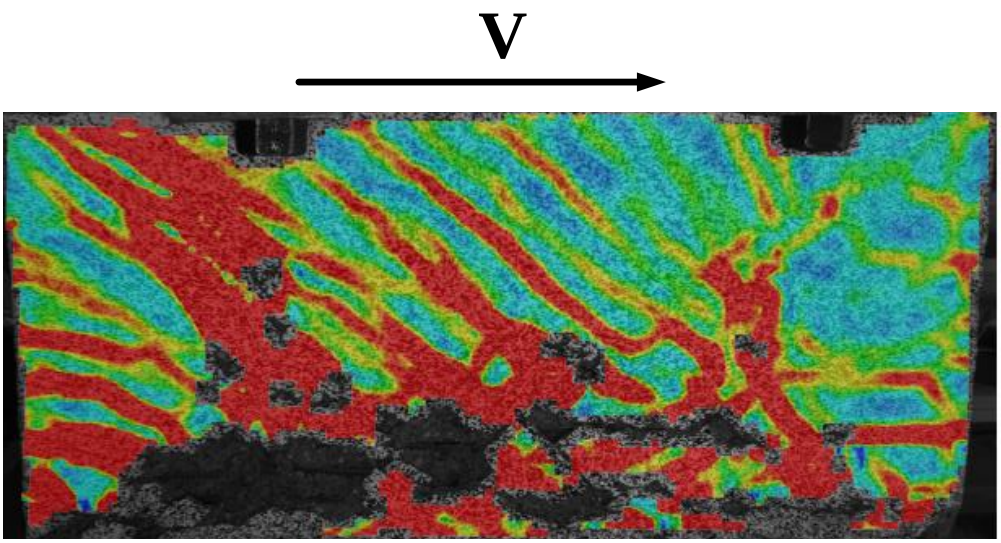

Drift ratio 1.75%

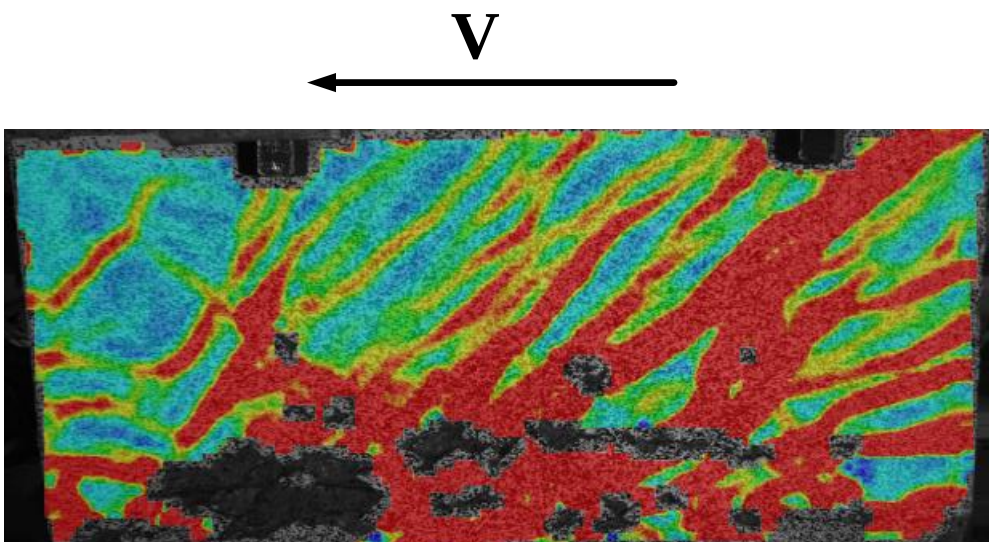

Drift ratio -1.75%

Figure 6-59 DIC major strain results of specimen SW-HP-0.5-2 at drift ratio 1.75%

6.6.2 DIC minor strain distribution

Cracks development at drift ratio 0.125%, 0.25%, 0.5%, 0.75%, 1%, 1.25%, and 1.5% are shown in Figure 6-60 to Figure 6-66. The diagonal blue lines refer to the axis of struts developed to transfer shear forces from wall's tip to the base. Diagonal struts remained undamaged until drift ratio 1.25%. Spalling of concrete cover started at 1.5% which prevents the DIC to capture the deformation of black dots on the wall face. All strain distributions have same legend values that shown at Drift ratio 0.125%.

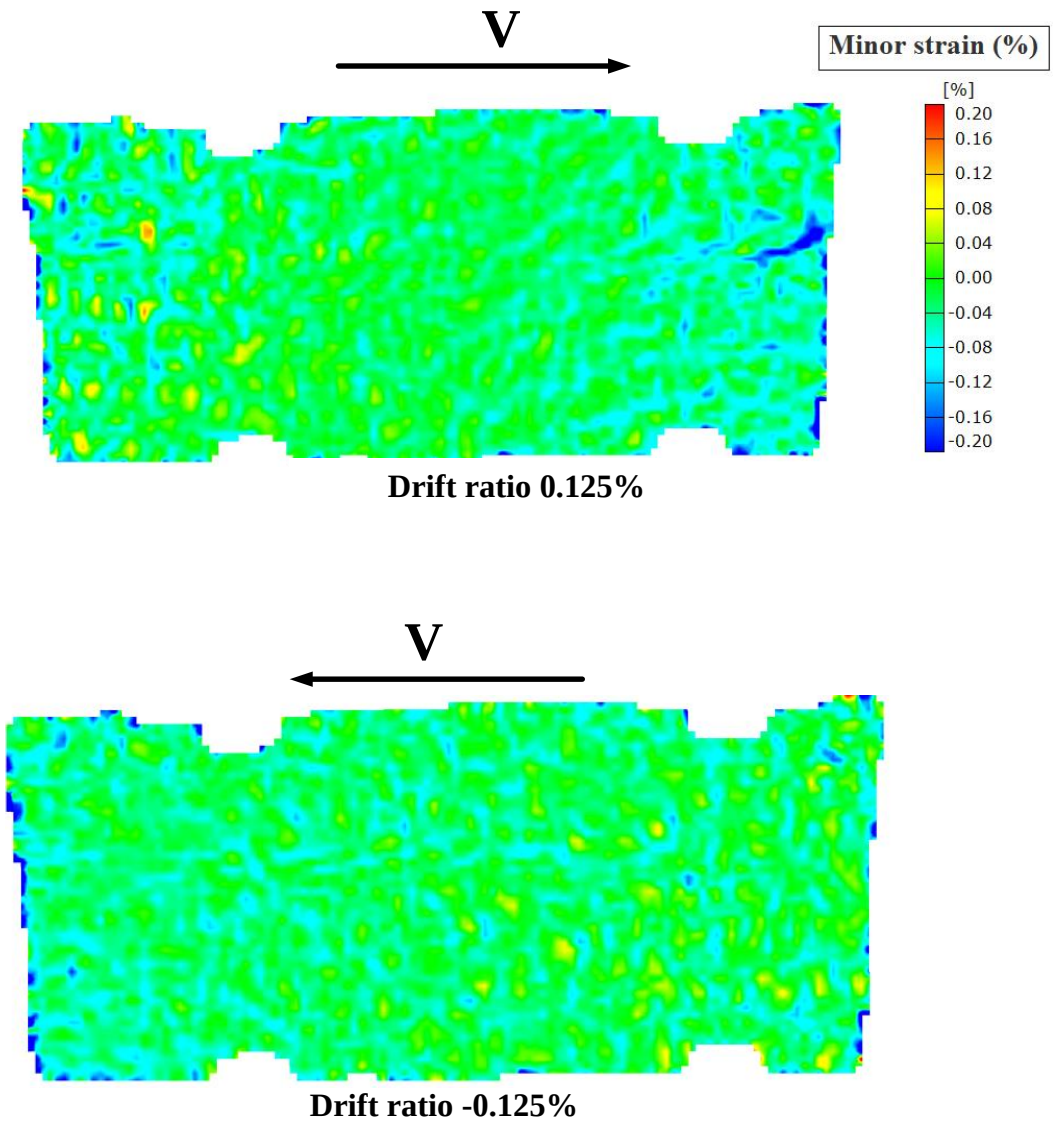

Figure 6-60 DIC minor strain results of specimen SW-HP-0.5-2 at drift ratio 0.125%

(positive strain is tension and negative strain is compression)

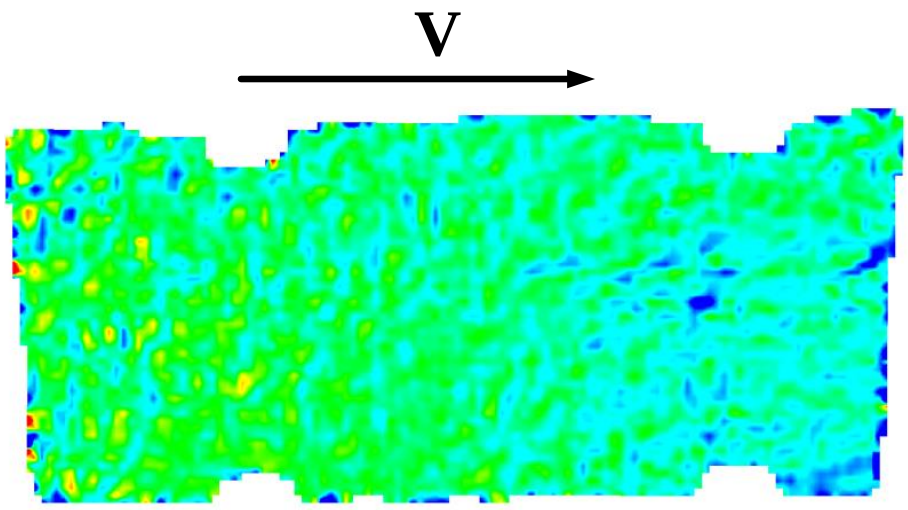

Drift ratio 0.25%

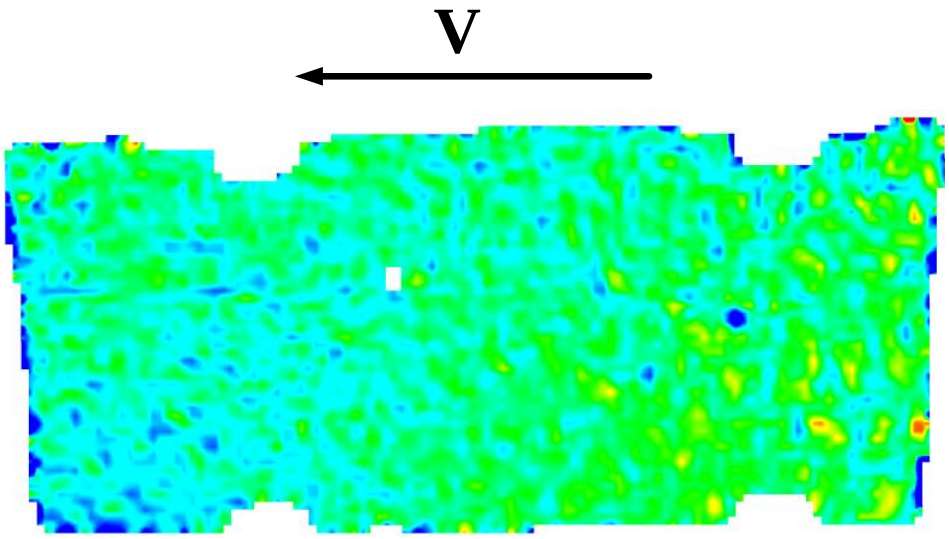

Drift ratio -0.25%

Figure 6-61 DIC minor strain results of specimen SW-HP-0.5-2 at drift ratio 0.25%

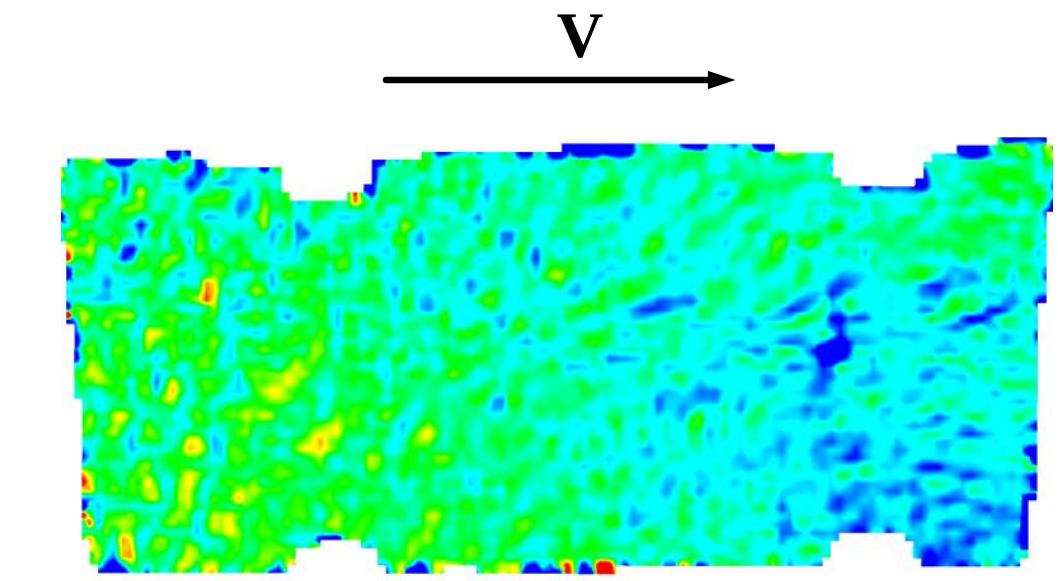

Drift ratio 0.5%

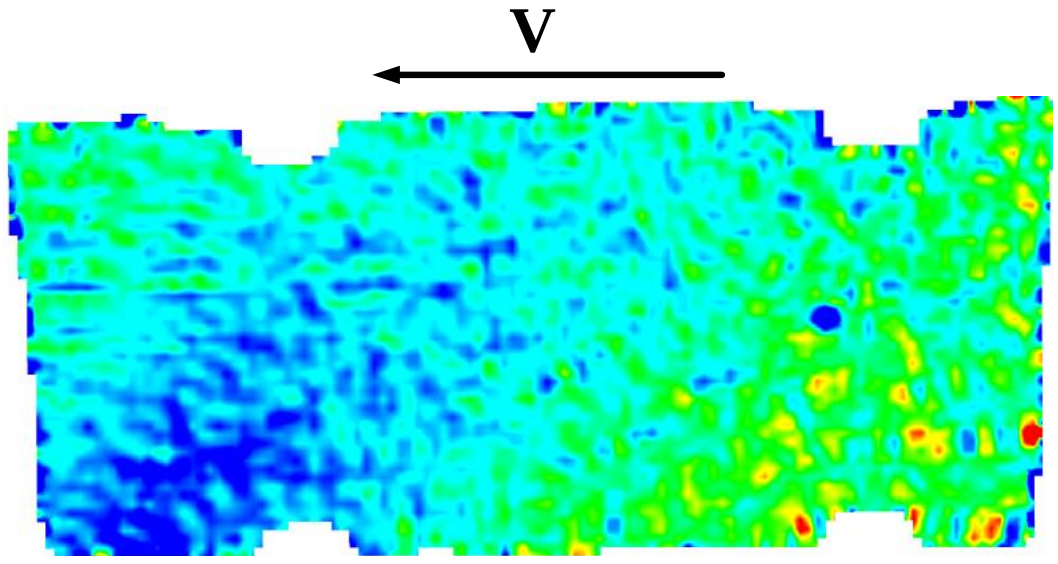

Drift ratio -0.5%

Figure 6-62 DIC minor strain results of specimen SW-HP-0.5-2 at drift ratio 0.5%

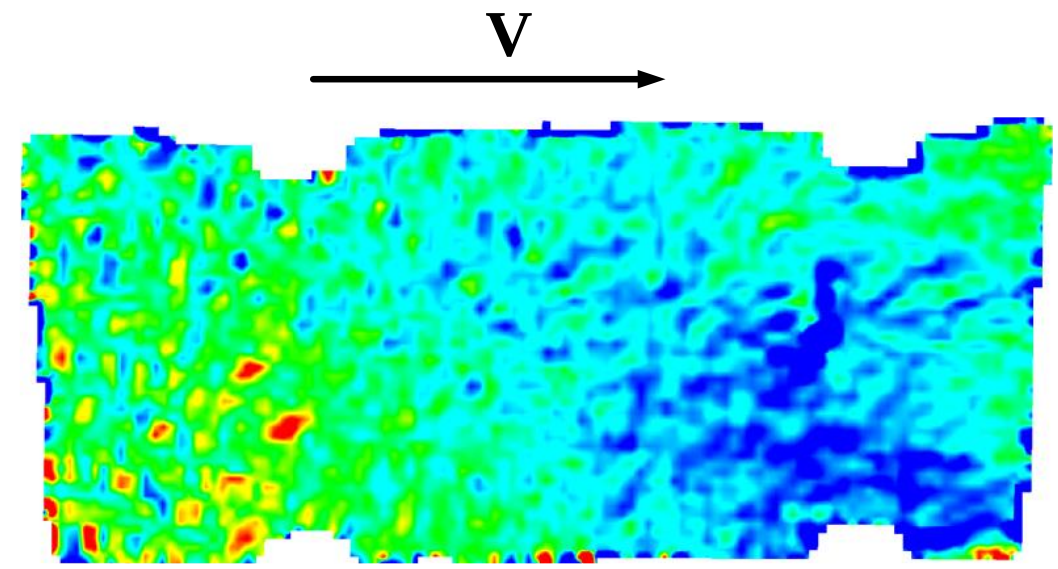

Drift ratio 0.75%

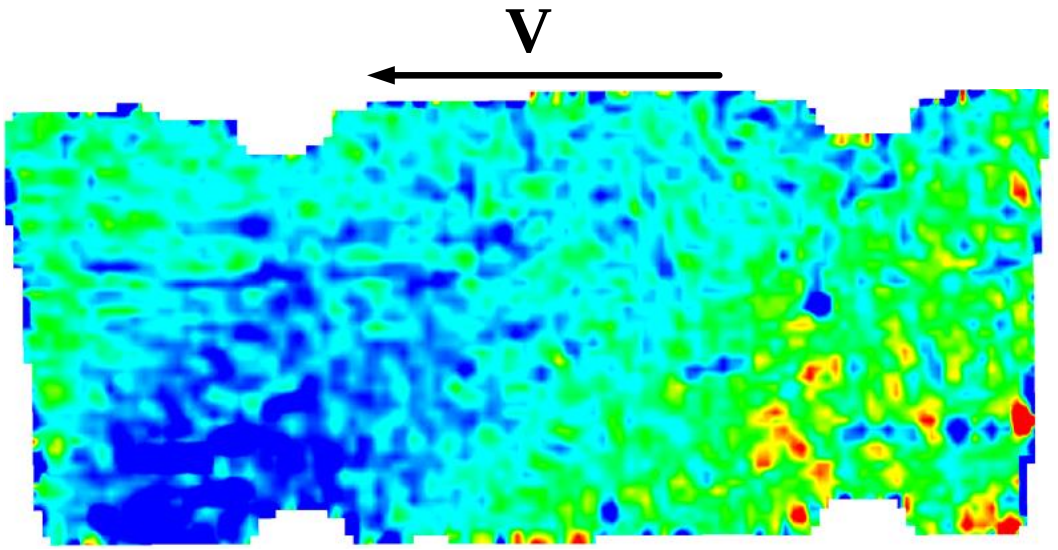

Drift ratio -0.75%

Figure 6-63 DIC minor strain results of specimen SW-HP-0.5-2 at drift ratio 0.75%

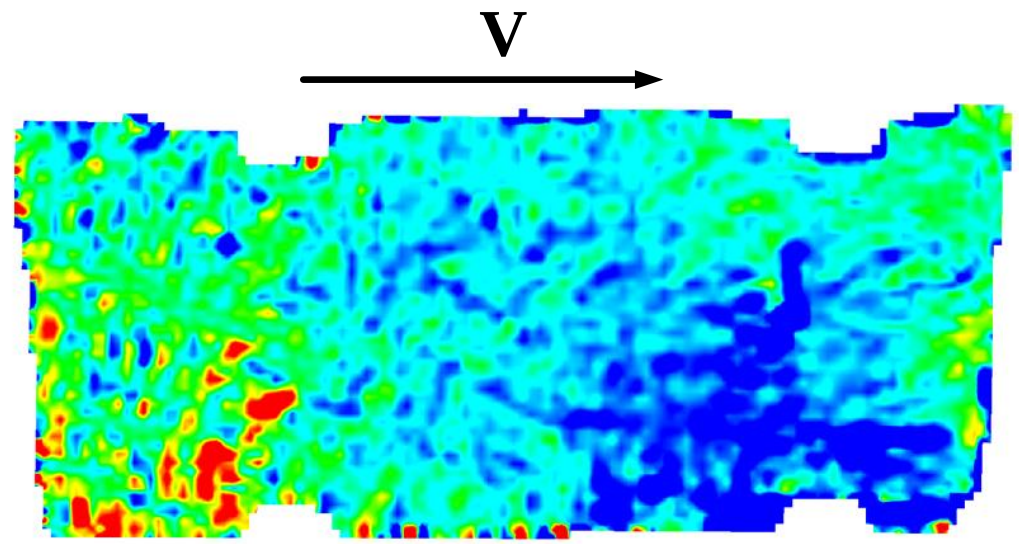

Drift ratio 1%

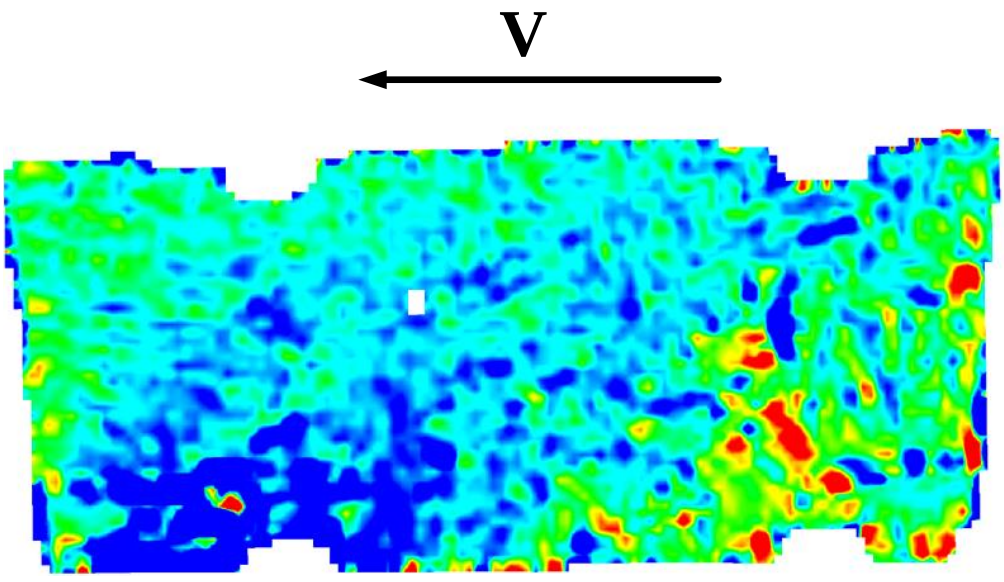

Drift ratio -1%

Figure 6-64 DIC minor strain results of specimen SW-HP-0.5-2 at drift ratio 1%

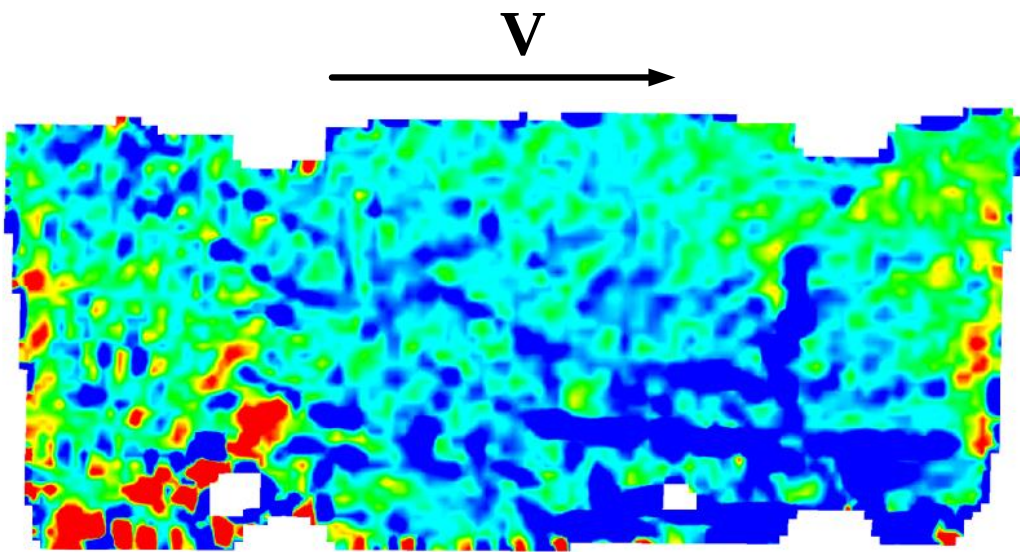

Drift ratio 1.25%

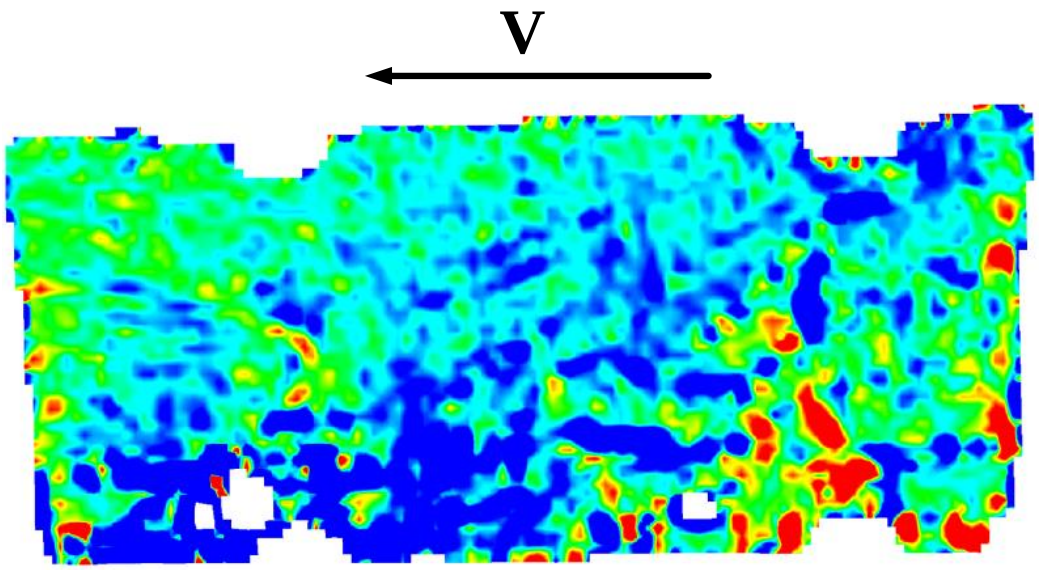

Drift ratio -1.25%

Figure 6-65 DIC minor strain results of specimen SW-HP-0.5-2 at drift ratio 1.25%

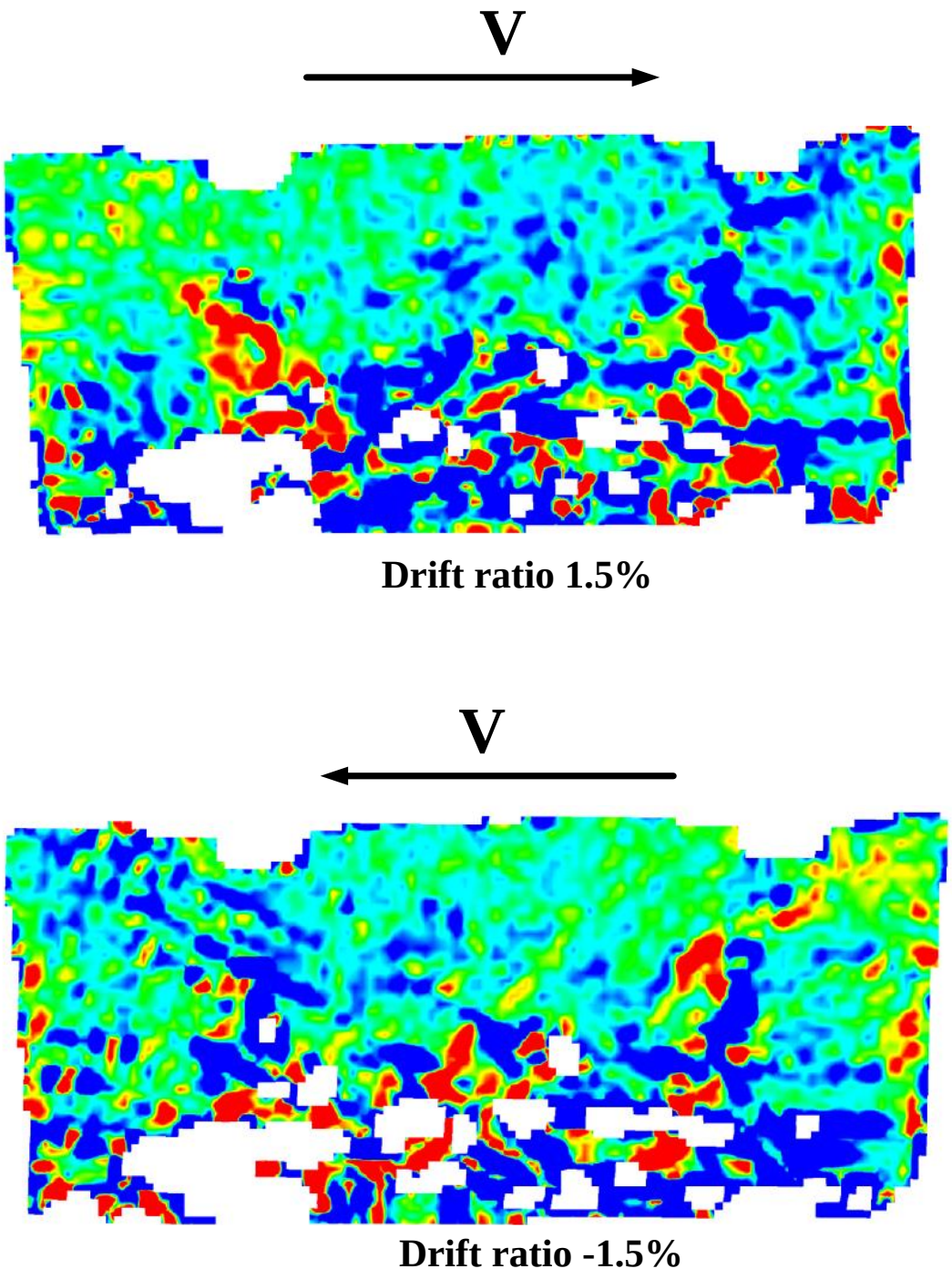

Figure 6-66 DIC minor strain results of specimen SW-HP-0.5-2 at drift ratio 1.5%

6.7 Specimen SW-MA-1.0

6.7.1 DIC major strain distribution

Cracks development at drift ratio 0.125%, 0.25%, 0.5%, 0.75%, and 1% are shown in Figure 6-67 to Figure 6-71. The diagonal red lines refer to the axis of struts developed to transfer shear forces from wall's tip to the base, while the horizontal red lines represent the flexural cracks due to bending stresses. Diagonal struts remained intact until drift ratio 0.75%. Sliding shear failure commenced at drift ratio 1%, DIC cannot capture deformations of crushed regions. All strain distributions have same legend values that shown at Drift ratio 0.125%.

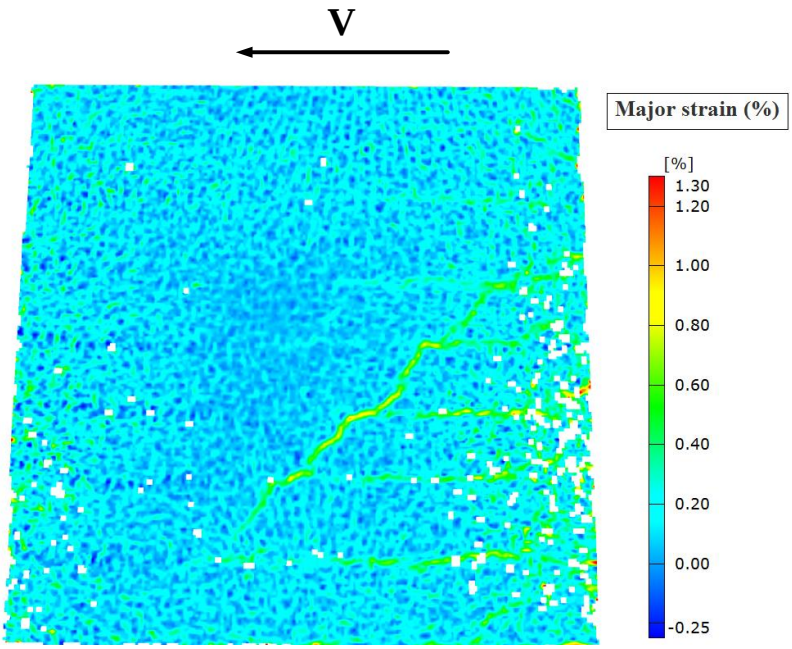

Drift ratio 0.125%

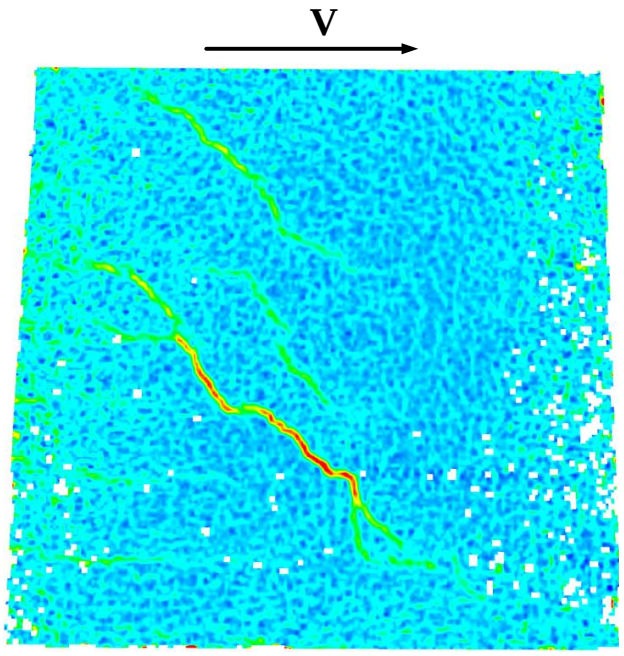

Drift ratio -0.125%

Figure 6-67 DIC major strain results of specimen SW-MA-1.0 at drift ratio 0.125% (positive strain is tension and negative strain is compression)

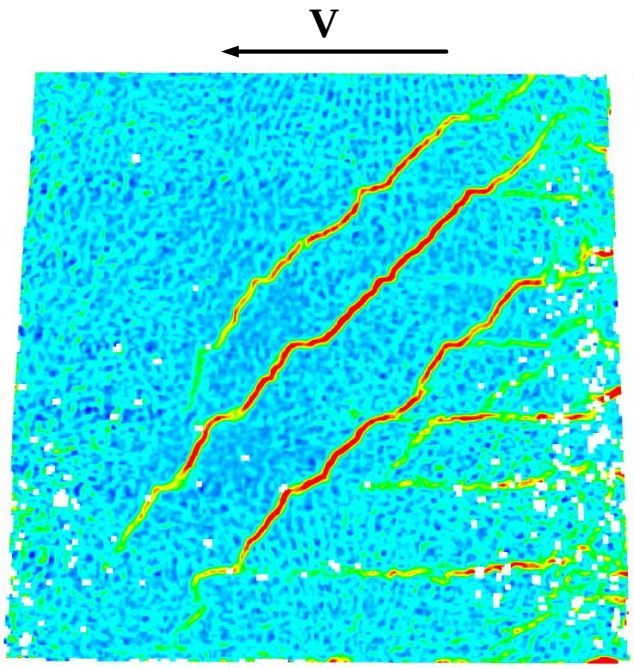

Drift ratio 0.25%

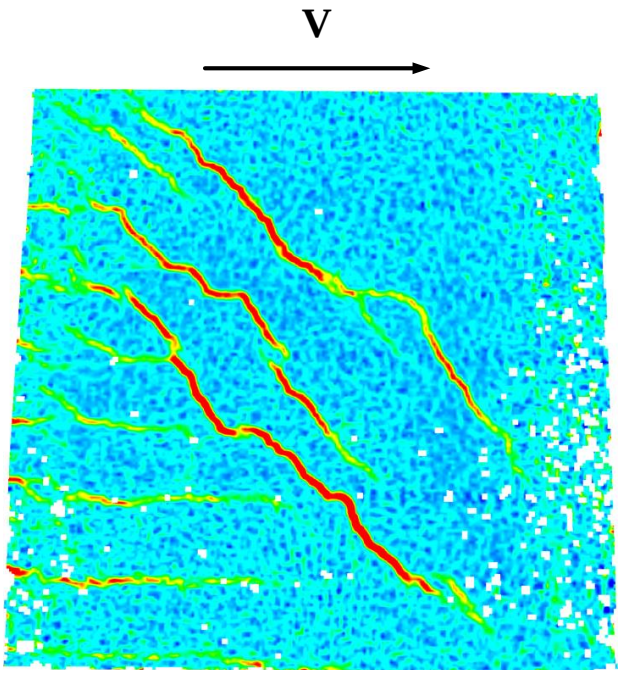

Drift ratio -0.25%

Figure 6-68 DIC major strain results of specimen SW-MA-1.0 at drift ratio 0.25%

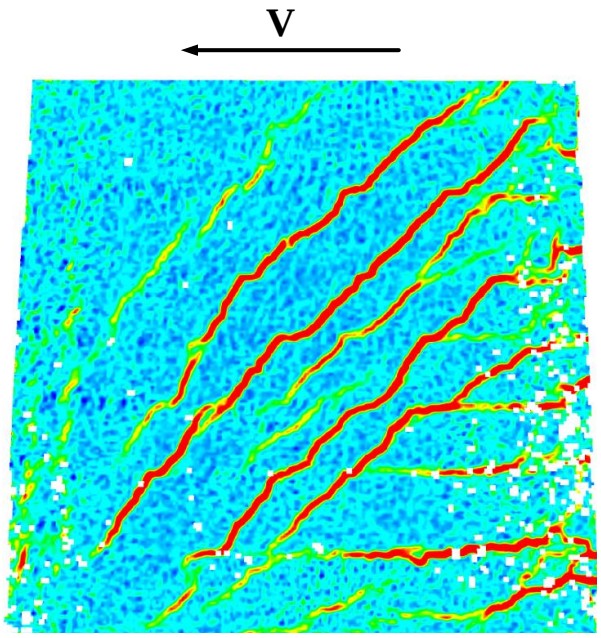

Drift ratio 0.5%

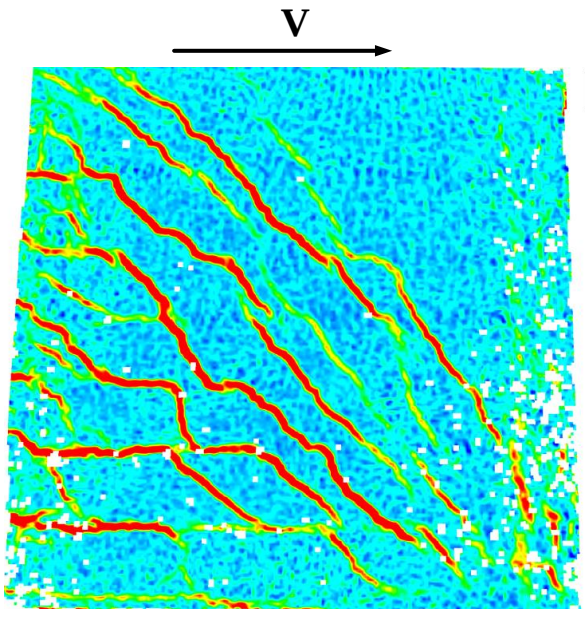

Drift ratio -0.5%

Figure 6-69 DIC major strain results of specimen SW-MA-1.0 at drift ratio 0.5%

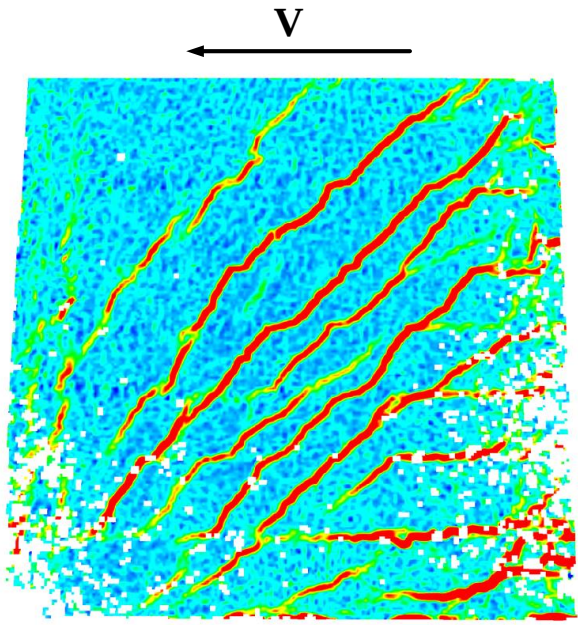

Drift ratio 0.75%

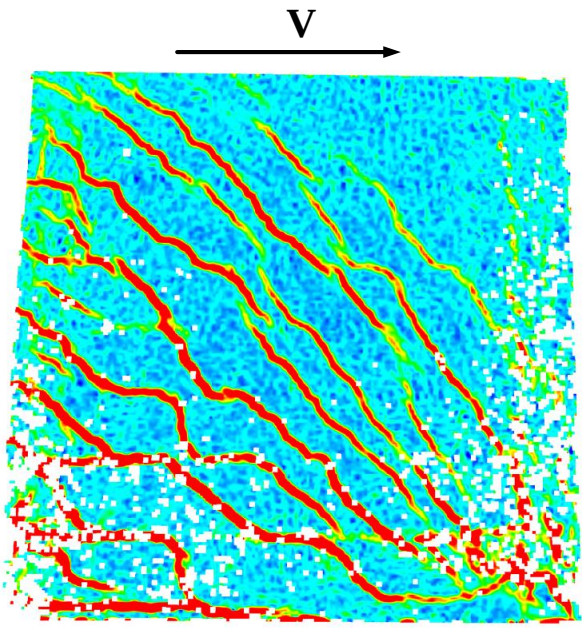

Drift ratio -0.75%

Figure 6-70 DIC major strain results of specimen SW-MA-1.0 at drift ratio 0.75%

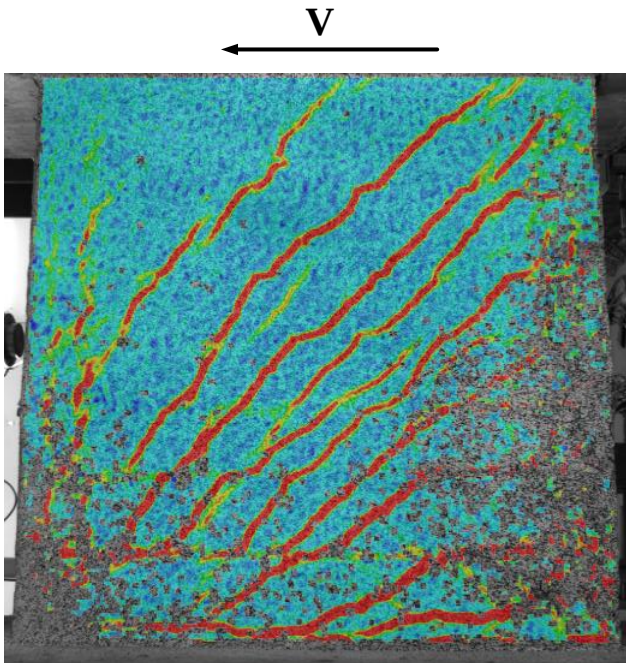

Drift ratio 1%

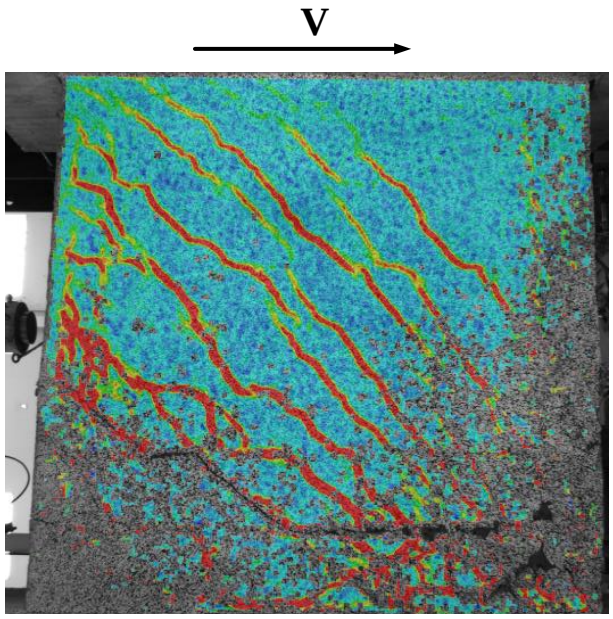

Drift ratio -1%

Figure 6-71 DIC major strain results of specimen SW-MA-1.0 at drift ratio 1%

6.8 Specimen SW-MP-1.0-1

6.8.1 DIC major strain distribution

Cracks development at drift ratio 0.125%, 0.25%, 0.5%, 0.75%, and 1% are shown in Figure 6-72 to Figure 6-76. Cracks developed along the diagonal compressive struts until 0.75% drift ratio. For walls of aspect ratio 1:1, it was observed that one inclined strut was responsible to carry forces from the tip of wall to its base, the base width is 0.25 wall length. The gap between steel cages was 5 inches which was not enough to confine the concrete at wall web. Therefore, a sudden shear strength drop observed at drift ratio 0.75% due to diagonal tension failure. All strain distributions have same legend values that shown at Drift ratio 0.125%.

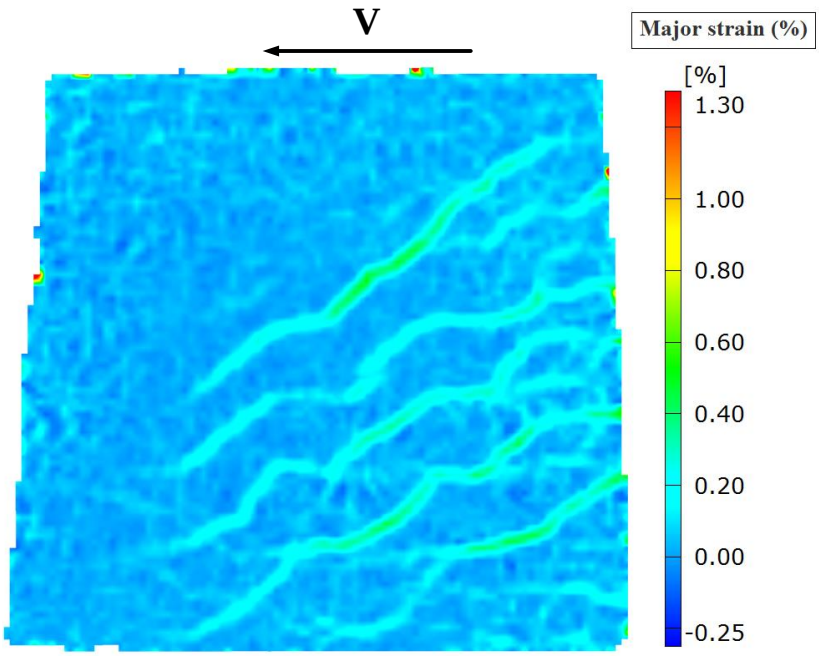

Drift ratio 0.125%

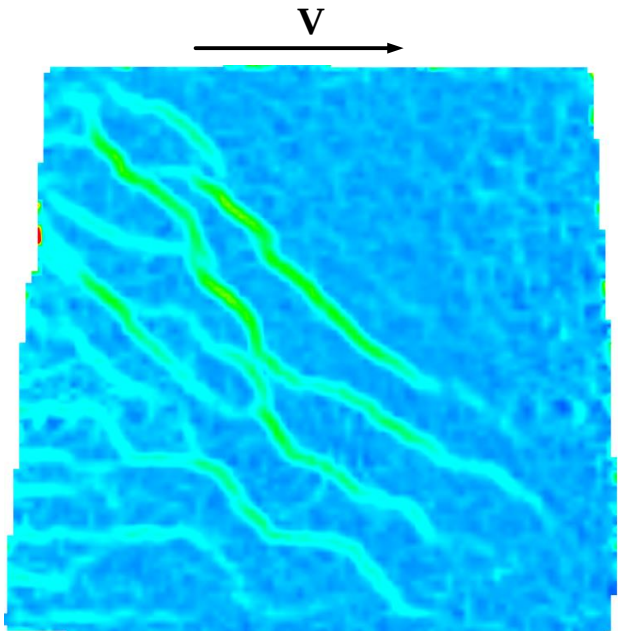

Drift ratio -0.125%

Figure 6-72 DIC major strain results of specimen SW-MP-1.0-1 at drift ratio 0.125% (positive strain is tension and negative strain is compression)

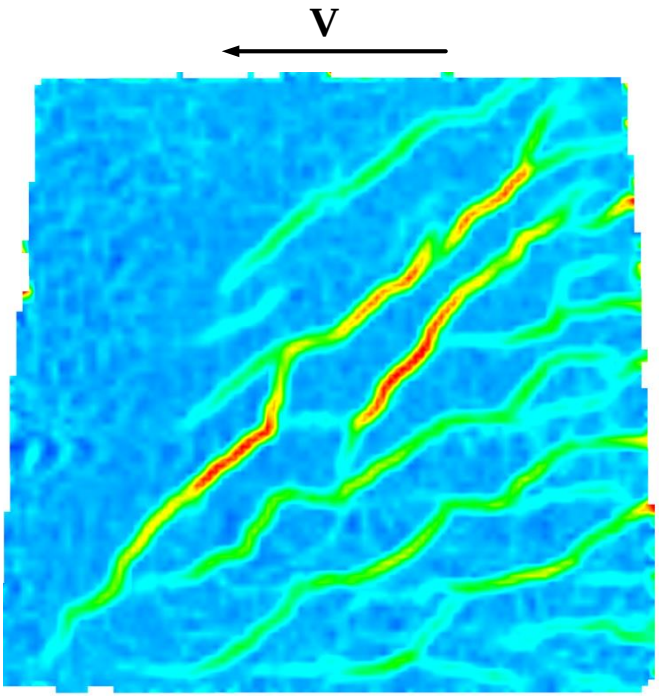

Drift ratio 0.25%

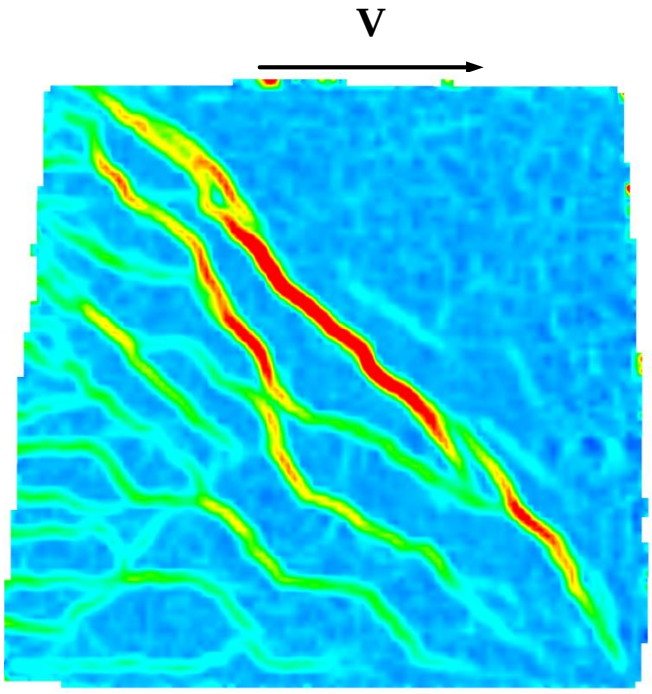

Drift ratio -0.25%

Figure 6-73 DIC major strain results of specimen SW-MP-1.0-1 at drift ratio 0.25%

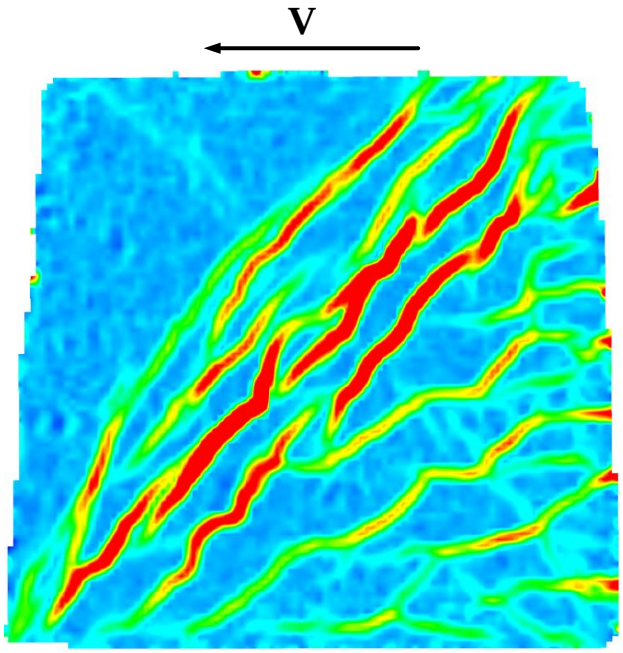

Drift ratio 0.5%

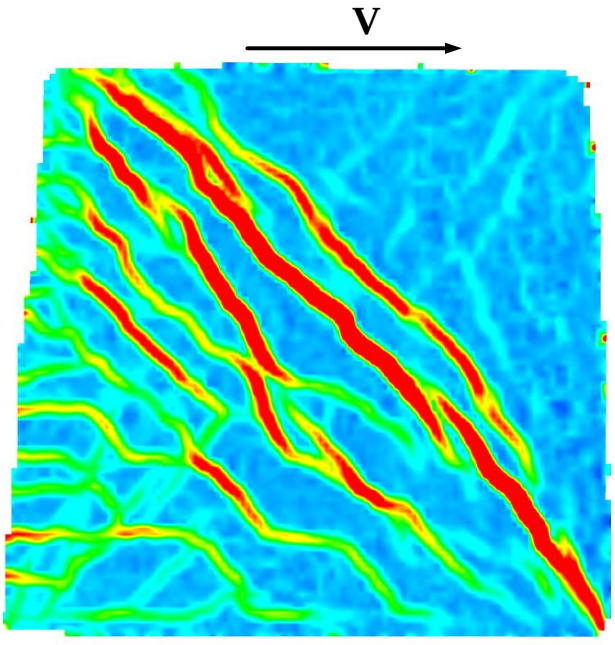

Drift ratio -0.5%

Figure 6-74 DIC major strain results of specimen SW-MP-1.0-1 at drift ratio 0.5%

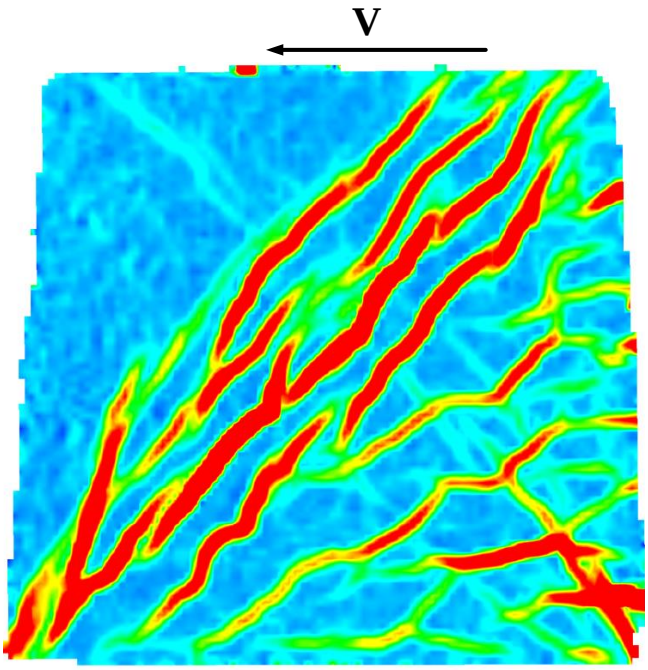

Drift ratio 0.75%

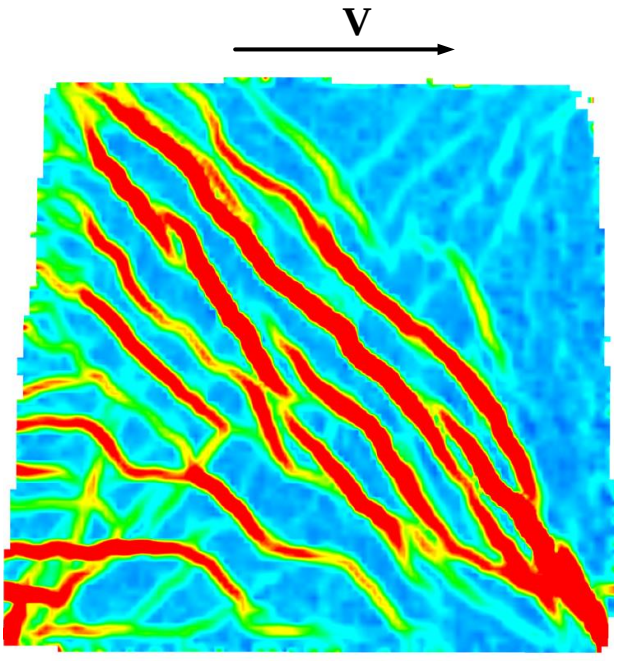

Drift ratio -0.75%

Figure 6-75 DIC major strain results of specimen SW-MP-1.0-1 at drift ratio 0.75%

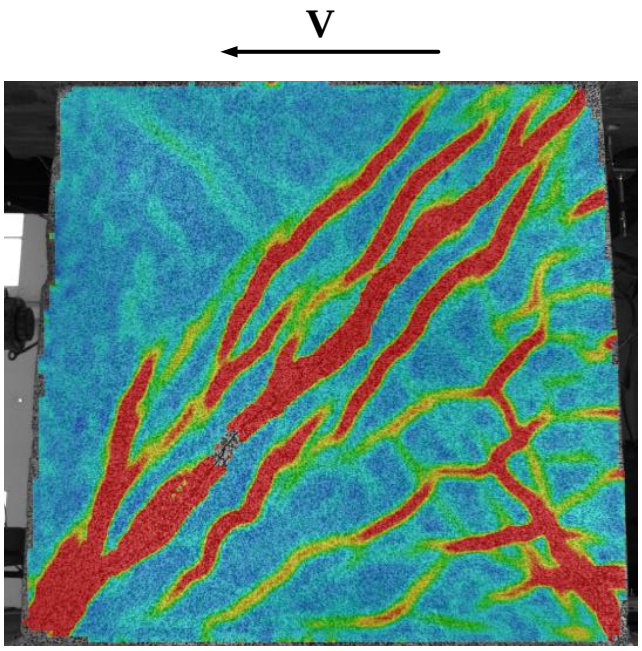

Drift ratio 1%

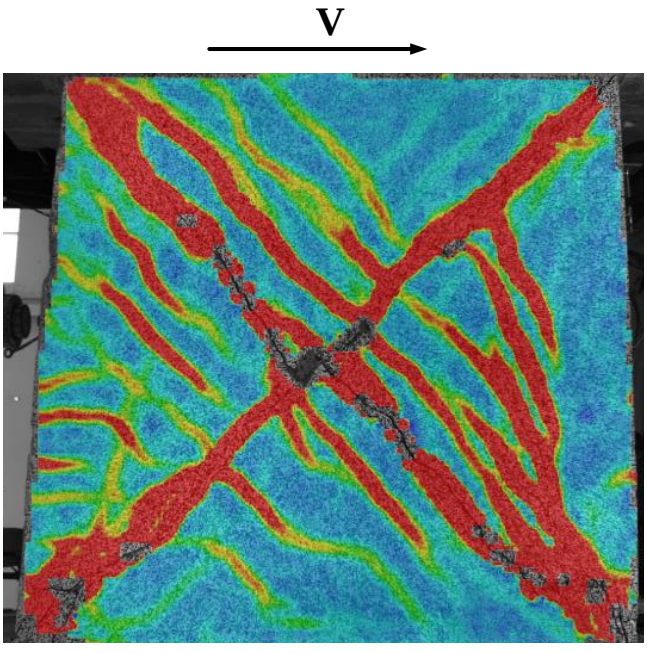

Drift ratio -1%

Figure 6-76 DIC major strain results of specimen SW-MP-1.0-1 at drift ratio 1%

6.8.2 DIC Minor strain distribution

Cracks development at drift ratio 0.125%, 0.25%, 0.5%, 0.75%, and 1% are shown in Figure 6-60 to Figure 6-66. The diagonal blue lines refer to the axis of struts developed to transfer shear forces from wall's tip to the base. Diagonal struts remained undamaged until drift ratio 0.75%. diagonal tension failure started at 1.0% which prevents the DIC to capture the deformation of black dots on the wall face. All strain distributions have same legend values that shown at Drift ratio 0.125%.

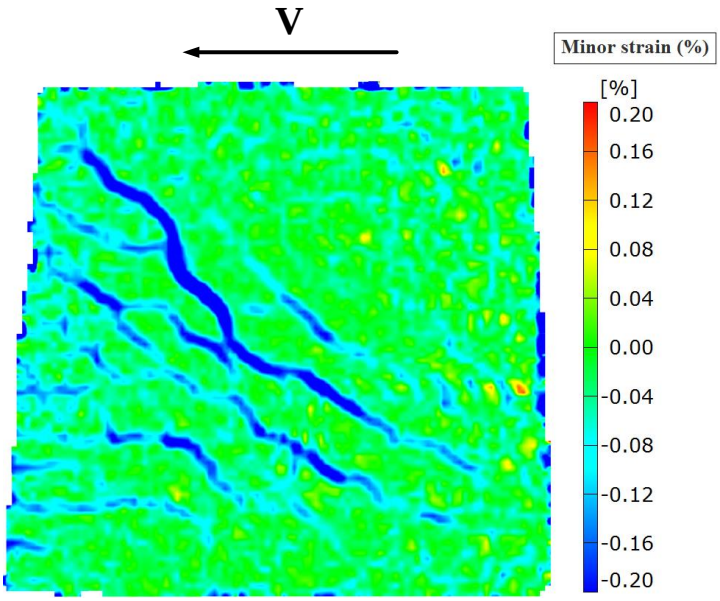

Drift ratio 0.125%

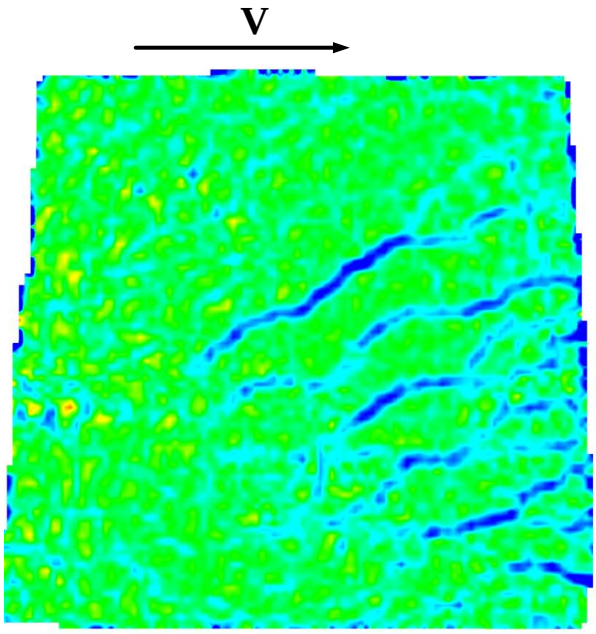

Drift ratio -0.125%

Figure 6-77 DIC minor strain results of specimen SW-MP-1.0-1 at drift ratio 0.125%

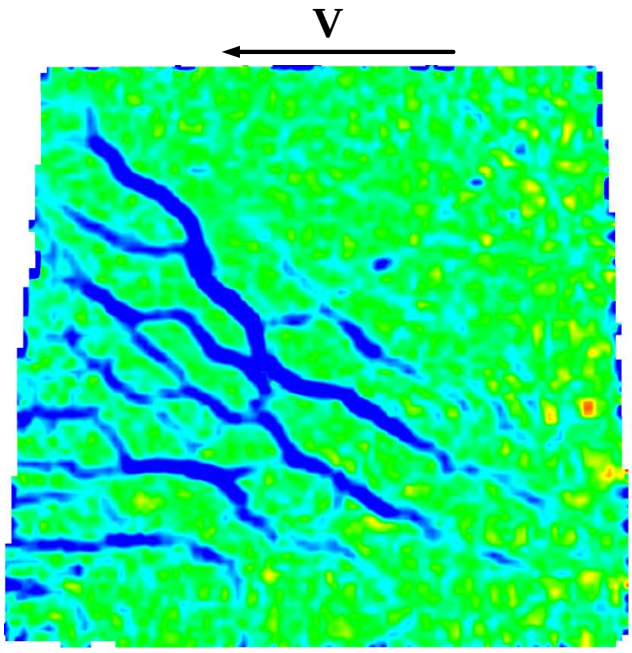

Drift ratio 0.25%

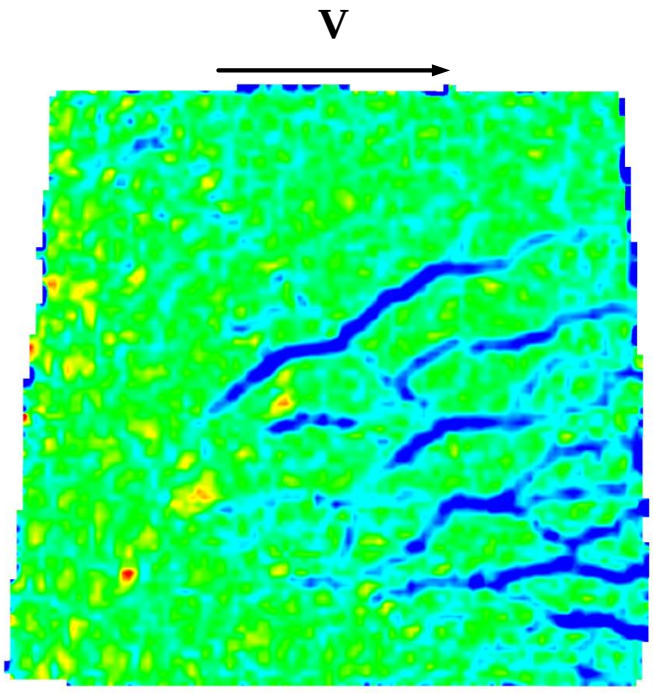

Drift ratio -0.25%

Figure 6-78 DIC minor strain results of specimen SW-MP-1.0-1 at drift ratio 0.25%

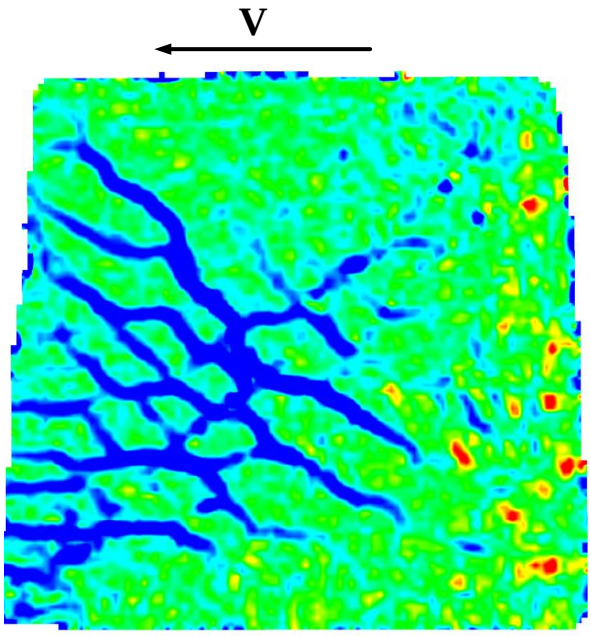

Drift ratio 0.5%

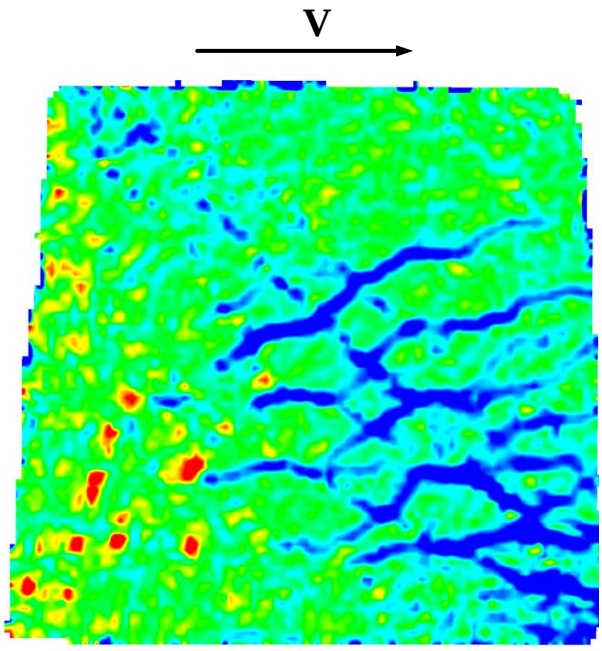

Drift ratio -0.5%

Figure 6-79 DIC minor strain results of specimen SW-MP-1.0-1 at drift ratio 0.5%

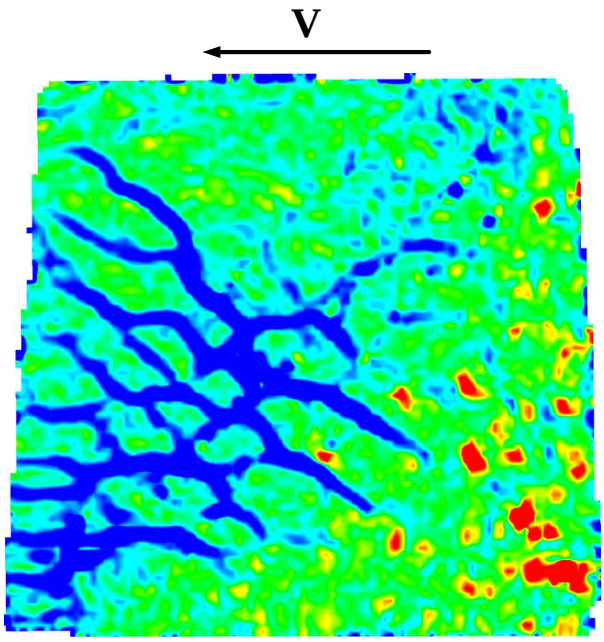

Drift ratio 0.75%

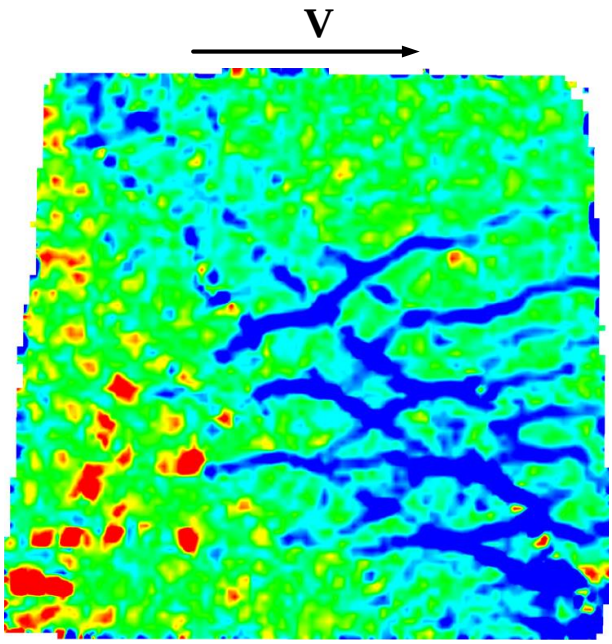

Drift ratio -0.75%

Figure 6-80 DIC minor strain results of specimen SW-MP-1.0-1 at drift ratio 0.75%

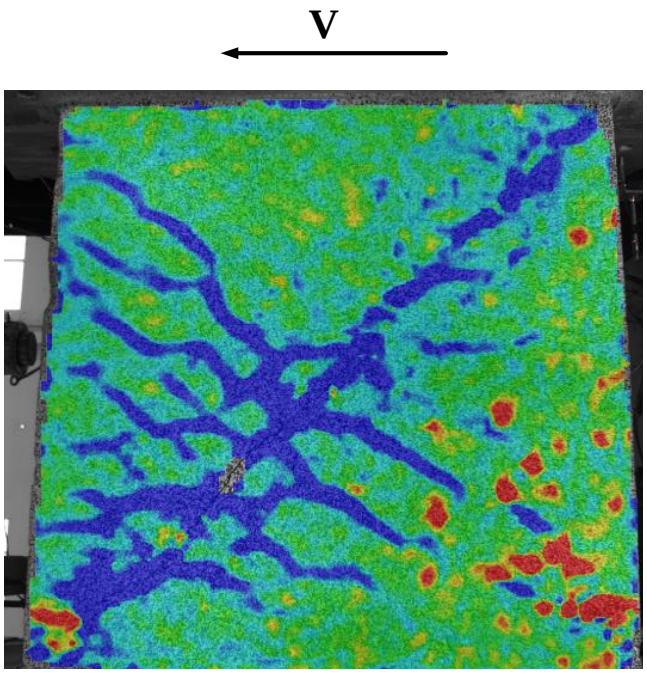

Drift ratio 1%

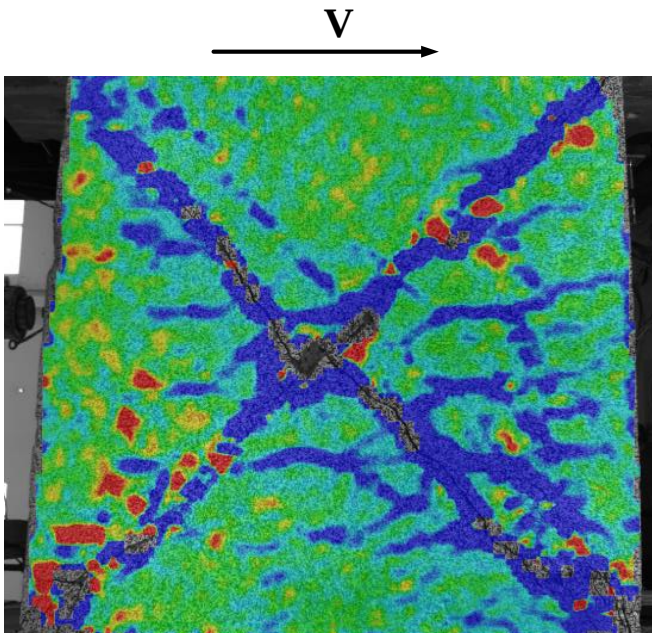

Drift ratio -1%

Figure 6-81 DIC minor strain results of specimen SW-MP-1.0-1 at drift ratio 1%

Chapter 7

Discussions and Analysis

7.1. Introduction

The available squat shear wall failure mechanisms are insufficient to precisely explain the sliding shear failure which is the most mode that squat walls suffer from. In this study an accurate sliding shear failure mechanism is presented based on the tested squat walls and using the sophisticated techniques to evaluate deformations and strain distribution over the wall face during the tests. In addition, the plausible flexural failure of the proposed walls was discussed.

Perform 3D software was used to model the squat wall having different shear force vs drift behavior (Proposed walls, ACI-compliant walls or Proposed walls with reduced strength), the analysis was carried on to study the effect of drift ductility on wall response due to earthquake records and to quantify the safety reduction factor for proposed walls compared to the ACI-compliant walls.

7.2. Sliding shear failure mechanism

Shear force transfer from the wall tip to its base follows the strut and tie model. The tie consists of longitudinal reinforcement located in two-thirds of wall length, while the struts have base width of L/2. as shown in Figure 7-1a and Figure 7-1b. In conventional walls designed by ACI 318-19 provisions, struts located at the wall web are less confined compared to the wall boundaries, as a result, wall shear strength drops due to crushing of web struts, as shown in Figure 7-1b. Consequently, struts crushing propagate toward wall boundaries due to the applied loading in the opposite direction as illustrated in Figure 7-1c, thereby leading to the sliding shear failure. Figure 7-1d highlights the most critical trapezoidal zone that causes sliding shear failures. The zone consists of three triangles;

the middle triangle which sustains only compressive stresses on both reversed cyclic directions, both outside triangles sustain flexural and compressive stresses. Strut crushing starts at the middle triangle if the web is not confined, while strut crushing commences at outside triangles if the boundaries are not well-confined.

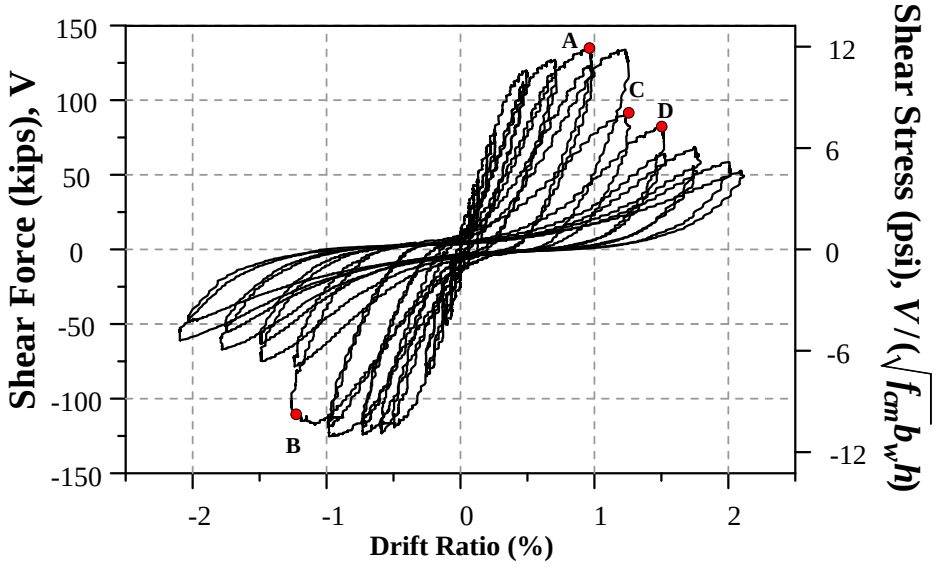

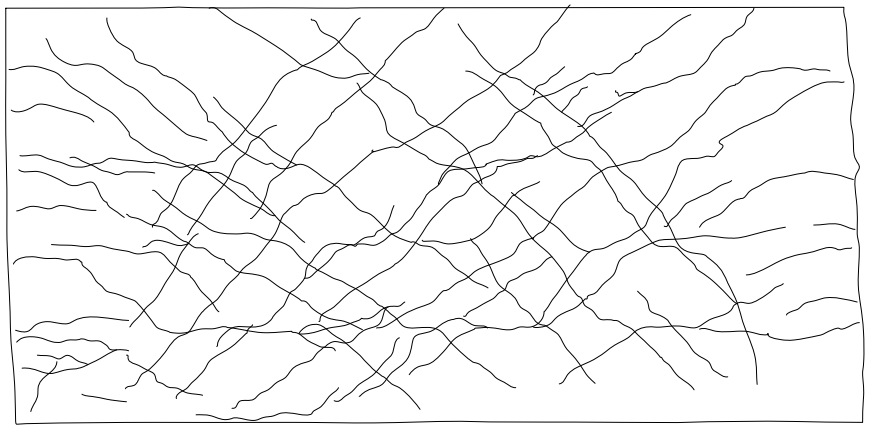

(a)

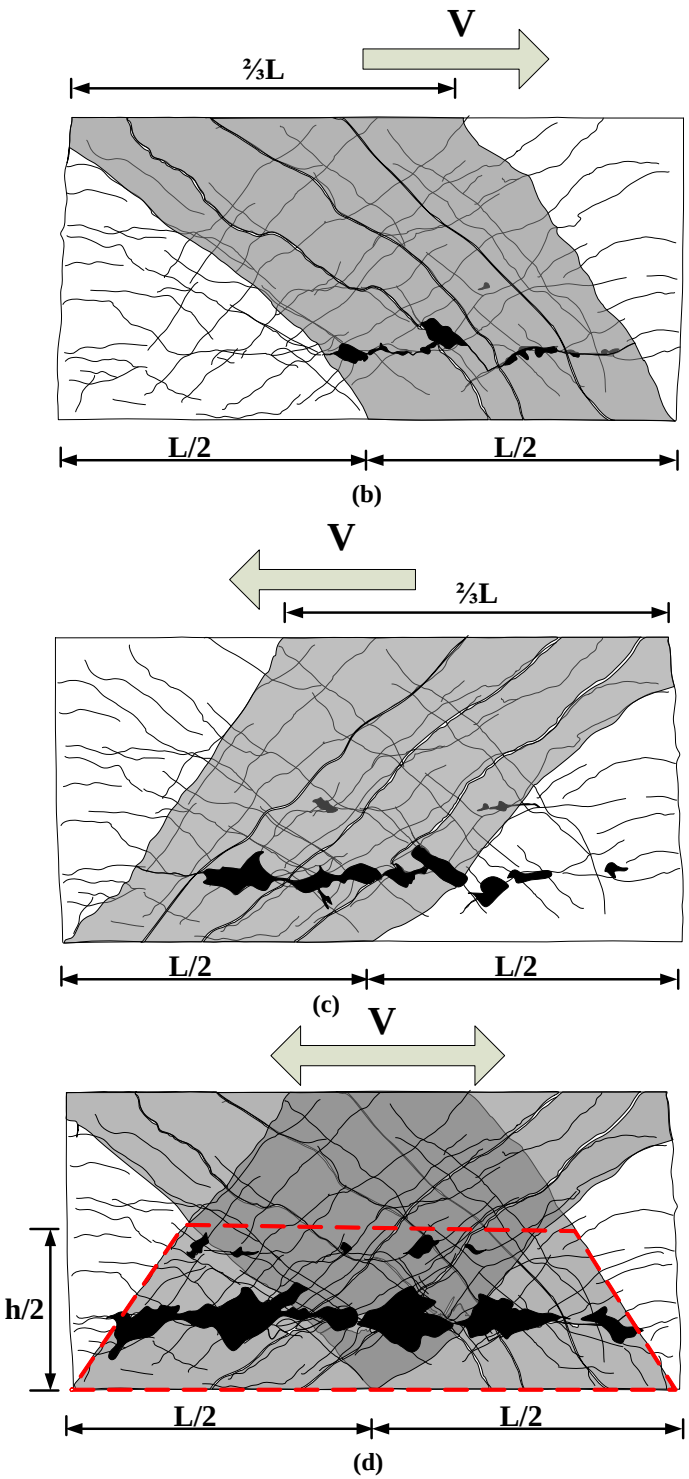

Figure 7-1 Sliding shear mechanism for ACI 0.5- aspect-ratio walls.

7.3. DIC-based Sliding shear failure mechanism

The Digital Image Correlation (DIC) is widely used to capture specimen displacement and strain during the test. One of each wall faces was painted by plain white then black dots, the X, Y, and Z displacement of each point on the wall face was recorded using two-calibrated cameras. The images were post-processed to measure strain profiles (Figure 7-2) after the end of each test. The tensile concrete strain with highest strain value of 0.01(for red bands) at different drift ratios. Figure 7-2 illustrates sliding shear formation for specimen SW-HA-0.5. The weakening zone (Figure 7-2c) developed due to cyclic flexural and compressive stresses at wall boundaries (Figure 7-2a and b). This weakening zone propagates to form the sliding plane due to connecting the diagonal compressive struts to the flexural cracks (Figure 7-2d) thereby leading the sudden sliding shear failure (Figure 7-2e).

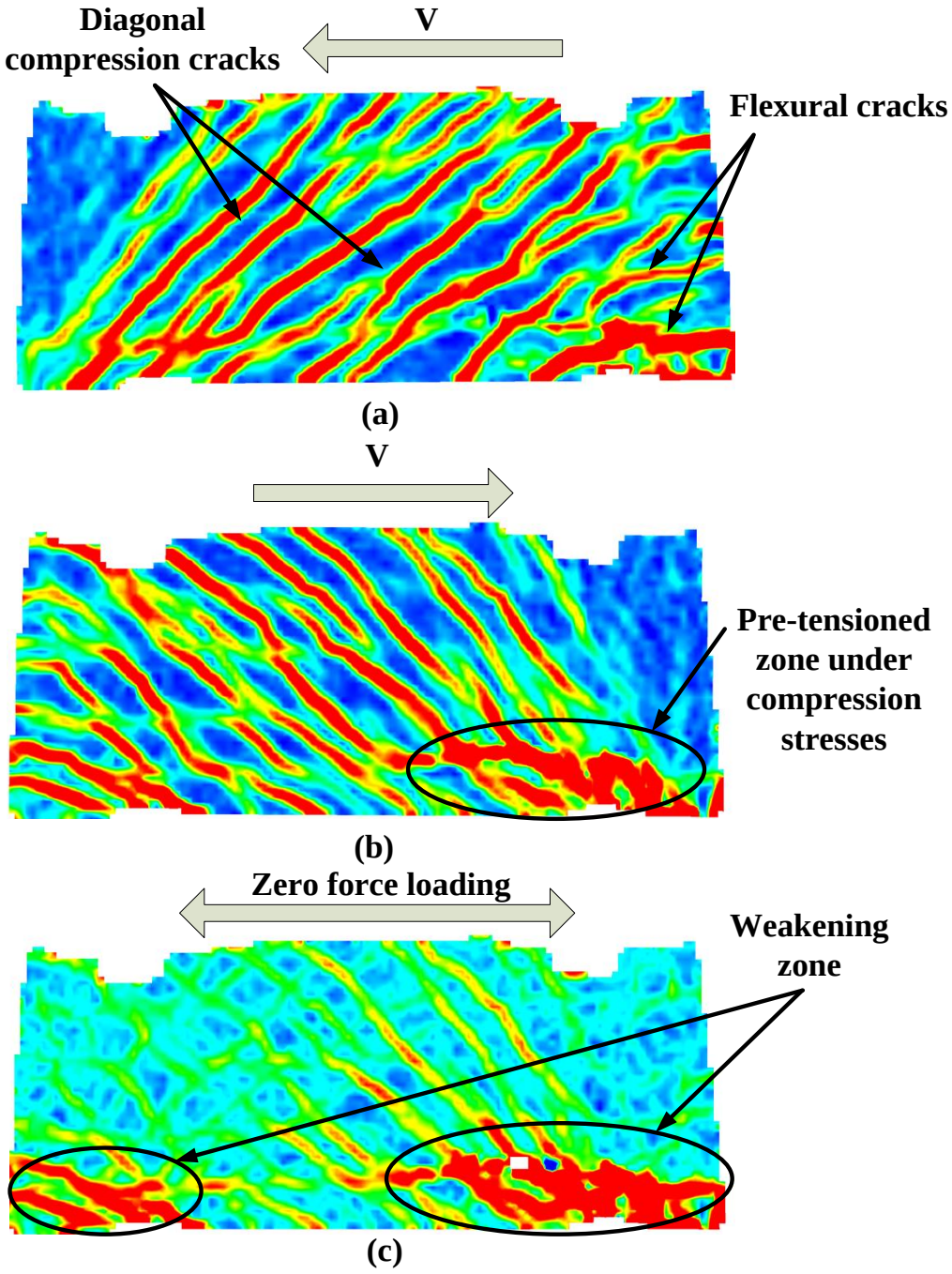
Diagonal
compression cracks
V
Flexural cracks
(a)
V
Pre-tensioned
zone under
compression
stresses
(b)
Zero force loading
Weakening
zone
(c)

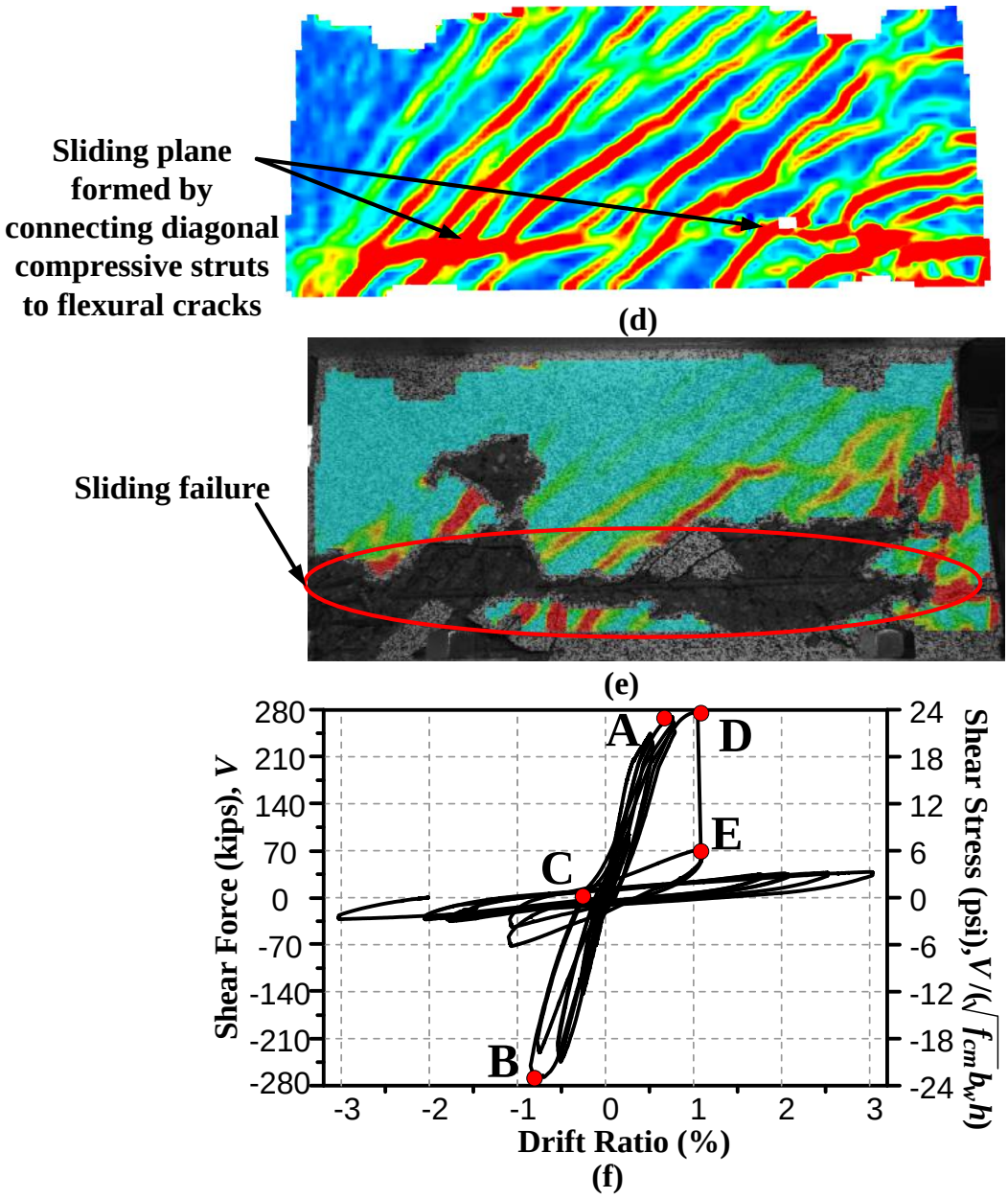

Figure 7-2 Formation of sliding shear failure for SW-HA-0.5.

7.4. Failure mechanism of Proposed squat shear walls

Diagonal and flexural cracks develop to transfer the shear stresses, the wall boundaries are the most highly stressed region, the stresses sources are 1) compressive stresses due to bending moment; 2) diagonal compressive stresses transferred throughout the diagonal struts. Wall boundaries and the web are well-confined, therefore concrete deterioration commences at the highly stressed boundaries as shown in (Figure 7-3a and b). Although the concrete crushing initiated at drift ratio 1.25%, the shear strength reached a plateau and did not drop before drift ratio 3% (Figure 7-3c and d), this indicates the benefit of web confinement to prevent sliding failure formation, instead the failure mode is flexural failure which represents the most plausible mode to prevent sudden failures and makes structural behavior of buildings more ductile.

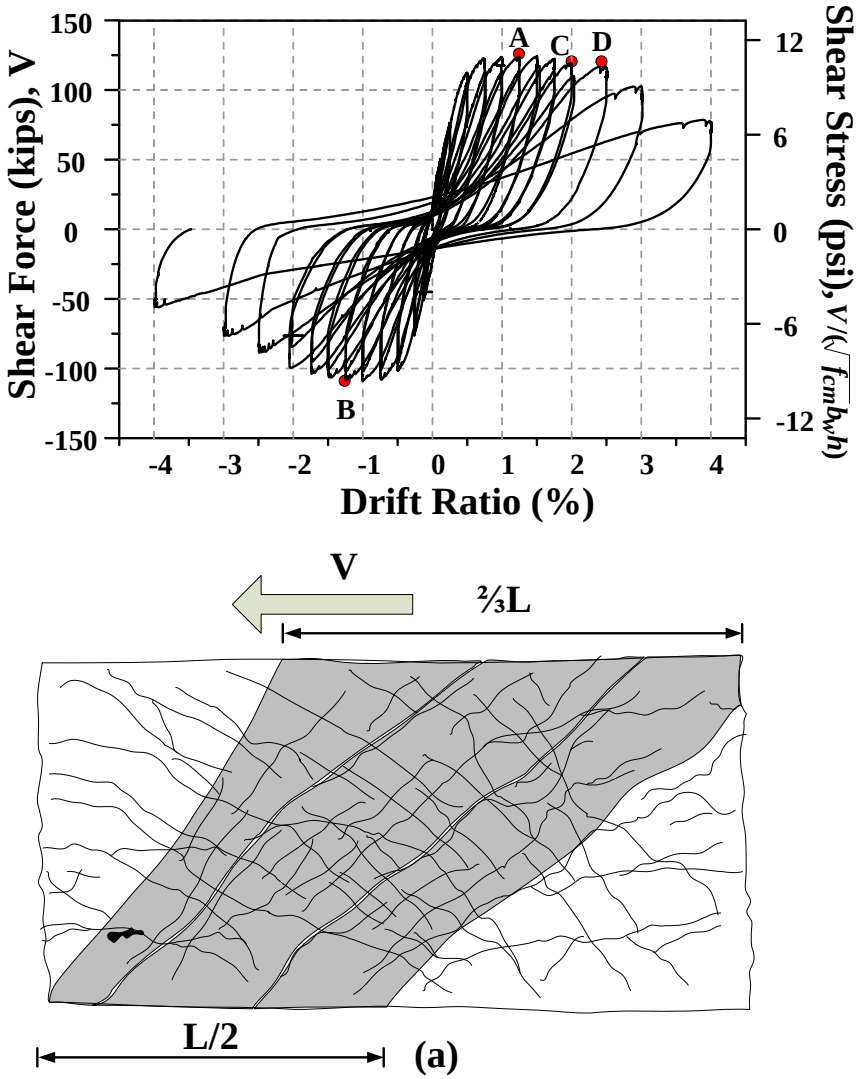
Shear Force (kips), V
Shear Stress (psi), $V/(\sqrt{f'_{cm}}b_w h)$
Drift Ratio (%)
150
100
50
0
-50
-100
-150
12
6
0
-6
-12
-4
-3
-2
-1
0
1
2
3
4
A
B
C
D
V
⅔L
L/2
(a)

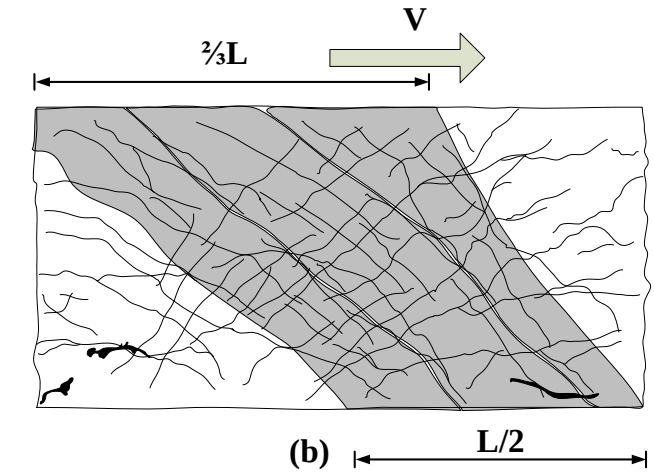

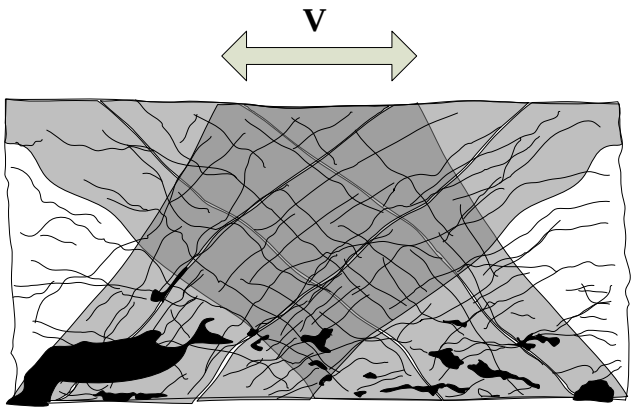

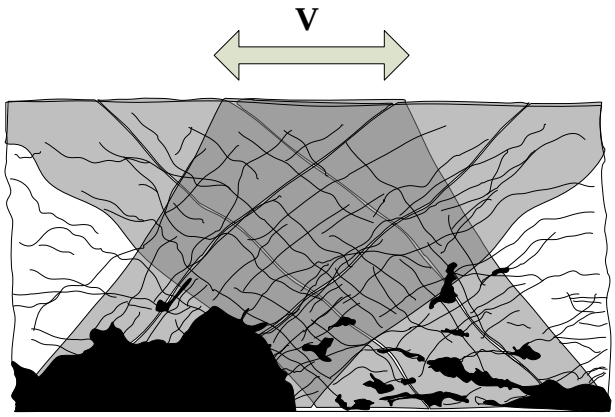

Figure 7-3 Flexural failure mechanism for Proposed Walls.

7.5 Response of Earthquake records

Figure 7-4 shows the Perform 3D model of squat shear walls. The model consists of plastic moment hinge, elastic elements, plastic shear hinge, and the slab mass. As shown in Figure 7-5, Four models with different shear hysteresis loops were selected to investigate the effect of drift ductility to resist LA16 earthquake response. Model 1 represents a tested ACI compliant wall, Model 2 is a tested proposed wall, both ACI and proposed walls have same longitudinal steel rebars but different horizontal reinforcement configuration. Model 3 and Model 4 are the hypothetical proposed walls with 0.65 and 0.5 reduced strength, respectively. It is worth to mention that drift ductility of reduced strength walls was conservatively selected to be same the tested proposed wall, but in reality, drift ductility increases for reduced strength walls. The drift ratio response due to LA16 earthquake record is shown in Figure 7-6. ACI compliant wall collapsed at time 6 sec. while the proposed wall sustained its strength until the end of LA16 time, 15 sec., with maximum drift ratio amplitude of 0.43%. The proposed wall 0.65 reduced also sustained its strength until 15 sec. with 2.6% maximum drift ratio, while the proposed wall 0.5 collapsed at 2.8 sec. These results indicate that the shear strength reduction factor, φ, for proposed walls is much higher than what ACI adopts for squat shear walls $\varphi = 0.65$.

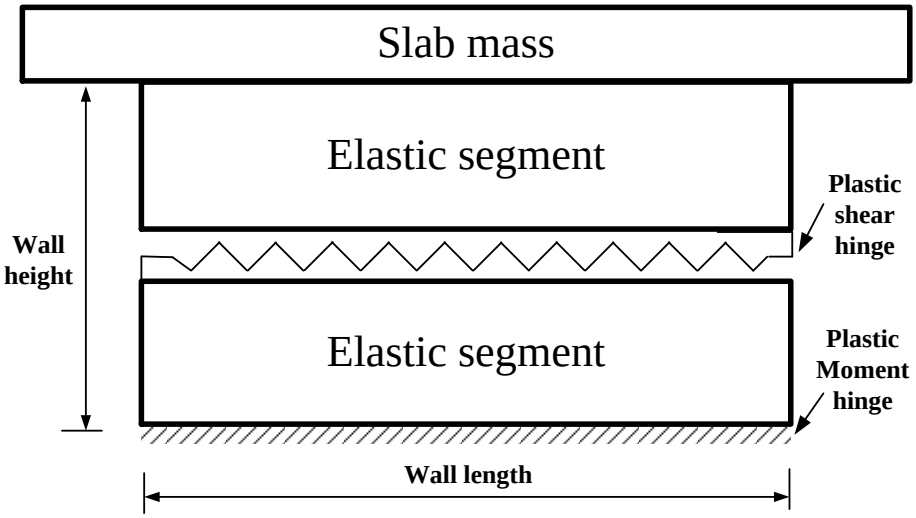

Figure 7-4 Perform 3D model of tested wall specimen.

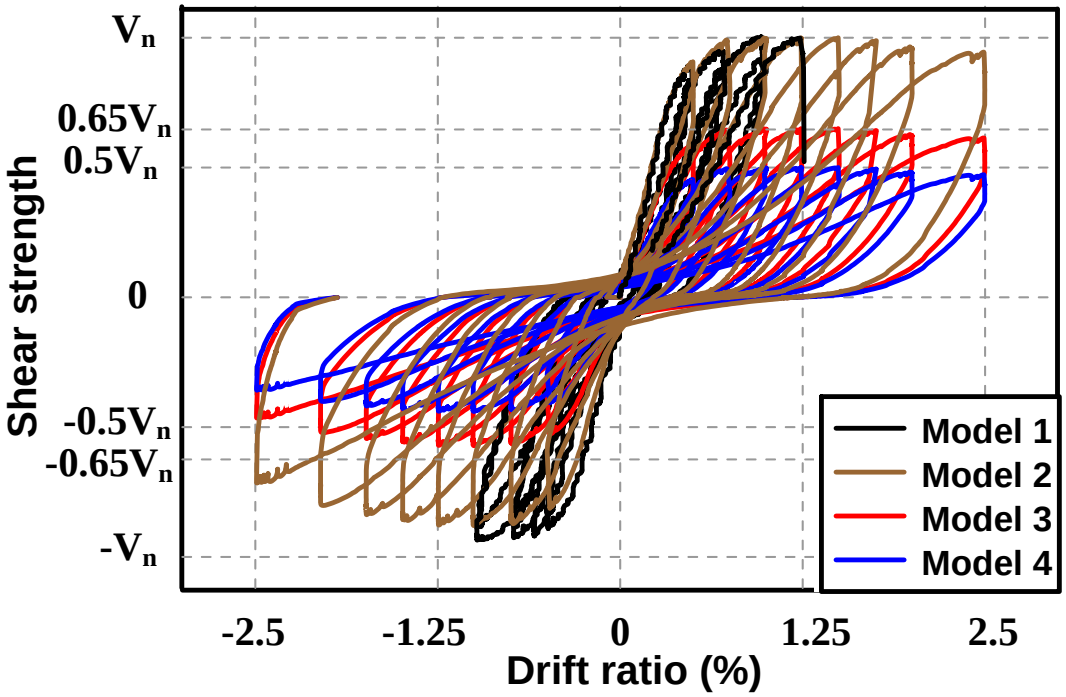

Figure 7-5 Flexural Shear strength and drift ratio response comparison between ACI provisions-based wall vs. reduced strength-proposed walls.

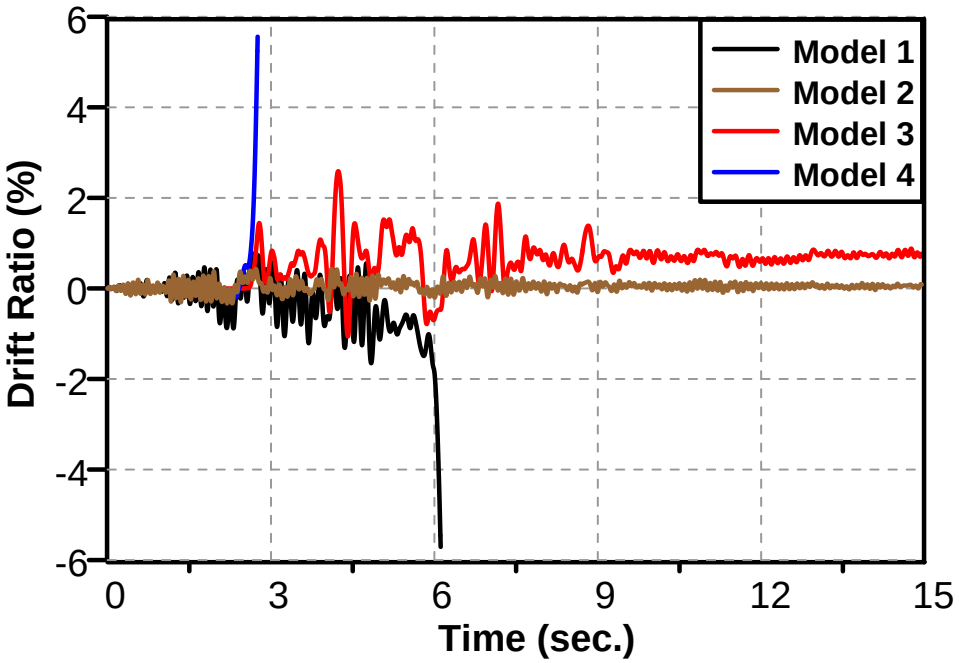

Figure 7-6 Drift ratio response comparison between ACI provisions-based wall vs. reduced strength-proposed walls.

Chapter 8

Proposed strut and tie model

8.1. Introduction

It is postulated that shear strength depends on strut and tie model. In general, the shear strength of walls controlled by the minimum strength of either tie or strut. The critical parts of a strut are at middle or base of strut. If the middle parts are sufficiently reinforced by horizontal steel bars, then the shear failure would be avoided, and the mode failure is governed by sliding. In contrast, if struts have no adequate horizontal reinforcements, then the shear failure will govern.

8.2. Derivation of the proposed equation

The proposed equation was derived based on several techniques including analyzing yielded steel reinforcement of tested specimens and Digital Image Correlation (DIC) of experimentally tested specimens using major and minor strain distributions. The proposed equation was compared to results of several tested specimens in literature, the equation shows significant predicting accuracy compared to ACI equations.

8.2.1 Derivation of proposed equation using DIC technique

The major strain distribution at drift ratio 1% and steel bars layout for each specimen, are shown in Figure 8-1 to Figure 8-6. In all 0.5-aspect-ratio walls, the vertical steel rebars that equilibrate struts compressive stresses, are located within wall length of 2/3L (Figure 8-1 to Figure 8-5). While in 1.0-aspect-ratio walls, the steel bars are concentrated at boundaries only (Figure 8-6). Same for the concrete strut, the strut width is about L/2 for 0.5-walls, while it is about L/4 for 1.0-aspect ratio walls.

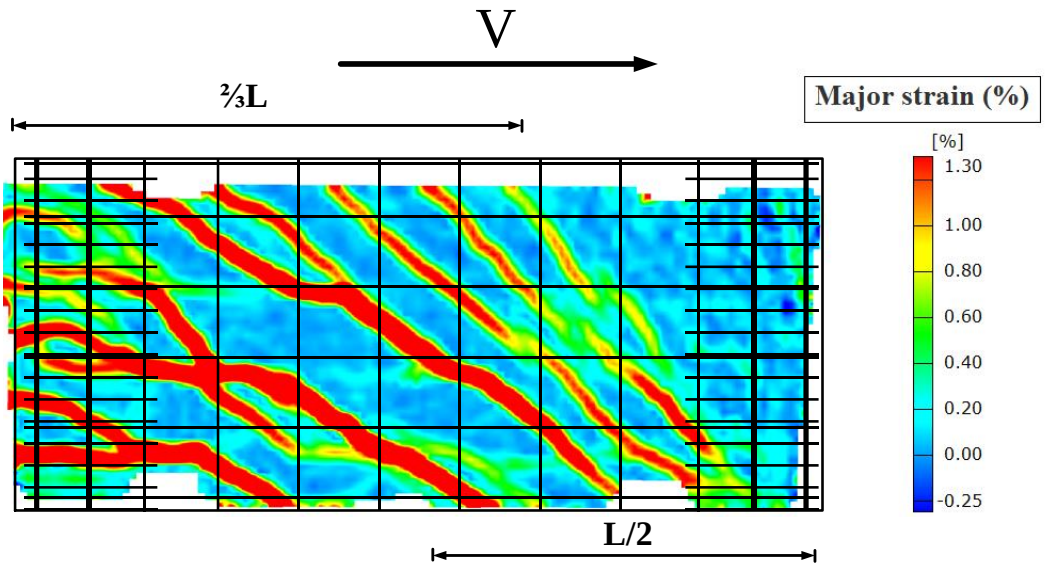

Figure 8-1 DIC major strain distribution of specimen SW-MA-0.5 at drift ratio 0.75%

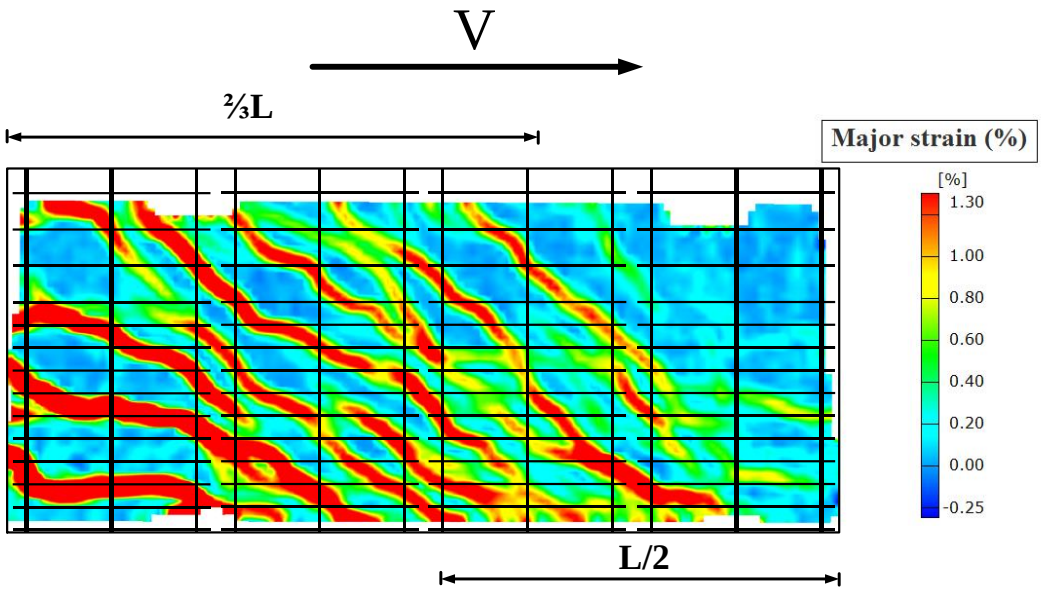

Figure 8-2 DIC major strain distribution of specimen SW-MP-0.5 at drift ratio 0.75%

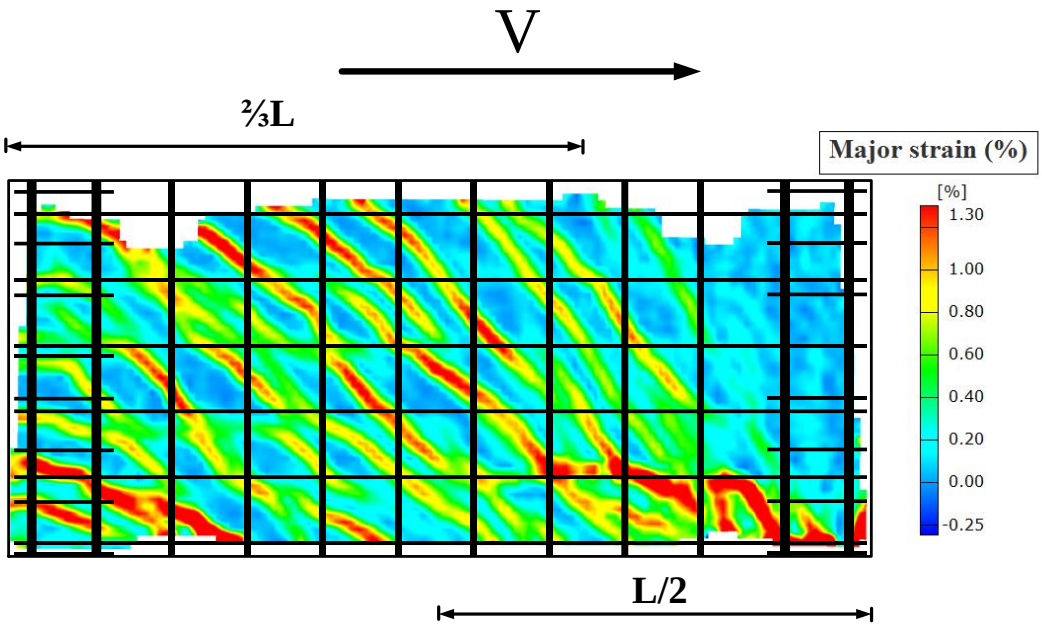

Figure 8-3 DIC major strain distribution of specimen SW-HA-0.5 at drift ratio 0.75%

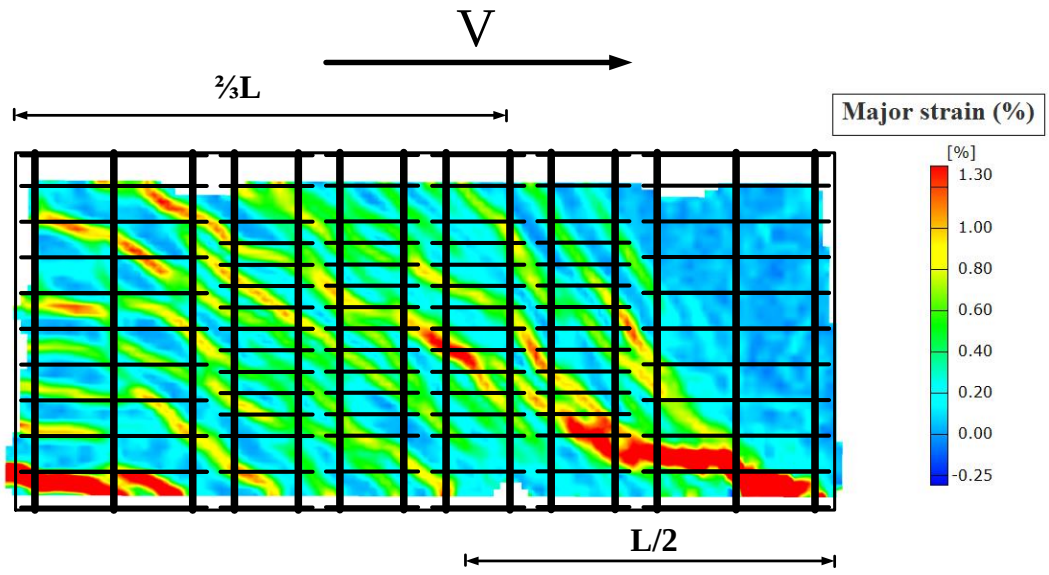

Figure 8-4 DIC major strain distribution of specimen SW-HP-0.5-1 at drift ratio 0.75%

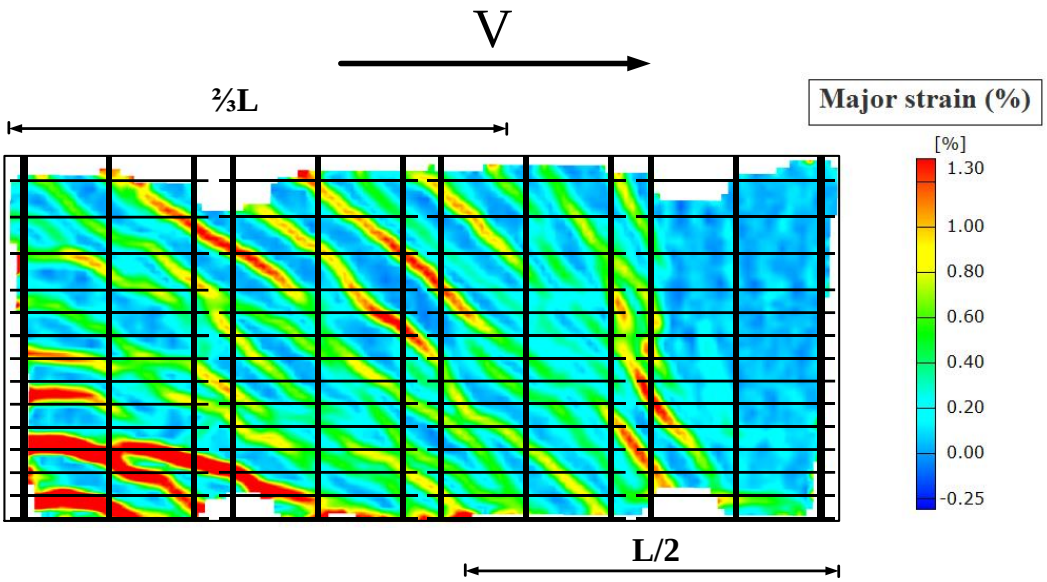

Figure 8-5 DIC major strain distribution of specimen SW-HP-0.5-2 at drift ratio 0.75%

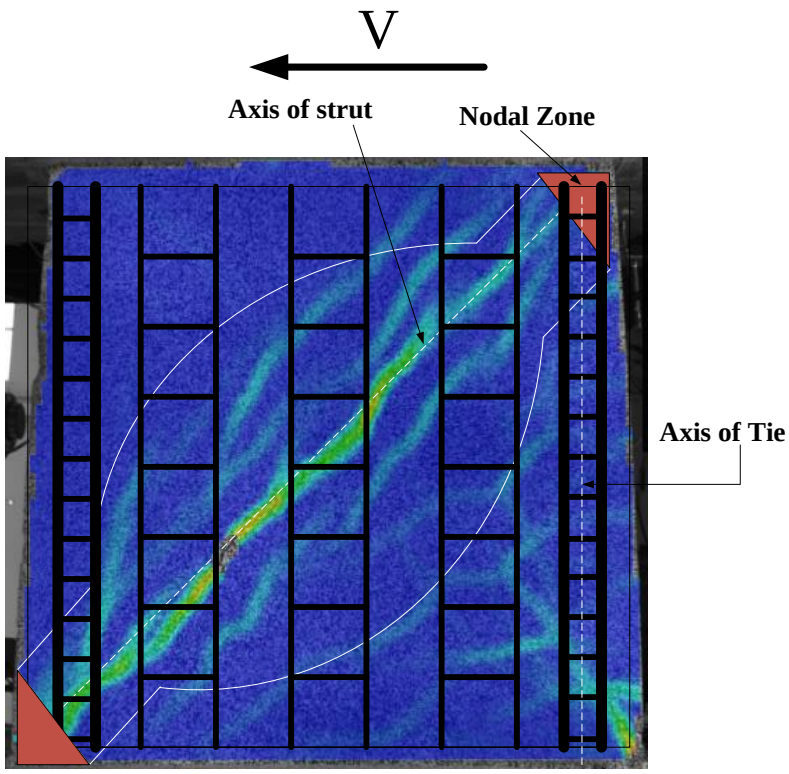

Figure 8-6 DIC major strain distribution of specimen SW-MA-1.0-1 at drift ratio 0.75%

8.2.2 Derivation of proposed equation using forces distribution of simple trusses

The minor strain distribution at drift ratio 0.75% for all specimens are shown in Figure 8-7. In all 0.5-aspect-ratio walls, the strut width is about 20 inches which represent L/2 as shown in Figure 8-7 (a - e). While in 1.0-aspect-ratio walls, while it is about L/4 for 1.0-aspect ratio walls (Figure 8-7 f).

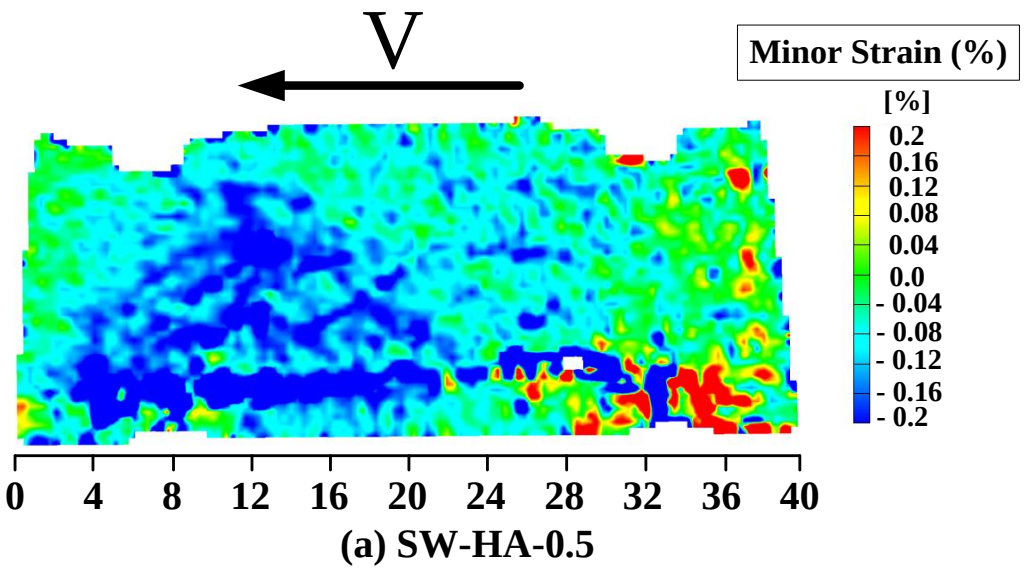

(a) SW-HA-0.5

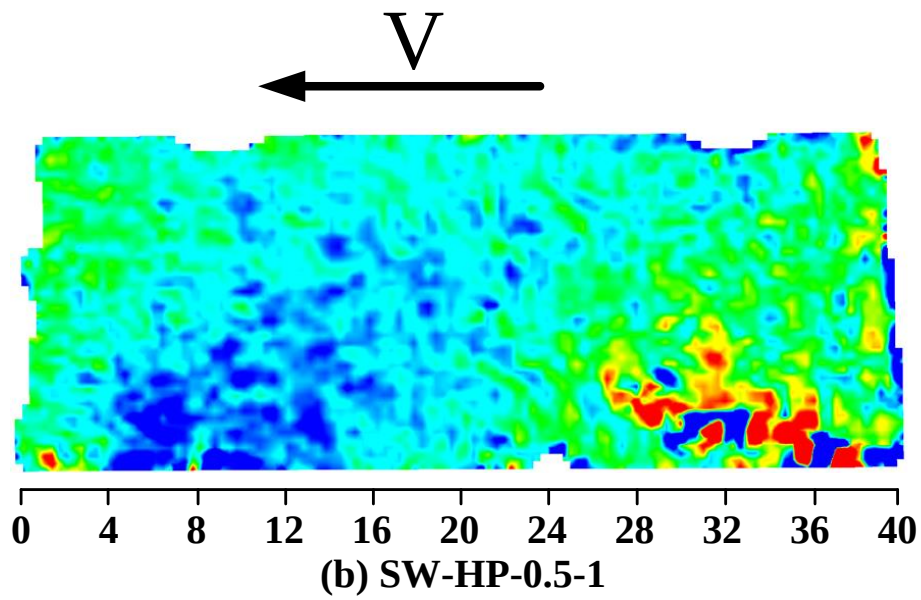

(b) SW-HP-0.5-1

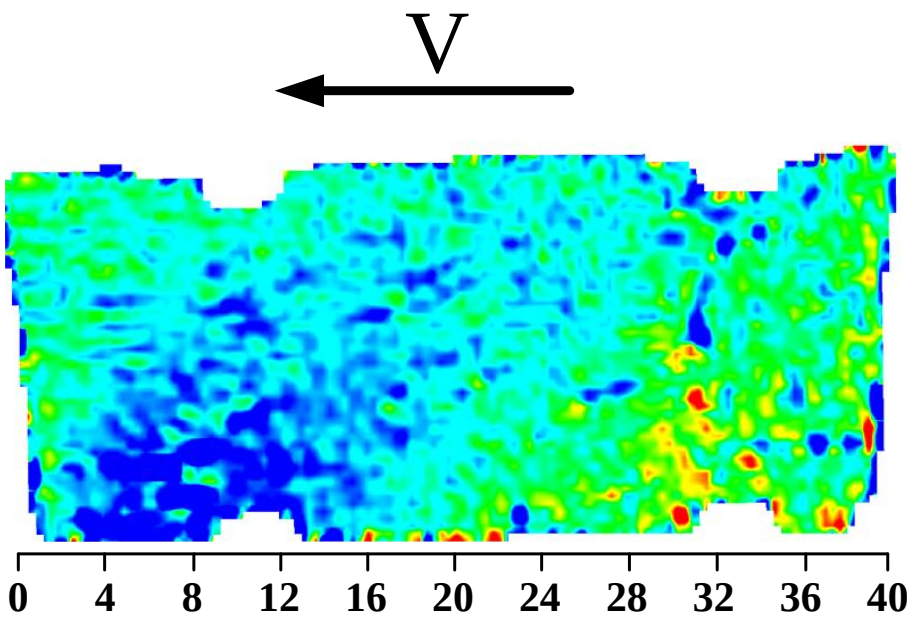

(c) SW-HP-0.5-2

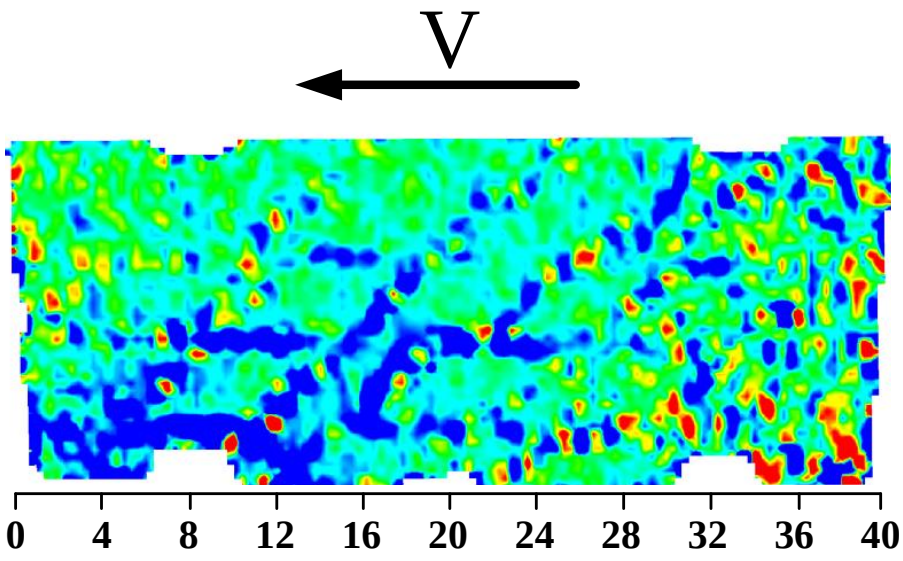

(d) SW-MA-0.5

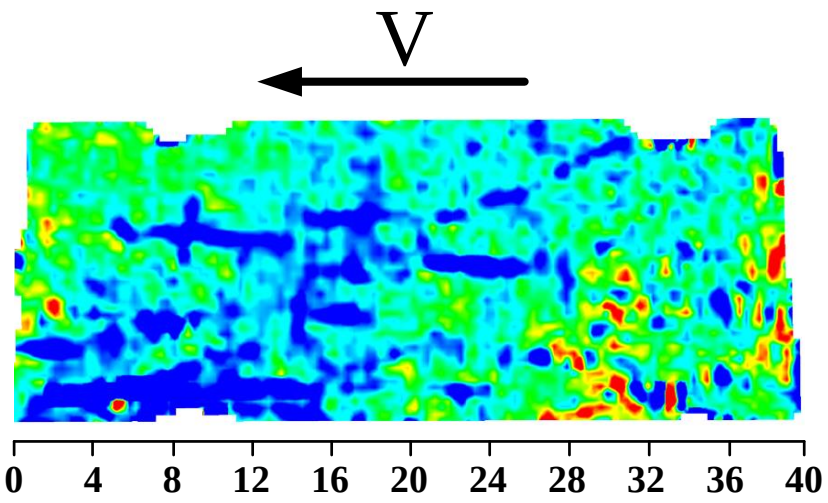

(e) SW-MP-0.5

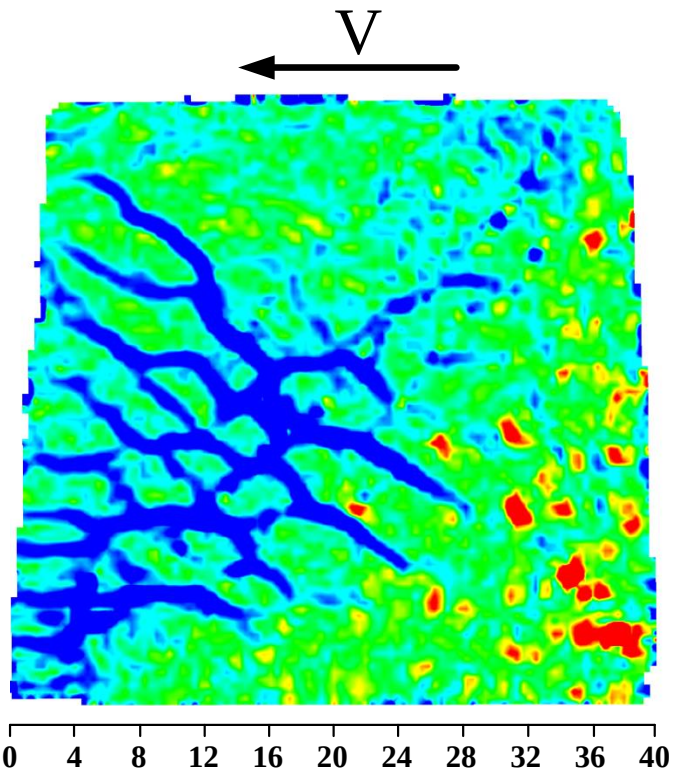

(f) SW-MP-1.0-1

Figure 8-7 DIC minor strain distribution at drift ratio 0.75% (positive strain is tension and negative strain is compression)

8.2.3 Derivation of proposed equation using analysis of yielded steel reinforcement

Strain gauges attached on longitudinal steel bars were used to measure stresses on steel bars. Figure 5-3 to Strain gauges were attached at boundaries, longitudinal and horizontal steel bars as shown in Figure 5-126. Strain gauges L1 to L12 are attached at vertical steel bars, while S13 to S16 are attached at boundaries and horizontal steel bars. The results of drift ratio and the attained steel stress in strain gauges L1 to S16 are shown in Figure 5-127 to Figure 5-142. All vertical steel bars yielded (reached the yielding strength of (60 ksi) except L9. None of strain gauges at boundaries or horizontal steel bars yielded.

Figure 5-126 illustrate longitudinal steel bars stresses along the wall length over different drift ratios. For 0.5-aspect-ratio walls, the yielded longitudinal steel bars are spread over 2/3 of wall length which represent the number of effective ties to transfer forces from wall tip to the base. On the other hand, the yielded steel bars on 1.0 aspect ratio walls are distributed on the boundaries (or 0.25L).

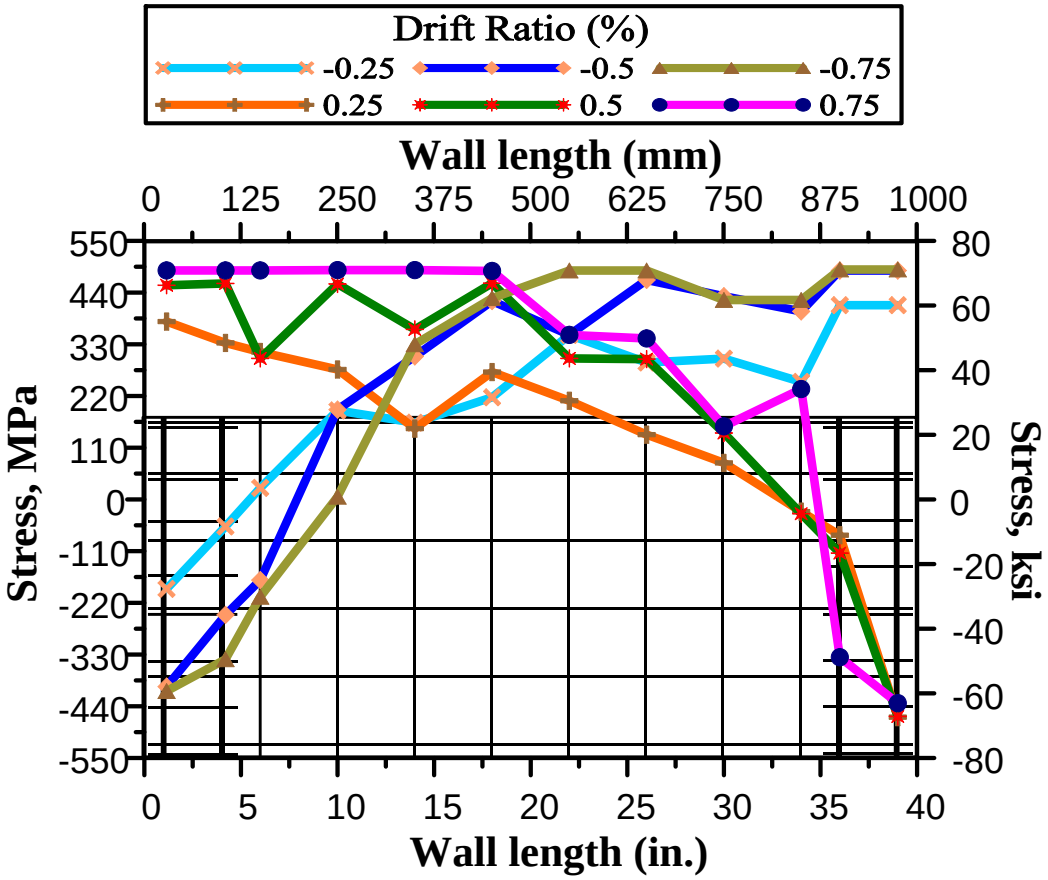

Figure 8-8 Measured stresses of vertical reinforcing steel bars for specimen SW-MA-0.5

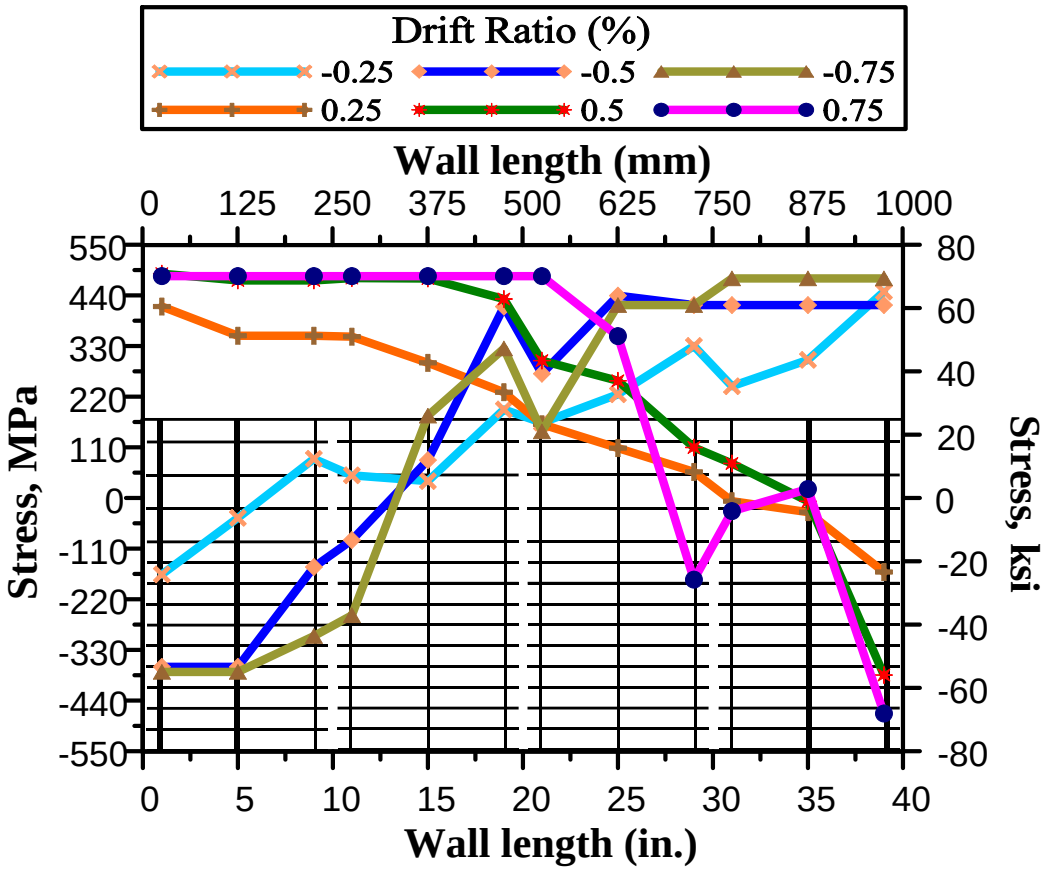

Figure 8-9 Measured stresses of vertical reinforcing steel bars for specimen SW-MP-0.5

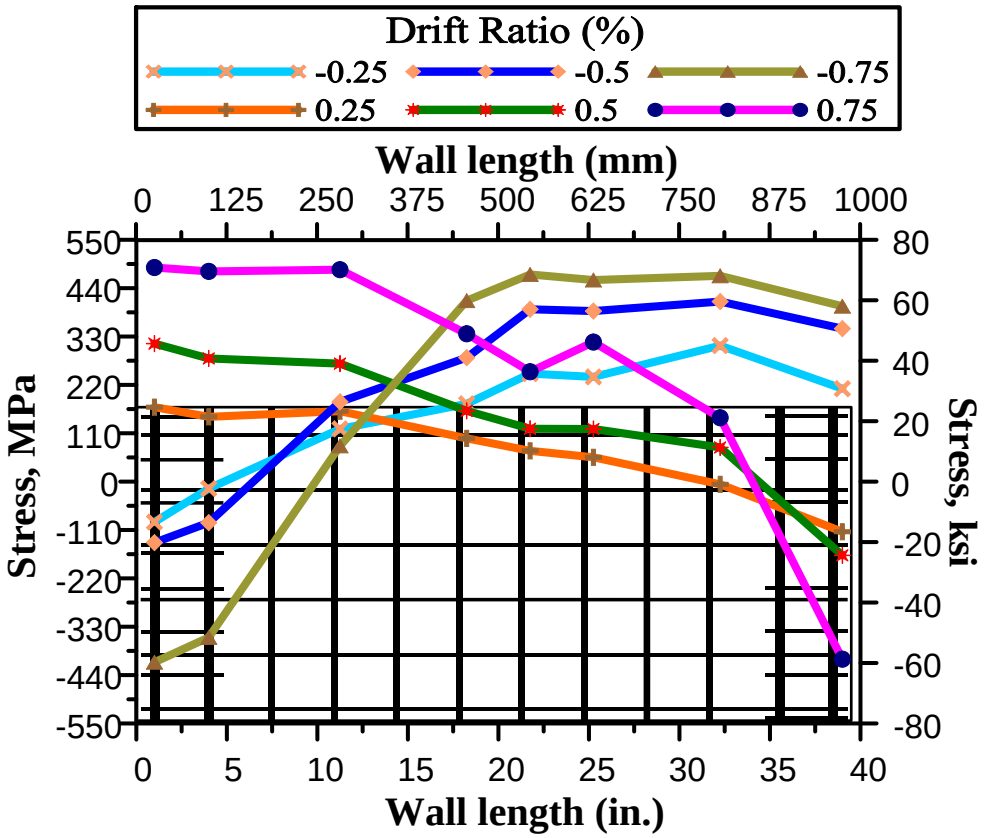

Figure 8-10 Measured stresses of vertical reinforcing steel bars for specimen SW-HA-0.5

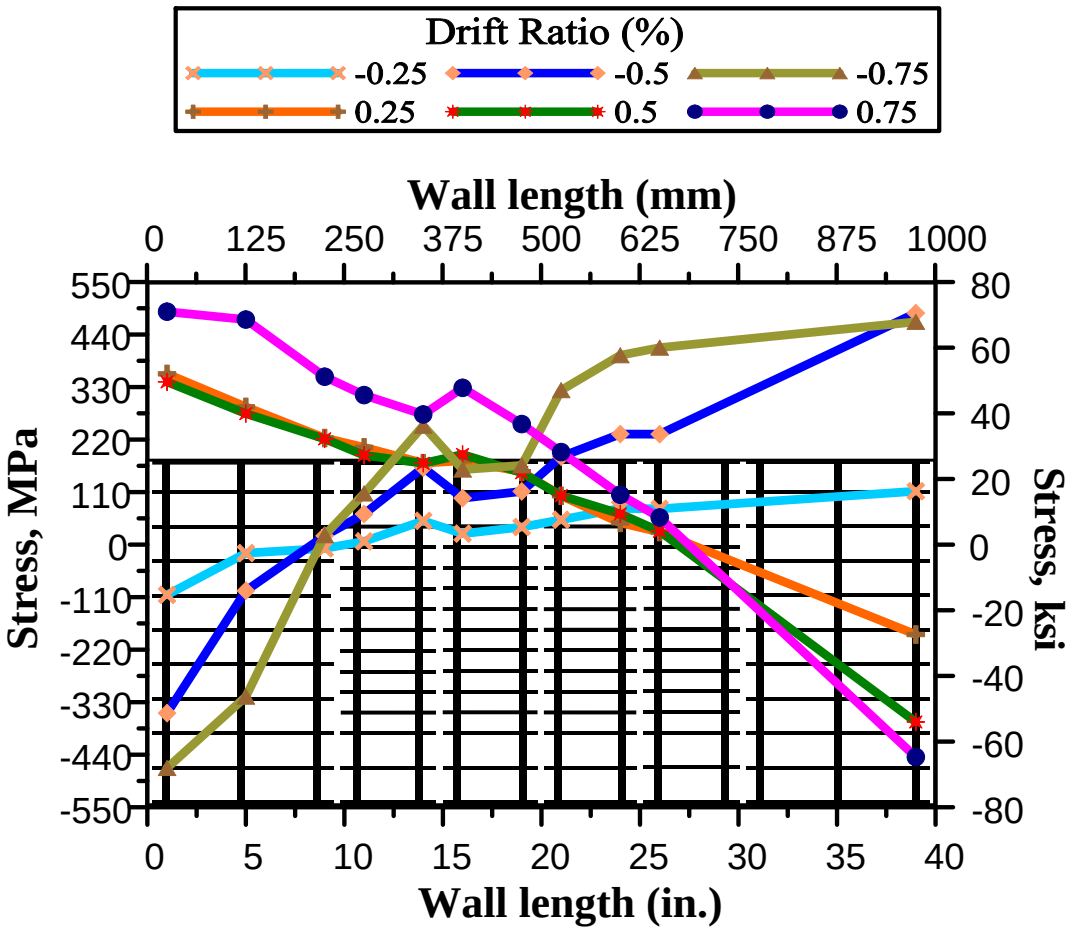

Figure 8-11 Measured stresses of vertical reinforcing bars for specimen SW-HP-0.5-1

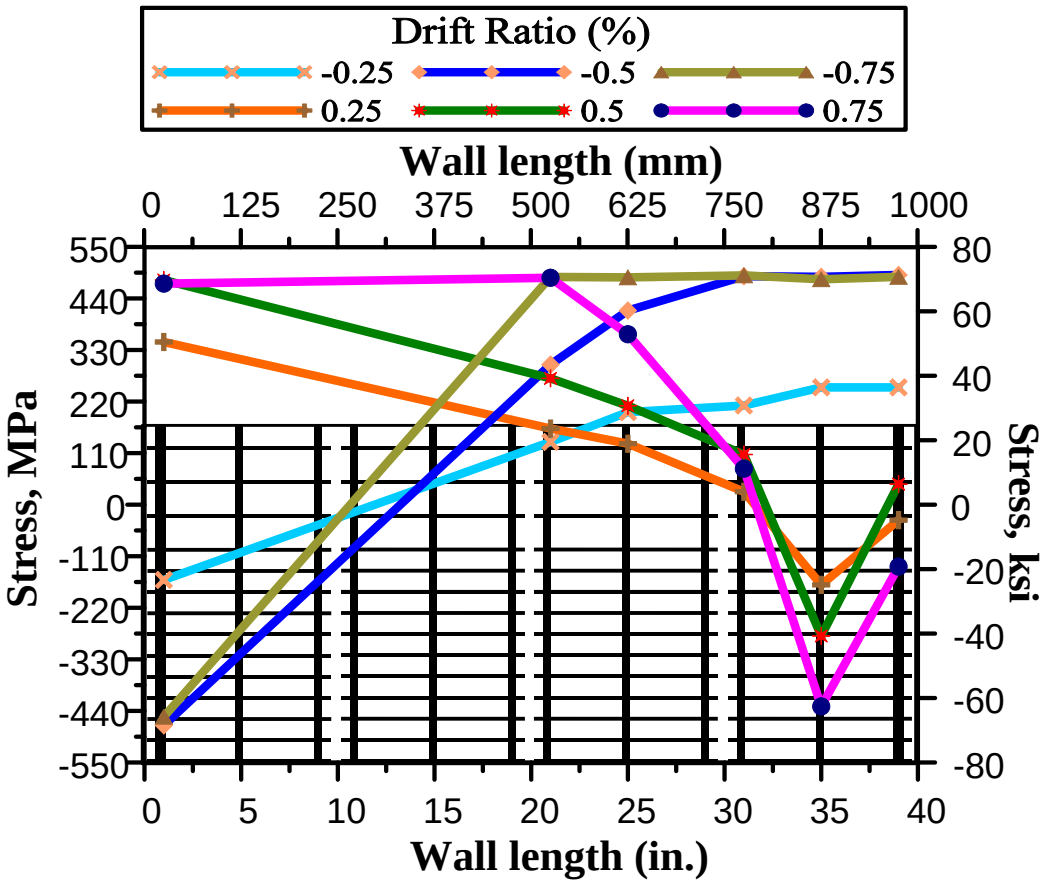

Figure 8-12 Measured stresses of vertical reinforcing bars for specimen SW-HP-0.5-2

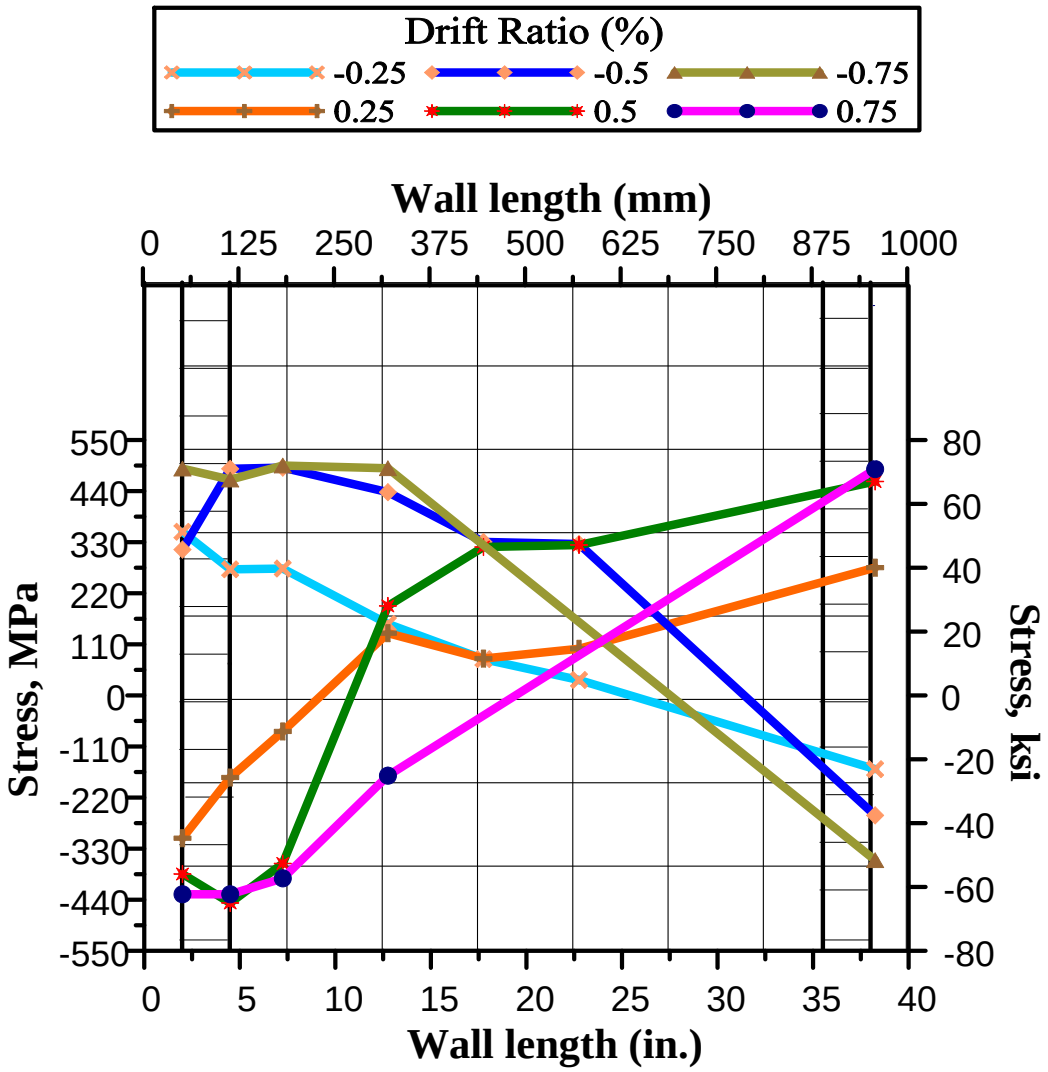

Figure 8-13 Measured stresses of vertical reinforcing bars for specimen SW-MA-1.0

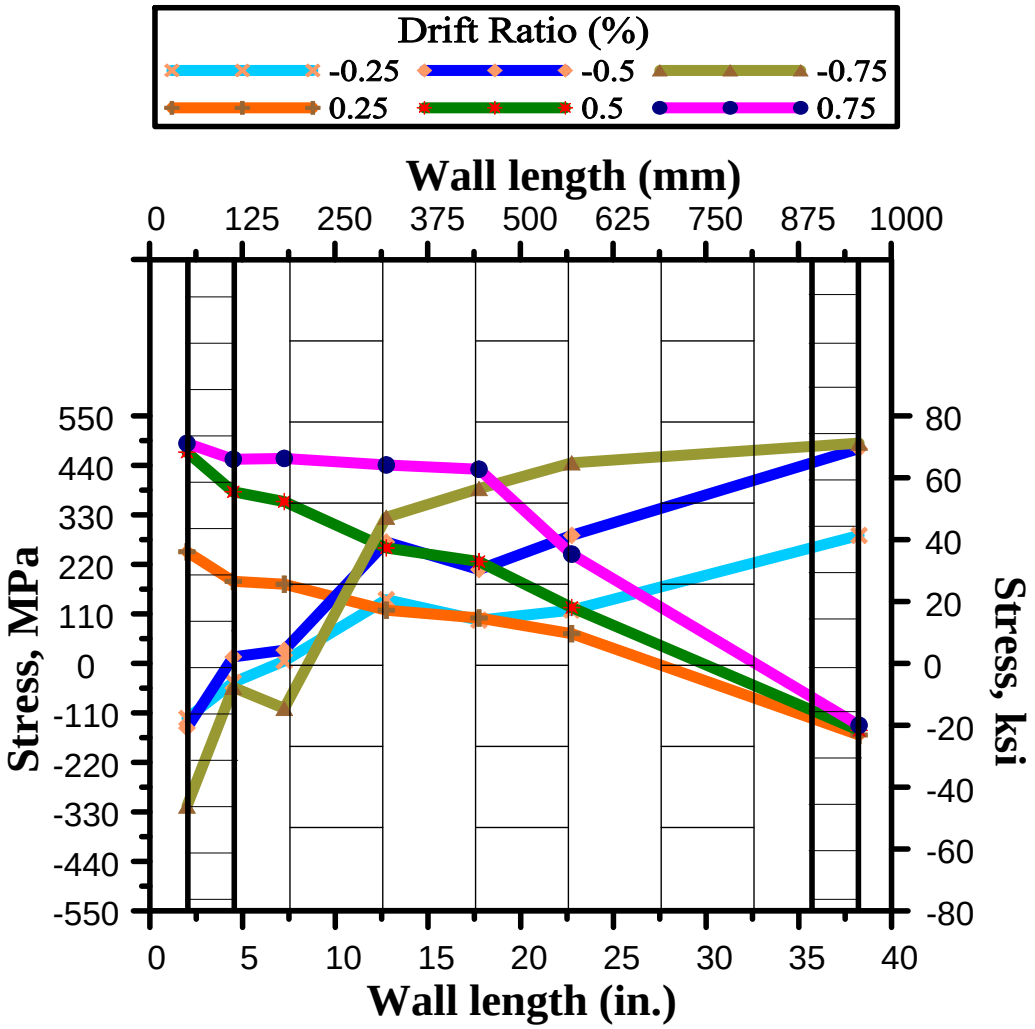

Figure 8-14 Measured stresses of vertical reinforcing bars for specimen SW-MA-1.0-1

8.3. The proposed equation based on Strut and Tie Model

As discussed in the previous sections, the tie width was 2/3L and boundary width (or 0.25L) for 0.5 and 1.0-aspect-ratio walls, respectively. Also, strut width was 0.5L and 0.25L for 0.5 and 1.0-aspect-ratio walls, respectively. A general strut and tie dimensions are shown in Figure 8-15.

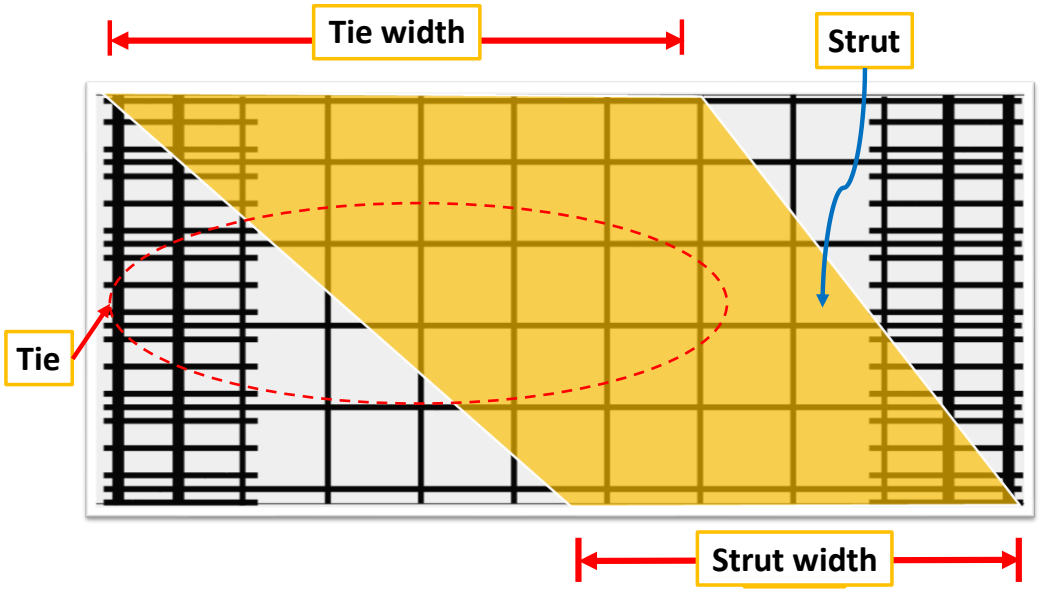

Figure 8-15 General strut and tie components

The proposed equation consists of two parts; tie strength and strut strength.

The following equation (Eq. 8-1) is to predict the shear strength of 0.5-aspect-ratio walls:

$$V_{proposed} = \text{minimum of} \begin{cases} V_{tie} = \dfrac{2}{3} A_{sv} F_{yv} \\ V_{strut} = 0.6(0.85) \dfrac{A_w}{2} f_c' \cos(45°) + 0.25 A_{sh} F_{yh} \end{cases} \quad \text{(Eq. 8-1)}$$

The following equation (Eq. 8-2) is to predict the shear strength of 1.0-aspect-ratio walls:

$$V_{proposed} = \text{minimum of} \begin{cases} V_{tie} = A_{sb} F_{yb} \\ V_{strut} = 0.6(0.85) \dfrac{A_w}{4} f_c' \cos(45°) + 0.5 A_{sh} F_{yh} \end{cases} \quad \text{(Eq. 8-2)}$$

Where:

$V_{proposed}$: the wall shear strength (kips).

$2/3A_{sv}$: area of vertical steel reinforcement located on 2/3 of wall area, in^2.

A_w: wall cross section (in^2).

A_{sb}: summation of steel bars area located at one boundary

45°: is the inclination angle of struts.

$0.25A_{sh}$ and $0.5A_{sh}$: quarter and half of horizontal reinforcements (in^2), respectively.

F_{yv}: actual steel yield strength of vertical reinforcements, ksi.

F_{yh}: actual steel yield strength of horizontal reinforcements, ksi.

F_{yb}: actual steel yield strength of boundary reinforcements, ksi.

f'c: concrete compressive strength (ksi)

Indeed, the 0.6 and 0.85 factors are used to be compatible to factors appeared on the ACI 318-19 equation 23.4.3 and Table 23.4.3 (c). βs considered to be 0.6 because the walls of this study are classified as "other cases"

The $0.25A_{sh}$ and $0.5A_{sh}$ are the contribution of horizontal steel reinforcement on the strut strength. The minor contribution of horizontal reinforcements of squat walls is compatible to the test results of horizontal reinforcements, where it was hard for horizontal bars to yield.

The following proposed equation (Eq. 8-3) valid for wall aspect ratios less or equal 0.75:

$$V_{proposed} = \text{minimum of} \begin{cases} V_{tie} = Y_1 A_{sv} F_{yv} \\ V_{strut} = 0.6(0.85) Y_2 A_w f'_c \cos(45°) + Y_3 A_{sh} F_{yh} \end{cases} \quad \text{(Eq. 8-3)}$$

Where:

Y_1 is the tie width and calculated by:

$$\frac{3L}{4} \geq Y_1 = \frac{4}{3}\left(1 - aspect\ ratio\right) \geq \frac{L}{3}$$

Y_2 is the strut width and calculated by:

$$\frac{3L}{4} \geq Y_2 = \frac{1}{4\left(aspect\ ratio\right)} \geq \frac{L}{3}$$

Y_3 is the horizontal reinforcement contribution of strut strength and calculated by:

$$0.5 \geq Y_3 = \frac{aspect\ ratio}{2} \geq 0.25$$

The following proposed equation (Eq. 8-4) valid for wall aspect ratio more than 0.75 and less than 2.0:

$$V_{proposed} = \text{ minimum of } \begin{cases} V_{tie} = \dfrac{A_{sb} F_{yb}}{aspect\ ratio} \\ V_{strut} = 0.6(0.85)\dfrac{A_w}{4} f_c' \cos(\alpha^\circ) \ + \ 0.5 A_{sh} F_{yh} \end{cases} \qquad \text{(Eq. 8-4)}$$

$\alpha = \tan^{-1}(aspect\ ratio)$

α is the strut inclination angle (degrees)

8.4. The proposed squat wall design

1) Calculate the required longitudinal steel reinforcement by equation (Eq. 8-5):

$$V_{tie} = \begin{cases} Y_1 A_{sv} F_{yv} & for\ aspect\ ratio \le 0.75 \\ \dfrac{A_{sb} F_{yb}}{aspect\ ratio} & for\ aspect\ ratio\ >\ 0.75 \end{cases} \qquad \text{(Eq. 8-5)}$$

$$\frac{3L}{4} \ge Y_1 = \frac{4}{3}(1 - aspect\ ratio) \ge \frac{L}{3}$$

2) Since the proposed squat walls have ductile behavior and strong strut, the calculation of strut is exempt as long as the hoops spacing satisfied the ACI 18.7.5.4 provisions in Table 8-1

Table 8-1 Calculation hoops spacing

In proposed walls, consider Pu = (Aspect ratio) (Vu)

Transverse Reinforcement	Conditions	Applicable expression	
$\frac{A_{sh}}{sb_c}$ ACI 18.7.5.4	$P_u \le 0.3A_g f_c'$ and $f_c' \le 10{,}000$ psi	Greater of (a) and (b)	$(a)\ 0.3\left(\frac{A_g}{A_{ch}} - 1\right)\frac{f_c'}{f_{yt}}$
	$P_u > 0.3A_g f_c'$ or $f_c' > 10{,}000$ psi	Greatest of (a), (b) and (c)	$(b)\ 0.09\frac{f_c'}{f_{yt}}$ $(c)\ 0.2k_f k_n \frac{P_u}{f_{yt} A_{ch}}$

3) Steel reinforcement layout

The proposed steel reinforcement layout (Figure 8-16) consists of several steel cages confined by hoops up 2/3 wall height, that satisfy ACI provisions for columns as

mentioned in step 2. The hoops spacing shall be relaxed over the remainder of wall height.

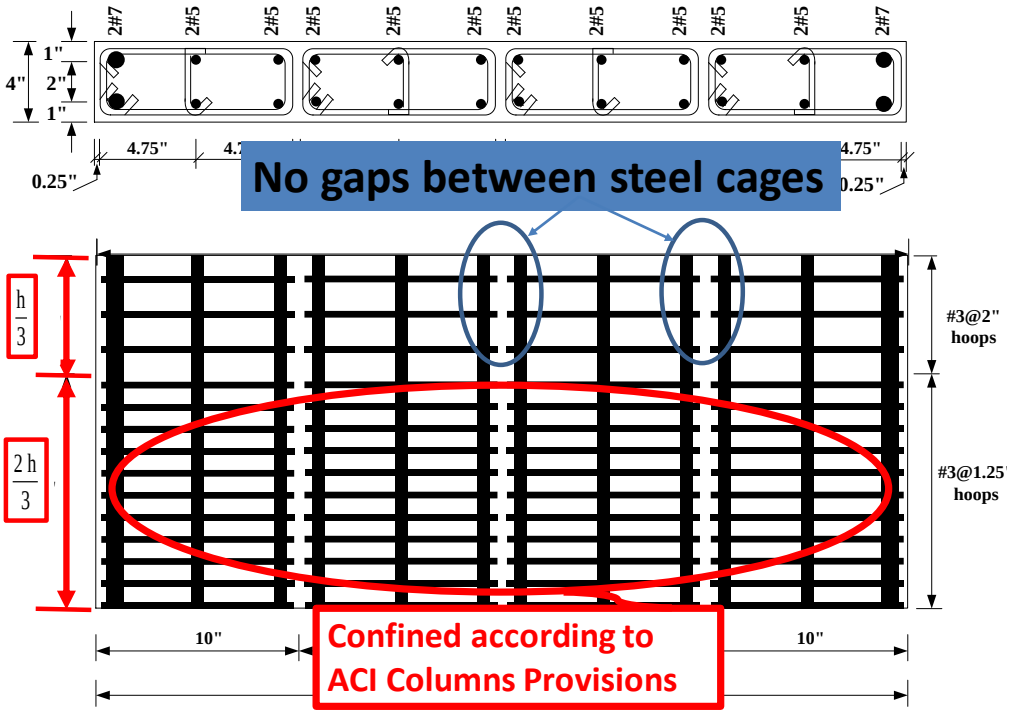

Figure 8-16 Steel reinforcement layout of Proposed walls.

8.5. Properties of tested walls in literature

Results of 54-tested squat shear walls were investigated to evaluate the accuracy of the proposed equation in addition to other commonly used equations (ACI 318-19, Wood 1990, and Gulec 2011). The walls height, length, thickness and aspect ratio are summarized in Table 8-2. Concrete compressive strength and Wall steel reinforcement at horizontal, vertical, and boundaries are shown in Table 8-3. The data of Alexander and Sheu walls were obtained from database of Gulec and Whittacker (2009). Also, axial forces and yielding steel stresses of horizontal, vertical, and boundaries are available in Table 8-4.

The tie, strut and the proposed strength are evaluated in Table 8-5, the predicted shear strength by other available equations (ACI 318-19, Wood 1990, and Gulec 2011) are listed in Table 8-6. Table 8-7 summarizes the ratio of experimental to the predicted shear strength by other equations, the dispersion parameters (Average, Standard deviation and Coefficient of variance) of these ratios are tabulated in Table 8-8. The result emphasizes the accuracy of the proposed equation to predict shear strength of squat walls compared to the other available equations. Where the average predicted strength is 1.137 with coefficient of variance 0.22. The ACI 318-19 overpredicts the shear strength.

Table 8-2 Walls dimensions

Wall number	Researcher	wall ID	h_w (in)	l_w (in)	Aspect Ratio	t_w (in)
1	Whyte and Stojadinovic (2014)	Wall 1	64	120	0.53	8
2	Whyte and Stojadinovic (2014)	Wall 2	64	120	0.53	8
3	Alexender	1	54	108	0.50	4
4	Sheu	98	19.7	39.4	0.50	3.94
5	Sheu	99	19.7	39.4	0.50	3.94
6	Sheu	101	19.7	39.4	0.50	3.94
7	Sheu	102	19.7	39.4	0.50	3.94
8	Sheu	103	19.7	39.4	0.50	3.94
9	Sheu	104	19.7	39.4	0.50	3.94
10	Sheu	105	19.7	39.4	0.50	3.94
11	Sheu	106	19.7	39.4	0.50	3.94
12	Sheu	107	19.7	39.4	0.50	3.94
13	Sheu	108	19.7	39.4	0.50	3.94
14	Sheu	109	19.7	39.4	0.50	3.94
15	Sheu	110	19.7	39.4	0.50	3.94
16	Sheu	111	19.7	39.4	0.50	3.94
17	Sheu	112	19.7	39.4	0.50	3.94
18	Sheu	113	19.7	39.4	0.50	3.94
19	Sheu	114	19.7	39.4	0.50	3.94
20	Baek et al. (2017)	NS0.5M	29.7	59	0.50	7.8
21	Baek et al. (2017)	HS0.5M	29.7	59	0.50	7.8
22	Baek et al. (2017)	NF0.5M	29.7	59	0.50	7.8
23	Baek et al. (2017)	HF0.5M	29.7	59	0.50	7.8
24	Baek et al. (2017)	HF0.5M-B	29.7	59	0.50	7.8
25	Baek et al. (2018)	H0.5MU	29.7	59	0.50	7.8
26	Baek et al. (2018)	H0.5HU	29.7	59	0.50	7.8
27	Baek et al. (2018)	H0.5MU-C	29.7	59	0.50	7.8
28	Baek et al. (2018)	H0.5MG-C	29.7	59	0.50	7.8
29	Baek et al. (2018)	H0.33MU	19.7	59	0.33	7.8
30	Baek et al. (2018)	H0.33HU	19.7	59	0.33	7.8
31	Baek et al. (2018)	H0.33MU-AS	19.7	59	0.33	7.8

Wall number	Researcher	wall ID	h_w (in)	l_w (in)	Aspect Ratio	t_w (in)
32	Baek et al. (2018)	H0.33HU-AS	19.7	59	0.33	7.8
33	Baek et al. (2018)	H0.33MU-AL	19.7	59	0.33	7.8
34	Baek et al. (2018)	N0.33MU	19.7	59	0.33	7.8
35	Baek et al. (2018)	N0.33MU-AL	19.7	59	0.33	7.8
36	Baek et al. (2018)	H0.33MR	19.7	59	0.33	7.8
37	Baek et al. (2017)	NF1M	59	59	1.00	7.8
38	Baek et al. (2017)	HF1M	59	59	1.00	7.8
39	Baek et al. (2017)	NS1M	59	59	1.00	7.8
40	Baek et al. (2017)	HS1M	59	59	1.00	7.8
41	Cheng et al. (2016)	M60	80	80	1.00	8
42	Cheng et al. (2016)	M115	80	80	1.00	8
43	Cheng et al. (2016)	H60	80	80	1.00	8
44	Cheng et al. (2016)	H115	80	80	1.00	8
45	Cheng et al. (2016)	H60X	80	80	1.00	8
46	Synge	121	59.1	118.1	0.50	3.94
47	Yoshizaki	133	31.5	63	0.50	2.36
48	Yoshizaki	134	31.5	63	0.50	2.36
49	Yoshizaki	135	31.5	63	0.50	2.36
50	Yoshizaki	136	31.5	63	0.50	2.36
51	Yoshizaki	137	31.5	63	0.50	2.36
52	Wiradinata	82	39.4	78.7	0.50	3.94
53	Current study	SW1	40	40	1.00	4
54	Current study	SW6	20	40	0.50	4

Table 8-3 Wall steel reinforcement and concrete compressive strength

Wall number	A_{sb} (in.^{2})	A_{sv} (in.^{2})	ρ_h (%)	f'_c (ksi)
1	0.00	6.43	0.67	7.43
2	0.00	6.43	0.67	7.59
3	0.00	1.30	0.3	3.00
4	0.00	1.10	0.71	3.61
5	0.00	1.10	0.71	4.91
6	0.00	0.67	0.57	3.77
7	0.00	0.67	0.57	3.91
8	0.00	0.67	0.57	3.77
9	0.00	0.67	0.57	3.95
10	0.00	1.20	1.03	3.84
11	0.00	1.20	1.03	3.87
12	0.00	1.20	1.03	3.95
13	0.00	1.20	1.03	4.10
14	0.00	1.23	0.57	3.78
15	0.00	1.18	0.57	3.91
16	0.00	1.23	0.57	3.78
17	0.00	1.21	0.57	3.84
18	0.00	1.18	0	4.69
19	0.00	1.18	1.14	4.55
20	2.82	3.72	0.93	6.70
21	2.82	2.40	0.68	5.40
22	0.62	3.72	0.93	5.60
23	0.40	2.40	0.68	5.60
24	0.80	2.40	0.68	5.40
25	0.00	4.65	0.68	6.10
26	0.00	2.76	0.38	6.10
27	0.00	3.13	0.68	6.10
28	0.00	3.13	0.68	5.60
29	0.00	3.50	0.71	6.10
30	0.00	2.35	0.43	6.10
31	0.00	3.50	0.71	6.10
32	0.00	2.35	0.43	6.10
33	0.00	3.50	0.71	6.60
34	0.00	4.88	1.01	6.60
35	0.00	4.88	1.01	6.60

Wall number	A_{sb} (in.^{2})	A_{sv} (in.^{2})	ρ_h (%)	f'_c (ksi)
36	0.00	3.50	0.71	6.40
37	2.48	3.72	0.93	7.40
38	2.48	2.40	0.68	7.40
39	8.46	3.10	0.93	7.70
40	8.46	2.00	0.68	7.70
41	3.28	1.32	0.31	5.70
42	1.86	0.66	0.15	5.50
43	5.40	3.60	0.83	6.40
44	2.79	2.00	0.42	6.40
45	5.40	3.60	0.83	6.10
46	0.70	3.17	1.61	3.95
47	0.39	0.26	0.23	3.70
48	0.44	0.95	0.82	3.70
49	0.66	0.44	0.41	3.70
50	0.66	0.95	0.82	3.70
51	0.70	1.39	1.17	3.70
52	0.62	1.24	0.26	3.63
53	1.24	1.32	1.1	4.13
54	1.02	1.32	1.38	5.00

Table 8-4 Steel yielding stresses and applied axial force

Wall Number	F_{yv} (ksi)	F_{yb} (ksi)	F_{yh} (ksi)	Axial Force (kips)
1	67.3	0	67.3	0
2	67.3	0	67.3	0
3	52	0	52	0
4	71.2	0	71.2	0
5	71.2	0	71.2	0
6	70.1	0	70.1	0
7	70.1	0	70.1	0
8	70.1	0	70.1	0
9	70.1	0	70.1	0
10	69.7	0	69.7	0
11	69.7	0	69.7	0
12	69.7	0	69.7	0
13	69.7	0	69.7	0
14	62.6	0	67.8	0
15	65.7	0	67.8	0
16	62.6	0	67.8	0
17	65	0	67.8	0
18	65.7	0	0	0
19	65.7	0	67.8	0
20	89.4	94.7	75	250
21	96.7	94.7	96	250
22	68	68	75	250
23	96.7	96.7	96	250
24	96.7	96.7	96	250
25	96.7	0	90.6	0
26	96.7	0	96.7	0
27	96.7	0	96.7	198
28	96.7	0	96.7	165
29	96.7	0	90.6	0
30	96.7	0	90.6	0
31	96.7	0	90.6	0
32	96.7	0	90.6	0
33	96.7	0	90.6	0
34	68.2	0	96.7	0

Wall Number	F_{yv} (ksi)	F_{yb} (ksi)	F_{yh} (ksi)	Axial Force (kips)
35	68.2	0	96.7	0
36	96.7	0	90.6	0
37	68.15	96.7	68	250
38	96.7	96.7	96	250
39	68.15	89	68	250
40	96.7	89	96	250
41	66	65	66	0
42	114	112	114	0
43	69	65	69	0
44	117	112	117	0
45	69	65	69	0
46	43.5	43.5	55.1	0
47	62.9	48.3	62.9	0
48	62.9	49.7	62.9	0
49	62.9	50.1	62.9	0
50	62.9	50.1	62.9	0
51	62.9	50.9	62.9	0
52	63.1	63.1	61.6	0
53	60	60	60	0
54	60	60	60	0

Table 8-5 Proposed, tie and strut strength

Wall Number	V_{tie}	V_{strut}	$V_{proposed}$
1	288.6	1343.7	288.6
2	288.6	1371.3	288.6
3	44.9	242.1	44.9
4	52.3	110.9	52.3
5	52.3	147.1	52.3
6	31.2	113.2	31.2
7	31.2	117.2	31.2
8	31.2	113.2	31.2
9	31.2	118.4	31.2
10	55.5	121.4	55.5
11	55.5	122.2	55.5
12	55.5	124.6	55.5
13	55.5	128.6	55.5
14	51.2	113.2	51.2
15	51.7	117.0	51.7
16	51.2	113.2	51.2
17	52.5	115.0	52.5
18	51.7	131.4	51.7
19	51.7	142.4	51.7
20	544.2	648.9	544.2
21	460.5	524.8	460.5
22	253.0	557.6	253.0
23	232.1	541.4	232.1
24	232.1	524.8	232.1
25	270.8	541.8	270.8
26	158.6	527.4	158.6
27	201.7	544.2	201.7
28	201.7	502.7	201.7
29	253.7	530.8	253.7
30	170.2	521.1	170.2
31	253.7	530.8	253.7
32	170.2	521.1	170.2
33	253.7	572.3	253.7
34	249.5	585.1	249.5

Wall Number	V_{tie}	V_{strut}	$V_{proposed}$
35	249.5	585.1	249.5
36	253.7	555.7	253.7
37	239.8	656.1	239.8
38	239.8	652.4	239.8
39	752.9	713.0	713.0
40	752.9	715.6	715.6
41	213.2	686.7	213.2
42	208.3	659.7	208.3
43	351.0	821.2	351.0
44	312.5	808.6	312.5
45	351.0	786.6	351.0
46	126.8	382.6	126.8
47	30.7	101.8	30.7
48	64.1	108.7	64.1
49	52.7	103.9	52.7
50	75.5	108.7	75.5
51	97.8	112.8	97.8
52	97.6	208.9	97.6
53	74.4	145.5	74.4
54	127.2	160.8	127.2

Table 8-6 Experimental, Wood (1990), Gulec (2011), ACI 318-19 and Proposed shear strength

Wall Number	V_{test}	Wood (1990)	Gulec (2011)	$V_{proposed}$	ACI 318-19
1	367	496.5	318.1	288.6	681.1
2	384	530.1	320.0	288.6	683.8
3	74	151.8	74.0	44.9	138.4
4	70.8	59.9	47.5	52.3	93.3
5	72.8	69.8	50.8	52.3	108.7
6	47.2	61.2	36.8	31.2	90.6
7	42.5	62.3	37.1	31.2	91.2
8	40.2	61.2	36.8	31.2	90.6
9	42.5	62.6	37.3	31.2	91.3
10	62.7	61.8	49.9	55.5	96.2
11	61.1	62.0	49.9	55.5	96.6
12	54.4	62.7	50.2	55.5	97.6
13	62	63.8	50.5	55.5	99.4
14	55.8	61.2	47.4	51.2	88.6
15	60.7	62.3	48.0	51.7	89.1
16	49.8	61.2	47.4	51.2	88.6
17	55.8	61.8	48.2	52.5	88.9
18	54.7	68.3	50.0	51.7	31.9
19	70.4	67.2	49.6	51.7	104.7
20	560	241.2	376.7	544.2	376.7
21	529	216.6	338.2	460.5	338.2
22	318	220.6	326.7	253.0	344.4
23	307	220.6	317.3	232.1	344.4
24	319	216.6	337.8	232.1	338.2
25	177	230.6	234.4	270.8	359.4
26	111	230.4	170.1	158.6	276.9
27	244	230.5	294.2	201.7	359.4
28	315	220.8	272.5	201.7	344.4
29	129	245.0	239.6	253.7	359.4
30	70	244.9	191.5	170.2	287.1
31	232	245.0	239.6	253.7	359.4
32	160	244.9	191.5	170.2	287.1
33	302	254.8	243.4	253.7	373.9

Wall Number	V_{test}	Wood (1990)	Gulec (2011)	$V_{proposed}$	ACI 318-19
34	218	254.8	241.0	249.5	373.9
35	297	254.8	241.0	249.5	373.9
36	254	250.9	241.9	253.7	368.2
37	326	395.9	318.7	239.8	395.9
38	294	395.9	313.3	239.8	395.9
39	511	403.8	403.8	713.0	403.8
40	475	403.8	403.8	715.6	403.8
41	252	339.6	179.5	213.2	275.9
42	248	323.2	173.3	208.3	251.8
43	443	512.0	279.3	351.0	512.0
44	406	501.5	260.3	312.5	468.1
45	439	499.9	277.5	351.0	499.9
46	173.8	187.5	127.9	126.8	292.3
47	40	58.0	35.8	30.7	48.6
48	72.3	58.0	52.6	64.1	90.4
49	62.8	58.0	47.7	52.7	65.5
50	87.8	58.0	59.0	75.5	90.4
51	89.7	58.1	70.4	97.8	90.4
52	119.7	119.8	89.4	97.6	105.7
53	76	61.7	65.0	74.4	102.8
54	133	72.7	86.6	127.2	113.1

Table 8-7 Ratio of Experimental to Wood (1990), ACI 318-19, Gulec (2011) and Proposed shear force

Wall Number	Wood (1990)	Gulec (2011)	$V_{proposed}$	ACI 318-19
1	0.739	1.154	1.272	0.539
2	0.765	1.200	1.331	0.562
3	0.521	1.000	1.647	0.535
4	1.265	1.489	1.353	0.759
5	1.116	1.433	1.392	0.669
6	0.825	1.284	1.513	0.521
7	0.730	1.144	1.362	0.466
8	0.703	1.094	1.289	0.444
9	0.726	1.141	1.362	0.465
10	1.086	1.257	1.129	0.652
11	1.055	1.223	1.100	0.633
12	0.929	1.084	0.979	0.557
13	1.040	1.227	1.116	0.624
14	0.975	1.178	1.090	0.630
15	1.042	1.265	1.175	0.681
16	0.870	1.051	0.973	0.562
17	0.967	1.157	1.063	0.628
18	0.857	1.095	1.059	1.714
19	1.120	1.419	1.362	0.672
20	2.478	1.487	1.029	1.487
21	2.607	1.564	1.149	1.564
22	1.539	0.974	1.257	0.923
23	1.486	0.967	1.323	0.891
24	1.572	0.944	1.375	0.943
25	0.821	0.755	0.654	0.492
26	0.515	0.653	0.700	0.401
27	1.131	0.829	1.209	0.679
28	1.524	1.156	1.561	0.915
29	0.598	0.538	0.509	0.359
30	0.325	0.366	0.411	0.244
31	1.076	0.968	0.915	0.645

Wall Number	Wood (1990)	Gulec (2011)	$V_{proposed}$	ACI 318-19
32	0.742	0.836	0.940	0.557
33	1.346	1.241	1.191	0.808
34	0.972	0.905	0.874	0.583
35	1.324	1.232	1.190	0.794
36	1.150	1.050	1.001	0.690
37	1.372	1.023	1.359	0.823
38	1.238	0.938	1.226	0.743
39	1.265	1.265	0.717	1.265
40	1.176	1.176	0.664	1.176
41	0.869	1.404	1.182	0.913
42	0.871	1.431	1.190	0.985
43	1.442	1.586	1.262	0.865
44	1.322	1.560	1.299	0.867
45	1.464	1.582	1.251	0.878
46	0.991	1.358	1.371	0.595
47	0.737	1.118	1.303	0.822
48	1.333	1.374	1.128	0.800
49	1.158	1.317	1.192	0.959
50	1.618	1.487	1.163	0.971
51	1.654	1.275	0.917	0.992
52	1.068	1.338	1.226	1.133
53	1.232	1.170	1.022	0.739
54	1.959	1.535	1.046	1.176

Table 8-8 Average, Standard deviation and Coefficient of variance of data listed in Table 8-7

Dispersion	Wood (1990)	Gulec (2011)	$V_{proposed}$	ACI 318-19
Average	1.135	1.172	1.137	0.778
Standard deviation	0.429	0.262	0.250	0.294
Coefficient of variance	0.378	0.224	0.220	0.378

Figure 6-1 illustrates the ratio comparison of the experimental to the predicted shear strength. Figure 8-18 summarizes the test results of the 54 squat walls and their predicted shear strength by the available equations in this study. Figure 8-19 to Figure 8-22 compares the experimental and predicted values for each equation.

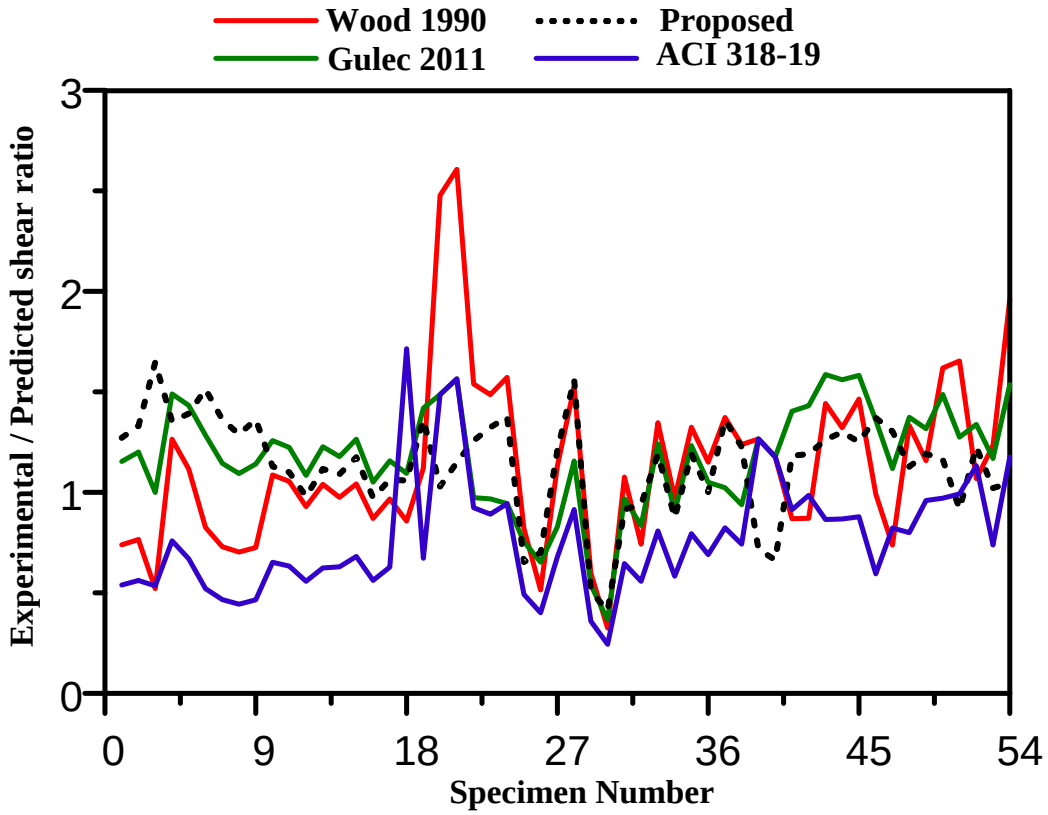

Figure 8-17 Ratio of Experimental to Wood (1990), ACI 318-19, Gulec (2011) and Proposed shear force

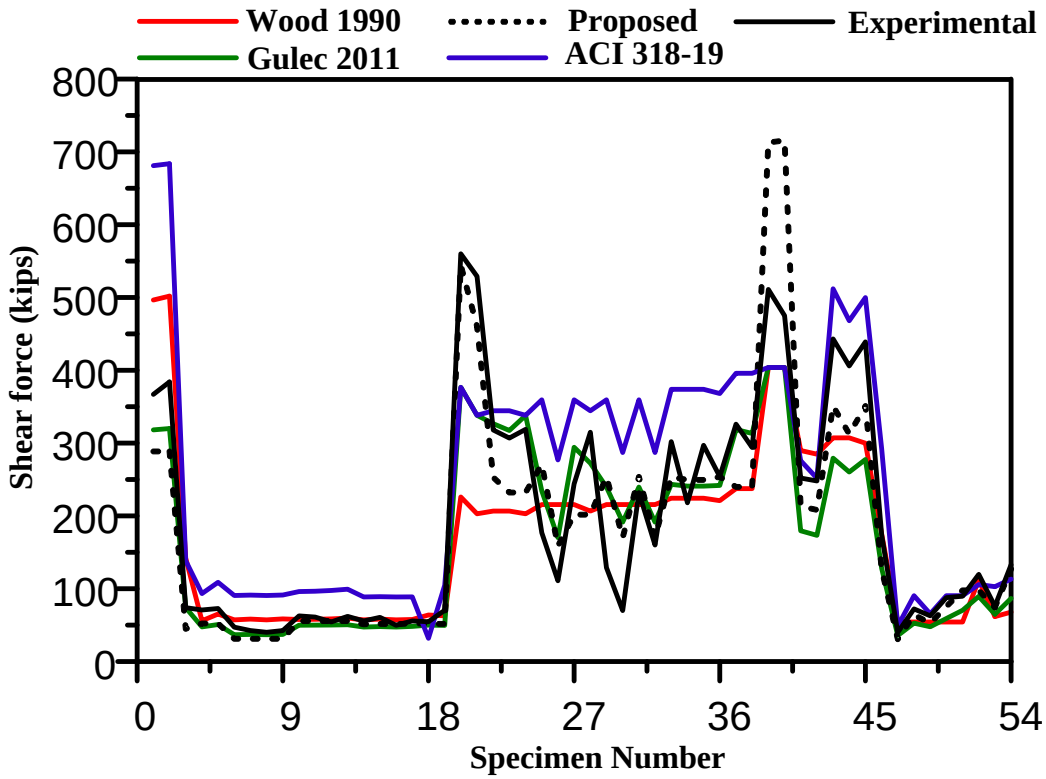

Figure 8-18 Experimental, Wood (1990), ACI 318-19, Gulec (2011) and Proposed shear strength

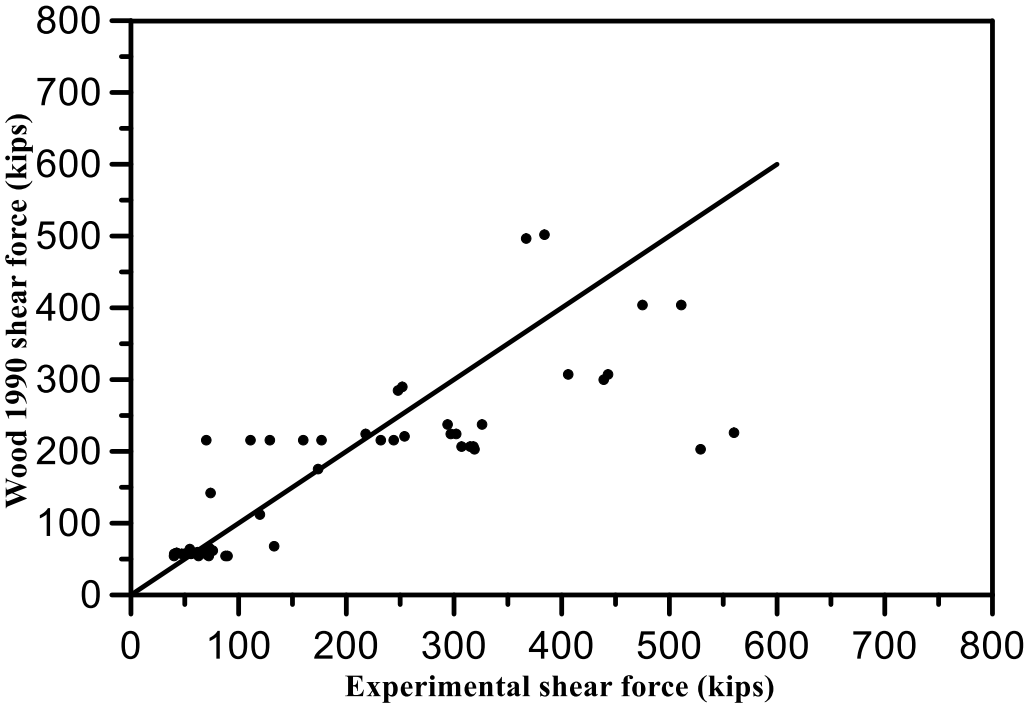

Figure 8-19 Experimental and Wood (1990) shear strength

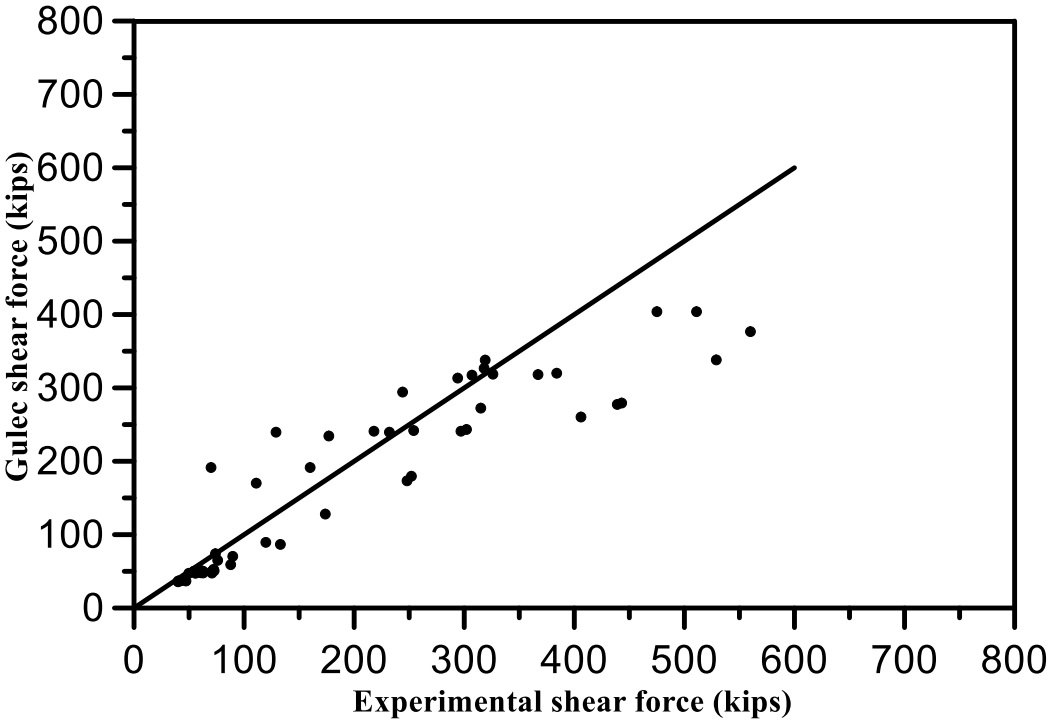

Figure 8-20 Experimental and Gulec (2011) shear strength

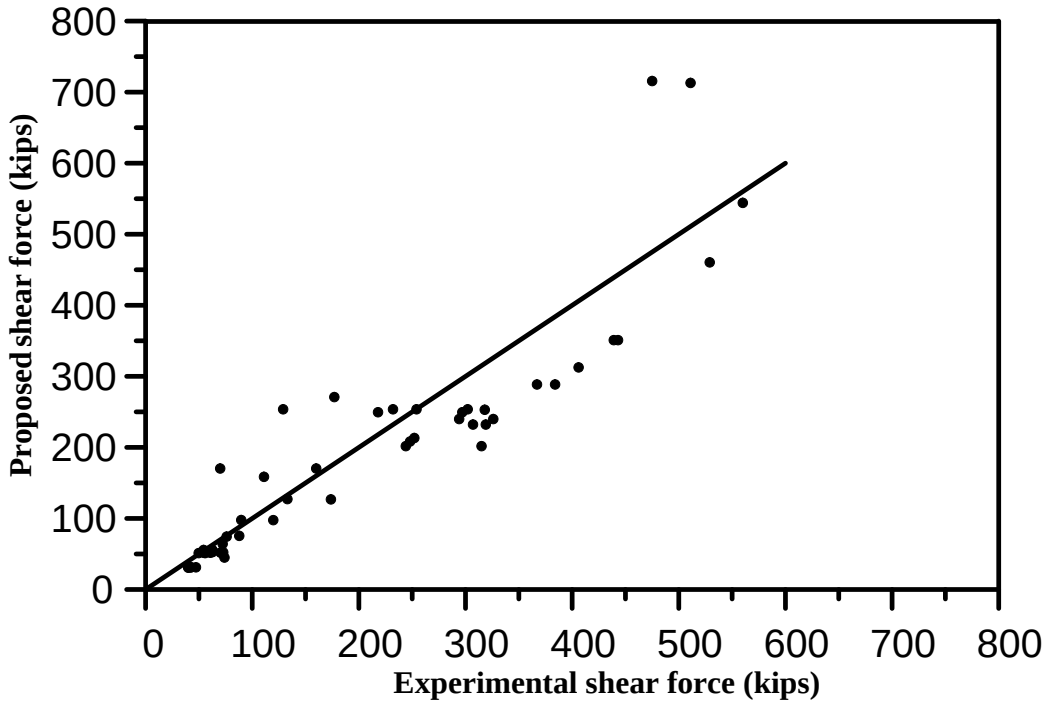

Figure 8-21 Experimental and Proposed shear strength

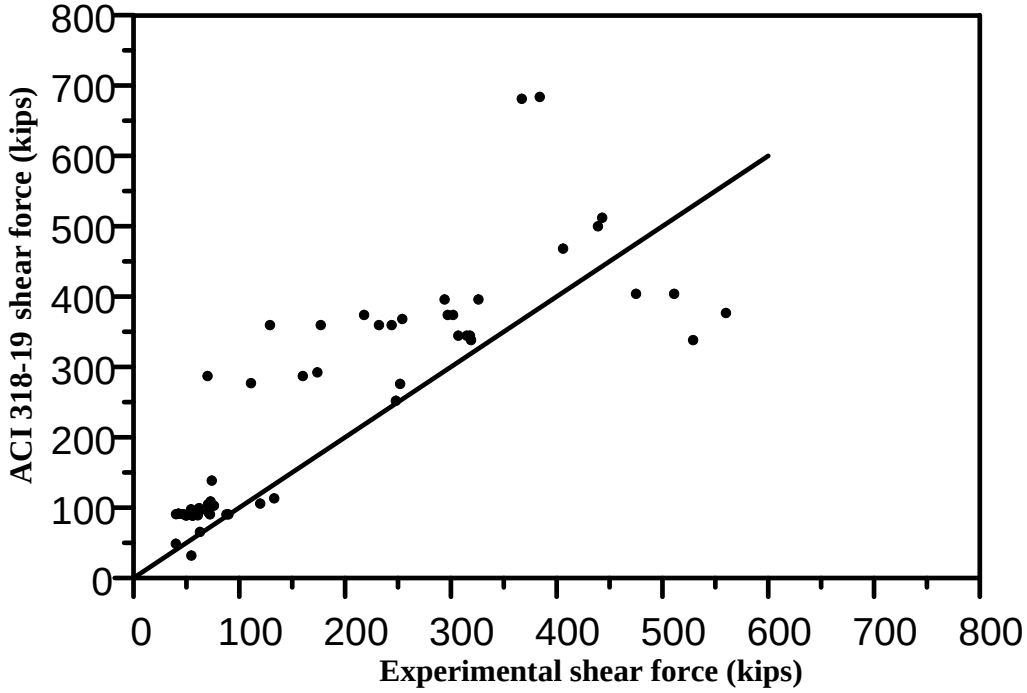

Figure 8-22 Experimental and ACI 318-19 shear strength

Chapter 9

Summary and Conclusions

This study investigated the proposal of ductile squat shear wall configuration which have several advantages over the conventional squat walls designed by ACI 318-19 provisions, specifically, having more ductile shear behavior, and easy to pre-fabricate steel cages. A total of seven squat walls were tested to explore the shear performance of ACI-compliant and proposed walls at medium and high design shear stresses. The typical conventional walls suffer from sliding shear failure as they are confined only at boundaries but are insufficient at the web. However, the proposed walls are confined at the critical regions to eliminate the implausible sliding shear failure.

The following conclusions are drawn from the study:

1. The sliding shear failure is the most common mode failure of well-reinforced squat walls, this study explained the factors of sliding behavior that are eliminated in the proposed squat walls.

2. The test results showed that proposed walls with medium demand shear stresses ($10\sqrt{f_{cm}}$ to $12\sqrt{f_{cm}}$, psi), reached drift ratio as twice as that ACI-compliant wall attained. This indicates the ductile shear behavior of the proposed walls; this merit is crucial to reduce the cost of wall reinforcement.

3. The proposed walls ductility advantage is also applicable to high demand shear stresses ($18\sqrt{f_{cm}}$ to $24\sqrt{f_{cm}}$, psi). This level of high shear stresses was

investigated even though ACI provisions limits the design shear strength to $10\sqrt{f_{cm}}$.

4. The strut and tie model is believed to be the most reliable criteria to explain shear force transfer in squat walls. In a 0.5 wall aspect ratio, the effective number of ties distributed over 2/3 of wall length for medium demand shear stress while ties distributed over 0.5 wall length for high demand shear stress, the effective number of ties was measured using strain gauges attached on longitudinal steel bars.

5. The DIC processed images were used to measure width of concrete struts, the width was determined to be 0.5 and 0.25 of wall length for 0.5- and 1.0-aspect ratio walls.

6. A Strut and Tie Model-based Proposed Equation was presented to predict the squat wall shear strength, the equation was derived based on experimental results of this study. Compared to the results of 54 squat wall results of tested wall in literature, the equation has an excellent prediction accuracy; where the average of experimental-to-predicted shear strength ratio is 1.137 and Coefficient of Variance 0.22. Based on the analyzed 54 wall results, the ACI 318-19 tends to overpredict squat walls shear strength.

References

1. American Concrete Institute. *Building Code Requirements for Structural Concrete (ACI 318-19) and Commentary,* Farmington Hills, Michigan, 2019.

2. Baek, J., Park, H., Lee, J., & Bang, C. (2017). Cyclic loading test for walls of aspect ratio 1.0 and 0.5 with grade 550 MPa shear reinforcing bars. ACI Structural Journal, 114(4), 969. doi:10.14359/51689680Cardenas A. E., Hanson J. M., Corley W. G., and Hognestad E., 1973, “Design Provisions for Shear Walls,” ACI Journal, Vol. 70, No. 23, Code Background Paper, Background Material used in preparing ACI 318-71, pp. 221-230.

3. Baek, J., Park, H., Shin, H., & Yim, S. (2017a). Cyclic loading test for reinforced concrete walls (aspect ratio 2.0) with grade 550 MPa (80 ksi) shear reinforcing bars. ACI Structural Journal, 114(3), 673. doi:10.14359/51689437

4. Barda F., Hanson J. M., and Corley W. G., 1977 “Shear Strength of Low-Rise Walls with Boundary Elements”, ACI Special Publications, Reinforced Concrete in Seismic Zones, SP-53-8, pp.149-202. (Also, Research and Development Bulletin, No. RD043.01D, Portland Cement Association.) Buffalo, NY, 2009, 291 pp.

5. Chandra, J., Chanthabouala, K., & Teng, S. (2018). Truss model for shear strength of structural concrete walls. ACI Structural Journal, 115(2), 323-335D. doi:10.14359/51701129

6. Cheng, M., Hung, S., Lequesne, R. D., & Lepage, A. (2016). Earthquake-resistant squat walls reinforced with highstrength steel. ACI Structural Journal, 113(5), 1065. doi:10.14359/51688825

7. Gulec, C. K., and Whittaker, A. S., “Performance-Based Assessment and Design of Squat Reinforced Concrete Shear Walls,” Report No. MCEER-09-0010, Multidisciplinary Center for Earthquake Engineering Research,

8. Gulec, C. K., and Whittaker, A. S., 2011, "Empirical Equations for Peak Shear Strength of Low Aspect Ratio Reinforced Concrete Walls," ACI Structural Journal, V. 108, No. 1, Jan.-Feb., pp. 80-89.

9. Gulec, C. K.; Whittaker, A. S.; and Stojadinovic, B., 2008, "Shear Strength of Squat Rectangular Reinforced Concrete Walls," ACI Structural Journal, V. 105, No. 4, July-Aug., pp. 488-497.

10. Gulec, C.K., Whittaker, A.S., and Stojadinovic, B., 2009" Peak Shear Strength of Squat Reinforced Concrete Walls with Boundary Barbells or Flanges," ACI Structural Journals, Vol. 106, No. 3, pp. 368-377.

11. Gupta, A. _1996_. "Behaviour of high strength concrete structural walls." Ph.D. thesis, Curtin Univ. of Technology, Perth, Australia.

12. Gupta, A., and Rangan, B. V. 1998. "High-strength concrete HSC structural walls." ACI Struct. J., 952, 194–205.

13. Hidalgo P. A., Ledezma C. A., and Jordan R. M., 2002 "Seismic Behavior of Squat Reinforced Concrete Shear Walls," Earthquake Spectra, Vol. 18, No. 2, pp. 287-308.

14. Hsu, T. T. C. (1996). Toward A unified nomenclature for reinforced-concrete theory. Journal of Structural Engineering, 122(3), 275-283. doi:10.1061/(ASCE)0733-9445(1996)122:3(275)

15. Hwang, S. J., and Lee, H. J. (1999). ''Analytical model for predicting shear strengths of exterior reinforced concrete beam-column joints for seismic resistance.'' ACI Struct. J., 96(5), 846–857.

16. Hwang, S. J., and Lee, H. J. (2000). ‘‘Analytical model for predicting shear strengths of interior reinforced concrete beam-column joints for seismic resistance.’’ ACI Struct. J., 97(1), 35–44.

17. Hwang, S., & Lee, H. (2002). Strength prediction for discontinuity regions by softened strut-and-tie model. Journal of Structural Engineering, 128(12), 1519-1526. doi:10.1061/(ASCE)0733-9445(2002)128:12(1519)

18. Hwang, S., Fang, W., Lee, H., & Yu, H. (2001). analytical model for predicting shear strength of squat walls. Journal of Structural Engineering, 127(1), 43.

19. Kassem, W. (2015). Shear strength of squat walls: A strut-and-tie model and closed-form design formula. Engineering Structures, 84, 430-438. doi:10.1016/j.engstruct.2014.11.027

20. Kassem, W. (2015). Shear strength of squat walls: A strut-and-tie model and closed-form design formula. Engineering Structures, 84, 430-438. doi:10.1016/j.engstruct.2014.11.027

21. Kassem, W., & Elsheikh, A. (2010). Estimation of shear strength of structural shear walls. Journal of Structural Engineering, 136(10), 1215-1224. doi:10.1061/(ASCE)ST.1943-541X.0000218

22. Lefas, I.D., Kotsovos, M.D. and Ambraseys, N.N., “Behavior of Reinforced Concrete Structural Walls: Strength, Deformation Characteristics and Failure Mechanism,” ACI Structural Journal, Vol. 87, No. 1, January-February 1990, pp. 23-31.

23. Li, Y. A., and Hwang, S. J. (2017). “Prediction of lateral load displacement curves for reinforced concrete short columns failed in shear.” J. Struct. Eng., 10.1061/(ASCE)ST.1943-541X.0001656, 04016164.

24. Luna, B. N., & Whittaker, A. S. (2019). Peak strength of shear-critical reinforced concrete walls. ACI Structural Journal, 116(2), 257-266. doi:http://dx.doi.org.ezproxy.uta.edu/10.14359/51712280

25. Luna, B. N.; Rivera, J. P.; and Whittaker, A. S., 2015, “Seismic Behavior of Low Aspect Ratio Reinforced Concrete Shear Walls,” ACI Structural Journal, V. 112, No. 5, Sept.-Oct., pp. 593-603. doi: 10.14359/51687709

26. Maikol Del Carpio Ramos , Andrew S. Whittaker & Cevdet K. Gulec (2012) Predictive Equations for the Peak Shear Strength of Low-Aspect Ratio Reinforced Concrete Walls, Journal of Earthquake Engineering, 16:2, 159-187, DOI: 10.1080/13632469.2011.613529

27. Mander, J. Priestley, M. and Park, R. “Theoritical stress – strain model for confined concrete”, Journal of structural engineering, Vol. 114, No. 8, 1988.

28. Moehle, J., 2015, Seismic Design of Reinforced Concrete Buildings, McGraw-Hill Education, New York, 760 pp.

29. Pauley T., Priestley M. J. N., Synge A. J., 1982 “Ductility in Earthquake Resisting Squat Shear walls,” ACI Journal, Vol. 79, No. 26, pp. 257-269.

30. Paultre, P., & Légeron, F. (2008). Confinement reinforcement design for reinforced concrete columns. Journal of Structural Engineering, 134(5), 738-749. doi:10.1061/(ASCE)0733-9445(2008)134:5(738)

31. Razvi, S., & Saatcioglu, M (1994) “Strength and deformability of confined high-strength concrete columns”, ACI structural journal, V.91, No.6.

32. Razvi, S., & Saatcioglu, M. (1999). Confinement model for high-strength concrete. Journal of Structural Engineering, 125(3), 281-289. doi:10.1061/(ASCE)0733-9445(1999)125:3(281)

33. Saatcioglu, M., & Razvi, S. R. (1992). Strength and ductility of confined concrete. Journal of Structural Engineering, 118(6), 1590-1607. doi:10.1061/(ASCE)0733-9445(1992)118:6(1590)

34. Sezen, H., and Moehle, J. P. (2006). “Seismic tests of concrete columns with light transverse reinforcement.” ACI Struct. J., 103(6), 842–849.

35. Teng, S., & Chandra, J. (2016). Cyclic shear behavior of high-strength concrete structural walls. ACI Structural Journal, 113(6), 1335. doi:10.14359/51689158

36. Vecchio, F. J., and Collins, M. P. (1993). ‘‘Compression response of cracked reinforced concrete.’’ J. Struct. Engrg., ASCE, 119(12), 3590–3610.

37. Vecchio, F. J., and Collins, M. P., “The Modified Compression Field Theory for Reinforced Concrete Elements Subjected to Shear,” ACI JOURNAL, Proceedings V. 83, No. 2, Mar.-Apr. 1986, pp. 219-231.

38. Weng, P., Li, Y., Tu, Y., & Hwang, S. (2017). Prediction of the lateral load-displacement curves for reinforced concrete squat walls failing in shear. Journal of Structural Engineering, 143(10), 4017141. doi:10.1061/(ASCE)ST.1943- 541X.0001872

39. Whyte, C. A., & Stojadinovic, B. (2014). Effect of Ground Motion Sequence on Response of Squat Reinforced Concrete Shear Walls. Journal of Structural Engineering, 140(8)

40. Wong, P. S. and Vecchio, F. J.,” VecTor2 & Formworks User’s Manual”, August 2002.

41. Wood, S. L., 1990, “Shear Strength of Low-Rise Reinforced Concrete Walls,” ACI Structural Journal, V. 87, No. 1, Jan.-Feb., pp. 99-107.

42. Yu, H., & Hwang, S. (2005). Evaluation of softened truss model for strength prediction of reinforced concrete squat walls. Journal of Engineering Mechanics, 131(8), 839-846. doi:10.1061/(ASCE)0733-9399(2005)131:8(839)

Biographical Information

Ghassan Almasabha got his Bachelor of Science in Civil Engineering from Alhussein bin Talal University in 2012, and the M.Sc. in Structural Engineering from the University of Jordan in 2014. He enrolled in the Civil Engineering PhD program at the University of Texas, Arlington, TX at Fall 2014. His research focuses on disaster resilient structures, large-scale experimental testing of shear walls, and steel members/frames especially eccentrically braced frame (EBF), Concrete Culverts and Finite Element Analysis (FEA).